

# THE JOURNAL OF PHYSICAL CHEMISTRY

(Registered in U. S. Patent Office)

## CONTENTS

J. H. Hildebrand 80th Birthday Symposium, Berkeley, Calif., September 13, 1961

<b>Kozo Shinoda and Eric Hutchinson:</b> Pseudo-phase Separation Model for Thermodynamic Calculations on Micellar Solutions. . . . .	577	<b>George Scatchard:</b> The Gibbs Adsorption Isotherm. . . . .	618
<b>F. Danon and Kenneth S. Pitzer:</b> Corresponding States Theory for Argon and Xenon. . . . .	583	<b>D. L. Andersen, R. A. Smith, D. B. Myers, S. K. Alley, A. G. Williamson, and R. L. Scott:</b> A Thermodynamic Study of the System 1-Hydro- <i>n</i> -perfluorohexane + Acetone. . . . .	621
<b>Otto Redlich:</b> Generalized Coordinates and Forces. . . . .	585	<b>O. K. Rice and J. T. MacQueen:</b> The Effect of an Impurity on the Phase Transition in a Binary Liquid System. II. . . . .	625
<b>Herbert S. Harned:</b> A Rule for the Calculation of the Activity Coefficients of Salts in Organic Solvent-Water Mixtures. . . . .	589	<b>Robert D. Dunlap and Robert L. Scott:</b> Internal Pressures of Perfluoro- <i>n</i> -hexane, <i>n</i> -Hexane, and their Mixtures. . . . .	631
<b>Joseph E. Mayer:</b> Heat Capacity and Open and Closed Ensemble Averages. . . . .	591	<b>Terrance B. Tripp and Robert D. Dunlap:</b> Second Virial Coefficients for the Systems: <i>n</i> -Butane + Perfluoro- <i>n</i> -butane and Dimethyl Ether + 1-Hydroperfluoropropane. . . . .	635
<b>E. B. Smith and John Walkley:</b> The Thermodynamic Properties of Gases in Solution. I. The Partial Molal Volume. . . . .	597	<b>Robert L. Scott and Robert D. Dunlap:</b> On the Determination of Second Virial Coefficients. . . . .	639
<b>Scott E. Wood:</b> The Energy-Temperature-Volume Surface for a Single Component System. . . . .	600	<b>J. M. Prausnitz:</b> Solubility Thermodynamics in Chemical Engineering. . . . .	640
<b>D. N. Glew:</b> Aqueous Solubility and the Gas-Hydrates. The Methane-Water System. . . . .	605	<b>Y. Kobatake and B. J. Alder:</b> Cell Potentials and Gas Solubility Theory. . . . .	645
<b>David Turnbull:</b> On the Relation between Crystallization Rate and Liquid Structure. . . . .	609		
<b>E. A. Allan and L. W. Reeves:</b> The Use of the Chemical Shift Parameter for Study of Intramolecular Hydrogen Bonds. . . . .	613		
-----			
<b>Warren G. Lee and Sidney I. Miller:</b> The Secondary Isotope Rate Effect in the Iodide Debromination of <i>sym</i> -Tetrabromoethane and <i>sym</i> -Tetrabromoethanes. . . . .	655	<b>S. Ehrenson:</b> A Closed Form Analysis of the LCAO-MO $\omega$ -Technique. I. Ionization Potentials and Electron Affinities. . . . .	706
<b>W. J. Svirbely and Shirley M. Read:</b> The Thermodynamic Properties of Liquid Ternary Zinc, Indium, and Gallium Solutions. . . . .	658	<b>S. Ehrenson:</b> A Closed Form Analysis of the LCAO-MO $\omega$ -Technique. II. Mechanics of the Technique. . . . .	712
<b>K. G. Mathai and E. Rabinowitch:</b> Studies of the Thionine-Ferrous Iron Reaction in a Heterogeneous System. . . . .	663	<b>A. Odajima, J. A. Sauer, and A. E. Woodward:</b> Proton Magnetic Resonance of Some Normal Paraffins and Polyethylene. . . . .	718
<b>A. R. Cooper, Jr., and W. D. Kingery:</b> Kinetics of Solution in High Viscosity Liquids: Sodium Chloride-Glycerol. . . . .	665	<b>David M. Mohilner:</b> Thermodynamic Treatment of the Electrocapillary Curve for Reversible Electrodes and Properties of the Double Layer. . . . .	724
<b>W. R. Gilkerson:</b> The Dielectric Constant and Conductance of Ion Pairs: An Extension of Onsager's Field Effect to Relaxation of Ion Pairs in an Alternating Field. . . . .	669	<b>Ronald A. Munson:</b> The Role of Adsorption in Constant Current Transition Time Studies—The Hydrogen Electrode. . . . .	727
<b>Paul H. Kasai:</b> Electron Paramagnetic Resonance Study of Mn <sup>2+</sup> Ion in Polycrystalline Calcium Fluorophosphate. . . . .	674	<b>Richard A. Holroyd:</b> Ethylene as a Scavenger in the Radiolysis of Liquid Cyclopentane. . . . .	730
<b>Leonard Peller and Lewis Barnett:</b> On Enzyme Catalyzed Equilibrium Polymerizations. I. Linear Polymers by Direct Reaction and through Primer Initiation. . . . .	680	<b>T. E. Hopkins, R. A. Pasternak, E. S. Gould, and J. R. Herndon:</b> X-Ray Diffraction Study of Arsenic Trisulfide-Iodine Glasses. . . . .	733
<b>Leonard Peller:</b> On Enzyme Catalyzed Equilibrium Polymerizations. II. Growth on a Branched Chain Primer and Copolymerization. . . . .	685	<b>P. J. McGonigal, A. D. Kirshenbaum, and A. V. Grosse:</b> The Liquid Temperature Range, Density, and Critical Constants of Magnesium. . . . .	737
<b>R. D. Doepker and Gilbert J. Mains:</b> Photolysis of Diethyl Ketone in Perfluorodimethylcyclobutane. . . . .	690	<b>E. G. Shafrin and W. A. Zisman:</b> Effect of Progressive Fluorination of a Fatty Acid on the Wettability of its Adsorbed Monolayer. . . . .	740
<b>I. P. Mayer, Ephraim Banks, and Ben Post:</b> Rare Earth Disilicides. . . . .	693	<b>Donald H. Payne and Edgar F. Westrum, Jr.:</b> Heat Capacities and Thermodynamic Properties of Globular Molecules. IV. Pentaerythrityl Chloride, Bromide, and Iodide from 6 to 300°K. . . . .	748
<b>Sydney Ross, Jeffrey K. Saelens, and James P. O'Neil:</b> On Physical Adsorption. XVIII. Limiting Isothermic Heats of Adsorption of Gases on Graphitized Carbon by the Chromatographic Method. . . . .	696	<b>J. H. Stern and A. A. Passchier:</b> The Heats of Formation of Triiodide and Iodate Ions. . . . .	752
<b>Assa Lifshitz and B. Perlmuter-Hayman:</b> The Kinetics of the Hydrolysis of Chlorine. III. The Reaction in the Presence of Various Bases, and a Discussion of the Mechanism. . . . .	701		
		<b>NOTES</b>	
		<b>D. L. Hildebrand and W. F. Hall:</b> The Vapor Pressure and Heat of Sublimation of Gold. . . . .	754
		<b>Everett R. Johnson:</b> Effect of Intensity on the Radiation Induced Decomposition of Inorganic Nitrates. . . . .	755

Contents continued on inside front cover

# THE JOURNAL OF PHYSICAL CHEMISTRY

(Registered in U. S. Patent Office)

W. ALBERT NOYES, JR., EDITOR

ALLEN D. BLISS

ASSISTANT EDITORS

A. B. F. DUNCAN

EDITORIAL BOARD

A. O. ALLEN  
C. E. H. BAWN  
J. BIGELEISEN  
F. S. DAINTON

D. D. ELEY  
D. H. EVERETT  
S. C. LIND  
F. A. LONG

J. P. McCULLOUGH  
K. J. MYSELS  
J. E. RICCI  
R. E. RUNDLE

W. H. STOCKMAYER  
E. R. VAN ARTSDALEN  
M. B. WALLENSTEIN  
W. WEST

Published monthly by the American Chemical Society at 20th and Northampton Sts., Easton, Pa. Second-class postage paid at Easton, Pa.

The *Journal of Physical Chemistry* is devoted to the publication of selected symposia in the broad field of physical chemistry and to other contributed papers.

Manuscripts originating in the British Isles, Europe, and Africa should be sent to F. C. Tompkins, The Faraday Society, 6 Gray's Inn Square, London W. C. 1, England.

Manuscripts originating elsewhere should be sent to W. Albert Noyes, Jr., Department of Chemistry, University of Rochester, Rochester 20, N. Y.

Correspondence regarding accepted copy, proofs, and reprints should be directed to Assistant Editor, Allen D. Bliss, Department of Chemistry, Simmons College, 300 The Fenway, Boston 15, Mass.

Advertising Office: Reinhold Publishing Corporation, 430 Park Avenue, New York 22, N. Y.

Articles must be submitted in duplicate, typed, and double spaced. They should have at the beginning a brief Abstract, in no case exceeding 300 words. Original drawings should accompany the manuscript. Lettering at the sides of graphs (black on white or blue) may be pencilled in and will be typeset. Figures and tables should be held to a minimum consistent with adequate presentation of information. Photographs will not be printed on glossy paper except by special arrangement. All footnotes and references to the literature should be numbered consecutively and placed in the manuscript at the proper places. Initials of authors referred to in citations should be given. Nomenclature should conform to that used in *Chemical Abstracts*, mathematical characters be marked for italic, Greek letters carefully made or annotated, and subscripts and superscripts clearly shown. Articles should be written as briefly as possible consistent with clarity and should avoid historical background unnecessary for specialists.

Notes describe fragmentary or incomplete studies but do not otherwise differ fundamentally from articles and are subjected to the same editorial appraisal as are articles. In their preparation particular attention should be paid to brevity and conciseness. Material included in Notes must be definitive and may not be republished subsequently.

Communications to the Editor are designed to afford prompt preliminary publication of observations or discoveries whose value to science is so great that immediate publication is imperative. The appearance of related work from other laboratories is in itself not considered sufficient justification for the publication of a Communication, which must in addition meet special requirements of timeliness and significance. Their total length may in no case exceed 1000 words or their equivalent. They differ from Articles and Notes in that their subject matter may be republished.

Symposium papers should be sent in all cases to Secretaries of Divisions sponsoring the symposium, who will be responsible for their transmittal to the Editor. The Secretary of the Division by agreement with the Editor will specify a time after which symposium papers cannot be accepted. The Editor reserves the right to refuse to publish symposium articles, for valid scientific reasons. Each symposium paper may not exceed four printed pages (about sixteen double spaced typewritten pages) in length except by prior arrangement with the Editor.

Remittances and orders for subscriptions and for single copies, notices of changes of address and new professional connections, and claims for missing numbers should be sent to the Subscription Service Department, American Chemical Society, 1155 Sixteenth St., N. W., Washington 6, D. C. Changes of address for the *Journal of Physical Chemistry* must be received on or before the 30th of the preceding month. Please include an old address label with the notification.

Claims for missing numbers will not be allowed (1) if received more than sixty days from date of issue (because of delivery hazards, no claims can be honored from subscribers in Central Europe, Asia, or Pacific Islands other than Hawaii), (2) if loss was due to failure of notice of change of address to be received before the date specified in the preceding paragraph, or (3) if the reason for the claim is "missing from files."

Subscription rates (1962): members of American Chemical Society, \$12.00 for 1 year; to non-members, \$24.00 for 1 year. Postage to countries in the Pan-American Union \$0.80; Canada, \$0.40; all other countries, \$1.20. Single copies, current volume, \$2.50; foreign postage, \$0.15; Canadian postage \$0.10; Pan-American Union, \$0.10. Back volumes (Vol. 56-65) \$30.00 per volume; foreign postage, per volume \$1.20, Canadian, \$0.40; Pan-American Union, \$0.80. Single copies: back issues, \$3.00; for current year, \$2.50; postage, single copies: foreign, \$0.15; Canadian, \$0.10; Pan-American Union, \$0.10.

The American Chemical Society and the Editors of the *Journal of Physical Chemistry* assume no responsibility for the statements and opinions advanced by contributors to THIS JOURNAL.

The American Chemical Society also publishes *Journal of the American Chemical Society*, *Chemical Abstracts*, *Industrial and Engineering Chemistry*, International Edition of *Industrial and Engineering Chemistry*, *Chemical and Engineering News*, *Analytical Chemistry*, *Journal of Agricultural and Food Chemistry*, *Journal of Organic Chemistry*, *Journal of Chemical and Engineering Data*, *Chemical Reviews*, *Chemical Titles*, *Journal of Chemical Documentation*, *Journal of Medicinal and Pharmaceutical Chemistry*, *Inorganic Chemistry*, *Biochemistry*, and *CA—Biochemical Sections*. Rates on request.

A. G. Tharp: The Structure of Lanthanum Family Silicides.....	758
Irving Fatt: A Modified Diffusion Time-Lag.....	760
J. J. Chesick: A Criticism of Heat of Immersional Wetting Practice.....	762
George Van Dyke Tiers: Fluorine N.m.r. Spectroscopy. VI. Fluorocarbon Sulfides.....	764
Arthur G. Maki and Earle K. Plyler: Formation Con-	

stant of the 1:1 Pyridine-Iodine Complex.....	766
P. J. Dyne: The Mechanism of the "Unimolecular" Yield of Hydrogen in the Radiolysis of Liquid Cyclohexane.....	767

## COMMUNICATION TO THE EDITOR

R. K. Harris: Variations in the Coupling Constant between <sup>14</sup> C and Directly-Bonded Fluorine.....	768
---	-----

---

---

# THE JOURNAL OF PHYSICAL CHEMISTRY

---

---

(Registered in U. S. Patent Office) (© Copyright, 1962, by the American Chemical Society)

VOLUME 66

APRIL 23, 1962

NUMBER 4

---

---

## PSEUDO-PHASE SEPARATION MODEL FOR THERMODYNAMIC CALCULATIONS ON MICELLAR SOLUTIONS<sup>1</sup>

BY KŌZŌ SHINODA<sup>2</sup> AND ERIC HUTCHINSON

*Department of Chemistry, Yokohama National University, Yokohama, Japan, and the Department of Chemistry, Stanford University, Stanford, California*

*Received August 21, 1961*

It is argued that the state of condensation in the micelles of detergent solutions most nearly corresponds to the liquid state. Thermodynamic equations are presented to show that the Krafft point, enthalpy, and entropy of micellization can be interpreted theoretically on a simple basis if the micelle is treated as a pseudo-phase, but that erroneous values for the enthalpy and entropy of micellization are obtained by assuming ideal behavior for the single species and micelles in the simpler treatments of this problem.

Micellar solutions such as sodium dodecyl sulfate solutions are particularly interesting from the theoretical viewpoint in that whereas below a well defined critical concentration (c.m.c.) the solute dissolves as single ions or molecules (depending on the chemical nature of the compound), above the c.m.c. it dissolves to form aggregates called micelles. The micelle is thermodynamically stable and reversible. A model has been advanced in which it is proposed to treat the micelle as a separate phase whose dimensions are very small compared with those normally characteristic of macroscopic phases.<sup>3-5</sup> The c.m.c. is considered to represent the maximum solubility of the single ions or molecules, and if this saturation point is exceeded a new phase, the micelle, appears. To this extent the formation of micelles resembles the formation of a sol of silver iodide when the solubility product of this latter is exceeded, but the interest in micelles largely derives from the differences between the micelle and a particle in a silver iodide sol. In the first place the micelle is a small entity, so that the extension of thermodynamic argument to such a small pseudo-phase is intrinsically interesting. This extension has some implications which have

not been very clearly appreciated. One of the important points in connection with micelles, for example, has to do with how the micellar pseudophase is specified in micellar solutions which are electrolytes. Some authors,<sup>6</sup> whose approach to the formation of micelles is *via* the mass action treatment, appear to define the micelle as the collection of surface active ions and the tightly bound gegenions. This micelle generally bears a net charge, and the charge and the size of the micelle vary with added electrolyte.<sup>7-10</sup> Another approach, suggested by Hutchinson<sup>5</sup> and Matijević and Pethica,<sup>11</sup> defines the micellar phase as comprising both this charged poly-ion and the gegenions in the diffuse double layer. This latter approach has the marked advantage that the system is describable in terms of uncharged components. There is a fundamental difference between these two approaches, because on the mass action model which concerns itself only with the micellar poly-ion this latter is a non-stoichiometric entity, and Matijević and Pethica<sup>11</sup> have advanced cogent criticisms of this model. In this paper we point out some of the implicit thermodynamic assumptions which must be made in order to reconcile the two approaches. These

(1) Presented before the Division of Colloid and Surface Chemistry, 139th National Meeting of the American Chemical Society, St. Louis, 1961.

(2) Department of Chemistry, Yokohama National University, Ooka-machi, Minami-ku, Yokohama, Japan.

(3) A. E. Alexander, *Trans. Faraday Soc.*, **38**, 54 (1942).

(4) K. Shinoda, *Bull. Chem. Soc. Japan*, **26**, 101 (1953).

(5) E. Hutchinson, A. Inaba, and L. G. Bailey, *Z. physik. Chem. (Frankfurt)*, **5**, 344 (1955).

(6) J. N. Phillips, *Trans. Faraday Soc.*, **51**, 561 (1955).

(7) E. Hutchinson and J. C. Melrose, *Z. physik. Chem. (Frankfurt)*, **2**, 363 (1954).

(8) D. Stigter and K. J. Mysels, *J. Phys. Chem.*, **59**, 45 (1955).

(9) D. Stigter, R. J. Williams, and K. J. Mysels, *ibid.*, **59**, 330 (1955).

(10) K. J. Mysels and L. H. Princen, *ibid.*, **63**, 169 (1959).

(11) E. Matijević and B. A. Pethica, *Trans. Faraday Soc.*, **54**, 589 (1958).

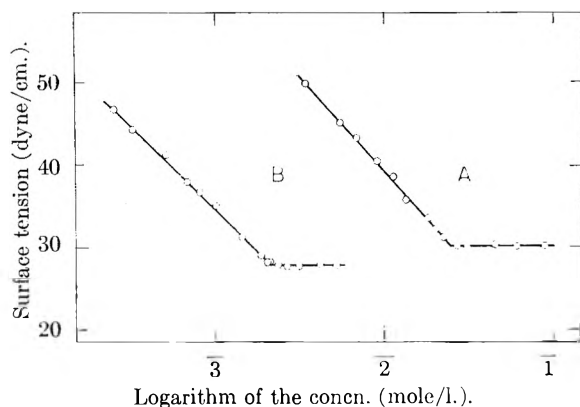


Fig. 1.—Surface tension vs. the logarithm of concentration curves of: A, octyl glucoside; B, decyl glucoside at 25°.

assumptions are involved in any thermodynamic calculations based on the c.m.c., e.g., the calculation of entropy and enthalpy of micellization, which is the subject of this paper.

Although the state of aggregation in detergent micelles is not yet clearly established, a liquid state model is strongly supported by a number of observations: (a) the solubilization phenomena exhibited by these solutions are consistent with a liquid state<sup>12</sup>; (b) micelle-forming ions can interact with a wide variety of additives to form mixed micelles.<sup>13</sup> It is not necessary that the additive be itself a liquid: in solution it is in the liquid state regardless of its properties in the pure state. Characteristic of the liquid state is the fact that a solvent may mix with solutes of markedly different molecular sizes to yield solutions in which the partial molal volumes are close to the molal volumes of the components,<sup>14</sup> whereas in the solid state it is well known that, with solute molecules differing markedly in size from the solvent, mixed crystals do not form readily. It seems probable, therefore, that the solubilizing properties of a micelle are due to its liquid nature.<sup>15</sup>

**A Phase Separation Model for the Micelle.**—A model which has been advanced to account for micelle formation treats the micelle as a separate phase which begins to form at the c.m.c., which then is regarded as a saturation concentration for the single solute particles.<sup>3-5</sup> Measurements of osmotic coefficients are consistent with this model.<sup>16</sup> The colligative properties of some colloidal surfactants do not deviate by more than about 5% from that of an ideal 1:1 electrolyte until the c.m.c. is reached,<sup>17</sup> although, as revealed by measurements of equivalent conductivity,<sup>18</sup> there are certain colloidal electrolyte solutions for which the evidence for the formation of dimer ions is strong. It is possible that di-

merization is not a universal phenomenon in solutions of detergents: it may depend on the molecular type to which the detergents belong, and, in any event, it seems likely that even when dimers are formed this process is to be distinguished from the initiation of micellar aggregation. Dimerization in those solutions in which it occurs may resemble the dimerization which occurs in acetic acid vapor, where, when the saturation vapor pressure is attained, liquid acetic acid separates out and is in equilibrium with both monomer and dimer molecules in the vapor. We propose to treat micellization as a similar phase separation, with the important distinction that micellization does not lead to an effectively infinite aggregation number, such as corresponds to true phase separation. Justification for this treatment may be found in curves describing the uptake of additives just below and above the c.m.c.<sup>13</sup>

It should follow from this model, if correct, that the activity of micelle-forming compounds should be practically constant above the c.m.c., and graphs relating the surface tension and concentration of solutions of these materials clearly illustrate that the activity does indeed remain constant above the c.m.c. This is illustrated in Fig. 1, which presents results for aqueous solutions of octyl and decyl glucosides.<sup>19</sup> The Gibbs' adsorption equation may be written in the form

$$-RT\Gamma_2 = \left( \frac{\partial \gamma}{\partial \ln a_2} \right)_T = \left( \frac{\partial \gamma}{\partial \ln X_2} \right)_T \left( \frac{\partial \ln X_2}{\partial \ln a_2} \right)_T \quad (1)$$

in which  $\Gamma_2$  and  $\gamma$  have their usual meaning, and  $X_2$  and  $a_2$  are the mole fraction and activity of the solute, respectively. Experiments involving the use of radiotracers indicate that  $\Gamma_2$  has large nearly constant values over a wide range of values of  $X_2$  in excess of the c.m.c.<sup>20,21</sup> Accordingly, if  $\Gamma_2$  is finite and if  $(\partial \gamma / \partial \ln X_2)_T$  is zero, it follows that  $(\partial \ln a_2 / \partial \ln X_2)_T$  also is zero. This last conclusion which is equivalent to the statement that  $a_2$  is independent of  $X_2$  above the c.m.c. is an impressive evidence of phase separation model.

**The Physical Meaning of the Krafft Point.**—By analogy with the phase diagram for the ice-water system, we may imagine that as the temperature is increased the difference between the saturation concentration of the supercooled micelles and that of the hydrated solid compound decreases. In the case of the solution, concentration is playing the role played by pressure in the one-component system. As shown in Fig. 2,<sup>22,23</sup> above the Krafft point the saturation of the micelles is smaller than that of the (hypothetical) superheated hydrated solid, so that the micelle is the thermodynamically preferred form. Hence above the Krafft point the addition of detergent beyond the c.m.c. produces neither a large increase in the concentration of monomers nor the hydrated solid agent, but rather it produces increasing numbers of micelles. Moreover, since the

(12) M. E. L. McBain and E. Hutchinson, "Solubilization and Related Phenomena," Academic Press, Inc., New York, N. Y., 1955.

(13) W. D. Harkins, R. W. Mattoon, and R. Mittelman, *J. Chem. Phys.*, **15**, 763 (1947). K. Shinoda, *J. Phys. Chem.*, **58**, 1136 (1954).

(14) K. Shinoda and J. H. Hildebrand, *ibid.*, **62**, 295 (1958).

(15) G. S. Hartley, "Aqueous Solutions of Paraffin Chain Salts," Hermann et Cie, Paris, 1936.

(16) M. E. L. McBain, W. B. Dye, and S. A. Johnson, *J. Am. Chem. Soc.*, **61**, 3210 (1939).

(17) S. A. Johnson and J. W. McBain, *Proc. Roy. Soc. (London)*, **A181**, 119 (1942).

(18) P. Mukerjee, K. J. Mysels, and C. I. Dulin, *J. Phys. Chem.*, **62**, 1390 (1958).

(19) K. Shinoda, T. Yamaguchi, and R. Hori, *Bull. Chem. Soc. Japan*, **34**, 237 (1961).

(20) G. Nilsson, *J. Phys. Chem.*, **61**, 1135 (1957).

(21) D. J. Salley, A. J. Weith, Jr., A. A. Argyle, and J. K. Dixon, *Proc. Roy. Soc. (London)*, **A203**, 42 (1950).

(22) H. V. Tartar and K. A. Wright, *J. Am. Chem. Soc.*, **61**, 539 (1939).

(23) H. B. Klevens, *J. Phys. Chem.*, **52**, 130 (1948).

activity of the solute remains almost constant above the c.m.c.,<sup>24</sup> and since the addition of more agent in dissolved form leaves the activity practically unaltered, the solubility of the agent increases very rapidly with change of temperature. In the present model the concentration of the monomer above the Krafft point may either decrease or increase moderately, subject only to the requirement that the activity of the solute remain constant. The Krafft point now can be interpreted as the point at which solid hydrated agent and micelles are in equilibrium with monomers: in terms of the phase rule, with two components the equilibrium hydrated solid  $\rightleftharpoons$  monomers  $\rightleftharpoons$  micelles is univariant, so that at a given pressure the point is fixed. The usual hysteresis effects associated with phase changes are readily reproduced in these systems, *e.g.*, it is quite easy to maintain supercooled micelles in solution below the Krafft point for long periods of time before hydrated solid agent appears. This corresponds to a supercooling of the micelle below its normal freezing point. Although the freezing points of micelles may be affected by the type and concentration of gegenions, as has been demonstrated in the case of the cetane sulfonates,<sup>25</sup> nevertheless there should be a rough parallelism between the freezing of micelles and the freezing of hydrocarbon chains, and this has been demonstrated in the case of fatty acid soaps.<sup>26</sup> Moreover, just as the freezing point of a pure component is decreased by the presence of additives, so also should the Krafft point, *i.e.*, the freezing point of the micelles, be decreased by the presence of additives. We have demonstrated this readily by measurements of the solubility of sodium dodecyl sulfate in the presence of increasing amounts of *n*-hexanol at 12°, which is very close to the Krafft point of this compound. As shown in Fig. 3, the solubility of the sodium dodecyl sulfate increases with increasing hexanol concentration, since a solution which contains hexanol has a lower c.m.c. than a solution of pure sodium dodecyl sulfate, and consequently, can contain more sodium dodecyl sulfate at a given temperature.<sup>27</sup> In support of the notion that the Krafft point represents a freezing of the micelles, we may note that the heats of fusion of fatty acids and their esters increase by about 1 kcal. per mole per increased CH<sub>2</sub> group, and that the heat of solution corresponding to solid hydrated agent  $\rightarrow$  micelles increases by 0.9 kcal. per mole per increased CH<sub>2</sub> group.<sup>28</sup>

Slightly above the Krafft temperature the micelle may be somewhat more stable than the infinitely large hydrated solid agent, as suggested above. Nevertheless, the concentration of gegenions increases with the stoichiometric amount of colloidal electrolyte in solution: hence, since the Krafft point is dependent on gegenion concentration, it shifts to higher temperatures with increasing solute (gegenion) concentration, so that at a higher temperature we can again, in the saturated solution, encounter

(24) E. Hutchinson, *Z. physik. Chem.* (Frankfurt), **21**, 38 (1959).

(25) R. C. Murray and G. S. Hartley, *Trans. Faraday Soc.*, **31**, 183 (1935).

(26) F. Krafft and H. Wiglow, *Ber.*, **28**, 2566 (1895).

(27) We are indebted to Mr. Stephen Filseth for making these measurements.

(28) E. Hutchinson, K. E. Manchester, and L. Winslow, *J. Phys. Chem.*, **58**, 1124 (1954).

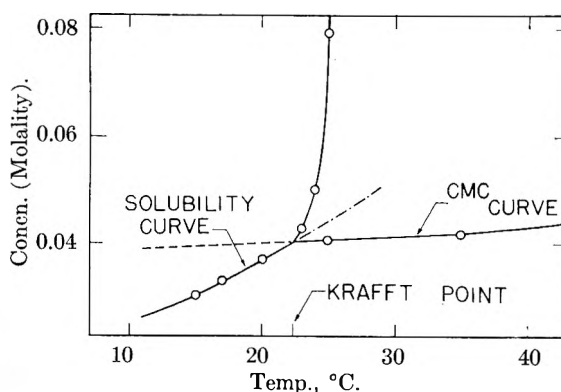


Fig. 2.—Phase diagram close to the Krafft point of sodium decyl sulfonate.

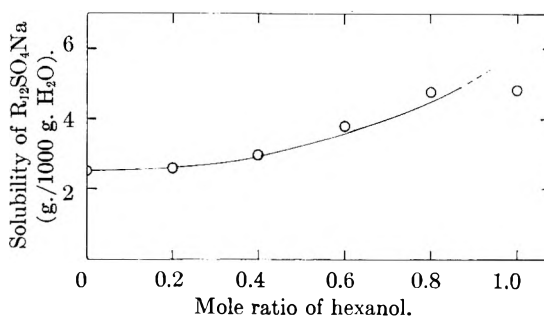


Fig. 3.—Solubility of sodium dodecyl sulfate vs. mole ratio of hexanol to R<sub>12</sub>SO<sub>4</sub>Na at 12°.

the monomer-micelle-hydrated solid equilibrium point at which the solid again becomes the preferred thermodynamic form.

**The Enthalpy and Entropy of Micellization.**—A number of suggestions have been made in the literature for methods of estimating the enthalpy and entropy of micellization, but there is still some confusion about the thermodynamic basis for such estimates. There are essentially two cases to be considered: (1) *Phase separation treatment.* The case of a non-ionic agent is readily obtainable just as in the ordinary substances. In the case where the micelle forming compound is an electrolyte, the micelle may be regarded either as neutral or charged. (2) *Mass action treatment.* The micelle is treated by mass action model in the case of a non-ionic agent. It is shown that both treatments give the same conclusion if the aggregation number is fairly large.

**Uncharged Phase Separation Model.**—We begin with the general experimental problem in which we deal with a solution containing water (component 1), detergent (component 2), and added salt. The micelle is treated as a separate phase and the c.m.c. as a saturation concentration which, if exceeded, leads to the production of the new phase. It should be noted, however, that the micellar phase comprises both the poly-ion and the gegenions in the diffuse double layer, so that the micellar phase, defined in this way, has zero net charge. One effect of added salt is to change the thickness of the double layer and hence the size of the micelle. On this model the micellar phase, the continuous aqueous phase surrounding the micelles, and the total system are describable in terms of uncharged components. A typical system would consist of water (1), sodium dodecyl sulfate (2), and sodium chloride

(3). In a solution above the c.m.c. in which both micelles and monomers are present we have

$$\mu_{2\pm}^\alpha = \mu_{2\pm}^\beta \quad (2)$$

where

$\mu_{2\pm}^\alpha$  = chemical potential of detergent in the micelle  
 $\mu_{2\pm}^\beta$  = chemical potential of detergent in the aqueous phase

For any arbitrary change in conditions

$$d\mu_{2\pm}^\alpha = d\mu_{2\pm}^\beta \quad (3)$$

A convenient set of independent intensive variables is given by  $P$ ,  $T$ ,  $X_2$ ,  $X_3$ , where

$P$  = pressure  
 $T$  = absolute temperature  
 $X_2$  = stoichiometric mole fraction of the detergent monomer  
 $X_3$  = stoichiometric mole fraction of the added salt

Phase  $\alpha$ , the micelle, has an intensive state determined solely by  $T$  and  $P$ .

$$\mu_{2\pm}^\alpha = \mu_{2\pm}^\alpha(T, P)$$

But

$$\mu_{2\pm}^\beta = \mu_{2\pm}^\beta(T, P, X_2, X_3)$$

Hence, from eq. 3

$$\left(\frac{\partial \mu_{2\pm}^\alpha}{\partial T}\right)_P dT + \left(\frac{\partial \mu_{2\pm}^\alpha}{\partial P}\right)_T dP = \left(\frac{\partial \mu_{2\pm}^\beta}{\partial T}\right)_{P, X_2, X_3} dT + \left(\frac{\partial \mu_{2\pm}^\beta}{\partial P}\right)_{T, X_2, X_3} dP + \left(\frac{\partial \mu_{2\pm}^\beta}{\partial X_2}\right)_{P, T, X_3} dX_2 + \left(\frac{\partial \mu_{2\pm}^\beta}{\partial X_3}\right)_{P, T, X_2} dX_3$$

$\therefore$

$$\left\{ \left(\frac{\partial \mu_{2\pm}^\alpha}{\partial T}\right)_P - \left(\frac{\partial \mu_{2\pm}^\beta}{\partial T}\right)_{P, X_2, X_3} \right\} dT = \left\{ \left(\frac{\partial \mu_{2\pm}^\beta}{\partial P}\right)_{T, X_2, X_3} - \left(\frac{\partial \mu_{2\pm}^\alpha}{\partial P}\right) \right\} dP + \left(\frac{\partial \mu_{2\pm}^\beta}{\partial X_2}\right)_{P, T, X_3} dX_2 + \left(\frac{\partial \mu_{2\pm}^\beta}{\partial X_3}\right)_{P, T, X_2} dX_3 \quad (4)$$

$$- \left(\frac{H_{2\pm}^\alpha - H_{2\pm}^\beta}{T}\right) dT - (V_{2\pm}^\beta - V_{2\pm}^\alpha) dP + \left(\frac{\partial \mu_{2\pm}^\beta}{\partial X_2}\right)_{P, T, X_3} dX_2 + \left(\frac{\partial \mu_{2\pm}^\beta}{\partial X_3}\right)_{P, T, X_2} dX_3 \quad (5)$$

Where  $H_{2\pm}^\alpha$ ,  $V_{2\pm}^\alpha$ , and so on refer to partial molal enthalpies and volumes of component 2. Writing  $\Delta H_m = (H_{2\pm}^\beta - H_{2\pm}^\alpha)$ , and confining attention to systems at constant pressure<sup>29</sup>

$$-\frac{\Delta H_m}{T} = \left(\frac{\partial \mu_{2\pm}^\beta}{\partial X_2}\right)_{P, T, X_3} \left(\frac{\partial X_2}{\partial T}\right)_P + \left(\frac{\partial \mu_{2\pm}^\beta}{\partial X_3}\right)_{P, T, X_2} \left(\frac{\partial X_3}{\partial T}\right)_P \quad (6)$$

Now suppose that components 2 and 3 are both 1:1 electrolytes and that they have a common ion, *e.g.*,  $\text{Na}^+$  in the system sodium dodecyl sulfate-sodium chloride. Then

$$X_{2+} = X_2 + X_3$$

$$X_{2-} = X_2$$

$$X_{2\pm}^2 = X_2(X_2 + X_3) = X_2^2 + X_2X_3 \quad (7)$$

And, assuming ideality

$$\mu_{2\pm}^\beta = \mu_{2\pm}^0 + RT \ln(X_{2\pm}^2)$$

$$= \mu_{2\pm}^0 + RT \ln(X_2^2 + X_2X_3) \quad (8)$$

$$\left(\frac{\partial \mu_{2\pm}^\beta}{\partial X_2}\right)_{P, T, X_3} = RT \frac{2X_2 + X_3}{X_2^2 + X_2X_3}$$

$$\left(\frac{\partial \mu_{2\pm}^\beta}{\partial X_3}\right)_{P, T, X_2} = RT \frac{X_2}{X_2^2 + X_2X_3}$$

$$-\frac{\Delta H_m}{RT^2} = \frac{2X_2 + X_3}{X_2^2 + X_2X_3} \left(\frac{\partial X_2}{\partial T}\right)_P + \frac{X_2}{X_2^2 + X_2X_3} \left(\frac{\partial X_3}{\partial T}\right)_P \quad (9)$$

A number of special cases may be noted.

(1)  $X_3 = 0$ , so that we have a solution of pure detergent electrolyte.

$$\therefore -\frac{\Delta H_m}{RT^2} = \frac{2}{X_2} \left(\frac{\partial X_2}{\partial T}\right)_P = 2 \left(\frac{\partial \ln X_2}{\partial T}\right)_P \quad (10)$$

If now  $X_2$  is equated, as we suggest, with the c.m.c. value

$$-\frac{\Delta H_m}{RT^2} = 2 \left(\frac{\partial \ln \text{c.m.c.}}{\partial T}\right)_P$$

This is similar to the result obtained by Matijević and Pethica.<sup>11</sup> (2)  $X_3$  is constant and  $X_3 \gg X_2$ . This corresponds to a solution of detergent in the presence of "swamping electrolyte."

$$-\frac{\Delta H_m}{RT^2} = \frac{X_3}{X_2X_3} \left(\frac{\partial X_2}{\partial T}\right)_P = \left(\frac{\partial \ln X_2}{\partial T}\right)_P$$

$$\text{or } -\frac{\Delta H_m}{RT^2} = \left(\frac{\partial \ln \text{c.m.c.}}{\partial T}\right)_P \quad (11)$$

This equation was used by Matijević and Pethica<sup>11</sup> for the case which they describe as "complete ion exchange," and incorrectly used by Stainsby and Alexander<sup>30</sup> for systems containing no added salt.

**Charged Phase Separation Model.**—In this case the term micellar phase is restricted to the surface active ion. If now we choose as components, detergent ion = 2, gegenion = 3, simili-ion = 4, we have as the equilibrium conditions

$$\tilde{\mu}_2^\alpha = \tilde{\mu}_2^\beta, d\tilde{\mu}_2^\alpha = d\tilde{\mu}_2^\beta \quad (12)$$

where  $\tilde{\mu}_2^\alpha$ ,  $\tilde{\mu}_2^\beta$  are electrochemical potentials of the surface active ions in the micellar state and in the aqueous phase, respectively.

As the heat, entropy, and free energy (including electrical energy) are insensitive to the concentration of simili-ion, the entropy and the enthalpy of micellization are related by the equation as before

$$\Delta S_m = \frac{\Delta H_m}{T} = - \left(\frac{\partial \Delta \tilde{G}_m}{\partial T}\right)_{P, X_2, X_3} = \left(\frac{\partial \Delta \tilde{G}_m}{\partial \ln X_2}\right)_{P, X_3, T} \left(\frac{\partial \ln X_2}{\partial T}\right)_{P, \Delta \tilde{G}_m} + \left(\frac{\partial \Delta \tilde{G}_m}{\partial \ln X_3}\right)_{P, X_2, T} \left(\frac{\partial \ln X_3}{\partial T}\right)_{P, \Delta \tilde{G}_m} \quad (13)$$

The next step is to derive  $\Delta \tilde{G}_m$  as a function of  $X_2$  and  $X_3$ . Both theoretically and experimentally,<sup>4,31</sup> we know that

$$\Delta \tilde{G}_m = \tilde{\mu}^\alpha - \tilde{\mu}^\beta = -RT \ln X_2 - K_g RT \ln X_3 + \text{Const}(P, T) \quad (14)$$

Where  $K_g$  is an experimental constant determined from the change of the c.m.c. with the concentration of univalent gegenions. Accordingly

$$-\Delta S_m = -\frac{\Delta H_m}{T} = RT \left(\frac{\partial \ln X_2}{\partial T}\right)_{P, \Delta \tilde{G}_m} + K_g RT \left(\frac{\partial \ln X_3}{\partial T}\right)_{P, \Delta \tilde{G}_m} \quad (15)$$

(29) Measurements by one of us, *J. Colloid Sci.*, **11**, 352 (1956), suggest that  $V_{2\pm}^\alpha - V_{2\pm}^\beta \approx 0$ , so that the constant pressure requirement may be an unnecessary refinement.

(30) G. Stainsby and A. E. Alexander, *Trans. Faraday Soc.*, **46**, 587 (1950).

(31) K. Shinoda, *J. Phys. Chem.*, **60**, 1439 (1956).

In the case where no salts are added, so that we have a solution of pure detergent electrolyte,  $X_2 = X_3$ .

$$-\Delta S_m = -\frac{\Delta H_m}{T} = (1 + K_g) RT \left( \frac{\partial \ln X_2}{\partial T} \right)_{P, \Delta G_m} \quad (16)$$

If  $X_3$  is kept constant the second term in eq. 15 is zero, so that

$$-\Delta S_m = -\frac{\Delta H_m}{T} = RT \left( \frac{\partial \ln X_2}{\partial T} \right)_{P, \Delta G_m} \quad (17)$$

The exact thermodynamic eq. 6 and 13 are identical, as they should be. Equations 15-17, which correspond to 9-11, agree with each other if  $K_g = 1$ . The difference simply results from the models assumed.

The heat of micellization in aqueous solutions of various ionic compounds has been measured by direct calorimetric determinations of heat of dilution.<sup>28,32,33</sup> Because the concentrations characteristic of the c.m.c. are generally small, calorimetric measurements, though thermodynamically important, do not provide very accurate values of  $\Delta H_m$ .

Values of  $\Delta H_m$  obtained from the temperature dependence of the c.m.c. are not very accurate, either, because of the rather small change in the c.m.c. over convenient temperature gaps and because in general the plot of  $\ln$  c.m.c. vs. temperature is not linear.

**Mass Action Model.**—Suppose we have a solution in which the total stoichiometric concentration of detergent is measured by  $X_2$ , and in which  ${}_1X_2$  is the mole fraction of monomer and  ${}_nX_2$  the mole fraction of the micellar  $n$ -mer. If we take as the standard state for the solution a concentrated solution above the c.m.c., then the activity of the monomer remains constant, as we have seen, while the activity of the micellar phase also is constant. Hence if  ${}_1a_2$  and  ${}_na_2$  are the appropriate activities we have

$$\frac{{}_1a_2^n}{{}_na_2} = K$$

where  $K$  is a constant. By choosing the standard state suggested above,  $K = 1$ , hence

$$({}_1a_2)^n = {}_na_2$$

Replacing the activity by the mole fraction and activity coefficient

$$\frac{({}_1f_2 \cdot {}_1X_2)^n}{{}_nf_2 \cdot {}_nX_2} = 1$$

For the micellar phase, as for any pure phase we may take  ${}_nf_2 = 1$

$${}_1f_2 \cdot {}_1X_2 = ({}_nX_2)^{1/n} \quad (18)$$

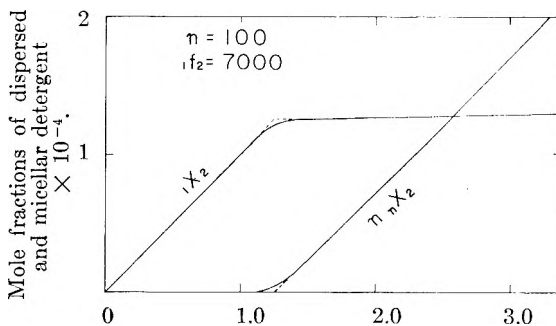
For values of  $n$  of the order of magnitude 25-100 or more  $({}_nX_2)^{1/n} \approx 1$ , so that  ${}_1f_2 \approx 1/{}_1X_2$ . And, since  ${}_1X_2 + n \cdot {}_nX_2 = X_2$

$${}_1X_2 + n({}_1f_2 \cdot {}_1X_2)^n = X_2 \quad (19)$$

Clearly, if we know the aggregation number  $n$  and c.m.c., from which we can calculate the activity coefficient  ${}_1f_2$ , we can calculate the population of

(32) E. D. Goddard, C. A. J. Hoeve, and B. C. Benson, *J. Phys. Chem.*, **61**, 593 (1957).

(33) P. White and G. C. Benson, *J. Colloid Sci.*, **13**, 584 (1958); *Trans. Faraday Soc.*, **55**, 1025 (1959).



Total concn. of detergent in mole fraction unit  $\times 10^{-4}$ .

Fig. 4.—The relation between monomeric and micellar detergent. The calculations were performed assuming that the aggregation number is 100 and the c.m.c. is about 0.008 mole/l., typical values for common detergents.

the solution in monomers and micelles by the aid of eq. 19, as shown in Fig. 4. The c.m.c. is the intersection of the two lines in Fig. 4. The system is a hypothetical one, but the aggregation number and the c.m.c. value are close to those of sodium dodecyl sulfate. At the c.m.c.,  ${}_1X_2$  is practically identical with  $X_2$ , and the ratio  ${}_1X_2/X_2$  is almost independent of  $n$ . By arguments parallel to those used in the case of the phase separation model we can show that in this case

$$\Delta S_m = \frac{\Delta H_m}{T} = -\left( \frac{\partial \Delta G_m}{\partial T} \right)_{P, X_2} = + \left( \frac{\partial \Delta G_m}{\partial \ln {}_1X_2} \right)_{P, T} \cdot \left( \frac{\partial \ln {}_1X_2}{\partial T} \right)_{P, \Delta G_m} \quad (20)$$

$$= -RT \left( \frac{\partial \ln {}_1a_2}{\partial \ln {}_1X_2} \right)_{P, T} \left( \frac{\partial \ln {}_1X_2}{\partial T} \right)_{P, \Delta G_m} \quad (21)$$

Although we can calculate  ${}_1X_2$  from  $X_2$  provided the aggregation number is known,  ${}_1X_2$  and  $X_2$  are so close in value at the c.m.c. that any errors introduced by employing the alternative form of eq. 21 are negligible. There then remains the problem of calculating the derivative  $(\partial \ln a_2 / \partial \ln X_2)_{P, T}$ .

For a non-ionic solute we may write<sup>34</sup>

$$\ln a_2 = \ln X_2 + \frac{B}{RT} \phi_1^2 \quad (22)$$

where  $B$  is a constant, independent of  $X_2$ , and  $\phi_1$  is the volume fraction of the solvent.<sup>35</sup> The first of these terms reflects the entropy of mixing, whereas the second reflects the enthalpy of mixing of solute and solvent. Since it recently has been found<sup>36</sup> that the entropy of mixing is not seriously dependent on the molecular volumes of solute and solvent, we have used  $\ln X_2$  as an entropy term. Then

$$\left( \frac{\partial \ln a_2}{\partial \ln X_2} \right)_{P, T} = 1 - 2\phi_1^2 \phi_2 \cdot \frac{B}{RT} = 1 - 2\phi_2 \ln \frac{a_2}{X_2}$$

Accordingly, as  $a_2 \approx 1$  at  $X_2 = \text{c.m.c.}$

$$\Delta S_m = -RT(1 + 2\phi_2 \ln \text{c.m.c.}) \left( \frac{\partial \ln X_2}{\partial T} \right)_{P, \Delta G_m} \quad (23)$$

So that an accurate value of  $\Delta S_m$  is in principle derivable from the temperature dependence of the

(34) J. H. Hildebrand and R. L. Scott, "The Solubility of Non-electrolytes," Reinhold Publ. Corp., New York, N. Y., 1950.

(35) There are additional enthalpy and entropy factors which occur in aqueous solutions of paraffin chain compounds ascribable to the ice-like structure of surrounding water molecules, but both are functions of  $\phi_1^2$  and they largely cancel each other.

(36) K. Shinoda and J. H. Hildebrand, *J. Phys. Chem.*, **61**, 789 (1957).

c.m.c., some values of  $(\partial \ln a_2 / \partial \ln X_2)_{P,T}$  are given in Table I. If the c.m.c. value is small, the correction due to  $(\partial \ln a_2 / \partial \ln X_2)_{P,T}$  is small as shown in Table I.<sup>37</sup> There is no paper which reports the

in which the enthalpy changes are as indicated:  $\Delta_1 H_2$  can be obtained calorimetrically or from the temperature dependence of the solubility below the Krafft point.  $\Delta H_m$  is obtained from the difference between the partial molal heats of solution above and below the c.m.c. or from the temperature dependence of the c.m.c.  $\Delta_n H_2$  is obtained either algebraically from  $\Delta_1 H_2$  and  $\Delta H_m$  or from the partial molal heat of solution above the c.m.c. From the experimental results it may be concluded that  $\Delta H_m$  is small compared with  $\Delta_1 H_2$  or  $\Delta_n H_2$  and that the major portion of both  $\Delta_1 H_2$  and  $\Delta_n H_2$  is ascribable to the heat of fusion of the hydrated solid agent. This latter

TABLE I

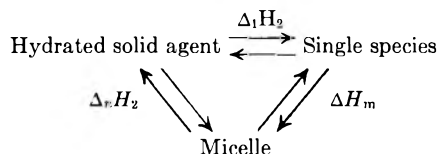
Compound	C.m.c. ( $X_2$ )	$(\frac{\partial \ln a_2}{\partial \ln X_2})$ at c.m.c.	Ref.
R <sub>8</sub> -glucoside	0.00045	0.89	19
R <sub>10</sub> -glucoside	.00004	.99	19
R <sub>12</sub> -glucoside	.0000034	.999	19
R <sub>10</sub> O(CH <sub>2</sub> CH <sub>2</sub> O) <sub>12</sub> CH <sub>3</sub>	.000018	.993	37a
R <sub>7</sub> COO(CH <sub>2</sub> CH <sub>2</sub> O) <sub>7.6</sub> CH <sub>3</sub>	.00018	.963	37b

TABLE II

Compound	HEAT OF MICELLIZATION, $\Delta H_m$			Method	Ref.
	Medium	Temp., °C.	$\Delta H_m$ , kcal./mole		
R <sub>8</sub> SO <sub>4</sub> Na	H <sub>2</sub> O	25	0.8	Calorimetry	32
R <sub>8</sub> SO <sub>4</sub> Na	0.694 <i>m</i> NaCl	25	0.3	Calorimetry	32
R <sub>10</sub> SO <sub>4</sub> Na	H <sub>2</sub> O	25	0.5	Calorimetry	32
R <sub>7</sub> COOK	0.033 <i>m</i> KOH	25	2.1 $(\frac{\partial \ln a_2}{\partial \ln X_2})$	Temp. depend.	33
R <sub>7</sub> COOK	0.0417 <i>m</i> KOH	25	1.7	Calorimetry	32
R <sub>7</sub> COOK	1.802 <i>m</i> KCl + 0.042 <i>m</i> KOH	25	1.5	Calorimetry	33
R <sub>7</sub> COOK	0.033 <i>m</i> KOH	50	-2.0 $(\frac{\partial \ln a_2}{\partial \ln X_2})$	Temp. depend.	35
R <sub>7</sub> COOK	0.033 <i>m</i> KOH	50	1.0	Calorimetry	33
C <sub>10</sub> H <sub>21</sub> O(CH <sub>2</sub> CH <sub>2</sub> O) <sub>12</sub> CH <sub>3</sub>	H <sub>2</sub> O	10~40	3.3	Temp. depend.	37a
C <sub>7</sub> H <sub>15</sub> COO(CH <sub>2</sub> CH <sub>2</sub> O) <sub>7.6</sub> CH <sub>3</sub>	H <sub>2</sub> O	27	2.3	Temp. depend.	37b

heat of micellization of non-ionic agents by calorimetric measurement. The temperature dependence of the c.m.c. was reported for a few non-ionic agents, from which the heat of micellization was calculated with the aid of Table I and shown in Table II. Only a few experimental values for the calorimetric heat of micellization of ionic agents are reported and shown in Table II. As the heat of micellization is small, the values are not very accurate. The accurate values of the temperature dependence of the c.m.c. also are craved for to check the theory. The data for comparison are insufficient. Values of R<sub>7</sub>COOK at 25° agree each other if  $(\partial \ln a_2 / \partial \ln X_2)$  is about 0.8, which seems a reasonable value. Smaller values are to be expected for the heat of micellization of ionic materials in the presence of salts, owing to a reduction in the electrical repulsion in the micelle, and this appears to be borne out in the case of sodium octyl sulfate and potassium octanoate.<sup>32,33</sup>

We can construct the familiar triangle



(37) (a) T. Nakagawa and K. Shinoda, Chapter 2 in "Colloidal Surfactants," Academic Press, Inc., New York, N. Y., 1962; (b) T.

result accords with the view of the Krafft point given above.

The small heat of micellization can be explained in terms of the structural effects in water discussed by Frank and Evans.<sup>38</sup> Water molecules tend to form a kind of ice structure around the molecules of non-polar solutes, and with single paraffin chains this structure decreases the enthalpy and entropy of solution and gives rise to an extra heat capacity effect owing to the gradual breakdown of the structure with rise in temperature. The enthalpy and entropy contributions from the ice-like structures are large, but essentially cancel each other in the free energy term. It has been shown experimentally<sup>38</sup> that the enthalpy change on dissolving non-polar gases in water is considerably larger than in organic solvents and that the aqueous solutions have a larger partial molal heat capacity. Corresponding effects for the heat capacity of aqueous solutions of long chain ions are to be expected.<sup>32,39</sup>

**Acknowledgment.**—Portions of this work were supported by the National Science Foundation, to whom grateful acknowledgment is made.

Nakagawa, H. Inoue, K. Tori, and K. Kuriyama, *J. Chem. Soc. Japan*, **79**, 1194 (1958).

(38) H. S. Frank and M. W. Evans, *J. Chem. Phys.*, **13**, 507 (1945).

(39) D. B. Flockhart and A. R. Ubbelohde, *J. Colloid Sci.*, **8**, 428 (1953).



## CORRESPONDING STATES THEORY FOR ARGON AND XENON

BY F. DANON AND KENNETH S. PITZER<sup>1</sup>*Department of Chemistry and Lawrence Radiation Laboratory, University of California, Berkeley, California**Received September 18, 1961*

Recent experimental results allow a more precise check than was previously possible on the conformity of argon and xenon to the principle of corresponding states. The data show agreement within experimental error except at very high pressures where small differences are found for some but not for other measurements.

Precise check on the theory of corresponding states for the rare gases until recently has been limited by the lack of experimental volumetric data for argon at low reduced temperatures. Consequently the recent volumetric measurements of Levelt<sup>2</sup> are of particular interest. Other relevant data also will be considered.

**Compressibility Factor.**—Unfortunately the compressibility factor comparisons of Levelt's results<sup>2</sup> with values for xenon were made in ways which introduced unnecessary inaccuracies from auxiliary data. Consequently it seemed desirable to present the comparison of the compressibility factor data of Ar and Xe on the basis of reduced temperature and pressure. It was been pointed out<sup>3</sup> that the critical temperature and pressure are readily measured with high accuracy, hence the selection of these reduced variables introduces little error. By contrast the critical volume frequently is much less accurately known than the volumetric data at other temperatures and pressures.

The critical properties used in our calculations are

	Ar	Xe
$T_c$ , °K.	150.86	289.74
$P_c$ , atm.	48.34	57.64
$z_c$	0.2913	0.287

The values for argon are from Levelt's work; those for xenon are from Habgood and Schneider,<sup>4</sup> and are the same as Levelt used. The substantial difference in the  $z_c$  values is apparent at once. A comparison of the compressibility factor of argon with that for xenon at a variety of reduced temperatures and pressures is shown in Table I. These values were obtained by calculating the  $P_r$  values corresponding to Levelt's tabulated values of  $z$  at even  $T_r$  and  $d_r$ . These  $z$  values then were interpolated to even  $P_r$  values.

The results in Table I show essentially perfect conformity to the principle of corresponding states at densities substantially less than critical density. At higher densities, however,  $z$  for argon rises from 2 to 3% above that for xenon. These differences are much smaller than those reported by Levelt on the basis of comparison in terms of reduced temperature and density where a difference of about 10% is found at  $T_r = 1.05$  and  $d_r = 2.0$ . This point is near  $T_r = 1.05$ ,  $P_r = 6.0$ , where Table I shows less than 1% difference.

(1) Rice University, Houston, Texas.

(2) J. M. H. Levelt, *Physica*, **26**, 361 (1960); Thesis, Amsterdam, 1958.(3) R. F. Curl, Jr., and K. S. Pitzer, *Ind. Eng. Chem.*, **50**, 265 (1958); "Thermodynamic and Transport Properties of Fluids," Inst. Mech. Engr., London, 1958, p. 1.(4) H. W. Habgood and W. G. Schneider, *Can. J. Chem.*, **32**, 98, 164 (1954).

TABLE I  
COMPARISON OF COMPRESSIBILITY FACTORS FOR ARGON AND XENON

$P_r$	$T_r = 1.05$		$T_r = 1.20$		$T_r = 1.45$	
	Ar	Xe	Ar	Xe	Ar	Xe
0.9	0.665	0.666	0.860	0.860	0.906	0.906
1.5	.308	.304	.613	.615	.847	.847
3.0	.465	.453	.541	.532	.753	.750
6.0	.816	.809	.809	.791	.857	.842
9.0	---	---	1.095	1.066	1.071	1.046

**Second Virial Coefficient.**—The second virial coefficients of argon and xenon<sup>5</sup> also were compared on the reduced basis  $B^* = BP_c/RT_c$ . The results are shown in Fig. 1 as differences from values calculated by the empirical second virial equation presented by Pitzer and Curl.<sup>6</sup>

While the xenon values average a little above those for argon at the higher temperatures, the difference appears to be within the experimental uncertainties. Indeed there is a much larger difference between the Ottawa and the Amsterdam measurements at the lowest temperatures where no Ar–Xe differences are found in the data of either laboratory.

While it was not our primary purpose to test further the empirical equation of Pitzer and Curl, we may note that the differences from the empirical equation remain below 0.005 except for the Ottawa measurements near the critical temperature. Thus we find agreement in this respect also within the range of experimental error.

**Solid State Properties.**—Further support for conformity to the principle of corresponding states is obtained from a study of the solid state properties of the noble gases. Guggenheim and McGlashan<sup>7</sup> recently have considered the interaction energy between pairs of argon atoms using experimental data both on the equilibrium properties of the crystalline solid and on the gas phase. The potential function which they obtained then was used for the calculation of several thermodynamic properties, e.g., entropy and energy of the crystal as a function of temperature and pressure and the temperature dependence of the second virial coefficient.

In a later publication<sup>8</sup> by the same authors, their results on the interaction energy between argon atoms

(5) J. M. H. Levelt (ref. 1); E. Whalley, Y. Lupien, and W. G. Schneider, *Can. J. Chem.*, **31**, 723 (1953); **33**, 633 (1955); J. A. Beattie, R. J. Barrault, and J. S. Brierly, *J. Chem. Phys.*, **19**, 1222 (1951); A. Michels, Hk. Wijker, and Herb. Wijker, *Physica*, **15**, 627 (1949).(6) K. S. Pitzer and R. F. Curl, Jr., *J. Am. Chem. Soc.*, **79**, 2369 (1957).(7) E. A. Guggenheim and M. L. McGlashan, *Proc. Roy. Soc. (London)*, **A255**, 456 (1960).(8) E. A. Guggenheim and M. L. McGlashan, *Mol. Phys.*, **3**, 563 (1960).

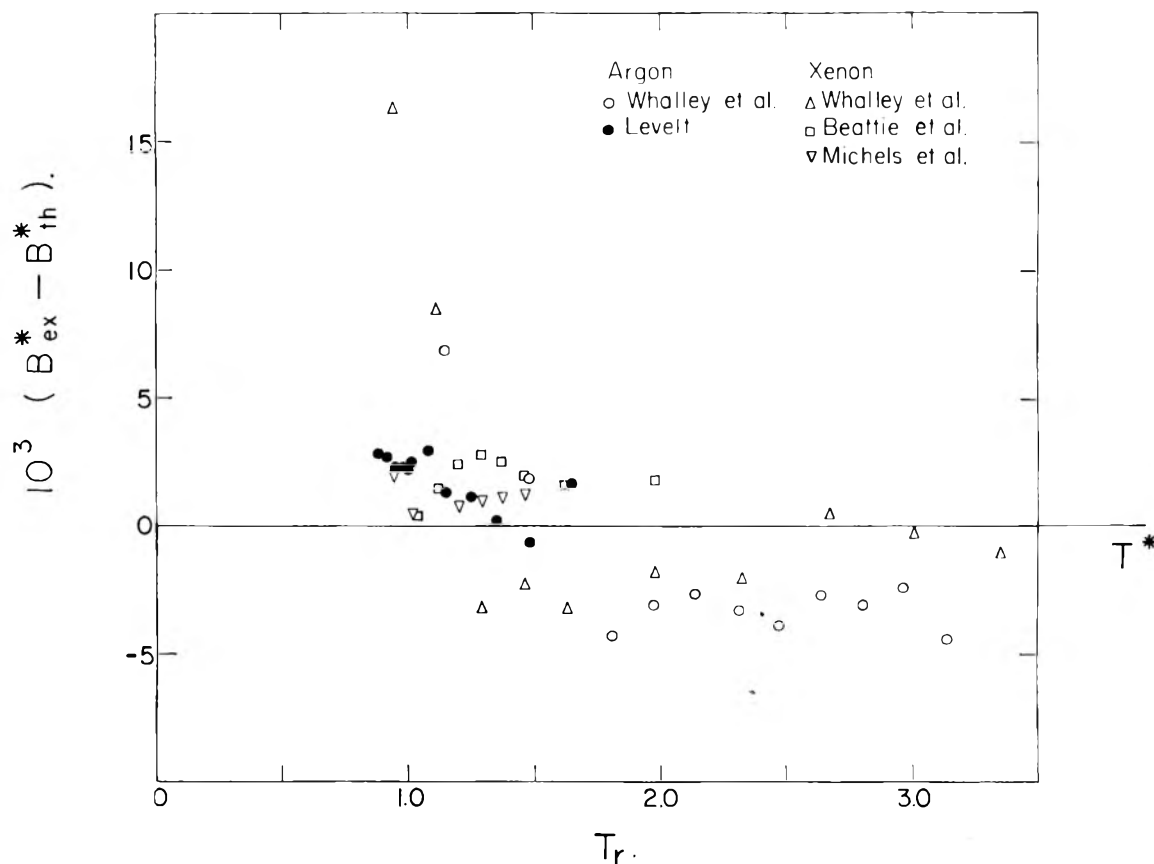


Fig. 1.—Reduced second virial coefficients of argon and xenon compared as differences from the empirical equation of Pitzer and Curl.

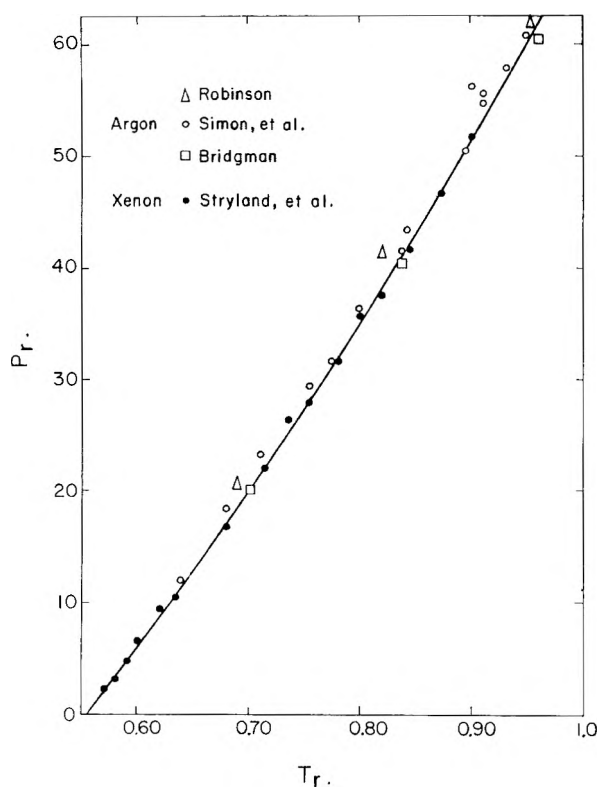


Fig. 2.—Melting curve for argon and xenon compared in terms of reduced pressure and temperature.

together with the principle of corresponding states are applied to the evaluation of thermodynamic properties of xenon. They obtained an agreement between calculated and measured values of the entropy and the enthalpy within the limits of the experimental error from the triple point temperature down to about 20°K. For the molar volume the agreement is of the order of 1%. This larger deviation is, however, as these authors point out, not surprising considering that the equilibrium molar volume is determined by minimizing the free energy and a small inaccuracy in the shape of the potential curve would give rise to a much greater inaccuracy in the position of the minimum.

The variation of the melting temperature of argon with pressure was measured by several investigators.<sup>9</sup> There had not been, however, any similar study made for xenon, until very recently Stryland, *et al.*,<sup>10</sup> reported the results of their measurements. This makes possible a comparison of the melting curve for both substances, which is shown in reduced form,  $P_r = P/P_c$ ,  $T_r = T/T_c$ , in Fig. 2. The curve through the single series of xenon points lies within the range of the several series of results for argon. Hence any deviation from corresponding states must be less than present experimental error. Since this comparison extends to 50 times the criti-

(9) D. W. Robinson, *Proc. Roy. Soc. (London)*, **A225**, 393 (1954); P. W. Bridgman, *Phys. Rev.*, **46**, 930 (1934); F. E. Simon, M. Ruhemann, and N. A. M. Edwards, *Z. physik. Chem.*, **B6**, 62, 331 (1930).

(10) J. C. Stryland, J. F. Crawford, and M. A. Mastoor, *Can. J. Phys.*, **38**, 1546 (1960).

cal pressure, it is a real test of the correspondence of the repulsive portions of the intermolecular potential curves.

The application of the principle of corresponding states to solid inert gases at very low temperature, where quantum effects have to be considered, also has been made in two recent independent studies by Bernardes<sup>11</sup> and Zucker<sup>12</sup>; their results also support the general validity of the principle.

### Discussion and Conclusions

We note first that the corresponding states principle (as extended by the acentric factor<sup>13</sup> where applicable) still may be recommended as a reliable basis for estimating volumetric data provided accurate critical temperature and pressure values are available. Since critical volume data usually are relatively inaccurate, comparisons on the basis of reduced volume or reduced density should be avoided.

From the viewpoint of microscopic theory, exact conformity to the corresponding states principle has been shown<sup>14</sup> to follow for the heavier rare gases if their intermolecular potentials are pairwise additive and are given by an expression of the type

(11) N. Bernardes, *Phys. Rev.*, **120**, 807 (1960).

(12) I. J. Zucker, *Proc. Phys. Soc. (London)*, **77**, 889 (1961).

(13) K. S. Pitzer, *J. Am. Chem. Soc.*, **77**, 3427 (1955). For a complete discussion of the properties of fluids in terms of the acentric factor see G. N. Lewis and M. Randall, "Thermodynamics" revised by K. S. Pitzer and L. Brewer, 2nd Ed., McGraw-Hill Book Co., New York, N. Y., 1960, App. 1, p. 605.

(14) K. S. Pitzer, *J. Chem. Phys.*, **7**, 583 (1939).

$$V = E_0\phi(r/r_0) \quad (1)$$

where  $\phi$  is a universal function but  $E_0$  and  $r_0$  are characteristic energy and distance parameters for each substance. The London theory yields a general inverse sixth power dependence on  $r$  at long distances which is in accordance with the concept of a universal function  $\phi$ . Unfortunately, the theory of intermolecular interaction at short distances is not precise enough to show whether this assumption of a universal function is exact or merely a good approximation.

The molecular theory also predicts pairwise additivity of potential interactions only as an approximation. It is possible that differences between Ar and Xe with respect to the importance of triple interaction and still higher terms may be significant.

The differences in compressibility factor at the highest pressures, which were noted in Table I, may arise from one or more of the sources just noted. However, the data on the melting curve, which shows no significant deviation from corresponding states, extend to even higher pressures and densities than those on the fluid density. Hence further experimental work seems to be indicated before concluding that any deviation of Ar and Xe from corresponding states behavior exists.

**Acknowledgment.**—This research was carried out under the auspices of the U. S. Atomic Energy Commission. The aid of a Fulbright Travel Grant to one of us (F. D.) is gratefully acknowledged.

## GENERALIZED COÖRDINATES AND FORCES

BY OTTO REDLICH\*

*Shell Development Company, Emeryville, California*

*Received September 23, 1961*

The terms "generalized coördinates" and "generalized forces" have replaced what early authors called "extensities" or "capacities" and "intensities." But the change in names has not yet been accompanied by the necessary clarification of the concepts. An explicit formulation of the meaning of these concepts is presented.

Classical or phenomenological or "pure" thermodynamics always has been praised as the model of a strict science. Yet an attentive observer is able to notice a certain uneasiness showing up time and again in its whole history. Carathéodory's great achievements have not answered some of the most elementary questions. They can be used rather to illustrate the problem.

Indeed, Carathéodory has lucidly shown how the concepts of *energy* and *heat* can be derived from the concept of *work* on the basis of the First Law. Work, of course, is, in modern language, the integral of a generalized *force* along the conjugate generalized coördinate. But what are these forces and coördinates? Everybody has learned to enumerate certain forces and coördinates. But this is not enough.

The defect is quite obvious in teaching. No intelligent student can be satisfied by parroting a list of forces and coördinates. Yet no textbook of

thermodynamics explains the meaning of these terms. If the student goes back to analytical mechanics, where the same words have been used before, he finds that a generalized *force* is defined as the negative derivative of a *potential function* with respect to the conjugate generalized coördinate.

Obviously there is a serious circle definition involved since the potential function is a special kind of energy. Moreover, terms defined in the narrow field of mechanics are glibly and without any discussion applied in the whole field of physics and chemistry.

This confusion is not only a didactic problem since textbook writers may justly plead that they cannot find an answer in the literature. Thermodynamics plainly needs some solid underpinnings. The often heard objection "Defining is a recurrent operation and you must stop somewhere" does not discharge us of the obligation to make clear in plain English what we mean by the words we are using, such as generalized force and generalized coördinate. We may say that a concept is explained

\* Department of Chemical Engineering, University of California, Berkeley, California.

if we have given sufficient instructions of how to measure the quantity involved. We need not be pedantic about this matter, yet we should be articulate enough to go beyond the enumeration of examples.

**Previous Discussions.**—Helm<sup>1</sup> saw quite clearly the need for introducing the general concepts which nowadays are called generalized forces and coordinates. He introduced the terms "Intensitäten" and "Extensitäten" and tried to explain the meaning of these terms. But his discussion does not strike the significant points and is not even correct (he states wrongly that conservation laws exist for the extensities). His concepts (and still more Ostwald's<sup>2</sup> discussions) are so vague that no specific objections need or can be raised to their terms.

Quite a few modern authors, however, replaced Helm's terms by "intensive" and "extensive" properties. These terms have been precisely defined by Lewis and Randall. A simple consideration of two galvanic cells shows that forces are not always intensive and coordinates not always extensive. If we switch the cells in series, the voltage is extensive and the charge intensive though the voltage is always the force and the charge always the coordinate. Stress and strain of two rods present the same situation. But even if the classification intensive-extensive were correct, it would be neither characteristic nor sufficient: there are many other intensive and extensive quantities!

Carathéodory's famous paper<sup>3</sup> did not change this situation. Ehrenfest<sup>4</sup> knew this paper well when he wrote with admirable frankness: "Eine mich völlig befriedigende Definition dieser Begriffe habe ich weder in der Literatur finden können noch auch selber zuwege gebracht." This discussion was much later taken up by Planck<sup>5</sup> and Mrs. Ehrenfest-Afanassjewa and Mrs. de Haas-Lorentz.<sup>6</sup> Unquestionably the existence of the problem was felt by the participants in this discussion but a clarification has not been achieved.

In particular, the meaning of the term "generalized coordinate" has never been even approximately outlined. Obviously a coordinate is one variable of a set of independent variables used for the description of the state of an object. But why should the path, the surface area, the electric charge be coordinates while the specific resistivity or the resistance or the dielectric constant are not? Any of these properties can be a member of a set of independent variables.

**The Method.**—There is a way of building a system of concepts such as we need: It is simply to describe in plain words and in a logical arrangement what we are really doing in thermodynamic research. The objective of this discussion will be reached if the reader will recognize, in a Kantian sense, that this system of concepts is inevitable as a

basis of any orderly knowledge of physical nature, and at the same time that these concepts imply at every turn some idealization and even limitation, and that they therefore necessarily fall short of a complete description of nature.

Concepts of such a general nature appear only in strictly classical thermodynamics, properly called thermostatics by Kohnstam. On the other hand, these concepts build the base for the whole field of physics and chemistry, and the split into the various branches occurs only when we proceed from statics to kinetics and dynamics, to the description of dependent properties, and to molecular, atomic, and nuclear theory.

Such a discussion of the basic concepts is believed to be an indispensable precursor of any fundamental or axiomatic theory.

**Isolation and Interaction.**—Since we cannot describe the whole universe in a single instant we are bound to concentrate our attention to a part of it that we are able to study by itself; that is, we examine, at first, an *isolated object*. By "object" we shall understand any part of the world which we can isolate arbitrarily. The term "isolate" implies an idealizing assumption, namely, that we are able to establish conditions under which any object behaves always in the same way whatever may happen in the rest of the world, *i.e.*, its surroundings. What such conditions are we leave to the experimenter, ignoring the wistful smile of the man who has attempted to design such a simple thing as a good calorimeter. But even so we notice at this first step that we are not exactly timid with our idealizing assumptions. The isolation of an atom or a galaxy is a quite far-reaching idea. Yet it is obvious that we cannot dispense with it. Our ability to describe the world cannot go farther than our ability to isolate objects.

When we introduce the term "interaction" we imply that we can design devices which connect two otherwise isolated objects in such a manner that the behavior of one object depends on the state of the other object. Such a device is, for instance, a hook and eye which can be used for connecting a weight and spiral spring hanging down from the ceiling (Fig. 1). Another example is a pair of copper wires and a switch, connecting a storage cell and a capacitor. Another example is a glass tube and a stopcock connecting two bulbs containing some gas.

We require also that these interaction devices are so small that their size, shape, and nature have no influence on the behavior of the two objects. We leave to the experimenter the chore of realizing all these assumptions, of checking his compliance with them, and of correcting for all shortcomings as far as he is able to do so. Gladly we let him assume responsibility for uncorrected shortcomings, which we include in his "experimental errors."

**Coordinates.**—Establishing interaction between two otherwise isolated objects means then that a condition is imposed upon two otherwise independent properties  $x'$  and  $x''$  of the two objects. In illustrating this definition by an example we shall not in the least restrict its generality. As an example we take the spiral spring (Fig. 1); its length is called  $x'$ . A weight is hooked into the lower end

(1) G. Helm, "Die Energetik," Veit & Co., Leipzig, 1898, pp. 253-274, especially p. 257.

(2) W. Ostwald, *Z. physik. Chem.*, **9**, 563; **10**, 363 (1892). Also "Lehrbuch der allgemeinen Chemie," 1890.

(3) C. Carathéodory, *Math. Ann.*, **67**, 355 (1909).

(4) P. Ehrenfest, *Z. physik. Chem.*, **77**, 237 (1911).

(5) M. Planck, *Ann. Physik*, **19**, 759 (1934); *Physica*, **2**, 1029 (1935).

(6) T. Ehrenfest-Afanassjewa and G. L. de Haas-Lorentz, *ibid.*, **2**, 743 (1935).

of the spring; its height over the floor is  $x''$ . As long as the weight is not hooked in, the two variables  $x'$  and  $x''$  are independent. After interaction is established a condition is imposed on them, which in the particular example is

$$x' + x'' = H \tag{1}$$

The special form of this condition is unessential; it will be discussed however in the following section.

In the definition of *coordinates*  $x'$  and  $x''$  the important point is that we have an actual device of imposing a condition upon the previously independent properties  $x'$  and  $x''$ . We have such devices for different *modes of interaction*, for example, for the transfer of electric charges, for changing surface areas or volumes and other properties.

Previous independence, however, is not enough to endow a property with the quality of a *coordinate*. In the simple example of Fig. 1 we could take some other property, either some property trivially connected with  $x'$  such as the number of coils per cm., or some less trivially connected property such as the electrical resistivity of the spring. Actually it would not matter which of these properties we call *coordinate* as long as we restrict ourselves entirely to the case of Fig. 1. But the arbitrariness disappears as soon as the range of interest is extended. The extension necessarily proceeds in two directions: The same object (weight) can interact by the same mode of interaction with different other objects (with another weight by means of a balance, with a gas by means of a piston). And the same object can interact simultaneously with other objects by different modes. The composite object "capacitor-weight" shown in Fig. 2 can interact with other objects in two different modes.

In order to forge a useful tool, we have to restrict the concept of a *coordinate* to a variable that *always* is involved in a certain mode of interaction and *never* in any other mode. In other words, a set of independent variables is a set of *coordinates* if for any mode of interaction all members of the set but one are constant.

In the capacitor-balance of Fig. 2, for instance, we may arrest the balance and keep the balance position  $h$  constant. At the same time we may connect the two capacitor plates by thin wires with a storage cell and add or remove some electric charge. Conversely we can isolate the capacitor and let the balance move. There are properties, such as the voltage, which change in both modes of interaction. To be sure, one can keep the voltage constant: but in this case the object changes in *both* modes of interaction; the capacitor charge *and* the balance position change according to a specific relation to be imposed on them. A *coordinate*, however, will be defined in such a manner that it is distinguished from other properties by the exclusive connection with a single mode of interaction.

Again the introduction of the concept of generalized *coordinates* is a requirement, not an assumption or an axiom. This is demonstrated easily by the fact that we cannot always satisfy the requirement. Indeed, no *coordinate* exists for thermal interaction. Neither heat nor temperature is a *coordinate*. In fact, thermal interaction requires an entirely different consideration, beyond the scope

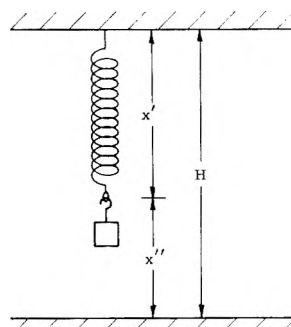


Fig. 1.—Spring and weight.

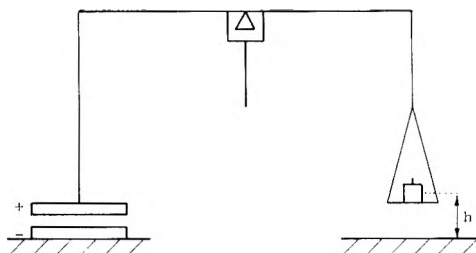


Fig. 2.—Capacitor balance.

of the present paper. Thermal interaction therefore is excluded from the whole of the following discussion.

An earlier statement on *coordinates* can be reformulated in the following way: Each mode of interaction for which a conjugate *coordinate* exists influences an object only through this *coordinate*. The behavior of an object therefore is determined solely by its own properties, and by its environment only as far as interacting *coordinates* are influenced.

**Interaction Conditions.**—It has been mentioned before that the special form of the interaction condition (1) is unessential. Actually we could replace any variable  $x$  in the present discussion by a monotonically increasing function  $y(x)$  such as  $e^x$  or  $\log x$  and so on. We shall make certain specific choices for convenience. While the general interaction condition would be

$$G(x', x'') = 0 \tag{2}$$

we shall always choose our *coordinates*  $x'$  and  $x''$  so that the interaction condition becomes

$$dx' + dx'' = 0 \tag{3}$$

We did so in eq. 1.

If  $x'$  and  $x''$  are extensive, eq. 3 can be interpreted as a conservation condition. But this interpretation is unessential, particularly since  $x'$  and  $x''$  need not be extensive.

**Equilibrium and Force.**—As soon as interaction between two objects is established, they undergo, in general, a change. In accord with condition 3,  $x'$  may become greater and  $x''$  smaller, or conversely. The exceptional case that no change at all occurs on establishing interaction is called equilibrium. By observation we can establish a function  $F(x', x'')$  such that the three conditions

$$F > 0; F = 0; F < 0 \tag{4}$$

correspond with the three cases of decreasing  $x'$ , equilibrium, and increasing  $x'$ .

We may define a property  $f'$  of the first object

and  $f''$  of the second object such that the three conditions (4) are replaced by

$$f' > f''; f' = f''; f' < f'' \quad (5)$$

The logical content of (4) is different from that of (5). The conditions (5) imply that two equilibria between three objects

$$f' = f'' \text{ and } f'' = f''' \quad (6)$$

necessarily imply the third equilibrium

$$f' = f''' \quad (7)$$

while the conditions (4) do not permit the conclusion that equilibrium between I and II, and between II and III, also satisfies the condition for equilibrium between I and III. But the difference is just an expression of the requirement that the first object is influenced by any other one *only* through the coordinate  $x'$  and therefore behaves in the same way whether interaction is established with object II or III. It is for this reason that we may introduce a property  $f'$  of the first object which depends only on the coordinates of the first object. The relations between the two objects are exhaustively expressed by (3) and (5).

In plain words, the spring in Fig. 1 does not know whether it is pulled down by a brass weight or a platinum weight or by my finger.

The relations (5) are sufficient for an experimental definition of the functions  $f$ , which are called generalized forces. Again any monotonic function would serve as well as  $f$ . The choice essentially is arbitrary and a matter of convenience. A standard force (gravitational force of a certain piece of platinum) is defined and a procedure of assigning numbers to larger and smaller forces is chosen. Other forces then are measured by establishing equilibrium with a suitable standard object (standard weight, mercury column, or calibrated spring in a pressure gage, standard cell, and so on).

Forces are distinct from all other properties in that their measurement requires establishment of equilibrium between two objects. This distinction is characteristic as well as obvious, yet it appears that it has never been pointed out.

**Concluding Remarks.**—At this point we again may illustrate the nature of our basic concepts.

Let us suppose that a balance indicates equilibrium between weights I and II, and between weights II and III, but not between I and III. Of course, we shall not abandon condition (5). Instead we shall look for interference of another mode of interaction. For instance, we may find that the last weighing is impaired by electrostatic charges, eliminated in the first two weighings by radioactivity of weight II. Thus the basic concepts are neither axioms nor the result of experimental facts but practical requirements which we impose on our observations. They are at the same time arbitrary and necessary: arbitrary because they are neither logically nor experimentally justified, and necessary because they are indispensable for the orderly array of our observations.

After reading the present paper, one may quite naturally have the impression that all this has been very well known before. It is of course true that the concepts of forces and coordinates actually always have been used as meaning precisely what has been attributed to them here. But the uneasiness and the efforts mentioned in the Introduction emphasize the need for an articulate formulation.

This need becomes manifest in the discussion by Ehrenfest,<sup>4</sup> Planck,<sup>5</sup> Ehrenfest-Afanassjewa, and de Haas-Lorentz.<sup>6</sup> Initially the subject of this discussion was the principle of Braun and Le Chatelier. The participants themselves pointed out that this principle did not deserve an elaborate discussion such as they were carrying on. Yet one cannot fail to see that from the beginning they felt that they were struggling with some fundamental problem. Only the last paper of that discussion indicates more directly that the real problem of the whole discussion was the meaning of the terms of generalized coordinates and forces.

An explicit introduction of forces and coordinates prepares the access to the other fundamental concepts of thermodynamics. A similar analysis of these concepts still is believed to present an important problem.

The author expresses his sincere thanks to Dr. F. H. Stross for numerous clarifying, helpful, and encouraging discussions.

# A RULE FOR THE CALCULATION OF THE ACTIVITY COEFFICIENTS OF SALTS IN ORGANIC SOLVENT-WATER MIXTURES

BY HERBERT S. HARNED

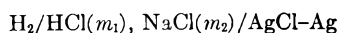
Contribution No. 1688 from the Department of Chemistry of Yale University, New Haven, Conn.

Received October 2, 1961

Consideration of the properties of systems containing two electrolytes in water and in organic solvent-water mixtures leads to the conclusion that the ratio of the activity coefficients of the electrolytes at a given salt concentration and temperature is constant over a considerable range of composition of the solvent. Therefore, if the activity coefficient of one of the electrolytes is known in the organic solvent-water mixture, that of the second electrolyte may be computed from the activity coefficient ratio determined in aqueous solution. Since the activity coefficient of hydrochloric acid has been determined with high accuracy in many organic solvent-water mixtures, the above rule has a wide range of applicability. Comparison of results for lithium, sodium, and potassium chlorides computed by the rule is made with those derived from amalgam cell measurements in methanol-water mixtures containing 10 and 20% methanol. The agreement is quite satisfactory.

Precise determinations of the activity coefficient of hydrochloric acid in a number of organic solvent-water mixtures have been obtained from electromotive force measurements of the hydrogen-silver chloride cell.<sup>1</sup> On the other hand, no precise determinations of the activity coefficients of salts in these mixed solvents are available. The isopiestic vapor pressure method is not applicable for solutions of electrolytes in two volatile solvents nor are the freezing point and boiling point methods readily adaptable. Flowing amalgam cells may be used in some instances but accurate determinations by this method are difficult to obtain and to extrapolate.

Examination of the properties of solutions containing hydrochloric acid and an alkali metal chloride in water and in water-organic solvent mixtures indicates that the activity coefficient of the salt may be computed from that of the acid by a very simple rule if the activity coefficient ratio of the acid to the salt in water is known. From precise measurements of the electromotive forces of the cells



Akerlof, Teare, and Turck<sup>2,3</sup> found that the activity coefficient of hydrochloric acid,  $\gamma_1$ , in sodium chloride solutions at one molal total concentration,  $m$ , with methyl alcohol-water mixtures as solvents varied linearly with the acid concentration according to the equation

$$\log \gamma_1 = \log \gamma_{1(0)} - \alpha_{12(0)}m_2 \quad (1)$$

where  $\gamma_{1(0)}$  is the activity coefficient of the acid in the absence of the salt,  $m_2$  is the sodium chloride concentration, and  $\alpha_{12(0)}$  is constant at a given temperature. The results were extended over a temperature range from 0 to 40° at 5° intervals. The weight percentage of methyl alcohol was varied from 0 to 60%.

A most significant feature of these results is that the parameter  $\alpha_{12(0)}$  has the same value in all these solutions at a given temperature. Thus, if the activity coefficient of the acid is known in the salt-free solution, its value in the acid-salt mixtures may be computed using the value of  $\alpha_{12(0)}$  found in pure water as solvent. As a result, it is reason-

able to assume that the parameters which represent the variation of the activity coefficient of the salt also are independent of the percentage of methyl alcohol in these solutions.

In aqueous solutions, the activity coefficients of the acid and salt in hydrochloric acid-sodium chloride<sup>4</sup> and hydrochloric acid-potassium chloride<sup>5</sup> systems at 1 and 2 *m* constant total molalities may be expressed by the equations

$$\log \gamma_1 = \log \gamma_{1(0)} - \alpha_{12(0)}m_2 \quad (2)$$

$$\log \gamma_2 = \log \gamma_{2(0)} - \alpha_{21(0)}m_1 - \beta_{21}m_1^2 \quad (3)$$

where the subscripts 1 and 2 refer to the acid and salt, respectively. If, as we shall assume, the parameters  $\alpha_{12(0)}$ ,  $\alpha_{21(0)}$ , and  $\beta_{21}$  are the same in the organic solvent-water mixtures as in water, both  $\gamma_1$  and  $\gamma_2$  may be computed in all these systems provided that the activity coefficient of the acid in the salt-free solution and the activity coefficient of the salt in the acid-free solution are known. Precise values of  $\gamma_{1(0)}$  in many of these solvents are available, so there remains the problem of determining  $\gamma_{2(0)}$ . At the limits when

$$m_1 \rightarrow m, \text{ or } m_2 \rightarrow m$$

eq. 2 and 3 become

$$\log \gamma_{0(1)} = \log \gamma_{1(0)} - \alpha_{12(0)}m \quad (4)$$

$$\log \gamma_{0(2)} = \log \gamma_{2(0)} - \alpha_{21(0)}m - \beta_{21}m^2 \quad (5)$$

where  $\log \gamma_{0(1)}$  is the activity coefficient of the acid at zero concentration in the salt solution and  $\gamma_{0(2)}$  is the activity coefficient of the salt at zero concentration in the acid solution. The experimental results indicate that the relation<sup>6</sup>

$$\log \gamma_{0(1)} = \log \gamma_{0(2)} \quad (6)$$

is valid within narrow limits. Combination of this equation with eq. 4 and 5 yields

$$\log \frac{\gamma_{1(0)}}{\gamma_{2(0)}} = (\alpha_{12(0)} - \alpha_{21(0)} - \beta_{21}m)m \equiv B'm \quad (7)$$

Thus, if eq. 6 is valid the activity coefficient ratio of the hydrochloric acid in the absence of salt to that of salt in the absence of the acid,  $\gamma_{1(0)}/\gamma_{2(0)}$ , may be calculated from the mixture data. But this quantity also can be calculated from activity coefficients determined individually.

(1) H. S. Harned and B. B. Owen, "The Physical Chemistry of Electrolytic Solutions," 3rd Ed., Reinhold Publ. Corp., New York, N. Y., 1958, pp. 717-720.

(2) G. Akerlof, J. W. Teare, and H. Turck, *J. Am. Chem. Soc.*, **59**, 1916 (1937).

(3) Ref. 1, Fig. (14-4-5) on p. 601.

(4) H. S. Harned, *J. Phys. Chem.*, **63**, 1299 (1959).

(5) H. S. Harned, *ibid.*, **64**, 102 (1960).

(6) Cf. Fig. 14-5-1-b, page 605, ref. 1.

Thus

$$\log \frac{\gamma_{1(0)}}{\gamma_{2(0)}} = Bm \quad (8)$$

Comparison of values of  $B$  and  $B'$  for hydrochloric acid-sodium chloride and hydrochloric acid-potassium chloride mixtures at 1 and 2  $m$  total molalities from 0 to 40° is shown in Table I. Considering the

TABLE I

COMPARISON OF  $(\alpha_{12(0)} - \alpha_{21(0)} - \beta_{21}m) \equiv B'$  AND  $B$  IN AQUEOUS SOLUTIONS AT 2  $m$  TOTAL MOLALITY FROM 0 TO 40°

	HCl-NaCl		HCl-KCl	
	$B$	$B'$	$B$	$B'$
0	0.1156	0.1131	0.1473	0.1440
10	.1041	.1019	.1363	.1350
20	.0937	.0923	.1260	.1260
25	.0895	.0878	.1228	.1224
30	.0841	.0830	.1175	.1170
40	.0756	.0748	.1102	.1105

complicated nature and sensitivity of the calculation, the agreement is quite good. Therefore, if our assumption that the parameters,  $\alpha_{12(0)}$ ,  $\alpha_{21(0)}$ , and  $\beta_{21}$  at a constant concentration,  $m$ , do not vary with the composition of the organic solvent-water mixture, then the ratio,  $\gamma_{1(0)}/\gamma_{2(0)}$  is also invariant. Thus

$$\log \left[ \frac{\gamma_{1(0)}}{\gamma_{2(0)}} \right]_{P,T,m} = [Bm]_{P,T,m} = \text{constant} \neq f(X) \quad (9)$$

where  $X$  is the weight percentage of organic solvent.

The rule given by eq. 9 should have a considerable degree of validity in mixtures which have dielectric constants between 80 and 20. It should hold for any pair of strong electrolytes.

**The Activity Coefficients of Lithium, Sodium, and Potassium Chlorides in Methanol-Water Mixtures at 25°.**—Values of the parameter,  $B$ , necessary for the calculation of the activity coefficients of the designated salts in non-aqueous solvent-water mixtures are listed in Table II. The activity coefficients of the acid and the salts were those given by Harned and Owen.<sup>7</sup>

TABLE II

VALUES OF 25° OF THE PARAMETER,  $B$ , IN EQUATION 9

$m$	LiCl	NaCl	KCl
0.01	0.02	0.09	0.15
.02	.02	.09	.14
.05	.02	.09	.14
.1	.033	.099	.134
.2	.0285	.1015	.1435
.5	.021	.0920	.1338
1.0	.019	.0904	.1269
1.5	.019	.0901	.1244
2.0	.0198	.0895	.1228

In Table III, the activity coefficients of lithium, sodium, and potassium chlorides in 10 and 20 weight % methyl alcohol-water mixtures are recorded. The required values of the activity coefficient of hydrochloric acid, obtained from the electromotive force measurements of Harned and Thomas,<sup>8</sup> are listed in the second column of the table.

Fortunately, for these methanol-water solutions

(7) Ref. 1, Tables (11-4-1A), (12-3-1A), (12-1-1), and (12-2-2).

(8) H. S. Harned and H. C. Thomas, *J. Am. Chem. Soc.*, **57**, 1366 (1935); **58**, 761 (1936).

TABLE III

ACTIVITY COEFFICIENTS OF HYDROCHLORIC ACID (OBSD.) AND OF LITHIUM, SODIUM AND POTASSIUM CHLORIDES (COMPUTED) IN 10 AND 20% METHANOL-WATER MIXTURES AT 25°

$m$	X = 10			
	HCl	LiCl	NaCl	KCl
0.01	0.897	0.897	0.895	0.894
.02	.866	.865	.862	.860
.05	.819	.817	.811	.806
.1	.780	.774	.762	.756
.2	.747	.737	.713	.699
.5	.737	.719	.663	.632
1.0	.783	.750	.636	.585
1.5	.861	.806	.631	.560
2.0	.966	.882	.641	.599
X = 20				
0.01	0.888	0.888	0.886	0.885
.02	.856	.855	.852	.851
.05	.806	.804	.798	.794
.1	.762	.751	.745	.739
.2	.727	.717	.694	.680
.5	.708	.691	.637	.607
1.0	.747	.715	.607	.558
1.5	.814	.762	.596	.530
2.0	.911	.832	.603	.517

there are a few experimental data available for comparison with the values computed by our rule. From the amalgam cell measurements of Akerlof,<sup>9</sup> values of the activity coefficients in these solutions have been computed and listed in Table IV. Since the extrapolation of the amalgam cell measurements was very uncertain, the activity coefficients derived from them have been revised to conform with the results of the present calculation. The values in parentheses in Table IV were used as standard and the others calculated from the activity coefficient ratio determined by Akerlof. The agreement between the two sets of values for lithium and sodium chlorides is quite good, while that for potassium chloride is not good. This discrepancy may be due to the difficulty in obtaining good amalgam cell

TABLE IV

COMPARISON WITH ACTIVITY COEFFICIENTS OBTAINED FROM AMALGAM CELLS<sup>a</sup>

	LiCl		NaCl		KCl	
	(a)	(b)	(a)	(b)	(a)	(b)
X = 10						
0.02	0.865	...	0.862	0.865	0.860	(0.860)
.05	.817	...	.811	(0.811)	.806	.797
.1	.774	.777	.762	...	.756	...
.2	.737	...	.713	.714	.699	...
.5	.719	.718	.663	.656	.632	...
1.0	.750	(.750)	.631	...	.584	...
X = 20						
0.02	0.855	...	0.852	0.856	0.851	(0.851)
.05	.804	...	.797	(.797)	.794	.778
.1	.751	...	.745	.748	.739	...
.2	.717	...	.694	.696	.680	...
.5	.691	(0.691)	.637	.636	.607	...
1.0	.715	.719	.607	...	.558	...

<sup>a</sup> (a) Present method; (b) amalgam cell method.

(9) G. Akerlof, *ibid.*, **52**, 2353 (1930).



measurements at concentrations lower than 0.1  $M$ . Energy Commission under contract AT-(30-1) 1375.  
This contribution was supported by the Atomic

## HEAT CAPACITY AND OPEN AND CLOSED ENSEMBLE AVERAGES

BY JOSEPH E. MAYER

*Department of Chemistry, University of California, San Diego, La Jolla, California*

*Received October 7, 1961*

It is well known that the heat capacity is given by  $C_V = k[\langle(\beta E)^2\rangle_{AV} - \langle\beta E\rangle_{AV}^2]$  with  $\beta = 1/kT$ , where the average is that of an ensemble of closed systems of fixed  $N, V, T$ . One also may express  $C_V$  as the same average in an ensemble of open systems of fixed  $V, \mu, T$  plus calculable correction terms. Any numerical calculation of the mutual potential energy contribution using reduced probability densities always will give only the open ensemble averages, unless explicit account is taken of the long range correlations of order  $N^{-1}$  in these probability densities for the closed ensemble. A general method of obtaining these long range correlation terms to every order of  $N^{-1}$  is presented, and it is shown that their introduction does indeed give the same expression for  $C_V$  that is obtained by the computation with the ensemble of open systems.

### Introduction

In statistical mechanics one frequently requires the average value,  $\bar{F}^2$ , of the square of some function,  $F$ , that is a sum of functions of the coordinates (or of coordinates and momenta) of single molecules, or of pairs, triples, etc. Sometimes the average,  $\langle F_1 F_2 \rangle$  of the product of two such functions is required. More usually, if not invariably, the quantity of interest is  $(\bar{F}^2 - \bar{F}^2)$  where  $\bar{F}$  is the average value of  $F$ . In general moments such as  $\langle \prod_{\alpha} (F_{\alpha} - \bar{F}_{\alpha}) \rangle$  occur. A particular example of such a use is the well known expression for the heat capacity

$$\partial E / \partial T = kT^2 \langle (E - \bar{E})^2 \rangle = kT^2 (\bar{E}^2 - \bar{E}^2) \quad (1.1)$$

which usually is proved early in any course on statistical mechanics. The proof usually is made using the ensemble of closed systems of fixed  $N, V, T$ , in which case the omitted subscripts in (1) on the partial derivative are  $V, N$ , namely the left-hand side is  $(\partial E / \partial T)_{V, N}$  and the averages on the right are those of the closed ensemble. One may equally well prove (1) for an ensemble of open systems, of fixed  $V, \mu, T$ , with  $\mu$  the chemical potential, in which case one finds on the left of (1) the rather horrible partial derivative at constant  $V$  and  $\mu/kT$ , whereas the right-hand side involves the average in the open system. By itself the difference is not alarming, since the averages in the closed ensemble and open ensemble are not expected to be equal.

What is, however, disturbing, is that when one attempts to evaluate the averages one finds identical equations in terms of the probability density functions of the molecules.

The origin of the discrepancy is not hard to find. For instance, one of the terms of  $\bar{E}^2$  is the average of the product of the potentials of two independent pairs of molecules, say 1,2 and 3,4, and this term  $T_4$ , turns out to be, with  $\rho_4$  the four particle probability density

$$T_4 = \frac{1}{4} \iiint \int_V d\mathbf{r}_1 d\mathbf{r}_2 d\mathbf{r}_3 d\mathbf{r}_4 \rho_4(\mathbf{r}_1, \mathbf{r}_2, \mathbf{r}_3, \mathbf{r}_4) u(r_{12}) u(r_{34}) \quad (1.2)$$

This integral is proportional to  $N^2$ . Subtract from this the square,  $\bar{U}^2$ , of the average pair potential. This average,  $\bar{U}$ , is

$$\bar{U} = \frac{1}{2} \iint d\mathbf{r}_1 d\mathbf{r}_2 \sigma_2(r_{12}) u(r_{12}) \quad (1.3)$$

where we assume the system is fluid so that  $\rho_2$  depends only on the distance  $r_{12} = |\mathbf{r}_1 - \mathbf{r}_2|$ . One finds for the difference

$$\beta^{-2} \Psi_4 = T_4 - \bar{U}^2 = \frac{1}{4} \int \dots \int d\mathbf{r}^{(4)} [\rho_4(\mathbf{r}_1, \mathbf{r}_2, \mathbf{r}_3, \mathbf{r}_4) - \rho_2(r_{12}) \rho_2(r_{34})] u(r_{12}) u(r_{34}) \quad (1.4)$$

Now the potentials  $u(r_{12}), u(r_{34})$  are short range, so that the integrand of (4) is non-zero only if  $r_{12}$  and  $r_{34}$  are small, but if the distance  $r_{ab} = \frac{1}{2} |\mathbf{r}_1 + \mathbf{r}_2 - \mathbf{r}_3 - \mathbf{r}_4|$  is large  $\rho_4$  becomes equal to  $\rho_2(r_{12}) \rho_2(r_{34})$ , and the integrand again approaches zero value. The integrand is appreciable only when all four molecules are close, and the value of the integral is proportional to the size of the system,  $N$ .

Now the statement

$$\rho_4(\mathbf{r}_1, \mathbf{r}_2, \mathbf{r}_3, \mathbf{r}_4) - \rho_2(r_{12}) \rho_2(r_{34}) \rightarrow 0, r_{ab} \gg \rho^{-1/3} \quad (1.5)$$

is exact for an open system, and the contribution to the integral of (4) in the open ensemble does come only from the region of integration for which  $r_{ab}$  is small. However (5) is correct only to order  $\rho^4/N = \rho^3/V$  in a closed system, and since the volume for which  $r_{ab} \gg \rho^{-1/3}$  is of order  $V = N/\rho$ , the contribution from the region of large  $r_{ab}$  values is of the same order of magnitude as that from small values, even in the limit that  $N \rightarrow \infty, V = N/\rho \rightarrow \infty$ , for which limit (5) is satisfied.

The inference for a hypothetical computing machine calculation of the term is obvious. Even if  $\rho_4$  were given to many significant decimal digits the difference, (5), would be zero to the accuracy of the machine, and computation would yield the value appropriate to the open system and hence to the computation of  $(\partial E / \partial T)_{V, \mu/kT}$  and not to  $C_V$ .

The statement above that (5) is exactly correct for the open system but only to order  $N^{-1}$  in the closed system is more intuitively obvious, and in all detail understandable, if we consider instead  $\rho_2(r_{12}) - \rho^2$  at large  $r_{12}$  values. The pair probability density,  $\rho_2(\mathbf{r}_1, \mathbf{r}_2) = \rho_2(r_{12})$  is the simultaneous probability density of finding a molecule at  $\mathbf{r}_1$  and one at  $\mathbf{r}_2$ . That of finding the first molecule at  $\mathbf{r}_1$  may be written as  $\rho = N/V$ , but then there are only  $N - 1$  molecules left to occupy the position  $\mathbf{r}_2$ , and since

on the average the first molecule at  $\mathbf{r}_1$  excludes a volume  $v_0$ , these are distributed in a volume  $V - v_0$ , so that

$$\rho_2^{(Cl)}(r) = \rho \frac{N-1}{(V-v_0)} \cong \rho^2 \left[ 1 - \frac{1}{N}(1 - \rho v_0) \right], \quad r \gg \rho^{-1/3} \quad (1.6)$$

In general then, one may write, for the closed system

$$\rho_2^{(Cl)}(\mathbf{r}_1, \mathbf{r}_2) = \rho^2 [1 + g_2(r_{12}) - N^{-1}(1 - \rho v_0)] \quad (1.7)$$

where  $g_2(r)$  goes strictly to zero at large  $r$  values, and  $v_0$  is some average volume excluded by a single molecule.

The open system is confined to a large but finite volume  $V$ , in equilibrium through permeable walls with an infinite reservoir of the same chemical potential,  $\mu$ . Hence its probability density functions  $\rho_n$  are those of an infinite closed system, namely that of (7) in the limit  $N \rightarrow \infty$  so that

$$\rho_2^{(O)}(\mathbf{r}_1, \mathbf{r}_2) = \rho^2 [1 + g_2(r_{12})] \quad (1.7')$$

For the closed system the pair probability density,  $\rho_2^{(Cl)}(\mathbf{r}_1, \mathbf{r}_2)$ , exactly obeys the relation

$$\int_V d\mathbf{r}_2 \rho_2^{(Cl)}(\mathbf{r}_1, \mathbf{r}_2) = (N-1)\rho \quad (1.8)$$

so that by integration of (7) one has

$$N\rho + \rho^2 \int 4\pi r^2 dr g_2(r) - \rho(1 - \rho v_0) = (N-1)\rho$$

$$\rho v_0 = -\rho \int 4\pi r^2 dr g_2(r) \quad (1.9)$$

and the "long range" term  $N^{-1}(1 - \rho v_0)$  is determined uniquely by the "short range" function,  $g_2(r)$ . Similarly, the exact relation

$$\int d\mathbf{r}_3 \rho_3(\mathbf{r}_1, \mathbf{r}_2, \mathbf{r}_3) = (N-2)\rho_2(\mathbf{r}_1, \mathbf{r}_2) \quad (1.10)$$

can be used to determine uniquely the terms of order  $N^{-1}$  and of  $N^{-2}$  in  $\rho_3$ . The author has been unable to succeed in using such a direct method of finding even the terms of order  $N^{-1}$  in  $\rho_4$ . The condition

$$\int d\mathbf{r}_4 \rho_4(\mathbf{r}_1, \mathbf{r}_2, \mathbf{r}_3, \mathbf{r}_4) = (N-3)\rho_3(\mathbf{r}_1, \mathbf{r}_2, \mathbf{r}_3) \quad (1.11)$$

is inadequate.

One can, however, without too great difficulty, evaluate  $(\partial E / \partial T)_{V, \mu/kT}$  by thermodynamic means as  $C_V$  plus a correction, eq. 2.21, and the correction can be evaluated in terms of integrals over probability densities of the open system. Therefore, since  $C_V$  is given by (1) to which the integral (4) contributes a finite "long range" contribution, and can be evaluated in terms of the "short range" open system integrals, it follows that the "long range" value of the integrand of (4) is uniquely determined by the short range values.

In sections 5 and 6 of this paper a method is given whereby these long range correlations in  $\rho_n$ , for any  $n$ , to order  $N^{-k}$  with  $1 \leq k \leq n-1$ , are determined. An entirely different method has been used by Lebowitz and Percus<sup>1</sup> to determine the terms of order  $N^{-1}$ .

The purpose of this paper is then threefold: (1) to emphasize that any numerical computation of  $C_V$  using (1) *must* be made by directly or indirectly going through the open system ensemble equations; (2) to show exactly what are the open ensemble integrals entering  $C_V$ ; (3) to answer the

(1) J. L. Lebowitz and J. K. Percus, *Phys. Rev.*, **122**, 1675 (1961).

question of how the "long range" terms of  $\rho_n^{(Cl)}$  can be evaluated.

**Thermodynamic Derivatives and Moments.**—We use, for convenience, a set of symbols which are tailored to make the statistical mechanical equations look most simple. The number density,  $\rho$ , is  $N/V$  in the closed ensemble, but  $\bar{N}/V$  in the open one, and we always compare ensembles of equal  $\rho$ . We use

$$\beta = 1/kT$$

$$\phi = I'\beta$$

$$\nu = -\mu\beta \quad (2.1)$$

$$\epsilon = \beta E/N$$

$$a = -\mu\beta + \phi\rho^{-1} = \beta A/N$$

where  $\mu$  is the chemical potential and  $A$  the Helmholtz free energy. The probability densities for the complete set of  $N$  molecules in  $V$  are then

$$W_N^{(O)} = \exp - [\varphi V + N\nu + \beta H_N] \quad (2.2)$$

and

$$W_N^{(Cl)} = \exp - [Na + \beta H_N] \quad (2.2')$$

in the open and closed ensembles, respectively, with  $H_N$  the Hamiltonian function for the  $N$  molecules. We use  $\{N\}$  to represent the complete phase space, the coordinate-momentum set of all the  $N$  molecules, and define an integration operator,  $\mathcal{G}_N$ , as

$$\mathcal{G}_N \equiv \int \cdots \int_V (h^{3N} N!)^{-1} d\{N\} \quad (2.3)$$

The normalization condition requires that

$$\sum_N \mathcal{G}_N W_N^{(O)} = 1 \quad (2.4)$$

$$\mathcal{G}_N W_N^{(Cl)} = 1 \quad (2.4')$$

for the two cases, and these determine  $\varphi(\nu, \beta)$  and  $a(\rho, \beta)$ , respectively. The definition of an average of any function,  $F_{N\alpha} \{N\}$ , of the phase space is that

$$\bar{F}_\alpha^{(O)} = \sum \mathcal{G}_N W_N^{(O)} F_{N\alpha} \quad (2.5)$$

$$\bar{F}_\alpha^{(Cl)} = \mathcal{G}_N W_N^{(Cl)} F_{N\alpha} \quad (2.5')$$

and, to terms of order  $N^{-1}$  if  $\rho, \beta$  are equal in the two cases

$$\bar{N}^{-1} \bar{F}_\alpha^{(Cl)} = N^{-1} \bar{F}_\alpha^{(O)} + 0(N^{-1}) \quad (2.6)$$

We shall hence omit the superscripts, and write the averages  $\bar{F}^{(O)} = \bar{F}^{(Cl)} = \bar{F}$ . We define moments,  $I\{n\}$  and  $J\{n\}$ ,  $\{n\} = 1, 2, \dots, \alpha, \dots, n$  of functions  $F_{N\alpha} \{N\}$ , in the two ensembles

$$I\{n\} = \left\langle \prod_{\alpha=1}^{\alpha=n} (F_{N\alpha} - \bar{F}_\alpha) \right\rangle^{(O)} \quad (2.7)$$

$$J\{n\} = \left\langle \prod_{\alpha=1}^{\alpha=n} (F_{N\alpha} - \bar{F}_\alpha) \right\rangle^{Cl} \quad (2.7')$$

Since (4) must hold for all  $\nu, \beta$ , we have that for any change  $d\nu, d\beta$

$$0 = \sum_N \mathcal{G}_N dW_N^{(O)} = - \sum_N \mathcal{G}_N W_N^{(O)} [Vd\varphi + Nd\nu + H_N d\beta]$$

$$= - [Vd\varphi + d\nu + \bar{E}d\beta]$$

$$V(\partial\varphi/\partial\nu)\beta = -\bar{N} = -V\rho \quad (2.8)$$

$$V(\partial\varphi/\partial\beta)\nu = -\bar{E} = -\bar{N}\epsilon\beta^{-1} \quad (2.9)$$

whereas for the system of constant  $N, V$

$$0 = g_N dW_N^{(Cl)} = -g_N W_N^{(Cl)} [N da + H d\beta] \\ N(\partial a/\partial \beta)_\rho = -\bar{E} = -N\epsilon\beta^{-1} \quad (2.10)$$

Differentiation of  $\bar{E}$ , computed in the closed ensemble, with respect to  $\beta$  gives

$$(\partial \bar{E}/\partial \beta)_{v,N} = g_N H_N (\partial W_N^{(Cl)}/\partial \beta) \\ = -g_N W_N^{(Cl)} H_N [N(\partial a/\partial \beta) + H_N] \\ = -J \{E^2\} = -(1/k\beta^2)(\partial \bar{E}/\partial T)_{v,N}$$

from (10), (7'), and  $T = 1/k\beta$ . We have, then, for the heat capacity at constant volume,  $c_V$ , per molecule in units of  $k$

$$c_V = (Nk)^{-1} (\partial \bar{E}/\partial T)_{v,N} = N^{-1} \{J(\beta E)^2\} \quad (2.11)$$

On the other hand, using the open ensemble averages, and (8) and (9) for  $Vd\phi$

$$(\partial \bar{E}/\partial \beta)_{v,\nu} = \sum_N g_N H_N (\partial W_N^{(o)}/\partial \beta)_\nu \\ = - \sum_N g_N W_N^{(o)} H_N [V(\partial \phi/\partial \beta)_\nu + H_N] \\ = -I \{E^2\} \quad (2.12)$$

$$(\partial \bar{N}/\partial \nu)_{v,\beta} = \sum_N g_N N (\partial W_N^{(o)}/\partial \nu) \\ = - \sum_N g_N W_N^{(o)} N [V(\partial \phi/\partial \nu) + N] \\ = -I \{N^2\} \quad (2.13)$$

$$(\partial \bar{N}/\partial \beta)_{v,\nu} = (\partial \bar{E}/\partial \nu)_{v,\beta} = -V(\partial^2 \phi/\partial \nu \partial \beta) \\ = \sum_N g_N N (\partial W_N^{(o)}/\partial \beta)_\nu = \\ \sum_N g_N H_N (\partial W_N^{(o)}/\partial \nu)_\beta \\ = -I \{N, E\} \quad (2.14)$$

so that with  $\rho = \bar{N}/V_2$  and eq. 1, 8, and 9, we have

$$d\phi = -\rho d\nu - \rho \epsilon d \ln \beta \quad (2.15)$$

$$(\partial \ln \rho/\partial \nu)_\beta = -\bar{N}^{-1} I \{N^2\} \quad (2.16)$$

$$(\partial \ln \rho/\partial \ln \beta)_\nu = (\partial \epsilon/\partial \nu)_\beta = -\bar{N}^{-1} I \{N, \beta E\} \quad (2.17)$$

$$(\partial \epsilon/\partial \ln \beta)_\nu = \epsilon - \bar{N}^{-1} I \{(\beta E)^2\} \quad (2.18)$$

The quantity  $c_V$  of (11) is

$$c_V = -(\partial \epsilon/\partial \ln \beta)_\rho + \epsilon \quad (2.19)$$

The usual partial derivative manipulation gives

$$(\partial \epsilon/\partial \ln \beta)_\rho = (\partial \epsilon/\partial \ln \beta)_\nu + (\partial \epsilon/\partial \nu)_\beta (\partial \nu/\partial \ln \beta)_\rho = \\ (\partial \epsilon/\partial \ln \beta)_\nu - (\partial \epsilon/\partial \nu)_\beta (\partial \ln \rho/\partial \ln \beta)_\nu (\partial \ln \rho/\partial \nu)_\beta^{-1} \quad (2.20)$$

$$\bar{N} c_V = I \{(\beta E)^2\} - [I \{N, \beta E\}]^2 [I \{N^2\}]^{-1} \quad (2.21)$$

or with (11)

$$J \{(\beta E)^2\} = I \{(\beta E)^2\} - [I \{N, \beta E\}]^2 [I \{N^2\}]^{-1} \quad (2.22)$$

**Kinetic Energy Moments.**—The difference between the two moments  $I \{(\beta E)^2\}$  and  $J \{(\beta E)^2\}$  for the open and closed ensembles, respectively, is particularly easy to understand in detail for the case of a hard sphere fluid in which there is no potential energy. Define  $\kappa_i$

$$\kappa_i = \mathbf{p}_i \cdot \mathbf{p}_i / 2m \quad (3.1)$$

as the kinetic energy of a single molecule  $i$ . With the classical Gaussian distribution

$$w_p(\mathbf{p}_i) = (\beta/2\pi m)^{3/2} \exp -(\beta \mathbf{p}_i \cdot \mathbf{p}_i / 2m) \quad (3.2)$$

in the momentum space of a single molecule one finds

$$\beta \bar{\kappa} = 3/2 \quad (3.3)$$

$$\beta^2 \bar{\kappa}^2 = 15/4 \quad (3.4)$$

and recognizes the value of  $c_V$  as

$$c_V = \beta^2 [\bar{\kappa}^2 - \bar{\kappa}^2] = 3/2 \quad (3.5)$$

For a system of  $N$  molecules the total kinetic energy  $K_N$  is

$$K_N = \sum_{i=1}^{i=N} \kappa_i \quad (3.6)$$

so that

$$\beta \bar{K}_N = N \beta \bar{\kappa} = (3/2)N \quad (3.7)$$

The average of  $K_N^2$  is

$$\overline{K_N^2} = \left\langle \sum_{i=1}^{i=N} \kappa_i \sum_{j=1}^{j=N} \kappa_j \right\rangle \quad (3.8)$$

which has  $N$  terms  $\kappa_i^2$ , when  $i = j$ , and  $N^2 - N$  terms  $\kappa_i \kappa_j$  with  $i \neq j$ , whose average kinetic energies are independent. One finds, then

$$\overline{K^2} - \bar{K}^2 = N(\bar{\kappa}^2 - \bar{\kappa}^2) + (N^2 \bar{\kappa}^2) - (N \bar{\kappa})^2 \quad (3.9)$$

In the closed system of fixed  $N$  the last two terms cancel identically, and

$$J \{(\beta K)^2\} = N \beta^2 (\bar{\kappa}^2 - \bar{\kappa}^2) \quad (3.10)$$

but in the ensemble of open systems they do not, and

$$I \{(\beta K)^2\} = \bar{N} \beta^2 [\bar{\kappa}^2 - \bar{\kappa}^2] - I \{N^2\} \bar{\kappa}^2 \quad (3.11)$$

Since, in the open ensemble

$$I \{N, \beta K\} = I \{N^2\} \beta \bar{\kappa} \quad (3.12)$$

one verifies (2.22).

Had we, however, not counted the terms in  $\bar{K}^2$ , but attempted to evaluate the moments by integration over volume elements, we would in both cases have become involved with the integration of  $(\rho_2 - \rho^2) \bar{\kappa}^2$  over the volume. The differences in this integral due to the "long range" term,  $(\rho^2/N)(1 - \rho\nu_0)$  of eq 1.6, would have accounted for the difference between  $J \{(\beta K)^2\}$  and  $I \{(\beta K)^2\}$ . Since, for the potential energy the average values of the product for two different pairs is not the product of the averages, no simple counting of terms is possible, and we must necessarily recourse to the volume integrals involving such cases as that of (1.4).

**Reduced Probability Densities and Averages.**—For a classical system, the distribution in the momentum space of the center of mass of the molecules is a product of the single molecule functions,  $w_p(\mathbf{p}_i)$  of (3.2). We will be concerned with reduced probability densities,  $\rho_n \{n\}$ , in the coordinate space,  $\{n\} = \mathbf{r}_1, \dots, \mathbf{r}_n$  of the centers of mass of  $n$  molecules, defined for the open system by

$$\rho_n \{n\} = \iint \dots \int_{-\infty}^{+\infty} \prod_{i=1}^{i=n} d\mathbf{p}_i \sum_{N=0} g_N W_{N+n}^{(o)} \quad (4.1)$$

so that

$$\iint_V \dots \int d\{n\} \rho_n = \langle N! / (N - n)! \rangle^{(o)} \quad (4.2)$$

whereas for the closed system the definition is

$$\rho_n^{(Cl)} \{n\} = \iint_{-\infty}^{+\infty} \dots \int_{i=1}^{i=n} \prod d\mathbf{p}_i g_{N-n} W_N^{(Cl)} \quad (4.3)$$

and

$$N^{-1} \int d\mathbf{r}_n^{(Cl)} \rho_{n+1} \{n, \mathbf{r}_n\} = [1 - (n/N)] \rho_n^{(Cl)} \{n\} \quad (4.4)$$

is an exact relation. For the open systems, in the

same integral over  $\rho_{n+1}$ , the term of order  $\bar{N}^{-1}$  does not have the analytical form of  $\rho_n$ .

It is convenient to introduce cluster functions,  $G_n \{n\}$  and  $g_n \{n\}$  of the coordinates of  $n$  molecules. Use  $\{k\{\nu_i\}_n\}_u$  to indicate a partition of the  $n$  numbered molecules of the set  $\{n\}$  into  $k$  unconnected subsets,  $\{\nu_i\}_n$ ,  $1 \leq i \leq k$ ,  $\sum_i \nu_i = n$ , and  $\Sigma\{k\{\nu_i\}_n\}_u$  to indicate the sum over all possible such partitions for given  $k$  and  $n$ .

Define, then

$$\rho^n g_n \{n\} = G_n \{n\} = \sum_{k=1}^{k=n} \Sigma \{k\{\nu_i\}_n\}_u (-)^{n-1} (k-1)! \times \prod_{i=1}^{i=k} \rho_{\nu_i \{ \nu_i \}_n} \quad (4.5)$$

so that

$$\rho_n \{n\} = \sum_{k=1}^{k=n} \Sigma \{k\{\nu_i\}_n\}_u \prod_{i=1}^{i=k} G_{\nu_i \{ \nu_i \}_u} \quad (4.6)$$

and

$$G_i(\mathbf{r}) = \rho_i(\mathbf{r}) = \rho, \quad g_i \equiv 1 \quad (4.7)$$

in a fluid for which the density is independent of position. In the open system, for which these are defined (except in the neighborhood of a critical point) the functions  $g_n$  go sufficiently rapidly to zero if any distance  $r_{ij}$  between molecules of the set  $n$  goes to infinity, so that the integral

$$g_n^{(1)} \{n\} = \rho \int_{-\infty}^{+\infty} d\mathbf{r}_n g_{n+1} \{n\} \mathbf{r}_n, \quad n \geq 1 \quad (4.8)$$

exists. In (1.9) we already have used the first of these, namely

$$g_1^{(1)} = \rho \int 4\pi r^2 dr g_2(r) \quad (4.8')$$

Writing  $\rho_2(r) = \rho^2 [1 + g_2(r)]$  from (6), and using (2) we have, since

$$\rho \int_V d\mathbf{r} = \bar{N} \quad (4.9)$$

that

$$\bar{N}^2 + \bar{N}\rho \int 4\pi r^2 dr g_2(r) = \bar{N}^2 + \bar{N}g_1^{(1)} = \bar{N}^2 - \bar{N} \quad (4.10)$$

or

$$(\bar{N}^2 - \bar{N}^2) = I\{N^2\} = \bar{N}[1 + g_1^{(1)}] \quad (4.11)$$

The moment  $I\{N^2\}$  is related to the isothermal compressibility. From (2.12) and (2.13) we have

$$-\bar{N}^{-1} I\{N^2\} = (\partial \ln \rho / \partial \nu)_\beta = (\partial \ln \rho / \partial \varphi)_\beta (\partial \varphi / \partial \nu)_\beta = -(\partial \rho / \partial \varphi)_\beta \quad (4.12)$$

or

$$(\partial \rho / \partial \varphi)_\beta = -kT\rho[V^{-1}(\partial V / \partial P)_T] = \bar{N}^{-1} I\{N^2\} \quad (4.12')$$

The Hamiltonian,  $H_N \{N\}$ , is the sum of kinetic plus potential energies

$$H_N = K_N + U_N \quad (4.13)$$

so that

$$\beta \bar{E} = \beta \bar{K} + \beta \bar{U} \quad (4.14)$$

$$I\{N, \beta E\} = I\{N, \beta K\} + I\{N, \beta U\} \quad (4.15)$$

$$I\{(\beta E)^2\} = I\{(\beta K)^2\} + 2I\{\beta K, \beta U\} + I\{(\beta U)^2\} \quad (4.16)$$

The kinetic energy averages,  $\bar{k}$ , of the single molecules are completely independent of their coordinate positions, so that

$$I\{\beta K, \beta U\} = \beta \bar{k} I\{N, \beta U\} \quad (4.17)$$

Use these equations with (3.11) and (3.12) in (2.21) for  $c_V$ . One finds, as must be the case, that one can write  $c_V$  as the sum of two independent terms,  $c_{V_k}$  and  $c_{V_u}$  due to the kinetic and potential energies, respectively

$$c_V = c_{V_k} + c_{V_u} \quad (4.18)$$

$$c_{V_k} = \beta^2 (\bar{k}^2 - \bar{k}) = 3/2 \quad (4.19)$$

$$c_{V_u} = \bar{N}^{-1} [I\{(\beta U)^2\} - [I\{N, \beta U\}]^2 I\{N^2\}]^{-1} \quad (4.20)$$

If the potential,  $U_N$ , consists of the sum of mutual pair terms only

$$U_N \{N\} = \sum_{N \geq 2} \sum_{j \geq 1} u(r_{ij}) \quad (4.21)$$

we obtain for the average  $\beta \bar{U}$ , from (1) for  $\rho_2$ , that

$$\beta \bar{U} = \frac{1}{2} \int_V \int_V d\mathbf{r}_1 d\mathbf{r}_2 \rho_2(r_{12}) \beta u(r_{12}) \quad (4.22)$$

If (4.21) for  $U_N$  is squared, one finds for every one of the  $\frac{1}{2}N(N-1)$  pairs,  $i, j$ , a term  $u^2(r_{ij})$ , for every one of the  $N(N-1)(N-2)/6$  triples,  $i, j, k$ , six terms of the type  $u(r_{ij})u(r_{jk})$  (namely two each of the three possibilities with the three indices  $i, j, k$ , occurring twice), and for each of the  $N(N-1)(N-2)(N-3)/24$  quadruplets there are six terms of type  $u(r_{ij})u(r_{kl})$ . Subtract the square of (22) from the last of these, and note that the integration over the last coordinate always leads to a factor  $V$ . We find

$$I\{(\beta U)^2\} = \bar{N}(\Psi_2 + \Psi_3 + \Psi_4) \quad (4.23)$$

$$\Psi_2 = \rho^{-1} \int 4\pi r^2 dr \rho_2(r) \beta^2 u^2(r) \quad (4.24)$$

$$\Psi_3 = \rho^{-1} \int \int d\mathbf{r}_2 d\mathbf{r}_3 \rho_3(\mathbf{r}_1, \mathbf{r}_2, \mathbf{r}_3) \beta u(r_{12}) \beta u(r_{23}) \quad (4.25)$$

$$\Psi_4 = \frac{1}{4} \rho^{-1} \int \int \int d\mathbf{r}_2 d\mathbf{r}_3 d\mathbf{r}_4 [\rho(\mathbf{r}_1, \mathbf{r}_3, \mathbf{r}_4) - \rho_2(r_{12}) \rho_2(r_{34})] \beta u(r_{12}) \beta u(r_{34}) \quad (4.26)$$

in which all integrals can be extended to infinite limits.

The potential energy,  $U$ , consists of  $\frac{1}{2}N(N-1)$  term,  $u(r_{ij})$ , so that

$$\langle NU \rangle^{(0)} = \frac{1}{2} \sum_{N \geq 2} g_N N^2 (N-1) u(r_{12}) W_N \quad (4.27)$$

writing  $N^2(N-1) = N(N-1)(N-2) + 2N(N-1)$  we have with (3) for  $\rho_n$ , that

$$\langle NU \rangle^{(0)} = \int \int \int d\mathbf{r}_1 d\mathbf{r}_2 \rho_2(r_{12}) u(r_{12}) + \frac{1}{2} \int \int \int d\mathbf{r}_1 d\mathbf{r}_2 d\mathbf{r}_3 \rho_3(\mathbf{r}_1, \mathbf{r}_2, \mathbf{r}_3) u(r_{12})$$

subtracting  $\bar{N}\bar{U}$  from the latter we write, for the moment

$$I\{N, \beta U\} = \bar{N}(X_2 + X_3) \quad (4.28)$$

$$X_2 = \rho^{-1} \int 4\pi r^2 dr \rho_2(r) \beta u(r) = 2\beta \bar{U} / \bar{N} \quad (4.29)$$

With these in (20) we have with (11) that

$$X_3 = \frac{1}{2\rho} \int d\mathbf{r}_2 d\mathbf{r}_3 [\rho_3(\mathbf{r}_1, \mathbf{r}_2, \mathbf{r}_3) - \rho \rho_2(r_{12})] \beta u(r_{12}) \quad (4.30)$$

$$c_{V_u} = \Psi_2 + \Psi_3 + \Psi_4 + (X_2 + X_3)^2 [\bar{N} / I\{N^2\}] \quad (4.31)$$

For numerical purposes (31), with the expressions (24) to (30) for the individual terms, and with (8) and (11)

$$\bar{N}^{-1} I\{N^2\} = 1 + \rho^{-1} \int 4\pi r^2 dr [\rho_2(r) - \rho^2] \quad (4.32)$$

are adequate to compute  $c_V$ , the contribution due to the potential energy to the heat capacity at constant volume, per molecule in units  $k$ . There remains, however, the somewhat unsatisfactory situation that  $c_{V_u} = I\{(\beta U)^2\}$ , and this involves the "long range" contribution that would appear in

$\Psi_4$  if closed ensemble probability density functions,  $\rho_u^{(Cl)}$ , were used. One would like to see more directly that these contributions are equal to  $-(X_2 + X_3)^2 [\bar{N}/I\{N^2\}]$ .

**The Difference  $J\{n\} - I\{n\}$  for any  $n$ .**—We use a mathematical artifice by writing

$$\ln W_N^{(0)} = -[\varphi V + Nu + \beta H] + \sum_{\alpha} \lambda_{\alpha} F_{\alpha} \quad (5.1)$$

$$\ln W_N^{(Cl)} = -[Na + \beta H] + \sum_{\alpha} \lambda_{\alpha} F_{\alpha} \quad (5.1')$$

so that for  $\lambda = \lambda_1, \lambda_2, \dots, \lambda_{\alpha} \equiv 0$  the probability densities are those of the equilibrium system. The normalization conditions (2.4) and (2.4') now determine  $\phi(\nu, \beta, \lambda)$  and  $a(\rho, \beta, \lambda)$ , and following the method by which (2.8), (2.9), and (2.10) were obtained we find immediately that

$$V(\partial\varphi/\partial\lambda_{\alpha})_{\nu, \beta, \lambda} = \bar{F}_{\alpha} \quad (5.2)$$

$$N(\partial a/\partial\lambda_{\alpha})_{\rho, \beta, \lambda - \lambda_{\alpha}} = \bar{F}_{\alpha} \quad (5.2')$$

With these and the procedure of obtaining (2.11) to (2.14) one finds

$$(\partial\bar{F}_{\alpha}/\partial\lambda_{\alpha})_{\nu} = I\{\alpha, \gamma\} \quad (5.3)$$

$$(\partial\bar{F}_{\alpha}/\partial\lambda_{\gamma})_{\rho} = J\{\alpha, \gamma\} \quad (5.3')$$

$$-(\partial\bar{F}_{\alpha}/\partial\nu)\lambda = (\partial\bar{N}/\partial\lambda_{\alpha})_{\nu} = I\{N, \alpha\} \quad (5.3'')$$

The rule of differentiation

$$(\partial/\partial\lambda_{\alpha})_{\rho} = (\partial/\partial\lambda_{\alpha})_{\nu} - (\partial \ln \rho / \partial\lambda_{\alpha})(\partial \ln \rho / \partial\nu)^{-1} (\partial/\partial\nu) \quad (5.4)$$

then gives

$$J\{\alpha, \beta\} = I\{\alpha, \beta\} - I\{N, \alpha\} I\{N, \beta\} [I\{N^2\}]^{-1} \quad (5.5)$$

as a generalization of (2.22).

To continue we extend the notation of (2.7) with  $N$  held distinct as a unique function, namely

$$I_{\mu}\{n\} = \left\langle (N - \bar{N})^{\mu} \prod_{\alpha, c\{n\}} (F_{\alpha} - \bar{F}_{\alpha}) \right\rangle^{(0)} \quad (5.6)$$

so that

$$(\partial I_{\mu}\{n\} / \partial\lambda_{\alpha})_{\nu, \lambda - \lambda_{\alpha}} = I_{\mu}\{n, \alpha\} \quad (5.7)$$

$$-(\partial I_{\mu}\{n\} / \partial\nu)\lambda = I_{\mu+1}\{n\} \quad (5.8)$$

whereas, at constant  $\rho$

$$(\partial J\{n\} / \partial\lambda_{\alpha})_{\rho, \lambda - \lambda_{\alpha}} = J\{n, \alpha\} \quad (5.9)$$

Number the  $\alpha$ 's sequentially  $1, 2, \dots, n, \dots$  and use the notation introduced in (4.6). Define, for given  $n$  and given  $k$ , with  $1 \leq k \leq n$ , the sums

$$S(n, k) = \sum \{k\{\nu_i\}_n\}_u \prod_{i=1}^{i=k} I_1\{\nu_i\}_n \quad (5.10)$$

$$T(n, k) = (\partial S(n-1, k) / \partial\lambda_{\alpha})_{\nu}, \quad (T(n, n) = 0) \quad (5.11)$$

$$R(n, k) = I_1(n) S(n-1, k-1), \quad (R(n, 1) = 0) \quad (5.12)$$

so that

$$S(n, n) = R(n, n) \quad (5.13)$$

$$S(n, k) = R(n, k) + T(n, k) \quad (5.13')$$

and, in this notation, (5) becomes

$$J\{1, 2\} = I\{1, 2\} - I_2^{-1} S(2, 2) \quad (5.14)$$

If we define the operators

$$\mathcal{L} = -I_2^{-1} (\partial/\partial\nu)_{\nu, \lambda} \quad (5.15)$$

$$\mathcal{O}_n = (\partial/\partial\lambda_n)_{\nu, \nu, \lambda - \lambda_n} - I\{n\} \mathcal{L} \quad (5.16)$$

then (4) becomes

$$(\partial/\partial\lambda_n)_{N, \nu, \lambda - \lambda_n} = \mathcal{O}_n \quad (5.17)$$

Since

$$(\partial/\partial\lambda_n) I_2^{-1} = -I_2^{-2} I_2(n) = \mathcal{L} I_1(n) \quad (5.18)$$

we have for any  $S(n-1, k)$ ,  $k \leq n-1$ , using (11) and (12)

$$\begin{aligned} \mathcal{O}_n I_2^{-1} S(n-1, k) &= I_2^{-1} T(n, k) - [\mathcal{L} I_1(n)] S(n-1, k) - \\ I_1(n) [\mathcal{L} S(n-1, k)] &= I_2^{-1} (T(n, k) - \mathcal{L} [I_1(n) S(n-1, k)]) \\ &= I_2^{-1} T(n, k) - \mathcal{L} R(n, k+1) \end{aligned} \quad (5.19)$$

and since

$$\mathcal{O}_n I\{n\} - 1 = I\{n\} - I_2^{-1} I_1(n) S(n-1, 1) = I\{n\} = I_2^{-1} R(n, k) \quad (5.20)$$

we have for  $n=3$ , using (13) and (13')

$$J\{3\} = I\{3\} - I_2^{-1} S(3, 2) + \mathcal{L} I_2^{-1} S(3, 3) \quad (5.21)$$

Since one can check that  $\mathcal{O}_n$  and  $\mathcal{L}$  commute

$$\mathcal{O}_n \mathcal{L} = \mathcal{L} \mathcal{O}_n \quad (5.22)$$

one has, for any  $n$ , that

$$J\{n\} = I\{n\} - \sum_{k=0}^{k=n-2} (-)^k \mathcal{L}^k I_2^{-2} S(n, k+2) \quad (5.23)$$

**Closed System Ensemble Cluster Functions.**—The moments defined by (2.7) also may be written

$$I\{n\} = \sum_{k=1}^{k=n} \sum \{k\{\nu_i\}_n\}_u (-)^{k-1} (k-1)! \times \prod_{i=1}^{i=k} \left\langle \prod_{\alpha \in C\{\nu_i\}_n} F_{\alpha} \right\rangle^{(0)} \quad (6.1)$$

Choose

$$F_{\alpha}\{N\} = \sum_{i=1}^{i=N} \delta(\mathbf{r}_{\alpha} - \mathbf{r}_i) \quad (6.2)$$

$$\mathbf{r}_{\alpha} \neq \mathbf{r}_{\beta}, \quad \alpha \neq \beta \quad (6.2')$$

so that

$$\left\langle \prod_{\alpha \in C\{\nu\}} F_{\alpha} \right\rangle^0 = \rho_{\nu}\{\nu\} \quad (6.3)$$

$$\{\nu\} = \{\mathbf{r}_{\alpha 1}, \mathbf{r}_{\alpha 2}, \dots, \mathbf{r}_{\alpha \nu}\} \quad (6.3')$$

and comparing (1) with (4.5) for  $G_n$ , one has

$$I\{n\} = G_n\{n\} = \rho^n g_n\{n\} \quad (6.4)$$

$$I_1\{n\} = -(\partial G_n\{n\} / \partial\nu)_{\beta} \quad (6.4')$$

Use (4.1) for  $\rho_n$ , and, since

$$(\partial W_{N+n}^{(0)} / \partial\nu)_{\beta} - W_{N+n}^{(0)} [-V(\partial\varphi/\partial\nu)_{\beta} - n - N] = W_{N+n}^{(0)} [\bar{N} - n - N] \quad (6.5)$$

one finds

$$(\partial\rho_n / \partial\nu)_{\beta} = (\bar{N} - n)\rho_n - \int_V d\mathbf{r} \rho_{n+1}\{\{n\}, \mathbf{r}\} \quad (6.5')$$

Use (4.6) to write

$$\begin{aligned} \rho_{n+1}\{\{n\}, \mathbf{r}\} &= \rho\rho_n\{n\} + G_{n+1}\{\{n\}, \mathbf{r}\} + \\ &\sum_{m=n-2}^{m=n-1} \sum_{\{m_i\}_n} G_{m+1}\{\{m_i\}_n, \mathbf{r}\} \rho_{n-m}\{n-m\}_n \end{aligned} \quad (6.6)$$

$$\begin{aligned} n\rho_n\{n\} &= nG_n\{n\} + \\ &\sum_{m=1}^{m=n-1} \sum_{\{m_i\}_n} m_i G_{m_i}\{m_i\}_n \rho_{n-m}\{n-m\}_n \end{aligned} \quad (6.6')$$

and

$$\begin{aligned} (\partial\rho_n\{n\} / \partial\nu)_{\beta} &= (\partial G_n\{n\} / \partial\nu)_{\beta} + \\ &\sum_{m=1}^{m=n-1} \sum_{\{m_i\}_n} \left( \frac{\partial G_{m_i}\{m_i\}}{\partial\nu} \right)_{\beta} \rho_{n-m}\{n-m\}_n \end{aligned} \quad (6.6'')$$

and since  $N\rho_n = \rho_n \rho \int_V d\mathbf{r}$ , one finds by iteration

$$-(\partial G_n\{n\} / \partial\nu)_{\beta} = \rho^n [n g_n\{n\} + g_n^{(1)}\{n\}] \quad (6.7)$$

where  $g_n^{(1)}$ , defined by (4.8), is the integral of  $\rho g_{n+1}$  over one coordinate,  $\mathbf{r}$ .

The case  $n = 1$  of (6.7), with  $G_1 = \rho, g_1 = 1$

$$-(\partial G_1 / \partial \nu)_\beta = -(\partial \rho / \partial \nu) = \rho(1 + g_1^{(1)}) \quad (6.8)$$

has been encountered in (4.11) and (4.12). Since  $1 + g_1^{(1)}$  occurs so regularly in the equations we give it a special symbol

$$B = 1 + g_1^{(1)} = 1 + \rho \int 4\pi r^2 dr g_2(r) = -(\partial \ln \rho / \partial \nu)_\beta \quad (6.9)$$

so that

$$-(\partial G_1 / \partial \nu) = \rho B = V^{-1} I_2 \quad (6.10)$$

and the operator  $\mathcal{L}$  of (5.15) is

$$\mathcal{L} = -I_2^{-1} (\partial / \partial \nu)_{\mathbf{v}, \beta} = V^{-1} (\partial \rho / \partial \nu)^{-1} \beta (\partial / \partial \nu)_{\mathbf{v}, \beta} = V^{-1} (\partial / \partial \rho)_{\mathbf{v}, \beta} \quad (6.11)$$

Introducing

$$S'(n, k) = \sum \{k\{\nu_i\}_n\} \prod_{i=1}^{i=k} [\nu_i g_{\nu_i}\{\nu_i\}_n + g_{\nu_i}^{(1)}\{\nu_i\}_n] \quad (6.12)$$

and noting that for the functions of equation 2

$$J\{n\} = \rho^n g_n^{(Cl)}\{n\} \quad (6.13)$$

namely the cluster functions  $g_n^{(Cl)}$  defined by (4.5) with  $\rho_n^{(Cl)}$  replacing  $\rho_n$ , one has from (5.23) that

$$g_n^{(Cl)} = g_n\{n\} - N^{-1} B^{-1} S'(n, 2) - \sum_{k=n-2}^{k=1} (-)^k N^{-(k+1)} \rho^{k+1-n} (\partial^k / \partial \rho^k)_{\mathbf{v}, \beta} B^{-1} \rho^{n-1} S'(n, k+2) \quad (6.13)$$

The operator  $(\partial / \partial \rho)_{\mathbf{v}, \beta}$  can be used on  $S'$  and  $B$  as

$$(\partial / \partial \rho)_{\mathbf{v}, \beta} = -(\rho B)^{-1} (\partial / \partial \nu)_{\mathbf{v}, \beta} \quad (6.14)$$

with

$$-(\partial g_n\{n\} / \partial \nu)_\beta = g_n^{(1)}\{n\} - n(B-1) g_n\{n\} = \rho \int dr_i [g_{n+1}\{n, r_i\} - \sum_{i=1}^{i=n} g_n\{n\} g_2(r_{ii})] \quad (6.15)$$

from (7) and (9) with  $G_n = \rho^n g_n$ , and

$$-(\partial B / \partial \nu) = -(\partial g_1^{(1)} / \partial \nu) = -\int 4\pi r^2 dt [\partial \rho g_2(r) / \partial \nu] = g_1^{(2)} - [g_1^{(1)}]^2 + g_1^{(1)} = g_1^{(2)} - B^2 + 3B - 2 \quad (6.16)$$

$$g_1^{(2)} = \rho^2 \int \int dr_1 dr_2 g_3(r, r_1, r_2) \quad (6.16')$$

With these expressions in (4.6) for  $\rho_n^{(Cl)}$  in terms of the  $g_n$  functions we find

$$\rho_2^{(Cl)}(r) = \rho_2(r) - N^{-1} \rho^2 B = \rho^2 [1 + g_2(r) - N^{-1} B] \quad (6.17)$$

in agreement with (1.7) with (1.9) and (9) that  $1 - \rho V_0 = B$ . For  $\rho_3^{(Cl)}$  we find

$$\rho_3^{(Cl)}(r_1, r_2, r_3) = \rho_3(r_1, r_2, r_3)$$

$$-N^{-1} \rho^3 \left\{ 3B + \sum_{i=1}^{i=3} [2g_2(r_{jk}) + g_2^{(2)}(r_{jk})] \right\} + N^{-2} \rho^3 [2g_1^{(2)} + 6B - 4] \quad (6.18)$$

and for  $\rho_4^{(Cl)}$

$$\rho_4^{(Cl)}(r_1, r_2, r_3, r_4) = \rho_4(r_1, r_2, r_3, r_4) - N^{-1} \rho^4 \left\{ 6B + \sum_{i=1}^{i=4} [3g_3(r_i, r_k, r_l) + g_3^{(1)}(r_i, r_k, r_l)] \times \sum_{\substack{i > j > k \\ i > j > l}} 1/2 B^{-1} [2g_2(r_{ij}) + g_2^{(1)}(r_{ij})] [2g_2(r_{kl}) + g_2^{(1)}(r_{kl})] - [(2+B)g_2(r_{ij}) + g_2^{(1)}(r_{ij})] + [(2+B)g_2(r_{kl}) + g_2^{(1)}(r_{kl})] \right\} + C(N^{-2}) \quad (6.19)$$

**The Integrals in  $J\{(\beta U)^2\}$ .**—Since  $c_{VU} = N^{-1} J\{(\beta U)^2\}$  we can compute it as

$$c_{VU} = \Psi_2^{(Cl)} + \Psi_3^{(Cl)} + \Psi_4^{(Cl)} \quad (7.1)$$

where the terms  $\Psi_n^{(Cl)}$  are integrals defined by equations (4.24), (4.25), (4.26) replacing  $\rho_n$  by  $\rho_n^{(Cl)}$ . Since  $u(r_{ij})$  is a short range function we see that

$$\Psi_2^{(Cl)} = \Psi_2, \Psi_3^{(Cl)} = \Psi_3 \quad (7.2)$$

but in the integrand of  $\Psi_4^{(Cl)}$  there are, from (6.19), terms of order  $N^{-1}$  which are present when  $r_{ab} = 1/2 [r_1 + r_2 - r_3 - r_4] \gg \rho^{-1/2}$ . These terms in  $\rho_4^{(Cl)}$  from (6.19) are  $-N^{-1} \rho^4$  times  $6\beta$  plus the terms in the double sum over  $i, j$  when  $i = 2, j = 1$  and the equal terms when  $i = 4, j = 3$ . Add to these the terms of order  $N^{-1}$  in  $-\rho_2^{(Cl)}(r_{12}) \rho_2^{(Cl)}(r_{34})$ , which, from (6.17), are  $+N^{-1} \rho^2 B [2 + g_2(r_{12}) + g_2(r_{34})]$ .

One finds that

$$\Psi_4^{(Cl)} - \Psi_4 = -1/4 \rho^{-1} \int \int dr_2 dr_3 dr_4 N^{-1} \rho^4 \{ 4B + 2[2g_2(r_{12}) + g_2^{(1)}(r_{12})] + 2[2g_2(r_{34}) + g_2^{(1)}(r_{34})] + B^{-1} [2g_2(r_{12}) + g_2^{(1)}(r_{12})] [2g_2(r_{34}) + g_2^{(1)}(r_{34})] \} \beta U(r_{12}) \beta U(r_{34}) = -B^{-1} X^2 \quad (7.3)$$

where

$$X = 1/2 \rho \int 4\pi r^2 dr [2g_2(r) + g_2^{(1)}(r) + 2B] \beta U(r) \quad (7.4)$$

With (6.9) that  $B = 1 + g_1^{(1)}$  and with (4.8) for  $g_2^{(1)}$  and  $g_1^{(1)}$  one may write

$$X = X_2 + X_3 \quad (7.5)$$

$$X_2 = \rho \int 4\pi r^2 dr [1 + g_2(r)] \beta u(r) \quad (7.6)$$

$$X_3 = 1/2 \rho^2 \int dr_2 dr_3 [g_3(r_1, r_2, r_3) + g_2(r_{12}) + g_2(r_{23})] \beta u(r_{12}) \quad (7.7)$$

With (4.6) in (4.29) and (4.30) one sees that the integrals  $X_2$  and  $X_3$  of (6) and (7) are indeed identical with those defined in (4.29) and (4.30). One then has from (1) to (7)

$$c_{VU} = \Psi_2 + \Psi_3 + \Psi_4 - B^{-1} (X_2 + X_3)^2 \quad (7.8)$$

in agreement with (4.31) since  $B = \bar{N}^{-1} I\{N^2\}$ .

# THE THERMODYNAMIC PROPERTIES OF GASES IN SOLUTION. I. THE PARTIAL MOLAL VOLUME

By E. B. SMITH

*Physical Chemistry Laboratory, South Parks Road, Oxford*

AND JOHN WALKLEY

*Department of Chemistry, Imperial College, London, S.W. 7*

*Received October 7, 1961*

An understanding of the partial molal volume of gases in solution is of considerable importance in the study of the thermodynamic properties of such solutions. The available experimental data for gases in non-polar solvents are summarized and the applicability of various theories is examined. An inconsistency in the predictions of regular solution theory is observed. Finally, a simple free volume model is presented which enables the partial molal volume of dissolved gases to be predicted in a satisfactory manner.

Largely as a result of the research of Professor J. H. Hildebrand over the last half-century, a general understanding of the properties of solutions is now possible. Regular solution theory has provided a basis by which solubility can be predicted with a remarkable over-all success. Many details remain to be filled in and we may be confident that Professor Hildebrand will, in future years, be active in their solution as he has been in the past.

The more recent research of Professor Hildebrand and co-workers on the properties of gases dissolved in non-polar solvents has shown that the development of an adequate theory for these systems remains one of the outstanding problems of solution theory. Progress in this field long has been hampered by a lack of reliable data, but the recent research of Hildebrand,<sup>1</sup> of Clever,<sup>2</sup> and of Gjaldbaek<sup>3</sup> now has produced accurate solubility data extending over a wide range of solvent and solute molecules. These workers confirm, in general, the earlier data of Lannung<sup>4</sup> and of Horiuti.<sup>5</sup> As yet no detailed theoretical analysis has been made for gases in solution though several workers<sup>2,3</sup> have applied regular solution theory to their experimental results. In all cases, however, the actual prediction of gas solubility has involved the use of most unrealistic parameters which, as will be discussed later, lead to completely unacceptable values when used in the prediction of other relevant data.

The volume change on mixing for a dissolved gas is a most important thermodynamic property, yet only a few workers have produced experimental values for the partial molal volumes of gases dissolved in non-polar solvents (Table I), and these of limited accuracy.<sup>1b,5-7</sup> No attempt has been made to interpret such data on the basis of an ac-

ceptable model using fundamental gas and solvent parameters.

TABLE I

EXPERIMENTAL	PARTIAL MOLAL VOLUME AT 25° (CM. <sup>3</sup> )						
	$\delta$	$A_T$	N <sub>2</sub>	CH <sub>4</sub>	CF <sub>4</sub>	H <sub>2</sub>	D <sub>2</sub>
C <sub>7</sub> F <sub>16</sub>	6.0	54	66.1	68.4		54.4	52.9
C <sub>7</sub> F <sub>14</sub>	6.1	51					
<i>i</i> -C <sub>8</sub> H <sub>18</sub>	6.9	50		56.6	85.4		
C <sub>7</sub> H <sub>16</sub>	7.5			55.4	86.4		
CCl <sub>4</sub>	8.6	44	52.5	52.4	79.7	38	
C <sub>6</sub> H <sub>6</sub>	9.2	43	53	52	83.2	35.2	32.7
CS <sub>2</sub>	10.0	45		56.1	85.4		
			CO	O <sub>3</sub>	C <sub>2</sub> H <sub>4</sub>	CO <sub>2</sub>	N <sub>2</sub> O
CCl <sub>4</sub>	8.6	52.5	45.3	61	48	47	

**Regular Solution Theory.**—In the case of liquid and solid solutes considerable success in the understanding of solubility has been obtained by the use of the regular solution theory.<sup>8-10</sup>

This theory gives for the solubility of a gas<sup>11</sup>

$$-\log X_2 = -\log X_2^{\text{id}} + V_2(\delta_1 - \delta_2)^2/4.575T \quad (1)$$

where  $X_2$  is the mole fraction of a gas in a saturated solution,  $X_2^{\text{id}}$  is the ideal solubility,  $V_2$  is the molal volume of the gas in its reference state (the pure liquid), and  $\delta_1$  and  $\delta_2$  are the solubility parameters of the solvent and solute, respectively. The main difficulty in the application of eq. 1 is the choice of a suitable value for  $V_2$ . Clever<sup>2</sup> selected the critical volume of the gas and was able to find a solubility parameter for each gas which gave a reasonable prediction of the solubility in a series of solvents, using a comparative method to eliminate  $X_2^{\text{id}}$ . Gjaldbaek<sup>3</sup> took  $V_2$  to be equal to the partial molal volume of the gas in CCl<sub>4</sub> solvent and evaluated  $\delta_2$  directly, since  $X_2^{\text{id}}$  can be estimated for the gases he examined. For a gas in a series of solvents a reasonably consistent value of  $\delta_2$  was obtained. Table II gives a list of the values obtained by the above mentioned workers.

Using the assumptions of regular solution theory it is possible to evaluate the excess volume change on mixing.<sup>12</sup> In terms of solubility parameters the

(1) (a) L. W. Reeves and J. H. Hildebrand, *J. Am. Chem. Soc.*, **79**, 1313 (1957); (b) J. E. Jolley and J. H. Hildebrand, *ibid.*, **80**, 1050 (1958); (c) Y. Kobatake and J. H. Hildebrand, *J. Phys. Chem.*, **65**, 331 (1961).

(2) (a) H. L. Clever, R. Battino, J. H. Saylor, and P. M. Gross, *ibid.*, **61**, 1078 (1957); (b) H. L. Clever, J. H. Saylor, and P. M. Gross, *ibid.*, **62**, 89 (1958); (c) H. L. Clever, *ibid.*, **62**, 375 (1958).

(3) (a) J. C. Gjaldbaek and J. H. Hildebrand, *J. Am. Chem. Soc.*, **71**, 3147 (1949); (b) J. C. Gjaldbaek, *Acta Chem. Scand.*, **8**, 1398 (1952).

(4) A. Lannung, *J. Am. Chem. Soc.*, **52**, 68 (1930).

(5) J. Horiuti, *Sci. Papers Inst. Phys. Chem. Research Tokyo*, **17**, 125, No. 341 (1931).

(6) R. H. Schumm and O. L. I. Brown, *J. Am. Chem. Soc.*, **75**, 2520 (1953).

(7) J. Walkley and J. H. Hildebrand, *ibid.*, **81**, 4439 (1959).

(8) J. E. Jolley and J. H. Hildebrand, *J. Phys. Chem.*, **61**, 791 (1957).

(9) K. Shinoda and J. H. Hildebrand, *ibid.*, **61**, 789 (1957).

(10) E. B. Smith and J. Walkley, *Trans. Faraday Soc.*, **56**, 220 (1960).

(11) Hildebrand and Scott, "Solubility of Non-electrolytes," Reinhold Publishing Corporation, New York, N. Y., 1950, p. 224.

(12) Reference 11, p. 138.

TABLE II

(Gas)	H <sub>2</sub>	O <sub>2</sub>	CO <sub>2</sub>	CO	Gas He	Ne	Ar	Kr	Xe
$\delta$	5.1	5.7	5.7	5.8	3.2	4.9	7.0	7.5	8.0
Ref.	3	3	3	3	2	2	2	2	2

partial molal volume of a solute in dilute solution,  $\bar{V}_2$ , is given by

$$(\bar{V}_2 - V_2) = n\beta_1\phi_1^2V_2(\delta_1 - \delta_2)^2 \quad (2)$$

where  $V_2$  is the volume of the solute in the pure liquid state,  $\beta_1$  is the compressibility of the pure solvent, and  $\phi_1$  the volume fraction of the solvent.  $n$  is the ratio  $(\partial E/\partial V)_T/(E/V)$ , which for most non-polar liquids is approximately equal to unity. For solid and liquid solutes eq. 2 has been used with success in the prediction of the partial molal volume.<sup>13,14</sup> The application of this equation to gases leads to anomalous results when used in conjunction with the solubility parameters given in Table II. For most of the gases the calculated partial molal volume is less in solvents of low solubility parameter, such as the fluorocarbons, than in carbon tetrachloride or benzene, a trend in direct contradiction to the experimental results. For nitrogen, with an estimated solubility parameter of 5.8, we calculate the partial molal volume to be (in cm.<sup>3</sup>)

C <sub>7</sub> F <sub>16</sub>	C <sub>7</sub> H <sub>16</sub>	CCl <sub>4</sub>	C <sub>6</sub> H <sub>6</sub>	CS <sub>2</sub>
52	53	54	55	55

$V_2$  was taken to be 52 cm.<sup>3</sup>, in keeping with Gjaldbaek's assumption. For hydrogen the predicted partial molal volume is 2 cm.<sup>3</sup> less in C<sub>7</sub>F<sub>16</sub> than in CCl<sub>4</sub>, while for argon the estimated solubility parameter lies between those of the liquids considered and thus the variation in the calculated partial molal volume is very small (Table IV).

**Simple Free Volume Theory.**—An evaluation of the partial molal volume of the dissolved gas at what is virtually infinite dilution requires a treatment in which the properties of the solution are evaluated explicitly for a cell with the gas molecule at the center and the solvent molecules as the surrounding neighbors.<sup>15</sup> Certain regularities in the experimental data suggest, however, that the values of the partial molal volumes of gases in solution depend mainly upon two simple parameters: (a) the size of the gas (solute) molecule, and (b) the solubility parameter, or internal pressure of the solvent. Uhlig<sup>16</sup> and Eley<sup>17</sup> both have developed theories for gases in solution and have evaluated the energy required to make a "cavity" in solution from the surface tension and the internal pressure of the solvent. The success of these approaches and the regularities mentioned above suggest that it is appropriate to consider a simple cell model in which the gas molecule at the center of the cell, treated as a hard sphere, generates a pressure equal to the internal pressure of the solvent in which the gas will be dissolved. Having evaluated the molal volume of the gas at the internal pressure of the

solvent we may consider mixing to occur with no further volume change. The internal pressure of a liquid is defined by

$$(\partial E/\partial V)_T = T(\partial P/\partial T)_V - P$$

The external pressure term  $P$  may be ignored in comparison to  $T(\partial P/\partial T)_V$ . The free volume of a system of hard sphere molecules is given by

$$V_f = \int_0^{a-\sigma} 4\pi r^2 dr = 4\pi(a-\sigma)^3/3$$

where  $\sigma$  is the collision diameter of the molecule and  $a$  the nearest neighbor distance.<sup>18</sup> The pressure generated may be evaluated

$$P = RT \partial \ln V_f / \partial V = (RT/V)(1 - \sigma/a)^{-1}$$

Equating this pressure to the internal pressure of the solvent we may obtain an estimate of the molal volume of the gas,  $V_2$ , under these conditions

$$\frac{V_2}{V_0} = \left[ 1 - \frac{R}{V_2} \left( \frac{\partial P}{\partial T} \right)_V^{-1} \right]^{-3} \quad (3)$$

where  $V_0 = \gamma N \sigma^3$  and  $V_2 = \gamma N a^3$ .  $\gamma$  is a constant depending on the geometry of the lattice and  $V_0$  is equal to the volume of the gas at absolute zero. From a knowledge of the collision diameter of the gas and the  $(\partial P/\partial T)_V$  of the solvent,  $V_2$  may be evaluated numerically from eq. 3. The values of  $(\partial P/\partial T)_V$  for most common solvents are readily available.<sup>19</sup> The choice of  $\sigma$  for each gas is more difficult as in certain cases the reported values show considerable variation. Three sources have been used. The most reliable are the values of  $\sigma$  obtained from gas imperfection and transport data,<sup>20</sup> the third source is the volume of the solid at low temperatures. For Ar, N<sub>2</sub>, CO, and CH<sub>4</sub> there is substantial agreement between all three methods if the packing parameter  $\gamma$  is taken as unity. For N<sub>2</sub>O and C<sub>2</sub>H<sub>4</sub>, however, a wide discrepancy exists between the gas imperfection and transport values, but in both cases the values from the transport data were in agreement with the volume of the solids at low temperatures and thus were used in the theory. For H<sub>2</sub> and D<sub>2</sub> the volume of the solids were used. Values of the molal volume of the various gases at 25° obtained from this simple model are given in Table III. A comparison with the experimental partial molal volume data in Table I shows that the agreement between the two sets of data is good, except in the case of CO<sub>2</sub>. This confirms the original supposition that on going into solution there will be no further change in volume of this hypothetical hard sphere (pure solute) liquid and the molal volume thus is equal to the partial molal volume of the dissolved gas. Further, for every gas the correct trend of the experimental data is reproduced.

### Discussion

The application of regular solution theory to solutions of gases is illustrated in Table IV where

(13) E. B. Smith and J. Walkley, *Trans. Faraday Soc.*, **56**, 1276 (1960).

(14) E. B. Smith, J. Walkley, and J. H. Hildebrand, *J. Phys. Chem.*, **63**, 703 (1959).

(15) J. Walkley, *Trans. Faraday Soc.*, in press.

(16) H. H. Uhlig, *J. Phys. Chem.*, **41**, 1215 (1937).

(17) D. D. Eley, *Trans. Faraday Soc.*, **35**, 1281 (1939); **35**, 1421 (1939).

(18) Reference 11, p. 75.

(19) (a) J. H. Hildebrand and J. M. Carter, *J. Am. Chem. Soc.*, **54**, 3592 (1932); (b) B. J. Alder, E. W. Haycock, J. H. Hildebrand, and H. Watts, *J. Chem. Phys.*, **22**, 1060 (1954); (c) E. B. Smith and J. H. Hildebrand, *ibid.*, **31**, 145 (1959).

(20) J. O. Hirschfelder, C. F. Curtiss, and R. B. Bird, "The Molecular Theory of Gases and Liquids," John Wiley and Sons, Inc., New York, N. Y., 1954, p. 1100.



TABLE III

PARTIAL MOLAL VOLUMES FROM INTERNAL PRESSURE OF THE SOLVENT AT 25° (CM.<sup>3</sup>)

	Ar	N <sub>2</sub>	O <sub>2</sub>	CO	CH <sub>4</sub>	CO <sub>2</sub>	C <sub>2</sub> H <sub>4</sub>	CF <sub>4</sub>	N <sub>2</sub> O	H <sub>2</sub>	D <sub>2</sub>
$V_0 = \gamma N \sigma^3$	25 <sup>a</sup>	32 <sup>a</sup>	28 <sup>a</sup>	32 <sup>a</sup>	35 <sup>a</sup>	40 <sup>b</sup>	40 <sup>c</sup>	63 <sup>b</sup>	33 <sup>b</sup>	23 <sup>c</sup>	20 <sup>c</sup>
C <sub>7</sub> F <sub>16</sub>	53	60	56	60	64	69	69	94	62	51	48
C <sub>7</sub> F <sub>14</sub>	51	59	55	59	63	68	68	92	61	50	47
C <sub>7</sub> H <sub>16</sub>	49	57	52	57	60	65	65	89	58	47	44
CCl <sub>4</sub>	44	51	47	51	54	59	59	83	52	42	39
C <sub>6</sub> H <sub>6</sub>	42	49	46	49	53	58	58	81	51	40	37
CS <sub>2</sub>	42	49	46	49	53	58	58	81	51	40	37
CHBr <sub>3</sub>	40	47	43	47	50	55	55	78	48	38	35

<sup>a</sup> From gas imperfection data: ref. 20, assuming  $\gamma = 1$ . <sup>b</sup> From transport properties: ref. 20, assuming  $\gamma = 1$ . <sup>c</sup> From the volume of the solid.

the partial molal volumes of argon in various solvents, calculated using eq. 2, are compared with the experimentally observed values. It can be seen that the well defined trend of the experimental data is not reproduced. In general it is impossible to obtain solubility parameters for gases that lead to acceptable values for both the partial molal volumes and the solubility. Also included in Table IV are the partial molal volume values for argon calculated using the Prigogine-Scott model.<sup>21</sup> This model, by making use of the thermodynamic properties of the pure components, gives a theory with only the minimum dependence upon the cell model. The free energy of a second liquid may be related to that of a reference liquid by expanding in a double power series in the characteristic molecular parameters of energy,  $\epsilon$ , and volume,  $\sigma^3$ . The volume change on mixing may be obtained by a suitable differentiation of the free energy, thus

$$\frac{\Delta V^m}{x_1 x_2} = V^p \left( \eta \xi + \frac{11}{6} \xi^2 \right) + T \left( \frac{\partial V}{\partial T} \right)_p [3\eta \xi + 4\xi^2 - 2\eta^2] \quad (4)$$

$$\text{where } \xi = (\sigma_{11}^3 - \sigma_{22}^3 / \sigma_{11}^3 + \sigma_{22}^3) \\ \text{and } \eta = (\epsilon_{11} - \epsilon_{22} / \epsilon_{11} + \epsilon_{22})$$

As terms higher than the second power of  $\xi$  and  $\eta$  have been neglected, the application of this model to solutions of gases takes it beyond its range of applicability since from the large differences in the size of the molecules concerned  $\xi$  may be as high as 0.8. It may be seen that this model greatly overestimates the expansion caused by the differences in the size of the solvent and solute molecules. Higher terms in the expansion would, no doubt, tend to correct this feature but it is unlikely that a correction would be obtained to the extent necessary to give agreement with the experimental values.

(21) R. L. Scott, *J. Chem. Phys.*, **25**, 193 (1956).

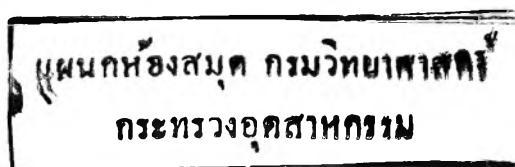
TABLE IV

THE PARTIAL MOLAL VOLUME OF ARGON AT 25° (CM.<sup>3</sup>)

	CS <sub>2</sub>	C <sub>6</sub> H <sub>6</sub>	CCl <sub>4</sub>	C <sub>7</sub> H <sub>16</sub>	<i>i</i> -C <sub>8</sub> H <sub>18</sub>	C <sub>7</sub> F <sub>16</sub>
Observed	45	43	44	..	50	54
This work, eq. 3	42	42	44	49	51	53
Prigogine-Scott, eq. 4	43	31	105	165	..	250
Regular soln. theory, eq. 2	45	45	44.5	44.5	44.5	44.5

It is considered that the success of the simple free volume theory arises from its neglect of the differences in the size of the solvent and solute molecules due to its consideration of the properties of the isolated pure solute under the conditions appropriate to the solution. The model of a hypothetical pure solute at the  $(\partial P / \partial T)_V$  of the solvent gives a naive explanation of the solubility "quantum differences" observed experimentally since the gas is considered not at 1 atmosphere but at an effective pressure of some 2-3000 atmospheres. The quantum differences are introduced only through the  $V_0$  values used (those of the solid at a low temperature) and in view of the simplicity of the model the agreement between the theoretical and experimental partial molal volume values, though not as good as those for the classical gases, certainly confirms the experimentally measured differences.<sup>7</sup> It seems unlikely that such a simple model could be an adequate basis for the complete evaluation of the thermodynamic properties of gases in solution. Nevertheless it has a considerable predictive value in the case of partial molal volume, an area of solubility study where both theoretical and experimental investigation has been lacking.

Both authors wish to thank Professor J. H. Hildebrand for the hospitality he extended to them as his research workers at the University of California.



# THE ENERGY-TEMPERATURE-VOLUME SURFACE FOR A SINGLE COMPONENT SYSTEM<sup>1</sup>

By SCOTT E. WOOD

*Department of Chemistry, Illinois Institute of Technology, Chicago 16, Illinois*

*Received October 12, 1961*

The thermodynamic energy-temperature-volume surface for a one component system is developed and its properties discussed. The energy of a single phase system is simply represented by a primitive surface, that of a two phase system by a ruled surface, and that of a three phase system by a triangular area lying within a plane drawn perpendicular to the temperature axis at the temperature of the triple point. The energy is continuous at the intersections of the different surfaces but the first partial derivatives of the energy are discontinuous.

When a macrocanonical ensemble is used in a statistical mechanical study, the independent variables are the volume and temperature for a closed system. The thermodynamic variable which is obtained directly in such a study is the Helmholtz free energy; however, the derived functions, energy and entropy, are more informative from a molecular point of view. In such a case the energy and the entropy must be considered as functions of the temperature and volume.

The importance of the volume in interpreting the behavior of solutions has been considered in many papers, only a few of which can be mentioned here. Hildebrand<sup>2</sup> defined a regular solution in terms of the transfer of a small amount of a component to a regular solution from an ideal solution of the same composition without any change in the total volume. Scatchard<sup>3</sup> was the first to calculate the difference in the changes of the thermodynamic functions on mixing at constant pressure and on mixing at constant volume. Wood and Gray<sup>4</sup> showed for the three binary systems formed from benzene, carbon tetrachloride, and cyclohexane that the changes of the energy and entropy on mixing at constant volume were more dependent upon the volume than upon the temperature. Subsequently, Wood, Sandus, and Weissman<sup>5</sup> concluded that the dependence of the energy and the entropy of pure liquids on the volume also was greater than that on the temperature.

If the volume is taken as an independent variable in addition to the temperature and the mole numbers of the components, a general change of state for the formation of a binary solution from the components would be

$$n_1A(T, \bar{V}_1) + n_2B(T, \bar{V}_2) = (n_1 + n_2)S(T, \bar{V}_3, x)$$

In this equation  $A$ ,  $B$ , and  $S$  represent the two pure components and the solution, respectively, and  $\bar{V}_1$ ,  $\bar{V}_2$ , and  $\bar{V}_3$  the corresponding molar volumes. Changes of state under arbitrary constant pressures or under arbitrary constant volumes would be special cases of this general change of state. Scott<sup>6</sup> has studied various changes of state, all of which involve mixing at constant volume, and

which can be represented by the general change of state. Such studies emphasize the need to consider the energy and entropy of the pure liquids and solutions as functions of the volume and temperature. Indeed  $P$ - $V$ - $T$  measurements of pure liquids and solutions over as wide a range of temperature and volume as possible would be very informative.

A study of the Helmholtz free energy, the energy, and the entropy as functions of the volume and temperature for pure substances and solutions thus is important. Moreover the general considerations discussed here are applicable to solid phases as well as liquid phases. Consequently this paper presents a qualitative study of a general energy-temperature-volume surface for a single component system. The general concepts of the Helmholtz free energy surface and the entropy surface would be similar but of course the details would be different. The substance is assumed to have one solid phase in addition to the fluid phases (liquid and gas).

These fluid phases are considered as a single phase except in those regions where two phases are in equilibrium with each other. The general concepts of the surface for such a system are developed but the details cannot be determined without the knowledge of an equation of state. Throughout the paper a closed system, containing presumably one mole of the substance, is considered.

A three-dimensional, rectangular coordinate system is used in which the energy, temperature, and volume are represented by the three axes. For one and two phase systems, the energy is a continuous function of the temperature and volume and therefore the individual surfaces representing such systems are continuous.<sup>7</sup> The differential of the energy for such systems is given by the equation

$$dE = C_VdT + \left(\frac{\partial E}{\partial V}\right)_T dV \quad (1)$$

Thus the slope of the curve formed by the intersection of the surface with a plane at constant volume is the heat capacity of the system at constant volume. Similarly, the slope of the curve formed by the intersection of the surface with a plane at constant temperature is  $(\partial E/\partial V)_T$  for the system. Moreover, the conditions for thermal and mechanical stability<sup>8</sup> must be satisfied. These are

(7) The energy will be continuous at the boundaries between the surfaces representing the one and two phase system, but the first derivatives of the energy will be discontinuous at the boundaries.

(1) Presented at the symposium held at the University of California at Berkeley, September, 1961 in honor of Professor Joel H. Hildebrand on the occasion of his eightieth birthday.

(2) J. H. Hildebrand, *J. Am. Chem. Soc.*, **51**, 66 (1929).

(3) G. Scatchard, *Trans. Faraday Soc.*, **33**, 160 (1937).

(4) S. E. Wood and J. A. Gray, III, *J. Am. Chem. Soc.*, **74**, 3733 (1952).

(5) S. E. Wood, O. Sandus, and S. Weissman, *ibid.*, **79**, 1777 (1957).

(6) R. L. Scott, *J. Phys. Chem.*, **64**, 1241 (1960).

that both the heat capacity at constant volume and the isothermal compressibility must be positive. Finally, the condition of equilibrium also must be satisfied. When the temperature and the volume are used as independent variables, this condition is expressed most easily in terms of the Helmholtz free energy rather than the energy. When the stabilities of two possible systems at the same temperature and volume are to be compared, the Helmholtz free energy of the stable system must be less than that of the unstable system. Thus if the stable system is designed by a prime and the unstable system by a double prime, then  $A' < A''$ . Either of the two inequalities

$$(E' - E'') < T(S' - S'') \quad (2)$$

or

$$T(S'' - S') < (E'' - E') \quad (3)$$

then may be used to determine the relative stability of the two possible systems. It is not possible to represent or determine the difference in the entropies in the energy-temperature-volume diagram and the difference must be calculated according to an equation of state along a reversible path between the two systems. Part of this path would be either metastable or unstable. Consequently a general proof of equilibrium is not possible and conditions for the various equilibria are not discussed in this paper except in the more simple cases.

**One-Phase Systems.**—The energy of the fluid phase expressed as a function of the volume at constant temperature is represented by the heavy line in Fig. 1a. This curve is applicable particularly above the critical point with the exclusion of any solid-fluid equilibrium. Only portions of such a curve will be physically realizable below the critical point or if a solid-fluid equilibrium is present along the isotherm. At large volumes the energy approaches that of the substance in the ideal gas state. As the volume decreases the energy decreases to a minimum and then rapidly increases. The slope of the curve is given by

$$\left(\frac{\partial E}{\partial V}\right)_T = T \left(\frac{\partial P}{\partial T}\right)_P - P \quad (4)$$

For an ideal gas this quantity is zero and thus the slope of the curve must approach zero as the volume approaches infinity. For the liquid or high-density fluid state,  $T(\partial P/\partial T)_V$  is generally positive and larger than the pressure.<sup>9</sup> Under these conditions the slope is positive. The negative slope at small volumes may be realized in two ways: (1) at high pressures  $T(\partial P/\partial T)_V$  may be smaller than the pressure and (2)  $(\partial P/\partial T)_V$  may itself become negative. The first case has been observed by Cutler, McMickle, Webb, and Schiessler.<sup>10</sup> Water below the temperature of maximum density is representative of the second case. According to the condition of mechanical stability the isothermal compressibility must be positive but the coefficient of expansion is negative for

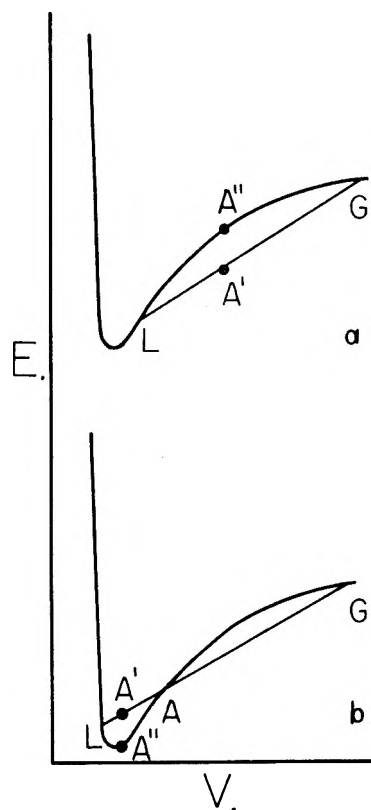


Fig. 1.—A simple energy-volume isotherm.

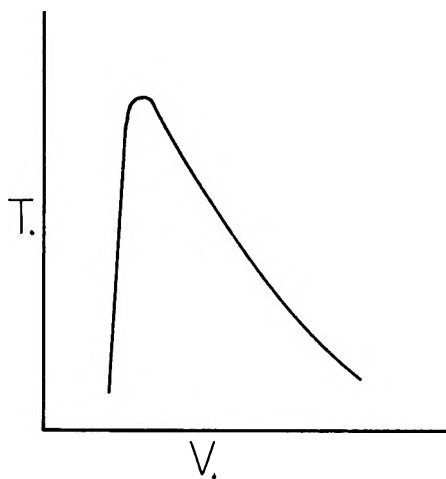


Fig. 2.—A temperature-volume curve at constant energy.

water below the temperature of maximum density. Under these conditions  $(\partial P/\partial T)_V$  is negative and, hence,  $(\partial E/\partial V)_T$  is also negative.

A concept of the energy surface for the single fluid phase may be obtained from the knowledge that similar curves exist at each temperature. The slope of this surface at constant volume is given by the heat capacity of the system at constant volume and consequently always must be positive. The change of this slope with temperature is given, of course, by the temperature derivative of the heat capacity at constant volume. The slope of the curve formed by the surface and a plane at constant energy is given by

(8) J. A. Rowlinson, "Liquids and Liquid Mixtures," Academic Press, Inc., New York, N. Y., 1959, p. 19.

(9) J. H. Hildebrand and R. L. Scott, "Solubility of Nonelectrolytes," Reinhold Publ. Corp., New York, N. Y., 1950, pp. 98-100.

(10) W. G. Cutler, R. H. McMickle, W. Webb, and R. W. Schiessler, *J. Chem. Phys.*, **29**, 727 (1958).

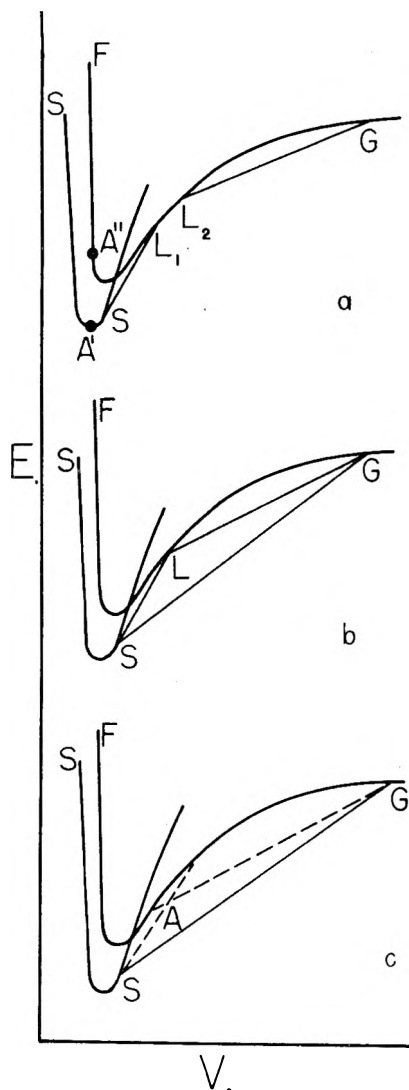


Fig. 3.—Energy-volume isotherms in the neighborhood of the triple point when the volume of the liquid is larger than that of the solid at the triple point.

$$\left(\frac{\partial T}{\partial V}\right)_E = -\frac{(\partial E/\partial V)_T}{C_V} \quad (5)$$

To the left of the minimum of the energy-volume curve,  $(\partial E/\partial V)_T$  is large and negative, while to the right of the minimum, it is smaller and positive. Consequently,  $(\partial T/\partial V)_E$  is large and positive to the left of the minimum and somewhat smaller and negative to the right of the minimum. At the point where the plane at constant energy intersects the surface at a minimum,  $(\partial T/\partial V)_E$  is zero. Such an intersection is illustrated in Fig. 2.

Vaidhyanathan<sup>11</sup> has shown from limited compressibility data for benzene, cyclohexane, iso-octane, and carbon tetrachloride that the depth of the minimum relative to the energy of the substance in the ideal gas state decreases with increase of temperature and that the volume at the minimum increases with increase of the temperature. This behavior probably is generally true for many substances but the proof of an absolute rule re-

(11) V. S. Vaidhyanathan, Ph.D. thesis, Illinois Institute of Technology, 1960.

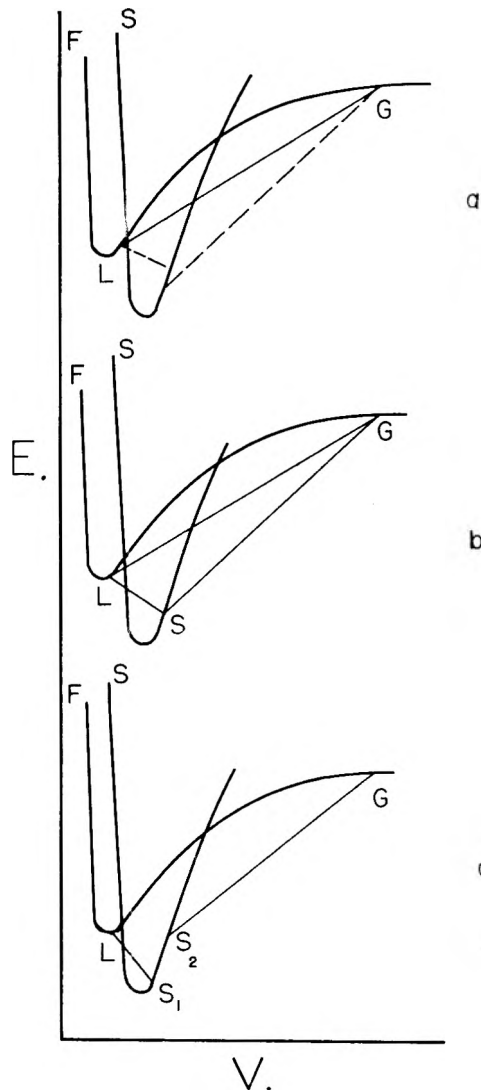


Fig. 4.—Energy-volume isotherms in the neighborhood of the triple point when the volume of the liquid is smaller than that of the solid at the triple point.

quires the knowledge of an adequate equation of state.

The surface for a solid phase has the same characteristics as the surface for the fluid phase except that the surface at extremely large volumes has no meaning for the solid phase. The curves marked SS in Fig. 3 and 4 illustrate the energy of a solid phase as a function of the volume at constant temperature.

When it is known that only one surface exists in a given range of temperature and volume, a point on the surface is an equilibrium point. However, such a surface may be extended into regions where two surfaces, one for the solid phase and the other for the fluid phase, may overlap. This is illustrated in the extreme left hand side of Fig. 3 and 4 where the curve marked SS represents the solid phase and that marked FG represents the fluid phase. Under such circumstances the phase having the lower energy presumably will be the stable phase. Thus in Fig. 3 the solid phase would be stable and in Fig. 4 the fluid phase would be

stable. Certainly this conclusion is the logical one obtained from consideration of two-phase systems which are discussed in the next section, but a general proof is not possible. The problem is illustrated in Fig. 3a at the points A'' and A'. Here the temperature and volume are the same and equation 3 would have to be satisfied if the solid phase at A' is stable in respect to the fluid phase at A''. The proof necessitates the calculation of  $(S'' - S')$  along the path A'SL<sub>2</sub>A'', but this can be done only with adequate equations of state for the two phases.

The surfaces described in this section may be called primitive surfaces in accordance with Gibbs.<sup>12</sup>

**Two-Phase Systems.**—The energy of a closed one component, two-phase system may be expressed as a function of the temperature and volume of the system. Moreover, the molar energies of the two saturated phases are also functions of the temperature and molar volumes of the saturated phases. The energy of the two-phase system at a given temperature is given by the equation

$$E = n'\bar{E}' + n''\bar{E}'' \quad (6)$$

with the conditions that

$$n = n' + n'' \quad (7)$$

and

$$V = n'\bar{V}' + n''\bar{V}'' \quad (8)$$

In these equations the non-primed quantities represent the system and the primed quantities the separate phases, the tilde is used to represent molar quantities, and  $n$  represents the number of moles. With these equations

$$\left(\frac{\partial E}{\partial V}\right)_{T,n} = \frac{\bar{E}'' - \bar{E}'}{\bar{V}'' - \bar{V}'} \quad (9)$$

The equilibrium line then is a straight line which lies within the plane at constant temperature and has a slope given by equation 9. Each end of the line will lie on a primitive surface and will designate the energy of the corresponding saturated phase. The straight lines shown in the two parts of Fig. 1 represent such lines for the equilibrium between the gas and liquid phases under two possible conditions. In Fig. 1a  $(\partial E/\partial V)_T$  is taken to be positive for the liquid phase while in Fig. 1b it is taken to be negative. Similar lines for two-phase equilibria (solid-liquid, solid-gas, and liquid-gas) are shown in Fig. 3 and 4. These latter figures are discussed more fully in the next section. It is evident in these figures that, in order to define the thermodynamic state of a two-phase, single component system completely, values must be assigned to one extensive variable, in this case the volume, in addition to the number of moles.

The problem of proving that the equilibrium conditions are satisfied may be discussed in terms of Fig. 1. The curve between L and G in Fig. 1a represents the energy of a single-phase system unstable with respect to the two-phase system. Such a system is represented at the point A'', while a two-phase system at equilibrium at the same temperature and volume is represented at the point A'. For equilibrium according to equa-

tion 2,  $T(S'' - S')$  must be less than  $(E'' - E')$ . The difference in the entropies would have to be calculated along either of the reversible paths A'LA'' or A'GA''. But this cannot be done without a suitable equation of state for the unstable states. Similar arguments would have to be used for the situation illustrated in Fig. 1b with the use of equation 3.

The situation at the point A in Fig. 1b where the one-phase curve and the two-phase line intersect presents a special case. If the point A on the curve represented a phase at equilibrium, then three phases would be at equilibrium along the line. Moreover  $\Delta E/\Delta V$  (equation 9) would have to be the same for each of the three possible phase transitions. Since such a situation has not been observed, the point A on the curve cannot represent an equilibrium point but it does represent a two-phase equilibrium point on the line.

Similar two-phase equilibrium lines can be drawn at each temperature within a certain temperature range. Such lines will produce a ruled surface which represents the energy of a two-phase system as a function of the temperature and volume. Such a surface may be called a derived surface in conformity with the nomenclature of Gibbs.<sup>12</sup> The slope of the curve formed by the intersection of the surface with a plane drawn perpendicular to the volume axis at a given volume will represent the heat capacity of the system at this constant volume. Such a heat capacity will be positive and in general larger than that of a single-phase system. It will be a discontinuous function of the temperature at the intersection of the derived surface with a primary surface. Such a discontinuity has been observed for the liquid-gas system of helium.<sup>13</sup>

**The Triple Point and Neighboring Regions.**—The molar energy and volume of each of the three phases at the triple point are different but the temperature is the same. The triple point is represented then by a triangular area which lies in the plane drawn perpendicular to the temperature axis at the triple point. Such an area is represented in Fig. 3b by the triangle SLG for the case that the molar volume of the liquid is larger than that of the solid at the triple point. A similar triangle is shown in Fig. 4b for the case in which the molar volume of the liquid is smaller than that of the solid. Each of the lines, LS, LG, and SG, represents the last line of the derived surface for the corresponding two-phase system. Because the triangular area is perpendicular to the temperature-volume plane and thus parallel to the energy axis, it is evident that two extensive variables, in this case the energy and volume of the system, must be assigned values in order to define the state of a single-component system at a triple point.

When the temperature is increased from the triple point for systems in which the molar volume of the liquid phase is greater than that of the solid phase, the solid-gas equilibrium no longer exists. There are two two-phase equilibria, solid-liquid and liquid-gas, and three single-phase equilibria

(12) J. Willard Gibbs, "Collected Works," Longmans, Green and Co., New York, N. Y., 1931, p. 36.

(13) R. W. Hill and O. V. Lounasmaa, *Phil. Trans. Roy. Soc. (London)*, **252**, 357 (1960); *J. Chem. Phys.*, **33**, 443 (1960).

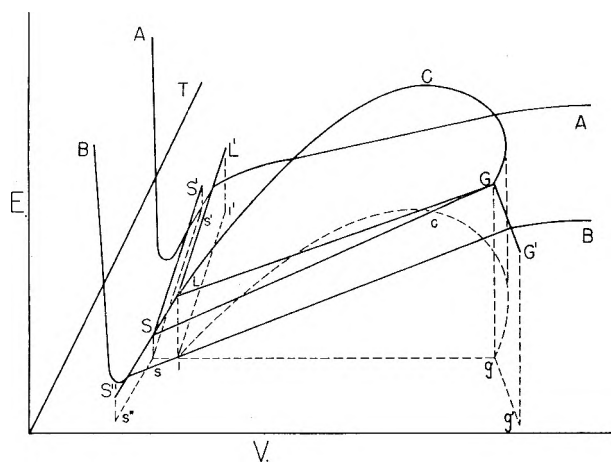


Fig. 5.—The energy-temperature-volume surface when the volume of the liquid is larger than that of the solid at the triple point.

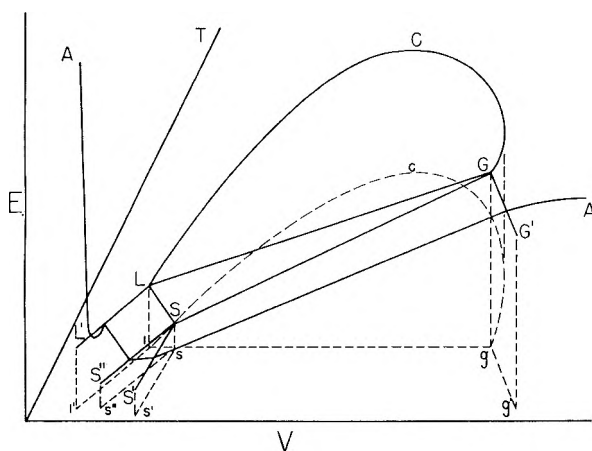


Fig. 6.—The energy-temperature-volume surface when the volume of the liquid is smaller than that of the solid at the triple point.

at such a temperature. The phases that are present in any specific case would depend upon the volume of the system. An isotherm for the conditions discussed here is illustrated in Fig. 3a. The stable isotherm is the path designated as  $SSL_1L_2G$ .<sup>14</sup> A single solid phase would be present along  $SS$ , a solid-liquid equilibrium between  $S$  and  $L_1$ , a single liquid phase between  $L_1$  and  $L_2$ , and a liquid-gas equilibrium between  $L_2$  and  $G$ . Beyond  $G$  a single gas phase would exist.

A stable liquid phase does not occur below the triple point for the same type of systems. At temperatures below the triple point, the only two-phase system is that of a solid and gas. An isotherm at such a temperature is represented in Fig. 3c along the path  $SSG$ . The dotted lines, representing possible solid-liquid or liquid-gas equilibria, are included to show how the relative position of such lines changes with temperature. They have no physical significance and, indeed, four phases would be in equilibrium at  $A$ , the point

(14) Figures 3, 4, 5, and 6 have been drawn for the case in which the energy of any liquid phase and any solid phase in equilibrium with a second phase lies on the portion of the curve for which  $(\partial E/\partial V)_T$  is positive. Other cases in which  $(\partial E/\partial V)_T$  is negative are, of course, possible. The general representation of the surfaces would be the same.

where the two lines intersect, if these lines had meaning.

Figure 4 represents a similar set of isotherms for temperatures above (a), at (b), and below (c) the triple point for systems in which the molar volume of the liquid is less than that of the solid at the triple point. The stable isotherm for temperatures above the triple point is along the path  $FLG$ . The liquid phase is stable from  $F$  to  $L$ , the liquid-gas system is stable along the line  $LG$ , and the gas phase is stable beyond  $G$ . At the temperature of the triple point, a liquid phase is stable from  $F$  to  $L$  and a gas phase beyond  $G$ . Any system represented by a point within the triangle  $LSG$  is a three-phase system. At temperatures below the triple point, the stable isotherm is designated by the path  $FLS_1S_2G$ . A liquid phase is stable from  $F$  to  $L$ , the liquid-solid equilibrium is present along the line  $LS_1$ , a single solid phase is stable from  $S_1$  to  $S_2$ , the solid-gas equilibrium is present along the line  $S_2G$ , and the gas phase is stable beyond  $G$ . The intersections of the various curves and lines have no meaning in these diagrams and are not equilibrium points. The dotted two-phase lines in Fig. 4a are included to show again how such lines may move relative to each other as the temperature is changed.

**The Energy Surface.**—With the foregoing description of the relationships of the energy with the temperature and volume, the general features of the energy-temperature-volume surface can be described. Figure 5 represents the case in which the molar volume of the liquid is larger than that of the solid at the triple point and Fig. 6 the case in which the molar volume of the liquid is smaller than the solid. The primitive surface for the solid phase lies to the left of the two curves<sup>15</sup>  $S'S'S'$  in Fig. 5 and is bounded by the same two curves in Fig. 6. The primitive surface for the fluid phase lies above the curves designated by  $L'LCGG'$  in each figure. The derived surface for the gas-liquid systems is bounded by the curve  $LCG$  and the straight line  $LG$ . The derived surface for solid-liquid systems lies within the curves  $S'SLL'$  in Fig. 5 and  $S'S'L'L'$  in Fig. 6. The derived surface for solid-gas systems lies within the curve  $S'S'S$ , the line  $SG$ , and the curve  $GG'$  in Fig. 5. In Fig. 6 the first of these curves is designated  $S'S$ . In each diagram, systems at the triple point are located in the vertical triangular area  $SLG$ . Isotherms described in Figs. 3a and 3c also are drawn in Fig. 5 and designated as  $AA$  and  $BB$ . The isotherm described in Fig. 4c is drawn in Fig. 6 and labeled  $AA$ .

The projection of the intersections of the primitive and derived surfaces onto the temperature-volume plane has been drawn with dashed lines. Small letters have been used to label the curves rather than capital letters; otherwise the designations are the same. The areas bounded by the curves represent the corresponding systems described in the previous paragraph. If the Helmholtz free energy-temperature-volume or the

(15) The intersections of the primitive and derived surfaces, except for the liquid-gas system, have been drawn as straight lines in these diagrams for convenience. They would not be straight lines necessarily for any actual system.

entropy-temperature-volume surfaces were developed, the intersections of the primitive and derived surfaces would have to be similar to those described in this paper because the projection of such surfaces onto the temperature-volume plane would have to be identical.

## AQUEOUS SOLUBILITY AND THE GAS-HYDRATES. THE METHANE-WATER SYSTEM<sup>1</sup>

By D. N. GLEW

*Contribution No. 56 from the Exploratory Research Laboratory, Dow Chemical of Canada, Limited, Sarnia, Ontario, Canada  
Received October 13, 1961*

A model for aqueous solution consistent with the nature of the hydrogen-bonded liquid water solvent is formulated and developed with particular reference to the energetic and volumetric properties of aqueous methane. The standard enthalpy functions for methane hydrate equilibria are derived and show the hydrate to be  $\text{CH}_4 \cdot 5.75\text{H}_2\text{O}$ . A correlation at  $0^\circ$  is given between the heat of hydrate decomposition to ice and the heat of solute evolution from aqueous solution for methane and other hydrate-formers, which thermochemically requires that the heat of melting of these gas hydrates  $M \cdot n\text{H}_2\text{O}$  is equal to the heat of melting of  $n$  mole of ice.

### Introduction

The tetrahedral nearest neighbor coordination of water exhibited in ices I, II, and III, cubic ice and in the solid gas hydrates,<sup>2,3</sup> together with the small energy changes for the high pressure ice transitions, indicate that the water molecule invariably exerts a tetrahedrally directed force field in which the four hydrogen bonds with nearest neighbors do not rupture<sup>4</sup> and are not critically sensitive to angular distortions as large as  $31$  to  $-39^\circ$  from the regular tetrahedral angle. The persistence of general three-dimensional tetrahedral fourfold coordination of nearest neighbors in liquid water postulated by Bernal and Fowler<sup>5</sup> has received support from later X-ray scattering<sup>6,7</sup> and Raman spectral measurements,<sup>8,9</sup> which may be interpreted<sup>10</sup> in terms of complete tetrahedral fourfold coordination of nearest water neighbors at lower temperatures with thermal distortion and bending of hydrogen bonds  $\pm 26^\circ$  without significant rupture.

Eley<sup>11</sup> presented an aqueous solubility theory for the inert gases, consistent with the Bernal and Fowler water model, in which the water at low temperatures was assumed to occupy quasi-lattice sites maintaining tetrahedral coordination and where the solute occupied interstitial sites or cavities formed at low energy expenditure within the hydrogen-bonded solvent water structure. In this way Eley was able to physically interpret (i) the invariably positive enthalpy of transfer  $\Delta H_2^0$  ( $l_1 \rightarrow g$ ) of aqueous solute to the gas phase at lower

temperatures, (ii) the anomalously large positive entropies of transfer  $\Delta S_2^0$  ( $l_1 \rightarrow g$ ) predominantly responsible for the poor solvent properties of water for weakly-interacting solutes, and (iii) the very large solute molar heat capacities responsible for the large negative heat capacity changes  $\Delta Cp_2^0$  ( $l_1 \rightarrow g$ ) characteristic of aqueous solubility. Frank and Evans<sup>12</sup> considered the large  $\Delta S_2^0$  ( $l_1 \rightarrow g$ ) values in terms of generalized iceberg formation of the water next to the solute and the large aqueous heat capacities deriving from the energy requirement to break down such structures at higher temperatures. Powell and Latimer<sup>13</sup> showed that the addition of weakly-interacting solutes to water decreased the free-volume of the solution which was interpreted in the sense that the presence of a solute reduces the librational freedom of the water, or that the water molecules are more restricted when adjacent to the weakly-interacting solutes.

Independent evidence regarding the nature of aqueous solvation was deduced from reaction kinetics<sup>14</sup> and consequent solubility work<sup>15</sup> independently and simultaneously indicated<sup>16</sup> that the nature of the water solvent surrounding weakly interacting aqueous solutes should be likened geometrically to those coordination polyhedra experimentally observed<sup>2,3</sup> in the solid gas-hydrates. Such water polyhedra containing no rupture hydrogen bonds provide a natural interpretation of the low energy cavities of Eley's solution theory,<sup>11</sup> consistent with a three-dimensionally hydrogen-bonded liquid water phase.<sup>5,10</sup> The obvious cooperative alignment of the water molecules within such polyhedra or hydration shells likewise provides an interpretation of the larger entropy losses characteristic of aqueous solutes and the reduced librational freedom<sup>13</sup> of the water adjacent to the solute, in that the preferred regular

(1) Presented at Professor J. H. Hildebrand's 80th Birthday Symposium, Lewis Hall, University of California, Berkeley, September 13, 1961.

(2) (a) W. F. Claussen, *J. Chem. Phys.*, **19**, 259, 662, 1425 (1951);

(b) L. Pauling and R. E. Marsh, *Proc. Natl. Acad. Sci.*, **38**, 112 (1952).

(3) M. v. Stackelberg and H. R. Müller, *Z. Elektrochem.*, **58**, 25 (1954).

(4) R. L. McFarlan, *J. Chem. Phys.*, **4**, 60, 253 (1936).

(5) J. D. Bernal and R. H. Fowler, *ibid.*, **1**, 515 (1933).

(6) J. Morgan and B. E. Warren, *ibid.*, **6**, 666 (1938).

(7) C. L. van Panthaleon van Eck, H. Mendel, and J. Fahrenfort, *Proc. Roy. Soc. (London)*, **A247**, 472 (1958).

(8) M. Magat, *Trans. Faraday Soc.*, **33**, 114 (1937).

(9) E. F. Gross, "Hydrogen Bonding," ed. D. Hadzi, Pergamon Press, London, 1959, p. 203.

(10) J. A. Pople, *Proc. Roy. Soc. (London)*, **A205**, 163 (1951).

(11) D. D. Eley, *Trans. Faraday Soc.*, **35**, 1281 (1939).

(12) H. S. Frank and M. W. Evans, *J. Chem. Phys.*, **13**, 507 (1945).

(13) R. E. Powell and W. M. Latimer, *ibid.*, **19**, 1139 (1951).

(14) D. N. Glew and E. A. McElwyn-Hughes, *Proc. Roy. Soc. (London)*, **A211**, 254 (1952).

(15) D. N. Glew and E. A. McElwyn-Hughes, *Discussions Faraday Soc.*, No. **15**, 150 (1953).

(16) W. F. Claussen and M. F. Polglase, *J. Am. Chem. Soc.*, **74**, 4817 (1952).

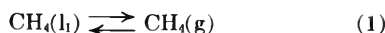
TABLE I  
STANDARD ENTHALPY AND HEAT CAPACITY CHANGES FOR METHANE EVOLUTION FROM AQUEOUS SOLUTION

$t, ^\circ\text{C.}$	Winkler-Morrison and Billet		Claussen and Polglase-Culberson and McKetta		Four sets combined		Eley model
	$\Delta H_2^0,$ cal./mole	$\Delta Cp_2^0,$ cal./deg.-mole	$\Delta H_2^0,$ cal./mole	$\Delta Cp_2^0,$ cal./deg.-mole	$\Delta H_2^0,$ cal./mole	$\Delta Cp_2^0,$ cal./deg.-mole	$\Delta Cp_2^0,$ cal./deg.-mole
0	4690	-61.6	4491	-57.0	4621	-60.7	-62.7
25	3206	-59.8	3124	-52.4	3173	-55.0	-57.8
50	1833	-55.3	1872	-47.8	1869	-49.3	-52.1
75	571	-50.6	735	-43.2	707	-43.6	-45.7
100	-580	-43.8	-287	-38.6	-312	-37.9	-38.5
125	...	...	-1194	-34.0	-1188	-32.2	-30.7
$\frac{d\Delta Cp_2^0}{dT}$ (cal./deg. <sup>2</sup> -mole)	+ 0.18		+ 0.18		+ 0.23		+0.18 to 0.33

tetrahedral hydrogen-bond forming directions of the water molecule (ice I, cubic ice) force alignment and increase orientation of those water molecules adjacent to the solute in maintaining their three hydrogen bonds with nearest water neighbors also adjacent to the solute, the fourth bonds radially directed away from the solute maintain bonding of the hydration shell with the external bulk water. The central attractive forces between the solute and the surrounding hydration shell further cooperatively stabilize the water members in a manner tending to promote intra-shell hydrogen bonding and the allied reduction of hydration water librational freedom. In no sense is it considered that the water molecules adjacent to the solute are permanently immobilized or rigid as in solid structures, but rather as being subject to greater orientational constraints permitting reduced hydrogen bond bending as compared with those water molecules within the bulk liquid.

**Solubility of Methane in Water.**—The implications of this aqueous solution model will be examined with reference to the quantitative values for the thermodynamic functions for the solubility and the gas hydrate equilibria of the methane-water system.

Analysis of the unit pressure Henry law constants  $H_2$  for the aqueous methane solubility equilibrium



characterized by the generalized standard thermodynamic function change denoted  $\Delta X_2^0(l_1 \rightarrow g)$ , showed that the measurements of Winkler<sup>17</sup> between 0 and 50° agreed to within 0.22% with those of Morrison and Billet,<sup>18</sup> while those measurements of Culberson and McKetta<sup>19</sup> and of Claussen and Polglase<sup>16</sup> again agree closely with each other, but show a 4.5% greater methane solubility than the former authors'. The solubility data thus were fitted with respect to temperature variation equations in pairs and finally all data were combined. In obtaining a true representation of the variation of aqueous methane solubility with temperature it was necessary to use an equation of the type  $\log H_2 = A/T + B \log T + CT + D$ , which implies that  $\Delta Cp_2^0(l_1 \rightarrow g)$  is a linear function of absolute temperature  $T$ .

In Table I are presented the standard enthalpy,

(17) L. W. Winkler, *Ber.*, **34**, 1408 (1901).

(18) T. J. Morrison and F. Billet, *J. Chem. Soc.*, 3814 (1952).

(19) O. L. Culberson and J. J. McKetta, Jr., *J. Petrol. Technol. Trans. A.I.M.E.*, **192**, 223 (1951).

heat capacity, and temperature derivative of heat capacity changes for reaction 1 as derived by standard methods<sup>20</sup> from the solubility temperature equations for the Winkler-Morrison and Billet measurements, for the Claussen and Polglase-Culberson and McKetta measurements, and for all data sets combined. In the final column of Table I are shown theoretical values for  $\Delta Cp_2^0(l_1 \rightarrow g)$  calculated by Eley's method<sup>11</sup> using the equation

$$\Delta Cp_2^0(l_1 \rightarrow g) = R - C_c = R - \frac{d}{dT} \left[ \frac{\alpha_1^{11}}{\beta_1^{11}} TV_2 \right]^{11} \quad (2)$$

which had been derived assuming that the aqueous methane heat capacity is equal to the sum of that heat capacity  $Cv_2^g$  due to the methane inside the water cavities considered as square wells plus the heat capacity  $C_c$  necessary to maintain the cavity volume  $V_2^{11}$  against thermal collapse.  $\alpha_1^{11}$  and  $\beta_1^{11}$  are the respective coefficients of thermal expansion and compressibility of the water solvent<sup>21</sup> and  $V_2^{11}$  is the aqueous methane molar volume derived in the next section.

The measure of agreement between the standard enthalpy changes and their temperature derivatives in Table I obtained from the two independent solubility data sets allows confidence to be placed in the values for the heat capacity changes  $\Delta Cp_2^0(l_1 \rightarrow g)$  and in the reality of an experimentally significant change of  $\Delta Cp_2^0(l_1 \rightarrow g)$  with temperature, which is demonstrated here for the first time for aqueous solute transfer to the gas phase. The excellent agreement of the Eley model values for both the absolute value for  $\Delta Cp_2^0(l_1 \rightarrow g)$  and for its temperature derivative gives a *posteriori* support for the model which indicates that the anomalously large aqueous solute heat capacities derive predominantly from the energy requirement to maintain the solute cavity against thermal breakdown.

The model similarly shows that  $\frac{d}{dT} \Delta Cp_2^0(l_1 \rightarrow g)$  should be positive for all weakly-interacting aqueous solutes having positive aqueous molar volumes.

**Molar Volume of Aqueous Methane.**—The high pressure aqueous methane solubility measurements of Culberson and McKetta<sup>19</sup> were treated by standard thermodynamic methods<sup>22</sup> to yield the aqueous

(20) D. N. Glew and R. E. Robertson, *J. Phys. Chem.*, **60**, 332 (1956).

(21) N. E. Dorsey, "Properties of Ordinary Water-Substance," Reinhold Publ. Corp., New York, N. Y., 1940.

(22) I. R. Krichevsky and S. S. Kasarnovsky, *J. Am. Chem. Soc.*, **57**, 2168 (1935).



methane molar volumes, denoted  $V_2^1$ , shown with standard errors in Table II. These molar volumes fitted as a linear function of  $T$  give a methane molar volume  $V_2^1 = 34.37 \pm 0.54$  ml. at  $0^\circ$  and an aqueous methane thermal expansion coefficient  $\alpha_2^1 = 1180 \pm 190 \times 10^{-6} \text{ deg.}^{-1}$ .

The third and fourth columns in Table II show the aqueous methane molar volumes, denoted  $\phi_2^1$ , as directly determined by dilatometry<sup>23</sup> and by densitometry,<sup>24</sup> which, excepting one low value, are 1.6 ml. greater than the  $V_2^1$  values, this difference being significantly larger than the experimental errors. Kritchevsky and Iliinskaya<sup>23</sup> were first to note this difference for a number of other weakly-interacting aqueous solutes and have provided a theoretical explanation for the effect.

TABLE II

COMPARISON OF AQUEOUS METHANE MOLAR VOLUMES			
$t$ , °C.	$V_2^1$ , ml./mole <sup>19</sup>	$\phi_2^1$ , ml./mole <sup>23</sup>	$\phi_2^1$ , ml./mole <sup>24</sup>
0	$(34.4 \pm 0.5)$	$36 \pm 0.5$	
16.8			33.2
23.0			36.3
25	$35.6 \pm 0.4$	$37 \pm 0.5$	
29.1			38.0
35.1			38.2
37.8	$35.4 \pm 0.4$		
50		$38 \pm 0.5$	
71.1	$37.4 \pm 0.8$		
104.4	$40.3 \pm 0.9$		
137.8	$39.4 \pm 0.5$		

A simpler alternative is suggested here, consistent with our solution model. Since the  $\phi_2^1 - V_2^1$  difference is observed in other aqueous systems it is reasonably assumed to derive as a general effect from the water solvent rather than from any special nature of the solute species. Apparently the  $\phi_2^1$  values were derived<sup>23,24</sup> using the pure water molar volume  $V_1^0$  for the water in the dilute methane solutions, the difference between this and the water partial molar volume  $V_1^1$  having been neglected. When the volume of aqueous methane solutions is expressed in terms of the partial molar quantities, the dilatometric measurements<sup>23,24</sup> and solubility pressure coefficient measurements<sup>19</sup> are consistent provided that

$$V_1^1 = V_1^0 + (\phi_2^1 - V_2^1) n_2/n_1 \quad (3)$$

that is, the water partial molar volume  $V_1^1$  expands linearly with the solute mole ratio of the solution. Such an increase of water molar volume has been demonstrated<sup>25</sup> for aqueous ethyl alcohol and is absent for aqueous hydrogen peroxide; this locates the expansion in the vicinity of the weakly-interacting ethyl group.

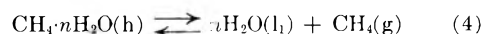
Accordingly our model for the dissolution of methane in water at  $0^\circ$  is considered as involving (i) interstitial expansion of  $V_2^1 = 34.37$  ml./mole within the water to form cavities occupied by the methane solute, (ii) this cavity formation being associated with the concomitant 1.6 ml. water

expansion arising from the orientation and reduction of bending freedom of the hydration shell water.

The presence of the solute within the water structure at lower temperatures thus is visualized as orienting the hydration shell members and, through radial hydrogen bonding, the shell's near water neighbors, in the sense of reducing the average hydrogen-bond bending from the  $\pm 26^\circ$  characteristic<sup>10</sup> of the bulk to some smaller value, this reduced bending moving second nearest water neighbors further away thereby increasing the water molar volume<sup>25</sup> and reducing the water free-volume.<sup>13</sup>

Evidence further supporting a more ordered hydration shell in the vicinity of weakly-interacting solutes is provided by (i) the increase<sup>25</sup> of maximum density temperature for water by addition of small quantities of ethyl alcohol the order in the vicinity of the ethyl group being enhanced, (ii) the increased<sup>26</sup> viscosity of aqueous solutions of benzene and of diethyl ether above that for pure water, these liquid solutes themselves being less viscous than water, and (iii) the decreased<sup>27</sup> compressibility of aqueous diethyl ether solution below the value for pure water, the solute decreasing the bending angles of adjacent water, compression requiring increase of the water bending angles.

**Methane Hydrate-Water-Gas Equilibrium.**—Examination of the methane hydrate<sup>28-32</sup> equilibrium constants for the reaction



characterized<sup>33</sup> by the thermodynamic functions  $\Delta X^0(h \rightarrow l, g)$  showed that no set of hydrate equilibrium measurements with water yet exists of sufficient accuracy or over a sufficiently large temperature range to justify evaluation of more than the standard enthalpy change  $\Delta H^0(h \rightarrow l, g)$  appropriate to the average data temperature. The hydrate equilibrium measurements were treated by standard methods developed earlier<sup>33</sup> adapted to higher pressure systems in which corrections for gas phase fugacity, gas and solution phase compositions, and condensed phase volumes have been included. The equilibrium constants were fitted in sets as functions of temperature to yield average  $\Delta H^0(h \rightarrow l, g)$  values which have been reduced to  $0^\circ$  using<sup>33</sup>  $\Delta Cp^0(h \rightarrow l, g) = +48.2 \text{ cal/deg.-mole}$ .

The equilibrium measurements of Villard<sup>28</sup> yield a standard enthalpy change  $\Delta H^0(h \rightarrow l, g) = 12,896 \text{ cal./mole at } 0^\circ$ ; those of Roberts, Browncombe, and Howe,<sup>29</sup> 12,818; Deaton and Frost,<sup>30</sup> 13,093; McLeod and Campbell,<sup>31</sup> 2,420; the four measurements of Kobayashi and Katz<sup>32</sup> were over insufficient temperature range to justify an independent

(26) H. M. Chadwell, *J. Am. Chem. Soc.*, **48**, 1912 (1926).

(27) T. W. Richards and H. M. Chadwell, *ibid.*, **47**, 2283 (1925).

(28) P. Villard, *Compt. rend.*, **107**, 395 (1888).

(29) O. L. Roberts, E. R. Browncombe, and L. S. Howe, *Oil and Gas J.*, **38**, No. 12, 37 (1940).

(30) W. M. Deaton and E. M. Frost, Jr., "Gas Hydrates and their Relation to the Operation of Natural-Gas Transmission Lines," U.S. Bureau of Mines Monograph 8, 1946.

(31) H. O. McLeod, Jr., and J. N. Campbell, *J. Petrol. Technol.*, **13**, 590 (1961).

(32) R. Kobayashi and D. L. Katz, *J. Petrol. Technol. Trans. A.I.-M.E.*, **186**, 66 (1949).

(33) D. N. Glew, *Can. J. Chem.*, **38**, 208 (1960).

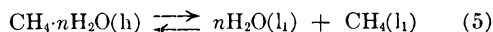
(23) I. Kritchevsky and A. Iliinskaya, *Acta Physicochim. U.R.S.S.*, **20**, 327 (1945).

(24) W. L. Masterson, *J. Chem. Phys.*, **22**, 1830 (1954).

(25) A. G. Mitchell and W. F. K. Wynne-Jones, *Discussions Faraday Soc.*, No. **15**, 161 (1953).

enthalpy change evaluation. These values of  $\Delta H^0(h \rightarrow l, g)$  were weighted in direct proportion to the number of measurements to yield a mean value and standard error  $\Delta H^0(h \rightarrow l, g) = 12,830 \pm 140$  cal./mole at  $0^\circ$ .

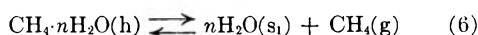
**Methane Hydrate-Water Equilibrium.**—The equilibrium reaction



is representative of methane hydrate melting to liquid water and aqueous methane and is characterized by the thermodynamic functions  $\Delta X^0(h \rightarrow l_1)$ . Reaction 5 also may be considered the difference of reaction equations 4 and 1 and the function  $\Delta X^0(h \rightarrow l_1)$  the difference  $\Delta X^0(h \rightarrow l, g) - \Delta X_2^0(l_1 \rightarrow g)$ .

Each of the hydrate equilibrium measurements<sup>28-32</sup> with water was evaluated to yield the equilibrium constant for (5) and these equilibrium constants were fitted in sets as functions of temperature. The standard enthalpy changes  $\Delta H^0(h \rightarrow l)$  from each data set were derived and averaged as previously to yield the standard enthalpy change  $\Delta H^0(h \rightarrow l_1) = 8228 \pm 130$  cal./mole for methane hydrate melting to aqueous solution at  $0^\circ$ .

**Methane Hydrate-Ice-Gas Equilibrium.**—The methane hydrate equilibrium measurements<sup>30</sup> with ice for the reaction



characterized by the thermodynamic functions  $\Delta X^0(h \rightarrow s_1, g)$ , were treated by standard methods<sup>33</sup> to yield the equilibrium constants for (6). In combination with<sup>33</sup>  $\Delta Cp^0(h \rightarrow s_1, g) = -2$  cal./deg.-mole the standard enthalpy change for hydrate decomposition to ice and gaseous methane is  $\Delta H^0(h \rightarrow s_1, g) = 4553 \pm 102$  cal./mole at  $0^\circ$ .

The difference of reaction equations 4-6 represents the fusion reaction of  $n$  mole of ice to yield  $n$  mole of water, while correspondingly the difference  $\Delta H^0(h \rightarrow l, g) - \Delta H^0(h \rightarrow s_1, g) = 8277 \pm 172$  cal. at  $0^\circ$  is the standard enthalpy of fusion<sup>21</sup> of  $n$  mole of ice and is  $n1435.7$  cal., whence the hydrate formula number  $n = 5.765 \pm 0.120$ . This experimental value for  $n$  agrees with the ideal crystallographic value 5.75 expected from structural work.<sup>2a,3</sup> The cavities within the methane hydrate lattice at  $0^\circ$  thus are indicated by presently available data to be 99.7% occupied by methane with a standard error of  $\pm 2.1\%$ , in contrast to the 83% occupancy predicted theoretically.<sup>34,35</sup>

**Comparison of Aqueous Solution and Gas Hydrate Properties.**—Comparison of the heat requirement (8277 cal.) for the melting of  $n$  mole of ice to water with  $\Delta H^0(h \rightarrow l_1) = 8228$  cal. at  $0^\circ$  for the melting of solid  $\text{CH}_4 \cdot n\text{H}_2\text{O}$  to liquid aqueous methane reveals that the presence of methane in the hydrate melting reaction little affects the heat requirement for melting of  $n$  mole of solid water to the liquid state.

The thermochemically equivalent comparison of  $\Delta H^0(h \rightarrow s_1, g) = 4553$  cal. for reaction 6 with that  $\Delta H_2^0(l_1 \rightarrow g) = 4621$  cal. for reaction 1 at  $0^\circ$  sug-

gests that the interaction energy of aqueous methane with its hydration shell in solution is equal to that of methane with its solid coordination polyhedra in the hydrate. This equality arises from environmental similarity in respect to coordination and spatial geometry of the solution hydration shells with those completely hydrogen-bonded hydrate polyhedra. Since the aqueous methane molar volume 34.37 ml. at  $0^\circ$  corresponds closely with that of the 20 coordinated sites of both the structure I and II hydrate lattices<sup>3</sup> and is significantly smaller than the 40-55 ml. volume range<sup>2b,3</sup> for the 24 coordinated sites it is inferred that aqueous methane is 20 coordinated by water at lower temperatures.

To ascertain the more general validity of the solution model already applied to methane, values for  $\Delta H_2^0(l_1 \rightarrow g)$  and  $\Delta H^0(h \rightarrow s_1, g)$  have been derived from the literature for other hydrate-formers and are presented in Table III. The second column under C gives the aqueous solution hydration numbers assigned from the known gas hydrate structures.<sup>2,3</sup> All  $\Delta H_2^0(l_1 \rightarrow g)$  values have been obtained from the earlier work,<sup>15</sup> except those values for ethane and propane,<sup>18</sup> sulfur dioxide,<sup>36</sup> and ethyl chloride,<sup>37</sup> which have been derived from primary data. The errors on the solubility enthalpy changes at  $0^\circ$  are assessed at  $\pm 200$  cal., except for ethyl chloride where the error is  $\pm 500$  cal. The  $\Delta H^0(h \rightarrow s_1, g)$  values have been derived from the hydrate measurements indicated, hydrogen sulfide<sup>38</sup>; chlorine, bromine, and sulfur dioxide<sup>39</sup>; ethane and propane.<sup>30</sup> The corrected enthalpy change values given by von Stackelberg<sup>40</sup> have been used for methyl bromide, methyl iodide, and ethyl chloride. The errors on the hydrate enthalpy changes are larger and are assessed at  $\pm 500$  cal.

TABLE III  
ENTHALPY CHANGE FOR SOLUBILITY AND HYDRATE EQUILIBRIA

Gas	Temperature $0^\circ$		
	C solution	$\Delta H_2^0(l_1 \rightarrow g)$ , cal./mole	$\Delta H^0(h \rightarrow s_1, g)$ , cal./mole
CH <sub>4</sub>	20	4621	4553
H <sub>2</sub> S	20	5140	5550
C <sub>2</sub> H <sub>6</sub>	24	5560	5850
Cl <sub>2</sub>	24	6180	6500
SO <sub>2</sub>	24	7420	7700
CH <sub>3</sub> Br	24	7390	8100
Br <sub>2</sub>	24	8750	8300
C <sub>3</sub> H <sub>8</sub>	28	6860	6300
CH <sub>3</sub> I	28	8500	7300
C <sub>2</sub> H <sub>5</sub> Cl	28	8400	8700

The correlation in Table III thermochemically necessitates, as for methane, that these larger, more polarizable, and dipolar solutes do not significantly change the enthalpy of hydrate melting from that value for the melting of the equivalent  $n$  mole of ice. Thus in the same way as the hydrate-former stabil-

(36) C. E. Maas and O. Maass, *J. Am. Chem. Soc.*, **50**, 1352 (1928).

(37) N. Nicloux, *Znn. physiol. physicochim. biol.*, **5**, 434 (1929).

(38) F. E. C. Scheffer and G. Meyer, *Verlag Gewone Vergader. Afdel. Naturk. Koninkl. Ned. Akad. Wetenschap.*, **27**, 1104, 1305 (1919).

(39) H. W. B. Rozzeboom, *Rec. trav. chim.*, **4**, 65 (1885).

(40) M. v. Stackelberg, *Naturwiss.*, **36**, 359 (1949).

(34) J. H. van der Waals and J. C. Platteeuw, "Advances in Chemical Physics," Vol. II, ed. I. Prigogine, Interscience Publishers Inc., New York, N. Y., 1959, p. 1.

(35) D. N. Glew, *Nature*, **184**, 545 (1959).

izes the more open hydrogen-bonded solid hydrate lattices, so these aqueous solutes stabilize and orient their hydration shells in aqueous solution.

In conclusion it would appear just as liquid water at lower temperatures has been considered a broken-down ice-like (not necessarily ice I-like) structure maintaining short range order through fourfold hydrogen-bonding of water nearest neigh-

bors, so may aqueous solutions of non-hydrogen-bonding non-electrolytes be considered as consisting of individually hydrated solute species, in which the hydration shell adjacent to the solute contains no ruptured hydrogen bonds and can be likened to broken-down gas-hydrate type polyhedra maintaining orientational short range order through intra-shell hydrogen-bonding.

## ON THE RELATION BETWEEN CRYSTALLIZATION RATE AND LIQUID STRUCTURE

BY DAVID TURNBULL

*General Electric Research Laboratory, Schenectady, New York*

*Received October 13, 1961*

Most liquids, including many which crystallize to close-packed structures, exhibit, when mote-free, a high resistance to the initiation of crystallization even though the crystallization front, once formed, propagates at a very high velocity. The implications of this behavior to the validity of various models for liquids are discussed. Also the conditions for glass-formation, the knowledge on the interior stability of superheated crystals, and the relation between crystal growth rate and viscosity for various types of liquids are reviewed.

In connection with investigations made by him and his associates<sup>1-3</sup> on the crystallization rate of liquid white phosphorus, Professor Hildebrand pointed out that the crystallization behavior of simple liquids has important implications concerning the validity of some models for the structure of liquids. In view of this and the author's own interest in the subject it seems appropriate to try to review the knowledge on the relation of the crystallization rate of pure liquids to the arrangement and structure of the constituent molecules.

Actually in the light of some common conceptions of liquid structure the crystallization behavior of simple liquids exhibits some striking features. Perhaps the most striking feature is the extraordinary resistance of these liquids to the initiation of crystallization even though the crystallization front once formed propagates at a very high velocity. For example, the rate of initiation of crystallization in mote-free metallic liquids is detectable only if the undercooling exceeds 10 to 30%, depending on the metal, of the thermodynamic crystallization temperature,  $T_m$ . Further some liquids composed of structurally simple molecules, even though they are very fluid at  $T_m$ , can be undercooled to the glassy state. In marked contrast with this behavior the propagation velocity of the crystallization front in these substances is at least as large as expected from the molecular mobility indicated by the liquid-state fluidity and self-diffusion coefficient. This behavior and what it seems to suggest about liquid state models are discussed more fully in what follows.

To begin the mode of crystallization of a pure liquid should be recalled. Thermodynamically

this crystallization is a first-order transition and it occurs, even at wide departures from equilibrium, by a process of nucleation and growth; that is, it begins at and propagates from certain centers, all reaction occurring at crystal-liquid interfaces. To describe the rate of crystallization then two constants are needed: the frequency of appearance (nucleation),  $I$ , of crystallization centers and the rate,  $u$ , of propagation of the crystal-liquid interface from these centers.

**Crystal Growth Rate.**—Experience indicates that in many instances the rate of growth of crystals into undercooled liquids is proportional to the liquid state fluidity,  $\phi$ . However, to establish a theoretical relation<sup>4</sup> between  $u$  and  $\phi$  some important assumptions must be made. First we suppose that the transfer of a molecule from the liquid to the crystal occurs in the following two steps: (1) reorientation of the molecule to a position favorable for the second step which is (2) the incorporation of the molecule into the crystal. Assuming that step 2 can occur only at a certain fraction,  $\alpha$ , of the surface sites and that the reaction rate at these sites is governed by the reorientation process (1) the following expression for  $u$  is obtained<sup>5</sup>

$$u = \frac{\alpha D_u}{a} [1 - \exp(\Delta g/kT)] \quad (1)$$

where  $\Delta g$  is the molecular free energy change,  $a$  is the molecular displacement, and  $D_u$  is the kinetic constant (in units of distance<sup>2</sup>/time) for the process. When the molecules are structurally complex the molecular reorientation step (1) may require motions very similar to those which are necessary for liquid state self-diffusion. If we assume that  $D_u$  actually is identical with the liquid state self-diffusion coefficient,  $D$ , and that  $D$  and the fluidity

(1) J. H. Hildebrand and G. J. Rotariu, *J. Am. Chem. Soc.*, **73**, 2524 (1951).

(2) R. E. Powell, T. S. Gilman, and J. H. Hildebrand, *ibid.*, **73**, 2525 (1951).

(3) J. H. Hildebrand, (a) *Discussions Faraday Soc.*, No. 15, 9 (1953); (b) "Growth and Perfection of Crystals," edited by Doremus, Roberts, and Turnbull, John Wiley & Sons, New York, N. Y., 1958, pp. 310-318.

(4) For derivation and references to older literature, see references 5 and 6.

(5) W. B. Hillig and D. Turnbull, *J. Chem. Phys.*, **24**, 914 (1956).

(6) D. Turnbull and M. H. Cohen, "Modern Aspects of the Vitreous State," edited by J. D. Mackenzie, Butterworths, London, 1960, pp. 38-62.

are related by the Stokes-Einstein equation, the connection between  $u$  and  $\phi$  can be established

$$u = \frac{\alpha k T \phi}{3 \pi a d} [1 - \exp(\Delta g / k T)] \quad (2)$$

where  $d$  is the average diameter of the molecule.

Not enough is understood about the nature of the liquid-crystal interface to evaluate  $\alpha$ . If it is assumed that molecules can be incorporated only at the edges of steps formed by screw dislocations emergent in the crystal surface,  $\alpha$  should increase approximately linearly with the undercooling,  $\Delta T$ . This assumption leads at small undercooling (so that  $kT \gg |\Delta g|$ ) to the relation obtained by Hillig and the author<sup>5</sup>

$$u = \left(\frac{\Delta s}{2\pi}\right)^2 \frac{(\Delta T)^2 \phi}{v d \sigma} \quad (3)$$

where  $v$  is the molecular volume,  $\Delta s$  is the molecular entropy of crystallization, and  $\sigma$  is the free energy/area of the step edges.

In experience it often is difficult to specify  $\Delta T$  at the crystal-liquid interface because of the heating due to the liberation of the heat of crystallization during growth. If the growth rate is governed entirely by the rate of flow of heat away from the moving interface the crystal will assume a form, *e.g.*, of a spike or blade, which facilitates this process. In this case Fisher<sup>7</sup> showed by a simple analysis that the velocity of the leading edge, of optimum form, of the crystal should be given by

$$u = \frac{\kappa (\Delta T)^2}{4 \pi T \sigma} \quad (4)$$

where  $\kappa$  is the thermal conductivity of the undercooled liquid and  $\Delta T$  is now the *nominal* undercooling; *i.e.*, the difference between  $T_m$  and the temperature of the undercooled liquid far from the interface. Thus a  $(\Delta T)^2$  growth law, which was found by Powell, Gilman, and Hildebrand<sup>2</sup> and others,<sup>5,8</sup> could arise in at least two different ways; *i.e.*, either by heat flow control or by the operation of a dislocation mechanism.

**Growth in Molecularly Complex Liquids.**—The observed velocities of crystal growth in these liquids are far below the limiting values calculated from the Fisher equation. Further for those liquids having high viscosities the calculated difference in temperature between the crystallization front and the body of the liquid is negligible. Thus the results for these systems should be suitable for testing the growth velocity-fluidity relation (eq. 2 and 3). However, in this testing it should be recognized that the effects of impurity traces and crystal-interface orientation on the crystal growth rate were not evaluated in most of the investigations.

It is found that for glycerin, salol, selenium, and some silicates the crystal growth velocities indeed are described by eq. 2 with values of  $\alpha$  less than unity and increasing with undercooling.<sup>9</sup> Further the results for at least glycerin and salol at small undercooling are described satisfactorily by eq. 2 with  $\sigma$  values having the expected order of magni-

tude.<sup>5</sup> These results are consistent with but do not prove the screw dislocation mechanism for growth in these systems.

Under ordinary conditions cristobalite grows into fused silica at rates which are  $10^3$  to  $10^4$  times those given by the velocity-fluidity relation with  $\alpha$  equal to unity.<sup>10</sup> However, it has been demonstrated<sup>11,12</sup> that this process in silica is strongly catalyzed by small amounts of water and/or oxygen. When these impurities are removed from the external gas phase the growth rate is reduced to a level which is no more than a factor of 10 to 100 above the theoretical level.<sup>11</sup> It is possible that the discrepancy would be reduced further if residual impurities within the silica were removed. This action of impurities in fused silica is in marked contrast with that in most other systems which is to inhibit rather than to promote crystal growth. That such promotion is possible in covalently bound systems had been pointed out by Cohen and the author.<sup>13</sup>

There have been several investigations<sup>5,14,15</sup> of the rate of growth of ice crystals into undercooled water. In this system pronounced interface orientation effects have been demonstrated,<sup>14</sup> the rate of growth being at least an order of magnitude greater in directions lying within than in the direction normal to the basal plane of the ice structure. This behavior may reflect differences in the  $\alpha$  values for different crystal faces. The observed growth rate in directions within the basal plane does increase as the square of the apparent undercooling, but it still is not clear to what extent this rate is governed by the dissipation of the crystallization heat.<sup>15</sup> To describe the observed rates, which can be no larger than the actual rates at the nominal undercooling, by eq. 3 it is necessary to choose a value of the interfacial tension  $\sigma$  which is about an order of magnitude smaller<sup>5</sup> than that deduced from nucleation experiments. A possible explanation for this discrepancy is provided by the treatment of Cahn<sup>16</sup> according to which the thermodynamic barrier to the lateral growth of island monolayers on crystal surfaces will be substantially reduced if the interface is somewhat diffuse; that is if the change from crystal to liquid properties in a traverse of the interface requires more than two molecular layers.

Thus, taken as a whole, the crystal growth rates in molecularly complex liquids are of the magnitude expected from the growth-rate-fluidity relation. This indicates that the process is governed primarily by molecular reorientation in the liquid adjacent to a site in the crystal surface favorable for the reception of the molecule.

**Growth in Molecularly Simple Liquids.**—Molecularly simple liquids are those in which the molecules

(10) S. D. Brown and S. S. Kistler, *J. Am. Ceram. Soc.*, **42**, 263 (1959).

(11) N. G. Ainslie, C. R. Morelock, and D. Turnbull, *ibid.*, in press. (1961-62).

(12) F. Wagstaff, I. B. Cutler, and S. D. Brown, presented at Am. Ceram. Soc. Meeting, Toronto, 1961.

(13) D. Turnbull and M. H. Cohen, *J. Chem. Phys.*, **29**, 1049 (1958).

(14) W. B. Hillig, ref. 3b, pp. 350-360.

(15) C. S. Lindenmeyer, G. T. Orrok, K. A. Jackson, and B. Chalmers, *J. Chem. Phys.*, **27**, 822 (1957).

(16) J. W. Cahn, *Acta Met.*, **8**, 554 (1960).

(7) J. C. Fisher, unpublished.

(8) A. Rosenberg and W. C. Winegard, *Acta Met.*, **2**, 342 (1954).

(9) The detailed comparisons are described in references 5 and 6 where also may be found the references to the original crystal growth measurements.

either are single atoms or delineate a figure with a regular polyhedral shape. In these systems the crystal growth rates are very high and, under most conditions, probably governed by the dissipation of the crystallization heat. Thus the reported rates must be considered minimal for the corresponding nominal undercoolings. These minimal rates do increase approximately with the square of the nominal undercooling, but they are orders of magnitude larger than calculated from eq. 3 with reasonable values for  $\sigma$ . Further, values of  $\alpha$  much greater than unity would be required to fit eq. 2 to the results. For example, the velocity 200 cm./sec. in white phosphorus at undercooling of 20°, reported by Powell, Gilman, and Hildebrand,<sup>2</sup> would require  $\alpha \sim 10$ . The crystal growth rate of 4000 cm./sec. in pure nickel at nominal undercooling 175°, recently measured by Walker,<sup>17</sup> would require  $\alpha \sim 50$ . These results indicate that in molecularly simple liquids the molecular motions necessary for crystal growth are much more rapid than those required in diffusion and fluid flow.

**Nucleation Rate.**—To measure the intrinsic or homogeneous frequency of crystal nucleation in liquids it is necessary to circumvent the catalysis of nucleation on the surfaces of impurities (*e.g.*, container walls or suspended notes) in the liquid. This perhaps is most readily accomplished by using the droplet technique,<sup>18,19</sup> and here shall be cited only the experience obtained with this technique.

This experience has shown that the homogeneous nucleation frequency rises very steeply with increasing undercooling. For example, this rise is a factor of 5 per degree for mercury at 80° undercooling<sup>20</sup> and a factor of 7000 per degree for *n*-octadecane at 13° undercooling.<sup>21</sup> Thus the range of undercooling in which the nucleation frequency is readily measurable is very narrow. We shall take an undercooling,  $\lambda$ , in this range, corresponding to a nucleation frequency  $\sim 10^6$  cm.<sup>-3</sup> sec.<sup>-1</sup>, as the index of the resistance of a liquid to crystal nucleation.

There are listed in Table I the range and average of the reported  $\lambda$  values, expressed in units of the thermodynamic crystallization temperature for four classes of liquids.

TABLE I

RANGE AND AVERAGE VALUES OF THE UNDERCOOLING,  $\lambda$ , IN UNITS OF  $T_m$ , AT WHICH HOMOGENEOUS NUCLEATION FREQUENCY REACHES VALUE  $\sim 10^6$  CM.<sup>-3</sup> SEC.<sup>-1</sup>

Liquid type	Range	Average
Metallic <sup>22</sup>	0.13 to 0.32	0.19
Alkali Halide <sup>23</sup>	0.14 to 0.24	.18
Simple Molecular <sup>24</sup>	0.12 to 0.32	.21
<i>n</i> -alkanes <sup>21</sup>	0.037 to 0.043	.041

(17) J. L. Walker, to be published.

(18) B. Vonnegut, *J. Colloid Sci.*, **3**, 563 (1948).(19) D. Turnbull, *J. Appl. Phys.*, **20**, 817 (1949).(20) D. Turnbull, *J. Chem. Phys.*, **20**, 411 (1952).(21) D. Turnbull and R. L. Cormia, *ibid.*, **34**, 820 (1961).(22) For review of this work and references to original literature see: (a) J. H. Hollomon and D. Turnbull, *Progr. in Metal Phys.*, **4**, 333 (1953); (b) D. Turnbull, "Solid State Physics," Vol. 3, Academic Press, New York, N. Y., 1956, pp. 225-306.(23) E. R. Buckle and A. R. Ubbelohde, *Proc. Roy. Soc. (London)*, **259A**, 325 (1960).

These results show the extraordinary resistance, already alluded to in the Introduction, of structurally simple liquids, including many which crystallize to close packed structures, to the initiation of crystallization. Professor Hildebrand<sup>1,3</sup> has emphasized that this behavior is incompatible with the defective crystal models<sup>25</sup> of the liquid state. According to such models the molecular motions which initiate crystallization should occur with about the same net frequency as those which propagate crystallization. This implies, contrary to the experience just cited, that crystallization within clean liquids would begin at slight undercooling. Thus to account for crystallization behavior it is necessary either to modify the defective crystal model or to use an entirely different model for the liquid state.

From the phenomenological viewpoint, the large undercooling required for detectable nucleation reflects a relatively large liquid-crystal interfacial tension,  $\sigma_{LS}$ . With simple nucleation theory this tension can be calculated from the value of  $\lambda$ . There are no directly measured values of  $\sigma_{LS}$  with which to compare the values so calculated. However, there are relations<sup>26</sup> between  $\sigma_{LS}$  and certain other measured interfacial tensions which must be fulfilled at the thermodynamic crystallization temperature,  $T_m$ . For example,  $\sigma_{LS} \geq \sigma_{gb}/2$  at  $T_m$  where  $\sigma_{gb}$  is the grain boundary tension. Actually the values obtained by extrapolating the measured  $\sigma_{gb}$ 's to  $T_m$  are somewhat larger than  $2\sigma_{LS}$ , but the differences are hardly more than might be accounted for by the experimental uncertainties and the possible effects of crystal boundary orientation on  $\sigma_{LS}$ .<sup>27</sup> The interfacial free energy per molecule in the crystal-liquid interface, calculated from the nucleation  $\sigma_{LS}$ , is 1/3 to 1/2 of the molecular heat of fusion.<sup>26</sup> This result has been justified<sup>28,29</sup> crudely by application of the nearest neighbor model.

From the atomistic viewpoint the large values of  $\lambda$  seem to indicate that a substantial local rearrangement of molecules is required for crystal nucleation. Frank<sup>30</sup> pointed out that such a rearrangement would indeed have to occur if the symmetry of the predominant local configurations (*i.e.*, the polyhedra formed by the immediate neighbors of a molecule) in liquids is pentagonal. Since they cannot fill space such configurations do not exist in close-packed crystals. Recently Bernal<sup>31</sup> showed that the radial distribution functions of simple liquids indeed can be approximated by that of structures in which pentagonal symmetry elements are prominent. The possible importance of these elements

(24) (a) D. G. Thomas and L. A. K. Stavely, *J. Chem. Soc.*, 4569 (1952); (b) H. J. DeNordwall and L. A. K. Stavely, *ibid.*, 224 (1954).(25) For review of these models and references to original literature see: (a) H. N. V. Temperley, "Changes of State," Cleaver-Hume Press, London, 1956; (b) D. Turnbull, *Trans. Met. Soc. A.I.M.E.*, **221**, 422 (1961).(26) D. Turnbull, *J. Appl. Phys.*, **21**, 1022 (1950).(27) For further discussion see J. E. Hilliard and J. W. Cahn, *Acta Met.*, **6**, 772 (1958).(28) K. A. Jackson and B. Chalmers, *Can. J. Phys.*, **34**, 473 (1956).(29) A. S. Skapski, *Acta Met.*, **4**, 576 (1956).(30) F. C. Frank, *Proc. Roy. Soc. (London)*, **215A**, 43 (1952).(31) J. D. Bernal, *Nature*, **183**, 141 (1959).

in amorphous structures also has been stressed by Tilton<sup>32</sup> and Ginell.<sup>33</sup>

Liquid white phosphorus exhibits an exceptionally large, relative to other simple liquids, resistance to crystal nucleation. This was shown by the observations of Hildebrand and Rotariu<sup>1</sup> that some droplets of white phosphorus remain liquid at undercooling  $>0.367T_m$ . A possible cause for this large undercooling is that white phosphorus apparently crystallizes to the  $\alpha$ -manganese structure,<sup>34</sup> which has an exceptionally large unit cell (58 molecules). As yet there is no satisfactory crystal chemical explanation for the formation of this structure by phosphorus.

The relative smallness of the  $\lambda$  values (see Table I) of the  $n$ -alkanes (16 to 32 carbon atoms) has been accounted for qualitatively<sup>6</sup> by use of the concept, advanced earlier for polymer systems,<sup>35</sup> that crystal nucleation in systems of linear molecules occurs by the aggregation of relatively short chain segments. It would follow from this concept that the crystal nucleation frequency would be relatively high for all systems of linear polymers; for example  $\lambda$  for polyethylene would be of the same order of magnitude as the values for the  $n$ -alkanes. However, there is the possibility in linear polymer systems that the folding of chains, which often occurs in the crystal growth process,<sup>36</sup> also may be required for crystal nucleation. Such a requirement might be imposed, for example, by the large strain energy<sup>37,38</sup> which develops from the propagation of a crystallization front along the polymer chains. It would lead to  $\lambda$  values for linear polymers which are much larger than those of the short chain homologs.

**Glass Formation.**—It is remarkable at first sight that many liquids, including some of the simple van der Waals type, which are quite fluid at  $T_m$  can be undercooled to a temperature range in which they solidify to a glass.<sup>6</sup> An explanation for this behavior, based on a simple free volume model for the amorphous phase, was proposed by Cohen and the writer.<sup>39,40</sup> According to this model all liquids would solidify to glasses at sufficient undercooling. Whether or not this undercooling actually is reached will be determined by the magnitude of the cooling rate and the crystallization kinetic constants.

The fluidities of simple molecular substances at one atmosphere pressure appear to be approximately a single function<sup>6,40</sup> of a reduced temperature defined as

$$\tau = kT/h_v \quad (5)$$

where  $h_v$  is the molecular heat of vaporization. Experience indicates, in accord with the reduced relation, that glass formation in these systems takes place at a roughly constant reduced temperature

(32) L. W. Tilton, *J. Research Natl. Bur. Standards*, **59**, 139 (1957).

(33) R. Ginell, *J. Chem. Phys.*, **34**, 992 (1961).

(34) D. E. C. Corbridge and E. J. Lowe, *Nature*, **170**, 629 (1952).

(35) For review of Crystal Nucleation in Polymers see L. Mandelkern in ref. 3b, pp. 467–497.

(36) For review see A. Keller, ref. 3b, pp. 499–532.

(37) F. C. Frank, ref. 3b, pp. 529–530.

(38) J. D. Hoffman and J. I. Lauritzen, Jr., *J. Research Natl. Bur. Standards*, **65A**, 297 (1961).

(39) M. H. Cohen and D. Turnbull, *J. Chem. Phys.*, **31**, 1164 (1959).

(40) D. Turnbull and M. H. Cohen, *ibid.*, **34**, 120 (1961).

which is  $\tau_g \sim 0.025$ . In contrast with the reduced glass and boiling temperatures the reduced thermodynamic crystallization temperature,  $\tau_m$ , varies widely with the substance. Cohen and the writer<sup>6,40</sup> have made the generalization that the glass forming tendency should be greater the smaller is  $\tau_m$ . This generalization is supported, at least qualitatively, by experience. It follows, in part, from the hypothesis that all classical liquids are capable of the glass transition and from the principle of corresponding states for fluid behavior alluded to above. According to this theory the effect of molecular constitution upon glass forming tendency is simply a reflection of its effect upon  $1/\tau_m$ . Indeed Cohen and the writer<sup>6,40</sup> have so interpreted molecular constitutive effects on glass formation.

Simple molecular substances with  $\tau_m \lesssim 0.05$  usually form glasses quite readily. At the undercooling required for copious crystal nucleation in liquids with a wide fluid range below  $\tau_m$  (see Table I) the reduced temperature in the strong glass formers is  $\gtrsim 0.033$ , which is above the glass transition temperature by a considerable amount. However, at  $\tau \sim 0.033$  the fluidity is about 3 orders of magnitude smaller than at  $\tau_m$  and falling quite rapidly with decreasing temperature. In addition to this there is another effect, pointed out by Hoffman,<sup>41</sup> which will reduce the rate of increase of nucleation frequency with undercooling at low temperature. It is that the rate of change of the free energy of crystallization with undercooling decreases with decreasing temperature. This effect becomes especially marked in molecular systems as the glass transition temperature is approached. By taking these effects into account the crystal nucleation behavior of molecular substances with strong glass forming tendencies can be explained without invoking especially large liquid-crystal interfacial tensions.

**Melting.**—If a substantial local rearrangement of molecules occurs in the liquid-crystal transition the interior of perfect crystals should withstand quite large superheating without the initiation of melting. That most crystals actually melt at slight superheating merely reflects that, in contrast with the converse process, the formation of a thin liquid film on the free surface of a crystal needs only a negligible motivating free energy. Thus in ordinary melting a liquid film immediately forms over the crystal surface and grows inward. If the growth is governed by the rate of supply of the heat of fusion, as is most often so, the crystal interior cannot be superheated appreciably by the external heat source. In this case little is proved about the interior stability of the crystal.

If, on the other hand, the crystal melts to a very viscous liquid the movement of the crystal-liquid interface is slow and not controlled by the flow of heat. In this case the resistance of the crystal interior to superheating can be tested easily. Actually some, at least, of these crystals do withstand large superheating. For example, crystals of the feldspar albite<sup>42</sup> have been superheated

(41) J. D. Hoffman, *ibid.*, **29**, 1192 (1958).

(42) A. L. Day and E. T. Allen, *Carnegie Inst. Washington Publ.* **31**, 1905.

more than one hundred degrees for considerable periods. Recently Ainslie, Mackenzie, and the writer<sup>43</sup> investigated the melting of the two crystalline forms of silica, cristobalite and quartz, by a microscopic technique. We found that melting began at and propagated from free surfaces and grain boundaries, but there was no evidence of melting within crystals of either form at the largest superheating investigated (40° for cristobalite and 400° for quartz). The full significance of these results is not yet clear since the systems are structurally complex and the role of transformation strain energy has not been evaluated.

A different and very ingenious method of investigating the interior stability of crystals was proposed<sup>44</sup> by Bridgman.<sup>45</sup> It is to observe melting

(43) N. G. Ainslie, J. D. Mackenzie, and D. Turnbull, *J. Phys. Chem.*, **65**, 1718 (1961).

when the crystal is made metastable, relative to the liquid, by sudden pressure changes. Bridgman actually applied this method to the water system and observed that ice, when made metastable by compression, apparently melted only from the external surfaces. The amount of superheating was not stated.

Some other interesting instances of crystal superheating have been described by Khaikin and Benet,<sup>46</sup> Sears,<sup>47</sup> and Stranski and his associates.<sup>48</sup>

(44) The author is indebted to J. W. Cahn for calling attention to this proposal.

(45) P. W. Bridgman, "Physics of High Pressures," Bell and Sons, London, 1949, p. 210.

(46) S. E. Khaikin and H. P. Benet, *Compt. rend. Acad. Sci. U.R.-S.S.*, **23**, 31 (1939).

(47) G. W. Sears, *J. Phys. and Chem. Solids*, **2**, 37 (1957).

(48) I. Karutz and U. N. Stranski, *Z. anorg. u. allgem. Chem.*, **292**, 330 (1957).

## THE USE OF THE CHEMICAL SHIFT PARAMETER FOR STUDY OF INTRAMOLECULAR HYDROGEN BONDS

BY E. A. ALLAN AND L. W. REEVES

*Department of Chemistry, University of British Columbia, Vancouver 8, B. C.*

*Received October 14, 1961*

The chemical shift of protons in intramolecular hydrogen bonds has been measured in 34 compounds of the phenol type. The change in chemical shift " $\Delta\sigma_{\text{OH}}$ " on formation of these hydrogen bridges is taken as the difference between the infinite dilution chemical shift in the parent phenol compound in  $\text{CCl}_4$  solution and the chemical shift measured for the proton in the intramolecular hydrogen bonds. Corrections have been made for ring current effects. This change in chemical shift is correlated with the corresponding frequency shift  $\Delta\nu_{\text{OH}}$  in the  $-\text{O}-\text{H}$  stretching region of the vibrational spectrum. The dilution chemical shifts for the  $-\text{O}-\text{H}$  proton in the *ortho*-halophenols have been investigated over a concentration range 1–5 mole % in  $\text{CS}_2$  and a temperature range  $-53$  to  $+107^\circ$ . The chemical shift at infinite dilution of this proton is used to determine equilibrium constants for the *cis-trans* conversion. Values of  $\delta_{\text{cis}}$ ,  $\delta_{\text{trans}}$ , and  $\Delta H$ , the heat of formation of the hydrogen bonds, have been obtained from p.m.r. measurements alone.

### Introduction

The changes in chemical shift of a proton involved in the formation of a hydrogen bond are large<sup>1</sup> and serve as an indication of hydrogen bond formation in a similar manner to the changes in  $\text{X}-\text{H}$  stretching frequency on formation of the bond  $\text{X}-\text{H} \cdots \text{Y}$ .<sup>2</sup> It is necessary that the lifetime of an exchanging species be long compared to the various proton resonance shift differences in order that distinct resonances can occur for each chemical environment.<sup>3</sup> In the solutions where extensive hydrogen bonding occurs the lifetime of individual species is generally very short. The average chemical shift observed is not sufficient information to allow estimates of equilibrium constants involving hydrogen bonding.<sup>1,2</sup> In the infrared spectrum a band for each type of hydrogen bond can be observed, and the free  $-\text{X}-\text{H}$  stretching band also can be measured.<sup>2,4</sup> The equilibrium constants obtained from infrared intensity data suffer from two main disadvantages. The occurrence of polymeric chains of hydrogen bonded molecules in a non-polar solvent leaves a terminal  $-\text{X}-\text{H}$  stretching band which does not differ appreciably

from the monomer value. The hydrogen bonded band is considerably intensified and broadened and rarely is resolved cleanly into the different types of hydrogen bonds.<sup>2</sup>

Intramolecular hydrogen bonds formed by molecules in dilute non-polar solutions are a simple case and have been studied by several workers using infrared spectroscopy.<sup>5–8</sup> Even in this simple situation, however, there is a lack of agreement of the equilibrium constant for the *cis-trans* conversion in *ortho*-halophenols and disparity among the enthalpies of formation of the internal hydrogen bond. It appears that part of this disagreement may be due to impurities.<sup>5,8</sup>

The shift in the stretching frequency of the  $\text{X}-\text{H}$  group on formation of a hydrogen bond has been correlated with many other parameters including heats of formation.<sup>1</sup> In earlier papers<sup>9</sup> the change in chemical shift on formation of a hydrogen bond

(4) G. F. Hilbert, O. R. Wulf, S. B. Hendricks, and U. Liddel, *J. Am. Chem. Soc.*, **58**, 548 (1936).

(5) G. Rassmy, W. Lüttke, and R. Mecke, *J. Chem. Phys.*, **21**, 1606 (1953).

(6) A. W. Baker, *J. Phys. Chem.*, **62**, 744 (1958).

(7) A. W. Baker and W. W. Kaeding, *J. Am. Chem. Soc.*, **81**, 5904 (1959).

(8) D. A. K. Jones and J. G. Watkinson, *Chem. & Ind. (London)*, 661 (1961).

(9) L. W. Reeves, *Can. J. Chem.*, **38**, 736 (1960); L. W. Reeves, E. A. Allan, and K. O. Strømme, *ibid.*, **38**, 1249 (1960).

(1) J. A. Pople, W. G. Schneider, and H. J. Bernstein, "High Resolution Nuclear Magnetic Resonance," McGraw-Hill Book Co., New York, N. Y., 1959.

(2) G. C. Pimentel and A. L. McClellan, "The Hydrogen Bond," W. H. Freeman & Co., San Francisco, 1960.

(3) H. S. Gutowsky and A. Saika, *J. Chem. Phys.*, **21**, 1688 (1953).

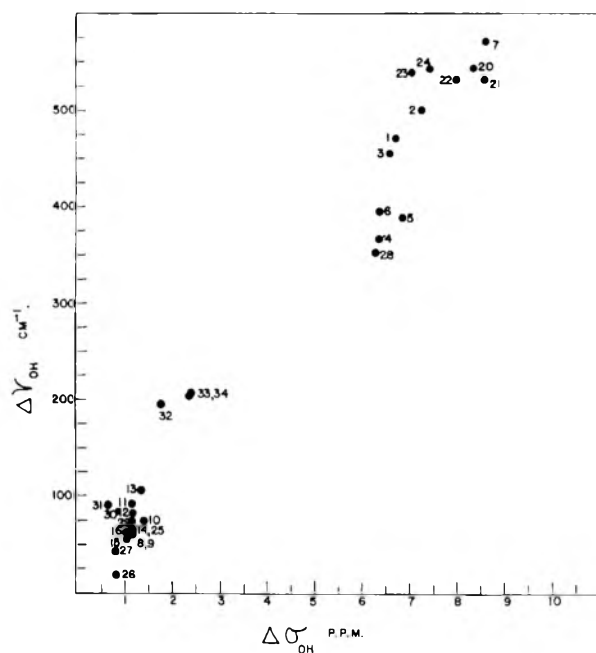


Fig. 1.—The change in chemical shift " $\Delta\sigma_{OH}$ " and the frequency shift of the  $-O-H$  " $\Delta\nu_{OH}$ " stretching band in 34 compounds. The numbered points on the figure refer to the numbered compounds below.

Table of Compounds

1. Salicylaldehyde	
2. 5-Nitrosalicylaldehyde	
3. 5-Bromosalicylaldehyde	
4. <i>o</i> -Nitrophenol	
5. 2,4-Dinitrophenol	
6. Methyl salicylate	
7. <i>o</i> -Bromobenzoic acid	
8. <i>o</i> -Chlorophenol	
9. 2,4-Dichlorophenol	
10. 2,4,6-Trichlorophenol	
11. <i>o</i> -Bromophenol	
12. 2,4-Dibromophenol	
13. <i>o</i> -Iodophenol	
14. <i>o</i> -Methoxyphenol	
15. 2,6-Dimethoxyphenol	
16. <i>o</i> -Allylphenol	
17. <i>o</i> -Cresol	
18. <sup>a</sup>	
19. <sup>a</sup>	
20.	
21.	
22.	
23. 1-Nitro-2-naphthol	
24. 2,4-Dinitro-1-naphthol	
25. 2,5-Dichlorophenol	
26. <i>o</i> -Fluorophenol	
27. <i>o</i> -Phenylphenol	
28. 4-Chloro-2-nitrophenol	
29. 2-Bromo-4-phenylphenol	
30. 1-Bromo-2-naphthol	
31. 2,4-Dibromo-1-naphthol	
32. <i>o</i> -(Methylthio)-phenol	
33. 2-Methyl-6-(methylthio)-phenol	
34. <i>o</i> -(Isopropylthio)-phenol	

<sup>a</sup> The values of  $\Delta\nu_{OH}$  were not obtainable because of overlap with the  $-C-H$  stretching frequencies. The chemical shifts  $\Delta\sigma_{OH}$  are 9.42 and 8.47, p.p.m. respectively.

has been correlated with the frequency shift in the infrared spectrum for intramolecular hydrogen bonds. In this work this correlation is extended to other compounds. A similar correlation for intermolecular hydrogen bonds now has appeared<sup>10</sup> in the literature.

(10) I. Gränacher, *Helv. Phys. Acta*, **34**, 272 (1961).

## Experimental

*ortho*-Fluoro-, chloro-, and bromophenol were purified by at least two passes through a "Beckmann Megachrom" gas chromatograph column. *o*-Iodophenol was purified by recrystallization from chloroform. All other phenols used were obtained by recrystallizing analytical grade material from cyclohexane, chloroform, ether, ethyl alcohol, or acetone, depending on which solvent was most suitable. The solvents used, carbon disulfide and carbon tetrachloride, were subjected to fractional distillation and a small middle cut selected.

A standard Varian 40 Mc./sec. spectrometer was modified by replacing the filament supply to the R-F unit with 12-volt batteries. This gave the base line stability required for this work. The variable temperature probe was similar to that used by Reid and Connor.<sup>11</sup>

Chemical shifts were measured from an internal cyclohexane reference ( $\sim 1$  mole %) in the solvent. Simultaneous measurement of the side band frequencies was made possible by employing suitable blocking condensers in the electronic counter circuit (Hewlett Packard 522B). Spectra were taken on a Leeds and Northrup Speedomax model H recorder. A side band was placed before and after the  $-OH$  resonance peak and the sweep rate was arranged such that the distance on the chart paper was 1 cm./cycle with the distance between side bands 10–12 cm. For the temperature measurements five to eight spectra were taken, and then averaged, with a standard deviation of  $\pm 0.1$  c.p.s. This precision could not be obtained in the case of *o*-fluorophenol since the half width of the signal was 4–6 c.p.s. In the work on correlation of chemical shift changes with infrared frequency shifts, one measurement on two independent solutions was deemed sufficient.

## Results

**1. Chemical Shifts and Infrared Measurements of Intramolecular Hydrogen Bonds.**—Some 34 intramolecularly hydrogen bonded phenols have been studied, and the chemical shift of the hydrogen bonded proton determined. The change in chemical shift on formation of each hydrogen bond is taken, as before,<sup>9</sup> as the difference between the infinite dilution chemical shift of the parent phenol,  $\alpha$ - or  $\beta$ -naphthol, in  $CCl_4$  and the chemical shift with the *ortho*-substituent in 1–2 mole % solution in  $CCl_4$ . Corrections have been made to eliminate ring current effects.<sup>9</sup> The change in chemical shift so obtained is correlated with the corresponding change in the stretching frequency of the  $-O-H$  band. Many of the infrared measurements are taken from the work of A. W. Baker and co-workers,<sup>12</sup> some were checked using a Perkin-Elmer 21 instrument, and others are measurements made by us. In the case of the *ortho*- $CH_3S$ ,  $-(CH_3)_2CHS$ - and  $2CH_3S-6CH_3$ -substituted phenols the values were obtained by private communication with Dr. Baker prior to his publication.

Figure 1 shows graphically the correlation obtained between the two chosen parameters for all the compounds studied. The points on the diagram are numbered and referred to a legend of the compounds measured.

**2. Analysis of *cis-trans* Equilibrium in the *o*-Halophenols.**—The dilution chemical shifts of the  $-O-H$  proton in the four *o*-halophenols have been studied at approximately 5, 4, 3, 2, and 1 mole % in carbon disulfide at temperatures between  $-53$  to  $+107^\circ$ . The internal reference was 1 mole % cyclohexane. The results for *o*-chlorophenol are shown in Fig. 2, *o*-bromophenol in Fig. 3, and *o*-

(11) C. Reid and T. M. Connor, *J. Mol. Spectry*, **7**, 32 (1961).

(12) A. W. Baker and A. J. Shulgin, *J. Am. Chem. Soc.*, **80**, 5358 (1958).



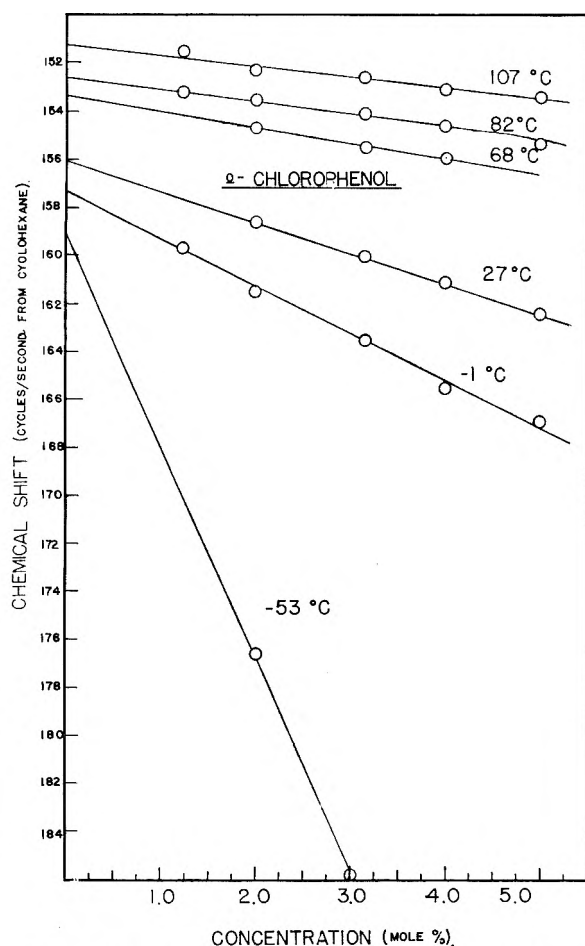


Fig. 2.—Dilution chemical shifts at 6 temperatures for the  $-O-H$  proton in *o*-chlorophenol at 5–1 mole % of the phenol in  $CS_2$ . The numbers refer to cyclohexane as an internal standard.

fluoro- and *o*-iodophenol in Fig. 4. The main object of these studies has been to define as accurately as possible the infinite dilution chemical shift of the  $-O-H$  proton at various temperatures. In the only previous study of these compounds, Huggins, Pimentel, and Shoolery have noted that the dilution shifts of *o*-chlorophenol have zero slope over this concentration range at room temperature.<sup>13</sup> The figures show that the slope is finite and constant in three of the phenols from 3–4 mole % to 1 mole %. There is also a strong temperature dependence of this finite slope. The  $-OH$  proton resonance in *o*-fluorophenol is considerably broader ( $\sim 5$  c.p.s. half-width) than in the other phenols studied. The dilution shifts are not linear in concentration except at the highest temperature and the curvature of the plot at lower temperatures is opposite to that in the other three phenols. The large half width of the signal prevented observation of the chemical shift in 1 mole % solutions at a 40 Mc./sec. proton resonance frequency. The solid points in Fig. 4 represent measurements made at 60 Mc./sec. and reduced to 40 Mc./sec. for the purpose of inclusion on the same figure.<sup>14</sup> These measurements show no change of curvature even at 1 mole % concentration

(13) C. H. Huggins, G. C. Pimentel, and J. N. Shoolery, *J. Phys. Chem.*, **60**, 1311 (1956).

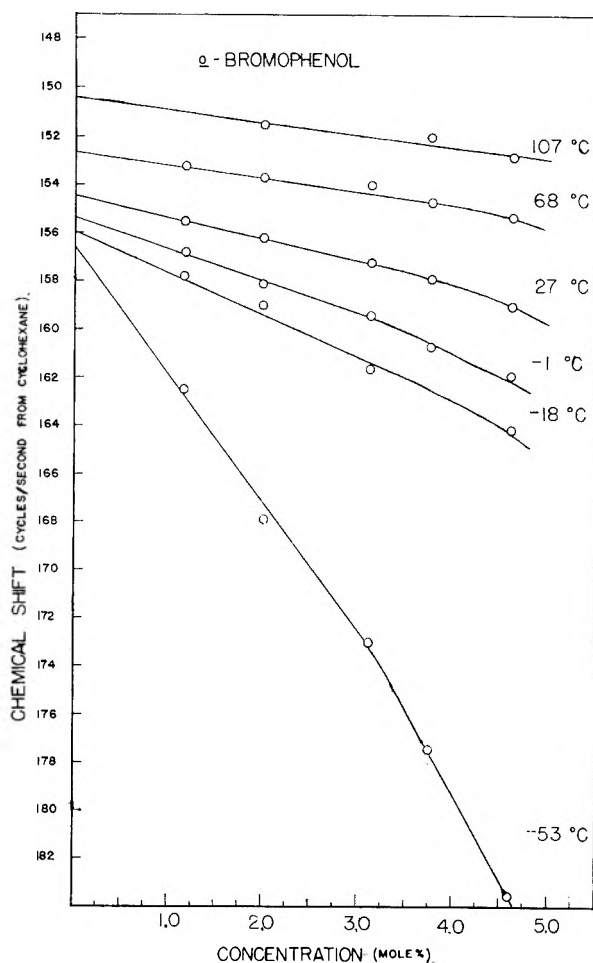


Fig. 3.—Dilution chemical shifts at 6 temperatures for the  $O-H$  proton in *o*-bromophenol.

of the phenol. The *o*-iodophenol solutions were studied below  $-1^\circ$  but the curvature in the dilution chemical shift curves occurred below 3 mole % phenol and the slope at zero concentration was too high to enable reliable infinite dilution chemical shifts to be obtained by extrapolation. The use of graphical extrapolation might be improved slightly by fitting the chemical shifts to a three-constant equation in concentration but it is felt that this would not improve our extrapolation considerably provided the dominant term is linear in concentration at 4 mole % or below. In all three cases shown in Fig. 2, 3, and 4 this approximation is seen to be quite good.

In order to treat the data for obtaining constants for the *cis-trans* equilibrium, the infinite dilution chemical shift at a low enough temperature to obtain almost 100% *cis* form is required. Figure 5 shows a plot of the infinite dilution chemical shift from *o*-bromophenol from Fig. 3 against temperature. In order to find the point at low temperature where this has zero slope the points are fitted to a three-constant equation in temperature. A fit of all points within 0.1 c.p.s. is obtained with

$$\delta_{M\infty} = 151.6 + (5.75 \times 10^{-2})T - (1.6 \times 10^{-4})T^2 \quad (1)$$

(14) The authors are indebted to Dr. W. G. Schneider for allowing one of us (L. W. R.) to make these measurements at 60 Mc./sec. in his laboratory.

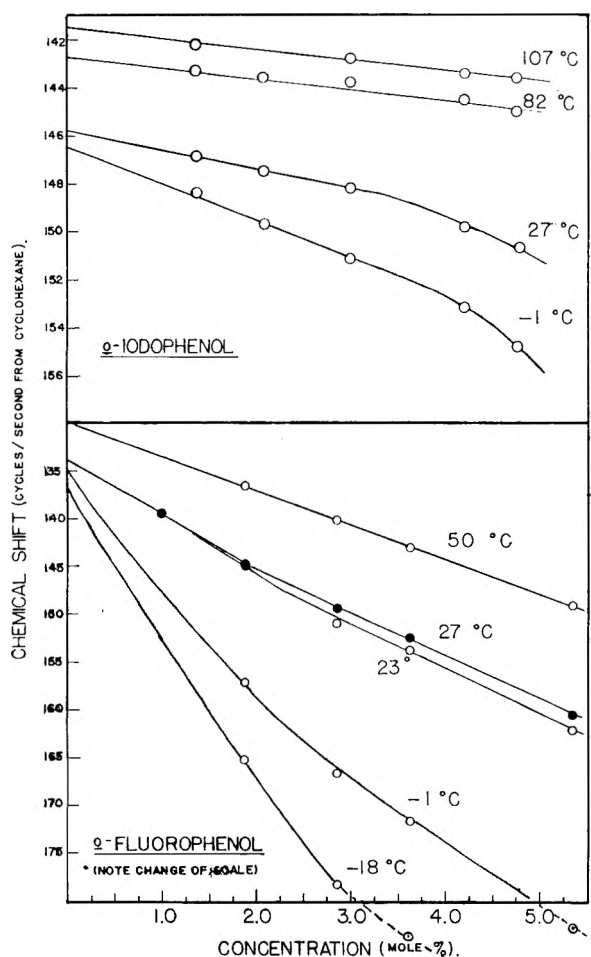


Fig. 4.—Dilution chemical shifts for the  $-O-H$  proton in *o*-iodo- and *o*-fluorophenol.

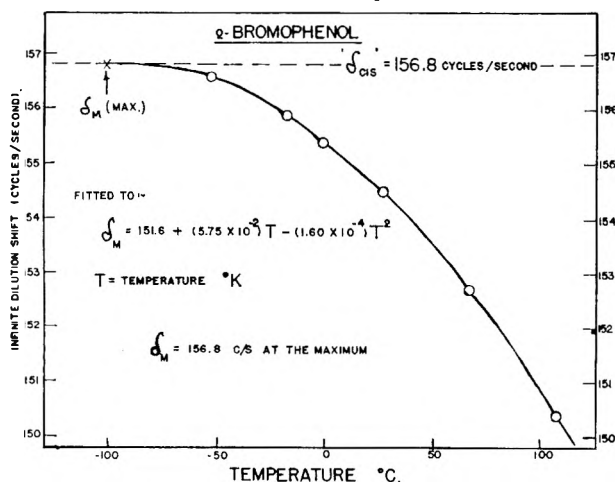


Fig. 5.—The values of " $\delta_{M\infty}$ " obtained from Fig. 3 plotted against temperature.

Zero slope  $[d(\delta_{M\infty})/dT]$  occurs when

$$\delta_{M\infty} = \delta_c = 156.8 \text{ at } 172^\circ\text{K.}$$

$\delta_{M\infty}$  = measured infinite dilution chemical shift  
 $T$  = temperature, °Kelvin

156.8 c.p.s. to low field from the cyclohexane proton resonance will be taken as  $\delta_{cis}$ , the chemical shift of the  $-OH$  proton in the *cis* proton.

Similar procedures were followed with results for *o*-chloro- and *o*-iodophenols.

The equation expressing  $\delta_{M\infty}$  as a function of temperature was accurate to  $\pm 0.1$  c.p.s. in the case of *o*-chlorophenol for all experimental points and correct to  $\pm 0.2$  c.p.s. for the *o*-iodophenol results.

The equations fitted to the experimental results are

$$\delta_{M\infty} = 153.6 + (6.83 \times 10^{-2})T + (2.00 \times 10^{-4})T^2 \quad (2)$$

for *o*-chlorophenol

$$\delta_c = 159.5 \text{ c.p.s. at } +171^\circ\text{K.}$$

and

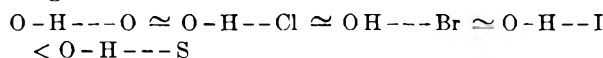
$$\delta_{M\infty} = 147.4 + (2.41 \times 10^{-2})T + (9.86 \times 10^{-6})T^2 \quad (3)$$

for *o*-iodophenol with  $\delta_{cis} = 148.9$  c.p.s. at  $121^\circ\text{K.}$

## Discussion

**1. Correlation of Chemical Shift Changes with the Infrared Data.**—The compounds studied embrace several types of hydrogen bonds including;  $-O-H \cdots Cl$ ,  $O-H \cdots Br$ ,  $O-H \cdots I$ ,  $O-H \cdots S$ ,  $O-H \cdots O$ , and perhaps  $O-H \cdots F$  in 5-membered chelated rings and  $O-H \cdots O$  and  $O-H \cdots N$  in six-membered hydrogen bonded rings. Except in cases where the frequency shift  $\Delta\nu_{OH}$  is small and rather similar values result as in the *o*-halo-phenols and substituted derivatives, the larger the  $\Delta\nu_{OH}$ , the larger the change in chemical shift  $\Delta\sigma_{OH}$ . It is evident that over a large range of hydrogen bonding energies the change in chemical shift is a direct indication of these energies in a similar manner to the frequency shift.<sup>2</sup>

In the weak hydrogen bonds of the 5-membered ring systems the frequency shift and chemical shift range indicate an order



for the heats of formation of these hydrogen bonds. The frequency shift in the infrared region is known to be anomalous because of inter-orbital repulsion between donor orbitals and the orbitals on the acceptor proton.<sup>7</sup> In a corresponding manner the diamagnetic anisotropies of the *ortho* C-X bond vary widely in the above series and in hydrogen bonds of rather similar energy can cause small anomalies in the over-all correlation. It is evident that the  $O-H \cdots S$  hydrogen bond is considerably stronger than all others measured for 5-membered chelated rings. This is attributed to the size effect of the sulfur atom being the best compromise for the strongest hydrogen bond.

The hydrogen bonds formed with 6-membered chelated rings are always stronger presumably because the donor orbital can be accommodated by the molecule at a much more favorable distance for hydrogen bond formation. In these larger rings the proton can lie much nearer the line joining the X and Y atoms across which the hydrogen bridge is formed. The directional nature of the donor orbitals in these compounds also favors stronger hydrogen bonds if we assume that electrostatic forces predominate.<sup>15</sup>

There are two compounds which are interesting exceptions to the 5- and 6-membered rings. *o*-Allylphenol, which appears to have a  $\Delta\sigma_{OH}$  and

(15) (a) J. Lennard-Jones and J. A. Pople, *Proc. Roy. Soc. (London)*, **205A**, 155 (1951); (b) W. G. Schneider, *J. Chem. Phys.*, **23**, 26 (1955).

$\Delta\nu_{\text{OH}}$  similar to those in the 5-membered *o*-halophenols is actually a 6.5-membered ring where hydrogen bonding occurs with the  $\pi$ -electrons of the double bond. *o*-Bromobenzoic acid has a 6-membered ring for internal hydrogen bonding if we consider an O-H...Br hydrogen bridge but even in dilute solution the acid dimers are still present, as indicated by the hydrogen bonded band in the infrared spectrum. The large  $\Delta\sigma_{\text{OH}}$  and  $\Delta\nu_{\text{OH}}$  is therefore the result of the strong hydrogen bond in the dimer.

**2. Enthalpies of Formation of Hydrogen Bonds in *o*-Halophenols.**—At infinite dilution in carbon disulfide the measured chemical shift  $\delta_{\text{M}\infty}$  is characteristic of the *cis-trans* equilibrium according to the equation.<sup>3</sup>

$$\delta_{\text{M}\infty} = X_{\text{C}} \delta_{\text{C}} + X_{\text{T}} \delta_{\text{T}} \quad (4)$$

$X_{\text{C}}$  = mole fraction of infinitely diluted phenol in the *cis* form  
 $X_{\text{T}} = (1 - X_{\text{C}})$  = mole fraction of phenol in the *trans* form  
 $\delta_{\text{C}}$  = chemical shift (referred to the internal cyclohexane reference) of the OH proton in the *cis* form. This is assumed to be temperature invariant.

$\delta_{\text{T}}$  = corresponding chemical shift in the *trans* form

The equilibrium constant may be written

$$K_1 = \frac{[\textit{trans}]}{[\textit{cis}]} = \frac{(\delta_{\text{M}\infty} - \delta_{\text{C}})}{(\delta_{\text{T}} - \delta_{\text{M}\infty})} \quad (5)$$

In the *cis-trans* conversion in a non-polar solvent we may assume the solvation of the *trans* form to be negligible.<sup>16</sup> There also will be small changes in force constants in the molecule but both these terms, which affect  $\Delta S$ , the entropy of conversion, are small enough to be neglected. The simple thermodynamic system is obtained in which

$$-R \frac{d(\log K_1)}{d(1/T)} = \Delta H = -RT \log K_1 \quad (6)$$

Values of  $K_1$ ,  $\delta_{\text{C}}$ , and  $\delta_{\text{T}}$  are to be determined.  $\delta_{\text{C}}$  may be taken, as a first approximation, to be the experimental value of the -OH proton chemical shift derived at low temperatures from equations 1, 2, and 3 of this paper. Values of  $\delta_{\text{T}}$  have been selected such that  $-RT \log K_1$  is constant for all values of  $\delta_{\text{M}\infty}$  at the various temperatures. The values of  $\log K_1$  obtained also were plotted against  $1/T$  to check the value of  $\Delta H$ . In this manner  $\delta_{\text{C}}$ ,  $\delta_{\text{T}}$ , and  $K_1$  could be determined from three temperatures and adjusted eventually to obtain the best value of  $\Delta H$  which fitted experimental data. The results for *o*-chloro- and *o*-iodophenol did not require further adjustment of the  $\delta_{\text{C}}$  obtained from the values in equations 1 and 2. The *o*-bromophenol results were best fitted by changing  $\delta_{\text{C}}$  by 0.4 to 157.1 c.p.s. This further adjustment is within the estimated error of the extrapolation.

In Table I the values of the enthalpies  $\delta_{\text{C}}$  and  $\delta_{\text{T}}$  obtained for the three compounds are listed. The enthalpies obtained agree with those of Baker<sup>6</sup> and the values of  $\delta_{\text{C}}$  and  $\delta_{\text{T}}$  are internally consistent. The larger the value of  $\Delta H$  the larger the  $(\delta_{\text{T}} - \delta_{\text{C}})$ . The fact that  $\delta_{\text{C}}$  for the three compounds is in the order *o*-iodo at highest field followed by *o*-bromo

and then *o*-chlorophenol is also the correct order for the strength of the hydrogen bonds. The absolute values of  $\delta_{\text{T}}$  are, however, surprising since in *o*-chlorophenol the *trans* -O-H peak is calculated to appear on the high field side of cyclohexane. The calculated  $\delta_{\text{T}}$  is very sensitive to the extrapolated  $\delta_{\text{C}}$  value since the equilibrium constant is so small. The absolute value of this chemical shift therefore is unreliable but the computed enthalpy is relatively insensitive to this uncertainty and agreement with the values of Baker<sup>6</sup> indicates that this feature of the results is available in high accuracy.

TABLE I  
*o*-CHLOROPHENOL

Temp., °K.	$\Delta H$ , cal. mole <sup>-1</sup>
380	2334
355	2320
341	2308
300	2392
272	2432

Mean value  $\Delta H = 2356$  cal. mole<sup>-1</sup>

$K_1 = 1/56$  at 25°

$\delta_{\text{C}} = -159.5$  c.p.s.  $\delta_{\text{T}} = +34$  c.p.s.

$(\delta_{\text{T}} - \delta_{\text{C}}) = 193.5$  c.p.s.

*o*-BROMOPHENOL

Temp., °K.	$\Delta H$ , cal. mole <sup>-1</sup>
380	2011
353	2095
341	2161
300	2182
272	2284

Mean value  $\Delta H = 2141$  cal. mole<sup>-1</sup>

$K_1 = 1/38$  at 25°

$\delta_{\text{C}} = -157.2$  c.p.s.  $\delta_{\text{T}} = -51.9$  c.p.s.

$(\delta_{\text{T}} - \delta_{\text{C}}) = 105.3$  c.p.s.

*o*-IODOPHENOL

Temp., °K.	$\Delta H$ , cal. mole <sup>-1</sup>
380	1529
341	1581
300	1748
272	1746

Mean value  $\Delta H = 1651$  cal. mole<sup>-1</sup>

$K_1 = 1/19$  at 25°

$\delta_{\text{C}} = -148.9$  c.p.s.  $\delta_{\text{T}} = -84.9$  c.p.s.

$(\delta_{\text{T}} - \delta_{\text{C}}) = 64.0$  c.p.s.

The results in Fig. 4 for *o*-fluorophenol show no evidence of a hydrogen bonded interaction with the *o*-fluoro group. It appears that the repulsive interaction between the bonding orbital in the -O-H group and the non-bonding donor orbital is the most important factor in determining the strength of the bond in *o*-iodophenol. In *o*-fluorophenol the proton fluorine separation in the *cis* position is too great for hydrogen bond formation.

**Acknowledgment.**—This research has been supported by the Petroleum Research Fund of the American Chemical Society. We are grateful for this generous grant.

16) H. H. Jaffe, *J. Am. Chem. Soc.*, **79**, 2373 (1957).

THE GIBBS ADSORPTION ISOTHERM<sup>1</sup>

BY GEORGE SCATCHARD

*Department of Chemistry and Laboratory of Nuclear Science, Massachusetts Institute of Technology, Cambridge, Mass.**Received October 16, 1961*

The Gibbs adsorption isotherm is derived directly and simply from the chemical potentials and surface tension of Gibbs' model of a phase boundary when the derivation is not complicated by the discussion of stability. The advantages of expressing surface concentrations in units of length are illustrated for the vapor-liquid boundary of water-ethanol. A discussion of Gibbs which is reputed to be vague is shown to be very precise.

Gibbs' treatment of surfaces<sup>2</sup> is often considered difficult and abstract. The chief reason seems to be that the development of the equations alternates with proofs of stability. I hope that it can be resolved by this more limited presentation.

When Gibbs neglects surface effects (62) he considers a system "enclosed in a rigid and fixed envelope, which is impermeable to and unaltered by any of the substances enclosed, and perfectly non-conducting to heat." It is difficult to justify this neglect when the volume is made to approach zero in his derivation of the Gibbs-Duhem equation (87). When he considers surface effects Gibbs avoids these difficulties (278) by considering a system separated by imaginary surfaces from other regions with the same density of energy, of entropy, and of each component as the adjacent portion of the system. We will follow him in limiting the discussion at first to fluids unaffected by gravity. Then, if the system is all in one bulk phase, conditions of equilibrium are that the temperature, pressure, and potential of each component are the same throughout the system. The "extensive" properties are rigorously extensive or mathematically homogeneous.

**Boundaries between Two Fluid Phases.**—If the system includes a boundary between two phases, the temperature and potential of each component are the same in the two phases and in the boundary (with the usual limitation for a possible, but not actual, component of any phase that its potential is not less than in a phase in which it is present), but the pressure is not the same in the two phases if the boundary is curved.

Gibbs recognizes that the boundary, though very thin, is not a mathematical surface. He selects a point in (or very near) the boundary and imagines "a geometrical surface to pass through this point and all other points which are similarly situated with respect to the condition of the adjacent matter" (219). He calls this the dividing surface,  $S$ . He also imagines a closed surface with cuts off a portion,  $s$ , of the surface  $S$ . It is composed of a surface  $n$  "such as may be generated by a moving normal to  $S$ " "as far as there is any want of perfect homogeneity in the fluid masses." It is convenient to close the surface  $n$  by two surfaces,  $S'$  and  $S''$ , each parallel to  $S$ . The system is that matter enclosed by this closed surface. It is divided into two parts by the surface  $S$ , with

volumes  $V'$  and  $V''$  and pressures  $p'$  and  $p''$ . This is illustrated in Fig. 1a.

The properties of this system are mathematically homogeneous if changes in its volume are made by shifting the surface  $n$ , changing the size but not the position of the surfaces  $S$ ,  $S'$ , and  $S''$ . The surface may be made an independent variable if this change is accompanied by a movement of the planes  $S'$  and  $S''$  sufficient to maintain  $V'$  and  $V''$  each constant. We then may write immediately

$$G = \sum_i n_i \mu_i + \alpha \gamma \quad (1)$$

in which  $G$  is the Gibbs free energy,  $n_i$  the number of units of component  $i$ ,  $\mu_i$  the chemical potential of one unit of  $i$ ,  $\alpha$  is the area of the surface, and  $\gamma$  the surface free energy or surface tension.

$$dG = \sum_i (\mu_i dn_i + n_i d\mu_i) + \gamma d\alpha + \alpha d\gamma \quad (2)$$

By the definitions of  $\mu$  and  $\gamma$ , however, at constant  $t$  and  $p$ ,

$$dG = \sum_i \mu_i dn_i + \gamma d\alpha \quad (3)$$

so

$$0 = \sum_i n_i d\mu_i + \alpha d\gamma \quad (4)$$

Equation 4 is the equivalent of the Gibbs-Duhem equation, and reduces to it if  $\alpha$  is zero.

It is convenient to imagine a second, comparison, system with the same geometry as the first system but with each part moved completely into the appropriate region of perfect homogeneity, as shown in Fig. 1b. We will designate properties which differ in the two parts by ' or ''.

Then

$$G' = \sum_i n_i' \mu_i \quad (5)$$

$$G'' = \sum_i n_i'' \mu_i \quad (6)$$

$$0 = \sum_i n_i' d\mu_i = \sum_i n_i'' d\mu_i \quad (7)$$

again at constant  $t$  and  $p$ 's. We will attribute to the surface and designate by a superscript  $\alpha$ , the difference between any quantity in the first and in the second system. Thus

$$V^\alpha = V - V' - V'' = 0 \quad (8)$$

$$n_i^\alpha = n_i - n_i' - n_i'' \quad (9)$$

$$G^\alpha = G - G' - G'' = \sum_i n_i^\alpha \mu_i + \alpha \gamma \quad (10)$$

$$0 = \sum_i n_i^\alpha d\mu_i + \alpha d\gamma = \sum_i \Gamma_i d\mu_i + d\gamma \quad (11)$$

at constant  $t$  and  $p$ 's,

in which  $\Gamma_i = n_i^\alpha/\alpha$  is the surface concentration. Equation 11 is the most general form of Gibbs' adsorption isotherm. We may eliminate one potential by assuming a variation in the comparison system of  $p'$  and  $p''$  with  $(p' - p'')$  constant. Then

$$dp = \sum_i (n_i'/V') d\mu_i = \sum_i c_i' d\mu_i = \sum_i c_i'' d\mu_i \quad (12)$$

so

(1) Presented in part before the Division of Colloid Chemistry, American Chemical Society, Boston, Massachusetts, April 3, 1951.

(2) "The Collected Works of J. Willard Gibbs," Longmans Green and Co., New York, N. Y., 1928, pp. 219-331. Reference will be made to this reprint rather than to the less accessible original (1878) and page numbers will be given as (219), etc.

$$\sum_i (c_i' - c_i'') d\mu_i = 0$$

$$d\mu_k = \sum_{i \neq k} \frac{(c_i' - c_i'')}{(c_k' - c_k'')} d\mu_i \quad (13)$$

Equation 11 becomes

$$0 = \sum_{i \neq k} \left( \Gamma_i - \frac{(c_i' - c_i'')}{(c_k' - c_k'')} \Gamma_k \right) d\mu_i + d\gamma \quad (14)$$

**Plane Boundaries.**—We will now limit our discussion to systems with a plane dividing surface. The position of the surface  $S$  is arbitrary as long as its normal is unchanged and it is in (or very near) the phase boundary. Gibbs chose the position for which  $\Gamma_1$  is zero and considered the case in which all  $d\mu$ 's other than  $d\mu_1$  and  $d\mu_2$  are zero. He defined  $\Gamma_2$  as so determined as  $\Gamma_{2(1)}$ , and the Gibbs isotherm has the more familiar form

$$\Gamma_{2(1)} d\mu_2 = -d\gamma \quad (15)$$

For the adsorption of an unsaturated vapor, such as water, on a relatively non-volatile liquid, such as mercury, it is natural to make the surface concentration of the liquid zero. Making that of the vapor zero would shift the dividing surface a long distance from the phase boundary. Water-mercury was possibly the only system studied experimentally at the time of Gibbs' paper.

Recently, however, emphasis has been placed on systems in which the concentration of either component may be relatively high in either phase. Then Gibbs' definition is analogous to bulk composition expressed as molality or mole ratio, and becomes increasingly inconvenient as the concentration becomes large. We may then speak equally well of  $\Gamma_{2(1)}$  or  $\Gamma_{1(2)}$ , or we may choose other conditions which keep constant the total number of moles, the total mass, or the total volume in the liquid phase. This was first noted by Guggenheim and Adam.<sup>3</sup> The last of these is the most interesting. We will call these surface concentrations  $\Gamma_{1(v)}$  and  $\Gamma_{2(v)}$ . It is instructive to choose as measure of the quantity of a component the volume of the pure liquid at some temperature and pressure. The bulk concentration then becomes the volume fraction and the surface concentration is expressed as volume/surface, or length. The convenient unit is the Ångstrom.

The system water (1)-ethanol (2), vapor-liquid has been particularly well studied, and was used in (3). Figure 2 shows  $\Gamma_{2(1)}$  and  $\Gamma_{1(2)}$  for this system as dashed lines, and  $\Gamma_{2(v)}$  and  $\Gamma_{1(v)}$  =  $-\Gamma_{2(v)}$  as full lines.  $\Gamma_{2(1)}$  is nearly proportional to  $\phi_2$  (the volume fraction) for small values of  $\phi_2$ , goes through a maximum and then decreases to a finite value for pure alcohol.  $\Gamma_{1(2)}$  is negative. It also is nearly proportional to  $\phi_1$  for small values of  $\phi_1$  but it becomes increasingly larger (more negative) and reaches a value  $-40$  Å. for pure water. The difference between  $\Gamma_{1(2)}$  and  $\Gamma_{2(1)}$  is probably a rough measure of the thickness of the phase boundary—a few Ångstroms or a few millimicrons. For small values of  $\phi_2$ ,  $\Gamma_{2(v)} = -\Gamma_{1(v)}$  is equal to  $\Gamma_{2(1)}$ , for large values it is equal to  $-\Gamma_{1(2)}$ . The maximum is at about 20 volume % alcohol. It is so near the water end because it is much easier

(3) E. A. Guggenheim and N. K. Adam, *Proc. Roy. Soc. (London)*, **A139**, 231 (1933).

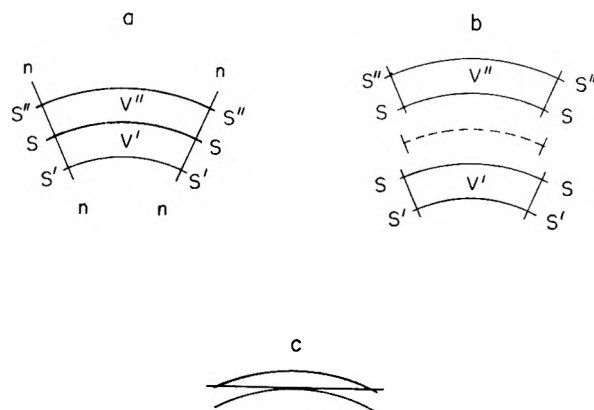


Fig. 1.—a, The system; b, comparison system; c, variations by bending.

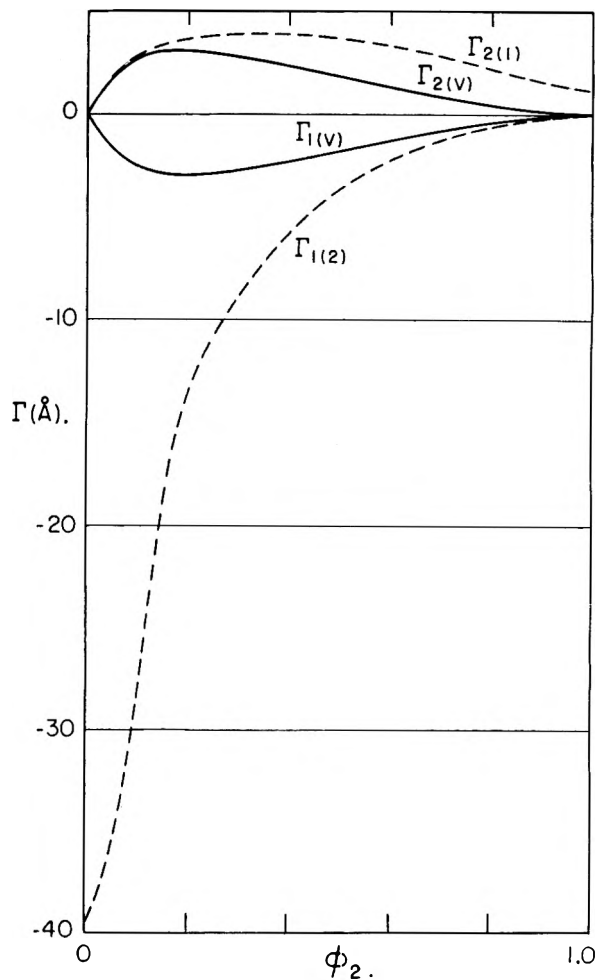


Fig. 2.—Surface concentrations,  $\text{Å}^3/\text{Å}^2 = \text{Å}$ . Water (1)-ethanol (2), vapor-liquid.

to obtain a positive surface concentration than a negative one of the same magnitude.

The effect of pressure on the potentials of liquids is so small that a two component liquid-liquid interface is essentially univariant with the surface tension fixed by the temperature as is that at a one component gas-liquid interface. For polycomponent systems the principles are the same for liquid-liquid as for liquid-gas interfaces.

The system water-phenol-sodium chloride

liquid-vapor gives further evidence of the small thickness of the boundary.<sup>4</sup> The surface concentration of the phenol at constant phenol activity appears to be independent of the salt concentration up to 25 g./100 ml., and the surface concentration of the water relative to the salt is about 4 Å., nearly independent of the phenol activity.

**Curved Surfaces.**—Although the experimental measurements of surface tension depend upon the relation of the pressure difference across a surface to the curvature of the surface, and often upon the effect of gravity upon this surface, neither curvature nor gravity is important for surface concentrations. A surface is always compared with a bulk phase which is at very nearly the same gravitational potential, and at measurable curvatures  $p' - p''$  is very small. This was stated by Gibbs (233), and has been iterated by Guggenheim, whose digest of the thermodynamics of curved surfaces<sup>5</sup> gives a good survey of the subject.

Certain limitations should be considered. From Fig. 1 we see that the distance to the region of perfect homogeneity must be smaller than the shortest radius of curvature or there will be no such region. This limitation depends upon the system and not upon the position of the dividing surface. The position of the dividing surface does affect the surface free energy, however. Since it cannot affect the total free energy or the number of units or the potential of any component, it cannot by equation 1 affect the product  $\alpha\gamma$ . Since it does change  $\alpha$ , it must also change  $\gamma$ .

This process should be distinguished from that used in the derivation of the fundamental surface tension equation. This derivation considers the reversible work, energy at constant entropy or Helmholtz free energy at constant temperature, for a normal shift of the dividing surface in which the quantity of each component on each side of the dividing surface is kept constant, and only the volumes  $V'$  and  $V''$  and the surface  $\alpha$  are considered to vary. Then

$$\delta V'' = -\delta V' = (c_1 + c_2) d\alpha \quad (16)$$

in which  $c_1$  and  $c_2$  are the principal curvatures, the reciprocals of the principal radii of curvature. So

$$\gamma(c_1 + c_2) = p' - p'' \quad (17)$$

**Solid-Fluid Interfaces.**—It is usually difficult and often impossible to measure the work of extending a solid-fluid interface reversibly. It is therefore customary to reverse the procedure used for fluid-fluid interfaces and to measure directly the surface concentration of a gas or a solute in a liquid solution. It is natural to choose the dividing surface so that the surface concentration of the solid is zero. The advantage that the ratio of surface to volume may be made much larger for solids than for fluids is partially offset by the disadvantage that the surfaces are very much less homogeneous.

**The Vagueness of Gibbs.**—Guggenheim,<sup>6</sup> who considers Gibbs' treatment of surface concentrations "abstract" and prefers another which I consider much inferior, criticizes particularly Gibbs' proof that it is possible to so choose a dividing surface in (or very near) the boundary that a variation in the curvature of the surface does not affect the surface energy, or free energy. Gibbs says, "also at and about the surface let the state of the matter *so far as possible be the same* as at and about the plane surface in the initial state of the system" (226). The italics are by Guggenheim, who says, "The words written in italics are in their vagueness unlike Gibbs' usual style. The whole treatment of Gibbs like the treatment in this book postulates complete equilibrium throughout the entire system." However, the next two sentences of Gibbs are, "(Such a variation in the system may evidently take place negatively as well as positively, as the surface may be curved toward either side. But whether such a variation is consistent with the maintenance of equilibrium is of no consequence, since in the preceding equations only the initial state is supposed to be one of equilibrium.)"

I think the first sentence of Guggenheim is as erroneous as the one flatly contradicted by Gibbs. Gibbs is considering the effect of varying a plane surface without displacing it. Figure 1c shows two extreme ways of bending the surface, one keeping its center in the original plane, the other keeping its ends there. If the surfaces were in a homogeneous region the best choice would be to keep the net volume between the surfaces zero. Since the surfaces are in a film of unspecified inhomogeneity the best and most precise way of defining the variation is that of the words italicized.

(4) A. K. Goard and E. K. Rideal, *J. Chem. Soc.*, **127**, 1668 (1925).

(5) E. A. Guggenheim, *Research*, **10**, 478 (1959).

(6) E. A. Guggenheim, *Trans. Faraday Soc.*, **36**, 408 (1940); "Thermodynamics," Third Edition, North Holland Publishing Company, Amsterdam, 1957, pp. 46-57, 261-272.

# A THERMODYNAMIC STUDY OF THE SYSTEM 1-HYDRO-*n*-PERFLUOROHEPTANE + ACETONE<sup>1</sup>

By D. L. ANDERSEN,<sup>2</sup> R. A. SMITH, D. B. MYERS, S. K. ALLEY, A. G. WILLIAMSON, AND R. L. SCOTT

*Department of Chemistry, University of California, Los Angeles 24, California*

*Received October 16, 1961*

The excess Gibbs free energy at 0° and volume changes of mixing at 20° and heats of mixing at 0 and 35° have been determined for 1-hydro-*n*-perfluoroheptane + acetone. The free energy, determined from total vapor pressures at 0°, is positive and sharply skewed toward acetone ( $G^E_{\max} = 90$  cal. at  $x_{\text{acetone}} = 0.75$ ). Volume changes are less positive than those observed for fluorocarbon + hydrocarbon systems ( $V^E_{\max} = 1.83$  cm.<sup>3</sup> at  $x_2 = 0.70$ ). Heats of mixing are S-shaped with minima near  $x_2 = 0.30$  and maxima near  $x_2 = 0.90$ . Nuclear magnetic resonance (n.m.r.) data yielded equilibrium constants at -20, 30, and 80° for the formation of a hydrogen-bonded complex  $C_7F_{15}H \cdots OMe_2$  with a heat of formation of  $-2.5 \pm 0.5$  kcal./mole for the hydrogen bond. Symmetric exothermic heats of complexing calculated from the n.m.r. results were subtracted from the observed heats, giving a skewed "physical" endothermic curve which agrees well with observed heats of mixing for fluorocarbon + hydrocarbon systems. The additivity of chemical and "physical" heats of mixing was confirmed by measuring the heat of mixing perfluoroheptane and acetone outside the two-phase region at 35°.

## Introduction

Hydrogen bonding long has been known to be a major cause of non-ideality in aqueous and alcoholic solutions. Hydrogen bonds involving hydrogen attached to carbon (CH $\cdots$ B, where B is a Lewis base) also can cause deviations from ideality in non-electrolyte solutions. Pimentel and McClellan<sup>3</sup> document the existence of such bonds and conclude that halogen-activated C-H, acetylenic C-H, and S-H should be included in the usual list (OH, NH, and HF) of groups capable of hydrogen bonding to Lewis bases. Chloroform + acetone is perhaps the classic example of C-H participation in such bonding. The large deviations from ideality observed for this system are characteristic of associated systems:  $G^E$ ,  $\bar{H}^E$ ,  $T\bar{S}^E$  and  $\bar{V}^E$  are -133, -437, -304 cal., and -0.2 cm.<sup>3</sup>, respectively, at 35° and  $x_2 = 1/2$ .

Fluorocarbon + hydrocarbon interactions are not nearly so well understood. Scott<sup>4</sup> discussed the anomalous behavior of these solutions and concluded (1958) that more work, experimental and theoretical, was needed before the problem could be clearly understood; this situation still is true. Perfluoro-*n*-heptane + isooctane (2,2,4-trimethylpentane) provides a good illustration of the unexpectedly large excess functions to be explained:  $G^E$ ,  $\bar{H}^E$ ,  $T\bar{S}^E$ , and  $\bar{V}^E$  are 326, 508, 182 cal., and 4.8 cm.<sup>3</sup> at 30° and  $x_2 = 1/2$ . There is an upper critical point at  $t_c = 22.7^\circ$  and  $x_c = 0.63$ .

As part of our continuing program of research on fluorocarbon solutions, we have studied the thermodynamic properties of a system in which hydrogen bonding competes with "fluorocarbon + hydrocarbon" interactions: 1-hydro-*n*-perfluoroheptane + acetone ( $C_7F_{15}H + OMe_2$ ). Strong association does not occur in either of the pure components, so the observed properties of mixing are directly related to the competition between the hydrogen bonding (exothermic) and the "fluorocarbon + hydrocarbon" (endothermic) interactions. We will

refer to the former as chemical, the latter as "physical" interactions.

## Experimental

**Materials.**—"Baker Analyzed" reagent grade acetone was dried before using by distilling from a Linde Molecular Sieve following the procedure of Howard and Pike.<sup>5</sup> Density at 25°, 0.7834 g./cm.<sup>3</sup> (Howard and Pike reported 0.7842),  $n^{25}_D$  1.3558.

1-Hydroperfluoroheptane was prepared by decarboxylating the sodium salt of perfluoroheptanoic acid (original sample given to us by the Minnesota Mining and Manufacturing Company; subsequent samples purchased from Matheson Coleman & Bell) in ethylene glycol. Final distillation from a Linde Molecular Sieve through a glass-packed column gave 70-80% yields of  $C_7H_{15}H$ , boiling range 94.7-95.0°, density at 25°, 1.7278 g./cm.<sup>3</sup>,  $n^{25}_D$  1.2702. The original perfluoroheptanoic acid contained about 30% branched isomers<sup>7</sup> and the hydrofluorocarbon used also was thought to contain about 30% branched isomers. Nuclear magnetic resonance (n.m.r.) spectra<sup>8</sup> indicate that most of the branching in these impurities occurs at the end of the molecule away from the hydrogen. Such branching probably has a negligible effect on the thermodynamic behavior of hydroperfluoroheptane + acetone. We prepared *n*-perfluoroheptanoic acid by fractional recrystallization<sup>9</sup> and verified this assumption for the heats of mixing.<sup>9</sup> 1-Hydro-*n*-perfluoroheptane prepared from recrystallized acid distilled at 94.9° and had a lower refractive index than the impure material,  $n^{25}_D$  1.2690.

Perfluoroheptane ( $C_7F_{16}$ ), obtained from Union Carbide and Carbon Chemicals, was distilled from a Linde Molecular Sieve and a cut taken between 82.3 and 82.8°; density at 25°, 1.721 g./cm.<sup>3</sup>,  $n^{25}_D$  1.2593. This product is known to contain branched isomers (Blumkin, *et al.*,<sup>10</sup> report 20% of branched isomers in a sample with a boiling range of 6°), but the presence of a small amount of these should have a negligible effect upon the thermodynamic properties we have measured.

**Vapor Pressures.**—Crude total vapor pressure-liquid composition data were obtained by a simple procedure that required less than 20 cm.<sup>3</sup> of hydroperfluoroheptane.  $C_7F_{15}H$  and  $OMe_2$  were weighed into a small bulb (about 5 cm.<sup>3</sup>) containing a stirring bar and attached to a closed-end mercury manometer. Before evacuating the bulb-manometer system to eliminate air, the mixture was frozen in liquid  $N_2$ . Pressure readings were made with a meter stick after equilib-

(5) K. S. Howard and F. P. Pike, *ibid.*, **63**, 311 (1959).

(6) J. D. LaZerte, L. J. Hals, T. S. Reid, and G. H. Smith, *J. Am. Chem. Soc.*, **75**, 4525 (1953).

(7) J. D. LaZerte, private communication.

(8) S. K. Alley, Doctoral Dissertation, University of California, Los Angeles, May, 1961, p. 136.

(9) Observed heats of mixing with acetone at 35°: 49 and 70 cal./mole at  $x_{\text{acetone}} = 0.952$  and 0.835, respectively, for *n*- $C_7F_{15}H$ ; 47 and 68 cal./mole (calculated from the coefficients in Table I) for  $C_7F_{15}H$ , including the branched isomers.

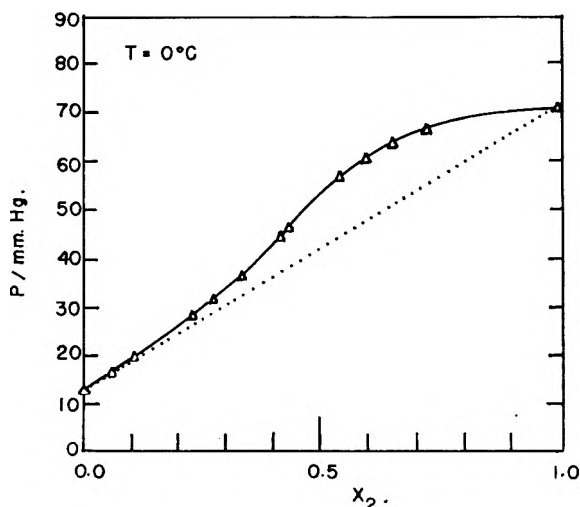
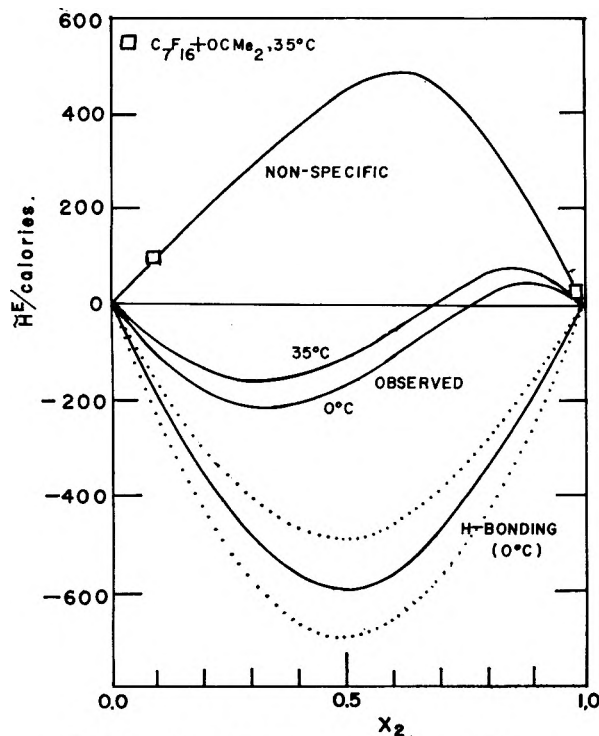
(10) S. Blumkin, N. C. Orrick, J. W. Grisard, and J. D. Gibson, "Purification of Hexadecafluoroheptane," Report K-557, Union Carbide and Carbon Chemicals, 1950, p. 6.

(1) This work was supported in part by the U. S. Atomic Energy Commission, in part by the American Chemical Society Petroleum Research Fund, and in part by the National Science Foundation Undergraduate Research Program.

(2) Participant in the National Science Foundation Undergraduate Summer Research Program.

(3) G. C. Pimentel and A. L. McClellan, "The Hydrogen Bond," W. F. Freeman and Company, San Francisco, Calif., 1960, Chapter 6.

(4) R. L. Scott, *J. Phys. Chem.*, **62**, 136 (1958).

Fig. 1.—Total vapor pressure of  $C_7F_{15}H + OCMe_2$ .Fig. 2.—Heats of mixing for  $C_7F_{15}H + OCMe_2$ .

bration at  $0^\circ$  (fluctuations were less than 2 mm.). No correction was made for liquid which vaporized; liquid compositions are good to  $\pm 0.005$ . One of us (Williamson) is building a vapor-liquid equilibrium still so that a careful determination of vapor pressures can be made for this and other hydrofluorocarbon systems.

**Heats of Mixing.**—The calorimeter and auxiliary equipment have been described.<sup>11</sup> The thermostat was filled with an ice + water mixture for the  $0^\circ$  measurements. Heats of mixing are precise to  $\pm 2\%$ , mole fractions to  $\pm 0.0005$ .

**Nuclear Magnetic Resonance (N.m.r.) Measurements.**—Permanent samples of mixtures were sealed in Pyrex tubes after adding approximately 0.25 mole % cyclohexane as an internal standard. A Varian Associates V-4300-B High Resolution n.m.r. spectrometer with auxiliary equipment (including a variable temperature probe) was used for measuring chemical shifts due to hydrogen bonding. A copper-constantan thermocouple sensed the probe temperature. Complete details of technique and the method of

calculating equilibrium constants for the hydrogen-bonded complex are given in reference 8 and a paper to be published shortly. Temperature readings were at least good to one degree; estimated uncertainties in the equilibrium constants are given in Table III.

**Volume Changes.**—Two calibrated capillaries were attached vertically to either side of a glass bulb with a thin glass membrane in the middle and a glass-enclosed soft iron rod in one side. The capillaries had ground-glass fitted caps with 1 mm.-diameter "breather" holes to equalize pressures on both sides of the membrane before making measurements. Pure liquids were weighed in the apparatus after insertion with a syringe and fine glass tube. Heights of the liquids in the capillaries were read with a cathetometer after allowing at least 8 hr. for thermal equilibrium to be reached in a water-bath. The iron rod served as a breaker and stirrer; tilting the whole assembly ensured mixing of the material in the arms. The uncertainties in  $\bar{V}^E$  near  $x_2 = 1/2$  and in composition were  $\pm 0.01 \text{ cm.}^3$  and  $\pm 0.005$ , respectively. A null measurement (acetone in both sides) gave  $\bar{V}^E = 0.008 \text{ cm.}^3$  at  $x_2 = 1$ .

Several trial measurements were made on the system benzene + cyclohexane at  $25^\circ$  and the results agree well with those of Mathieson and Thynne<sup>12</sup> (our maximum volume change was  $0.68 \text{ cm.}^3/\text{mole}$ , theirs  $0.66 \text{ cm.}^3/\text{mole}$ , both at  $x = 1/2$ ).

**Phase Diagram.**—Phase separations were observed for mixtures in sealed Pyrex tubes (8 cm. long, 4 mm. i.d.) cooled in a water-bath at a rate of one degree/min. or less. Stirring was accomplished by continuously tilting the tubes, moving two glass beads through the liquids. Temperatures were determined with an uncalibrated mercury thermometer and are precise to  $\pm 0.1^\circ$ , accurate to  $\pm 0.5^\circ$ . The main concern in this work was to locate the sides of the phase diagram for  $C_7F_{16} + OCMe_2$  so that phase separation could be avoided in measuring heats of mixing in that system. Uncertainties in the composition (determined by weighing the tubes after addition of each component) were  $\pm 0.005$ .

## Results and Discussion

**Excess Gibbs Free Energies.**—Crude vapor pressure-liquid composition data at  $0^\circ$  allowed us to estimate  $\bar{G}^E$  for  $C_7F_{15}H + OCMe_2$ . A modified Barker method calculation<sup>13,14</sup> of partial pressures and excess Gibbs free energies gave the coefficients for the Guggenheim-Scatchard expansion  $\bar{G}^E = x_1x_2 \sum_n g_n (x_1 - x_2)^n$  in Table I and the total pressure curve in Fig. 1.

TABLE I  
THERMODYNAMIC PROPERTIES OF  $C_7F_{15}H + OCMe_2$

$Y$ ( $t$ , $^\circ\text{C.}$ )	$G(0)$	$H(35)$	$H(0)$	$TS(0)$	$V(20)$ , $\text{cm.}^3$
$y_0$	193	-497	-707	-900	6.60
$y_1$	-433	-960	-945	-512	-5.73
$y_{1/2}$	309	683	413	104	0.25
$y_{3/2}$	116	-200	-499	-614	2.01
$\sigma_Y$	0.8	3 cal.	8 cal.	...	0.07
					$\text{cm.}^3$

$\sigma_Y = \sqrt{d_i^2/(n - m)}$  where  $m$  = no. parameters,  $n$  = no. observations,  $d_i$  = deviations of observations from the calculated curve.

**Heats of Mixing.**—Table II gives the observed heats of mixing at 0 and  $35^\circ$ . Coefficients for the Guggenheim-Scatchard expansion  $\bar{H}^E = x_1x_2 \sum_n$

(12) A. R. Mathieson and J. C. J. Thynne, *J. Chem. Soc.*, 3708 (1956).

(13) Data processing was done on the IBM 7090 digital computer at the Computing Facility, University of California, Los Angeles.

(14) A. G. Williamson and R. L. Scott, *J. Phys. Chem.*, **65**, 275 (1961).

(11) A. G. Williamson and R. L. Scott, *J. Phys. Chem.*, **64**, 440 (1960).



$h_n(x_1 - x_2)^n$  were determined by the method of least squares<sup>13</sup> and are given in Table I. The smooth S-shaped curves in Fig. 2, calculated from the coefficients in Table I, fit the data within experimental errors.

TABLE II  
HEATS OF MIXING FOR  $C_7F_{15}H + OCM_e_2$   
 $P = 1$  atmosphere

$t =$	$0^\circ$		$35^\circ$	
$x_2$	$\bar{H}^E$ , cal.	$x_2$	$\bar{H}^E$ , cal.	
	0.0767	-96.3	0.0960	-78.2
	.1638	-191.0	.2332	-153.4
	.3196	-218.5	.3400	-167.1
	.3985	-205.8	.4247	-152.0
	.5261	-172.6	.4625	-140.5
	.5593	-142.4	.6284	-43.5
	.6662	-73.1	.6925	-2.4
	.7372	-18.4	.7440	26.3
	.8150	24.6	.7795	48.8
	.8914	46.6	.8536	71.9
	.9102	57.6	.9371	60.9
	.9868	7.2	.9700	40.6

It was possible to separate the observed total heats of mixing curve into a chemical (hydrogen bonding) part and a "physical" part due to non-specific interactions (Fig. 2). Molar equilibrium constants (Table III) defined by eq. 1, where  $C$  is the number of moles of hydrogen-bonded complex

$$K = \frac{[C][A + B - C]}{[A - C][B - C]} \quad (1)$$

formed when  $A$  moles of  $C_7F_{15}H$  and  $B$  moles of  $OCMe_2$  are mixed, were determined from n.m.r. measurements at  $-20$ ,  $30$ , and  $80^\circ$  and from these

TABLE III<sup>15</sup>

MOLAR EQUILIBRIUM CONSTANTS FOR  $C_7F_{15}H + OCM_e_2 = C_7F_{15}H \cdots OCM_e_2$

$t$ , $^\circ C$ .	$K$
80	$1 \pm 0.4$
30	$2 \pm 0.6$
-20	$4 \pm 1.0$

$\Delta H_{H \text{ bond}}^f = -2.5 \pm 0.5$  kcal./mole

values a heat of formation of the hydrogen bond was estimated to be  $\Delta H_{H \text{ bond}}^f = -2.5$  kcal./mole. The symmetric exothermic curve in Fig. 2 was calculated from eq. 2 and subtracted from the ob-

$$\bar{H}_{H \text{ bond}}^E = \Delta H_{H \text{ bond}}^f \left( \frac{C}{A + B} \right) \quad (2)$$

served total heats, giving the upper skewed curve. The indicated width (dotted lines) of the exothermic curve (and thus also of the non-specific curve) is due to the 0.5 kcal./mole uncertainty in  $\Delta H_{H \text{ bond}}^f$ .

Table IV gives values of  $\bar{H}_{\text{Obs.}}^E$  at  $x_2 = 1/2$  for various fluorocarbon systems in which hydrogen bonding cannot occur; these values lie very close to the "physical" endothermic curve for  $C_7F_{15}H + OCM_e_2$ . Heats determined by the "vapor pressure" method were estimated from the temperature dependence of the Gibbs free energies.

The shape of the "physical" part of the heat of mixing agrees well with the van-Laar-Scatchard-

(15) S. K. Alley, Doctoral Dissertation, page 50.

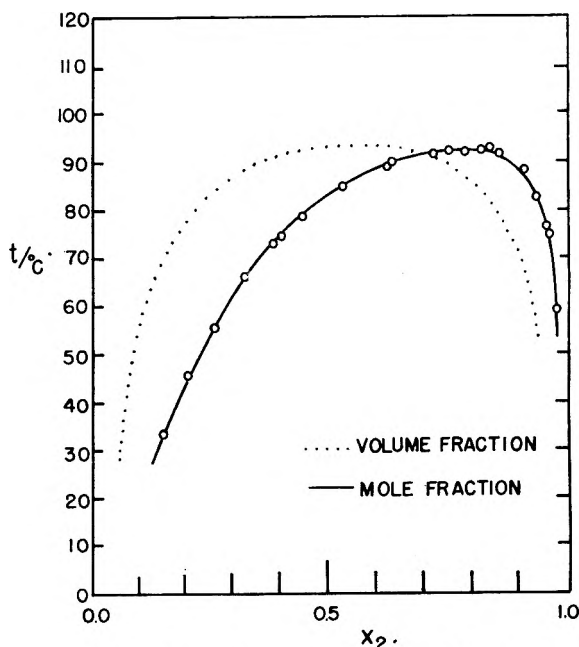


Fig. 3.—Phase diagram for  $C_7F_{16} + OCM_e_2$ .

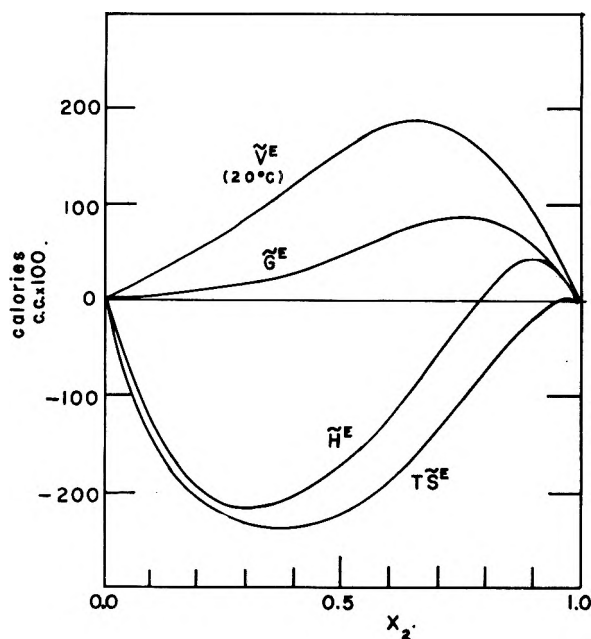


Fig. 4.—Excess functions for  $C_7F_{15}H + OCM_e_2$ ,  $0^\circ$ .

TABLE IV

HEATS OF MIXING FOR FLUOROCARBON SYSTEMS

System	$x_2 = 1/2$		Method	Refer.
	$t$ , $^\circ C$ .	$\bar{H}^E$ , cal.		
$C_7F_{16} + i-C_8H_{18}$	30, 50	508	Calorimeter	14
$C_6F_{14} + C_6H_{14}$	25, 35	516	Calorimeter	14
$C_5F_{12} + Si(CH_3)_4$	0	465	Vapor pressure	4
$C_5F_{12} + C_5H_{12}$	4	370	Vapor pressure	4
$C_4F_{10} + C_4H_{10}$	-27	504	Vapor pressure	4

Hildebrand equation for the energy of mixing in a regular solution

$$E^M = A \frac{x_1 \bar{V}_1 x_2 \bar{V}_2}{x_1 \bar{V}_1 + x_2 \bar{V}_2} \quad (3)$$

For such an expression, with a concentration-inde-

pendent  $A$ , the maximum occurs at

$$x_{\max} = \frac{\sqrt{\bar{v}_1}}{\sqrt{\bar{v}_1} + \sqrt{\bar{v}_2}} \quad (4)$$

At 25°,  $\bar{v}_{\text{C}_7\text{F}_{15}\text{H}} = 214 \text{ cm.}^3$ ,  $\bar{v}_{\text{OCMe}_2} = 74 \text{ cm.}^3$ , yielding  $x_{\max} = 0.63$ , in excellent agreement with the observed maximum at  $x_2 = 0.61$ .

A further test of the additivity of chemical and "physical" heats was made by measuring the heat of mixing for  $\text{C}_7\text{F}_{16} + \text{OCMe}_2$  on both sides of the two-phase region in Fig. 3. At 35°, the heats were 90.8 and 15.5 cal. at  $x_2 = 0.097$  and 0.993, respectively. These values are shown in Fig. 2. Phase separation would have caused low results, vaporization high results (a small bubble appeared in the  $x_2 = 0.097$  run).

**Volume Changes.**—Excess volumes for fluorocarbon + hydrocarbon mixtures are positive and unusually large; values of 3 to 6  $\text{cm.}^3/\text{mole}$  at  $x_2 = 1/2$  have been reported.<sup>4</sup> The reason for these unusually large volume changes is not entirely understood, but the combination of the large positive excess free energy with the large coefficient of thermal expansion of fluorocarbons appears to be the most significant factor.<sup>16</sup>

In contrast to the situation with the heat of mixing, the "chemical" contribution to the volume change, while probably negative, would be expected to be small in comparison with these large "physical" effects. Hydrogen-bonded mixtures usually show small negative volume changes over all or most of the composition range (*e.g.*,  $\text{Cl}_3\text{CH} + \text{OCMe}_2$ ,  $\bar{v}^E = -0.2 \text{ cm.}^3$  at  $x = 1/2$  and 35°). Figure 4 shows the volume changes observed for  $\text{C}_7\text{F}_{15}\text{H} + \text{OCMe}_2$  at 20°.  $\bar{v}^E$  decreases with decreasing temperature. A small region of negative volume change near  $x_2 = 0$  is possible within the experimental error of our data at 20°.

**Excess Entropy of Mixing.**—The excess functions for  $\text{C}_7\text{H}_{15}\text{H} + \text{OCMe}_2$  at 0° (volume changes at 20°) are shown in Fig. 4. These curves were calculated from the coefficients in Table I. The large negative excess entropy is of course due to the loss of

rotational freedom when the hydrogen bond is formed.

**Solubility.**—Fluorocarbon + hydrocarbon systems usually show partial miscibility with upper critical temperatures of 300 to 400°K. for  $\text{C}_6$  or higher compounds.<sup>4</sup> Phase separation was *not* observed for  $\text{C}_7\text{F}_{15}\text{H} + \text{OCMe}_2$  from freezing to boiling at atmospheric pressure and up to 100° in sealed tubes over a wide mole fraction range. Perfluoroheptane itself, however, is only partially miscible with acetone. Figure 3 shows our phase diagram for  $\text{C}_7\text{F}_{16} + \text{OCMe}_2$  ( $t_c = 93.5^\circ$ ,  $x_c = 0.82$ ). The dotted line is the same data plotted against volume fraction as abscissa; this illustrates the approximate volume-fraction symmetry previously observed by Hildebrand, Fisher, and Benesi<sup>17</sup> for perfluoroheptane + hydrocarbon systems. It is interesting to note that the phase diagram for  $n\text{-C}_7\text{H}_{16} + \text{OCMe}_2$  is very symmetrical in mole fraction with  $t_c = -27.6^\circ$  and  $x_c = 0.50$ , and has a broad, flat top, much flatter than that of  $\text{C}_7\text{F}_{16} + \text{OCMe}_2$ .<sup>18</sup>

Lower critical points require that at low temperatures  $\bar{H}^E$  and  $\bar{S}^E$  be negative, but that  $\bar{G}^E$  become increasingly positive as the critical temperature is approached.<sup>19</sup> The sort of behavior observed for  $\text{C}_7\text{F}_{15}\text{H} + \text{OCMe}_2$  fits such a requirement although the unusual composition dependence precludes the application of a simple model. So far phase separation has not been observed for  $\text{C}_7\text{F}_{15}\text{H} +$  acetone, 2-butanone, 3-pentanone, 4-heptanone, diethyl ether, or triethylamine. Benzene and mesitylene (where the proton of  $\text{C}_7\text{F}_{15}\text{H}$  associates with the  $\pi$  electrons<sup>20</sup>) and dioxane have upper critical points near room temperature; this does not preclude lower critical points, but we have not observed any above the freezing temperatures of these mixtures (only equivolume mixtures were studied).

(17) J. H. Hildebrand, B. B. Fisher, and H. A. Benesi, *J. Am. Chem. Soc.*, **72**, 4348 (1950).

(18) H. Wolf and K. Bernstorff, *Z. physik. Chem. (Frankfurt)*, **14**, 208 (1953).

(19) J. L. Copp and D. H. Everett, *Discussions Faraday Soc.*, No. **15**, 182 (1953).

(20) S. K. Alley, Doctoral Dissertation, page 111.

(16) I. M. Croll and R. L. Scott, *J. Phys. Chem.*, **62**, 954 (1958).

# THE EFFECT OF AN IMPURITY ON THE PHASE TRANSITION IN A BINARY LIQUID SYSTEM. II<sup>1,2</sup>

BY O. K. RICE AND J. T. MACQUEEN

*Department of Chemistry, University of North Carolina, Chapel Hill, North Carolina*

*Received October 16, 1961*

Two expressions have been derived for  $dT_c/dc_3$  (where  $T_c$  is critical solution temperature and  $c_3$  is concentration of an impurity) in a binary liquid system, one by Wagner on a general thermodynamic basis, and one by one of us based on a consideration of the effect of the impurity on the interfacial tension of the interface between the phases assuming that even at the critical point there is a difference in composition of the coexisting phases (*i.e.*, there is a critical range of concentrations). A new derivation is given for Wagner's relation, and the relation between the two equations is discussed. They are shown to be equivalent under certain limiting conditions. This proof depends upon the assumptions that the solubility of the impurity and the molal entropy of the mixture are the same at a point in the interface as in a bulk phase of the same composition. The validity of the latter assumption is considered in detail, and certain necessary conditions for there to be a critical range of concentrations are discussed. Some experiments are presented in which  $dT_c/dc_3$  is measured, for water in the cyclohexane-aniline system. Measurements also were made in which the solutions were saturated with water. These experiments are discussed in the light of the theory developed, the negative adsorption of water at the interface is obtained, and an estimate is obtained for the thickness of the interface at the critical temperature.

## Introduction

In a recent paper<sup>3</sup> the effect of a third component in small concentration (an "impurity") on the critical temperature of a binary liquid system was treated as a surface effect. At the critical temperature the interfacial tension is zero; by considering the rate of change of interfacial tension with temperature and with the concentration of the third component and balancing these against each other, the effect of the concentration on the critical temperature can be found. It was shown<sup>3,4</sup> that where

$$dT_c/dc_3 = RT(\Gamma_3/c_3)(\partial\sigma/\partial T)_{c_3}^{-1} \quad (1.1)$$

$T$  is the temperature,  $T_c$  the critical temperature,  $c_3$  the concentration of the third component,  $R$  the gas constant,  $\sigma$  the interfacial tension, and  $\Gamma_3$  the interfacial adsorption of the third component, defined with respect to a certain dividing surface, placed so as to make the adsorption of the main components as nearly zero as possible, and in any case to cause their effects to cancel.

On the other hand, Wagner<sup>5</sup> has shown by a thermodynamic analysis of the ternary system that, when the impurity is dilute, we may write<sup>6</sup>

$$dT_c/dc_3 = - \frac{(RT/\lambda)d^2\lambda/dx_1^2}{d^2\Delta S/dx_1^2} \quad (1.2)$$

where  $x_1$  is the mole fraction of the first component,  $\lambda$  is proportional to the solubility of the third component, and  $\Delta S$  is the entropy of mixing of  $x_1$  moles of the first component with  $x_2 = 1 - x_1$  moles of the second, being given by

$$\Delta S = x_1\bar{s}_1 + x_2\bar{s}_2 - x_1s_1^0 - x_2s_2^0 \quad (1.3)$$

where  $\bar{s}_1$  and  $\bar{s}_2$  are partial molal entropies and  $s_1^0$  and  $s_2^0$  are molal entropies of the pure components.

(1) This work was supported by the U. S. Army Research Office, Durham, North Carolina.

(2) This paper was presented by one of us (O. K. R.) at the symposium held in Berkeley, California, September, 1961, to honor Professor Joel Hildebrand on the occasion of his eightieth birthday. It is dedicated to Professor Hildebrand with admiration and affection.

(3) J. T. MacQueen, F. R. Meeks, and O. K. Rice, *J. Phys. Chem.*, **65**, 1925 (1961). Referred to as I.

(4) D. Atack and O. K. Rice, *Discussions Faraday Soc.*, **15**, 210 (1953).

(5) C. Wagner, *Z. physik. Chem.*, **132**, 273 (1928).

(6) Wagner expressed his equation in terms of the enthalpy of mixing ( $\Delta H$ , called by him  $Q$ ) instead of the entropy of mixing. The equation given here is equivalent since  $\partial^2G/\partial x_1^2$  (where  $G$  is the Gibbs free energy) vanishes at the critical point.

It will be noted that eq. 1.1 and 1.2 are not quite equivalent to each other, for Wagner has assumed that the coexistence curve is rounded in the neighborhood of the critical point, whereas we assume that the coexistence curve is truncated or flattened at the critical temperature<sup>7</sup>; *i.e.*, we assume that at the critical temperature there are still two distinct phases, and a range of critical compositions. The vanishing of the interfacial tension at  $T_c$ , due to cancellation of the energy and entropy parts, causes the two phases to "emulsify" into each other. It is clear that, though eq. 1.1 and 1.2 are not precisely equivalent, they are closely related to each other. It will be the purpose of this paper to explore the relationship between them, and to discuss the application of some new data to the elucidation of the situation.

## New Derivation of Wagner's Relation.—

Before proceeding to the ends indicated above, we wish to present a derivation of Wagner's equation, (1.2), based upon a simpler, though possibly a slightly more restricted, criterion for the critical point, than that used by him, though again assuming a rounded coexistence curve.<sup>8</sup> If there are two phases in equilibrium with each other, containing two principal components and a small amount of a third component, the third component also is in equilibrium between the phases. Since the third component will have a different concentration in each of the two phases, it is awkward to attempt to define a concentration of the third component in the system. Its activity,  $a_3$ , is, however, the same in the two phases, and we may think of  $a_3$  as being fixed in some particular way, as the activity of water in the cyclohexane-aniline system was controlled by Meeks, Gopal, and Rice<sup>9</sup> by using a mixture of  $\text{Li}_2\text{SO}_4$  and  $\text{Li}_2\text{SO}_4 \cdot \text{H}_2\text{O}$ . We can use the activity of the third component, then, as an independent variable, rather than its concentration, and consider the phase equilibrium in the presence of this fixed activity. At any temperature, we have the relations between the chemical potentials

(7) See O. K. Rice, *J. Chem. Phys.*, **23**, 164 (1955).

(8) A still different derivation has been given by B. Widom, private communication.

(9) F. R. Meeks, R. Gopal, and O. K. Rice, *J. Phys. Chem.*, **63**, 992 (1959).

$$\begin{aligned}\mu_1' &= \mu_1'' \\ \mu_2' &= \mu_2''\end{aligned}\quad (2.1)$$

where the single prime indicates the phase richer in component 1 and the double prime indicates the phase richer in component 2. The critical point, then, is a point at which

$$(\partial\mu_1/\partial x_1)_{a_3} = (\partial\mu_2/\partial x_1)_{a_3} = 0 \quad (2.2)$$

At this point, of course, there is a definite concentration  $c_3$  of the third component, and it will be possible to consider how the partial differential coefficient  $(\partial\mu_1/\partial x_1)_{a_3}$  changes with  $c_3$ ,  $T$ , and  $x_1$ .

We define  $x_1$  and  $x_2$  as the mole fractions of the binary system, so that  $x_1 + x_2 = 1$ , and  $c_3$  as the number of moles of third component per mole of binary system. We also will wish to refer to the numbers of moles,  $n_1$ ,  $n_2$ , and  $n_3$ . Since the activity will be used at different temperatures, it must be defined carefully. We will take the activity equal to the concentration of the vapor of third component, assumed ideal. Then, assuming an ideal, or dilute, solution

$$c_3 = a_3\lambda \quad (2.3)$$

where  $\lambda$  is the solubility of the third component and is a function of  $x_1$ , say, and  $T$ . It also is possible to write

$$\mu_3 = \mu_3^0 + RT \ln a_3 = \mu_3^0 + RT \ln c_3 - RT \ln \lambda \quad (2.4)$$

Taking  $x_1$ ,  $a_3$ , and  $T$  as independent variables, we may write, following the locus of the critical point

$$\frac{\partial^2\mu_1}{\partial a_3\partial x_1} da_3 + \frac{\partial^2\mu_1}{\partial T\partial x_1} dT + \frac{\partial^2\mu_1}{\partial x_1^2} dx_1 = 0 \quad (2.5)$$

It also is true that  $\partial^2\mu_1/\partial x_1^2 \equiv (\partial^2\mu_1/\partial x_1^2)_{a_3,T}$  vanishes at the critical point. It is possible for  $dx_1/dT_c$  to be very large, but we will show in Section 3 that it is never of a large enough order to make the last term appreciable. Therefore we may write

$$\frac{dT}{da_3} = - \frac{\partial^2\mu_1/\partial a_3\partial x_1}{\partial^2\mu_1/\partial T\partial x_1} \quad (2.6)$$

If  $c_3$  is very small, then from eq. 2.3

$$dc_3 = \lambda da_3$$

so

$$\frac{dT}{dc_3} = - \frac{\partial^2\mu_1/\partial a_3\partial x_1}{\lambda\partial^2\mu_1/\partial T\partial x_1} \quad (2.7)$$

Now we may write

$$\begin{aligned}\left(\frac{\partial\mu_1}{\partial a_3}\right)_{x_1,T} &= \lambda \left(\frac{\partial\mu_1}{\partial c_3}\right)_{x_1,T} = \lambda \left(\frac{\partial\mu_1}{\partial n_3}\right)_{n_1,n_2,T} (n_1 + n_2) = \\ &\quad \lambda \left(\frac{\partial\mu_3}{\partial n_1}\right)_{n_2,n_3,T} (n_1 + n_2) \\ &= RT\lambda(\partial \ln c_3/\partial n_1 - \partial \ln \lambda/\partial n_1)(n_1 + n_2) \\ &= -RT\lambda[1 + x_2(\partial \ln \lambda/\partial x_1)_{T,c_3}]\end{aligned}\quad (2.8)$$

The last expression arises because  $c_3 = n_3/(n_1 + n_2)$  and  $x_1 = n_1/(n_1 + n_2)$ . From the above we may write

$$\partial^2\mu_1/\partial x_1\partial a_3 = -x_2 RT \partial^2\lambda/\partial x_1^2 \quad (2.9)$$

Now to evaluate  $\partial^2\mu_1/\partial T\partial x_1$  we note that  $(\partial\mu_1/\partial T)_{x_1,a_3}$  is equal to  $(\partial\mu_1/\partial T)_{x_1,c_3}$  when  $c_3 \rightarrow 0$ , and

$$(\partial\mu_1/\partial T)_{x_1,c_3} = -\bar{s}_1 \quad (2.10)$$

where  $\bar{s}_1$  is the partial molal entropy. The entropy

of solution  $\Delta S$  is given by eq. 1.3, and using the Gibbs–Duhem equation applied to entropy

$$\partial\Delta S/\partial x_1 = \bar{s}_1 - \bar{s}_2 - (s_1^0 - s_2^0) \quad (2.11)$$

and

$$\begin{aligned}\partial^2\Delta S/\partial x_1^2 &= \partial\bar{s}_1/\partial x_1 - \partial\bar{s}_2/\partial x_1 \\ &= (\partial\bar{s}_1/\partial x_1)(1 + x_1/x_2)\end{aligned}$$

(from the Gibbs–Duhem relation)

$$= x_2^{-1}\partial\bar{s}_1/\partial x_1 \quad (2.12)$$

Thus

$$\partial^2\mu_1/\partial T\partial x_1 = -\partial\bar{s}_1/\partial x_1 = -x_2\partial^2\Delta S/\partial x_1^2 \quad (2.13)$$

From eq. 2.7, 2.9, and 2.13, Wagner's equation (1.2) follows.

#### Higher Derivatives of the Chemical Potential.—

As we have noted  $(\partial^2\mu_1/\partial x_1^2)_{a_3}$  also may be expected to vanish at a critical point, and if we follow this derivative along the locus of the critical point we may write

$$\frac{\partial^2\mu_1}{\partial a_3\partial x_1^2} da_3 + \frac{\partial^3\mu_1}{\partial T\partial x_1^2} dT + \frac{\partial^3\mu_1}{\partial x_1^3} dx_1 = 0 \quad (3.1)$$

If all the derivatives are finite and non-vanishing this offers no unusual features, and with the use of eq. 1.2 would enable one to determine  $dx_1/dT_c$  or  $dx_1/da_3$  along the locus of critical points. However, there is some indication, since most coexistence curves are cubic rather than quadratic,<sup>7,10</sup> that  $\partial^3\mu_1/\partial x_1^3$  also will vanish.<sup>11</sup> In this case, if we are interested in a region very close to the critical point of the binary system, we would substitute<sup>12</sup>  $1/2(\partial^4\mu_1/\partial x_1^4)(dx_1)^2$  for the last term in eq. 3.1, recognizing, however, that  $\partial^4\mu_1/\partial x_1^4$  would have to have a discontinuity, being positive if  $x_1 > x_{1,c}$ , where  $x_{1,c}$  is the value at the critical point, and negative if  $x_1 < x_{1,c}$ . Thus the resulting equation which is substituted for (3.1) would have a real solution only for  $dx_1$  either positive or negative, depending on the signs of the other terms, and  $dx_1$  would start off as  $(dT_c)^{1/2}$ . However, this depends on at least one of  $\partial^3\mu_1/\partial a_3\partial x_1^2$  and  $\partial^3\mu_1/\partial T\partial x_1^2$  being different from zero. There is no doubt that  $\partial^2\mu_1/\partial a_3\partial x_1$  and  $\partial^2\mu_1/\partial T\partial x_1$  are different from zero, but a turning point for  $\mu_1$  will persist as the temperature of the binary system is raised above its critical temperature, and while this may not occur exactly at the critical composition it certainly will be very close to it; thus, if  $\partial^3\mu_1/\partial T\partial x_1^2$  is not actually zero at the critical point, it probably will be very close to it. In a similar manner,  $\partial^3\mu_1/\partial a_3\partial x_1^2$  also might be expected to be very small. Thus, though the locus of the critical point may start off with  $dx_1/dT_c$  infinite, it still will not be a very noticeable infinity. Widom<sup>13</sup> has shown that if the critical point be defined as the maximum of a temperature–composition curve with fixed value of  $c_3$  rather than of  $a_3$ , then along the critical locus  $dx_1$  starts out as  $(dT_c)^{1/2}$ , but this also depends on the non-vanishing of a differential coefficient.

It may be noted that with  $dx_1 \sim (dT_c)^{1/2}$  the last term of eq. 2.5 will remain negligible. Since in

(10) J. D. Cox and E. F. G. Herington, *Trans. Faraday Soc.*, **52**, 926 (1956).

(11) O. K. Rice, *J. Chem. Phys.*, **23**, 169 (1955).

(12) Cross terms involving  $dx_1$  and  $dT$  or  $dx_1$  and  $da_3$  always will be of higher order.

(13) B. Widom, private communication.

this case  $\partial^3\mu_1/\partial x_1^3$  vanishes, we would substitute for the last term<sup>12</sup>  $1/6(\partial^4\mu_1/\partial x_1^4)(dx)^3$ , which would be of the order  $(dT_c)^{3/2}$  and hence of higher order than the other terms.

**Relation between the Equations.**—We turn now to the principle point in our theoretical investigation, namely the relation between eq. 1.1 and 1.2. It will be recalled that these have a slightly different basis, eq. 1.1 being grounded on the assumption that there is still a surface at the critical temperature, so we can expect coincidence only as a first approximation. We also shall find it necessary, in order to avoid considerable complication, to make the simplifying assumption that the density of the solution is constant throughout, although we would not expect this to be necessary from a fundamental point of view.

Let us first consider  $\Gamma_3$ . This quantity is defined as the excess in the amount of the third component at the surface over what it would be if its concentration had the respective bulk values right up to the selected dividing surface. We may write

$$\Gamma_3 = \int_{-\infty}^0 (c_3\rho - c_3'\rho') dz + \int_0^{\infty} (c_3\rho - c_3''\rho'') dz \quad (4.1)$$

where  $z$  is the coordinate normal to the surface ( $z = 0$  at the selected dividing surface),  $c_3$  is the number of moles of component 3 per mole of binary mixture, and  $\rho$  is the molar density of the binary mixture, both considered as functions of  $z$ , while  $c_3'$ ,  $c_3''$ ,  $\rho'$ , and  $\rho''$  are values characteristic of the bulk phases. Now  $a_3$  is constant throughout, and we may write  $c_3 = \lambda a_3$ . If  $\rho$  is taken as a constant throughout, we may write

$$\Gamma_3 = a_3\rho \left[ \int_{-\infty}^0 (\lambda - \lambda') dz + \int_0^{\infty} (\lambda - \lambda'') dz \right] \quad (4.2)$$

If  $\rho$  is constant, then

$$\int_{-\infty}^0 (x_1 - x_1') dz + \int_0^{\infty} (x_1 - x_1'') dz \cong 0 \quad (4.3)$$

This is the condition that we have set our dividing surface at the position where  $\Gamma_1$  and, hence (if  $\rho$  is constant),  $\Gamma_2$  are both zero.

If we expand  $\lambda - \lambda'$  and  $\lambda - \lambda''$  in Taylor series we obtain

$$\lambda - \lambda' \cong (\partial\lambda/\partial x_1)'(x_1 - x_1') + 1/2(\partial^2\lambda/\partial x_1^2)'(x_1 - x_1')^2 \quad (4.4)$$

and

$$\lambda - \lambda'' \cong (\partial\lambda/\partial x_1)''(x_1 - x_1'') + 1/2(\partial^2\lambda/\partial x_1^2)''(x_1 - x_1'')^2 \quad (4.5)$$

assuming, in this approximation, that  $\partial^2\lambda/\partial x_1^2$  is constant, but taking account of the difference in  $\partial\lambda/\partial x_1$  in the two bulk phase. The latter values will be related by

$$(\partial\lambda/\partial x_1)'' = (\partial\lambda/\partial x_1)' + (\partial^2\lambda/\partial x_1^2)(x_1'' - x_1') \quad (4.6)$$

If we insert (4.4), (4.5), and (4.6) into eq. 4.2, then, noting eq. 4.3, we find

$$\Gamma_3 \cong a_3\rho(\partial^2\lambda/\partial x_1^2)I \quad (4.7)$$

and

$$\Gamma_3/c_3' = \rho\lambda'^{-1}(\partial^2\lambda/\partial x_1^2)I \quad (4.8)$$

where

$$I = 1/2 \int_{-\infty}^0 (x_1 - x_1')^2 dz + 1/2 \int_0^{\infty} [(x_1 - x_1'')^2 + 2(x_1'' - x_1')(x_1 - x_1'')] dz \quad (4.9)$$

Now  $(x_1'' - x_1')(x_1 - x_1'')$  always is negative, and it always is larger in absolute value than  $(x_1 - x_1'')^2$  or  $(x_1 - x_1')^2$ . Therefore  $I$  is negative.

We turn now to the term  $(\partial\sigma/\partial T)_{c_3}$  for  $c_3 \rightarrow 0$ . This is equal to the negative of the surface entropy

$$\partial\sigma/\partial T = -s_\sigma \quad (4.10)$$

We can set up an equation analogous to (4.1)

$$s_\sigma = \int_{-\infty}^0 [(x_1\bar{s}_1 + x_2\bar{s}_2)\rho - (x_1'\bar{s}_1' + x_2'\bar{s}_2')\rho'] dz + \int_0^{\infty} [(x_1\bar{s}_1 + x_2\bar{s}_2)\rho - (x_1''\bar{s}_1'' + x_2''\bar{s}_2'')\rho''] dz \cong \rho \left[ \int_{-\infty}^0 (\Delta S - \Delta S') dz + \int_0^{\infty} (\Delta S - \Delta S'') dz \right] \quad (4.11)$$

using the definition of eq. 1.3. In just the same way that eq. 4.7 was derived from eq. 4.2, we now obtain

$$s_\sigma = \rho(\partial^2\Delta S/\partial x_1^2)I \quad (4.12)$$

Now noting eq. 2.13 and combining eq. 1.1, 4.8, 4.10, and 4.12, we see that eq. 1.1 reduces to eq. 1.2. As noted, certain approximations enter this result, but, except for the assumption of constant  $\rho$ , which should not be necessary, but which we have not been able to remove, they reflect the true but small differences between (1.1) and (1.2), which will of course be less the smaller the critical range of concentrations.

**Validity of the Approximations.**—In the above deduction the assumption has been made that the solubility and the entropy at a point in the surface were the same as they would be in a bulk phase of the same composition. Such an assumption seems reasonable at the critical temperature, which is the last temperature at which a surface exists if there is a range of critical concentrations. At the critical temperature one may expect that, even if there are still two phases in equilibrium, concentration gradients will be small. However, some further consideration of this approximation is desirable.

Cahn and Hilliard<sup>14</sup> showed that a formal theory of interfacial tension could be developed by taking into account the fact that the free energy at a point at which concentration gradients exist in general will be different from that of a bulk phase having the concentration existing at this point. If  $\Delta_0 F$  is the difference in free energy<sup>15</sup> between such a bulk phase, characterized by the concentration at a specific point in the interface, and the bulk phases which are actually present and in equilibrium with each other, then the true difference in free energy, taking into account the effects of gradients, can be shown to be given by<sup>14,16</sup>

$$\Delta_0 F + \kappa(\partial x_1/\partial z)^2 + \text{terms of higher order}$$

where  $\kappa$  is a coefficient depending on  $x_1$  and  $T$ , and the surface tension will be given ( $\rho$  constant) by

$$\sigma = \min \rho \int_{-\infty}^{\infty} [\Delta_0 F + \kappa(\partial x_1/\partial z)^2] dz \quad (5.1)$$

(14) J. W. Cahn and J. E. Hilliard, *J. Chem. Phys.*, **28**, 258 (1958).

(15) In a condensed phase we do not need to distinguish between Gibbs and Helmholtz free energy.

(16) O. K. Rice, *J. Phys. Chem.*, **64**, 976 (1960).

Minimization of this expression by the calculus of variations yields

$$\Delta_0 F - \kappa(\partial x_1/\partial z)^2 = \text{const} = 0 \quad (5.2)$$

(the constant is zero by the boundary conditions), and hence

$$\sigma = 2\rho \int_{-\infty}^{\infty} \Delta_0 F dz \quad (5.3)$$

The interfacial tension can be written as the sum of an energy and an entropy term, thus

$$\sigma = e_\sigma - Ts_\sigma \quad (5.4)$$

and if the two terms on the right-hand side cancel each other before the two phases become identical we have the phenomenon of a flat top in the coexistence curve, representing the range of concentrations at the last temperature (the critical temperature) at which two phases can be observed. Equation 5.3 shows that certain conditions must hold, in addition, because  $\Delta_0 F$  cannot be negative without creating a more stable phase, so if  $\sigma = 0$ , we see that  $\Delta_0 F$  must be zero for all  $z$ . Then we see that, unless  $\kappa = 0$ , we would have  $\partial x_1/\partial z = 0$ , hence no gradient. Thus vanishing of  $\kappa$  is a further condition for a critical range of concentrations.

We already have discussed reasons for expecting  $\kappa$  to vanish at the critical point, even if there is no critical range,<sup>16</sup> and have shown that experimental data on the interfacial tension are in accord with this assumption. According to our formulation we could write for the free energy at any point (using chemical potentials which do not include the effects of concentration gradients)

$$F \cong x_1\mu_1 + x_2\mu_2 + \kappa(\partial x_1/\partial z)^2 \quad (5.5)$$

and similarly for energy and entropy

$$E \cong x_1\bar{e}_1 + x_2\bar{e}_2 + \kappa_e(\partial x_1/\partial z)^2 \quad (5.6)$$

and

$$S \cong x_1\bar{s}_1 + x_2\bar{s}_2 + \kappa_s(\partial x_1/\partial z)^2 \quad (5.7)$$

If  $\kappa$  is to be zero at the critical point we must have  $\kappa_c = T\kappa_s$ . It was suggested in earlier work<sup>16</sup> that the departure of  $\kappa$  from zero depended upon the breakdown of this relation as one leaves the critical point.

As we have noted, it appears that the coexistence curve is cubic.<sup>7,10</sup> This means, setting  $\Delta x_1 = x_1'' - x_1'$ , that  $(\Delta x_1)^3$  is proportional to  $\Delta T$ , where  $\Delta T = T_c - T$ . This, of course, neglects any flat top in the coexistence curve. It is found that  $\sigma$  is about proportional to  $(\Delta T)^{3/2}$ , and this can be shown<sup>16</sup> to correspond to

$$\kappa \propto (\Delta x_1)^2 \propto (\Delta T)^{2/3} \quad (5.8)$$

where  $\kappa$  is evaluated at the critical concentration near the critical temperature. The change in  $\kappa$  for a relatively small value of  $\Delta T$  can be effected by small changes in  $\kappa_e$  and  $\kappa_s$ .

Strictly, of course, we should write instead of eq. 4.11

$$s_\sigma = \int_{-\infty}^{\infty} [\Delta_0 S + \rho\kappa_s(\partial x_1/\partial z)^2] dz \quad (5.9)$$

where  $\Delta_0 S = (x_1\bar{s}_1 + x_2\bar{s}_2)\rho - (x_1'\bar{s}_1' + x_2'\bar{s}_2')\rho'$  or  $(x_1\bar{s} + x_2\bar{s})\rho - (x_1''\bar{s}_1'' + x_2''\bar{s}_2'')\rho''$  is the integrand of (4.11), and we need to inquire whether the last term in the integral of eq. 5.9 is likely to play any role at the critical point. For this purpose, it will

be sufficient to ignore the flat top to the coexistence curve, since this occurs only a few thousandths of a degree below what would be the rounded top of the curve.

The assessment of the significance of the last term in eq. 5.9 is most easily made by comparing the integral  $\int_{-\infty}^{\infty} \kappa_s(\partial x_1/\partial z)^2 dz$  with  $s_\sigma$  itself. If  $\sigma \propto (\Delta T)^{3/2}$ , then, since  $d\sigma/dT = -s_\sigma$ , we see that

$$s_\sigma \propto (\Delta T)^{1/2} \quad (5.10)$$

We can write, assuming  $\kappa_s$  to be approximately constant

$$\int_{-\infty}^{\infty} \kappa_s(\partial x_1/\partial z)^2 dz \cong \kappa_s(\partial x_1/\partial z)_{\text{max}}^2 \Delta z \quad (5.11)$$

$(\partial x_1/\partial z)_{\text{max}}$  being the largest value of  $\partial x_1/\partial z$  in the interface and  $\Delta z$  being defined as the thickness of the interface. But obviously

$$(\partial x_1/\partial z)_{\text{max}} \cong \Delta x_1/\Delta z \quad (5.12)$$

We have shown that,<sup>16</sup> if  $\sigma$  varies as  $(\Delta T)^{3/2}$ , and  $\Delta z$  as  $(\Delta T)^{1/2}$ , the thickness of the interface is proportional to  $\Delta T^{-1/2}$ , so

$$\kappa_s(\partial x_1/\partial z)_{\text{max}}^2 \Delta z \propto (\Delta T)^{5/4} \quad (5.13)$$

Comparing this with eq. 5.10 it is seen that if  $\Delta T$  is small enough the contribution of the last term in eq. 5.9 must be negligible. It is true that if the coexistence curve is truncated, these quantities will not have reached their limiting values at  $T_c$ , but they should be close to them.

#### Experimental Procedure and Results<sup>17</sup>

In I we reported experiments on two cyclohexane-aniline mixtures to which water was added and the resulting transition temperatures determined.<sup>3</sup> At the same time that these mixtures were prepared several other mixtures in the critical range of concentration also were prepared, and these were available for further experiments. They had been sealed off in their tubes for some period of time when these experiments were begun, and the separation temperatures were found to be up to 0.02° low, even after redrying with CaO *in vacuo*. Since our principal interest was to obtain values of the change of transition temperature with  $c_3$  it was not believed that this slight discrepancy would make any difference.

Altogether, successful measurements were made with five samples, which are labelled 1 to 5, the samples previously reported<sup>3</sup> being 2 and 4. The final results gave a consistent set of data for all the samples except for sample 3. Suspecting that an error might have been made in preparing this sample, it was decided to analyze samples (1, 3, and 5) by titration for aniline. The other samples were lost in the course of the experiments before the analysis could be run.

The method used was that described by Reilley and Sawyer<sup>18</sup> for pyridine, using glacial acetic acid as a solvent, and following the progress of the titration with perchloric acid by means of a standard pH meter. This method was checked against known samples of aniline, and was found to be unaffected by addition of cyclohexane and water. Samples 1, 3, and 5, after completion of the experiments (known amounts of water being present), were collected in weighed tubes, with constriction and breakseal, equipped with standard joints which were fitted with polyethylene sleeves and covered on the outside with Apiezon W wax to hold the vacuum. After the sample was distilled into such a tube, the constriction was sealed, and the tube was removed and reweighed. Glacial acetic acid then was poured into the space above the breakseal, which was broken; the tube then was thoroughly rinsed with glacial acetic acid and the

(17) For more detail see J. T. MacQueen, Thesis, University of North Carolina, 1961. Some minor corrections in the calculations have been made here.

(18) C. N. Reilley and D. T. Sawyer, "Experiments for Instrumental Methods," McGraw-Hill Book Co., New York, N. Y., 1961, p. 26.

TABLE I  
 EXPERIMENTAL DATA<sup>a</sup>

Sample	1			2			3			4			5		
$n_1 + n_2$	27.37			43.00			(24.01)			47.41			34.83		
$(n_1 + n_2)$	(27.25)												(34.90)		
$x_1$	0.4081			0.4158			(0.4386)			0.4351			0.4373		
$(x_1)$	(0.4077)												(0.4358)		
$T$ (°C.)	29.563			29.593			29.593			29.595			29.575		
	$x_1 \times 10^3$	$\Delta T$	$dT/dx_1$	$x_1 \times 10^3$	$\Delta T$	$dT/dx_1$	$x_1 \times 10^3$	$\Delta T$	$dT/dx_1$	$x_1 \times 10^3$	$\Delta T$	$dT/dx_1$	$x_1 \times 10^3$	$\Delta T$	$dT/dx_1$
	0.522	0.168	322	0.395	0.131	(332)	0.587	0.165	281	0.367	0.105	286	0.396	0.114	288
	1.00	.322	322	0.774	.243	314	1.152	0.325	282	0.719	.206	287	0.777	.221	284
	2.75	.766	(27E)	1.138	.364	320	5.86	1.67	285	1.056	.303	287	1.651	.481	291
	21.65	6.28	290	1.502	.474	316	21.60	5.94	275	1.380	.403	292	14.21	4.05	285
	42.80	12.80	295				45.97	12.58	274	1.691	.492	291	35.34	9.84	278
	53.9*	15.94					56.7*	15.55					55.5*	15.62	
	52.4* (cor.)						55.1* (cor.)						54.4* (cor.)		
	Av.		322	Av.		317	Av.		283	Av.		289	Av.		288
	Av. (cor.)		332	Av. (cor.)		323	Av. (cor.)		292	Av. (cor.)		294	Av. (cor.)		294

<sup>a</sup> Subscripts: 1 refers to aniline, 2 to cyclohexane, 3 to water.  $x_3 = n_3/(n_1 + n_2 + n_3)$ . Units of  $n_1 + n_2$  are millimoles. Compositions in parentheses were obtained by analysis, and were used in calculating  $x_3$  only in sample 3.  $T$  is separation temperature of binary system,  $\Delta T$  is separation temperature of ternary system minus that of binary system. Values of  $x_3$  with asterisk are saturation values. The second value (cor.) is corrected for water in the vapor phase and the extra amount of cyclohexane in the vapor at 45.5°. At 45.5° the values of  $x_1$  are about 0.001 larger than at 29.5°. The average values of  $dT/dx_3$  were obtained by averaging all values for  $x_3$  less than  $6 \times 10^{-3}$ , except those enclosed in parentheses, which seemed to be in error. They were corrected by assuming the same percentage correction as would obtain at 45.5°. The values of  $dT/dx_3$  were obtained merely by dividing  $\Delta T$  by  $x_3$ .

titration made. Except for sample 3, the results of the analysis agreed, within the limits of error of the analysis, with the originally recorded compositions.

For the first additions, water was added to the mixtures of cyclohexane and aniline by a method in principle the same as that previously used,<sup>3</sup> but for larger amounts an ampoule containing a weighed amount of water was broken *in vacuo* and the entire amount condensed into the mixture. Samples 1, 3, and 5 eventually were saturated with water, the final measurements being made in the presence of a small amount of a phase rich in water. Once such an excess of water was present, the temperature of transition (now from a three-phase to a two-phase system) remained essentially independent of the excess of water added. From the amount of water necessary in order to attain this situation, the solubility of water at the transition temperature in a cyclohexane-aniline solution having the given over-all composition could be determined.

The experimental results are shown in Table I. For comparison, the solubility of water in cyclohexane<sup>19</sup> and in pure aniline<sup>20</sup> at 45.5° correspond to  $x_3$  equal to 0.00152 and 0.250, respectively. The compositions given for the mixtures have been corrected for the amount of water and the amount of cyclohexane in the vapor phase, which had a volume of about 12 cc. The partial pressure of water must be nearly equal to the vapor pressure of pure water, which is 73.7 mm., at 45.5°, which would give  $4.5 \times 10^{-6}$  mole of water in the vapor space, giving corrections of 2.9, 3.1, and 2.2% for samples 1, 3, and 5, respectively. The data of Rowden and Rice<sup>21</sup> for the vapor pressure of a sample containing only cyclohexane and aniline (mole fraction of aniline = 0.439) were extrapolated to 45.5°. A value of 208 mm. was estimated, which corresponds to  $1.2 \times 10^{-4}$  mole of cyclohexane in the vapor.

In I we corrected the results for samples 2 and 4 for the water in the vapor phase. This was based on the vapor pressure of water, about 2.25 mm. from a  $\text{LiSO}_4\text{-LiSO}_4\text{-H}_2\text{O}$  mixture which, it may be recalled, raised the critical temperature by about 0.29 to 29.9°. It appears from the results on the solutions saturated with water that the correction which we made may have been too large. The solubility of water in cyclohexane increases, from 29.9 to 45.5°, by a factor of 2.09, the solubility in aniline increases by a factor of 1.11, while the vapor pressure of water increases by a factor of 2.3 over the same range. The concentration of water vapor changes by a factor of 2.2. It thus appears that the solubility of water vapor decreases with increasing tem-

perature so that the correction for the water in the vapor phase should be greater, if anything, at 45.5 than at 29.9°. However, if we use the vapor pressure, 2.25 mm., of the salt mixture at 29.9°, it is found that the corrections are 5.2, 5.7, and 3.8% for samples 1, 3, and 5, while, as noted, the corrections at 45.5° are 2.9, 3.1, and 2.2%, respectively. This seems inexplicable, and if we assume that the correction should be the same at the two temperatures we find that it corresponds to a water vapor pressure from the solution of about 1.5 mm. at 29.9°, considerably lower than the reported vapor pressure of the  $\text{LiSO}_4\text{-LiSO}_4\text{-H}_2\text{O}$  mixture.

Another possible explanation of the results is that the observed change in separation temperature in the presence of the lithium sulfate mixture was not due to water vapor alone. A check was made<sup>3</sup> for solution of  $\text{LiSO}_4$  in a cyclohexane-aniline mixture by evaporating a mixture which had been in contact with the salt, and no residue was found. Perhaps a more sensitive test would have been to place a cyclohexane-aniline mixture in contact with anhydrous salt to see whether the separation temperature was affected, but this would not necessarily test the possibility that the hydrate itself is soluble. In any case, it is clear that these possible disturbing factors need further investigation.

Included in Table I are the initial slope  $dT/dc_3$  of the transition-temperature vs. water-concentration curve for the several mixtures. In reference 4 we gave some arguments which would indicate that, at least for the two solutions studied there, the values of  $dc_3/dT$  would be almost exactly proportional to the solubility, since they would give the relative amounts of water to be added to the solution to bring them up to a point where they would be in equilibrium with each other at 29.9°. If the presence of the  $\text{LiSO}_4$  complicates the situation, this particular argument may break down, but the proportionality nevertheless must exist over the critical range of compositions. For  $dT/dc_3$  is, by our definition of  $T_c$ , independent of  $x_1$ , and in the region where  $a_3$  is small,  $da_3 = dc_3/\lambda$ , hence  $\lambda dT_c/dc_3$  does not change with  $x_1$ . Furthermore, we see that, since  $c_3 = a_3\lambda$ , and  $T_c$  is defined in terms of a situation where  $a_3$  is constant,  $c_3 dT_c/dc_3$  will be independent of  $x_1$  and eq. 1.1 will remain valid if applied at any composition within the critical range.

## Discussion

In Fig. 1 we plot the solubilities at 45.5° (or the saturation temperature for the mixtures) against the composition. This figure probably affords us the best opportunity to estimate the relative curvature of the solubility with respect to composition, for use in eq. 4.8, even though it is not for the critical temperature. The curve shown gives

$$\lambda^{-1} \partial^2 \lambda / \partial x_1^2 = 14 \quad (7.1)$$

(19) W. F. Hoot, A. Azarnoosh, and J. J. McKetta, *Petrol. Refiner.*, **36**, 255 (1957).

(20) N. V. Sidgwick, P. Pickford, and B. H. Wilsdon, *J. Chem. Soc. (London)*, **99**, 1122 (1911).

(21) R. W. Rowden and O. K. Rice, "Changements de Phases," *ociété de Chimie Physique, Paris, 1952*, p. 78.

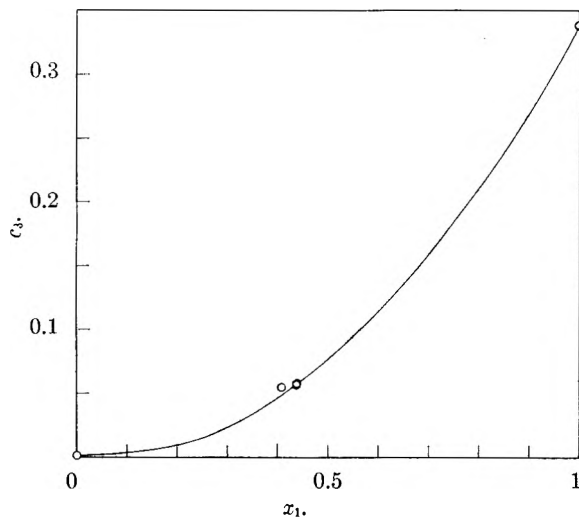


Fig. 1.—Concentration of water (moles per mole of mixture) as a function of aniline mole fraction in cyclohexane-aniline mixtures. Equation of curve:  $c_3 = 0.0015 - 0.031x_1 + 0.366x_1^2$ .

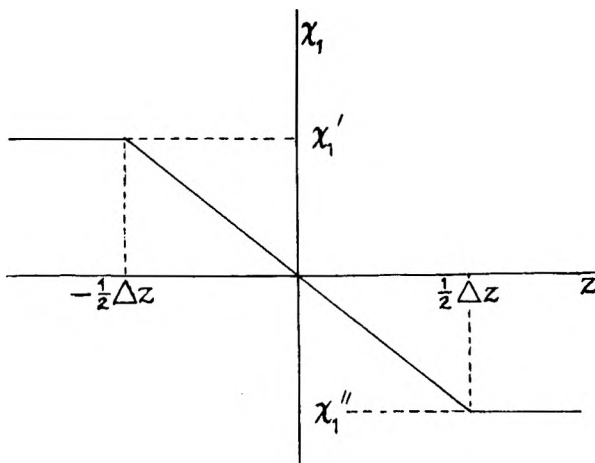


Fig. 2.—Schematic drawing showing change of mole fraction of aniline across the interface.

We now wish in the light of the new data and new theoretical insights to make a somewhat more detailed comparison than was made in I between  $\Gamma_3$ , as obtained from eq. 1.1, and the value of  $\lambda''^{-1} \partial^2 \lambda / \partial x_1^2$ , which means essentially that we wish to test eq. 4.8 which, however, we prefer to write in the form

$$\Gamma_3 / \Delta c_w = (c_w'' / \Delta c_w) \lambda''^{-1} (\partial \lambda^2 / \partial x_1^2) I \quad (7.2)$$

where the double-primed phase has been substituted for the single-primed, and where  $c_w = \rho c_3$ , having thus the same meaning as in I, and  $\Delta c_w = c_w' - c_w''$ . It was shown in I that we could write

$$\Gamma_3 / \Delta c_w = -K(RT)^{-1} (\kappa/a) \tau^{1/3} x_1'' dT_c / dc_w \quad (7.3)$$

where  $K$ ,  $\kappa$  (not to be confused with the  $\kappa$  in section 5), and  $a$  were constant.  $a$  occurs in the equation

$$x_1' - x_1'' = a(T_c - T + \tau)^{1/2} \quad (7.4)$$

expressing the cubic form of the coexistence curve, corrected for the apparent truncation of this curve at the critical temperature  $T_c$  which is  $\tau$  below what the critical temperature would be if the curve were not truncated.  $\kappa$  occurs in the proposed expression for the interfacial tension

$$\sigma = \kappa(T_c - T + \tau)^{3/2}$$

This equation would not hold very close to  $T_c$  since  $\sigma$  must vanish at  $T_c$ . We believe that it perhaps would be more consistent with our method of handling the thickness of the transition layer to replace this equation by

$$\sigma = \kappa(T_c - T + \tau)^{3/2} - \sigma_\tau \quad (7.5)$$

where  $\sigma_\tau$  is a constant which causes  $\sigma$  to vanish at  $T_c$ . Then

$$(d\sigma/dT)_{T=T_c} = -(3/2) \kappa \tau^{1/2} \quad (7.6)$$

whereas before we had estimated the numerical factor as 2.

$K$  is the quotient of this numerical factor by the numerical factor in the empirical equation

$$\Delta c_w / c_w'' = \lambda_\Delta \Delta x_1 / x_1'' \quad (7.7)$$

where  $\Delta c_w = c_w' - c_w''$  and  $\Delta x_1 = x_1' - x_1''$ , and where our best estimate from the reciprocals of the values of  $dT/dc_3$  in Table I, allowing for the fact that the actual range of  $x_1$  in the critical range is greater than that covered by Table I, gives  $\lambda_\Delta = 2.2$ , which is in line with what we found in I. We then estimate  $K$  as 0.68, whereas it was given as 0.92 in I. The values of  $\kappa$ ,  $a$ , and  $\tau$ , as noted in I, are 0.0217 dynes  $\text{cm}^{-1} \text{deg}^{-3/2}$ , 0.327  $\text{deg}^{-1/3}$ , and  $0.005^\circ$ , respectively. We then find from the present work

$$\Gamma_3 / \Delta c_w = -1.0 \times 10^{-8} \quad (7.8)$$

We are now in a position to apply eq. 7.2. We may evaluate  $I$  roughly if we assume that the transition region of the surface has the character indicated in Fig. 2. One then need only integrate eq. 4.9 from  $-1/2 \Delta z$  to  $1/2 \Delta z$ , and the variable of integration can be changed by writing  $dz = -(\Delta z / \Delta x_1) dx_1$  where  $\Delta z$  is the "thickness" of the interface. We then find

$$I \cong -\frac{1}{12} (\Delta z) (\Delta x_1)^2 \quad (7.9)$$

If this be substituted along with (7.7) into eq. 7.2 we obtain

$$\Gamma_3 / \Delta c_w = -\frac{1}{12} (x_1'' / \lambda_\Delta) \Delta z \Delta x_1 \lambda''^{-1} (\partial^2 \lambda / \partial x_1^2) \quad (7.10)$$

The critical range of composition of the binary system extends from about 0.42 to 0.47 mole-fraction aniline, so  $\Delta x_1 = 0.05$ . All the other quantities in eq. 7.10 now are known, except  $\Delta z$ . Solving for this quantity we find

$$\Delta z = 9 \times 10^{-7} \text{ cm.}$$

As we have noted in Section 5,  $\Delta z$  may be expected to be proportional to  $(T_c - T)^{-1/6}$ , but if the coexistence curve is truncated, it seems reasonable, as in I, to substitute  $(T_c - T + \tau)^{-1/6}$ . The value of  $\Delta z$  obtained, which is, of course, the value at  $T_c$ , then implies that  $10^\circ$  below  $T_c$  the thickness of the interface is about  $2.6 \times 10^{-7}$  cm. This estimate is considerably greater than the one we made in I, but still is only around five molecular thicknesses. In any case it must be a rough estimate. It would, of course, be possible to put a curve through the points in Fig. 1 with considerably more curvature in the important concentration region, which would lower  $\Delta z$ ; on the other hand, it might be possible that the solubility curve was rather flat in the



critical region just as the density curve was found to be.<sup>22</sup> We had intended to have a better dis-

(22) M. E. Jacox, J. T. MacQueen, and O. K. Rice, *J. Phys. Chem.*, **64**, 972 (1960).

tribution of values of  $dT/dx_3$  in the critical range, but some accidents prevented this. When more data of this sort become available, it will be possible to fix  $\lambda''^{-1}\partial^2\lambda/\partial x_1^2$  more exactly.

## INTERNAL PRESSURES OF PERFLUORO-*n*-HEXANE, *n*-HEXANE, AND THEIR MIXTURES<sup>1</sup>

BY ROBERT D. DUNLAP

*Department of Chemistry, University of Maine, Orono, Maine*

AND ROBERT L. SCOTT

*Department of Chemistry, University of California, Los Angeles, California*

Received October 16, 1961

Values of  $(\partial P/\partial T)_V$  for perfluoro-*n*-hexane and *n*-hexane were determined at several temperatures between 10 and 50°. Ratios of the internal pressure,  $(\partial E/\partial V)_T$  to the cohesive energy density  $(-E/V)$  at 35° are 1.30 for the fluorocarbon and 1.09 for the hydrocarbon. The function  $V^2(\partial E/\partial V)_T$  decreased with increasing temperature for both liquids;  $V^3(\partial E/\partial V)_T$  was found to be nearly constant for *n*-C<sub>6</sub>F<sub>14</sub>. The values of  $-\ln(\partial E/\partial V)_T/d \ln V$  were found to be 3.17 for *n*-C<sub>6</sub>F<sub>14</sub> and 2.35 for *n*-C<sub>6</sub>H<sub>14</sub>. Measurements of  $(\partial P/\partial T)_V$  were obtained for five mixtures at temperatures near 25, 35, and 45° and were used to derive the thermodynamic functions for mixing at constant volume from those obtained experimentally at constant pressure. Values of  $TS^{VE}$  are negative to the extent of -60 cal., and the function is skewed toward the hydrocarbon. The discrepancy between the entropy of mixing at constant volume and the statistical value for random mixing is too small to account entirely for the failure of regular solution theory to predict the properties of this system.

Solutions of fluorocarbons and hydrocarbons previously studied have large positive deviations from Raoult's law. Large volume and energy changes accompany mixing and the mutual solubilities are much lower than those predicted by the Hildebrand-Scatchard solubility parameter theory<sup>2</sup> of regular solutions. Scott<sup>3</sup> in a recent review article has assembled most of the experimental data on these systems, and has critically reviewed the various attempts to explain their anomalous behavior. More recently, Kyle and Reed<sup>4</sup> have reported mutual solubilities and total vapor pressures for several additional fluorocarbon-hydrocarbon systems, and have postulated an empirical correlation of the existing data based on a negative excess entropy of mixing at constant volume.

This study was undertaken to supplement the studies of liquid vapor equilibrium<sup>5</sup> and heats of mixing<sup>6</sup> for this system, particularly in order to obtain the thermodynamic functions for mixing at constant volume.<sup>7</sup>

### Experimental

The apparatus was a modification of the one used by Benninga and Scott<sup>8</sup> in their study of carbon tetrachloride and similar to that described by Alder, Haycock, Hildebrand, and Watts.<sup>9</sup> The constant volume cell was a thermal regu-

lator; a spiral of 7-mm. Pyrex tubing having a volume of approximately 14 cm.<sup>3</sup>. In a typical experiment it contained some 10 to 12 cm.<sup>3</sup> of the liquid being studied, and the remaining space filled with mercury to enclose the liquid and serve as the electrical contact. The regulator was filled *in vacuo* with degassed liquid and covered with mercury before disconnecting it from the vacuum system. The exact amounts of liquid and mercury were determined by weighing the regulator and the container from which the liquid was removed. The regulator was enclosed in a steel bomb to which pressure was applied from a cylinder of nitrogen, the bomb immersed in a water thermostat, and its temperature regulated by the cell at various pressures from 1 to 65 atmospheres. The heating and cooling cycles were made very nearly equal and temperature was controlled within 0.1° in the bath and within 0.01° inside the bomb. The relay operated a signal so that the temperature could be determined at the times when contact was made and broken. The difference between these temperatures was never larger than 0.003°; the average was taken as the value of *t* at a given *P*.

Temperature was determined with a calibrated copper-constant thermocouple to 0.001° using a Leeds and Northrup K-2 potentiometer with a high sensitivity galvanometer. The pressure was determined within 0.01 atm. using a Refinery Supply Company #9010 dead weight gage. As an additional check, a calibrated Heise-Bourdon gage, kindly loaned to us by Professor George Kennedy, was conjoined during several of the experiments.

The perfluoro-*n*-hexane and *n*-hexane were the same liquids used for the previous studies.<sup>5,6,10,11</sup>

The *P* vs. *t* functions for the pure liquids and their mixtures were linear within the limits of experimental error. The largest deviation from the linear equations obtained by least squares was 0.05 atm. or 0.01°. The average deviation was 0.02 atm. Values of  $\Delta P/\Delta t$  so obtained were corrected for the volume changes of the glass and mercury using the relationship

$$\left\{ \frac{(\partial P/\partial T)_{V,P=1 \text{ atm}} = \Delta P/\Delta t}{1 + \frac{(1 + V_{\text{Hg}}/V_1)[\alpha_g - \beta_g(\Delta P/\Delta t)] - V_{\text{Hg}}/V_1}{\alpha_1 [\alpha_{\text{Hg}} - \beta_{\text{Hg}}(\Delta P/\Delta t)]}} \right\} \quad (1)$$

(1) These experiments were carried out in R.L.S.'s laboratory at the University of California at Los Angeles by R.D.D. while on sabbatical leave from the University of Maine.

(2) J. H. Hildebrand and R. L. Scott, "Solubility of Nonelectrolytes," 3rd Edition, Reinhold Publ. Corp., New York, N. Y., 1950.

(3) R. L. Scott, *J. Phys. Chem.*, **62**, 136 (1958).

(4) G. Kyle and T. M. Reed, III, *J. Am. Chem. Soc.*, **80**, 6170 (1958).

(5) R. D. Dunlap, R. G. Bedford, J. C. Woodbrey, and S. D. Furrow, *ibid.*, **81**, 2927 (1959).

(6) A. G. Williamson and R. L. Scott, *J. Phys. Chem.*, **65**, 275 (1961).

(7) R. L. Scott, *ibid.*, **64**, 1241 (1960).

(8) H. Benninga and R. L. Scott, *J. Chem. Phys.*, **23**, 1911 (1955).

(9) B. J. Alder, E. W. Haycock, J. H. Hildebrand, and H. Watts, *ibid.*, **22**, 1060 (1954).

(10) R. D. Dunlap, C. J. Murphy, and R. G. Bedford, *J. Am. Chem. Soc.*, **80**, 83 (1958).

(11) R. G. Bedford and R. D. Dunlap, *ibid.*, **80**, 282 (1958).

TABLE I  
THERMAL PRESSURE COEFFICIENTS FOR THE SYSTEM: PERFLUORO-*n*-HEXANE + *n*-HEXANE

Compositions are expressed in mole fractions of perfluoro-*n*-hexane.

$t, ^\circ\text{C.}$	$(\partial P/\partial T)_{V,P=1 \text{ atm.}}$ atm. deg. <sup>-1</sup>	(eq.-obsd.)	$t, ^\circ\text{C.}$	$(\partial P/\partial T)_{V,P=1 \text{ atm.}}$ atm. deg. <sup>-1</sup>
	<i>n</i> -C <sub>6</sub> H <sub>14</sub>			$x_1 = 0.2929$
8.423	8.928	-0.010	23.927	7.040
16.010	8.472	.014	27.212	6.790
22.030	8.148	.008	34.903	6.293
32.261	7.629	-.008	45.169	5.739
41.640	7.166	-.008		
50.333	6.749	.007		$x_1 = 0.5409$
	<i>n</i> -C <sub>6</sub> F <sub>14</sub>		27.763	6.210
			34.920	5.784
			44.873	5.253
11.567	6.978	-.008		$x_1 = 0.7444$
19.810	6.463	.016		
30.300	5.899	-.006		
39.505	5.420	-.006	27.023	5.961
48.630	4.969	.005	36.651	5.442
			45.842	5.015
				$x_1 = 0.8470$
$x_1 = 0.1478$			22.037	6.244
26.463	7.136		33.138	5.662
34.915	6.687		44.585	5.081
45.890	6.143			

$n\text{-C}_6\text{H}_{14} \quad (\partial P/\partial T)_{V,P=1 \text{ atm.}} = 9.420 - 0.06089t + 1.58 \times 10^{-4} t^2 \text{ atm. deg.}^{-1}$   
 $n\text{-C}_6\text{F}_{14} \quad (\partial P/\partial T)_{V,P=1 \text{ atm.}} = 7.706 - 0.06590t + 2.00 \times 10^{-4} t^2 \text{ atm. deg.}^{-1}$

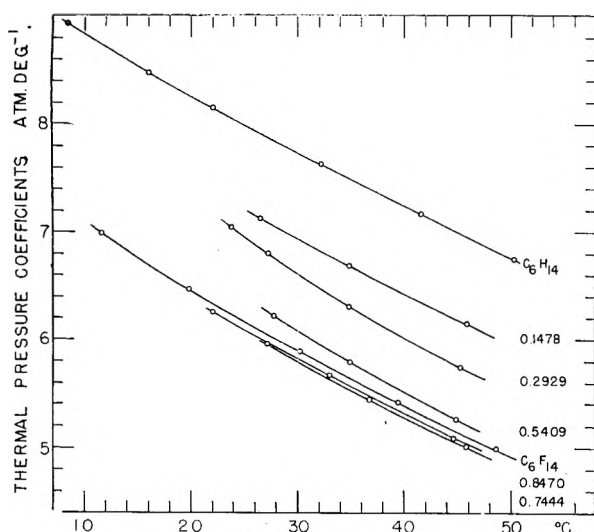


Fig. 1.—Thermal pressure coefficients for the system: perfluoro-*n*-hexane + *n*-hexane.

to give the thermal pressure coefficient,  $(\partial P/\partial T)_V$  at 1 atm. The  $V$ 's,  $\alpha$ 's, and  $\beta$ 's are the volumes, thermal coefficients of expansion, and compressibilities with subscripts Hg, g, and l for mercury, Pyrex glass, and liquid, respectively. Thermal coefficients of expansion of the liquids and mixtures were calculated from the volumetric data reported earlier.<sup>10,11</sup> The corrections, which depend largely upon the ratio of mercury to liquid, ranged from 2 to 5% and could be determined to better than 1%.

### Results and Discussion

**Thermal Pressure Coefficients.**—Experimental data are shown in Table I where the values of  $(\partial P/\partial T)_{V,P=1 \text{ atm}}$  are given for the temperature corresponding to  $P = 1$  atm. for each run. Equations of  $(\partial P/\partial T)_{V,P=1 \text{ atm}}$  as a function of  $t$  for each of the pure liquids were obtained using least squares and are shown at the bottom of Table I.

The goodness of fit is indicated by the deviations in column 3. Plots of the thermal pressure coefficients vs. temperature in Fig. 1 for the various compositions in mole fraction of perfluoro-*n*-hexane show increasing curvature as one approaches the critical solution composition of 0.37.

Values of the excess thermal pressure coefficients, viz.,  $\gamma_m - x_1\gamma_1 - x_2\gamma_2$  where  $\gamma_m$ ,  $\gamma_1$ , and  $\gamma_2$  are the smoothed values of  $(\partial P/\partial T)_{V,P=1 \text{ atm}}$  for the mixtures and pure liquids at 25, 35, and 45°, respectively, are shown in Fig. 2. Since  $(\partial P/\partial T)_V = (\partial S/\partial V)_T$ , these curves show that the increase in entropy per unit volume of the pure liquids is greater than that for their more expanded and less ordered mixtures. The 25° isotherm, at 2.35° above the critical solution temperature, has a double inflection in the region of the critical solution composition, an indication of higher ordering in the pre-unmixing region. The inflection is a consequence of steeper than average  $(\partial P/\partial T)_{V,P=1 \text{ atm}}$  vs.  $t$  curves for the mixtures (shown in Fig. 1) and is associated with the heat capacity and thermal expansion by the relation

$$C_P - C_V = T \left( \frac{\partial V}{\partial T} \right)_P \left( \frac{\partial P}{\partial T} \right)_V \quad (2)$$

Such behavior is qualitatively in accord with the large temperature dependence of the heat capacity and thermal coefficient of expansion observed by Hildebrand, *et al.*,<sup>12,13</sup> for similar solutions in their supra-critical region.

**Isothermal Compressibilities, Internal Pressures, and Related Functions.**—Isothermal compressibilities at 35° calculated from the thermal pressure coefficients and previously reported volumetric

(12) H. Schmidt, G. Jura, and J. H. Hildebrand, *J. Phys. Chem.*, **63**, 297 (1959).

(13) G. Jura, D. Fragi, G. Maki, and J. H. Hildebrand, *Proc. Natl. Acad. Sci.*, **39**, 19 (1953).

TABLE II  
INTERNAL PRESSURES AND RELATED ENERGY-VOLUME FUNCTIONS FOR  $n\text{-C}_6\text{F}_{14}$  AND  $n\text{-C}_6\text{H}_{14}$

Liquid	Temp., °C.	$(\partial P/\partial T)_V, P=1 \text{ atm.}$ atm. deg. <sup>-1</sup>	$(\partial E/\partial V)_T$ atm.	$V$ , cm. <sup>3</sup>	$V^2 (\partial E/\partial V)_T$ , atm. l. <sup>2</sup>	$(\partial E/\partial V)_T$ ( $-E/V$ )
$n\text{-C}_6\text{F}_{14}$	5	7.382	2052	195.33	78.29	1.321
	15	6.763	1948	198.67	76.89	1.314
	25	6.184	1843	202.23	75.37	1.306
	35	5.645	1739	205.96	73.76	1.299
	45	5.146	1636	209.95	72.11	1.292
	55	4.687	1537	214.19	70.51	1.290
$n\text{-C}_6\text{H}_{14}$	5	9.120	2536	127.96	41.52	1.084
	15	8.542	2460	129.76	41.42	1.088
	25	7.997	2383	131.56	41.25	1.091
	35	7.482	2305	133.43	41.03	1.095
	45	7.000	2226	135.37	40.79	1.098
	55	6.549	2148	137.38	40.53	1.103

data<sup>11</sup> are shown in Table III. The compressibility of perfluoro-*n*-hexane is 75% larger than that of the corresponding hydrocarbon, and mixtures of these liquids which contain more than 50 mole % fluorocarbon are even more compressible than perfluoro-*n*-hexane.

Internal pressures,  $(\partial E/\partial V)_T$ , calculated from the thermodynamic relation

$$(\partial E/\partial V)_T = T(\partial P/\partial T)_V - P \quad (3)$$

and values for two well known functions,  $V^2(\partial E/\partial V)_T = a$ , and  $(\partial E/\partial V)_T/(-E/V) = n$  are shown in Table II for each of the pure liquids. The former is van der Waal's  $a$ , and the drifts with temperature,  $-0.25\%$  deg.<sup>-1</sup> for  $n\text{-C}_6\text{F}_{14}$  and  $-0.05\%$  deg.<sup>-1</sup> for  $n\text{-C}_6\text{H}_{14}$ , are larger than observed for carbon tetrachloride.<sup>8</sup> Also where  $n$ , the ratio of the internal pressure to the cohesive energy density, was found to be reasonably constant over a 60° range for  $\text{CCl}_4$ , it decreases with temperature for perfluoro-*n*-hexane and increases with temperature for *n*-hexane.

Smith and Hildebrand<sup>14</sup> found that  $V^2(\partial E/\partial V)_T$  also decreased with increasing temperature for perfluoro-*n*-heptane and several chlorofluorocarbon liquids. They calculated values for the function  $V^{n+1}(\partial E/\partial V)_T$  which they found to be more nearly constant over the temperature range studied. For perfluoro-*n*-hexane, we find that  $V^3(\partial E/\partial V)_T$  is nearly temperature independent. When we plot  $\ln (\partial E/\partial V)_T$  vs.  $\ln V$ , remarkably straight lines are obtained and the slopes  $-[d \ln (\partial E/\partial V)_T/d \ln V]_P$  are 3.17 and 2.35 for perfluoro-*n*-hexane and *n*-hexane, respectively; these are somewhat larger than the corresponding values of  $n + 1$ , to which they should be equal if  $n$  were independent of  $V$  and  $(\partial^2 P/\partial T^2)_V$  were exactly zero.

**Excess Thermodynamic Properties.**—Excess thermodynamic functions and related thermodynamic properties at 35° are shown in Table III. Values of  $H_P^E(T, P^0)$ ,  $G_P^E(T, P^0)$ , and  $S_P^E(T, P^0)$ , the excess enthalpy, Gibbs free energy, and entropy of mixing at constant pressure, respectively, were calculated from equation 14 in the paper by Williamson and Scott.<sup>6</sup> These authors have combined the liquid-vapor equilibrium data at 25, 35, and 45° of Dunlap, *et al.*,<sup>5</sup> with their calorimetric

(14) E. B. Smith and J. H. Hildebrand, *J. Chem. Phys.*, **31**, 145 (1959).

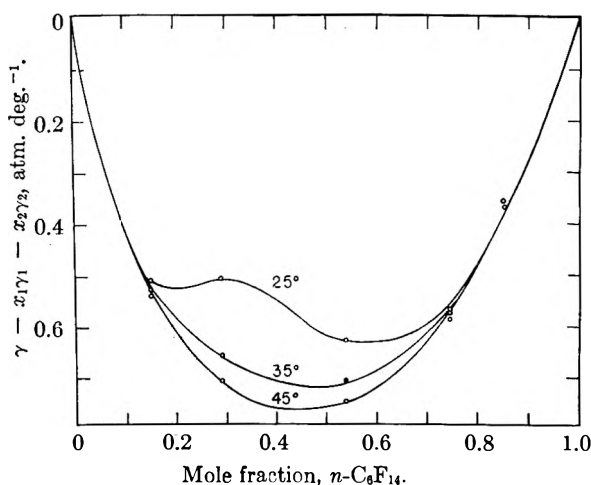


Fig. 2.—Excess thermal pressure coefficients for the system: perfluoro-*n*-hexane + *n*-hexane.

determinations of the heats of mixing at 25 and 35° to give a thermodynamically consistent representation of the properties in a single function,  $G_P^E(T, P^0, x)$ . Here  $P^0$  is practically one atmosphere.

Various constant volume processes and related thermodynamic functions have been described.<sup>7</sup> Two processes of interest to us are: IIA, in which both components are expanded (or compressed) isothermally to the same initial pressure at which the volume of the unmixed liquids equals the volume of the mixture at the final pressure and then mixed at constant volume; IIB in which the liquids are mixed at constant pressure and the mixture compressed (or expanded) isothermally to the volume of the unmixed liquids. The symbols correspond to those in the previous paper.<sup>7</sup> The mechanical properties of the pure liquids are employed to evaluate the thermodynamic functions for IIA while those of the mixture are used for IIB.

Values of excess thermodynamic functions for the constant volume processes shown in Table III were calculated from the relationships

$$A_{IIA}^{VE}(T, V_m^0) = G_P^E(T, P^0) + (VE)^2/(2 \langle V_P^0 \rangle) + \dots \quad (4)$$

$$A_{IIB}^{VE}(T, V_u^0) = G_P^E(T, P^0) - (VE)^2/(2 V_{Pm}^0) \quad (5)$$

TABLE III

THERMODYNAMIC AND MECHANICAL PROPERTIES FOR THE SYSTEM $n\text{-C}_6\text{F}_{14} + n\text{-C}_6\text{H}_{14}$ AT $35^\circ$							
Mole fraction $n\text{-C}_6\text{F}_{14}$	0.0000	0.1478	0.2929	0.5409	0.7444	0.8476	1.000
$(\partial P/\partial T)_{V,P-1 \text{ atm.}, \text{ atm. deg.}^{-1}}$	7.482	6.683	6.284	5.779	5.525	5.566	5.644
$[\partial \ln V/\partial T]_P \times 10^3, \text{ deg.}^{-1}$	1.427	1.665	1.828	1.963	1.959	1.931	1.876
$[\partial \ln V/\partial P]_T \times 10^3, \text{ atm.}^{-1}$	-1.907	-2.491	-2.909	-3.397	-3.546	-3.469	-3.324
$[\partial(\partial P/\partial T)_V/\partial T]_P,$ atm. deg. <sup>-2</sup>	-0.0498	-0.0516	-0.0606	-0.0568	-0.0514	-0.0513	-0.0519
$V, \text{ cm.}^3 \text{ mole}^{-1}$	133.43	147.14	159.25	178.03	191.89	198.12	205.96
$V^E, \text{ cm.}^3 \text{ mole}^{-1}$		2.99	4.57	5.37	4.47	3.26	
$G_{PE}(T, P^0), \text{ cal. mole}^{-1}$		187	282	312	233	157	
$H_{PE}(T, P^0), \text{ cal. mole}^{-1}$		309	450	514	409	283	
$TS_{PE}(T, P^0), \text{ cal. mole}^{-1}$		122	168	202	176	123	
$TS_{IIA}^{VE}(T, V_m^0), \text{ cal. mole}^{-1}$		-23	-36	-21	-7	-7	
$TS_{IIB}^{VE}(T, V_u^0), \text{ cal. mole}^{-1}$		-35	-63	-47	-18	-15	
$A_{IIA}^{VE}(T, V_m^0), \text{ cal. mole}^{-1}$		184	275	305	229	155	
$A_{IIB}^{VE}(T, V_u^0), \text{ cal. mole}^{-1}$		190	287	318	237	159	
$E_{IIA}^{VE}(T, V_m^0), \text{ cal. mole}^{-1}$		161	239	284	222	148	
$E_{IIB}^{VE}(T, V_u^0), \text{ cal. mole}^{-1}$		155	224	271	219	144	

$$S_{IIA}^{VE}(T, V_m^0) = S_{PE}(T, P^0) + \frac{\langle V_T^0 \rangle}{\langle V_P^0 \rangle} V^E + \frac{\langle V_P^0 \rangle \langle V_{TP}^0 \rangle - \langle V_T^0 \rangle \langle V_{PP}^0 \rangle}{2 \langle V_P^0 \rangle^2} (V^E)^2 \quad (6)$$

$$S_{IIB}^{VE}(T, V_u^0) = S_{PE}(T, P^0) - (\partial P/\partial T)_{V,P-1} V^E + (1/2) (\partial^2 S/\partial V^2)_T (V^E)^2 \quad (7)$$

where  $V_T$ ,  $V_P$ ,  $V_{PP}$ ,  $V_{PT}$ , are the derivatives  $(\partial V/\partial T)_P$ ,  $(\partial V/\partial P)_T$ ,  $(\partial^2 V/\partial P^2)_T$ , and  $\partial^2 V/\partial P \partial T$ , respectively, and symbol  $\langle V_T \rangle$  represents  $[x_1(V_T)_1 + x_2(V_T)_2]$ , *i.e.*, the mole fraction average of the  $V_T$  coefficients for the pure components. The superscript <sup>0</sup> represents the standard state, *viz.*, one atmosphere, and  $V_u^0$  and  $V_m^0$  are the volumes of the unmixed and mixed liquids at  $P^0$  and  $T$ , respectively.

Values of  $(\partial^2 S/\partial V^2)_T$  were calculated from the temperature derivatives of the thermal pressure coefficients shown in Table III using the relation

$$(\partial^2 S/\partial V^2)_T \cong [\partial(\partial P/\partial T)_V/\partial T]_P/(\partial V/\partial T)_P \quad (8)$$

which was derived<sup>7</sup> with the aid of the assumption that  $(\partial^2 P/\partial T^2)_V = 0$ . Although the  $P$  vs.  $T$  functions were linear within experimental error, this assumption is only moderately supported by this study because the pressure range of 65 atmospheres is relatively short.

The excess Gibbs free energy,  $G_{PE}$ , is very nearly halfway between the excess Helmholtz free energies for the two constant volume processes in the order

$$A_{IIA}^{VE} < G_{PE} < A_{IIB}^{VE} \quad (9)$$

The excess entropies for the two constant volume processes are negative and skewed toward the hydrocarbon, the values for process IIA at the larger volume being more positive than those for process IIB. The negative values for the excess entropies of mixing at constant volume are of un-

certain significance, but it is interesting to note that the sign is opposite to that which one would expect from the simple "Flory-Huggins" relation

$$S^{FH} = -R [x_1 \ln \phi_1 + x_2 \ln \phi_2] \quad (10)$$

where the  $\phi$ 's are volume fractions, when attempting to correct for the differences in the sizes of the molecules. This bears out the observation of Shinoda and Hildebrand<sup>15</sup> that the ideal entropy is better than the "Flory-Huggins" entropy when calculating critical solution compositions of similar mixtures.

The excess free energy,  $G_{PE}$ , is 318 cal./mole at  $x = 1/2$ , considerably larger than 85 cal. predicted from solubility parameters. If one adjusts the geometric mean approximation as suggested by Reed<sup>16</sup> to account for the differences in size and ionization potentials, the calculated excess free energy can be increased to 185 cal. Thus it can be concluded that the discrepancy between the entropy of mixing at constant volume and the statistical entropy for random mixing is too small to account for the failure of solubility parameter theory for this and other mixtures of fluorocarbons and hydrocarbons.

**Acknowledgments.**—Support of the National Science Foundation (R.D.D.) and the U. S. Atomic Energy Commission (R.L.S.) is gratefully acknowledged. The authors wish to thank Mr. S. D. Furrow of the University of Maine for helpful discussions. R.D.D. gives thanks and acknowledgment to the many members of the U.C.L.A. Chemistry Department for their stimulating discussions and assistance during the period of this study.

(15) K. Shinoda and J. H. Hildebrand, *J. Phys. Chem.*, **62**, 481 (1958).

(16) T. M. Reed, III, *ibid.*, **59**, 425 (1955).

# SECOND VIRIAL COEFFICIENTS FOR THE SYSTEMS: *n*-BUTANE + PERFLUORO-*n*-BUTANE AND DIMETHYL ETHER + 1-HYDROPERFLUOROPROPANE

BY TERRANCE B. TRIPP AND ROBERT D. DUNLAP

*Chemistry Department, University of Maine, Orono, Maine*

*Received October 16, 1961*

Second virial coefficients of *n*-butane, perfluoro-*n*-butane, dimethyl ether, 1-hydroperfluoropropane, an equal molar mixture of *n*-butane + perfluoro-*n*-butane, and an equal molar mixture of dimethyl ether + 1-hydroperfluoropropane were determined at 10, 30 and 50° from compressibility measurements obtained with a Boyle apparatus. Values of  $B_{12}$ , the cross-term second virial coefficients, characteristic of the interactions between dissimilar pairs of molecules, were indicative of weaker than average attractive forces in the *n*-butane + perfluoro-*n*-butane mixture and of hydrogen bonding in the 1-hydroperfluoropropane + dimethyl ether mixture. The association constants for the reaction  $(\text{CH}_3)_2\text{O} + \text{HC}_2\text{F}_7 \rightarrow (\text{CH}_3)_2\text{O} \cdot \text{HC}_2\text{F}_7$  were calculated from the virial coefficients at the three temperatures and the enthalpy of association estimated to be  $-4 \text{ kcal. mole}^{-1}$ .

## Introduction

In recent years, the large number of studies of liquid mixtures of fluorocarbons and hydrocarbons<sup>1-5</sup> have demonstrated that the attractive forces between the unlike molecules are weaker than the forces between the like molecules. A few investigations, however, produced evidence of hydrogen bonding. Zellhoeffer and Copley<sup>6</sup> in their calorimetric study of solutions of dichlorofluoromethane in tetraethylene glycol dimethyl ether found evidence of hydrogen bonding, as did Mastrangelo<sup>7</sup> from solubility studies of dichlorofluoromethane, difluorochloromethane, 2,2-dihydro-tetrafluoroethane, and 1-chloro-1-hydro-tetrafluoroethane in the same solvent. More recently Anderson, Smith, *et al.*,<sup>8</sup> found that the system 1-hydroperfluoro-*n*-heptane + acetone has a positive enthalpy of mixing for acetone-rich solutions and a negative enthalpy for 1-hydroperfluoro-*n*-heptane-rich solutions, the resulting curve being a superposition of specific and non-specific interactions.

In contrast to the large number of investigations of liquid mixtures containing fluorocarbons, the only study dealing with gaseous mixtures is that by Garner and McCoubrey<sup>9</sup> of *n*-pentane with perfluoro-*n*-pentane and with perfluoro-*n*-hexane. Such information is needed for the rigorous treatment of vapor pressure data when determining the thermodynamic properties of liquid mixtures; this being the reason for studying the system *n*-butane + perfluoro-*n*-butane. The intriguing possibility of hydrogen bonding between 1-hydroperfluoropropane and dimethyl ether prompted the study of these substances.

## Experimental

**Materials.**—The *n*-butane and dimethyl ether were

- (1) R. L. Scott, *J. Phys. Chem.*, **62**, 136 (1958).
- (2) R. D. Dunlap, R. G. Bedford, J. C. Woodbrey, and S. D. Furrow, *J. Am. Chem. Soc.*, **81**, 2927 (1959).
- (3) R. D. Bedford and R. D. Dunlap, *ibid.*, **80**, 282 (1958).
- (4) A. G. Williamson and R. L. Scott, *J. Phys. Chem.*, **65**, 275 (1961).
- (5) D. E. L. Dyke, J. S. Rowlinson, and R. Thacker, *Trans. Faraday Soc.*, **55**, 903 (1959).
- (6) G. F. Zellhoeffer and M. J. Copley, *J. Am. Chem. Soc.*, **60**, 1343 (1936).
- (7) S. V. R. Mastrangelo, *J. Phys. Chem.*, **63**, 608 (1959).
- (8) D. L. Anderson, R. A. Smith, D. B. Myers, S. K. Alley, A. G. Williamson, and R. L. Scott, *ibid.*, **66**, 621 (1962).
- (9) M. D. Garner and J. C. McCoubrey, *Trans. Faraday Soc.*, **55**, 1524 (1959).

Matheson Chemical Company C.P. grade (99 mole % pure). The perfluoro-*n*-butane was kindly furnished by the General Chemicals Research Laboratory of the Allied Chemical Corporation, and was a sample of the material used in the physical properties study of Brown and Mears.<sup>10</sup> The *n*-butane and perfluoro-*n*-butane were degassed by fractional distillation in the vacuum system and dried by repeatedly passing the vapors through a column of  $\text{P}_2\text{O}_5$  until the liquids appeared clear when cooled to Dry Ice temperature. The molecular weight of *n*-butane was found to be 58.07 g. mole<sup>-1</sup> from gas density balance measurements. The dimethyl ether was degassed by alternately freezing, pumping while frozen, and melting. Water was removed by the above procedure.

The 1-hydroperfluoropropane was prepared by decarboxylation of the ammonium salt of perfluorobutyric acid in ethylene glycol as described by LaZerte, *et al.*,<sup>11</sup> by Alan Wright of our Laboratory. The crude product was fractionally distilled and a middle cut was used in the compressibility measurements. The molecular weight of the sample determined by gas density measurements in a Dumas bulb and corrected for the gas imperfection herein reported was found to be 170.3 g. mole<sup>-1</sup> as compared to the theoretical 170.0.

**Compressibility Measurements.**—Measurements of gas compressibility were made in a Boyle's law apparatus similar to that described by Alexander and Lambert.<sup>12</sup> It consisted of a U-tube, having an inside diameter of 14 mm. One arm was constructed of Pyrex; the other arm, which served as the volumetric tube, was the remnants of an old 100-ml. soft glass gas buret with a neatly etched scale in tenths of ml., which could be read with the cathetometer to 0.005 ml. The tubes were enclosed in a cylindrical jacket through which water regulated to  $\pm 0.01^\circ$  at any temperature between 10 and 50° was circulated. Mercury was admitted to the system from a reservoir connected at the base of the U-tube. Pressures were measured with a Gaertner Model M 901 cathetometer capable of being set to 0.025 mm. For pressures above 400 mm. an additional manometer was connected in tandem.

The volumetric tube was calibrated at 7 points at room temperature by weighing the amount of mercury required to fill it to a desired volume. All measurements were taken within 0.1 ml. of the calibration points. Pressures and volumes were read six times at each point and the averages of these were taken as the values of  $P$  and  $V$  at that setting. Volumes at 50 and 10° were calculated using  $2.5 \times 10^{-5} \text{ deg.}^{-1}$  as the thermal coefficient of expansion of glass. The effect of pressure on the volume of the tube was calculated to be negligible in the range of interest.

The usual manometric corrections were made as well as corrections for the vapor pressure of mercury and the weight of the gas to give pressure in standard millimeters of mercury at the center of gravity of the vapor.

The compressibilities of *n*-butane, perfluoro-*n*-butane, and

- (10) J. A. Brown and W. H. Mears, *J. Phys. Chem.*, **62**, 960 (1958).
- (11) J. D. LaZerte, L. J. Hals, T. S. Reid, and G. N. Smith, *J. Am. Chem. Soc.*, **75**, 525 (1953).
- (12) E. A. Alexander and J. D. Lambert, *Trans. Faraday Soc.*, **37**, 421 (1941).

TABLE I

SECOND VIRIAL COEFFICIENTS IN CM.<sup>3</sup> MOLE<sup>-1</sup> FOR THE SYSTEMS: *n*-BUTANE + PERFLUORO-*n*-BUTANE AND DIMETHYL ETHER + 1-HYDROPERFLUOROPROPANE

Temp., °C.	Substance	10.00°		29.88°		50.05°	
		Pressure series eq. 1b	Concn. series eq. 1a	Pressure series eq. 1b	Concn. series eq. 1a	Pressure series eq. 1b	Concn. series eq. 1a
	<i>n</i> -C <sub>4</sub> H <sub>10</sub> Linear	-881 ± 11	-846 ± 10	-745 ± 6	-715 ± 5	-641 ± 12	-619 ± 11
	Quadratic	862 ± 68	862 ± 63	691 ± 27	695 ± 25	599 ± 72	602 ± 69
	<i>n</i> -C <sub>4</sub> H <sub>10</sub> + <i>n</i> -C <sub>4</sub> F <sub>10</sub> (1)	907 ± 12	873 ± 13	760 ± 3	736 ± 7	662 ± 9	644 ± 9
	<i>x</i> <sub>1</sub> = 0.4985	983 ± 66	976 ± 62	740 ± 43	741 ± 41	661 ± 58	660 ± 56
	<i>n</i> -C <sub>4</sub> F <sub>10</sub>	1164 ± 14	1098 ± 9	942 ± 19	900 ± 18	800 ± 6	770 ± 6
		1018 ± 45	1030 ± 40	894 ± 120	899 ± 110	772 ± 39	774 ± 37
	<i>B</i> <sub>12</sub>	792	766	678	666	593	604
		1018		686		636	
		10.10°		30.00°		50.00°	
	(CH <sub>3</sub> ) <sub>2</sub> O Linear	-542 ± 4	-531 ± 5	-466 ± 11	-457 ± 11	-411 ± 9	-405 ± 6
	Quadratic	591 ± 14	589 ± 13	515 ± 62	513 ± 61	508 ± 21	505 ± 20
	(CH <sub>3</sub> ) <sub>2</sub> O + C <sub>3</sub> F <sub>7</sub> H (1)	972 ± 6	934 ± 8	760 ± 13	737 ± 14	587 ± 13	573 ± 13
	<i>x</i> <sub>1</sub> = 0.4997	1022 ± 28	1019 ± 27	868 ± 65	861 ± 62	685 ± 62	681 ± 60
	C <sub>3</sub> F <sub>7</sub> H	788 ± 11	759 ± 10	674 ± 14	653 ± 14	577 ± 8	561 ± 8
		765 ± 68	766 ± 64	789 ± 61	781 ± 75	626 ± 35	632 ± 33
	<i>B</i> <sub>12</sub>	1280	1224	951	920	676	662
		1362		1080		800	

an equimolar mixture of these at 10.00, 29.88, and 50.05° and of 1-hydroperfluoropropane, dimethyl ether, and an equimolar mixture of these at 10.10, 30.00, and 50.00° were determined over the pressure range from 100 to 700 mm. The experimental data and other extensive details are available elsewhere.<sup>13</sup>

### Results

The problem of obtaining second virial coefficients from *PVT* measurements in the low pressure range has been discussed recently.<sup>14</sup> Our pressure-volume products, *PV*, were expressed as power series in the molecular concentration (*n/V*) and in the pressure *P* according to the relations

$$PV = nRT [1 + B(n/V) + C(n/V)^2 + \dots] \quad (1a)$$

$$PV = n[RT + \beta P + \gamma P^2 + \dots] \quad (1b)$$

The coefficients and their standard deviations were obtained for both series, terminating them at the linear terms as is customarily done,<sup>9,15-18</sup> and at the quadratic terms by the method of least squares on the Western Data Processing Center IBM 709 computer using a program written by Mr. D. B. Myers of the Chemistry Department at the University of California in Los Angeles. The pressure-volume product was found to be linear in *P* or in (*1/V*) within 0.05%; however, the second virial coefficients calculated from the linear equations in the pressure and concentration series, respectively, are different by a magnitude significantly larger than the uncertainties in the slopes of the apparent straight lines. Such differences have been referred to before.<sup>19,20</sup>  $\beta$  is larger than *B*; over the pressure

range of interest,  $B/\beta \cong (PV)_{1 \text{ atm.}}/RT$ . These quantities, though capable of being measured to high precision, and which represent very well the behavior of the gas in this range, must be considered as approximations to the coefficients of the infinite series. The infinite series values are of course needed for the calculation of the thermodynamic association constants. The best least squares fit to a quadratic equation removes the restriction that *C* or  $\gamma = 0$ . Very little, if anything, is learned about third virial coefficients; in fact if one were able to estimate these even crudely, one should incorporate them as fixed parameters in the expansions.

The second virial coefficients and standard errors are shown in Table I. Values obtained by terminating the series at the linear terms are given in the first row after each substance while those in the second row were obtained from the quadratic equations. The virial coefficients from the quadratic equations are in agreement with each other, though of course the standard errors are considerably larger than those obtained from the linear equations. Also, because of the small number of observations in each case, the experimental errors will not be distributed randomly and the best least squares fit to a quadratic may give values for second virial coefficients that are far less veritable than the ones obtained from the linear equations.

Reduced second virial coefficients are shown in Fig. 1. The smooth curves are through points obtained from linearization of the concentration series as is customarily done and the arrows indicate the location of points calculated from the quadratic equations. The critical constants selected are shown in Table II. The values for *n*-butane and dimethyl ether were from the review by Kobe and Lynn<sup>21</sup>; Brown and Mears<sup>10</sup> reported values for

(20) M. L. McGlashan and D. J. B. Potter, Presented at the Joint Conference of Thermodynamic and Transport Properties of Fluids, International Union of Pure and Applied Chemistry and The Institute of Mechanical Engineers, 1957.

(13) T. B. Tripp, M.S. Thesis, University of Maine, Orono, Maine, 1961.

(14) R. L. Scott and R. D. Dunlap, *J. Phys. Chem.*, **66**, 639 (1962).

(15) J. D. Lambert, G. A. H. Roberts, J. S. Rowlinson, and V. J. Wilkinson, *Proc. Roy. Soc. (London)*, **196A**, 113 (1949).

(16) J. H. P. Fox and J. D. Lambert, *ibid.*, **210A**, 557 (1951).

(17) J. D. Lambert, J. S. Clarke, J. F. Duke, C. L. Hicks, S. D. Lawrence, D. M. Mcorris, and M. G. T. Shore, *ibid.*, **249A**, 414 (1959).

(18) J. M. Prausnitz and W. B. Carter, *A.I.Ch.E. Journal*, **6**, 611 (1960).

(19) G. A. Bottomley and C. G. Reeves, *J. Chem. Soc.*, 3794 (1958).

perfluoro-*n*-butane, and the values for 1-hydroperfluoropropane were determined in our Laboratory by Hunt.<sup>22</sup> The cross-term second virial coefficients

TABLE II  
SELECTED CRITICAL CONSTANTS

	$T_c$ , °K.	$V_c$ , cm. <sup>3</sup> mole <sup>-1</sup>
<i>n</i> -C <sub>4</sub> H <sub>10</sub>	425.2	255
<i>n</i> -C <sub>4</sub> F <sub>10</sub>	386.4	378
(CH <sub>3</sub> ) <sub>2</sub> O	400.1	190
C <sub>2</sub> F <sub>5</sub> CF <sub>2</sub> H	377.6	276

were calculated from the relation

$$B_m = x_1^2 B_{11} + 2x_1 x_2 B_{12} + x_2^2 B_{22} \quad (2)$$

where  $B_m$ ,  $B_{11}$ , and  $B_{22}$  are the second virial coefficients of the mixture and pure components, respectively.  $B_{12}$  is related to the interactions between pairs of unlike molecules as  $B_{11}$  and  $B_{22}$  are to pairs of like molecules. The reduced cross-term second virial coefficients and reduced temperatures for the mixtures shown in Fig. 1 were calculated from the usual combining rules of Guggenheim and McGlashan<sup>23</sup>

$$V_{12}^c = 1/8 [(V_1^c)^{1/2} + (V_2^c)^{1/2}]^3 \quad (3)$$

and

$$T_{12}^c = (T_1^c T_2^c)^{1/2} \quad (4)$$

Values of  $B_{12}$  are subject to considerably larger errors than the pure component virial coefficients.

The dashed curve, shown for comparison, was calculated from the relation

$$B/V_c = 1/4 - 3/2 (T_c/T)^2 \quad (5)$$

an equation of the Berthelot form obtained by Guggenheim,<sup>24</sup> using  $0.282$  for  $P^c V^c / RT^c$  as an average of the values for a number of substances. Guggenheim pointed out that although this curve has no theoretical significance, it represents quite well the behavior of hydrocarbons in this reduced range.

### Discussion

***n*-Butane.**—The *n*-butane second virial coefficients from the quadratic equations,  $-693$  and  $-600$  cm.<sup>3</sup> mole<sup>-1</sup> at  $30$  and  $50^\circ$ , respectively, are in excellent agreement with the values  $-702$  and  $-596$  calculated from the equation given by McGlashan and Potter<sup>20</sup> at these temperatures and with the corresponding values  $-692$  and  $-610$  calculated from the Beattie-Bridgeman equation of state with the parameters given by Beattie and Stockmayer.<sup>25</sup> The latter represent a rather long extrapolation from the experimental temperatures and pressures but are probably correct to within 15 cm.<sup>3</sup>. Our value of  $-862$  at  $10^\circ$  is considerably larger than  $-823$  given by McGlashan and Potter and  $-807$  from the Beattie-Bridgeman equation, though it has a large uncertainty.

**Perfluoro-*n*-butane.**—The second virial coef-

(21) K. A. Kobe and R. E. Lynn, *Chem. Revs.*, **52**, 117 (1953).

(22) G. Hunt, B. S. Thesis, University of Maine, Orono, Maine, 1961.

(23) E. A. Guggenheim and M. L. McGlashan, *Proc. Roy. Soc. (London)*, **206A**, 448 (1950).

(24) E. A. Guggenheim, *J. Imp. Coll. Chem. Soc.*, **32**, 13, in *Sci. J. Roy. Coll. Sci.*, **23**, (1953).

(25) J. A. Beattie and W. H. Stockmayer, *J. Chem. Phys.*, **10**, 473 (1942).

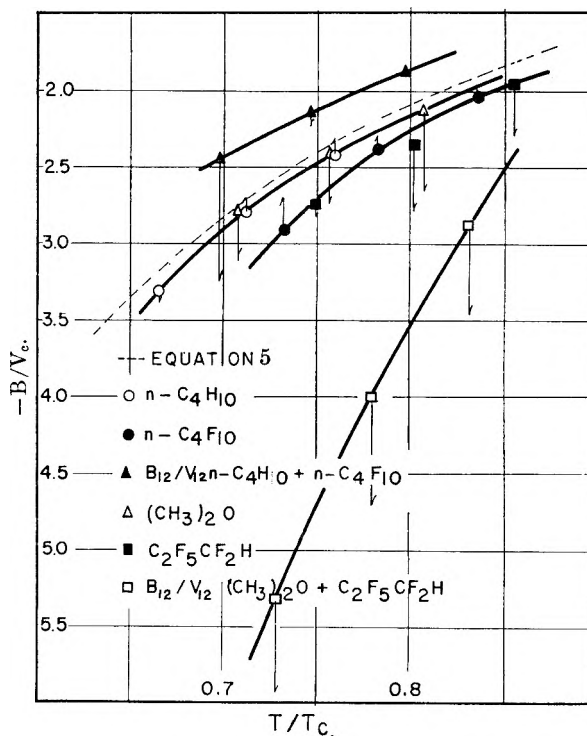


Fig. 1.—Reduced second virial coefficients.

ficients of perfluoro-*n*-butane at  $10$ ,  $30$ , and  $50^\circ$  agree reasonably with the values  $-1104$ ,  $-901$ , and  $-742$  cm.<sup>3</sup> mole<sup>-1</sup> calculated from the Martin-How equation of state used by Brown and Mears<sup>10</sup> to fit their  $PVT$  data near the critical region. Our reduced virial coefficients from the linear concentration series equation are more negative than the values for hydrocarbons at the same corresponding temperatures and fall between the values for perfluoro-*n*-pentane and perfluoro-*n*-hexane reported by Garner and McCoubrey.<sup>9</sup> These workers also linearized their data using the concentration series. The reduced values obtained from the quadratic equations, however, lie much closer to the hydrocarbon curves. Although it is to be expected that the reduced curves for the fluorocarbons will fall below those for the corresponding hydrocarbons, the differences may not prove to be as large as they now appear.

**Perfluoro-*n*-butane + *n*-Butane.**—The reduced cross-term second virial coefficients are in excellent agreement with those of Garner and McCoubrey,<sup>9</sup> whose values for the systems *n*-pentane + perfluoro-*n*-pentane and *n*-pentane + perfluoro-*n*-hexane fall on the same curve with our values for *n*-butane + perfluoro-*n*-butane. The large positive deviations from eq. 5 and from the curves for the pure components can be attributed to weaker attractive forces between pairs of unlike molecules than between pairs of like molecules.

Equation 4 is equivalent to the geometric mean approximation  $\epsilon_{12} = \epsilon_{11}^{1/2} \epsilon_{22}^{1/2}$ , where the  $\epsilon$ 's are the interaction energies characteristic of the pairs of molecular species. Reed<sup>26</sup> has suggested that failure of the geometric mean law for liquid mixtures of these substances may be due to the large

(26) T. M. Reed, III, *J. Phys. Chem.*, **59**, 425 (1955).

differences between the ionization potentials of fluorocarbons and hydrocarbons. Prausnitz<sup>27</sup> in his recognition of this suggested that eq. 4 be modified as

$$T_{12}^e = k(T_1^e T_2^e)^{1/2} \quad (6)$$

where

$$k = \left[ \frac{4V_1^e/V_2^e}{(1 + V_1^e/V_2^e)^2} \right] \left[ \frac{2(I_1/I_2)^{1/2}}{1 + I_1/I_2} \right] \quad (7)$$

The  $I$ 's are the ionization potentials of the molecules. This was derived from the London dispersion force equation for the attractive branch of the intermolecular potential function and neglects the repulsive branch. If we use Reed's estimate of 17.4 e.v. for the ionization potential of perfluoro-*n*-butane<sup>28</sup> with a value of 10.34 e.v. for *n*-butane, we calculate  $k = 0.92$ . The value of  $k$  required to superimpose the reduced curve for the mixture onto the Berthelot curve using eq. 6 is 0.94 and is constant over the reduced temperature range. No such simple adjustment was found for eq. 3, indicating that failure of the geometric mean approximation is primarily responsible for the observed behavior of these mixtures.

**Dimethyl Ether.**—The reduced second virial coefficients for dimethyl ether, calculated from the linear concentration series at 10, 30, and 50° are 2.86, 2.46, and 2.21, while the corresponding values given by Lambert, *et al.*,<sup>15</sup> for diethyl ether are 2.87, 2.47, and 2.14. They fall on the same reduced curve with *n*-butane. The values obtained using the quadratic, however, fall well below the curve for *n*-butane, as is expected for a polar substance.

**1-Hydroperfluoropropane.**—The reduced second virial coefficients for 1-hydroperfluoropropane obtained from the linear equation lie on the corresponding curve for the fluorocarbons; however, when one fits a quadratic to the data, they are found to be more negative and similar in behavior to dimethyl ether.

**Dimethyl Ether + 1-Hydroperfluoropropane.**—The second virial coefficients for the equimolar mixture of dimethyl ether and 1-hydroperfluoropropane are numerically larger than the values for either of the pure components, indicative of stronger attractive forces between pairs of molecules in the mixture than in the pure components. The plot of  $B_{12}^e/V_{12}^e$  vs.  $T/T_{12}^e$  calculated from equations 2, 3, and 4 and shown in Fig. 1 falls far below the curve given by eq. 5.

The large negative deviation from eq. 5 can be interpreted in terms of reversible association due to hydrogen bonding. The association constants were calculated using an equation similar to the one derived by Schäfer and Foz Gazulla<sup>29</sup> and Lambert, *et al.*,<sup>15</sup> relating the second virial coefficient to the association constant for dimerization. For the reaction

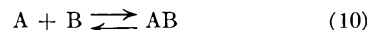


their equation can be written as

$$RTK_p = (B^e - B^o) \quad (9)$$

where  $B^e$  is the expected second virial coefficient for A should it not dimerize and  $B^o$  is the observed second virial coefficient. It applies when the concentration of dimers is small and the interaction between dimers and monomers is negligible.

The relation  $RTK_p = (B_{12}^e - B_{12}^o)$ , which resembles eq. 9 frequently has been used<sup>16-18</sup> to calculate association constants for equilibria of the type



However, if one considers for example, that in an equimolar mixture of A + B, the partial pressures of the interacting species are half of what they would be in a mixture of A + A, it is easily seen that the relation between the equilibrium constant  $K_p$  for associations between unlike species and the cross-term second virial coefficient is

$$RTK_p = 2(B_{12}^e - B_{12}^o) \quad (11)$$

There are several ways to estimate  $B_{12}^e$ . Lambert and co-workers<sup>15-17</sup> use the Berthelot equation. Prausnitz<sup>18</sup> has used the more refined acentric factor method of Pitzer and Curl.<sup>30</sup> We might assume, for example, that in the absence of hydrogen bonding, the mixture 1-hydroperfluoropropane + dimethyl ether would behave as a fluorocarbon + hydrocarbon mixture, and estimate  $B_{12}^e$  from the experimentally established reduced curves for these systems. Considering the accuracy of the values of  $B_{12}$  obtained from this kind of experiment, the method of selecting  $B_{12}^e$  is unimportant at present.

Values of  $B_{12}^o$  calculated from eq. 1 terminated at the quadratic term and eq. 2 are shown in column 2 of Table III. The corresponding values of  $B_{12}^e$  from eq. 5 are shown in column 3 and those from the reduced curve for mixtures of fluorocarbons and hydrocarbons in column 4. The association constants in columns 5 and 6 were calculated with the aid of eq. 11 from the values given in columns 3 and 4, respectively. Values of the enthalpy of association obtained from the temperature dependence of the association constants and the second law of thermodynamics are shown in the last row of Table III. The estimated error in  $\Delta H$  is on the order of 1 kcal. The decrease in entropy is on the order of 20 cal. deg.<sup>-1</sup> per mole of  $(CH_3)_2O \cdot HC_3F_7$  formed.

TABLE III  
DIMETHYL ETHER + 1-HYDROPERFLUOROPROPANE ASSOCIATION CONSTANTS AND ENTHALPY OF ASSOCIATION

$T, ^\circ C.$	$-B_{12}^o, \text{ cm.}^3$	$-B_{12}^e, \text{ cm.}^3$	$\text{mole}^{-1}$	$K_p \times 10^2, \text{ atm.}^{-1}$	
	Eq. 2	Eq. 5	Reduced curve for $C_4H_{10}$ + $C_3F_8$		
10	1362	591	481	6.6	7.6
30	1080	511	419	4.6	5.3
50	800	442	366	2.7	3.3
	$-\Delta H, \text{ kcal. mole}^{-1}$			4.2	4.1

**Acknowledgments.**—National Science Foundation support of the program of which this work was a part is gratefully acknowledged. We wish to thank the General Chemicals Division of the Allied Chemical Corporation for providing the perfluoro-*n*-butane, and Allen Wright, Miriam Doug-

(27) J. M. Prausnitz, *A.I.Ch.E. Journal*, **5**, 3 (1959).

(28) T. M. Reed III, *J. Phys. Chem.*, **59**, 428 (1955).

(29) K. Schäfer and O. R. Foz Gazulla, *Z. physik. Chem.*, **B52**, 299 (1942).

(30) K. S. Pitzer and R. F. Curl, *J. Am. Chem. Soc.*, **79**, 2369 (1957).



lass and Gardner Hunt for technical assistance. We are indebted to Professor Robert L. Scott and

Mr. D. B. Myers of the University of California for helpful discussion.

## ON THE DETERMINATION OF SECOND VIRIAL COEFFICIENTS

By ROBERT L. SCOTT AND ROBERT D. DUNLAP

Department of Chemistry, University of California, Los Angeles and  
Department of Chemistry, University of Maine, Orono, Maine

Received October 16, 1961

It is well known that the isothermal change of the pressure-volume product  $PV$  of a real gas can be expressed in either of two infinite power series, one in the pressure  $P$ , and one in the molar concentration  $n/V$

$$PV = nRT[1 + Bn/V + C(n/V)^2 + D(n/V)^3 + \dots] \quad (1a)$$

$$PV = n[RT + \beta P + \gamma P^2 + \delta P^3 + \dots] \quad (1b)$$

where for the infinite series the virial coefficients  $B$ ,  $C$ ,  $D$ , . . . and  $\beta$ ,  $\gamma$ ,  $\delta$ , . . . are related  $\beta = B$ ,  $\gamma = (C - B^2)/RT$ , etc.

Pressure-volume measurements in the low pressure region rarely are accurate enough to yield meaningful values of the third virial coefficients  $C$  or  $\gamma$ , so it is customary to terminate eq. 1a and 1b at the linear terms. However, even when the measurements are restricted to pressures below one atmosphere, these two linear equations can yield significantly different values for the two "second virial coefficients"  $B$  and  $\beta$ .

A little thought shows us that we are calculating average values of the slope  $PV/nRT$  vs.  $n/V$  and  $P/RT$ , respectively, while the second virial coefficients which have theoretical significance (arising from the interaction of an isolated pair of molecules) are the limiting slopes at  $n/V = 0$  and  $P/RT = 0$ ; only in this latter case must  $B$  equal  $\beta$ . For the average slope to equal the limiting slope, we must assume  $C = 0$  (for the concentration series) or  $\gamma = 0$  (for the pressure series). Since  $C - RT\gamma = B^2$ , manifestly  $C$  and  $\gamma$  cannot both be zero.

For example, if one determines  $PV$  over a set of pressures uniformly distributed between zero and a maximum pressure  $\hat{P}$ , the best (least squares) linear fit to eq. 1 (ignoring experimental "scatter") will yield apparent values for  $n$  and  $\beta$ .

$$n_{\text{app}} = n(1 - \gamma\hat{P}^2/6RT - \dots) \quad (2a)$$

$$\beta_{\text{app}} = (\beta + \gamma\hat{P} + 9\delta\hat{P}^2/10 + \dots)/(1 - \gamma\hat{P}^2/6RT - \dots) \quad (2b)$$

The difference between  $n_{\text{app}}$  and  $n$  normally is trivial, but the difference between  $\beta_{\text{app}}$  and  $\beta$  can be significant. Thus for  $\gamma = -B^2/RT$  (corresponding to  $C = 0$ )  $\beta_{\text{app}}$  would be in error by a factor approximately  $(1 - \beta\hat{P}/RT)$ , i.e.,  $nRT/PV$  at  $P = \hat{P}$ . For substances with large molecular size, like fluorocarbons, this can mean an error of as much as 10% in the calculated  $B$  or  $\beta$  at the normal boiling point.

One frequently encounters the statement<sup>1</sup> that the concentration series is markedly preferable to the pressure series. It indeed is true that at low

temperatures the concentration series shows gentler curvature than the pressure series and is better fit with two or three adjustable parameters. This conclusion, however, does not automatically extend to the low pressure region where we compare the two linear approximations. The relative magnitude of the ignored quadratic constants  $C$  and  $RT\gamma = C - B^2$  will depend upon the substance and the temperature in question.

Equation of state studies<sup>2</sup> on simple fluids (Ar and Kr) which should follow a law of corresponding states suggest that below a temperature near the critical point ( $T = 1.2T_c$ )  $C$  is smaller in magnitude than  $RT\gamma$ , and that at all temperatures above this, the reverse is true. One might conclude from this that below the critical point the linear concentration series is preferable, and that above this temperature the linear pressure series should be used. How far one can extrapolate this conclusion to polyatomic molecules is problematical. Moreover, in gases which exhibit a kind of "chemical" association in which an association constant  $K_2$  for dimerization is large compared with the  $K_3$  for trimers,  $RT\gamma \approx 3K_2^2 - 2K_3$  will be smaller than  $C = 4K_2^2 - 2K_3$ .

It is in the low reduced temperature low pressure region (e.g., near the normal boiling point) that  $B^2$  is large, producing a maximum uncertainty in a linear determination of  $B$ .

We recently have made measurements in our two laboratories<sup>3,4</sup> in which a least squares linearization of the  $PV$  data yielded markedly different values of  $B$  and  $\beta$ , yet the standard deviations for  $PV$  and for the "second virial coefficients" were so small and so nearly equivalent for the two methods as to offer no basis of choice.

The obvious resolution of this difficulty is to remove the inhibiting assumption that  $C$  (or  $\gamma$ ) is zero, and to obtain the best least squares fit to quadratic equations terminating in  $C(n/V)^2$  or  $\gamma P^2$ . This does not lead necessarily to more accurate values of the second virial coefficient, but the values of  $B$  and  $\beta$  are now in agreement. The standard deviations for  $B$  and  $\beta$  are of course larger but perhaps more realistic. Little significance, however, can be attached to  $C$  or  $\gamma$  calculated this way.

The different calculations for  $n$ -butane at 29.88° measured by Tripp and Dunlap<sup>3</sup> are shown in Table I.

Note that the standard deviations for  $B$  and  $\beta$  from the linear fit are surprisingly small; these represent the deviations for the average slope, not the limiting slope, which is determined much less well. The limiting slopes should be used for theoretical interpretation of the interactions of an isolated pair of molecules; the average slopes, if determined over

(2) J. A. Beattie, R. J. Barrault, and J. S. Brierley, *J. Chem. Phys.*, **19**, 1219 (1951); **20**, 1615 (1952).

(3) T. B. Tripp and R. D. Dunlap, *J. Phys. Chem.*, **66**, 635 (1962).

(4) C. Booth and R. L. Scott, to be published.

(1) J. S. Rowlinson, in "Encyclopedia of Physics XII," Springer, 1958, p. 1.

TABLE I  
VIRIAL COEFFICIENTS FOR *n*-BUTANE AT 29.88°

	Concn. series Eq. 1a	Pressure series Eq. 1b
Terminated at the linear term	$nRT = 14,796.7 \pm 1.5 \text{ cm.}^3 \text{ mm.}$ $\sigma PV = 2.1$ $B = -715 \pm 5 \text{ cm.}^3 \text{ mole}^{-1}$	$nRT = 14,801.1 \pm 2 \text{ cm.}^3 \text{ mm.}$ $\sigma PV = 2.8$ $\beta = -745 \pm 6 \text{ cm.}^3 \text{ mole}^{-1}$
Terminated at the quadratic term	$nRT = 14,793.5 \pm 4 \text{ cm.}^3 \text{ mm.}$ $\sigma PV = 2.2$ $B = -695 \pm 25 \text{ cm.}^3 \text{ mole}^{-1}$ $C/10^6 = -4 \pm 4 \text{ cm.}^6 \text{ mole}^{-2}$	$nRT = 14,793.2 \pm 4 \text{ cm.}^3 \text{ mm.}$ $\sigma PV = 2.2$ $\beta = -691 \pm 26 \text{ cm.}^3 \text{ mole}^{-1}$ $\gamma RT/10^6 = -10 \pm 5 \text{ cm.}^6 \text{ mole}^{-2}$

the relevant pressure range, should be used for correcting properties of real gases to the hypothetical ideal gas state.

We conclude: In the absence of information concerning the magnitude of the third virial coefficient (either from careful measurements at higher pressures or from clearly defensible assumptions which always should be stated) one cannot, from a linear plot of  $PV$  vs.  $1/V$  or  $PV$  vs.  $P$ , determine the true

(limiting) value of the second virial coefficient with anywhere near the accuracy which sometimes is claimed.

We wish to thank D. B. Myers of the University of California for helpful discussion and for making some of the calculations. Support of the U. S. Atomic Energy Commission (R.L.S.) and the National Science Foundation (R.D.D.) is gratefully acknowledged.

## SOLUBILITY THERMODYNAMICS IN CHEMICAL ENGINEERING

BY J. M. PRAUSNITZ

*University of California, Berkeley, California*

*Received October 27, 1961*

The semi-empirical approach of Hildebrand is highly suitable for engineering requirements and the chemical engineer who is familiar with Hildebrand's work is well prepared to attack many typical chemical engineering problems. Two examples are given which indicate the usefulness of some of Hildebrand's ideas; one of these deals with gas solubilities and the other with extractive distillation. The examples illustrate how a semi-empirical treatment of solution properties provides the necessary concepts for interpretation and correlation of useful solubility data.

Problems in phase equilibria play an important role in chemical engineering. A large part of the chemical engineer's task is to separate mixtures and the most common technique for performing such separations is by contacting the mixture with another phase which will preferentially dissolve one of the components of the mixture. Hence chemical engineers are interested in correlating and predicting solubilities as required in the design of technical chemical operations and it is not surprising that they turn to the work of Joel H. Hildebrand to seek aid in realizing their goal. The semi-empirical approach of Hildebrand and his co-workers is highly suitable for engineering requirements and the chemical engineer who is familiar with Hildebrand's work is well prepared to attack many typical phase equilibrium problems which arise in his professional practice. The great utility of Hildebrand's approach is that it provides not abstract and formal theories but rather concrete concepts and physical insights which can serve as theoretical foundations for practical interpretation and correlation of phase equilibrium data.

The potential applications of Hildebrand's solubility thermodynamics to chemical engineering problems are numerous. To illustrate how Hildebrand's work can be effectively utilized in the solution of practical problems two examples are described below.

**Solubility of Gases in Typical Non-polar Solvents.**—It frequently is desirable to estimate the

solubility of a gas in a liquid at a specified temperature and pressure. While many gas solubility data are in the literature, a significant fraction is of doubtful accuracy and the vast majority of the data were obtained at room temperature; as one proceeds to temperatures either higher or lower than about 25° the amount of data falls exponentially. It therefore frequently is necessary to estimate gas solubilities from little or essentially no information.

A technique for correlating reliable gas solubilities in non-polar systems<sup>1</sup> is provided by a combination of two concepts: the idea of corresponding states and the idea of a regular solution. The isothermal dissolution of a gaseous solute in a liquid solvent can be considered to take place in two consecutive steps: in the first step, the gas is "condensed" to a liquid-like volume and in the second step the "condensed" gas (or hypothetical liquid) is dissolved in the solvent. If the gas is initially at unit fugacity then the free energy for the first step is

$$\Delta G_1 = RT \ln f^{0L} \quad (1)$$

and that for the second step is

$$\Delta G_{11} = RT \ln \gamma_2 x_2 \quad (2)$$

where  $f^{0L}$  is the fugacity of the hypothetical liquid,  $x_2$  is the solubility (in mole fraction) of the gaseous solute denoted by subscript 2, and  $\gamma_2$  is the activity coefficient of the gaseous solute referred to the

(1) J. M. Prausnitz and F. H. Shair, *A.I.Ch.E. Journal*, **7**, 682 (1961).

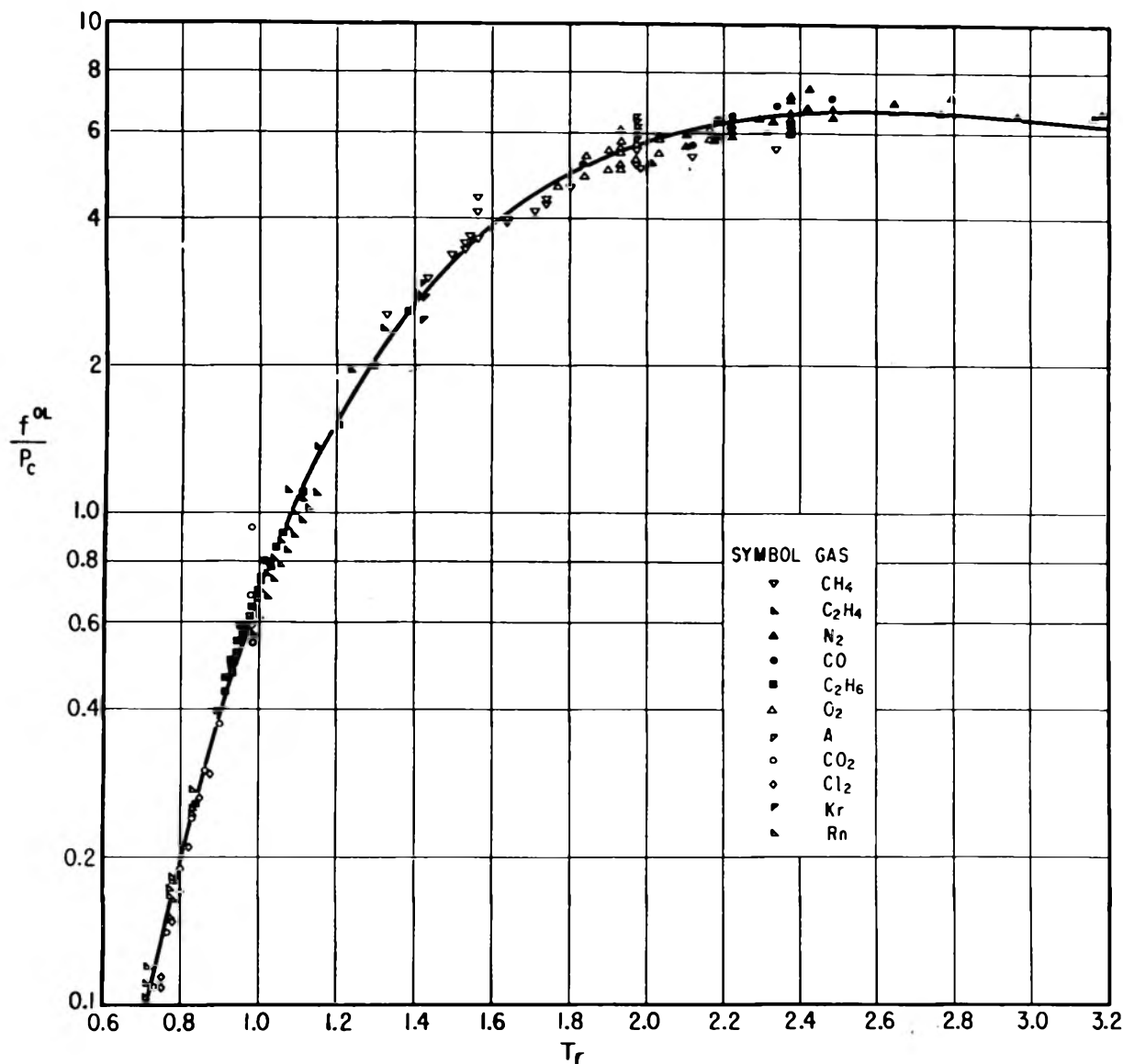


Fig. 1.—Fugacity of hypothetical liquid at pressure of 1 atmosphere.

hypothetical pure liquid. At equilibrium the free energy of the gas at unit fugacity is the same as that of the gaseous solute in the solvent and thus

$$\Delta G_{\text{I}} + \Delta G_{\text{II}} = 0 \quad (3)$$

The advantage of splitting the isothermal dissolution process into two steps is that the first step involves only properties of the pure gas and hence it is reasonable to expect that  $f^{0L}$  may be correlated within the framework of a corresponding states treatment; and that the second step may be described adequately by the regular solution equation. A correlation of gas solubilities in non-polar systems then may be constructed with the additional relations

$$\frac{f^{0L}}{P_c} = \Phi \left( \frac{T}{T_c} \right) \quad (4)$$

$$\ln \gamma_2 = \frac{V_2^L \phi_1^2 (\delta_1 - \delta_2)^2}{RT} \quad (5)$$

where  $P_c$  and  $T_c$  are the critical pressure and critical temperature of the gaseous solute,  $\Phi$  is a universal function,  $V_2^L$  and  $\delta_2$  are the molar volume and solu-

bility parameter of the hypothetical liquid, and  $\phi_1$  and  $\delta_1$  are the volume fraction and solubility parameter for the liquid solvent. Since  $x_2$  usually is very small,  $\phi_1$  is equal to unity for most practical purposes.

The correlating framework outlined by eq. 1 to 5 contains three unknown properties of the hypothetical liquid:  $f^{0L}$ ,  $V_2^L$  and  $\delta_2$ . All of these are temperature dependent but due to regular solution theory it is not necessary to consider the temperature dependence of  $V_2^L$  and  $\delta_2$ . According to regular solution theory,  $\ln \gamma$  is inversely proportional to temperature at constant composition and thus the term  $V_2^L \phi_1^2 (\delta_1 - \delta_2)^2$  may be considered independent of temperature. Accordingly  $V_2$  and  $\delta_2$  must be chosen at the same temperature as  $\delta_1$  and for convenience this arbitrary temperature as used here is 25°.

To obtain numerical values for the parameters,  $f^{0L}$ ,  $V_2$ , and  $\delta_2$  all available, reliable gas solubility data were correlated within the framework described above. The sources and temperature ranges

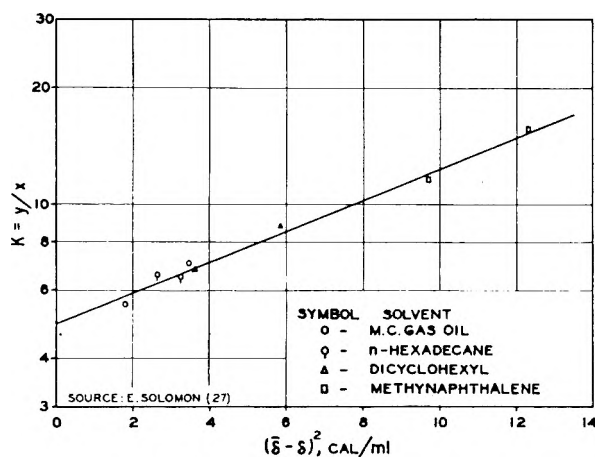


Fig. 2.—Effect of solubility parameter on  $K$  value of methane at 100°F. and 500 lb./sq. in. abs.

of the data used are given elsewhere<sup>1</sup> but Table I lists the molar volumes and solubility parameters which were obtained. The fugacities of the hypothetical liquid are correlated according to eq. 4 as shown in Fig. 1. Since most available data for hydrogen correspond to very high reduced temperatures they are not shown here but may be found in ref. 1.

TABLE I

LIQUID VOLUMES AND SOLUBILITY PARAMETERS FOR GASEOUS SOLUTES

Gas	$V^{0L}$ , cm. <sup>3</sup> /g. mole	$\delta$ , (cal./cm. <sup>3</sup> ) <sup>1/2</sup>
N <sub>2</sub>	32.4	2.59
CO	32.1	3.13
O <sub>2</sub>	33.0	4.00
Ar	57.1	5.33
CH <sub>4</sub>	52.0	5.68
CO <sub>2</sub>	55.0	6.00
Kr	65.0	6.40
C <sub>2</sub> H <sub>4</sub>	65.0	6.60
C <sub>2</sub> H <sub>6</sub>	70.0	6.60
Rn	70.0	6.83
Cl <sub>2</sub>	74.0	8.7

With the use of the information given in Table I and in Fig. 1 it is possible to compute the solubilities of many common gases in numerous non-polar solvents at any temperature where the solvent's vapor pressure is not too large. The solubility at one atmosphere pressure is calculated by combining eq. 1, 2, 3, and 5 to give

$$\frac{1}{x_2} = f^{0L} \exp \frac{V_2^L \phi_1^2 (\delta_1 - \delta_2)^2}{RT} \quad (6)$$

The large advantage of Fig. 1 is that it utilizes solubility data primarily obtained near room temperature to predict the solubility of gases at temperatures well removed from room temperature. This correlation scheme enables the chemical engineer to make predictions of gas solubilities over a wide temperature range. The accuracy is about 10%. Such predictions are of value in numerous common problems such as the preliminary design of absorption equipment. One example of such an application is given in Fig. 2, which compares calculated and observed  $K$  values for methane in several petroleum solvents.

**Solvent Selectivity in Extractive Distillation of Hydrocarbons.**—The separation of hydrocarbons from their mixtures usually is achieved by distillation but if two hydrocarbons have very nearly the same volatility ordinary distillation becomes extremely inefficient and, in the limiting case, where the volatilities of two hydrocarbons become identical, an azeotrope is formed and ordinary distillation fails completely. In such cases it has become a common procedure in the petrochemical industry to add deliberately another substance to the hydrocarbon mixture in the hope that this additional substance will favorably affect the volatility relations so that distillation may be used after all as a means of separation. This procedure is called extractive distillation and the added substance is called the solvent or entrainer. For the separation of hydrocarbons by extractive distillation an effective solvent must be a polar organic liquid which can induce strong deviations from Raoult's law and yet be sufficiently soluble in hydrocarbons without forming two liquid phases. When a separation by extractive distillation is contemplated the immediate question which arises is "What solvent is most effective?" Or, in other words, "What solvent will have the highest selectivity?" In trying to find an answer to these questions the chemical engineer can be greatly assisted by some of the concepts advanced by Joel Hildebrand.

The selectivity  $S$  is related to the relative volatility  $\alpha$  by

$$\alpha_{1,2} = \frac{\gamma_1 P_1^0}{\gamma_2 P_2^0} = S \frac{P_1^0}{P_2^0} \quad (7)$$

where subscripts 1 and 2 refer to the hydrocarbons to be separated,  $P^0$  is the vapor pressure, and  $\gamma$  the activity coefficient. A good solvent is characterized by a value of  $S$  well removed from unity; if a solvent has a selectivity  $S = 1$  it is worthless because it affects the volatility of both hydrocarbons equally and therefore does not facilitate separation.

At constant temperature, the selectivity will be a maximum when the polar solvent is present in excess and therefore it is most convenient to try to compute  $\gamma_1$  and  $\gamma_2$  for a solution where hydrocarbons 1 and 2 are infinitely dilute in the polar solvent designated by subscript 3.

Consider now a solution of hydrocarbon 1 (or 2) in polar solvent 3. The heat of mixing can be divided into two contributions: one from changes in potential energy and the other from changes in vibrational and rotational energy. Thus

$$\Delta H = \Delta H(\text{pot}) + \Delta H(\text{rot,vib}) \quad (8)$$

If now the simplifying assumptions are made that the excess entropy is given by

$$T \Delta S^E = \Delta H(\text{rot,vib}) \quad (9)$$

and that  $\Delta H(\text{pot})$  is given by a quadratic function of the volume fractions, then the excess free energy is given by

$$\Delta G^E = (x_1 V_1 + x_3 V_3) \phi_1 \phi_3 A_{13} \quad (10)$$

where  $A_{13} = c_{11} + c_{33} - 2c_{13}$ , the exchange energy per unit volume, and  $c$  stands for cohesive energy density. The selectivity now can be expressed as

$$S_{1,2} = \exp \left( \frac{V_1 A_{13} - V_2 A_{23}}{RT} \right) \quad (11)$$

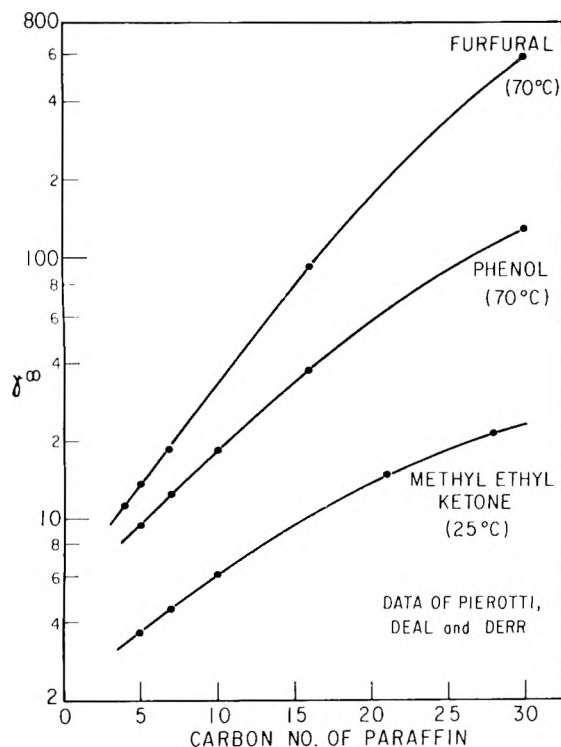


Fig. 3.—Size effect in solvent selectivity: activity coefficients of normal paraffins in polar solvents at infinite dilution.

Equation 10 is, of course, the Hildebrand-Scatchard solubility equation but the  $c$  terms now include contributions from polar as well as non-polar forces. Techniques for estimating quantitatively the strength of these forces are given elsewhere.<sup>2</sup>

**Induction Effects.**—As a first thought, one might expect that induction forces may be responsible for selectivity; if the polar solvent can induce a dipole in hydrocarbon 1 which is significantly different from that induced in hydrocarbon 2 then clearly a basis for good selectivity is established. But a moment's reflection indicates that this possibility is not promising. When a polar molecule of radius  $a$  having a dipole moment  $\mu$  is surrounded by a non-polar fluid having dielectric constant  $\epsilon$  the energy of induction is given by

$$\Delta E_{ind} = \left( \frac{\epsilon - 1}{2\epsilon - 1} \right) \frac{\mu^2}{a^3} \quad (12)$$

Thus preferential induction can occur only if the two hydrocarbons have considerably different dielectric constants. However, there is, in fact, very little variation in the dielectric constants of hydrocarbons and thus it appears that induction is not the key to good selectivity.

**Contributions to Selectivity: Effect of Molecular Size.**—If appropriate estimates of the  $c$  terms are made, it can be shown<sup>2</sup> that the selectivity can be expressed as the sum of three contributions: a polar, a non-polar, and induction term

$$RT \ln S_{12} = P + D + I \quad (13)$$

where

$$P = \delta_3 P^2 (V_1 - V_2) \quad (14)$$

$$D = V_1(\delta_3^n - \delta_1^n)^2 - V_2(\delta_3^n - \delta_2^n)^2 \quad (15)$$

(2) J. M. Prausnitz and R. Anderson, *A.I.Ch.E. Journal*, **7**, 96 (1961).

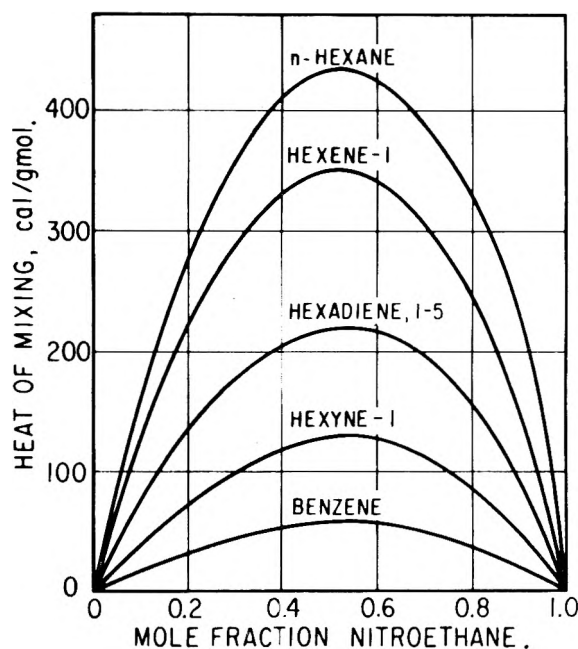


Fig. 4.—Effect of unsaturation of the hydrocarbon on the heats of mixing for nitroethane-hydrocarbon systems at 45°.

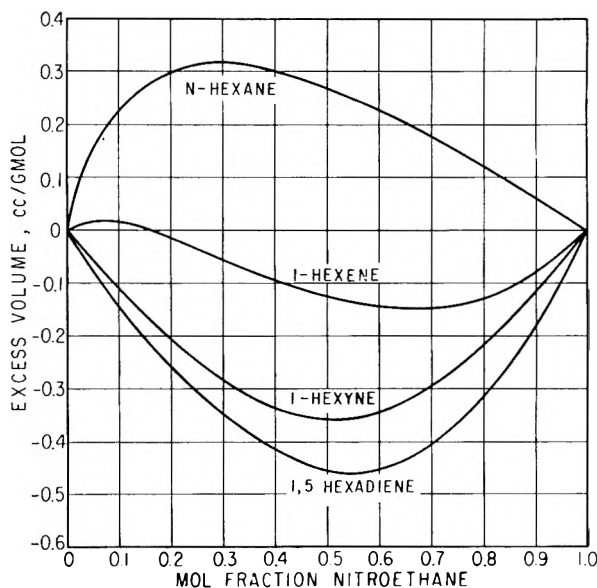


Fig. 5.—Volume change on mixing nitroethane with hydrocarbons at 25°.

$$I = 2V_2\zeta_{22} - 2V_1\zeta_{21} \quad (16)$$

In eq. 14 to 16  $\delta_3 P^2$  stands for the polar energy density,  $\delta^n$  for the non-polar energy density, and  $\zeta$  for the induction energy per unit volume.

Typical phase equilibrium data indicate that the polar term  $P$  is by far the most important term whenever the volumes of hydrocarbons 1 and 2 are not very near to each other. The contributions from  $D$  and  $I$  are then always small. It appears then that it is possible to separate hydrocarbons by extractive distillation on the basis of size difference; the selectivity rises as the difference in molar volumes of the two hydrocarbons increases and the most effective solvent is one having a high polar energy and a small volume. Thus, for ex-

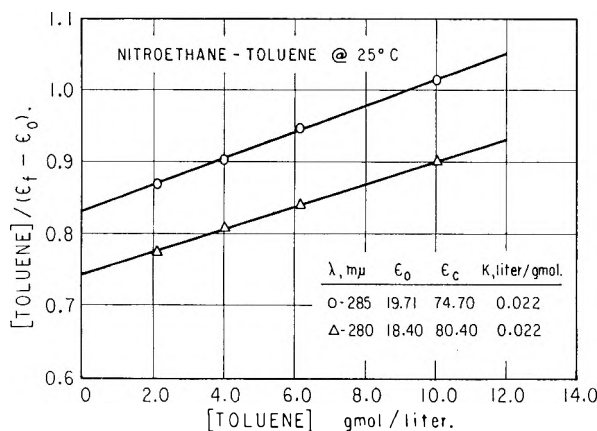


Fig. 6.—The evaluation of the equilibrium constant for the nitroethane-toluene system at 25°.

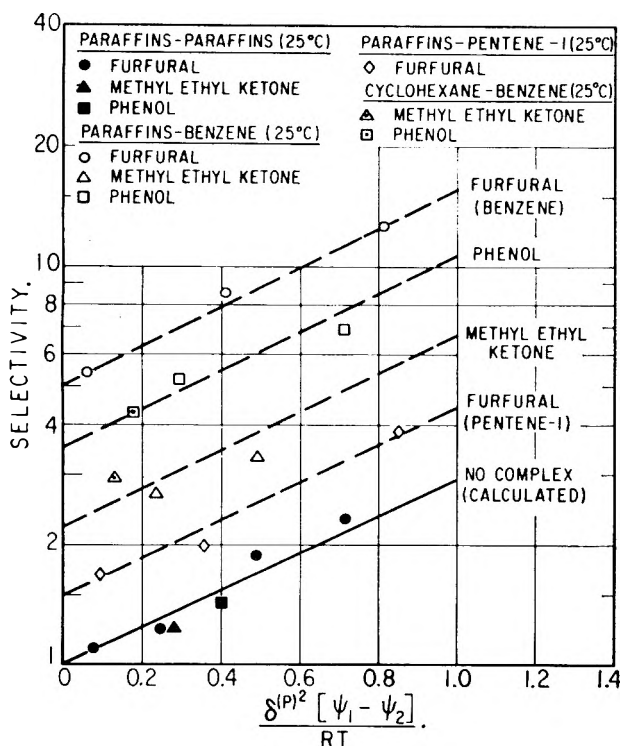


Fig. 7.—Effect of complex formation on solvent selectivity.

ample, eq. 13 predicts that acetone should be a more selective solvent than diethyl ketone and this prediction is in agreement with experiment. Further, eq. 13 says that in the absence of chemical effects the larger hydrocarbon has the larger activity coefficient and this too is supported by experimental evidence as shown in Fig. 3.

The effect of a polar molecule on a non-polar is to cause positive deviations from Raoult's law. The larger non-polar molecule presents a larger cross-section for interaction with the polar and thus a mechanical analog of the state of the solution is to think of the polar molecule wandering about "kicking" the hydrocarbon molecules; the larger hydrocarbon gets "kicked" more frequently than the smaller one and thus the larger hydrocarbon has the higher activity coefficient.

**Chemical Effects.**—The analysis of solvent selectivity given so far has considered only physical

effects; however, chemical effects also play a role in determining solution properties. Hildebrand's classic studies on iodine solubility show that complex formation is a common occurrence in solutions and therefore it is reasonable to suspect that complex formation plays an important role in determining solvent selectivity. The Lewis concept of acids and bases suggests that unsaturated hydrocarbons with pi electrons could serve as electron donors (bases) while typical polar solvents can act as electron acceptors (acids). If a hydrocarbon can form a complex its volatility is, of course, reduced and thus if a polar solvent forms a complex with one hydrocarbon and not with another a clear basis of selectivity is established.

There is considerable evidence to show that polar solvents do, in fact, complex with unsaturated hydrocarbons. Figure 4 shows some heat of mixing data for various  $C_6$  hydrocarbons with nitroethane.<sup>3</sup> Complex formation makes an exothermic (negative) contribution to the heat of mixing and Fig. 4 shows that as the unsaturation of the hydrocarbon increases the heat of mixing falls. Similarly, complex formation makes a negative contribution to the volume change on mixing and as shown by the data in Fig. 5 the volume change on mixing nitroethane with a saturated hydrocarbon is positive whereas that with unsaturated hydrocarbons is negative.<sup>3</sup> Finally, the presence of a complex frequently can be seen in the ultraviolet spectrum and Fig. 6 shows some spectral data for nitroethane-toluene which have been reduced according to the method of Benesi and Hildebrand.<sup>4</sup> From these data it has been possible to calculate an equilibrium constant for the nitroethane-toluene complex. Similar data for other unsaturated hydrocarbons<sup>5</sup> indicate that, as expected, complex stability rises as the ionization potential of the hydrocarbon falls.

It is evident, then, that chemical as well as physical effects play a role in determining solvent selectivity. In order to correlate solvent selectivity data a useful correlating equation has the form

$$\ln S_{12} = \frac{\delta_3^2 P^2 (\Psi_1 - \Psi_2)}{RT} + \Phi(K_{13}, K_{23}) \quad (17)$$

where  $\Psi$  is a collision volume which replaces the molar volume as given by eq. 14. The molar volume of a hydrocarbon is only a very crude measure of its molecular size as "seen" by the polar species and it is desirable to replace it by another term which more truly reflects the cross-section for interaction which the hydrocarbon possesses. The collision volume is defined by

$$\Psi = [V_w^{1/2} + V_f^{1/2}]^3 - k\beta P_1 V \quad (18)$$

where  $V_w$  is the van der Waals volume,  $V_f$  is the free volume,  $k$  is Meares' constant,  $\beta$  is the compressibility, and  $P_1$  is the internal pressure. This definition is quite arbitrary and is justified primarily by its utility.

The function  $\Phi$  is not specified but it depends on the equilibrium constants of the two hydrocarbons

(3) R. Anderson, R. Cambio, and J. M. Prausnitz, *A.I.Ch.E. Journal*, in press.

(4) H. Benesi and J. H. Hildebrand, *J. Am. Chem. Soc.*, **71**, 2703 (1949).

(5) R. Anderson, Dissertation, University of California, Berkeley, 1961.

for complex formation with the polar solvent. The function  $\Phi$  has the properties

If $K_{13} = 0$ and $K_{23} = 0$	then $\Phi = 0$
If $K_{13} = K_{23}$	then $\Phi = 0$
If $K_{23} > K_{13}$	then $\Phi > 0$
If $K_{23} < K_{13}$	then $\Phi < 0$

Figure 7 shows how eq. 17 may be used to correlate typical solvent selectivity data (5). The continuous line is a plot of eq. 17 with  $\Phi = 0$ ; that is, the continuous line gives the selectivity in those cases where there are no chemical effects. This calculated line correctly predicts the experimental selectivities for several systems containing only saturated hydrocarbons as indicated by the filled-in black points.

The dotted lines show the effect of complexing on selectivity. In the cases shown  $K_{23} > 0$  whereas  $K_{13} = 0$ ; that is, in all these cases the chemical and physical effects act in unison to raise the relative volatility of component 1 and therefore the experimental points lie above the calculated base

line for physical effects. Although such cases are not shown in Fig. 7 it is quite possible to have the chemical and physical effects act in opposite directions.

Analysis of the role of intermolecular forces in extractive separations cannot as yet eliminate the need for experimental data. However, such analysis can help in a preliminary screening of promising solvents and can contribute to minimizing experimental effort by providing a guide for the interpretation and correlation of phase equilibrium data.

**Conclusion.**—The examples given here illustrate the utility of solubility thermodynamics in typical chemical engineering problems. The semi-empirical treatment of solution properties as pioneered by Joel Hildebrand provides the necessary concepts for perceptive interpretation and subsequent useful correlation of solubility data as required in a variety of chemical engineering operations.

**Acknowledgment.**—The author is grateful to the donors of the Petroleum Research Fund for financial support.

## CELL POTENTIALS AND GAS SOLUBILITY THEORY<sup>1</sup>

BY Y. KOBATAKE AND B. J. ALDER

*University of California, Lawrence Radiation Laboratory, Livermore, California and University of California, Department of Chemistry, Berkeley, California*

*Received December 2, 1961*

A two-parameter cell potential in a free volume type theory is determined from two experimentally obtained thermodynamic quantities. For pure liquids further thermodynamic quantities are predicted quite accurately over a region of temperature by the Lennard-Jones-Devonshire form of the cell potential, although its harmonic oscillator modification gives better results. For a gas dissolved in a liquid, the cell potential yields values of the free volume of the gas molecule that are about 10 times larger than in a typical liquid. Moreover, it can be concluded that the gas molecule is surrounded by about 7 neighbors and that the solvent molecules surrounding the gas contribute importantly to the thermodynamic functions. The gas molecules perturb the solvent significantly over several molecular layers, while in dilute liquid mixtures the effect of the solute on the solvent is mainly confined to one molecular layer.

### Introduction

Recent developments in the theory of liquids have emphasized the inadequacy of a lattice model even when that theory is optimized.<sup>2</sup> The source of failure can be stated in terms of a significant contribution from the communal entropy term, that is, from higher order correlations which were not evaluated. However, it must be emphasized that the exact, single-occupancy problem has not yet been solved since the solutions so far involved spherical smoothing. There is reason to believe from machine computations on hard sphere systems<sup>3</sup> that the exact single occupancy solution differs significantly from the one obtained by spherical smoothing. In any case, these machine computations have shown that the communal entropy of the solid and the dense fluid do not differ very much.<sup>4</sup> If the contribution of higher order correlations were small in real dense liquids, the theory of liquids would be greatly simplified since attempts at estimating even a first correction for

the communal entropy involved such complex mathematics that this so far has been done only approximately with small quantitative improvement.<sup>5</sup> Since other theories of the liquid state are mathematically also very complex,<sup>6,7</sup> it is worthwhile to apply a one-particle theory to some real situations, still in the hope that it will be possible to estimate the contribution of various effects to the thermodynamic behavior.

In order to make the one-particle theory as realistic as possible some of the restrictions previously imposed on such theories have been removed. Basic to all existing cell theories is that the volume of the system is spanned by a virtual lattice and that the representative particle moves in the field of the other particles confined to the lattice cells. This imposes an arbitrary order on the particles which depends upon the lattice structure chosen and is particularly poor for a solution, when a lattice of equal sized cells for largely different size molecules is assumed, since that arrangement hardly accounts for the complex packing. The

(1) This work was performed under the auspices of the U.S. Atomic Energy Commission.

(2) J. S. Dahler and J. O. Hirschfelder, *J. Chem. Phys.*, **32**, 330 (1960).

(3) B. J. Alder and T. E. Wainwright, *ibid.*, **33**, 1439 (1960).

(4) B. J. Alder and T. E. Wainwright, UCRL report 6600 T (1961).

(5) (a) J. DeBoer, *Physica*, **21**, 137 (1955); (b) J. Pople, *Phil. Mag.*, **42**, 459 (1951).

(6) J. S. Dahler and E. G. D. Cohen, *Physica*, **26**, 81 (1960).

(7) J. M. Richardson and S. R. Brinkley, *J. Chem. Phys.*, **33**, 1467 (1960).

present alternative is to let the representative particle be confined to a spherical cell, not part of a lattice, whose size and whose number of surrounding neighbors are determined by forcing agreement to two measured thermodynamic quantities. In other words, a two-parameter cell potential is determined through experiment and further thermodynamic properties then are evaluated. A further advantage to this procedure is that it is no longer necessary to assume that the pair potential parameters determined from low density viscosity or second virial coefficient data apply at high density conditions. In fact, how the energy and length parameter in the cell potential are related to those of the pair potential never has to be evaluated but a discussion of it will be instructive.

The cell parameters obtained by fitting two kinds of thermodynamic data are effective parameters in that they reflect the higher order correlations of the molecules as well as the non pair-wise additive aspects of the potential of interaction. If these last two effects are small, a pair potential then can be deduced applicable to the condensed state. An important reason that the procedure outlined in the last paragraph was adopted is that this pair potential for the complex molecules composing the solutions for which most accurate and extensive thermodynamic data are available is not well known.

One of the necessary (but not sufficient) criteria that higher order correlations and non pair-wise additivity corrections are small is agreement of the calculated thermodynamic quantities with experiments. However, this agreement depends also on the form of the cell potential assumed. Although several forms of the two-parameter cell potential were investigated, most frequently that of the Lennard-Jones-Devonshire<sup>8</sup> theory was used, namely the form that results from the Lennard-Jones potential. This is partly a matter of convenience since it then is possible to use integrals previously tabulated.

Since the principal application of the model in this work is to studies of gas solubility in liquids, several kinds of cells should be considered. In a mixture, not only does the cell of the solute differ from that of the solvent but possibly solvent cells differ depending on their location relative to the solute molecule. Thus, a dissolved gas molecule introduces into a liquid solvent a tiny region of "weakness," that is, a gas molecule with the same kinetic energy as the solvent but a much smaller force field depopulates its immediate surrounding. (This is the reverse of the effect exerted by the strong force field of an ion upon surrounding water molecules, where electrostriction enhances the solvent density.) How far this region of "weakness" extends into the solvent, and hence how many different solvent cells have to be considered in order to evaluate the magnitude of their contribution to the partial molal thermodynamic properties of the solution, will be revealed by the present analysis. In order that these regions of weakness shall not overlap, consideration here is limited to dilute solutions, where solute-solute interaction can be neglected.

(8) J. E. Lennard-Jones and A. F. Devonshire, *Proc. Roy. Soc. (London)*, **A163**, 53 (1937).

Since each different cell in a mixture requires two thermodynamic solution properties to determine the two cell parameters, it is desirable to reduce the number of thermodynamic quantities with which the theory is forced to agree. For pure systems, the cell length parameter could be determined from the volume per particle. This means that the volume per particle determines the radius of the "cavity" of a molecule and the neighbors are spherically smoothed at a distance which is the Lennard-Jones potential radius beyond that. Since at the radius determined from the Lennard-Jones pair potential the force is very repulsive, the cavity molecule is pretty well confined to the particle volume. The sensitivity of the results to this choice of neighbor distance will be discussed. In gas solutions, the length parameter of the gas cell is determined in the same way except that the measured partial molal volume is used in conjunction with the solvent radius determined from its pure liquid properties. It is necessary in any case to study the properties of the pure solvent since one must know the difference between the behavior of a solvent molecule in bulk and in the neighborhood of a solute for the treatment of mixtures.

The cell picture of a liquid implies that a molecule remains surrounded by its neighbors for a period long compared to the traversal time of the cell. Escape out of the cell takes place infrequently by a series of small steps as in Brownian motion after which the molecule is again in a cell of the same average number of nearest neighbors but in a new position. From the time scale obtained from such transport data as the diffusion coefficient in dense fluids the above picture appears reasonable. The sufficiently long life time of a molecule in a cell in the liquid phase would make it possible to neglect the motion of the cell in its contribution to the thermodynamic behavior. However, this effect is only part of the communal entropy problem, since only a very special high order correlation of the molecules leads to interchange of particle position.

**Pure Liquids.**—The cell partition function leads to the following equations for the free energy, entropy, and pressure of a pure system<sup>9</sup>

$$\frac{A}{NkT} = \frac{3}{2} \ln \lambda - \ln v^f + \frac{W(0)}{2NkT} \quad (1)$$

$$\frac{S}{Nk} = -\frac{3}{2} \ln \lambda + \frac{3}{2} + \ln v^f + \left( \frac{\partial \ln v^f}{\partial \ln T} \right)_v \quad (2)$$

$$\frac{pv}{NkT} = \left( \frac{\partial \ln v^f}{\partial \ln v} \right)_T - \frac{1}{2NkT} \left( \frac{\partial W(0)}{\partial \ln v} \right)_T \quad (3)$$

where  $\lambda = h^2/2\pi mkT$  and  $v^f$  is the free volume

$$v^f = \int_{\text{cell}} \exp - [W(r) - W(0)]/NkT \, d\tau \quad (4)$$

$W(r)$  is the cell potential and  $W(0)$  is the potential at the center of the cell. The communal entropy has been assumed to be that of a solid. The other symbols have their usual meaning.

The vapor pressure is determined from the equilibrium condition that the free energy of the gas and liquid phase are the same. Assuming the gas to

(9) R. J. Buehler, R. H. Wentorf, J. O. Hirschfelder, and C. F. Curtiss, *J. Chem. Phys.*, **19**, 61 (1951).



be ideal and neglecting  $pv/NkT$  for the liquid, the vapor pressure,  $p_v$ , is given by

$$\ln \frac{p_v}{NkT} = -\ln v^l + \frac{W(0)}{2NkT} \quad (5)$$

The entropy of vaporization,  $\Delta S^v$ , in this case is identical with the excess entropy of the liquid over that of the ideal gas, namely

$$\frac{\Delta S^v}{Nk} = \left( \frac{\partial \ln v^l}{\partial \ln T} \right)_v + \frac{W(0)}{2NkT} - 1 \quad (6)$$

where the expression for the vapor pressure has been utilized. It is easily seen that the thermodynamic requirement of

$$\left( \frac{\partial \ln p_v}{\partial \ln T} \right)_v = \frac{-\Delta S^v}{Nk} \quad (7)$$

is satisfied.

The thermodynamic description of the system would be complete if  $W(r)$  were a known function of volume and temperature and its functional dependence on  $r$ , the distance from the center of the cell, were known. In previous applications  $W(r)$  was determined from a model and a known pair potential of interaction as, for example, in the Lennard-Jones-Devonshire theory.<sup>8</sup> It is the present intention to find  $W(r)$  so that agreement is obtained with some thermodynamic data and then to evaluate how well the  $W(r)$  so determined serves to predict other properties.

At least two parameters are needed for the description of the cell potential, one is a characteristic length and the other a characteristic energy. Restriction to a two-parameter cell potential clearly leads to a theory which is not better than the theory of corresponding states if the functional form of  $W(r)$  is maintained. Another consideration, which arises whenever parameters are determined in an average or effective potential, such as  $W(r)$ , is whether these parameters (since they are functions of volume and temperature) should be considered differentiable. For example, the energy parameter in  $W(r)$ , as in the pair potential, is a multiplicative factor in almost all models for the cell potential and it involves  $z\epsilon$ .  $z$  is the number of nearest neighbors and  $\epsilon$  is the well depth of the pair potential. The number of nearest neighbors is no longer considered as always 12 but varies with volume and temperature, however, arbitrarily, this is not taken into account in differentiating with respect to these variables.

Thus, adopting the Lennard-Jones-Devonshire form of  $W(r)$ , the thermodynamic functions have the same expressions as used in that theory before except that the reduced temperature is replaced by an effective reduced temperature  $T_e^* = 12NkT/z\epsilon$ , and also the reduced volume is replaced by an effective reduced volume,  $v_e^*$  (see eq. 10 for definition). The exception to the above is that the entire expression for the equation of state,  $pv/NkT$ , is multiplied by  $(\partial \ln v_e^*/\partial \ln v)_T$ , since the effective cell volume may no longer be simply related to the total volume. However, it is not necessary to know what this relation is for liquids under small external pressures, since then one of the thermodynamic pieces of information that is utilized for determining the parameters in the cell potential is that  $pv/NkT$  is, to a good approximation, zero.

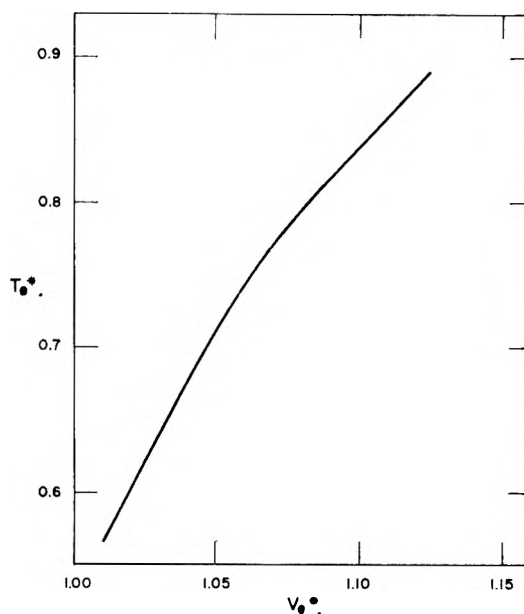


Fig. 1.—The relation between the effective reduced temperature and effective reduced volume obtained by setting  $pv/NkT = 0$  using the Lennard-Jones-Devonshire type of cell potential.

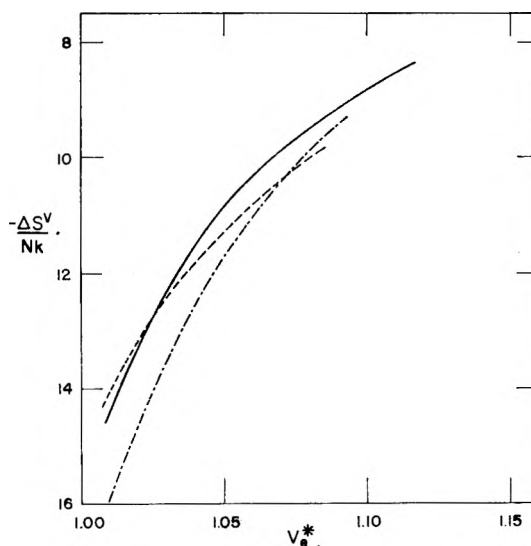


Fig. 2.—The entropy of vaporization plot vs. the effective reduced volume obtained by using the Lennard-Jones potential (—), the square well potential (---), and the harmonic oscillator potential (-·-·-).

Thus, by setting  $pv/NkT$  for the liquid equal to zero, a relation is obtained between the effective reduced temperature and effective reduced volume. This relationship for the Lennard-Jones-Devonshire form of  $W(r)$  is plotted in Fig. 1, where integrals previously tabulated<sup>9</sup> have been utilized. This relationship can be introduced into the equations for the other thermodynamic quantities, since all thermodynamic properties are expressed in terms of  $v_e^*$  and  $T_e^*$ . This is how the plot demonstrated in Fig. 2 is obtained, where the effective temperature parameter has been eliminated in order to obtain a relationship between the entropy of vaporization and the effective reduced volume.

An experimental value of the entropy of vaporiza-

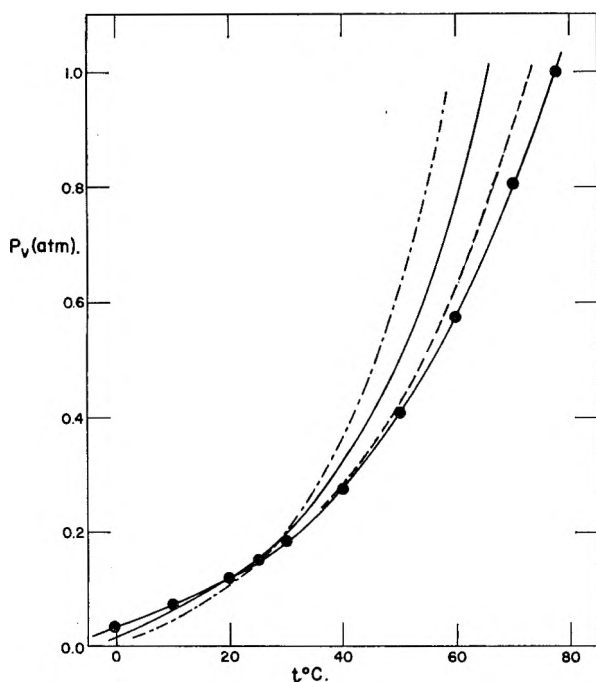


Fig. 3.—The calculated vapor pressure as a function of temperature using the Lennard-Jones potential (—), the square well potential (— · —), and the harmonic oscillator potential (---), compared to experiment (circles).

tion then allows the effective volume to be determined and this in turn determines the effective temperature, and hence all the other thermodynamic properties can be evaluated from a knowledge of these two parameters. Figure 2 shows also how the same procedure when used with a different functional form of  $W(r)$  leads to a different dependence of the entropy of vaporization on the effective volume.

There is one further minor consideration to take into account in the above calculations, namely, how to evaluate the contribution of more distant neighbors to  $W(r)$  when these neighbors are not part of a lattice structure. Although their contribution is relatively small in any case and, as shall be shown later, assuming them to contribute as if they were in a lattice structure does not significantly affect the results, a slightly better approximation than the lattice approximation was attempted for  $W(0)$ . The more remote neighbors were assumed to be distributed at the uniform density of the fluid starting at a distance from the central molecule such that, when the nearest neighbor distance,  $a$ , corresponded to that of a face-centered lattice,  $a_0$ , the same results were obtained as for the lattice. This distance from which to integrate the potential with a constant radial distribution function in order to obtain the further neighbor contribution to  $W(0)$  was taken as  $a + 0.341a_0$ .

Additional assumptions made concerning the contribution of further neighbors are that the number of further neighbors changes in the same proportion as the nearest neighbors deviate from the 12 particles of a close packed structure, and, that in ratios of integrals involving  $W(r)$ , the lattice approximation is satisfactory. The effect of these approximations are minor and they have been introduced only to employ the integrals already

tabulated for the Lennard-Jones-Devonshire theory.

The limited objective of this work then is to predict from two thermodynamic properties additional properties through the intermediate of the cell potential and also to gain some information about the cell potential itself. This procedure is similar in principle to the treatment of second virial data for information regarding pair potentials. For  $\text{CCl}_4$  at  $25^\circ$  the prediction of the vapor pressure from the entropy and the equation of state is very satisfactory. The calculation predicts 0.150 atm., while the experimental value is 0.155 atm. Had the procedure been reversed and the equation of state and vapor pressure been used to predict the effective parameters, the entropy comparison would have been  $\Delta S^\circ/Nk = -13.19$  calculated *vs.*  $-13.23$  experimental. When the further neighbor contribution in  $W(0)$  is calculated from the lattice model, the calculated  $\Delta S^\circ/Nk$  changes only slightly ( $-13.08$ ). Similar agreement has been found and can be expected for all liquids which are in corresponding states with  $\text{CCl}_4$  such as benzene and carbon disulfide. For argon, however, where one might have expected the Lennard-Jones potential to work best, the agreement is considerably worse. Of course, the lack of corresponding states between Ar and  $\text{CCl}_4$  already indicates that agreement cannot be expected for the same form of  $W(r)$  in both cases. It has been pointed out before<sup>10</sup> that the Lennard-Jones potential in the important region near the minimum does not adequately represent the properties of argon in the condensed state. The cell parameters for argon obtained from the equation of state and the vapor pressure give an entropy of  $\Delta S^\circ/Nk$  of  $-11.4$  at the melting point and  $-10.9$  at the boiling point, while the corresponding experimental values are  $-9.32$  and  $-8.93$ , respectively.

The fact that the Lennard-Jones form of  $W(r)$  yields the properties of  $\text{CCl}_4$  at  $25^\circ$  rather well is somewhat fortuitous. The identical procedure at other temperatures does not yield equally satisfactory agreement. This is illustrated in Fig. 3, where the two parameters were determined from equation of state and entropy data. The result means that the volume dependence of  $W(r)$  as given by the Lennard-Jones theory is not completely satisfactory. Having fitted the entropy of vaporization over a region of temperature in the above process to experimental data, it is, of course, evident that the theory also will yield the experimental value of the difference in the heat capacity of the gas and liquid states.

Although the major objective of this paper was not to find a form of  $W(r)$  which reproduces the pure liquid properties, a few attempts in that direction were made. It would be interesting to obtain as precise information as possible about  $W(r)$  by introducing not only the two parameters already described, which yield the volume and temperature dependence of  $W(r)$ , but further constants which describe the functional dependence of  $W$  or  $r$ . As many constants could be introduced as there are

(10) E. A. Guggenheim and M. L. McGlashan, *Proc. Roy. Soc. (London)*, **A255**, 466 (1960).

independent thermodynamic functions available. Since the data for gas solubility are mostly limited to 25° in those liquids for which the Lennard-Jones form of  $W(r)$  proved satisfactory, there is no present need to proceed further in the study of  $W(r)$  in order to understand the properties of the gas-liquid mixtures.

The two extreme, two-constant forms of  $W(r)$  to investigate are the square-well and harmonic oscillator forms. The square-well form of  $W(r)$

$$W(r) = W(0) \text{ for } r < \tau_0 \\ = \infty \text{ for } r > \tau_0$$

leads to a

$$v^f = \frac{4\pi}{3} \tau_0^3$$

where  $\tau_0$  is the distance parameter at which the potential becomes infinite. Since the free volume is not an explicit function of temperature,  $\Delta S^\gamma/Nk$  immediately determines  $W(0)$ , as can be seen from eq. 6. The vapor pressure, eq. 5, subsequently determines  $\tau_0$ . The volume dependence and hence derivatives of  $W(0)$  and  $\tau_0$  then can be found by carrying out this same process under the various conditions where experiments are available and then the equation of state can be checked by means of eq. 3. The agreement with experiments is poor showing that the square-well form of  $W(r)$  is not satisfactory.

On the other hand, the harmonic oscillator form of  $W(r)$  proved satisfactory.

$$W(r) = W(0) + \omega r^2$$

where  $\omega$  is the force constant. In that case  $v^f = (\pi kT/\omega)^{3/2}$  and

$$\left( \frac{\partial \ln v^f}{\partial \ln T} \right)_v = 1.5$$

Since the temperature derivative of the free volume is a constant, the same conditions prevail as in the square-well case, namely the entropy and vapor pressure determine  $W(0)$  and  $\omega$  over a region of volume.

The volume dependence of  $W(0)$  experimentally determined through the harmonic oscillator model agrees well with that obtained from the Lennard-Jones model for  $\text{CCl}_4$ , while for Ar the agreement is not too good. Using the criteria that the harmonic oscillator model for Ar gives fairly good results, the Lennard-Jones model does not seem accurate for Ar in the liquid state. The volume dependence of  $\omega$  over the limited region investigated agrees well with the form of the harmonic oscillator expansion of the Lennard-Jones model, namely

$$\omega = z\epsilon \left( \frac{20}{v_3^{*4}} - \frac{7}{v_6^{*2}} \right)$$

where, however, the numerical coefficients have been empirically adjusted. These forms of  $W$  and  $\omega$ , when substituted in the equation of state, give good agreement with experiment for  $\text{CCl}_4$ . In Fig. 4 the three different forms of  $W(r)$  are compared at two different densities. The harmonic oscillator model gives a satisfactory description of the thermodynamics in the region of normal liquid density and temperature. For argon, the harmonic oscillator model does not serve as well, but is better than the Lennard-Jones form.

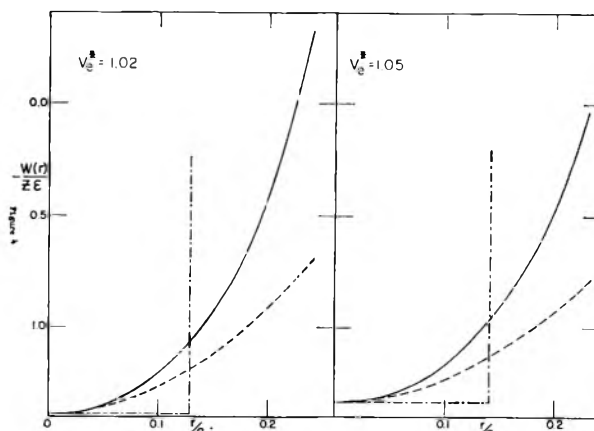


Fig. 4.—A plot of the effective cell potential for  $\text{CCl}_4$  as a function of the distance from the center of the cell at two different volumes for the Lennard-Jones potential (—), the square well potential (---), and the harmonic oscillator potential (-·-·).

In Fig. 2 and 3 a comparison is made between the various forms of  $W(r)$ , using comparable methods of calculation.  $W(0)$  was assumed in all cases to have the form of the Lennard-Jones model and  $\omega$  also to have the above form of the harmonic oscillator approximation to that model. The equation of state and entropy then were used to determine the parameters. Figure 2 then shows the dependence of  $\Delta S^\gamma/Nk$  on the effective volume. The calculated vapor pressure that results from the square-well model is shown in Fig. 3 and, as pointed out before, is in worse agreement with experiments on  $\text{CCl}_4$  than the Lennard-Jones potential, while the harmonic oscillator model gives better agreement.

The effective parameters experimentally evaluated now can be used to learn something about the arrangement of particles in the liquid provided the higher order correlations are not so important as to make use of the cell theory meaningless. The experimental agreement which was obtained is no evidence that these higher order correlations are small, since agreement with experiment always could be obtained by using enough parameters. The reasonableness of the parameters is, however, some indication that higher order correlations and the effects of non pair-wise additivity in the potential are not so serious that the cell theory description is not a valid first approximation. By reasonableness of the parameters is meant that they are within the uncertainties by which the pair potential and the number of nearest neighbors are known. The effective temperature can be used to calculate the number of nearest neighbors provided the energy parameter of the pair potential is assumed. Similarly, the effective volume can be used to verify a model for the geometric distribution of the particles around the cell, if the value of the distance parameter in the pair potential,  $\sigma$ , is assumed.

The model of the cavity mentioned in the introduction leads to a nearest neighbor distance of

$$a = R + \frac{\sigma}{2} \quad (8)$$

where  $R$  is determined from

$$v = \frac{4\pi}{3} NR^3 \quad (9)$$

and hence an effective reduced volume of

$$v_a^* = \frac{a^3}{\sigma^3 \sqrt{2}} \quad (10)$$

The introduction of the  $\sqrt{2}$  is not a consequence of any close-packing assumption, but merely a normalization to allow comparison with previously tabulated integrals. From the experimentally determined effective volume and known molar volume, a value of  $\sigma$  of 5.354 Å. for  $\text{CCl}_4$  at 25° is determined when the effective volume is evaluated from the pressure and the entropy, while a value of 5.350 Å. is obtained when the pressure and vapor pressure are used. The close agreement is merely a measure of the previously noted accuracy of the model for this system. For other liquids also the values of  $\sigma$  obtained in these two alternative ways are compared with previously postulated values.<sup>11,12</sup> In all cases the values found are within the uncertainties of  $\sigma$  obtained from other data. The case of argon shows the extraordinary sensitivity of the results to the value chosen for  $\sigma$ . Although it previously was shown that the agreement with experiment was very poor, only a 2% difference in the value of  $\sigma$  is found for the two different methods of calculation. This fact throws doubt upon any experimental evaluation of a liquid theory unless the potential is much more accurately known than is presently possible. Some credence in the model of the cell postulated is lent by the fact that the value of  $\sigma$  obtained from the pressure and entropy for  $\text{CCl}_4$  over the entire liquid region stayed constant within the four significant numbers carried.

From the effective temperature,  $\epsilon/k$  was calculated on the basis of the assumption of 12 nearest neighbors, and the results also are shown in Table I. It was felt that values of  $\epsilon/k$  are not well enough known for the systems here investigated to justify calculating the number of nearest neighbors, and hence by arbitrarily assuming 12 neighbors, a lower limit to  $\epsilon/k$  could be obtained which might not be too far from the correct value. The energy parameters are again within an acceptable range of values. If the effective temperature from the model in which the further neighbors are in a face-centered lattice is used to determine  $\epsilon/k$ , a value of 497 results instead of 490. This again shows the insensitivity of the results to the assumptions about neighbors.

**Gas Solubility.**—The system of a gas dissolved in a liquid represents one of the easiest mixtures to study from the theoretical point of view. However, only recently have these mixtures been investigated experimentally in great detail. This careful and extensive effort was largely carried out by Professor Hildebrand and his co-workers.<sup>13</sup>

(11) J. O. Hirschfelder, C. F. Curtiss, and R. B. Bird, "Molecular Theory of Gases and Liquids," John Wiley and Sons, New York, N. Y., 1954, p. 1110.

(12) Z. Salsburg and J. G. Kirkwood, *J. Chem. Phys.*, **21**, 2169 (1953).

(13) L. W. Reeves and J. H. Hildebrand, *J. Am. Chem. Soc.*, **79**, 1313 (1957); J. E. Jolley and J. H. Hildebrand, *ibid.*, **80**, 1050 (1958); Y. Kobatake and J. H. Hildebrand, *J. Phys. Chem.*, **65**, 331 (1961); H. L. Clever, *ibid.*, **62**, 375 (1958); J. C. Gjaldbaek and J. H. Hildebrand, *J. Am. Chem. Soc.*, **71**, 3147 (1949).

TABLE I

COMPARISON OF PAIR POTENTIAL PARAMETERS FROM CELL POTENTIAL WITH OTHER SOURCES

Substance	$\sigma^a$	$\sigma^b$	$\sigma^c$	$\sigma^d$	$\epsilon/k^a$	$\epsilon/k^b$	$\epsilon/k^c$	$\epsilon/k^d$
Ar <sup>e</sup>	3.50	3.42	3.43		122	126	120	
C <sub>2</sub> H <sub>6</sub> <sup>e</sup>		4.29	4.19			233	237	
Br <sub>2</sub>	4.33	4.31	4.27		490	466	520	
CS <sub>2</sub>	4.55	4.53	4.44	4.58	466	452	488	414
C <sub>6</sub> H <sub>6</sub>	5.22	5.22	5.27	5.26	501	504	440	494
CCl <sub>4</sub>	5.35	5.35	5.88	5.41	490	493	327	486
i-C <sub>8</sub> H <sub>18</sub>	6.42	6.44			504	519		
C <sub>7</sub> F <sub>16</sub>	7.07	7.11			473	505		

<sup>a</sup> The parameters are obtained from the effective cell potential under the assumption of 12 nearest neighbors from the equation of state and the vapor pressure. <sup>b</sup> Same as *a* except the equation of state and the entropy were used to determine the parameters. <sup>c</sup> The parameters are obtained from low density viscosity data or second virial coefficients.<sup>11</sup> <sup>d</sup> The parameters are obtained from a cell theory of Salsburg and Kirkwood.<sup>12</sup> <sup>e</sup> For all other gases the parameters also were close to the ones obtained from viscosity data.

These data are relatively easy to interpret because even at saturation under normal pressure conditions the system is dilute. Furthermore, since the gas molecule has a smaller attractive force than the liquid solvent and yet has the same kinetic energy, the dissolved gas molecule has a much larger free volume than a solute molecule in a liquid mixture. Such large free volumes make the calculations less sensitive to the assumptions of the geometric arrangements of the neighboring particles and less dependent on the uncertainties in the knowledge of the intermolecular cell potentials. The study of the behavior of a variety of gases in solution also offers the advantage of being able to assess theoretically the effects of a great range in intermolecular attraction. Finally, the interaction of the gas molecule with the solvent does not involve the arbitrary factor of 2 in  $W/2NkT$  as it does for pure systems (see eq. 1), since for the distinct gas particle no ambiguities arise about counting interactions twice.

An additional modification that must be made in the gas cell partition function,  $q$ , is that the degeneracy factor has to be taken into account. This arises because there are a large number of gas cells which can occur with equal probability, namely all those states where the gas molecule is located anywhere within the total volume of the system. Thus

$$q = \lambda^{-3/2} v_{gL} \frac{v_T}{\bar{v}_g} \exp\left[-\frac{W_{gL}(0)}{NkT}\right] \quad (11)$$

where the subscript  $gL$  refers to the gas molecule in the liquid,  $v_T$  is the total volume containing one mole of solute, and  $\bar{v}_g$  is the partial molal volume of the solute.  $\bar{v}_g/v_T$  is the volume fraction of solute,  $\varphi_g$ , which can be written to a good approximation in dilute solutions as

$$\varphi_g = \frac{x_g \bar{v}_g}{v_L} \quad (12)$$

where  $x_g$  is the mole fraction of solute and  $v_L$  is the molar volume of the solvent which is nearly identical to the partial molal volume of the solvent.

The gas cell contributions to the thermodynamic properties then become, analogous to eq. 1 to 3

$$\frac{A_{gL}}{NkT} = \frac{3}{2} \ln \lambda - \ln v_{gL}^f + \frac{W_{gL}(0)}{NkT} + \ln \varphi_g \quad (13)$$

$$\frac{S_{gL}}{Nk} = \frac{3}{2} \ln \lambda + \frac{3}{2} + \ln v_{gL}^f + \left( \frac{\partial \ln v_{gL}^f}{\partial \ln T} \right)_v - \ln \varphi_g \quad (14)$$

$$\left( \frac{pv}{NkT} \right)_{gL} = \left( \frac{\partial \ln v_{gL}^f}{\partial \ln v} \right)_T - \frac{1}{NkT} \left( \frac{\partial W_{gL}(0)}{\partial \ln v} \right)_T \quad (15)$$

The partial molal thermodynamic properties of the solute involve the properties not only of the gas cell but also of the solvent molecules surrounding the solute. Formally this arises because partial molal quantities imply differentiation of the thermodynamic functions with respect to the number of gas molecules. The number of solvent molecules influenced by the introduction of solute molecules is proportional in dilute solution to this number of gas molecules. Thus, the mixing process of the two pure substances involves the difference in properties of all the solvent molecules influenced by the solute and their properties in the pure or bulk state. The additional free energy in the mixing process due to the  $z_{ig}$  solvent molecules in the first neighboring shell surrounding a gas molecule within the cell approximation is hence, from eq. 1

$$\frac{A_s}{NkT} = z_{ig} \left[ \frac{W_{ig}(0)}{2NkT} - \frac{W(0)}{2NkT} - \ln \frac{v_{ig}^f}{v^f} \right] \quad (16)$$

Although the properties of each solvent molecule are changed only slightly from those in bulk, the fact that  $z_{ig}$  solvent molecules are affected results in a big contribution to the free energy. Further-than-nearest neighbors have their properties changed even to a smaller degree, however, because of their presence in large number their contribution to the partial molal thermodynamic properties cannot always be neglected. Thus, in general, the solvent contribution must be written as

$$\frac{A_s}{NkT} = \sum_{i=1}^{\infty} z_{ig} \left[ \frac{W_{ig}(0)}{2NkT} - \frac{W(0)}{2NkT} - \ln \frac{v_{ig}^f}{v^f} \right] \quad (17)$$

where the subscript  $i$  indicates the  $i$ th shell around a gas molecule.

The solubility now is determined as the vapor pressure was previously, by equating the chemical potential of the gas in solution with that in the gas phase, assuming the gas to be ideal. Hence

$$\ln \varphi_g = \ln \frac{p}{NkT} + \ln v_{gL}^f - \frac{W_{gL}(0)}{NkT} - \frac{A_s}{NkT} \quad (18)$$

where  $p$  is the pressure in the gas phase. The partial molal entropy of solution now can be calculated also, analogous to eq. 6, as

$$\frac{S_g}{Nk} = \left( \frac{\partial \ln v_{gL}^f}{\partial \ln T} \right)_v + \frac{W_{gL}(0)}{NkT} - 1 + \frac{S_s}{Nk} \quad (19)$$

where

$$\frac{S_s}{Nk} = \sum_{i=1}^{\infty} z_{ig} \left\{ \left[ \left( \frac{\partial \ln v_{ig}^f}{\partial \ln T} \right)_v + \frac{W_{ig}(0)}{2NkT} - 1 \right] - \left[ \left( \frac{\partial \ln v^f}{\partial \ln T} \right)_v - \frac{W(0)}{2NkT} - 1 \right] \right\}$$

and where the expression for  $\varphi_g$  has been substituted in the equation for entropy.

The equation analogous to eq. 7 is

$$\left( \frac{\partial \ln x_g}{\partial \ln T} \right)_v = - \frac{S_g}{Nk} \quad (20)$$

This thermodynamic requirement is satisfied by eq. 18 and 19 and is, in fact, experimentally used to determine the partial molal entropy of solution.

The procedure of calculation now is similar to that for the pure liquid case except that at least two different cells have to be considered and their effective parameters determined. For all the different cells under small external pressure the virial theory can be used to show that  $pv/NkT$  is very small. This is because the pressure is common to all these cells and the volumes accessible to a gas molecule in a cell, or to a solvent molecule in contact with the gas molecule, or to a solvent molecule in the vicinity of the gas molecule but only in contact with other solvents, all are comparable and close to liquid volumes, so that  $pv/NkT$  can be approximated as zero. Hence for each cell the equation of state gives a relation between the effective volume and temperature. For these cells too the contribution of further neighbors to  $W(0)$  was estimated similarly to the pure case except that the appropriate potential of interaction for mixtures has to be introduced when integrating with the constant radial distribution function.

For the gas cell, the measured partial molal volume was used to determine the length scale of the cavity, because the model worked out well for pure liquids. The partial molal volume was used to determine  $R$  in eq. 9 and the nearest neighbor distance in eq. 8 was obtained by adding on  $\sigma_L/2$ , where  $\sigma_L$  is the distance scale in the pair potential of the solvent molecule, as calculated from the pure liquid properties and given in Table I. The equation of state and the partial molal volume thus fix the gas cell potential. Although the partial molal volume reflects not only the solute's freedom of motion but also that of the surrounding solvent molecules, the above assignment of the partial molal volume entirely to the solute is not too serious since the results, as will be shown, are not sensitive to this arbitrary division.

As an illustration of the calculation, using the Lennard-Jones-Devonshire form of the cell potential, the Ar- $\text{CCl}_4$  system will be considered under a total pressure of one atmosphere. The partial molal volume of Ar in  $\text{CCl}_4$  of 43.6 cc. at 25° yields a value of  $R$  of 2.58 Å. from eq. 9 and a  $v_e^* = 1.221$  from eq. 10. The further-neighbor contributions to  $W(0)$  were evaluated as 0.0052 for the repulsive part of the potential and 0.1161 for the attractive part compared to 1 for the nearest neighbors. The equation of state then gave a  $T_e^* = 2.09$ . These values lead to a free volume of 1.922 cc. for the gas molecule in the liquid and this is about ten times larger than the free volume of a molecule in a pure liquid. Tables II and III show that the same magnitude of free volume also is found for other systems. The solubility and entropy relation now becomes

$$\ln x_g = -2.651 - \frac{A_s}{NkT}$$

$$\frac{S_g}{Nk} = -6.105 + \frac{S_s}{Nk}$$

Since the experimental values for  $\ln x_g$  and  $S_g/Nk$  are, respectively,  $-6.613$  and  $-0.25$ , it can be seen

that the contribution of the solvent is comparable to that of the solute.

The large free volume indicates that, as expected, the gas molecule almost digs a "hole" in the liquid. This suggestion has been made before<sup>14</sup> in theories of gas solubility and the solvent free energy contribution ought to be of the order of the surface energy necessary to create a cavity of the dimensions of the partial molal volume in the liquid. Hence equating  $A_s$  to  $4\pi R^2\sigma_0$  ought to give a reasonable interfacial tension,  $\sigma_0$ . Table IV shows that indeed this is the case for various gases in  $\text{CCl}_4$ . This apparent interfacial tension has a value somewhat less than the surface tension of  $\text{CCl}_4$  of 25.0 dynes/cm.<sup>2</sup>. This is to be expected since in the first place there is a correction due to the small size of the cavity and in the second place the interfacial tension is against a gas in a state equivalent to a fairly high density rather than against a gas of low density in the case of the surface tension.

TABLE II

THE NUMBER OF NEAREST  $\text{CCl}_4$  MOLECULES TO VARIOUS GAS MOLECULES AND THE FREE VOLUME OF THE GASES

Gas	$v^f$ (cc.)	$z$
$\text{CH}_4$	1.583	6.73
$\text{N}_2$	2.276	7.48
Ar	1.922	7.05
$\text{O}_2$	1.495	7.72
$\text{C}_2\text{H}_6$	1.582	5.16

TABLE III

THE NUMBER OF NEAREST SOLVENT MOLECULES TO AN AR MOLECULE AND THE AR FREE VOLUME

Solvent	$v^f$ (cc.)	$z$
$\text{CS}_2$	2.760	5.77
$\text{C}_6\text{H}_6$	2.407	6.29
$\text{CCl}_4$	1.922	7.05
<i>i</i> - $\text{C}_8\text{H}_{18}$	2.822	7.21
<i>n</i> - $\text{C}_7\text{F}_{16}$	3.258	7.78

TABLE IV

APPARENT INTERFACIAL TENSION,  $\sigma_0$ , OF VARIOUS GASES IN  $\text{CCl}_4$

Gas	$\sigma_0$ (dynes/cm. <sup>2</sup> )
$\text{CH}_4$	15.7
$\text{N}_2$	19.1
Ar	19.4
$\text{O}_2$	21.8

Another frequently used macroscopic argument is that the entropy contribution of the solvent can be calculated as if the solvent were expanded uniformly by the partial molal volume. This seems to work out very well for the Ar- $\text{CCl}_4$  system. Using the experimental value for the change of pressure with temperature at constant volume for pure  $\text{CCl}_4$  in the thermodynamic identity

$$\left(\frac{\partial S}{\partial v}\right)_T = \left(\frac{\partial p}{\partial T}\right)_v$$

yields a value of the solvent entropy contribution of 5.898 when the experimental value of the partial molal volume of Ar also is substituted. This solvent contribution makes the partial molal entropy

of solution  $-0.21$ ; close to the experimental value of  $-0.25$ .

To calculate the solvent contribution from the cell point of view, it is necessary to know  $z_{1g}$ . It hence is necessary to segregate the factors in the product of  $z_{1g}\epsilon_{1g}$  in  $T_0^*$  by estimating  $\epsilon_{1g}$  from the usual geometric mean rule of the pure  $\epsilon$ 's given in Table I. The cell parameters for a solvent molecule in contact with the solute are determined for an equivalent spherical cell although that solvent molecule is in an unsymmetrical force field since it is surrounded on all sides by solvent molecules except for one solute molecule. To determine the cell parameters, besides the pressure, an additional thermodynamic property has to be used. By insisting that the values of the parameters satisfy the experimentally determined solubility, it remains to check whether these parameters serve to predict correctly the partial molal entropy of solution.

In the example considered above, it was found from the effective temperature and the geometric mean rule that 7.05  $\text{CCl}_4$  molecules surround an Ar molecule. Tables II and III show that for other systems also, roughly 7 neighbors are adjacent to a gas molecule. The fact that this number of nearest neighbors is considerably smaller than 12 is due to the geometric impossibility that many large solvent molecules can surround a small cavity, and that the smaller force field of the gas molecule tends to depopulate the surroundings of solvent just as near a free surface of a liquid the density of particles is less than in the interior.

Each of these approximately 7 solvent molecules has only slightly different properties from a  $\text{CCl}_4$  molecule in the pure liquid as Table V shows. The free volume of the contact solvent molecule is about 10% larger than that of the pure solvent and the cell energy is about 5% less deep. These parameter changes are quite reasonable; however, they lead to a value of  $S_g/Nk$  of  $-1.50$  as compared to the experimental value of  $-0.25$ . Furthermore, in all of the other systems, as Fig. 5 and 6 show, the entropy discrepancy is about the same, making one suspect that a term has been omitted from the calculation. The entropy discrepancy becomes slightly less as the force field of the solvent and solute approach each other. To make this trend more apparent, it will be shown that in dilute liquid-liquid systems, where the force constants of solute and solvent are more nearly equal, the entropy discrepancy practically disappears. This fact leads one to surmise that the term in the entropy concerned with further neighbors cannot be omitted whenever a solute of largely different force field is introduced since then the perturbation extends over several molecular distances.

**Dilute Liquid Mixture.**—In the case of liquid-liquid mixtures, the formalism is entirely the same as in the gas-liquid mixture, except that the customary reference state of pure liquid has been chosen for the solute species. Thus

$$\ln \varphi_2 = \ln v_{12}^f - \ln v^f - \frac{W_{12}(0)}{NkT} + \frac{W(0)}{2NkT} - \frac{A_s}{NkT} \quad (21)$$

$$\frac{S_2}{Nk} = \left[ \left(\frac{\partial \ln v_{12}^f}{\partial \ln T}\right)_v + \frac{W_{12}(0)}{NkT} - 1 \right] -$$

(14) D. D. Eley, *Trans. Faraday Soc.*, **35**, 1421 (1939); H. H. Uhlig, *J. Phys. Chem.*, **41**, 1215 (1937).

$$\left[ \left( \frac{\partial \ln v^f}{\partial \ln T} \right)_v + \frac{W(0)}{2NkT} - 1 \right] + \frac{S_s}{Nk} \quad (22)$$

The system Br<sub>2</sub> in C<sub>7</sub>F<sub>16</sub> was chosen since all the relevant data<sup>15</sup> are available and the saturated solution is not too concentrated (x<sub>2</sub> = 0.049). The partial molal volume of Br<sub>2</sub> (73 cc.) is large compared to its molal volume (51.5 cc.) and accordingly the calculation shows again a large free volume for Br<sub>2</sub> in solution (1.313 cc.) compared to the free volume in the pure liquid (0.120 cc.). This is true in spite of the very similar potential energy depth in the pair interaction potentials. However, the length parameters in the solvent and solute potentials are very different, and thus the cohesive energy densities differ considerably. This is reflected in the low solubility and large partial molal volume.

TABLE V  
CELL PROPERTIES OF AR IN CCl<sub>4</sub> SYSTEM AT 25°

Cell	Ar	Bulk CCl <sub>4</sub>	Interfacial CCl <sub>4</sub>	2nd CCl <sub>4</sub>
v <sup>f</sup> (cc.)	1.922	0.222	0.245	0.223
$\left( \frac{\partial \ln v^f}{\partial \ln T} \right)_v$	0.897	1.322	1.308	1.324
$-\frac{W(0)}{NkT}$	6.00	27.02	25.69	26.94

By evaluating the solute contribution, one arrives at

$$\ln x_2 = -0.23 - \frac{A_s}{NkT}$$

$$\frac{S_2}{Nk} = 3.52 + \frac{S_s}{Nk}$$

Since the experimental values for ln x<sub>2</sub> and S<sub>2</sub>/Nk are -3.02 and 6.57, respectively, the solvent contribution again is comparable to that of the solute. The properties of the neighboring solvent molecules to the solute molecules are given in Table VI. The situation is very similar to that in gas mixtures except that the calculated entropy agrees perfectly with experiment. Hence, the region of perturbation due to the solute is pretty well confined to the solvent molecules adjacent to a solute molecule. To a second neighbor solvent molecule, the Br<sub>2</sub> molecule is about as distant as another second neighbor C<sub>7</sub>F<sub>16</sub> molecule, and since the potential depth is nearly the same, the presence of the foreign solute is hardly felt by C<sub>7</sub>F<sub>16</sub> molecules more distant from a Br<sub>2</sub> molecule.

TABLE VI  
CELL PROPERTIES OF BR<sub>2</sub> IN C<sub>7</sub>F<sub>16</sub>

Cell	Bulk Br <sub>2</sub>	Br <sub>2</sub> Cavity	Bulk C <sub>7</sub> F <sub>16</sub>	Interfacial C <sub>7</sub> F <sub>16</sub> <sup>a</sup>
v <sup>f</sup> (cc.)	0.120	1.313	0.561	0.601
$\left( \frac{\partial \ln v^f}{\partial \ln T} \right)_v$	1.315	1.082	1.309	1.290
$-\frac{W(0)}{NkT}$	26.90	9.70	25.90	24.72

<sup>a</sup> It was found that 5.34 molecules surround the cavity.

Discussion

Although the consistent entropy discrepancy of about two entropy units for all gas in liquid sys-

(15) L. W. Reeves and J. H. Hildebrand, *J. Phys. Chem.*, **60**, 949 (1956).

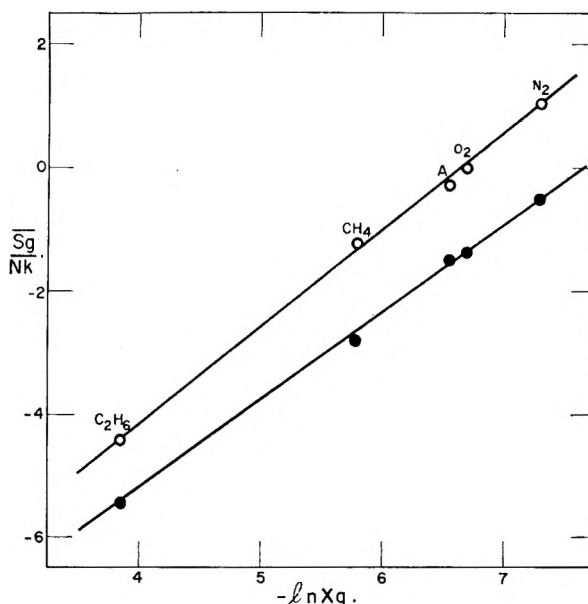


Fig. 5.—The calculated partial molal entropy of solution versus mole fraction for various gases in CCl<sub>4</sub> (closed circles) compared to the experimental values (open circles).

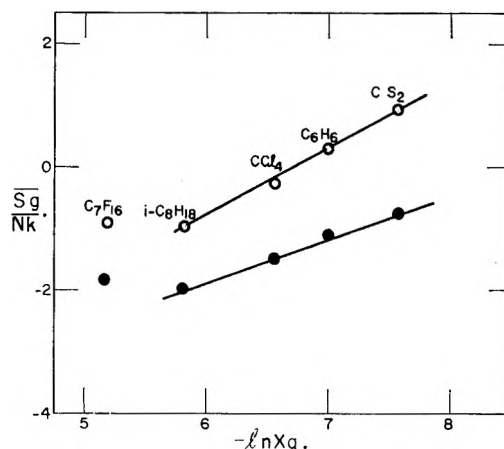


Fig. 6.—As Fig. 5 except for argon in various liquids.

tems and the lack of that discrepancy in the liquid mixture are good evidence that further neighbor contributions have to be considered in gas solubility theory, it is worthwhile to demonstrate that some of the arbitrary and approximate features of the crude model proposed could not be blamed for the entropy discrepancy. Moreover, an estimate of the more distant neighbor contributions is attempted in order to show that it is of the right magnitude.

As pointed out earlier, one of the arbitrary features of the model is the assignment of the entire partial molal volume to the solute. If, instead, 5% of the partial molal volume is assigned to the solvent, the free volume of the solute and solvent will change, as well as the number of nearest solvent neighbors and the well depths. However, following the same procedure as before, the resulting entropy change is less than 0.02 entropy unit, while the deficiency to be accounted for is about 100 times larger. Similarly, it is known that the geometric mean rule for the unlike pair interaction

potential is approximate. If it is assumed that the rule is inaccurate by 5%, then this will cause a 5% change in the number of nearest neighbors of the solute and, upon satisfying the experimental value of the solubility, the cell size of the contact solvent molecule will change. However, the entropy of solution here again varies only by about 0.02 entropy unit. Also, the estimate of the further neighbor contribution to  $W(0)$  is crude. Changing their contribution by 5% again changes the cell potential and again results in a final entropy change of less than 0.03 entropy unit. However, this insensitivity of the results to the approximations used in the model also indicates that the cell parameters found should not be considered as quantitatively accurate, but merely as a qualitative indication of their magnitude.

Further uncertainties arise from the functional form of the cell potential used and the spherical smoothing of the neighbors. There is no doubt that a different form of the two-parameter cell potential even if spherically smoothed could result in good agreement for the entropy too. For example, the exponents in the repulsive part of the cell potential could be altered till agreement is forced. However, the consistency of the picture obtained so far and the fact that the pure liquid properties are reproduced with much smaller entropy discrepancy for the same potential, makes it unlikely that the entire entropy discrepancy found is to be ascribed to the form of the potential.

The further-neighbor contribution should be significant merely on the ground that the first-neighbor contribution is so large. In the Ar-CCl<sub>4</sub> system it amounted to 9.16 entropy units. While in the Br<sub>2</sub>-C<sub>7</sub>F<sub>16</sub> system it also was large (6.06 entropy units), for reasons stated previously the further neighbor contribution is negligible. To evaluate the two-cell parameters of the second neighbors, only the pressure condition is available. Furthermore, it is necessary to know the number of such neighbors, which is hard to estimate, although, again, the calculation proved not sensitive to that number. Thus, all that can be done is to show that when the model also satisfies the experi-

mental entropy, the cell parameters approach those of the pure solvent as further neighbors are considered.

The procedure used was then as follows. Since pure CCl<sub>4</sub> had a  $v_e^*$  of 1.02186, and the contact solvent a  $v_e^*$  of 1.02292, a different  $v_e^*$  of 1.0226 for the contact solvent was assumed arbitrarily, since the previous value was overcorrected because, with only the first layer considered, the experimental solubility had to be satisfied. The second layer then yielded a  $v_e^*$  of 1.02194 in order that the experimental solubility was obtained.  $\bar{S}_g/Nk$  under these conditions is  $-1.03$ , better than the previous value of  $-1.50$  but not yet close to the experimental value of  $-0.25$ . This choice of  $v_e^*$  for the first neighbor yields a value of  $v_e^*$  for the second neighbor very close to the bulk value but slightly larger, as it must be. The properties of the second neighbor cell are given in Table V. If the first layer had a  $v_e^*$  of 1.0224, the second layer would have a  $v_e^*$  of 1.02214, which is a conceivable other extreme, where  $v_e^*$  falls off very slowly to the bulk value. Even then  $\bar{S}_g/Nk$  is hardly affected;  $-1.05$ . Moreover, the results are not sensitive to the number of second nearest neighbors to a gas molecule. In the above quoted calculations  $z_{2g}/z_{1g}$  was assumed to be 1. Changing the ratio to 2 gave  $\bar{S}_g/Nk = 0.90$ . Actually the entropy contribution of the second layer is somewhat larger than the above indicates since the first layer contributes somewhat less under the new cell parameter conditions. In any case, it is not unreasonable to assume that the further-than-second neighbors contribute about an equal amount to the entropy as the second layer and then the experimental entropy is obtained.

**Acknowledgment.**—The ideas incorporated in this work represent a crude quantitative measure of qualitative concepts that have been developed in frequent discussions between the authors and Professor Hildebrand, whose interest we gratefully acknowledge. We also are grateful to Dr. J. Walkley for participating in the early calculations in this project.



THE SECONDARY ISOTOPE RATE EFFECT IN THE IODIDE  
DEBROMINATION OF *sym*-TETRABROMOETHANE AND  
*sym*-TETRABROMOETHANE-*d*<sub>2</sub><sup>1,2</sup>

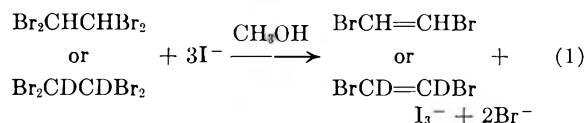
BY WARREN G. LEE AND SIDNEY I. MILLER

*Department of Chemistry, Illinois Institute of Technology, Chicago 16, Illinois*

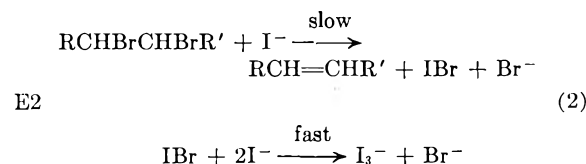
*Received July 10, 1961*

For the iodide-promoted debromination of *sym*-tetrabromoethane and *sym*-tetrabromoethane-*d*<sub>2</sub>, the secondary isotope rate factor  $k_H/k_D \approx 1.28$  at 81–111°. Over this temperature range, a decrease in  $k_H/k_T$  of ca. 6% was observed. The activation energies and entropies for the hydrogen and deuterium tetrabromoethanes are, respectively,  $25.5 \pm 0.5$  and  $26.2 \pm 0.5$  kcal. mole<sup>-1</sup> and  $-12.7$  and  $-11.2$  cal. deg.<sup>-1</sup> mole<sup>-1</sup>. A negative kinetic salt effect was observed. Calculations suggest that the observed value of  $k_H/k_D$  is characteristic of an elimination (E2) rather than a displacement (S<sub>N</sub>2) path for debromination. The rate data also appear to be more consistent with those from comparable E2 rather than S<sub>N</sub>2 systems.

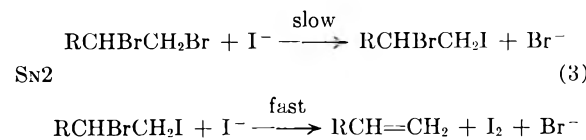
This paper is concerned with the secondary isotope effect and the reaction mechanism in the system



Because complete vibrational assignments for the reactants and products were available, we considered that calculations of  $k_H/k_D$  would be instructive: these are reported in another paper.<sup>3</sup> System 1 is an example of a large group of iodide ion debrominations of alkane dibromides.<sup>4</sup> This reaction has had synthetic utility.<sup>4,5</sup> It is perhaps more important theoretically as one of those early examples of stereospecific *trans* eliminations in which *D-L* or *threo*-dibromides generally yield *cis* products and *meso* or *erythro*-dibromides yield *trans* products. Originally, an E2 mechanism was accepted in which the bromine atoms were simultaneously removed in the *trans* sense



In 1955, Hine and Brader showed the S<sub>N</sub>2 mechanism applies to some terminal-type alkane dibromides.<sup>6</sup> These alternatives posed a mechanistic question which a kinetic isotope rate study could possibly resolve.



mechanistic question which a kinetic isotope rate study could possibly resolve.

### Experimental

**Materials.**—Reagent grade absolute methanol was further purified by the method of Lund and Bjerrum.<sup>7</sup> Sodium iodide was dried at 150° and stored in a desiccator; its purity was checked against standard silver nitrate. *sym*-Tetrabromoethane (500 g.) was washed, dried, and fractionated; a middle fraction (ca. 140 ml.) had b.p. 118° at 15 mm. and  $n_D^{20}$  1.6379 (lit.<sup>8</sup> b.p. 120° at 15 mm. and lit.<sup>9</sup>  $n_D^{20}$  1.6353). The preparation of *sym*-tetrabromoethane-*d*<sub>2</sub> has been described<sup>10</sup>; a middle fraction (ca. 50 ml.) had b.p. 52.8–53° (0.4 mm.) and  $n_D^{20}$  1.6356. An infrared spectrum of the deuterated sample as well as that of the derived dibromoethenes showed no protonated material (< 1%).<sup>11</sup>

**Rate Studies.**—Reactor 1 in the solvent methanol was studied in the range 75–10° by established procedures: the ampoule technique was used; 10<sup>-2</sup> mmole of iodine could be determined with standard thiosulfate to the “dead stop” end-point with an accuracy of 1%.<sup>12</sup> Apart from a few early ampoules in any given run for which the uncertainty in the time may be  $\pm 2$  min., this source of error was generally negligible. Calibrated thermometers were used in the thermostats: the temperature variation was ca.  $\pm 0.05^\circ$ .

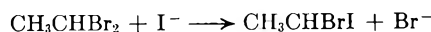
Methanol containing either sodium iodide or *sym*-tetrabromoethane produced no titratable iodine or bromide under the conditions of the experiments. However, within ca. 20 hr. at 110°, a methanol solution originally 1 mmole in iodine had lost 0.037 mmole of iodine and thereafter remained constant. As in previous studies,<sup>12,13</sup> a blank based on the temperature and reaction time was added to the iodine titer. The uncertainty in the rate constants due to this problem is smaller than the average deviation listed for the rate constants (Tables II and III).

A standard rate expression was used to treat the data<sup>12</sup>

$$kt = \frac{2.303}{(b-3x)} \log \frac{a}{b} \left( \frac{b-3x}{a-x} \right)$$

where  $a = [\text{C}_2\text{H}_2\text{Br}_4]_0$ ,  $b = [\text{NaI}]_0$ , and  $x = [\text{I}_3^-]$ , all in mole liter<sup>-1</sup>. The best value of  $k$  was determined by averaging the results of any one run and from  $kt$  vs.  $t$  plots. A typical run is given in Table I. The average rate constant was corrected to  $k_{\text{cor}}$  for the expansion of solvent.<sup>14</sup>

**Rate Study of 1,1-Dibromoethane and Sodium Iodide.**—One preliminary run of the following reaction was made at 101.1°



(7) H. Lund and J. Bjerrum, *Ber.*, **64**, 1210 (1931).

(8) T. E. Jordan, “Vapor Pressure of Organic Compounds,” Interscience Publishers, Inc., New York, N. Y., 1959, p. 35.

(9) A. I. Vogel, *J. Chem. Soc.*, 1850 (1948).

(10) S. I. Miller and W. G. Lee, *J. Am. Chem. Soc.*, **81**, 6313 (1959).

(11) J. M. Dowling, P. G. Puranik, A. G. Meister, and S. I. Miller, *J. Chem. Phys.*, **26**, 233 (1957).

(12) S. I. Miller and R. M. Noyes, *J. Am. Chem. Soc.*, **74**, 3403 (1952).

(13) R. T. Dillon, W. G. Young, and H. Lucas, *ibid.*, **52**, 1953 (1930).

(14) “Landolt-Bornstein Tabellen,” Julius Springer, Berlin, 1923, p. 278.

(1) (a) Presented in part at the 130th National Meeting of the American Chemical Society, Atlantic City, N. J., Sept., 1956. (b) Abstracted from a portion of the Ph.D. thesis of Warren G. Lee, Illinois Institute of Technology, 1961.

(2) Supported in part by the Research Corporation.

(3) S. I. Miller, *J. Phys. Chem.*, **66**, in press (1962).

(4) See W. G. Young, S. J. Cristol, and T. Skei, *J. Am. Chem. Soc.*, **65**, 2099 (1943), and S. Winstein, D. Pressman, and W. G. Young, *ibid.*, **61**, 1645 (1939), for earlier references.

(5) D. H. R. Barton and E. Miller, *ibid.*, **72**, 1066 (1950).

(6) J. Hine and W. H. Brader, *ibid.*, **77**, 361 (1955). See also W. M. Schubert, H. Steady, and B. S. Rabinovitch, *ibid.*, **77**, 5755 (1955).

TABLE I  
REACTION OF *sym*-TETRABROMOETHANE AND SODIUM IODIDE  
AT (76.37 ± 0.17)° IN METHANOL

$$a = 0.4160, b = 0.1028$$

Time, min.	(I <sub>3</sub> <sup>-</sup> )	k × 10 <sup>4</sup>
399	0.00278	1.70
964	.00750	1.94
1275	.00890	1.92
2937	.01668	1.94
4230	.02165	1.95
5558	.02471	1.91

$$k_{av} = 1.89 \pm 0.07$$

$$k_{cor} = 2.03 \pm 0.07 \text{ l. mole min.}^{-1}$$

The ampoule technique was used and an analysis of iodide in the presence of bromide was carried out.<sup>15</sup> On the basis that the reaction is first order in each reactant, the rate constant was found to be (15.6 ± 0.7) l. mole<sup>-1</sup> min.<sup>-1</sup> at 101.1°.

### Results and Discussion

Most of the previous studies of the iodide-catalyzed debromination reaction were not concerned with salt effects. However, Van Duin found that the rate constants increased slightly with ionic strength in the system potassium iodide with sodium 2,3-dibromopropionate.<sup>16</sup> Dillon reported a slight decrease in rate when neutral salt was added to the system potassium iodide and 1,2-dibromoethane: for example, at 40° in 60% aqueous ethanol at ionic strengths = 0.22 (KI), 0.33 (0.22 KI + 0.11 KCl), and 0.44 (0.22 KI + 0.22 KBr), the second-order rate constants were 80, 77.9, and 72.5 × 10<sup>3</sup> liter mole<sup>-1</sup> min.<sup>-1</sup>, respectively. Dillon considered all of these to be Brønsted salt effects.<sup>17</sup>

Our data for reaction 1 are given in Tables II and III. The rate constants clearly decrease with increasing initial concentrations of sodium iodide. The present state of the theory on salt effects in

TABLE II

KINETICS OF THE REACTION BETWEEN *sym*-TETRABROMOETHANE AND SODIUM IODIDE IN METHANOL

C <sub>2</sub> H <sub>2</sub> Br <sub>4</sub> , mole/l.	NaI, mole/l.	Temp., °C.	k × 10 <sup>4</sup> , l./mole min.
0.06249	0.06419	76.25 ± 0.17	2.24 ± 0.04
		92.94 ± .05	11.6 ± .4
		108.98 ± .09	57.2 ± 1.2
.4160	.1028	76.37 ± .17	2.03 ± 0.07
		92.64 ± .06	12.4 ± .6
		108.81 ± .07	59.0 ± 1.2
.1236	.2329	76.21 ± .10	1.83 ± 0.03
		92.02 ± .06	10.9 ± .4
		108.96 ± .04	50.0 ± 1.0
.3172	.3196	76.21 ± .10	1.87 ± 0.05
		78.72 ± .04	2.47 ± .03
		92.11 ± .06	10.1 ± .4
		108.92 ± .06	51.6 ± .6
.05196	.6743	76.77 ± .10	1.57 ± .08
		92.72 ± .07	9.00 ± .37
		108.88 ± .12	41.7 ± 1.1

(15) S. I. Miller and P. K. Yonan, *J. Am. Chem. Soc.*, **79**, 5931 (1957).

(16) C. F. Van Duin, *Rec. trav. chim.*, **43**, 341 (1924); **45**, 345 (1926); **47**, 715 (1928).

(17) R. T. Dillon, *J. Am. Chem. Soc.*, **54**, 952 (1932).

ion-molecule reactions is still inadequate. Even for solutions much more dilute than ours, opposing predictions have been made for the variations in *k* with ionic strength.<sup>18</sup> Therefore, we proceeded

TABLE III

REACTION BETWEEN *sym*-TETRABROMOETHANE-*d*<sub>2</sub> AND SODIUM IODIDE IN METHANOL

C <sub>2</sub> D <sub>2</sub> Br <sub>4</sub> , mole/l.	NaI, mole/l.	Temp., °C.	k × 10 <sup>4</sup> , l./mole min.
0.1336	0.1023	78.92 ± 0.05	2.16 ± 0.03
		90.10 ± .05	7.11 ± 0.14
		108.78 ± .05	45.9 ± 1.3
.2053	.1263	79.09 ± .10	2.23 ± 0.04
		90.05 ± .05	6.83 ± 0.20
		108.93 ± .05	49.7 ± 1.6
.07405	.1707	76.37 ± .07	1.56 ± 0.03
		78.72 ± .04	2.06 ± .04
		90.24 ± .02	6.69 ± .21
		92.18 ± .02	8.37 ± .25
.03538	.2317	108.96 ± .04	42.9 ± .7
		78.72 ± .04	2.00 ± .05
		90.24 ± .02	6.02 ± .22
.1054	.2344	108.96 ± .04	39.4 ± 1.3
		80.39 ± .02	2.29 ± 0.06
		90.11 ± .06	6.12 ± 0.17
.07210	.7595	109.86 ± .10	45.4 ± 1.1
		80.52 ± .09	2.00 ± 0.05
		90.10 ± .08	5.71 ± .15
		109.86 ± .10	40.1 ± .6

empirically and found log *k* to be linear in *b*, the concentration of sodium iodide, *i.e.*

$$\log k = \log k^0 + mb \quad (4)$$

To treat the data, it was necessary to make Arrhenius plots at constant ionic strength. The rate data were normalized at 80.82, 90.48, and 111.46°.

These isothermal data were fitted to eq. 4 by least squares. The slopes obtained for the three temperatures were: *m*<sub>H</sub> = -0.257, *m*<sub>D</sub> = -0.127 at 80.82°; *m*<sub>H</sub> = -0.243, *m*<sub>D</sub> = -0.142 at 90.48°; *m*<sub>H</sub> = -0.219, *m*<sub>D</sub> = -0.142 at 111.46°. The rate constants at zero ionic strength, derived activation parameters, and isotope rate factors are given in Table IV under Method 1. A plot of log *k*<sub>H</sub><sup>0</sup>/*k*<sub>D</sub><sup>0</sup> vs. 1/*T* was linear.

The lack of parallelism between the hydrogen and deuterium salt plots is difficult to reconcile with any existing theory. Intuitively, it seems improbable that the presence of deuterium in a molecule would greatly alter its sensitivity to salt effects. We have, therefore, applied a second least squares treatment of the ionic strength effect. Here it was assumed that the slopes of log *k* vs. *b* for the hydrogen and deuterium compounds at a given temperature were the same. The calculated slopes<sup>19</sup> at 80, 90, and 111° are -0.1556, -0.1583, and -0.1551 and essentially independent of temperature. This treatment reduced *k*<sub>H</sub>/*k*<sub>D</sub> and changed the activation parameters somewhat (see Table IV under Method 2).

Both methods of treating the data have their merits. By the first method *k*<sub>H</sub>/*k*<sub>D</sub> = 1.39-1.28;

(18) E. S. Amis, "Kinetics of Chemical Change in Solution," The Macmillan Co., New York, N. Y., 1949, Ch. 8.

(19) S. Ergun, *Ind. Eng. Chem.*, **48**, 11, 2063 (1956).

TABLE IV

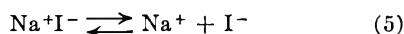
REACTION OF DEUTERATED AND NORMAL *sym*-TETRABROMOETHANE WITH SODIUM IODIDE IN METHANOL

Temp., °C.	$k_H^0 \times 10^4,^a$ l./mole min.	$k_D^0 \times 10^4,^a$ l./mole min.	$k_H^0/k_D^0$	$\Delta\Delta F^*,^b$ cal./mole
Method 1 <sup>c</sup>				
80.82	3.641	2.621	1.389	-231
90.48	10.05	7.439	1.351	-216
111.46	65.32	51.17	1.277	-186
$\Delta E_H = 25.5 \pm 0.5$ kcal./mole		$\Delta S_H = -12.7$ cal./deg. mole		
$\Delta E_D = 26.2 \pm 0.5$ kcal./mole		$\Delta S_D = -11.2$ cal./deg. mole		
Method 2 <sup>d</sup>				
80.82	3.415	2.669	1.28	-173
90.48	9.517	7.518	1.27	-172
111.46	62.78	51.17	1.23	-158
$\Delta E_H = 25.6 \pm 0.5$ kcal./mole		$\Delta S_H = -12.3$ cal./deg. mole		
$\Delta E_D = 26.0 \pm 0.5$ kcal./mole		$\Delta S_D = -11.6$ cal./deg. mole		

<sup>a</sup>  $k^0$ , rate constant at zero ionic strength. <sup>b</sup>  $\Delta\Delta F^*$  =  $-RT \ln k_H^0/k_D^0$ . <sup>c</sup>  $k^0$  from least squares treatment of 4. <sup>d</sup>  $k^0$  from least squares treatment of 4 in which a constant slope was required for the deuterated and normal tetrabromoethanes at a given temperature.

by the second  $k_H/k_D = 1.28-1.23$ . These experimental uncertainties render uncertain any estimates of the temperature dependent and independent parts of the isotope rate effect. We infer that these are limits on the isotope rate effect and that the true value lies between the two extremes, say  $k_H/k_D = 1.28$  in the range 80–111°. However, the trend in  $k_H/k_D$  with increasing temperature is clear: there is a decrease in  $k_H/k_D$  of ca. 4–8% over a 30° temperature interval.<sup>20</sup>

There is an alternative view of the medium effect, namely, that the sodium iodide is incompletely dissociated in methanol.



Accordingly

$$K = y^2/(b - y) \quad (6)$$

where no aggregates beyond dimers are assumed,  $y$  is the concentration of free iodide and only free iodide is effective in reaction 1.

Then

$$y/b = k/k^0 = m \quad (7)$$

Using  $k^0$  for the hydrogen compound at 80.82°, we calculate  $K = 1.7 \times 10^{-3}$  or  $2.5 \times 10^{-3}$  depending on the two methods of evaluating  $k^0$ . This is in the range of the dissociation constants of alkali iodides in similar solvents, e.g.,  $K = 5.3 \times 10^{-3}$  for sodium iodide in 1-propanol.<sup>21</sup> Although it would appear that association accounts nicely for the whole "medium" effect, it is probable that both a normal kinetic salt effect and ion aggregation diminish the effectiveness of added iodide in reaction 1.<sup>22</sup>

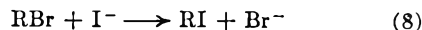
(20) The lower figure for the temperature coefficient is more probable.<sup>1</sup>

(21) M. B. Reynolds and C. A. Kraus, *J. Am. Chem. Soc.*, **70**, 1709 (1948); R. L. Kay, *ibid.*, **82**, 2099 (1960); T. A. Gover and P. G. Sears, *J. Phys. Chem.*, **60**, 330 (1956).

(22) S. Winstein, L. G. Savedoff, S. Smith, I. D. R. Stevens, and J. S. Gall, *Tetrahedron Letters*, 24 (1960).

**Debromination Mechanism.**—It is not obvious whether the E2 scheme in equation 2 or the SN2 scheme in 3 best represents the debromination process in tetrabromoethane. Three lines of argument, all favoring one of the mechanisms, will be developed.

Consider the displacement (SN2)<sup>6</sup>



The steric requirements of CH<sub>3</sub> and Br are closely similar—their Taft  $E_s$  parameters are identical—but CH<sub>3</sub> is electron-releasing compared with Br.<sup>23a</sup> In 8, the relative rates for different R groups are CH<sub>3</sub> (100), C<sub>2</sub>H<sub>5</sub> (1.65), *n*-C<sub>3</sub>H<sub>7</sub> (1.32), *i*-C<sub>4</sub>H<sub>9</sub> (0.059), and *i*-C<sub>3</sub>H<sub>7</sub> (0.022)<sup>23b</sup>: the important point is that alkyl substitution at the reacting center reduces the displacement rate sharply. This behavior is further illustrated for a series of known displacements: the rate constants per Br at 101.1° in l. mole<sup>-1</sup> min.<sup>-1</sup> follow the order, BrCH<sub>2</sub>CH<sub>2</sub>Br (1310),<sup>24</sup> Br<sub>2</sub>CHCH<sub>2</sub>Br (13.3),<sup>24</sup> CH<sub>3</sub>CHBrCH<sub>2</sub>Br (64),<sup>24</sup> and CH<sub>3</sub>CHBr<sub>2</sub> (7). If reaction 1 went through the displacement mechanism, one might predict Br<sub>2</sub>CHCHBr<sub>2</sub> (0.7–0.07) in this series. Since the observed rate constant is 7.5 on this scale, this argues against the displacement mechanism.

The elimination mechanism has been established in the reaction of iodide with the 2,3-dibromobutanes.<sup>6</sup> At 59.7°, relative rates are as follows: *meso*-CH<sub>3</sub>CHBrCHBrCH<sub>3</sub> (1.5),<sup>4</sup> *racemic*-CH<sub>3</sub>CHBrCHBrCH<sub>3</sub> (0.78),<sup>4</sup> and Br<sub>2</sub>CHCHBr<sub>2</sub> (0.37). Since the inductive effect of bromine is bond strengthening on a *gem*-bromine and opposite to that of methyl, this order is at least consistent for an elimination series.

In another paper, calculations for secondary isotope effects have been presented.<sup>3</sup> These suggest that  $k_H/k_D < 1$  for SN2 processes and  $k_H/k_D > 1$  for E2 processes. Data from the literature are consistent with these predictions.<sup>25,26</sup> The calculations also indicate that for an E2 process  $k_H/k_D$  should decrease as the temperature increases. This temperature dependence was found (see Table IV). This and the finding that  $k_H/k_D \approx 1.28$  for the debromination constitute the strongest argument for an E2 process in equation 1.<sup>3</sup>

Finally, addition reactions of alkenes are the reverse of E2 processes. The calculations<sup>3</sup> indicate that additions should have both a reverse secondary isotope effect, that is  $k_H/k_D < 1$ , and a reverse temperature dependence, i.e.,  $k_H/k_D$  should increase as  $T$  increases. The thiocyanate-catalyzed isomerization of maleic acid<sup>27</sup> or the bromine addition to stilbene<sup>28</sup> exhibit the expected behavior.<sup>29</sup> These authentic addition mechanisms provide

(23) (a) R. W. Taft, Jr., "Steric Effects in Organic Chemistry," M. S. Newman, Editor, John Wiley and Sons, New York, N. Y., 1956, p. 650; (b) E. L. Eliel, *ibid.*, pp. 73–77.

(24) D. Pressman and W. G. Young, *J. Am. Chem. Soc.*, **66**, 705 (1944).

(25) R. R. Johnson and E. S. Lewis, *Proc. Chem. Soc.*, 52 (1958).

(26) V. J. Shiner, *J. Am. Chem. Soc.*, **82**, 2655 (1960).

(27) S. Seltzer, *ibid.*, **83**, 1861 (1961).

(28) S. D. Denny and N. Tunkel, *Chem. & Ind. (London)*, 1383 (1959).

(29) The symmetry of elimination-addition processes is beautifully illustrated by these isotope effects.

another argument in favor of an E2 process for the debromination of tetrabromoethane.

**Acknowledgment.**—We wish to thank the Research Corporation for its financial support.

## THE THERMODYNAMIC PROPERTIES OF LIQUID TERNARY ZINC, INDIUM, AND GALLIUM SOLUTIONS

BY W. J. SVIRBELY AND SHIRLEY M. READ<sup>1</sup>

*Department of Chemistry, University of Maryland, College Park, Md.*

*Received July 24, 1961*

The ternary system zinc-indium-gallium and the binary systems zinc-indium and zinc-gallium have been investigated by electrode-potential methods over the temperature range of 420 to 520°. The properties,  $\Delta F^\circ$ ,  $\Delta H^\circ$ ,  $\Delta S^\circ$ ,  $\Delta F_i^\circ$ ,  $L$ , and activities were calculated from the experimental data for the systems at 470°. The corresponding properties of the gallium-indium binary system were obtained by calculation by means of Darken's procedure utilizing the experimental data.

### Introduction

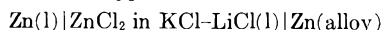
At the time this research was started, thermodynamic studies of liquid alloys involving more than two components were limited. The studies on the cadmium-lead-bismuth, cadmium-lead-tin, and the cadmium-lead-antimony systems had been reported by Elliott and Chipman<sup>2</sup> and the cadmium-bismuth-tin system by Mellgren.<sup>3</sup> Both papers made use of Darken's equations<sup>4</sup> developed for a single phase ternary system in which the composition of the third component is varied in a constant ratio mixture of the other two components.

In our Laboratory, attempts had been made to study the gallium-indium binary system directly by use of the electrode-potential method. We were not successful. However, values of this binary may be calculated<sup>4</sup> from experimental measurements on a ternary system involving gallium, indium, and some other more electropositive metal, for example, zinc.

Consequently, the present research was undertaken in order to determine: (1) the thermodynamic properties of the zinc-indium-gallium system; (2) the thermodynamic properties of the gallium-indium binary system.

**Materials.**—The sources of indium,<sup>5</sup> zinc, and gallium<sup>6</sup> already have been described. However, gallium of 99.99% purity, obtained from the Aluminum Co. of America, also was used in some of the runs. Spectrographic analyses indicated the complete absence of foreign elements in all three metals.

**Apparatus.**—The apparatus was essentially the same as before.<sup>5</sup> Cells of the type



were used. Details concerning the preparation of the cells already have been described.<sup>5</sup>

### Experimental

A series of measurements of the e.m.f. of cells of the above type were made over a temperature range of 420 to 520° using zinc-gallium, zinc-indium, and zinc-indium-gallium alloys. In the latter series, the measurements were performed on alloys having constant atomic ratios of  $N_{\text{Ga}}/N_{\text{In}}$

equal to 3/17, 1/3, 1/1, and 3/1. The mole fraction of zinc was varied from 0.100 to 0.900 in each of the binary and ternary systems.

The experimental e.m.f. for each alloy was plotted against the temperature. Linear plots were obtained. The temperature gradient and the e.m.f. for each alloy at the arbitrarily selected temperature of 470° were determined from the plots. These data are given in Table I.

TABLE I  
CELL COMPOSITION AND POTENTIALS AT 470°

$N_{\text{Zn}}$	E.m.f. (mv.)	$dE/dT$ mv./degree	$N_{\text{Zn}}$	E.m.f. (mv.)	$dE/dT$ mv./degree
Zinc-gallium series					
0.100	61.45	0.11532	0.100	47.75	0.11333
.200	41.25	.08188	.200	29.63	.08275
.300	30.26	.06400	.300	20.37	.06133
.370	24.97	.05425	.400	15.05	.04762
.400	22.76	.04888	.500	11.04	.03538
.500	17.45	.03838	.600	8.29	.02434
.600	12.91	.02722	.700	6.42	.01750
.700	9.26	.01916	.800	4.45	.00974
.800	6.08	.01195	.900	2.44	.00403
.900	2.89	.00505	$N_{\text{Ga}}/N_{\text{In}} = 1/3$		
Zinc-indium series					
0.100	38.92	0.11600	0.100	54.11	0.11300
.200	21.91	.08333	.200	35.23	.08000
.350	11.90	.05525	.300	25.18	.06300
.500	7.54	.03573	.400	18.84	.04938
.548	6.74	.0308	.500	13.99	.03644
.600	6.06	.02669	.600	10.45	.02663
.700	4.92	.01961	.700	7.48	.01815
.749	4.18	.01331	.800	5.06	.01030
.800	3.70	.01013	.900	2.74	.00425
.900	2.26	.00386	$N_{\text{Ga}}/N_{\text{In}} = 1/1$		
Zinc-indium-gallium series					
$N_{\text{Ga}}/N_{\text{In}} = 3/17$					
0.100	43.28	0.11422	0.100	58.43	0.11375
.200	26.88	.0838	.200	39.47	.08289
.300	18.93	.06371	.300	28.63	.06257
.400	13.19	.04788	.400	21.32	.04863
.500	10.0	.0361	.500	15.99	.03675
.600	7.49	.02556	.600	12.12	.02738
.700	5.90	.01825	.700	9.08	.01976
.800	4.09	.01044	.800	5.96	.01254
.900	2.50	.00454	.900	2.98	.00504

(1) Abstracted in part from a thesis submitted by Shirley M. Read to the Graduate School of the University of Maryland in partial fulfillment of the requirements for the degree of Doctor of Philosophy.

(2) J. F. Elliott and J. Chipman, *J. Am. Chem. Soc.*, **73**, 2682 (1951).

(3) S. Mellgren, *ibid.*, **74**, 5037 (1952).

(4) L. S. Darken, *ibid.*, **72**, 2909 (1950).

(5) W. J. Svirbely and S. M. Selis, *ibid.*, **75**, 1532 (1953).

(6) W. J. Svirbely and S. M. Selis, *J. Phys. Chem.*, **68**, 33 (1954).

When an alloy of a particular composition was chosen for analysis, part of the original sample was saved. After completion of a run, appropriate amounts of the used alloy

and the original sample were dissolved and analyzed by a comparative fluorescent X-ray spectrographic procedure.<sup>7</sup> Within the limits of accuracy of the method no significant changes in composition of the alloys were observed. Eight different alloys were analyzed between the mole fraction limits from 0.100 to 0.900 for each of the three metals. Thus the experimental method was found to cause no loss of material.

Check runs were made on twelve alloys. The number of runs made is designated by 2 and 4 on Fig. 2 and 3. Agreement between the  $E_{470}$  values is within 0.75% for all but one case (2.3%).

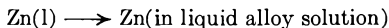
The zinc-gallium system has been studied previously.<sup>8</sup> At  $N_{Zn} = 0.370$ ,  $T = 761.4^\circ\text{K}$ ., the agreement between  $E$  and  $dE/dT$  values in the two studies is within 2% deviation from the mean. At  $N_{Zn} = 0.700$ , the agreement is less satisfactory, 3.6% for  $E$  and 15.8% for  $dE/dT$ . Our check run on this particular alloy is within 0.37% for  $E$  and identical for  $dE/dT$  with its duplicate.

The zinc-indium system also has been studied previously.<sup>8,9</sup> While compositions are not exactly alike, a comparison with the data of this research indicates average deviations of 5.5% for  $E_{700^\circ\text{K}}$  and 3.4% for  $dE/dT$  with those of Bohl and Hildebrandt and 2.1% for  $E_{700^\circ\text{K}}$  and 5.1% for  $dE/dT$  with those of Svirebely and Selis.

In all of our calculations involving the data of the above two binary systems, we have chosen to use the results of this research.

**Calculations.**—In all equations, the subscripts associated with a property refer to definite elements: 1 refers to gallium, 2 refers to zinc, and 3 refers to indium. The various constants in the equations have the following values:  $n = 2$ ,  $R = 1.986$  cal./mole-degree,  $T = 743.2^\circ\text{K}$ . and  $\mathfrak{F} = 23061.6$  cal./volt-degree.<sup>10</sup>

The cell reaction is



The partial molal free energy, the activity, the activity coefficient, the partial molal entropy, and the relative partial molal heat content of zinc in the alloys (the standard state in all cases is the pure metal) are obtained directly from the data by use of the equations

$$\Delta \bar{F}_2 = \bar{F}_2(1) - F_2^0(1) = -n\mathfrak{F}E \quad (1)$$

$$\log a_2 = \frac{-n\mathfrak{F}E}{2.3026 RT} \quad (2)$$

$$\alpha_2 = \frac{a_2}{N_2} \quad (3)$$

$$\Delta \bar{S}_2 = n\mathfrak{F} \left( \frac{dE}{dT} \right) \quad (4)$$

$$\bar{L}_2 = \Delta \bar{H}_2 = n\mathfrak{F} \left[ T \left( \frac{dE}{dT} \right) - E \right] \quad (5)$$

The activities of zinc in the binary and ternary systems are shown in Fig. 1.

Excess thermodynamic quantities are defined as the difference between the actual values and the values for an ideal solution of the same concentration. The excess partial molal properties of zinc were calculated by means of the equations

$$\Delta \bar{F}_2^x = 2.3026RT \log \alpha_2 \quad (6)$$

$$\bar{L}_2^x = \bar{L}_2 = \Delta \bar{H}_2 \quad (7)$$

(7) We acknowledge our indebtedness to Dr. W. J. Campbell and Mr. J. D. Brown, U. S. Bureau of Mines, College Park, Md., for the analyses.

(8) V. Genta, M. Fiorani, and V. Valenti, *Gazz. chim. ital.*, **85**, 103 (1955).

(9) R. W. Bohl and V. D. Hildebrandt, *J. Am. Chem. Soc.*, **79**, 2711 (1957).

(10) D. N. Craig, J. I. Hoffman, C. A. Law, and W. J. Hamer, *J. Research Natl. Bur. Standards*, **64A**, 381 (1960).

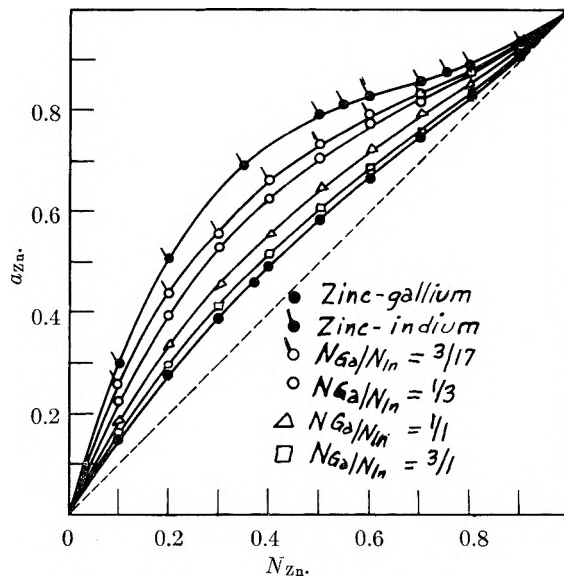


Fig. 1.—Activities of zinc at 470° in zinc-indium, zinc-gallium and in zinc-indium-gallium systems. Note: Symbolism on Fig. 2, 3, 4, and 5 is the same as above.

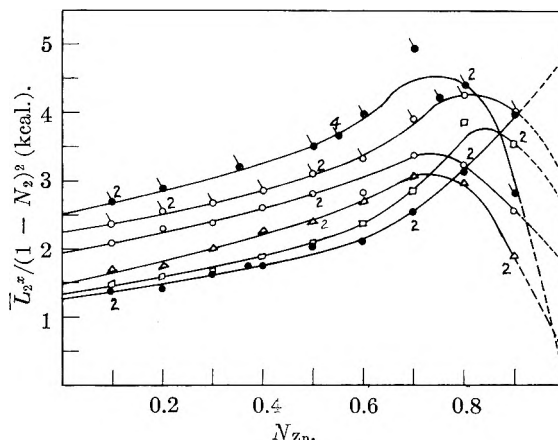


Fig. 2.—Heat of solution functions of zinc in the binary and ternary solutions.

$$\Delta \bar{S}_2^x = \frac{\bar{L}_2^x - \Delta \bar{F}_2^x}{T} \quad (8)$$

Values of the quantities  $\Delta \bar{F}_2^x / (1 - N_2)^2$  and  $\bar{L}_2^x / (1 - N_2)^2$  were calculated at each mole fraction for use in the graphical integrations of Darken's procedure. Graphs of such data vs.  $N_2$  are shown in Fig. 2 and 3 for the two binary systems and the four ternary systems investigated. Graphical integrations of the resulting plots were made and the results were used in the calculation of the values of the integral excess thermodynamic properties of the ternary systems in accordance<sup>4</sup> with eq. 9, namely

$$G^x = (1 - N_2) \left[ \int_1^{N_2} \frac{\bar{G}_2^x}{(1 - N_2)^2} dN_2 \right]_{N_1} + N_1 [\bar{G}_1^x]_{N_2=1} + N_3 [\bar{G}_3^x]_{N_2=1} \quad (9)$$

The binary constants,  $[\bar{G}_1^x]_{N_2=1}$  and  $[\bar{G}_3^x]_{N_2=1}$  were evaluated by the equations

$$[\bar{G}_1^x]_{N_2=1} = \left[ \int_0^1 \frac{\bar{G}_2^x}{(1 - N_2)^2} dN_2 \right]_{N_3=0} \quad (10)$$

and

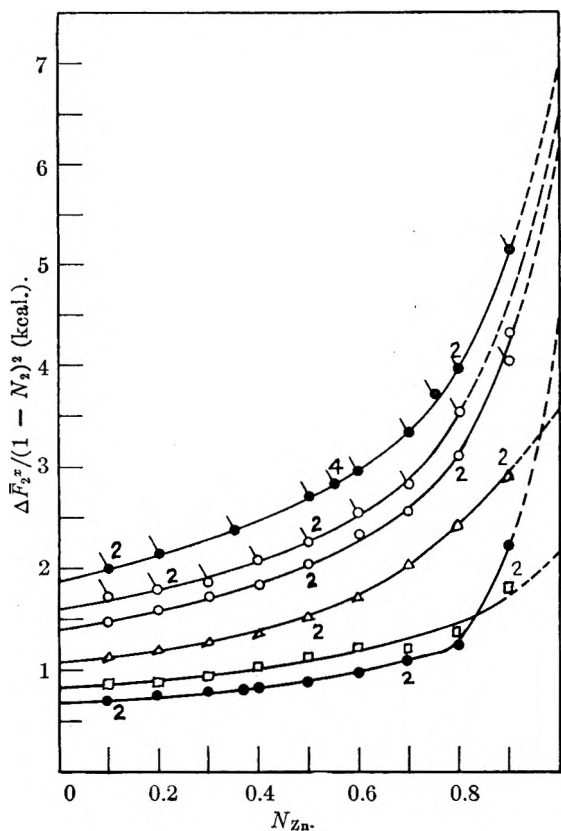


Fig. 3.—Excess free energy functions of zinc in the binary and ternary solutions.

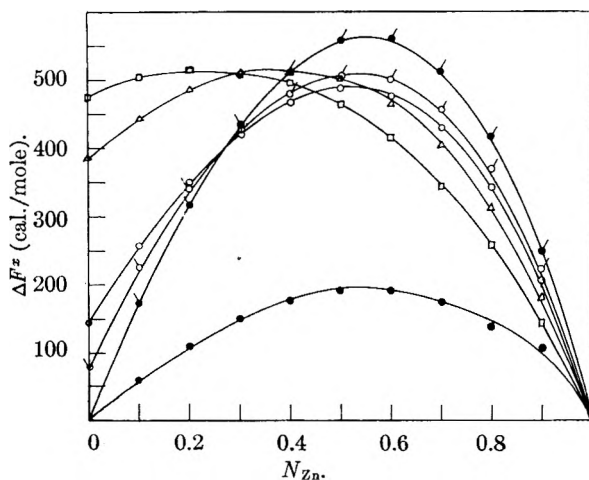


Fig. 4.—Integral excess free energies of mixing per mole of solution at 470° for binary and ternary solutions.

$$[\bar{G}_1^x]_{N_2=1} = \left[ \int_0^1 \frac{\bar{G}_2^x}{(1 - N_2)^2} dN_2 \right]_{N_2=0} \quad (11)$$

in which the values of the integrals are the total areas under the appropriate binary curves of Fig. 2 and 3. The values of the binary constants are

$$[\Delta \bar{F}_1^x]_{N_2=1} = 1177 \text{ cal./mole}; [\bar{L}_1^x]_{N_2=1} = 2308 \text{ cal./mole}$$

$$[\Delta \bar{F}_2^x]_{N_2=1} = 3120 \text{ cal./mole}; [\bar{L}_2^x]_{N_2=1} = 3286 \text{ cal./mole}$$

For the ternary curves of Fig. 2 and 3, graphical integrations were performed in 0.1 mole fraction intervals from  $N_2 = 1$  to  $N_2 = 0$ .

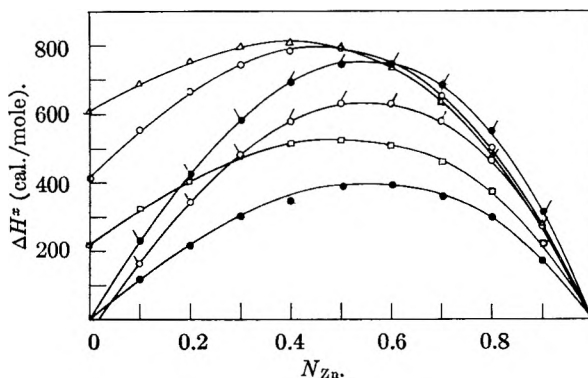


Fig. 5.—Integral heats of mixing per mole of solution at 470° for binary and ternary solutions.

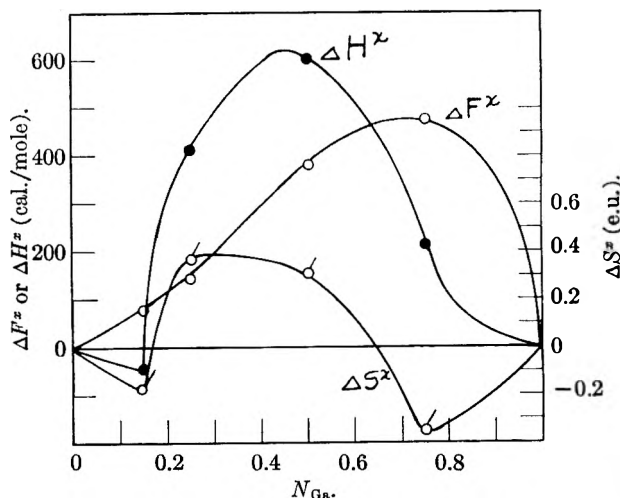


Fig. 6.—Integral thermodynamic functions of mixing per mole of solution at 470° for gallium-indium solutions.

The values obtained from the graphical integrations were multiplied by  $(1 - N_2)$ ,  $N_1$ , or  $N_3$  as appropriate in each case in accordance with eq. 9. The sum of the resulting three quantities is  $G^x$ , or more specifically, the excess integral molal free energy of solution  $\Delta F^x$ , and the integral molal heat of solution  $\Delta H = \Delta H^x$ . Excess integral molal entropies of solution,  $\Delta S^x$ , were calculated by eq. 12

$$\Delta S^x = \frac{\Delta H^x - \Delta F^x}{T} \quad (12)$$

The values of the excess integral free energies and enthalpies of solution for the ternary systems are plotted vs.  $N_2$  in Fig. 4 and 5.

The excess partial molal properties of gallium and indium in their respective binary systems with zinc were calculated from the experimental data by means of eq. 13.

$$\bar{G}_i^x = - \int_0^{N_2/N_1} \frac{N_2}{N_1} d\bar{G}_2^x \quad (13)$$

where  $\bar{G}_2^x$  is an excess partial molal property of zinc and  $i$  refers to either gallium or indium. The integral in eq. 13 was evaluated graphically in each case at intervals corresponding to 0.1 mole fraction unit of zinc from 0 to 0.900. The excess integral molal free energy and excess heat of solution for both binary systems were calculated by means of eq. 14 using these calculated excess partial molal

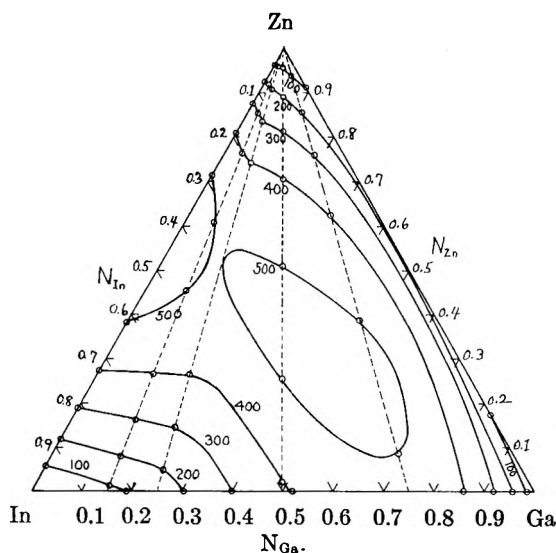


Fig. 7.—Excess integral free energy of mixing per mole of solution surface in 100-cal. steps at 470°.

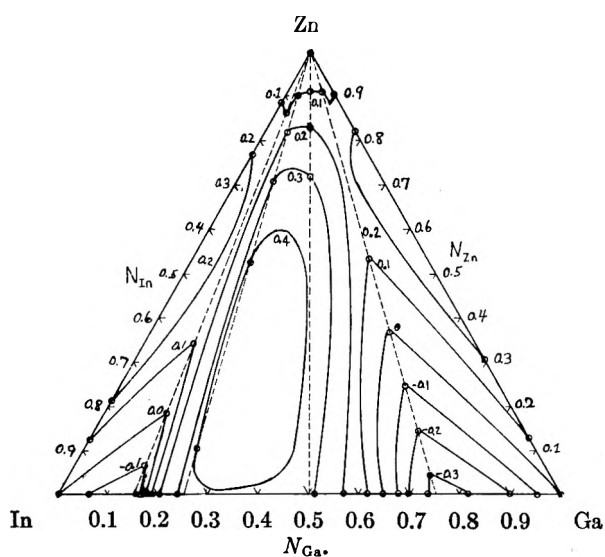


Fig. 9.—Excess integral entropy of mixing per mole of solution surface in 0.1-e.u. steps at 470°.

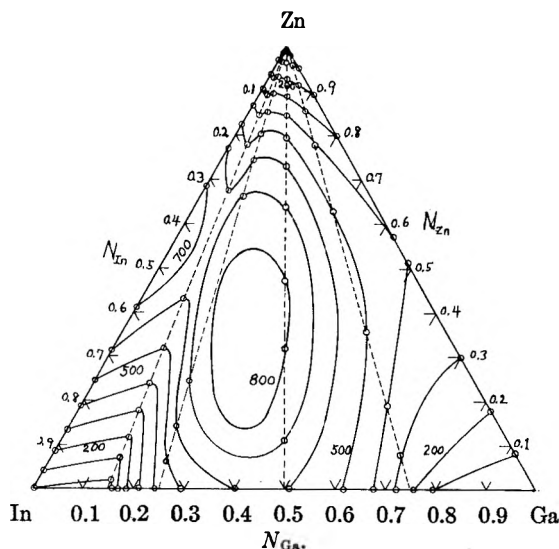


Fig. 8.—Integral heat of mixing per mole of solution surface in 100-cal. steps at 470°.

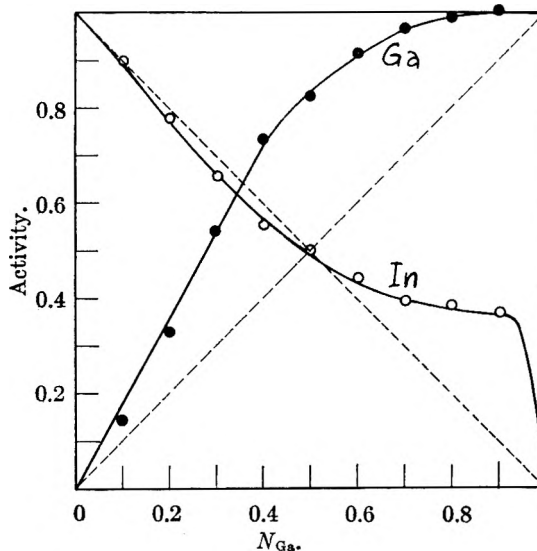


Fig. 10.—Activities of gallium and indium.

values. The final results also are shown on Fig. 4 and 5.

$$G^x = N_1\bar{G}_1^x + N_2\bar{G}_2^x \quad (14)$$

In the calculation of the excess thermodynamic properties of the gallium-indium binary system from the ternary data, use is made of eq. 9. The gallium-indium (binary 1-3 system) may be considered as the limiting case of the ternary 1-2-3 system in which  $N_2 = 0$ . Thus eq. 9 becomes eq. 15.

$$G_{1-3}^x = \left[ \int_1^0 \frac{\bar{G}_2^x}{(1-N_2)^2} dN_2 \right]_{N_1/N_3} + N_1[\bar{G}_1^x]_{N_2=1} + N_3[\bar{G}_3^x]_{N_2=1} \quad (15)$$

The binary constants remain the same as before, but  $N_1$  and  $N_3$  are the mole fraction values for the binary 1-3 system. The first term on the right is now the total area under the curve for a definite  $N_1/N_3$  ratio ternary system of plots of the type shown in Fig. 2 and 3. The values of the excess integral molal free energy of solution, heat of

solution, and excess entropy of solution for the gallium-indium binary system are plotted vs.  $N_{Ga}$  on Fig. 6.

Values of  $\Delta F^x$  and  $\Delta H^x$  in 100-cal. steps were picked from their respective curves and values of  $\Delta S^x$  in 0.1-e.u. steps were picked from similar plots. All such data are plotted in Fig. 7, 8, and 9. These ternary molal surface plots represent the excess integral thermodynamic properties of mixing per mole of solution for the zinc-indium-gallium ternary system at 470°. The values of the excess properties may be obtained at any composition by interpolation of the data shown on these triangular plots.

In the calculation of the excess partial properties of gallium and indium in the gallium-indium binary system, use was made of the plots shown on Fig. 6 for the excess molal solution properties. Tangents were drawn to the curves at 0.1 mole fraction intervals. The extension of these tangents to give intercepts on the  $N_{Ga} = 1$  and  $N_{In} = 1$  axes yields the values of the excess partial molal properties

of gallium and indium, respectively, in the binary solution of the selected concentration at the point of tangency. The application of eq. 6 to the  $\Delta\bar{F}_1^x$  values yielded the corresponding  $\alpha_1$  values which in turn yielded the activities of gallium and indium in the gallium-indium binary system. These final results are shown graphically in Fig. 10.

#### Discussion

**The Method.**—The functions plotted as ordinates in Fig. 2 and 3 are very sensitive to experimental error, particularly as  $N_{Zn} \rightarrow 1$ . Reference to Table I shows that at  $N_{Zn} = 0.9$ , the e.m.f. of all systems was between 2 and 3 mv. Since we believed that data obtained in the  $N_{Zn}$  region of 0.9 to 1.0 would lead to unreliable calculations for these functions and consequently influence the drawing of the whole curve, experimental data were not gathered in that region. Consequently, the extrapolation of these curves to  $N_{Zn} = 1.0$  must be based on the available data. Since the required area under the curves are from  $N_{Zn} = 1.0$ , it follows that such areas must be subject to some uncertainty. Chipman and Elliott<sup>2</sup> were able to check the reliability of the extrapolation method by ultimately calculating values of  $\Delta F^x$  and  $\Delta H^x$  for the lead-bismuth binary from measurements made on the cadmium-lead-bismuth ternary and comparing the predicted results with experimentally determined values. Their results for two different binary compositions indicated deviations between 5 and 7% for  $\Delta F^x$  and  $\Delta H^x$ , respectively. The agreement was considered excellent. Assuming that our derived results are no worse than those of Chipman and Elliott, the values of  $\Delta F^x$  and  $\Delta H^x$  shown on Fig. 6 would be in error by 5 and 7%. In the determination of the intercepts of the tangents to the curves, a very large difference in any intercept could result from just a small change in the shape of the curve. Thus no more than a semi-quantitative claim is made for the derived values of the activities of gallium and indium which are shown graphically in Fig. 10.

**Activities.**—Reference to Fig. 1 shows that the zinc-indium system, the zinc-gallium system, and all of the ternary systems exhibit positive deviations from Raoult's law for zinc over the entire concentration range with the largest deviation being exhibited by the zinc-indium binary system. Raoult's law is approached in each case as the solution composition approaches pure zinc. Furthermore, the zinc activity in the ternary system shows more positive deviation as  $N_{In}$  becomes greater in proportion to  $N_{Ga}$  in the pseudobinary systems.

**Isothermal Surfaces.**—The excess molal free energy surface (Fig. 7) and the molal heat of solution surface (Fig. 8) show positive values at all compositions. The excess molal entropy of solution surface (Fig. 9) shows mostly positive values.

**Other Comments.**—Reference to Fig. 5 shows that in the two different binary systems the maxima in the heats of mixing curves are displaced toward the side of the smaller atom,<sup>11</sup> *i.e.*, zinc. In Fig. 6 there are insufficient points to draw the curve for the gallium-indium binary system accurately enough to locate its maximum precisely and no claim is made by us concerning the position of the maximum.

Differences in the characteristic valences of the components of a mixture have been correlated approximately with the excess entropies of mixing in alloys of cadmium with indium, gallium, tin, thallium, lead, and bismuth.<sup>12</sup> In the cadmium-rich range, the solutes of higher valence than the solvent, cadmium, produce positive excess entropies of solution. For solutions of metals with lower valences than cadmium the excess entropies are negative. Referring now to our results, both indium and gallium have a characteristic valence of +3, while that of zinc is +2. Thus, contributions to the excess entropy of mixing should be positive in the zinc-rich range of composition. We find (Fig. 9) positive excess entropies of mixing in the zinc-indium and zinc-gallium binary systems.

Differences in space requirements have been observed to contribute to the large positive values of the excess entropy of mixing in the gold-lead system.<sup>13</sup> Packing problems originate<sup>14</sup> from the mixing of atoms with large differences in size and cause large positive excess entropies of mixing. The atomic volumes of zinc, indium, and gallium are 9.2, 15.7, and 11.8 cm.<sup>3</sup>, respectively. Differences in space requirements of each component of a mixture could cause the positive excess entropies of mixing which occur over most of the composition range.

**Acknowledgments.**—The financial support of the Research Corporation for materials and for the granting of the Frederick Gardner Cottrell Fellowship for the years 1957 to 1959 and of the Union Carbide Chemical Company for the granting of a fellowship from 1959 to 1960 to S. M. R. was greatly appreciated.

(11) O. J. Kleppa, *J. Am. Chem. Soc.*, **73**, 383 (1951).

(12) O. J. Kleppa, *Acta Met.*, **6**, 233 (1958).

(13) O. J. Kleppa, *J. Am. Chem. Soc.*, **71**, 3275 (1949).

(14) O. J. Kleppa, *ibid.*, **73**, 385 (1951).



# STUDIES OF THE THIONINE-FERROUS IRON REACTION IN A HETEROGENEOUS SYSTEM

BY K. G. MATHAI AND E. RABINOWITCH

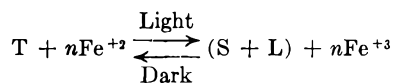
From the Photosynthesis Laboratory, Department of Botany, University of Illinois, Urbana, Ill.

Received July 28, 1961

The reversible photochemical oxidation-reduction reaction in the thionine-ferrous iron system can be made irreversible by the removal of the reduction products of thionine from the reaction mixture. One method is to distribute the products between immiscible solvents. The purple-colored thionine dye is insoluble in ether; but its reduction products are soluble. Since ferric ions also are insoluble in ether, the two products of the reaction can be separated by extraction with ether during the illumination; some stored light energy thus can be preserved. The ether extract containing the reduction products of thionine can be caused to form a homogeneous mixture with the mother liquor by adding methyl alcohol; the back reaction will then come to completion. A galvanic cell using stored light energy can be made by placing the ether extract (with some methyl alcohol added for increased conductivity) in one compartment and the aqueous mother liquor in the other, and connecting the two compartments with an agar bridge. Potential differences of 0.2434 to 0.3585 volt were measured in this cell, depending on the concentration of the reaction products. Another method of preventing the back reaction is to precipitate ferric ions, *e.g.*, by acetate. However, in this case the reaction cannot be reversed, and thus no direct proof of energy storage can be given. The relevance of these observations to the problem of energy storage in photosynthesis is discussed.

## Introduction

The photochemical oxidation-reduction system



where T is the purple-colored cation of thionine and S and L its colorless reduced forms (semithionine and leukothionine, respectively) was discovered by Weber,<sup>1</sup> and Weiss<sup>2</sup>; its kinetics were investigated by Rabinowitch,<sup>3</sup> Schlag,<sup>4</sup> Hardwick,<sup>5</sup> Ainsworth,<sup>6</sup> and others. Rabinowitch<sup>7</sup> also has investigated the photogalvanic effect in the thionine-iron system, under different conditions, including variations in the concentration of thionine, of ferrous and ferric ions, and of the pH. The present work is a continuation of these studies, using a heterogeneous system to stabilize the reaction products.

## Experimental

**A. Thionine-Iron Reaction in a Water-Ether System.**—Thionine (biological stain, National Aniline and Chemical Co., Inc.) was purified by repeated recrystallization, and the purity of the sample checked by spectroscopy. Ferrous sulfate (Analar reagent grade), methyl alcohol (analytical reagent grade 99.7% pure), and anhydrous ether (analytical reagent grade 99.5% pure) were used without further purification, as well as the "99.99% pure" Linde nitrogen gas.

Solutions of thionine and ferrous sulfate were prepared in deaerated, twice distilled water. Ether, methyl alcohol, thionine solution, and ferrous sulfate solution were stored in tonometers under nitrogen atmosphere. Samples to be bleached were prepared by transferring suitable aliquots of the stock solution into a glass cell (a cylindrical glass vessel with optically flat ends 5 cm. long and 3 cm. in diameter). One volume of ether was added to two volumes of the aqueous thionine-ferrous iron solution. The photolytic cell was placed in a bath through which water from a thermostat was circulated. The sample was stirred throughout the experiment by a stream of nitrogen. Actinic light (white light from a 1000-watt projection lamp) was passed through a heat filter and a 12-cm. condensing lens. The parallel beam fell on the flat end of the reaction cell and illuminated its surface uniformly. The optical density of aqueous solution at 600  $m\mu$ —the peak of the thionine absorption band—was measured every five minutes with a Beckman spectro-

photometer. For this measurement, the nitrogen stream was slowed enough to allow the ether layer to separate from the aqueous layer; a 4-ml. sample of the latter was taken by a syringe and transferred into the Beckman cuvette. It was returned into the reaction vessel after the measurement. The optical density decreased with time of exposure, but reached an almost constant value within half an hour. In the absence of ether, the photostationary state in the thionine-iron system is reached in less than a minute, but in the presence of ether this steady state is gradually changed by the extraction of reduced thionine into the ether phase, until a new stationary state is reached, in which the rate of extraction is balanced by the rate of diffusion of reduced thionine back into the aqueous phase. In this final state, the aqueous phase always remained slightly purple under the conditions of our experiments.

TABLE I  
BLEACHING OF THIONINE BY FERROUS IONS IN AN  
ETHER-WATER EMULSION

Expt.	Concn. of the reagent	Time of exposure, min.	Optical density	Potential diff.
1	$1 \times 10^{-5} M$ thionine	0.0	0.56	0.2634
		$5 \times 10^{-3} M$ ferrous sulfate	5.0	
	50 ml. of the above soln. + 25 ml. of ether	10	.22	
		15	.20	
	pH = 3.83	20	.19	
		25	.18	
		30	.17	
	returned to darkness	.55		
2	$2 \times 10^{-5} M$ thionine	0.0	1.13	0.3126
		$5 \times 10^{-3} M$ ferrous sulfate	5.0	
	50 ml. of the above soln. + 25 ml. of ether	10.0	.51	
		15.0	.39	
	pH = 3.75	20.0	.33	
		25.0	.31	
		30.0	.30	
	returned to darkness	1.08		
3	$3 \times 10^{-5} M$ thionine	0.0	1.70	0.3585
		$5 \times 10^{-3} M$ ferrous sulfate	5.0	
	50 ml. of the above soln. + 25 ml. of ether	10.0	0.83	
		15.0	0.62	
	pH = 3.75	20.0	0.52	
		25.0	0.49	
		30.0	0.47	
	returned to darkness	1.68		

- (1) K. Weber, *Z. physik. Chem.*, **B15**, 18 (1931).
- (2) J. Weiss, *Nature*, **136**, 794 (1935).
- (3) E. Rabinowitch, *J. Chem. Phys.*, **8**, 551 (1940).
- (4) J. Schlag, *Z. physik. Chem.*, (Frankfurt), **20**, 553 (1959).
- (5) R. Hardwick, *J. Am. Chem. Soc.*, **80**, 5667 (1958).
- (6) S. Ainsworth, *J. Phys. Chem.*, **64**, 715 (1960).
- (7) E. Rabinowitch, *J. Chem. Phys.*, **8**, 560 (1940).

At the end of each run in Table I, 20 ml. of the mother liquor was transferred into one half-cell of a galvanic cell, and 10 ml. of the ether extract plus 10 ml. of methyl alcohol were placed into the other half-cell. Bright platinum electrodes were used. The two half-cells were connected by an agar bridge<sup>8</sup> and the potential difference was measured.

After every experiment, the contents of the two compartments were mixed and the optical density of the mixture measured. This measurement showed that practically no thionine was lost in the cycle.

**B. Separation of the Reaction Products by Precipitation of Ferric Ions.**—Isolation of the reduction products of thionine by extraction with ether, reported in part A, was never complete under the conditions of our experiments, because reduced thionine drifted back into the aqueous solution.

A complete separation of the products of the thionine-ferrous iron reaction can be achieved by precipitation of the ferric ions, *e.g.*, with sodium acetate solution. In these experiments, thionine and ferrous sulfate were used in a molar ratio of 1:2 and a slight excess of sodium acetate was added to the reaction mixture. When the mixture was illuminated (under a nitrogen atmosphere), ferric acetate settled at the bottom of the reaction vessel. The clear colorless solution should be preserved under nitrogen atmosphere. The precipitate was analyzed and found to be ferric acetate.

When an aliquot of the supernatant was exposed to atmospheric oxygen, the purple color of thionine re-appeared in a few seconds. Another portion of the solution was treated with hydrogen peroxide. Here, too, the purple color of thionine returned immediately, 10 ml. of the same solution was treated with 2 ml. of ether and the ether layer separated from the aqueous layer. The latter did not become colored upon exposure to air, showing that practically all reduced thionine had been extracted into ether. The ether layer became pink in the presence of air. Addition of water to the aerated ether solution produced a dark purple color. These experiments confirm that the reduction products of thionine are highly soluble in ether.

To another portion of the colorless supernatant, some aqueous ferric chloride solution was added; the pink color of thionine re-appeared but disappeared again after exposure to light. This, too, suggests a very efficient removal of reduced thionine from the aqueous into the ether phase; at the low concentration of ferrous ions present in this experiment (only  $\text{Fe}^{2+}$  resulting from the reduction of  $\text{Fe}^{3+}$  by reduced thionine), bleaching in light would be unobservable in a homogeneous aqueous system; but extraction of the reduced dye into ether slows the back reaction so strongly that bleaching becomes apparent even when the forward photochemical reaction is very slow (because of the low concentration of ferrous ions).

### Discussion

The results summarized in Table I clearly prove that photochemical energy is stored—and can be preserved indefinitely—when the thionine-ferrous ion reaction is carried out in the water-ether system. Some free energy is, of course, lost in the extraction of the reduction products into ether (as well as in the process of stirring and in the mixing of ether and water by the addition of methanol); but the fact that the back reaction proceeds spontaneously after the mixing shows that a considerable fraction of the photochemical energy has been stored. The efficiency of the process remains to be determined; it is likely to depend on the rate of stirring, on temperature, and the concentration of the reagents.

Photosynthesis in plants is an important example of the storage of light energy in the form of potential chemical energy. Photochemical storage of energy had not been successfully achieved in

non-biological systems. It has been suggested that the difficulty lies not in finding a primary photochemical process, which would convert light into chemical energy, but in the prevention of back reactions which dissipate this energy. The above findings suggest how energy-rich products of an oxidation-reduction reaction can be separated and stored in a two-phase system. The key to the high efficiency of photosynthesis may lie in a similar separation of the primary oxidation and reduction products between two immiscible phases—for example, between a hydrophilic and a hydrophobic layer on two sides of a pigment monolayer (Rabinowitch<sup>9</sup>) or a bimolecular layer.<sup>10</sup>

The photogalvanic effect is a kind of Becquerel effect, in which the influence of light on the electrode potential results from a photochemical process in the body of the electrolyte (rather than on the surface of the electrode, as in the "photovoltaic" effect). The homogeneous thionine-ferrous iron system has a strong photogalvanic sensitivity. The "light potential"  $\Delta\epsilon = \epsilon^* - \epsilon$  (where  $\epsilon^*$  is the potential of the illuminated electrode and  $\epsilon$  that of a similar electrode in the dark) is always negative; *i.e.*, the illuminated half-cell always is negative in respect to the non-illuminated half-cell.

It seems that the light potential is determined primarily by the shift of the ratio [thionine]/[reduced thionine] in light, and less strongly affected by the shift in  $[\text{Fe}^{3+}]/[\text{Fe}^{2+}]$  (the first shift must lead to the illuminated half-cell becoming more negative, the second to it becoming more positive). In the heterogeneous system, the half-cell which contains the reduction products of thionine becomes negative in respect to the half-cell which contains the oxidation product of ferrous iron; in this case, the two component systems,  $[\text{Fe}^{2+}]/[\text{Fe}^{3+}]$  and [thionine]/[reduced thionine] tend to affect the potential in the same direction, making the aqueous half-cell more positive and the ether-methanol half-cell more negative.

From Table I, it is evident that the negative potential difference observed in the heterogeneous system increased with concentration of reduced thionine in the ether phase.

The photogalvanic potential of the heterogeneous system is another evidence of the storage of photochemical energy. However, the capacity of this system is likely to be small, since an attempt to take out current from it will cause rapid polarization, which could be relieved only by continuous mixing of the cathodic and anodic solutions.

The observations described in part B confirm the high efficiency with which the reduction products of thionine are extracted from the aqueous into the ether phase.

(9) E. Rabinowitch, *Discussions Faraday Soc.*, **27**, 161 (1959).

(10) E. Rabinowitch, paper presented at the 1962 Biophysical Society Meeting at Washington, D. C.

(8) L. Michaelis, M. P. Schubert, and S. Granick, *J. Am. Chem. Soc.*, **62**, 1802 (1940).

# KINETICS OF SOLUTION IN HIGH VISCOSITY LIQUIDS: SODIUM CHLORIDE-GLYCEROL

By A. R. COOPER, JR., AND W. D. KINGERY

*Ceramics Division, Department of Metallurgy, Massachusetts Institute of Technology, Cambridge 39, Massachusetts*

*Received August 21, 1961*

Dissolution of sodium chloride crystals in glycerol measured by forced convection (rotating disc) and free convection (stationary cylinder) experiments revealed that the rate was controlled by diffusion in the liquid for all cases from 10 to 50° and 0 to 5400 r.p.m. Experiments at the highest viscosity revealed that boundary layer analyses are satisfactory even when the calculated velocity boundary layer thickness greatly exceeds a characteristic dimension in the system. Diffusivity and viscosity vary with concentration in this system and correction factors to account for these variations were developed to modify solution rate expressions for constant properties. At the lowest temperature (11°) a selective solution process occurred. Development of the (100) and (110) faces on the originally cylindrical surfaces indicates that dissolution took place most slowly in directions normal to these planes.

## Introduction

The Noyes-Nernst<sup>1,2</sup> equation describing dissolution kinetics controlled by diffusion in the liquid has been found to apply in a wide variety of experimental conditions.<sup>3</sup> In terms of the flux density of solute entering the solvent,  $j$ , it states

$$j = -D \left( \frac{dC}{dy} \right)_0 = D \frac{\Delta C}{\delta_c^*} \quad (1)$$

The symbols have their usual meaning with the concentration differential,  $\Delta C = C_0 - C_\infty$ , representing the difference between interface and bulk concentration. When the concentration is given in units of fractional volume (volume pure solid/volume solution), the flux density is measured by the velocity of disappearance of a solute slab. The effective boundary layer thickness,  $\delta_c^*$ , is defined by the second half of eq. 1.

Motion in the fluid has an effect on  $\delta$  that has been analyzed in simple geometries with good agreement to experimental results.<sup>4</sup> The analyses depend on the assumption that the velocity boundary region,  $\delta_u$ , in which the motion in the system is affected by the presence of the solute is small in comparison to other experimental dimensions. In liquids of high viscosity this condition often is not satisfied, and there has been some doubt as to the appropriateness of using relations derived from boundary layer theory to predict diffusion controlled solution rates in viscous systems.

To examine this question, solution kinetics in the sodium chloride-glycerol system were studied. The effect on solution kinetics of a variation of viscosity and diffusivity with composition in the boundary layer proved an additional point of interest. Also, these studies with high viscosity liquids have a direct application to the solution of refractories in molten silicates at high temperatures.<sup>5</sup>

**Analysis. Forced Convection.**—A convenient method for causing a well described forced convec-

tion pattern about a dissolving sample is to rotate a disc face in the solvent. Cochran<sup>6</sup> has described the flow about a disc rotating at  $\omega$  radians/second

$$\delta_u \approx 4.0 (\nu/\omega)^{1/2} \quad (2)$$

Using Cochran's solution, Levich<sup>7</sup> has determined that the effective boundary layer thickness for transport to a rotating disc is

$$\delta_c^* = 1.611 (D/\nu)^{1/2} (\nu/\omega)^{1/2} \approx 0.4 (D/\nu)^{1/2} \delta_u \quad (3)$$

and others including Gregory and Riddiford<sup>8</sup> have confirmed this relation experimentally.

For the case where the diffusion coefficient varies with concentration, an appropriate weighted average diffusion coefficient,  $D^*$ , must be substituted in eq. 3. For unsteady state diffusion, a satisfactory value for  $D^*$  suggested by Phillip<sup>9</sup> is

$$D^* = \frac{1}{(\Delta C)^2} \int_{C_\infty}^{C_0} D(C - C_\infty) dC \quad (4)$$

As concentration distributions do not differ greatly in the forced convection and transient cases, eq. 3 will be used to determine  $D^*$ .

Viscosity variations seldom have been accounted for in boundary layer equations. The introduction of a variable viscosity in the Cochran-Levich solution is beyond the scope of this paper. It is, however, possible to introduce directly the complications of variable viscosity into the analogous but simpler case of flow over a flat plate. When this was done<sup>10</sup> for the case of viscous liquids where  $\delta_c \ll \delta_v$  it was found that the velocity boundary layer thickness was governed by the value for the bulk viscosity,  $\nu_\infty$ . This is not surprising since only a small fraction of the velocity boundary layer has variable viscosity. Thus, it is appropriate to use  $\nu_\infty$  in eq. 2. On the other hand, the viscosity value used in the Schmidt number ( $D/\nu$ ) does need to be modified to take into account the variation of viscosity and flow behavior in the immediate vicinity of the interface. The value of an effective viscosity,  $\nu^*$ , to compensate for this variation in the case of the flat plate is given by<sup>10</sup>

(1) A. A. Noyes and W. R. Whitney, *Z. physik. Chem.*, **23**, 689 (1897).

(2) W. Nernst, *ibid.*, **47**, 52 (1904).

(3) E. A. Moelwyn-Hughes, "The Kinetics of Reactions in Solution," Chapter 12, Clarendon Press, Oxford, 1947.

(4) L. L. Bircumshaw and A. C. Riddiford, *Quart. Revs.* (London), **6**, 157 (1952).

(5) A. R. Cooper, Jr., and W. D. Kingery, "Corrosion of Refractories by Liquid Slags and Glasses," a chapter in "Kinetics of High Temperature Processes," W. D. Kingery, Ed., John Wiley and Sons, Inc., New York, N. Y., 1959.

(6) W. G. Cochran, *Proc. Cambridge Phil. Soc.*, **30**, 365 (1934).

(7) B. Levich, *Discussions Faraday Soc.*, **1**, 37 (1947).

(8) G. G. Gregory and A. C. Riddiford, *J. Chem. Soc.*, 3756 (1956).

(9) J. R. Phillip, *Trans. Faraday Soc.*, **51**, 885 (1955).

(10) A. R. Cooper, Jr., Sc.D. Thesis, "Kinetics of Refractory Solution," Department of Metallurgy, M.I.T., 1960.

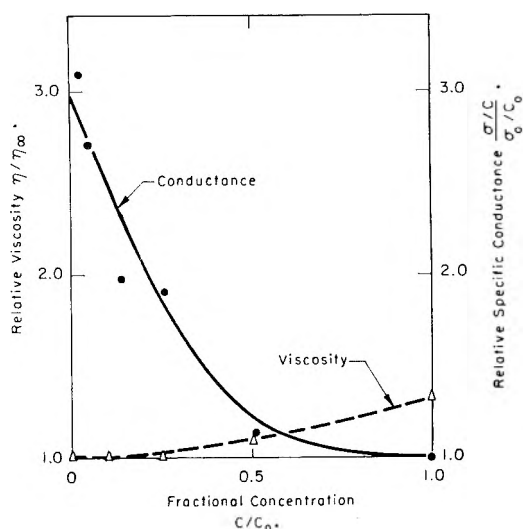


Fig. 1.—Dependence of specific conductance and viscosity on sodium chloride concentration.

$$\nu^* = \nu_{\infty}^2 \frac{\int_0^{\delta_c} (C_0 - C) \int \frac{1}{\nu} dy dy}{\int_0^{\delta_c} (C_0 - C) y dy} \quad (5)$$

Assuming that this effective viscosity  $\nu^*$  also is appropriate for the case of the rotating disc, eq. 3 and 1 give for the dissolution flux density of a rotating disc

$$j = 0.621 D_0 (\nu^*/D^*)^{1/3} (\omega/\nu_{\infty})^{1/2} \Delta C \quad (6)$$

For forced convection flow along a flat plate, boundary layer treatment leads to a similar relation<sup>11</sup> which is, after introducing the effective viscosity,  $\nu^*$ , and diffusivity,  $D^*$

$$j = 0.35 D_0 (\nu^*/D^*)^{1/3} (u_{\infty}/\nu_{\infty})^{1/2} \Delta C \quad (7)$$

where  $u_{\infty}$  is the bulk velocity and  $l$  is the distance from the leading edge of the plate. Equations 6 and 7 reveal two tests of diffusion control of solution; the solution rate of a rotating disc face is proportional to the square root of angular velocity and the solution rate of a plane plate in a flowing stream is inversely proportional to the square root of the distance from the leading edge.

**Free Convection.**—Analyses of free convection heat and mass transfer at vertical plane surfaces have been achieved by boundary layer approximations<sup>11</sup> and confirmed in recent experimental studies.<sup>12</sup> A cylindrical surface has the advantage of eliminating the edge effects that are present on narrow plates. Ellenbaas<sup>13</sup> has modified the flat plate free convection heat transfer solution to be appropriate for a cylindrical surface of radius  $r$  by adding an exponential term giving

$$\delta_c^* = 1.96 \left( \frac{D_0 \nu_0 l}{g \Delta \rho} \right)^{1/4} \exp \frac{2\delta_c^*}{2r + 1/2\delta_c^*} \quad (8)$$

where  $g$  is gravitational acceleration, and  $\Delta \rho = (\rho_0 - \rho_{\infty})/\rho_{\infty}$  is the fractional density difference between the saturated and bulk solution. Note

(11) E. Eckert, "Introduction to the Transfer of Heat and Mass," McGraw-Hill Book Co., New York, N. Y., 1950.

(12) (a) Y. S. Touloukian, G. A. Hawkins, and M. Jakob, *Trans. ASME*, **70**, 13 (1948); (b) C. Wagner, *J. Phys. Colloid Chem.*, **53**, 1030 (1949).

(13) W. Ellenbaas, *Phillips Res. Rept.*, **3**, 338 (1948); *J. Appl. Phys.*, **19**, 1148 (1948).

that eq. 8 for free convection follows Ellenbaas directly and does not use weighted average property values in determining the boundary layer thickness.

If we label the exponential correction term  $\lambda$ , and substitute in eq. 1, the solution rate is given by

$$j = 0.501 \lambda^{-1} D_0^{3/4} \left( \frac{g \Delta \rho}{l \nu_0} \right)^{1/4} \Delta C \quad (9)$$

Although the exponential term  $\lambda$  varies with the diameter, and hence with time, this effect is unimportant as long as the boundary layer thickness remains small in comparison to the diameter. Variation of the solution rate with the inverse quarter power of the distance from leading edge provides a simple test of diffusion control in free convection.

**Property Values.**—The solubility of sodium chloride in glycerol,  $\Delta C$ , is 0.044 cc./cc. ( $1.67 \times 10^{-3}$  mole/cc.) at 25°,<sup>14</sup> and the fractional increase in density of a saturated solution compared to pure glycerine,  $\Delta \rho$ , is 0.029 at 25°. The solubility is nearly constant from 20–25°, and experiments extending the range to –10° to –50° showed only a 2% change in solubility. The variation of glycerine density with temperature is well established.<sup>16</sup> The variation of the difference in density between the saturated and bulk solution with temperature,  $(d\Delta\rho/dT)$ , is not known, but with the relatively constant solubility of sodium chloride in glycerol, it seems reasonable to assume that this variation is slight. The 25° values for solubility and fractional density difference are used in this work and assumed to be independent of temperature.

The dynamic viscosity,  $\eta$ , of glycerol has been measured<sup>17</sup> over a wide range of temperature. At 0° it has a viscosity about 5,000 times greater than water, suggesting that velocity boundary layer thickness some 70 times greater than customarily obtained in aqueous solution experiments would be achieved. Wolkowa<sup>18</sup> found the diffusivity of sodium chloride in water-glycerol solutions between 15 and 30° to be inversely related to dynamic viscosity of pure glycerol; *i.e.*,  $D\eta = 6.5 \times 10^{-7}$ . It is assumed that this dependence can be extended from 10 to 50°.

Davis and Jones<sup>19</sup> reported that most cations, including sodium, increase the viscosity of glycerol. To confirm this result, we have made measurements of electrical conductivity,  $\sigma$ , and dynamic viscosity,  $\eta$ , at room temperature and corrected to 25°. The validity of the Nernst-Einstein relation was assumed; so that

$$\frac{\sigma/C}{\sigma_0/C_0} = \frac{D}{D_0}$$

Figure 1 shows the variation of diffusivity and viscosity with concentration obtained from our measurements and calculations. From these re-

(14) W. Hertz and M. Enoch, *Z. anorg. u. allgem. Chem.*, **45**, 267 (1905).

(15) "International Critical Tables," McGraw-Hill Book Co., New York, N. Y., 1928, Vol. III, p. 28.

(16) K. Holm, *Amer. J. Pharm.*, **94**, 139 (1922).

(17) M. L. Sheeley, *Ind. Eng. Chem.*, **24**, 1060 (1932).

(18) Z. V. Wolkowa, *Z. physik. Chem.*, **145**, 200 (1929); **147**, 206 (1930).

(19) P. B. Davis and H. C. Jones, *ibid.*, **81**, 68 (1912).

sults and graphical integration of eq. 4 and 5, factors to account for changes in properties with concentration were determined

$$\begin{aligned} \alpha &= D_0/D_\infty = 0.33 & \gamma &= \nu_0/\nu_\infty = 1.32 \\ \beta &= D^*/D_\infty = 0.65 & \epsilon &= \nu^*/\nu_\infty = 0.85 \end{aligned}$$

These ratios are presumed to be independent of temperature. Along with Wolkowa's relationship between diffusivity and viscosity of pure glycerol, the solubility data, these coefficients permit eq. 6 for forced convection to be rewritten for a disc rotating at 1200 r.p.m. ( $\omega = 124$ )

$$j = 2.3\alpha(\epsilon/\beta)^{1/3} \eta_\infty^{-5/6} \rho_\infty^{1/6} \times 10^{-6} \quad (10)$$

Since  $\beta$  and  $\epsilon$  tend to compensate for each other and their quotient is raised to the  $1/3$  power, the major influence of variable properties in the ratio of diffusion coefficients,  $\alpha = \bar{D}_0/D_\infty$ .

Substituting appropriate coefficients and property values into the free convection expression, eq. 9 at a distance 0.1 cm. below the leading edge yields

$$j = 1.9\lambda^{-1} \frac{\alpha^{3/4}}{\gamma^{1/4}} \eta_\infty^{-1} \rho^{1/4} \times 10^{-6} \quad (11)$$

The major influence from variable properties again occurs in the ratio,  $\alpha$ .

### Experimental Arrangements

Mallinckrodt reagent grade glycerol was used as the solvent. Viscosity measurements using a Brookfield Model RVF viscosimeter revealed a viscosity about 10% lower than values previously reported for pure glycerol—probably due to moisture pickup of about 0.5%. The log viscosity bore a linear relationship with temperature over the entire 10 to 50° range. Measured values of glycerol viscosity were interpolated as necessary and used in subsequent calculations.

Cylindrical sodium chloride single crystals (diameter 0.290 in.) obtained from Harshaw Chemical Company were sliced to length (0.5 in.) and machined to give a plane disc surface. A centrally located hole was drilled permitting the samples to be cemented to a steel shaft.

The glycerol was contained in a covered cylindrical brass vessel 7.5 cm. in diameter with depth of glycerol typically about 6.5 cm. The brass vessel was placed in a covered battery jar. Evaporation coils from a refrigerator unit and a simple heating element permitted the temperature to be varied from 0 to 60°; thermostats in the bell jar controlled the temperature. The temperature of the glycerol was uniform within 0.1°, and was controlled over long periods within  $\pm 0.5^\circ$ .

The sodium chloride samples were introduced into the glycerol through a set of bearings that permitted sample rotation by a constant speed motor at velocities up to 5400 r.p.m. All leads and connections to the battery jar were air-tight, and it contained several pounds of anhydrous calcium sulfate grains to keep humidity low.

Corrosion rates were determined from change in length in forced convection experiments and change in diameter in free convection experiments. Length and diameter of the sodium chloride samples were measured before and after immersion in glycerol with a micrometer which permitted vernier readings to 0.0001 in. Other measurements and profile tracings were made with an optical comparator, but these did not yield as reproducible results as the micrometer.

Greater precision of measurement of the change in length can be attained when the upper disc face is kept above the glycerol in forced convection experiments. Reproducibility of readings was  $\pm 0.0002$  in. for change in diameter and length under these conditions. Therefore, forced convection experiments in which only small amounts of solution were anticipated were conducted with the upper disc face out of the glycerol.

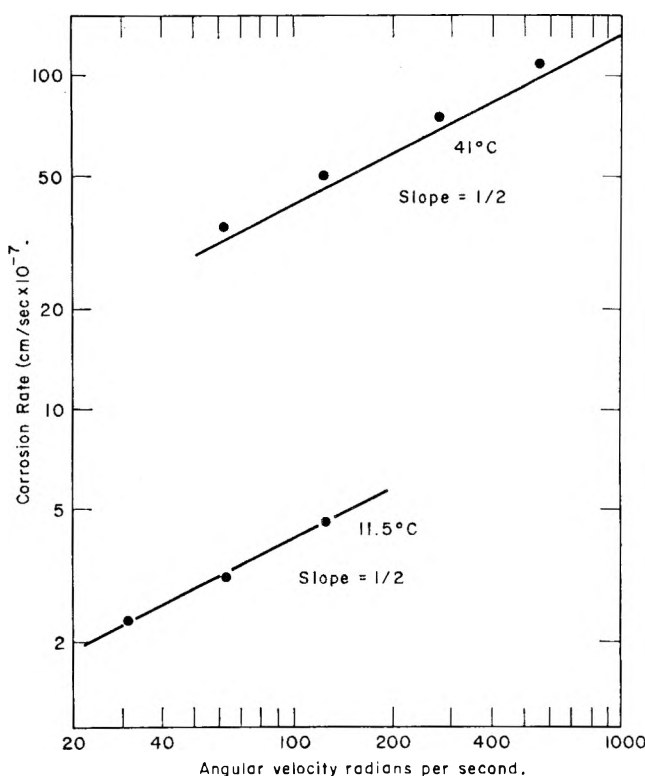


Fig. 2.—Dependence of log corrosion on log angular velocity at 11.5 and 41°.

### Results

**Effect of Experimental Variations.**—Two experiments to determine the effect of rotation eccentricity on transport to a rotating disc were made with sodium chloride samples totally immersed in glycerine. Results showed that for eccentricities up to 0.030 in., more than one-tenth the diameter, the effect of eccentricity at 41° and 1200 r.p.m. was insignificant. Changes in diameter of the container (made by inserting lengths of glass tubing) up to 1 cm. had no significant effect on corrosion rates.

When measurements of change in sample length were made after various times of corrosion, the initial rate always was significantly higher than the ultimate rate. This is believed to result from surface roughness of the disc face. Micrometer measurements read the upper peaks of this surface. Hence, there is less sodium chloride to be dissolved to obtain a given change in dimensions from a rough surface than would be the case if the surface were perfectly smooth. This premise is supported by observations that pock marks disappear from corroded surfaces at about the same time as the corrosion rate becomes stable. To account for this factor, the corrosion rate was determined by noting the difference in two readings after a steady state had been attained, or by requiring the total amount of corrosion to be in the vicinity of  $30 \times 10^{-3}$  cm. and subtracting  $2.5 \times 10^{-3}$  cm. as a correction for surface roughness.

Velocity boundary layers about 1.5 cm. thick are attained at 11° at 1200 r.p.m. Experiments were conducted in which glycerol was removed from the container following an experiment and the

succeeding sample positioned closer to the bottom of the container. In this way, the gap between the rotating disc face and the container bottom was reduced in four steps from 6.5 to 0.67 cm. The results corrected to 11.5° from temperatures between 10.7 and 11.6° revealed no significant change in corrosion rate. An increase of boundary layer thickness was attained at 0.7 cm. separation by reducing the speed of rotation to 600 and 300 r.p.m. The close dependence shown by the lower points of Fig. 2 of the corrosion rate on the square root of the angular velocity reveals that even when the velocity boundary layer is five times the distance between disc and container bottom, predictions from boundary layer theory based on diffusion control in the liquid remain useful for describing dissolution kinetics; this indicates that velocities immediately adjacent to a rotating disc are not substantially affected by the presence nearby of other surfaces.

**Forced Convection.**—A series of experiments was made at 41° in which the speed of rotation was changed in four steps from 600 to 5400 r.p.m. As shown by the upper points of Fig. 2, the dissolution rates of the disc face were proportional to the square root of angular velocity. This result, along with the results at 11°, gave confidence that diffusion control in the liquid boundary layer governs the dissolution rate over the entire temperature range.

The rates of dissolution from a disc face rotating at 1200 r.p.m. are summarized from 10 to 50° by the upper points of Fig. 3. Also shown are the predictions from eq. 10 with and without the correction factor associated with variable properties. The agreement between predicted and experimental results is reasonable, although the experimental data show a somewhat steeper temperature dependence than predicted. This may result from the fact that the velocity boundary layers produced at the sidewalls of the container interfere slightly with flow to the disc (the additional friction tending to decrease flow velocities). As temperature is reduced, these layers grow thicker and the interference is increased.

While the dissolution of the disc face is easier to measure and to analyze, interesting additional information is obtained by examination of the corrosion of the cylindrical surface. Totally immersed forced convection samples corrode most rapidly at the leading edge. Corrosion decreases gradually until a narrow region of abnormally low corrosion occurs about half way between the disc faces. It is believed that this band is caused by intersection of the flow streams from the top and bottom disc faces creating a region of virtual stagnation. Measurements of the corrosion rate of cylindrical surfaces agree well with the prediction of eq. 7; *i.e.*, corrosion rate is proportional to the inverse square root of distance from leading edge as shown by the upper points of Fig. 4, which also reveals the zone of abnormally low corrosion.

At 30° and above, the circular cylindrical surfaces persisted after corrosion; but in the vicinity of 10°, the samples developed eight facets along the originally cylindrical surfaces as the

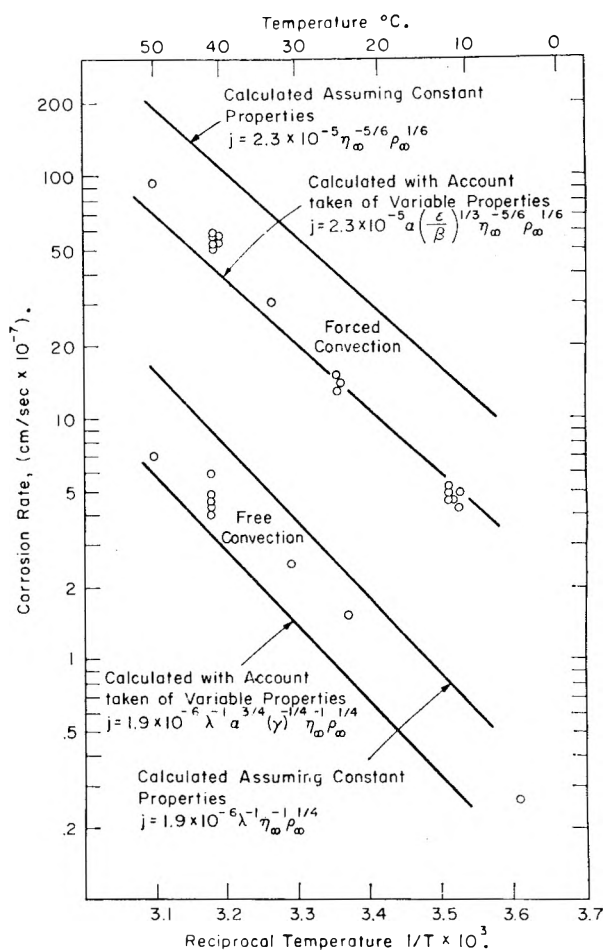


Fig. 3.—Effect of log distance from leading edge on log corrosion rate of sodium chloride cylinders in free and forced convection.

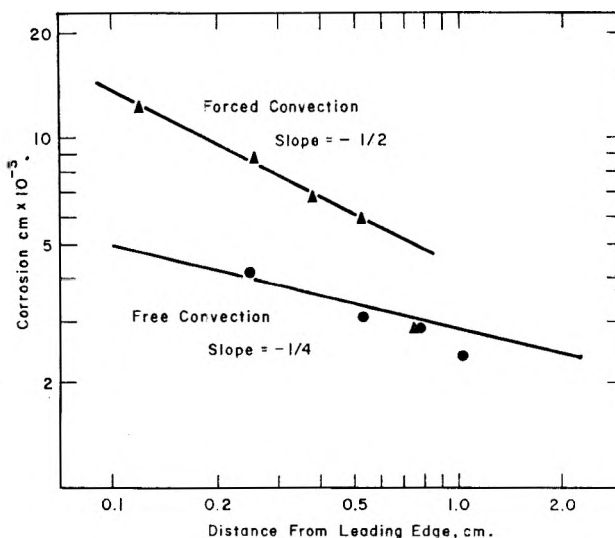


Fig. 4.—Dependence of free convection and free convection log corrosion rate of NaCl in glycerol on reciprocal temperature.

circular cross section transformed to an octagonal shape. Orientation of the faceted crystals with a Laue X-ray camera revealed that the facets where corrosion was lowest were (100) and (110) planes.

An additional second order effect was the appearance of screw markings on the cylindrical surfaces. A slight additional amount of corrosion occurred along a helix.

**Free Convection.**—Totally immersed samples and those with the liquid surface intersecting the sample showed a negligible difference in corrosion rate. Measurements of corrosion rate *vs.* distance from leading edge shown by lower points of Fig. 4 are proportional to the reciprocal fourth root of distance from the leading edge as predicted by eq. 9.

The data for solution rate 0.1 in. beneath the leading edge in free convection over the temperature range 0 to 50° are summarized in the lower half of Fig. 3, along with the results predicted by Ellenbaas's expression for free convection, eq. 11, with and without the correction factors. The experimental results show very nearly the predicted temperature dependence and are about midway between the predictions using bulk and interface property values.

The reasonable agreement of experimental results with those predicted and a lack of noticeable difference between partially and totally immersed samples indicates that buoyancy differences and not surface forces are the driving force for free convection in this system. The free convection corrosion rates are an order of magnitude lower than the rate of corrosion from a disc rotating at 1200 r.p.m. over the entire range of measurements.

### Conclusions

The geometry, time dependence, temperature dependence, and liquid velocity dependence of corrosion, and the agreement of experimental results with quantitative predictions all indicate that the kinetics of sodium chloride dissolving in glycerol are controlled by diffusion in the liquid. Relations derived from boundary layer theory for both free and forced convection adequately de-

scribe results over a 40° temperature range in this high viscosity liquid system. The presence of velocity boundary layers thick in comparison with experimental dimensions does not have an important effect on results.

Apparently the interface reaction occurs more slowly on the cube faces (010) and the face diagonal planes (011) than on the other available surfaces. With a rotating cylinder there is rapid convection transport in the tangential direction; this permits the selective solution process to occur even though radial diffusion limits the over-all rate of solution from the originally cylindrical surfaces. Free convection samples do not have this tangential convective transport and hence do not show any indication of selective solution. The development of (010) planes is consistent with the observation that the normal habit of rock salt is cubic, indicating that cube faces also are slowest growing during crystallization.

Typical experimental variations such as depth of immersion and eccentricity of rotation were shown to have only a slight effect on rates of solution.

Correction factors can be calculated to take into account variations in diffusivity and viscosity in the boundary layer. Better information regarding the concentration dependence of properties is required to further test these calculations, but it appears that agreement of calculated and experimental results is improved by using weighted average values of the properties rather than bulk or interface values alone.

**Acknowledgments.**—Appreciation is expressed to Michael Cable, who critically reviewed the manuscript, to Janis Kalnajs for the X-ray examination, and to the U. S. Atomic Energy Commission for sponsoring the research, which was conducted at M.I.T. under contract No. AT(30-1)-1852.

## THE DIELECTRIC CONSTANT AND CONDUCTANCE OF ION PAIRS; AN EXTENSION OF ONSAGER'S FIELD EFFECT TO RELAXATION OF ION PAIRS IN AN ALTERNATING FIELD<sup>1</sup>

By W. R. GILKERSON

*Department of Chemistry, University of South Carolina, Columbia, South Carolina*

*Received August 21, 1961*

Onsager's expression for the distribution function of ion pairs in an external field, in the form of a definite integral, has been solved and expressed as an infinite series, which reduces to the zero-field distribution and a term linear in the field for low field strengths. This result then is used to calculate the displacement current in the field direction in an alternating field, and equations for the resulting increase in dielectric constant and conductance as a function of frequency are derived. The resulting equations are compared to Pearson's, to the Debye-Falkenhagen equations, and to experimental results in the literature.

The distance of closest approach,  $a$ , is one of the principal parameters used to describe the behavior of ion pairs. One measure of this is the dipole moment of the ion pair.<sup>2-4</sup> The first thought

concerning the relation between the observed moment and the distance of closest approach is that it is  $ea$ , where  $e$  is the charge on either ion of a symmetrical electrolyte. It has been pointed

(1) This work has been supported in part by a grant from the U. S. Army Research Office, Durham, North Carolina.

(2) J. A. Geddes and C. A. Kraus, *Trans. Faraday Soc.*, **32**, 585 (1936).

(3) E. A. Richardson and K. H. Stern, *J. Am. Chem. Soc.*, **82**, 1296 (1960).

(4) W. R. Gilkerson and K. K. Srivastava, *J. Phys. Chem.*, **65**, 272 (1961).

out<sup>4</sup> that more realistic results are obtained if the effects of polarization are included in the equation for the moment.

Pearson has suggested<sup>5</sup> that the correct approach to the problem would be first to obtain an explicit solution for Onsager's distribution function of the ion pair system in an external electrical field,<sup>6</sup> and then to calculate the average moment of the pair using this distribution function. This is a report of results obtained as a consequence of Pearson's initial suggestion. The work actually went beyond the original intentions, leading naturally, it seems to the author, to the final results reported here.

Onsager gave the distribution function in the form of eq. 1

$$f(r, \vartheta) = n_1 n_2 r^{-1} \exp(2q/r + \beta r \cos \vartheta - \beta r) I \quad (1)$$

where

$$I = \int_0^{2q} J_0[(-8\beta s)^{1/2} \cos \vartheta/2] \exp(-s/r) ds$$

$n_1$  and  $n_2$  are the number of type 1 and 2 ions per cc.,  $r$  is the radial distance between the two ions,  $\vartheta$  is the angle between the line of centers and the direction of the external field,  $E_z$ , and  $J_0$  is the Bessel function of order zero. For the only case we consider here, that of symmetrical electrolytes, we also have  $2q = z^2 e^2 / \epsilon k T$ , and  $2\beta = zeE/kT$ . Note that the factor  $2q$  in eq. 1 is to be regarded as arising, not from Bjerrum's characteristic distance beyond which ions are no longer counted as pairs, but rather from Onsager's notation for expressing the reduced energy of interaction between two ions at a distance  $r$  as  $2q/r$ . The first part of the problem is to obtain an explicit solution for the integral  $I$ .

Let

$$z = [(-8\beta s)^{1/2} \cos \vartheta/2] = (\alpha s)^{1/2}$$

Then

$$I = 2\alpha^{-1} \int_{S=0}^{S=2q} J_0(z) \exp(-z^2/\alpha r) z dz$$

Now, making use of the relation<sup>7</sup>  $d[z^n J_n(z)] = z^n J_{n-1}(z) dz$ , and integrating by parts, we find

$$I = 2\alpha^{-1} \sum_{n=1}^{\infty} (2/\alpha r)^{n-1} z^n J_n(z) \exp(-z^2/\alpha r) \Big|_{z=0}^{z=2q} \quad (2)$$

That eq. 2 is really the solution for the integral  $I$  may be checked by differentiating eq. 2 with respect to  $z$ . Now, evaluating  $I$  between the limits and substituting in eq. 1, we obtain

$$f(r, \vartheta) = n_1 n_2 \exp(\beta r \cos \vartheta - 1) \sum_{n=1}^{\infty} (2q/r)^n \sum_{m=0}^{\infty} [2\beta q \cos \vartheta + 1]^{m/m} / (m+n)! \quad (3)$$

Now, we really desire  $f(r, \vartheta)$  for small  $\beta$ . Then

$$f(r, \vartheta) = f_0 \exp(2\beta r \cos \vartheta) - n_1 n_2 2\beta q (\cos \vartheta + 1) \quad (4)$$

where  $f_0 = n_1 n_2 [\exp(2q/r) - 1]$ . This latter result is correct to the first power of  $\beta$ . If eq. 4 is used to calculate the rate of dissociation in the

presence of an external field according to Onsager, one obtains his result, which is to be expected. The first term on the left in eq. 4 corresponds to a local Boltzmann distribution at small values of  $r$  and results in orientation of the ion pair dipole in the field. The second term is due to the increased flow of ions in the direction of the field. Following Onsager, the mean relative velocity is given by

$$(f_1 \vec{v}) = kT (\omega_1 + \omega_2) (f_1 \nabla U - \nabla f_1) \quad (5)$$

where  $f_1$  is the distribution function given by equation 4,  $\omega_1$  is the ion mobility, and  $U$  is the reduced potential energy, given by  $2q/r + 2\beta r \cos \vartheta$ . Onsager evaluated the average rate of dissociation by taking the surface integral of the radial component of eq. 5. This yielded a value which of necessity had to be independent of the direction of the field. As we shall show below, however, the flow is in the direction of the field and thus leads to polarization. We now wish to calculate the  $x$ ,  $y$ , and  $z$  components (where the field  $E$  is in the  $z$ -direction) of the mean relative velocity,  $(f_1 \vec{v}) = f_1 (\vec{i}u + \vec{j}v + \vec{k}w)$ , where  $\vec{i}$ ,  $\vec{j}$ , and  $\vec{k}$  are unit vectors in the  $x$ ,  $y$ , and  $z$  directions. We then shall show that the average over a spherical surface of the first two vanishes, while the latter has a non-zero value. For small  $r$

$$(f_1 v) = n_1 n_2 kT (\omega_1 + \omega_2) \{2q \cos \vartheta [1 + 2\beta q (\cos \vartheta + 1)/r^2 + 2\beta q (\cos^2 \vartheta + 1)/r]\}$$

$$(f_1 u) = n_1 n_2 kT (\omega_1 + \omega_2) \{2q \sin \vartheta \cos \varphi [1 + 2\beta q (\cos \vartheta + 1)/r^2 - 2\beta q \sin \vartheta \cos \varphi \cos \vartheta/r]\}$$

$$(f_1 w) = n_1 n_2 kT (\omega_1 + \omega_2) \{2q \sin \vartheta \sin \varphi [1 + 2\beta q (\cos \vartheta + 1)/r^2 - 2\beta q \sin \vartheta \cos \vartheta \sin \varphi/r]\} \quad (6)$$

Integration of say  $(f_1 w)$  over a spherical surface of radius  $r$  gives the net mean relative component of velocity in the  $y$ -direction. It is seen that

$$\int (f_1 w) r^2 \sin \vartheta d\vartheta d\varphi = \int (f_1 u) r^2 \sin \vartheta d\vartheta d\varphi = 0$$

This means that the components in the positive  $x$  and  $y$  directions balance out those in the opposite directions. This is not so in the case of the  $z$ -component.

Using the distribution function given by Onsager,<sup>6</sup>  $f_2 = n_1 n_2$ , for free ions, where  $n_1$  and  $n_2$  are the free ion concentrations, the  $z$ -component of the mean relative velocity is given by

$$(f_2 v) = n_1 n_2 kT (\omega_1 + \omega_2) [-2q \cos \vartheta/r^2 + 2\beta] \quad (7)$$

Now we introduce the value for  $n_1 n_2$  at small values of  $r$  in equation 6 as

$$n_1 n_2 = (v_0 - \Delta v) K_0$$

where  $v_0$  is the zero field ion pair concentration,  $\Delta v$  is the increase in free ion concentration due to the field effect, and  $K_0$  is the zero field ion pair dissociation constant. The value of  $n_1 n_2$  in eq. 7 then is  $(n_0 + \Delta v)^2$  where  $n_0$  is the zero field concentration of the free ions. We consider only the symmetrical electrolyte case. The net component of the flow of pairs in the  $z$ -direction is then  $(f_1 v) + (f_2 v)$ . Now, we will drop terms of the order of  $\beta \Delta v$ , and  $(\Delta v)^2$ , since these are second order. Also, following Onsager, we will drop the  $1/r$  term in comparison to the  $1/r^2$  term, since most of the effect occurs at small values of  $r$ . We then obtain

(5) R. G. Pearson, private communication.

(6) L. Onsager, *J. Chem. Phys.*, **2**, 599 (1934).

(7) E. T. Whittaker and G. N. Watson, "Modern Analysis," Cambridge Press, 4th ed., 1952, p. 360.



$$(fv) = kT(\omega_1 + \omega_2) \{ \nu_0 K_0 4\beta q^2 (\cos^2 \vartheta + \cos \vartheta) / r^2 - (K_0 + 2n_0) \Delta \nu 2q \cos \vartheta / r^2 + 2\beta(n_0 + \Delta \nu)^2 \} \quad (8)$$

The last term on the right will be seen to correspond to the ionic conductance of the free ions in the field. At equilibrium, the first two terms must go to zero, so that the equilibrium value of  $\Delta \nu$  is given by

$$\Delta \nu_e = \nu_0 K_0 2\beta q (\cos \vartheta + 1) / (K_0 + 2n_0)$$

The value of  $\Delta \nu$  to be substituted into eq. 8 is not  $\Delta \nu_e$  but is a function of the time and direction. When the field is first applied, there is a charging current which disappears at equilibrium. We will suppose that  $\Delta \nu = \Delta \nu(t) h(\vartheta, \varphi)$ . Comparison with  $\Delta \nu_e$  shows that  $h = (\cos \vartheta + 1)$ . We are principally interested in the  $z$ -component of the flow of ions, not pairs. Now the average number of ions per cc. having the component of velocity in the  $z$ -direction of  $v$  is

$$\overline{nv} = \int (fv) dV$$

The volume  $V (= 4\pi s^3/3)$  over which the integration is to be carried out is just the reciprocal of the free ion density, *i.e.*,  $1/(n_0 + \Delta \nu)$ . Separating  $(fv)$  into an ionic term and a charging term we get

$$(\overline{nv})_c = kT(\omega_1 + \omega_2) [16\pi \nu_0 K_0 \beta q^2 s/3 - (K_0 + 2n_0) \Delta \nu(t) 8\pi q s/3]$$

for the charging part. It is interesting to note that the value of the ionic part, at equilibrium, is just that given by Onsager.<sup>6</sup>

$$(\overline{nv})_i = kT(\omega_1 + \omega_2) 2\beta(n_0 + \Delta \nu_e)$$

where

$$\Delta \nu_e = \int \Delta \nu_e dV / \int dV = 2\beta q \nu_0 K_0 / (K_0 + 2n_0)$$

We thus see that the ratio of the equivalent conductance at high field strengths to that at low field strengths is given by

$$\Lambda(E)/\Lambda(0) = 1 + \Delta \nu_e / n_0 = 1 + (1 - \alpha) 2Bq / (2 - \alpha)$$

for fields not too large. Returning now to the charging portion, we may write

$$(\overline{nv})_c = \nu_0 k_d 2\beta q s / 3 - (k_d + 2n_0 k_r) s \Delta \nu(t) / 3 \quad (9)$$

where  $k_r = 8\pi q k T (\omega_1 + \omega_2)$ , the specific rate constant for ion recombination, in cc./ion sec., and  $k_d$  is the specific rate constant for pair dissociation. Now  $(\overline{nv})_c$  is the  $z$ -component of the mean ion flow due to the charging process. The specific relation between this quantity and  $\Delta \nu$  must be found before a solution of eq. 9 can be written down. Onsager's method of calculating the increased rate of dissociation due to the field is to integrate the normal component of the flow,  $f_i \bar{v}$ , over a spherical surface. If in this manner we calculate the rate of dissociation due to the  $z$ -component of the flow, we obtain

$$\int (f_i \bar{v}) \cos \vartheta r^2 \sin \vartheta d\vartheta d\varphi = \nu_0 k_d (1 + 2\beta q) / 3$$

This result is one-third of the total rate of dissociation. Thus

$$(\overline{nv})_c = (s/3) d \Delta \nu / dt$$

Now, inserting this result in eq. 9, and letting  $\Delta P = zes \Delta \nu / 3$ , then we obtain

$$d \Delta P / dt = \nu_0 k_d 2\beta q zes / 3 - (k_d + 2n_0 k_r) \Delta P \quad (10)$$

where  $\Delta P$  is the increased polarization density of the solution due to the development of  $\Delta \nu$ . Equa-

tion 10 is in suitable form to obtain  $\Delta P$  in an alternating field. Now in a field of circular frequency  $\omega (= 2\pi f, f$  in cycles per sec.)

$$E_z = E_0 \exp(i\omega t)$$

Now

$$d \Delta P / dt = K_1 E_0 \exp(i\omega t) - \Delta P / \tau'$$

The solution of this equation for  $\Delta P$ , aside from a transient which rapidly disappears is

$$\Delta P = K_1 \tau' E_0 \exp(i\omega t) / (1 + i\omega \tau')$$

The relaxation time for  $\Delta P$  is  $\tau'$ , the Langevin relaxation time. Separating  $\Delta P$  into its real and imaginary parts, and using the relation to the increase in the complex permittivity,<sup>8</sup>  $\Delta \epsilon = 4\pi \Delta P / E = \Delta \epsilon' - i \Delta \epsilon''$ , we obtain

$$\begin{aligned} \Delta \epsilon' &= 4\pi K_1 \tau' / (1 + \omega^2 \tau'^2) \\ \Delta \epsilon'' &= 4\pi K_1 \omega \tau'^2 / (1 + \omega^2 \tau'^2) \end{aligned} \quad (11)$$

where  $\Delta \epsilon'$  is the increase in dielectric constant and  $\Delta \epsilon''$  is the increase in loss factor due to the ion pair relaxation process.

### Discussion

We already have seen that the increase in ionic conductance due to the field effect calculated by the foregoing method is the same as that found by Onsager, *i.e.*,

$$\Lambda(E)/\Lambda(0) = 1 + (1 - \alpha) 2\beta q / (2 - \alpha)$$

The present treatment goes further and yields the effect of frequency on low field dielectric constant and loss factor due to relaxation of the ion pair equilibrium. These effects will be discussed in relation to the Debye-Falkenhagen<sup>9</sup> effect and the power loss due to ion pair relaxation as calculated by Pearson.<sup>10</sup> Taking the latter first, the power loss,  $\phi$ , in ergs/l. sec., as obtained by Pearson, is related to the loss factor,  $\Delta \epsilon''$ , by

$$\phi = 1000 \omega E_0^2 \Delta \epsilon'' / 8\pi$$

We then see that Pearson's loss factor is

$$\Delta \epsilon'' = 64z^2 e^2 q^2 N_a c \alpha_0 (2\omega \tau') / 9000 \pi k T (1 + 4\omega^2 \tau'^2) \quad (12)$$

while eq. 11 gives

$$\Delta \epsilon'' = 2\pi z^2 e^2 q s N_a c \alpha_0 \omega \tau' / 3000 k T (1 + \omega^2 \tau'^2) \quad (13)$$

where  $c$  is the stoichiometric salt concentration,  $\alpha_0$  the degree of dissociation, and the other factors have their usual significance. The differences between eq. 12 and 13 arise principally from Pearson's assumption that the only energy absorbed from the field was that in increasing  $\Delta \nu$  during the charging process. He neglected the energy dissipated in actually transporting the ions from the origin to the completely dissociated state. This is most apparent when one considers his statement regarding the corresponding calculation of  $\phi$  from the current-voltage integral. The voltage drop for dissociation is not "clearly  $Eg$ ." It is true that eq. 11 suffers from some uncertainty regarding the integration of eq. 8 over the volume. The distance parameter,  $s$ , thus introduced, should

(8) C. J. F. Bottcher, "Theory of Dielectric Polarization," Elsevier, New York, N. Y., 1952, p. 232.

(9) P. Debye and H. Falkenhagen, *Physik. Z.*, **29**, 121, 401 (1928). See also "Collected Papers of P. J. W. Debye," Interscience Publishers, Inc., New York, N. Y., 1954, p. 374, ff.

(10) R. G. Pearson, *Discussions Faraday Soc.*, **17**, 187 (1954).

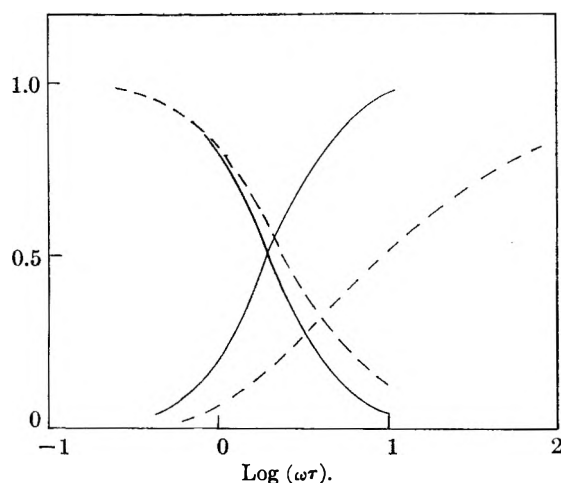


Fig. 1.—Frequency dependence of dissociation relaxation effect and Debye-Falkenhagen effect. Descending solid line has  $f(\omega\tau')$  as ordinate; ascending solid line is  $\omega^2\tau'^2f(\omega\tau')$ ; descending dashed line is  $g(\omega\tau)$ ; ascending dashed line is  $(1-h)$ ; all plotted as a function of frequency.

be some sort of average distance the dissociating ions attain during the charging process. There is a point which the author feels is strong justification for setting  $4\pi s^3/3 = 1/(n_0 + \Delta\nu)$ . This choice results in a value for the free ion current which is in agreement with Onsager's. In connection with this, it might be noted that if one confines the volume of integration to this value, then Bjerrum's distribution function,  $n_1n_2 \exp(-2q/r)$ , is normalized in a satisfactory manner. The frequency dependent terms in eq. 12 and 13 show that Pearson's relaxation time is twice that in eq. 13. This is a result of using the absolute value of the field in his calculation. It is true that the quantity  $\Delta\nu$  must be independent of the direction of the field, from the manner of its definition, but the charging current is dependent on field direction, and it is this latter quantity which determines the power loss in the field.

Comparison with the results of Debye and Falkenhagen<sup>9</sup> for the dispersion of the conductance and dielectric constant of a strong electrolyte shows some interesting parallels and differences. Let subscript 1 denote the Debye-Falkenhagen result, while 2 denotes that in eq. 11. Then, for the dielectric increment we have

$$\Delta\epsilon'_1 = z^2e^2\kappa g(\omega\tau)/24kT \quad (14)$$

where  $\kappa$  is characteristic of the ion atmosphere and  $g(\omega\tau)$  is a complicated function of  $\omega$  and the ion atmosphere relaxation time  $\tau$ . Now when the degree of dissociation is small, we find

$$\Delta\epsilon'_2 = z^2e^2\kappa^2sf(\omega\tau')/24kT \quad (15)$$

where  $f(\omega\tau') = 1/(1 + \omega^2\tau'^2)$ . Recalling that  $s$  is the result of integration over the volume containing a free ion, if we set  $s$  to be  $1/\kappa$ , which is the average radius of the ion atmosphere, then

$$\Delta\epsilon'_2/\Delta\epsilon'_1 = f(\omega\tau')/g(\omega\tau)$$

The two functions,  $f(\omega\tau')$  and  $g(\omega\tau)$ , are plotted vs.  $\log(\omega\tau)$  in Fig. 1, as the quantities decreasing as  $\log(\omega\tau)$  increases. For slightly dissociated electrolytes,  $\tau = 2\tau'$ . It is seen that even though the relaxation times,  $\tau$  and  $\tau'$ , are different, the

dielectric increments fall to one-half their low frequency value at about the same frequency, and with the assumption that  $s\kappa = 1$ , have about the same magnitude. The justification for assuming that  $s\kappa = 1$ , rather than  $s$  being the distance calculated from a cube-root law is the same as that involved in the original Debye-Hückel derivation<sup>11</sup> of the ion atmosphere potential.

The conductance functions, on the other hand exhibit different behavior. We will discuss these in the forms (assuming  $s\kappa = 1$ )

$$(\Delta G/G_0)_1 = z^2e^2\kappa(1-h)/10.24\epsilon_0kT \quad (16)$$

$$(\Delta G/G_0)_2 = z^2e^2\kappa\omega^2\tau'^2f(\omega\tau')/12\epsilon_0kT \quad (17)$$

where  $\Delta G/G_0$  is the relative increase in the conductance of the system,  $G_0$  being the low frequency value,  $h$  is the quantity  $\Lambda_{I\omega}/\Lambda_{I\omega} = 0$  tabulated in Harned and Owen,<sup>12</sup> and  $\epsilon_0$  is the solvent dielectric constant. The remaining are the same as in eq. 14 and 15. The magnitude of the two conductance increments are seen to be the same, except for the frequency dependency. The latter may be compared in Fig. 1 as the ascending curves with  $\log(\omega\tau)$ . It is seen that the ion pair relaxation effect reaches its maximum value faster than the Debye-Falkenhagen effect. An important question occurs at this point: do the two foregoing effects occur under the same experimental conditions? In the case of a weak electrolyte, the average lifetime of a free ion is  $\tau_i = 1/k_r n$ . Now if  $k_r$  is given by Onsager's value, then  $\tau_i$  is just the characteristic time of formation (or relaxation) of the ion atmosphere. It might appear that under these conditions, for a given ion, the only atmosphere it sees is that due to the oppositely charged ion from which it has just dissociated. But other free ions are being formed in the neighborhood also, so that on a time average basis, one would expect the Debye-Falkenhagen effect to be additive to the ion pair relaxation effect. One still might expect strange behavior in systems where the Debye-Hückel limiting law cannot apply at accessible concentrations such as solvents of low dielectric constant.

In systems where the degree of dissociation is large, then eq. 13, 15, and 17 must be modified to remove the assumption that  $\alpha$  is much less than one. Then

$$\tau' = (1-\alpha)\tau/(2-\alpha) \approx (1-\alpha)\tau/2$$

and is much smaller than  $\tau$ . As  $\alpha$  approaches unity, the ion pair relaxation effect disappears, so that only the Debye-Falkenhagen effect remains.

As an example of the expected effect of dielectric constant on the magnitude of  $(\Delta G/G_0)_2$ , the results of calculations for 0.001 *M* tetra-*n*-butylammonium picrate in benzene-*o*-dichlorobenzene solvent mixtures<sup>13</sup> for  $\omega\tau'$  much greater than unity are shown in Fig. 2 as a function of solvent dielectric constant. The ion pair dissociation constants range from  $1.9 \times 10^{-5}$  in *o*-dichlorobenzene to

(11) P. Debye and E. Hückel, *Physik. Z.*, **24**, 185 (1923).

(12) H. S. Harned and B. B. Owen, "Physical Chemistry of Electrolytic Solutions," Reinhold Publ. Corp., New York, N. Y., 1950, 2nd Ed., p. 132.

(13) W. R. Gilkerson and R. E. Stamm, *J. Am. Chem. Soc.*, **82**, 5295 (1960).

$1.8 \times 10^{-17}$  in benzene. Note the maximum. This is due to the fact that  $(\Delta G/G_0)_2$  is proportional to the half-power of the ion concentration (which increases with increasing  $\epsilon_0$ ) and is inversely proportional to the three-halves power of the dielectric constant.

**Comparison with Experiment**—Since recent data from this Laboratory will be the subject of another paper we confine ourselves here to a comparison of the calculations based on eq. 11 with those of Pearson<sup>10</sup> and the meager data available in the literature. It first must be noted that observations reported by this author<sup>14</sup> on boric acid in water must be regarded as in serious error. They cannot be reproduced. Efforts to find the source of the original absorption have proved fruitless.

The earliest available data are those of Whitmore,<sup>15</sup> as cited by Pearson,<sup>10</sup> on the conductance of propionic and tartaric acids in water relative to potassium iodide at 400 Mc. Assuming for the propionic acid an ionization constant of  $1.3 \times 10^{-5}$  and a recombination rate constant of  $10^{11} M^{-1} \text{ sec.}^{-1}$  (as Pearson did) then for a 0.1425  $M$  solution, using eq. 17, we calculate a relative increase in conductance of 0.72%. This is to be compared to Pearson's result of 0.1% and an observed increase of 1.1% for this concentration. There is enough scatter in the observed results to render any hope for a more detailed comparison fruitless.

Cole and Strobel<sup>16</sup> reported that tetra-*n*-butylammonium picrate ( $9.55 \times 10^{-3} M$ ) in anisole at 25° exhibited a minimum in  $\Delta\epsilon''$  around 10 Mc. It has been suggested<sup>17</sup> that the increase in  $\Delta\epsilon''$  toward lower frequencies possibly is due to ion pair relaxation. We subscribe to this and further will include the Debye-Falkenhagen effect. From low frequency conductance data<sup>18</sup> and assuming that all dissociating species behave identically in an external field, we calculate, at 1 Mc.,  $\Delta\epsilon'' = 0.037$  due to Debye-Falkenhagen effect, and  $\Delta\epsilon'' = 0.078$  due to ion pair relaxation. At 1.8 Mc., the lowest frequency observed, the  $\Delta\epsilon''$  was about 0.05. Since we calculate that the maximum should be around 0.8 Mc., the foregoing calculated values seem reasonable. Using Pearson's equation, one would calculate a value of  $\Delta\epsilon'' = 0.024$  due to ion pair relaxation. Comparison in this case, where the data are good, is difficult because of the complexity of concentrated electrolyte solutions in solvents having dielectric constants as low as anisole (4.30). Other maxima in the loss curves observed by Cole and associates<sup>16</sup> are at such high

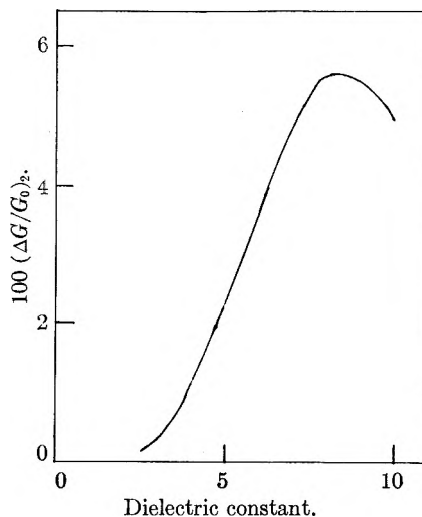


Fig. 2.—Relative maximum increase in conductance, calculated from eq. 17, of tetra-*n*-butylammonium picrate in benzene-*o*-dichlorobenzene as a function of solvent dielectric constant.

frequencies that they could not be due to the simple process treated here. The same may be said for recent observations<sup>17</sup> on 0.01  $M$  solutions of tetra-*n*-butylammonium bromide in benzene where a maximum was found around 7 Mc.

#### Conclusion

The definite integral form of the distribution function for ion pairs in an external field, as given by Onsager,<sup>6</sup> has been integrated to give a series form. This result has been used to derive equations for the increase in dielectric constant and conductance of a weak electrolyte in an alternating field due to relaxation of the ion pair equilibrium. These results are felt to be an improvement over Pearson's equation<sup>10</sup> for the conductance increase. There are three principal differences in the two approaches: the dielectric increment appears in the present work as a natural consequence of calculating the displacement current (it is absent in Pearson's treatment); the relaxation time for the present result is just the Langevin time  $\tau'$ , not  $2\tau'$  as in Pearson's; the magnitude of the effect for small degrees of dissociation has prospect of being much larger than Pearson indicated since the ratio of the maximum value of the conductance increase as calculated here to that calculated by Pearson is  $1/\kappa q$ . For instance, in water at 25°, for an ion concentration of  $10^{-5} M$ ,  $1/\kappa q$  is approximately 300.

The theory appears to be in agreement with the two experimental results known to the author. Much experimental work needs to be done to indicate the approaches that must be taken to improve the formulation of the problem. The uses to which dispersion measurements could be put in the kinetics of fast ionic reactions already has been discussed by Pearson.<sup>10</sup>

(14) W. R. Gilkerson, *J. Chem. Phys.*, **27**, 914 (1957).

(15) B. G. Whitmore, *Physik. Z.*, **34**, 649 (1933).

(16) R. H. Cole and H. A. Strobel, *Ann. N. Y. Acad. Sci.*, **54**, 807 (1949).

(17) M. Davies and G. Williams, *Trans. Faraday Soc.*, **56**, 1619 (1960).

(18) G. Bien, C. A. Kraus, and R. M. Fuoss, *J. Am. Chem. Soc.*, **56**, 1860 (1934).

# ELECTRON PARAMAGNETIC RESONANCE STUDY OF $Mn^{++}$ ION IN POLYCRYSTALLINE CALCIUM FLUOROPHOSPHATE

BY PAUL H. KASAI\*

*Hitachi Central Research Laboratory, Kokubunji, Tokyo, Japan*

*Received August 30, 1961*

The paramagnetic resonance spectrum of  $Mn^{++}$  ions in a polycrystalline sample of synthetic calcium fluorophosphate  $3[Ca_3(PO_4)_2] \cdot CaF_2$  has been investigated. It is found that most of the observed spectrum can be explained by a spin Hamiltonian for the case of axially symmetric crystalline field,  $\mathcal{H} = g\beta H \cdot S + D\{S_z^2 - \frac{1}{3}S(S+1)\} + A_{\parallel}S_zI_z + A_{\perp}(S_xI_x + S_yI_y)$ . The observed values are  $g = 2.0005 \pm 0.0005$ ,  $D = 428 \pm 2$  gauss,  $A_{\parallel} = 94.4 \pm 0.5$  gauss, and  $A_{\perp} = 92.4 \pm 0.5$  gauss at 290°K. This result implies that most of the  $Mn^{++}$  ions substitute for  $Ca^{++}$  ions at the Ca(I) site, since of the two non-equivalent sites for  $Ca^{++}$  ion in calcium fluorophosphate, the Ca(I) site has trigonal symmetry while the symmetry of the other site, Ca(II), is only rhombic. The analysis of the powder pattern with such a large fine structure spreading was made possible by noting that the signals corresponding to the angular orientations of  $\theta = \pi/2$  and 0 with respect to the static magnetic field can be identified easily from their characteristic shapes and signs.

## Introduction

Calcium fluorophosphate,  $3[Ca_3(PO_4)_2] \cdot CaF_2$ , has the structure and composition of mineral apatite and is one of the most commonly used fluorescent materials. In the rest of this article we shall often use the word "apatite" to mean specifically calcium fluorophosphate for the sake of simplicity. The fluorescent property of this compound comes about from the presence of the activating impurities  $Mn^{++}$  and  $Sb^{+++}$  ions, both of which are believed to occupy the sites for  $Ca^{++}$  ions substitutionally within the host crystal. The crystal structure of apatite is a hexagonal type and may be visualized as two types of planes A and B stacked alternately, parallel to each other, in the direction of the crystal axis.<sup>1</sup> Figure 1 shows these two planes schematically. As one can immediately recognize from the figure, there are two non-equivalent sites for  $Ca^{++}$  ions in apatite crystal, one site Ca(I) situating in the plane A, and the other Ca(II) situating in the plane B. Just which one of these sites is preferentially occupied, if there is such a preference, by these activating impurities has been the subject of many speculations,<sup>2,3</sup> though until very recently no definite experimental evidence has been presented.<sup>4</sup>

As is well known, the electron paramagnetic resonance (e.p.r.) spectrum of a paramagnetic ion dispersed in a dielectric medium is quite sensitive to its local environment. We therefore decided to look at the e.p.r. spectrum of  $Mn^{++}$  ions in apatite and to obtain some inference about the distribution of  $Mn^{++}$  ions between the Ca(I) and Ca(II) positions. The work of this nature should be straightforward, if one is in possession of a single crystal of the substance in question. A single crystal of apatite, however, was not available to us, and we thus were compelled to work with powdered sample. It was found that for a paramagnetic ion with a more or less isotropic  $g$ -value, the analysis of the e.p.r. spectrum of a polycrystalline sample could

be quite possible even under the influence of strong crystalline field, leading to a fairly accurate determination of the fine structure and the hyperfine structure constants. This paper reports on the results of our such work with the polycrystalline sample of calcium fluorophosphate.

## Theoretical Considerations

The ground state of  $Mn^{++}$  ion is  $(3d^5)^6S$ , and its spin degeneracy is known to split, under the combined influence of an externally applied magnetic field and a crystalline field, according to the spin Hamiltonian<sup>5</sup>

$$\mathcal{H} = g\beta H \cdot S + D\{S_z^2 - \frac{1}{3}S(S+1)\} + E(S_x^2 - S_y^2) + F(a) + AI \cdot S \quad (1)$$

Here  $g$  is the spectroscopic splitting factor,  $\beta$  is the Bohr magneton,  $H$  is the external magnetic field,  $S$  is the total spin operator, and  $I$  is the nuclear spin operator. The first term represents the Zeeman effect, and the next three terms represent the fine structure interaction induced by the crystalline field. Of the total crystalline field, the  $D$  term shows the effect of the axially symmetric part, while the  $E$  and  $F$  terms represent the effect of the rhombic and cubic part, respectively. The last term in equation 1 represents the hyperfine structure interaction between the electron spin and the  $Mn^{55}$  nuclear spin. As can be seen from Fig. 1, for our particular case of  $Mn^{++}$  ions incorporated in apatite crystal, the crystalline field which the ions experience would be axially symmetric, having  $C_3$  symmetry, if the ions are at the Ca(I) site. On the other hand if the  $Mn^{++}$  ions are at the Ca(II) site, the crystalline field would be rhombic, the only symmetry being that of reflection with respect to the plane B. Accordingly, if the  $Mn^{++}$  ions are at the Ca(I) site, the corresponding spin Hamiltonian in eq. 1 would be without the  $E$  and  $F(a)$  terms, while only the  $F(a)$  term may be omitted for the latter case. The selection rules for the observed transitions are  $\Delta M = \pm 1$  and  $\Delta m = 0$ , where  $M$  and  $m$  are the magnetic quantum numbers of the electron spin and the nuclear spin, respectively. Since  $S = 5/2$  and  $I = 5/2$  for  $Mn^{++}$  ion, there would be five fine structure components, each of which is split into six more or less equally spaced hyperfine components with equal intensity. Therefore con-

\* Union Carbide Research Institute, Tarrytown, New York.

(1) St. Naray-Szabo, *Z. Krist.*, **75**, 394 (1930).

(2) Keith H. Butler and Charles W. Jerome, *J. Electrochem. Soc.*, **97**, 265 (1950).

(3) W. L. Wanmaker, *J. phys. radium*, **17**, 636 (1956).

(4) After the completion of this work we learned that P. D. Johnson reported that the luminescent manganese in apatite substitutes for calcium in the Ca(I) position. His conclusion was based on the study of the polarization of the luminescence of synthetic single crystals of apatite; P. D. Johnson, *Bull. Am. Phys. Soc.*, [II] **6**, 30 (1961).

(5) B. Bleaney and D. J. E. Ingram, *Proc. Roy. Soc. (London)*, **A205**, 336 (1951).

sidering only the fine structure components, *i.e.*, the centers of each hyperfine group, we have as our general Hamiltonian

$$\mathcal{H} = g\beta H \cdot S + D \{S_x^2 - 1/3S(S+1)\} + E(S_x^2 - S_y^2) \quad (2)$$

The energy levels applicable to eq. 2 are evaluated by perturbation theory to second order in  $D$  and  $E$  terms, assuming that  $g$  is isotropic. The calculation yields for the resonance field corresponding to the transition  $M \rightarrow M - 1$ <sup>6</sup>

$$H_{M \rightarrow M-1} = H_0 - \left(M - \frac{1}{2}\right) \{D(3 \cos^2 \theta - 1) + 3E \sin^2 \theta \cos 2\phi\} - \frac{1}{2H_0} \{24M(M-1) + 9 - 4S(S+1)\} \{(E \cos 2\phi - D)^2 \cos^2 \theta \sin^2 \theta + E^2 \sin^2 \theta \sin^2 2\phi\} - \frac{1}{8H_0} \{2S(S+1) - 6M(M-1) - 3\} \{[D \sin^2 \theta + E(1 + \cos^2 \theta) \cos 2\phi]^2 + 4E^2 \cos^2 \theta \sin^2 2\phi\} \quad (3)$$

Here  $H_{M \rightarrow M-1}$  is the field at which the resonance is observed with the frequency  $\nu$  of the applied radiation, and  $H_0$  is given by  $h\nu/(g\beta)$  and is the resonance position in the absence of any fine structure interaction.  $D$  and  $E$  in eq. 3 differ from those of eq. 2 in that these are now divided by  $g\beta$  and are given in gauss.  $\theta$  is the angle between the magnetic field and the symmetry axis of the crystal field and  $\phi$  is the azimuthal angle. If our  $Mn^{++}$  ions are at the Ca(I) site, the resonance fields are then given by setting  $E = 0$  in eq. 3. This, of course, is identical with the expression given by Bleaney and Ingram<sup>5</sup> for the case of axial field, and the resonance field of each fine structure component varies with  $\theta$  as shown in Fig. 2a. The over-all pattern of this figure is independent of the sign of  $D$ . When  $\theta = \pi/2$ , the fine structure components occur in the order of, starting from the lowest field component,  $M = \mp 3/2 \leftrightarrow \mp 5/2$  (curve 1 in Fig. 2),  $M = \mp 1/2 \leftrightarrow \mp 3/2$  (curve 2),  $M = \pm 1/2 \leftrightarrow \mp 1/2$  (curve 3),  $M = \pm 3/2 \leftrightarrow \pm 1/2$  (curve 4), and  $M = \pm 5/2 \leftrightarrow \pm 3/2$  (curve 5), where the upper and lower signs hold for positive and negative  $D$ , respectively. The intensity ratio of these fine structure components are given by  $(S+M)(S-M+1)$  and are 5:8:9:8:5. On the other hand, if the  $Mn^{++}$  ions are at the Ca(II) site, the resonance field of each fine structure component depends upon both  $\theta$  and  $\phi$ , and no simple representation is possible as for the case of Ca(I) site.

As stated in the previous section, all of our experiments were carried out with powdered samples, for which the values of  $\theta$  and  $\phi$  of each grain may be considered to be completely at random. Then if our  $Mn^{++}$  ions are at the Ca(II) site, the only sharp signal which might be observed is the one corresponding to  $M = +1/2 \leftrightarrow -1/2$  for which the first-order effects of both  $D$  and  $E$  are non-existent. The other fine structure components probably yield no observable signal due to two additive anisotropy broadening effects of  $D$  and  $E$  terms.

(6) W. Low, "Paramagnetic Resonance in Solids," Academic Press New York, N. Y., and London, 1960. There are some inconsistencies in the expression given by W. Low for a similar spin Hamiltonian. We, therefore, re-evaluated the whole calculation.

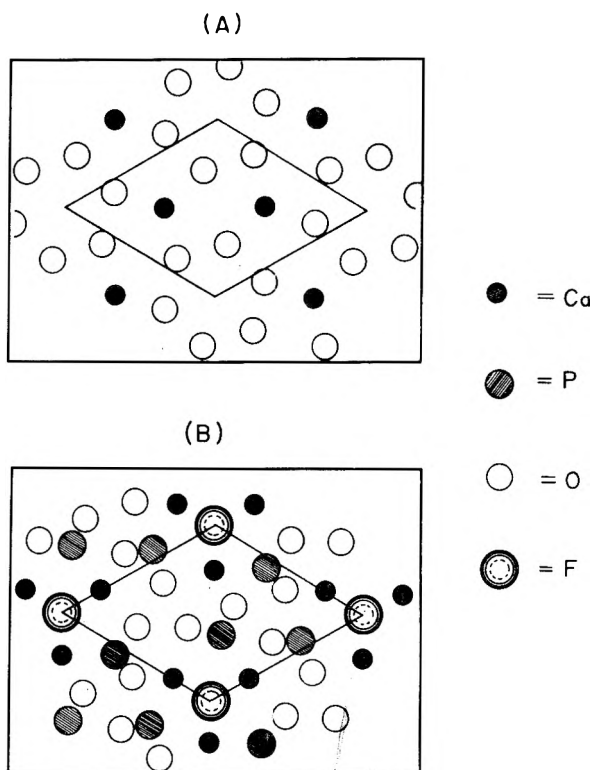


Fig. 1.—Crystal structure of calcium fluorophosphate. The structure is hexagonal and may be visualized as two types of planes A and B stacked alternatively in the direction of the crystal axis.

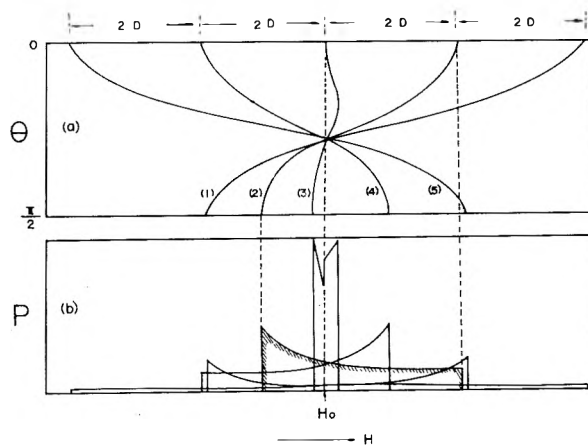


Fig. 2.—(a) The angular dependence of the fine structure for the case of axially symmetric crystalline field. (b) Distribution curve  $P$  of polycrystalline sample for each fine structure component.

If the  $Mn^{++}$  ions are at the Ca(I) site, however, the resonance field depends only upon  $\theta$ . For this case, one can calculate the distribution function  $P_{M \rightarrow M-1}$  of the crystal grains.

$$P_{M \rightarrow M-1} = \sin \theta \left| \frac{d\theta}{dH_{M \rightarrow M-1}} \right| = \left| \frac{d \cos \theta}{dH_{M \rightarrow M-1}} \right| \quad (4)$$

$P_{M \rightarrow M-1} \cdot dH$  gives the probability of a given crystal having the appropriate spatial orientation that would satisfy the resonance condition  $M \rightarrow M - 1$  at a given field of  $H$ . Equation 4 was evaluated from eq. 3 for each fine structure component, and the results are shown in Fig. 2b. The actual absorption spectrum then would be a superposition

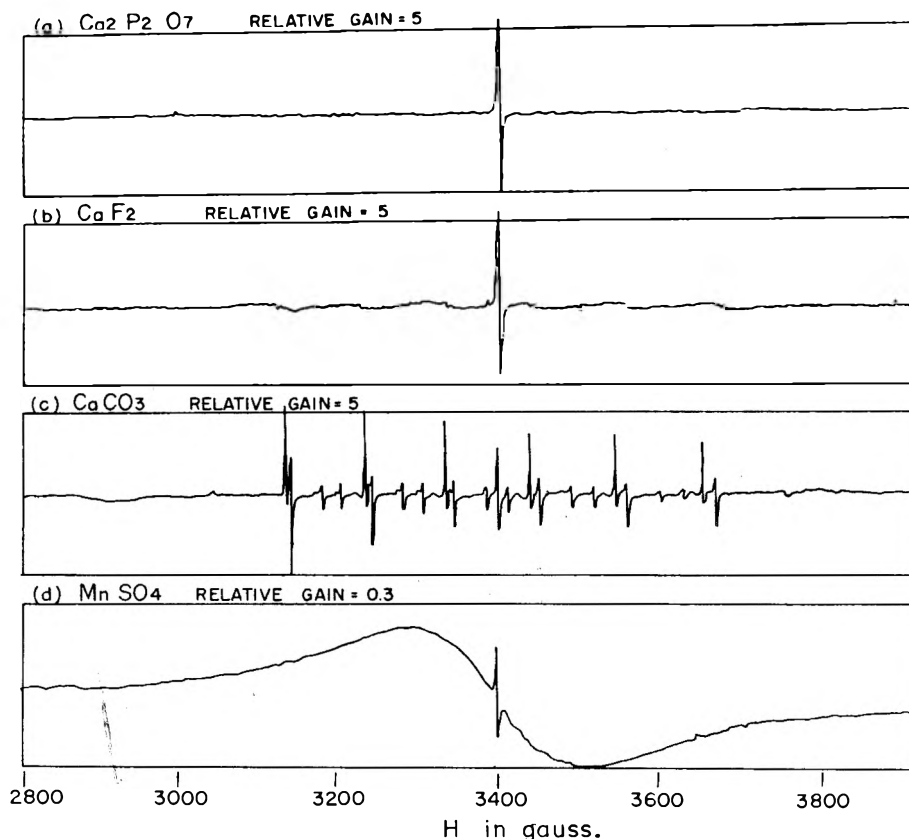


Fig. 3.—E.p.r. spectra of each material used in the firing reaction of apatite. The sharp signal at the center of each record is that of DPPH inserted as a reference.

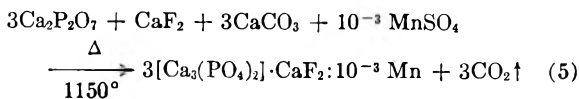
of many Lorentzian curves weighted by the distribution function  $P_{M \rightarrow M-1}$  and the quantum mechanical transition probability  $(S+M)(S-M+1)$ . However if the value of  $D$  is much larger, say by the order of two, than the intrinsic line width expected for a single crystal, the absorption spectrum of the polycrystalline sample should be well approximated with the superposition of these distribution curves, each of them weighted by the respective transition probability. We must recall here that, through the use of modulation technique, what we are observing is the first derivative of the absorptive curve. Consequently strong and sharp signals are expected only at the points corresponding to  $\theta = \pi/2$  of each distribution curve. The points corresponding to  $\theta = 0$  should also give sharp signals, but they ought to be much weaker compared to those corresponding to  $\theta = \pi/2$  and might not be observable. Then, referring to Fig. 2b, there would be strong and sharp "positive" signals at the points corresponding to  $\theta = \pi/2$  of the curves 1 and 2, whereas strong and sharp "negative" signals are expected at the points corresponding to  $\theta = \pi/2$  of the curves 4 and 5. The derivative curve expected for the curve 3 is rather complex. This, however, is no exception in that there again would be a strong and sharp positive signal at  $\theta = \pi/2$ . The signal due to the curve 3 would of course be the strongest. The signals due to the curves 1 and 5 would be the weakest, since they experience the widest fine structure spreading in addition to the smallest transition probability. Needless to repeat, in the actual

experimental observation, each of these signals is split into six equally spaced lines with equal intensity by the hyperfine interaction.

#### Instrumentation and Sample Preparation

The e.p.r. spectrometer used for this investigation was a Varian Model V-4500 equipped with a 100 kc. modulation unit. The cavity resonance frequency was about 9500 Mc./sec. The magnetic field was calibrated by measuring the frequency of the proton nuclear magnetic resonance. The width of the 100 kc./sec. modulation was about 0.6 gauss. All of the measurements were made at room temperature (290~300°K.). The sweeping of the d.c. magnetic field extended from 2,000 to 5,000 gauss with the sweep rate of about 50 gauss/min.

In calcium fluorophosphate ordinarily used for the fluorescent purpose, up to several per cent. of its  $\text{Ca}^{++}$  ions are replaced by  $\text{Sb}^{+++}$  and  $\text{Mn}^{++}$  ions. With such a high concentration of  $\text{Mn}^{++}$  ions, however, many of the details of the fine and the hyperfine structures of the resonance are lost due to the increased magnetic interactions between the ions. We, therefore, prepared a sample in which there are no  $\text{Sb}^{+++}$  ions and the amount of  $\text{Mn}^{++}$  ions is made as low as  $[\text{Mn}^{++}]/[\text{Ca}^{++}] = 10^{-4}$ . The reaction employed for the synthesis was



The firing was done in an atmosphere of dry nitrogen. Figure 3 shows the e.p.r. spectra of each material appearing in the left side of reaction 5. The sharp signal at the center of each record is that of DPPH (diphenyl-picrylhydrazyl) inserted as a reference. As should be expected,  $\text{MnSO}_4$  is the only sample which gives a strong absorption, though in this case the strong magnetic interaction between the spins destroys all the structures, resulting in a single extremely broad resonance. The weak signals observed in  $\text{CaF}_2$  and  $\text{CaCO}_3$  can be recognized as equally

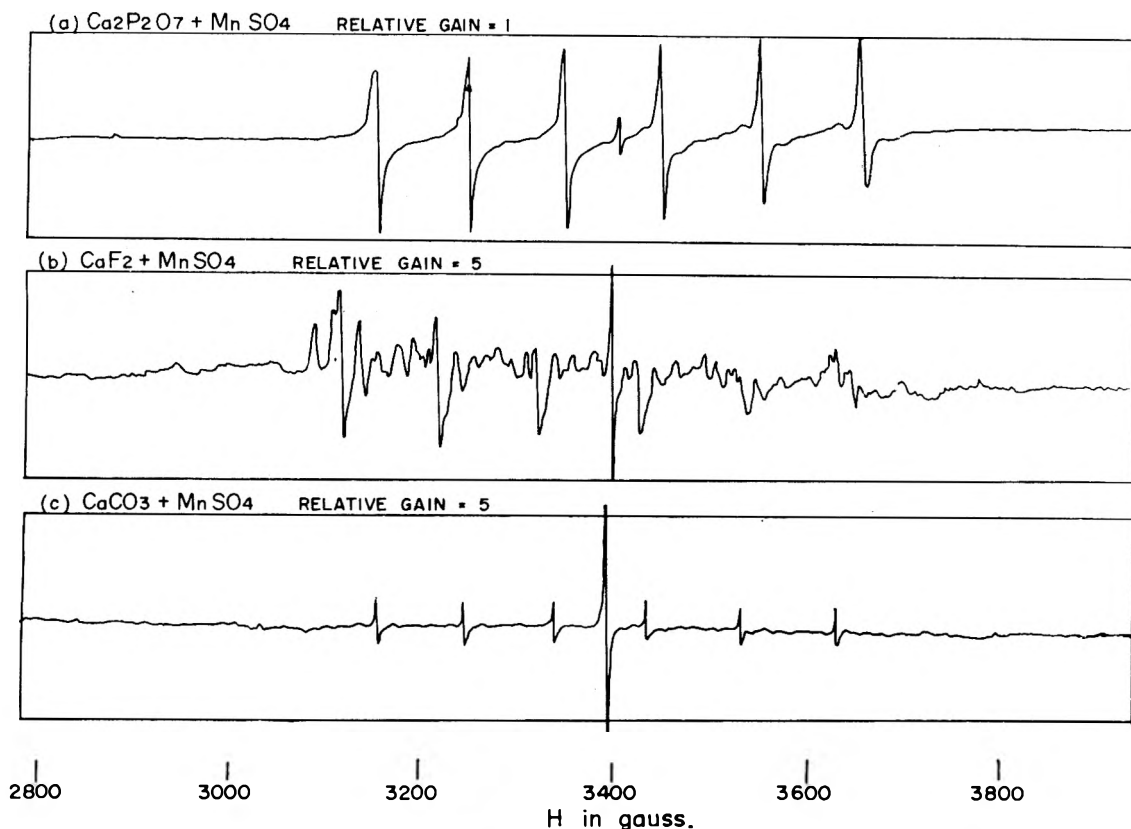


Fig. 4.—E.p.r. spectra of the samples prepared by firing each material mixed with a small amount of  $MnSO_4$ , separately for 10 min. at  $1150^\circ$ . The sharp signal at the center of each record is that of DPPH.

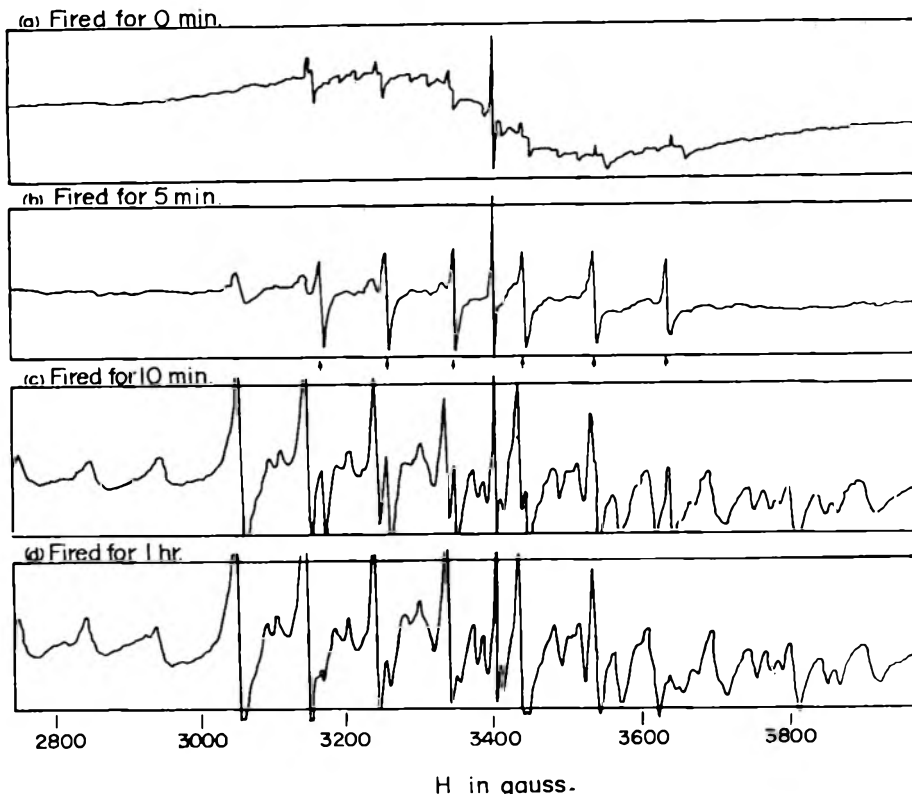


Fig. 5.—Change in the e.p.r. spectrum of the apatite's reaction mixture with the increase in the length of the firing period. The sharp signal at the center of each record is that of DPPH.

spaced six groups of lines, the center of which coincides with the DPPH signal. These signals, therefore, must be due to a trace of  $Mn^{++}$  ions already present in these mate-

rials. Then, for the purpose of comparison,  $10^{-4}$  mole fraction of  $MnSO_4$  was added to each of these materials and fired separately for 10 min. at  $1150^\circ$ . The e.p.r. spectra

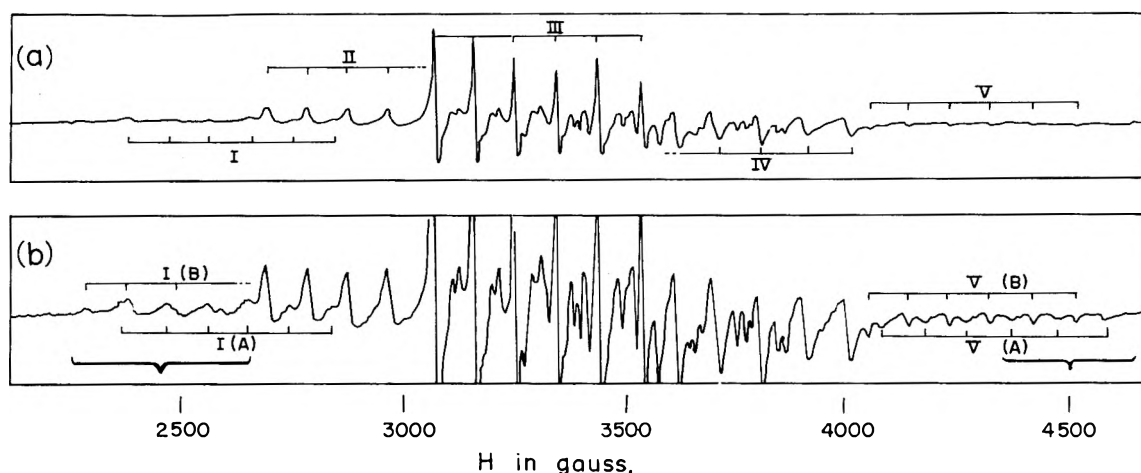


Fig. 6.—(a) The e.p.r. spectrum of  $Mn^{++}$  ion in a polycrystalline sample of calcium fluorophosphate. (b) Same spectrum observed with higher amplifier gain.

of the samples thus prepared are shown in Fig. 4. These records show that the diffusion of  $Mn^{++}$  ions takes place most rapidly into  $Ca_2P_2O_7$  and most slowly into  $CaCO_3$ , which should have been converted to  $CaO$  at this temperature. The complexity of the e.p.r. spectrum of  $Mn^{++}$  ions diffused into  $CaF_2$  probably is due to the super hyperfine interaction with  $F^{19}$  nuclei.

Figure 5 shows the e.p.r. spectra of the samples prepared by firing the mixture of the materials shown in the left side of equation 5 for 0, 5, 10, and 60 min., respectively, at  $1150^\circ$ . For 0 min. of firing, the spectrum is naturally the superposition of those of  $CaCO_3$  and  $MnSO_4$  shown in Fig. 3. After 5 min. of firing, these original spectra are completely gone and there are now two groups of signals, one group consisting of relatively sharp, equally spaced sextets (indicated by the arrows) and the other group consisting of relatively broad and weak signals. Comparison of this record with those of Fig. 4 leads us to the conclusion that the former group is due to  $Mn^{++}$  ions in  $Ca_2P_2O_7$  into which the diffusion was the easiest. None of the spectra in Fig. 4, however, resembles the latter group of broad signals. The latter group then must be attributed to  $Mn^{++}$  ions in apatite which already has begun to form. In fact with the increase in the length of the firing time, the  $Mn^{++}$  signals in  $Ca_2P_2O_7$  become weaker and the signals belonging to the latter group become progressively intensified. One therefore can conclude that the apatite's firing reaction of equation 5 is in near completion after 10 min. of firing at  $1150^\circ$ , and that with a sample which had been fired for more than 1 hr., its e.p.r. spectrum is almost entirely due to  $Mn^{++}$  ions incorporated in apatite.

#### Analysis of the Apatite Spectrum

Figure 6a shows the entire e.p.r. spectrum of the sample prepared by firing the mixture of equation 5 for 2 hr. at  $1150^\circ$ . One recognizes at once that the over-all pattern of the observed spectrum is exactly that expected when  $Mn^{++}$  ion is at the Ca(I) site. The groups of signals I, II, III, IV, and V in the figure correspond to the  $\theta = \pi/2$  positions of the curves 1, 2, 3, 4, and 5 of Fig. 2, respectively. As has been predicted, the groups I and II are showing only positive signals and the groups IV and V are showing only negative signals. The intensity ratios between the groups are also more or less in close agreement with the prediction. The magnetic field of the center of each of these groups then should be given by setting  $E = 0$  and  $\theta = \pi/2$  in equation 3. Figure 6b shows the same spectrum obtained with higher amplifier gain. A close look at the both ends of this record reveals that the groups I and V are each actually a superposition of two subgroups, I(A) and I(B),

and V(A) and V(B). The left and right end portions indicated by brackets in Fig. 6b therefore were investigated more carefully with much higher gain and slower sweep. Figures 7a and 7b show the results thus obtained for the left and the right end portions, respectively. When we pay attention only to the shapes of the signals, disregarding their intensities, we notice that the shape of the group I(A) signals is very similar to that of group V(A), while the shape of group I(B) signals resembles that of group V(B). Also the shapes of groups I(A) and V(A) are quite similar to those of groups II and IV. We therefore conclude that the  $\theta = \pi/2$  positions of the curves 1, 2, 3, 4, and 5 in Fig. 2 are represented by the groups I(A), II, III, IV, and V(A), respectively, and judging from Fig. 2b and eq. 3, groups I(B) and V(B) must correspond to  $\theta = 0$  positions of curves 4 and 2, respectively. The identification of the points corresponding to  $\theta = 0$  is quite fortunate since this enables us to evaluate eq. 3 in the absence of the second-order perturbation terms.

By letting  $E = 0$  and  $\theta = 0$  in eq. 3 and measuring the magnetic field of the centers of the groups I(B) and V(B), we obtained

$$\begin{aligned} H_0 &= 3398.8 \text{ gauss} \\ D &= 428.0 \text{ gauss} \end{aligned} \quad (6)$$

$$\text{when } \nu_{\text{microwave freq.}} = 9517.3 \text{ Mc./s.}$$

Once these values are known, eq. 3 can be used to predict the center field of each group when  $\theta = \pi/2$ . The comparisons of the values thus calculated and the experimentally measured values of the groups I(A), II, III, IV, and V(A) are shown schematically in Fig. 8. The experimental values are those corresponding to the maximum or the minimum points of the observed derivative curve, and the points truly corresponding to  $\theta = \pi/2$  probably would lie somewhat outside of them. The magnitude and the signs of the differences between the experimental values and the calculated ones thus are understandable, and the agreement must be said to be exceptionally good for the analysis of a polycrystalline sample.

If the fine structure spreading is totally due to the first order terms, the curves in Fig. 2 would be exactly symmetric and one would expect an



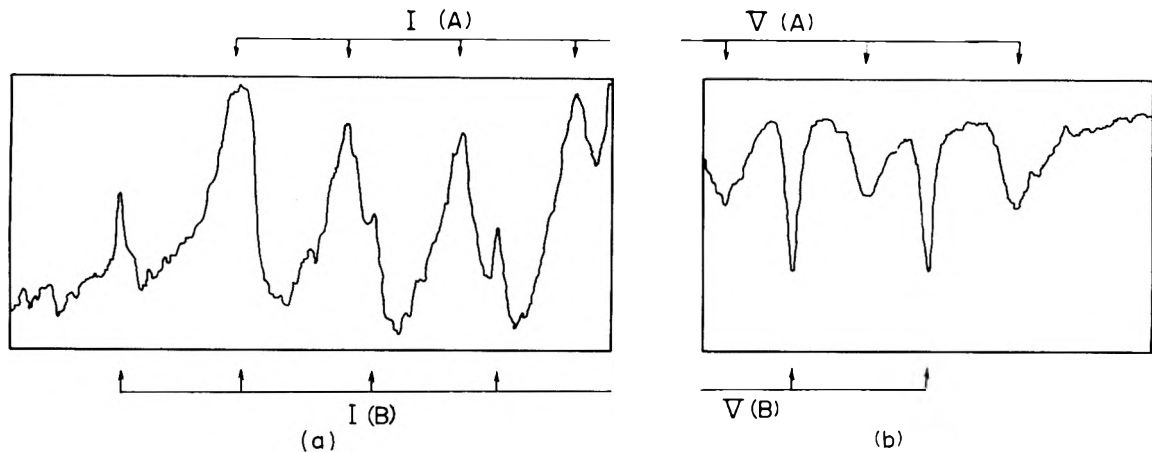


Fig. 7.—(a) A record showing the details of the left end portion indicated by a bracket in Fig. 6(b). (b) A record showing the details of the right end portion indicated by a bracket in Fig. 6b.

equal intensity for groups I(A) and V(A), and also for groups I(B) and V(B). Figure 7 shows, however, that the actual intensity ratios of these pairs are

$$\frac{I(A)}{V(A)} = \frac{2.5}{1} \quad \frac{I(B)}{V(B)} = \frac{1}{1.5} \quad (7)$$

The intensity of the group I(A), for example, should be proportional to the number of crystals having  $\theta$  that would just satisfy the resonance condition for curve 1 in the range of  $H_1(\pi/2)$  and  $H_1(\pi/2) + \Delta H$ . Here  $H_1(\pi/2)$  is the magnetic field corresponding to  $\theta = \pi/2$  of curve 1 and  $\Delta H$  is the modulation width. Then the intensity ratio between I(A) and V(A) should be given by

$$\frac{I(A)}{V(A)} = \frac{\int_{H_1(\pi/2)}^{H_1(\pi/2) + \Delta H} P_1 dH}{\int_{H_1(\pi/2) - \Delta H}^{H_1(\pi/2)} P_5 dH} \quad (8)$$

where  $P_1$  is the distribution function given by equation 4. Using eq. 3, in which  $E$  is set equal to zero, the integration of eq. 8 is straight forward. When  $\Delta H$  is small compared with  $D$  or  $q = D^2/H_0$ , it yields

$$\frac{I(A)}{V(A)} = \left( \frac{6D + 34q}{6D - 34q} \right)^{1/2} \cong \frac{2.5}{1} \quad (9)$$

and similarly for I(B) and V(B)

$$\frac{I(B)}{V(B)} = \frac{6D - 8q}{6D + 8q} \cong \frac{1}{1.5} \quad (10)$$

in exact agreement with the observed values.

Analysis of the hyperfine structure: Our analysis so far has been concerned only with the fine structure components, namely the centers of the observed hyperfine groups. In order to analyze the position of each hyperfine component one has only to add to equation 3<sup>5</sup>

$$-A_{\parallel} m - \frac{A_{\perp}^2}{2H_0} \left\{ \frac{35}{4} - m^2 + m(2M - 1) \right\} \quad (11)$$

when  $\theta = 0$ , and

$$-A_{\perp} m - \frac{A_{\perp}^2 + A_{\parallel}^2}{2H_0} \left\{ \frac{35}{4} - m^2 + m(2M - 1) \right\} \quad (12)$$

when  $\theta = \pi/2$ . From the observed hyperfine spreadings we determined

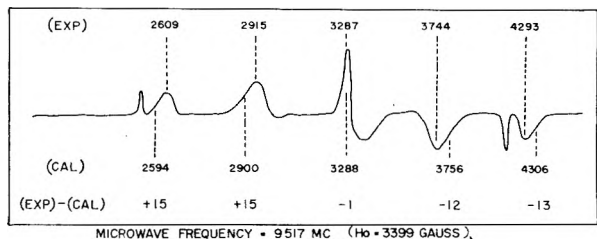


Fig. 8.—Comparison of the observed values and the calculated values for  $\theta = \pi/2$  of each fine structure component.

$$A_{\parallel} = 94.4 \text{ gauss} \quad \text{and} \quad A_{\perp} = 92.4 \text{ gauss} \quad (13)$$

Also from this analysis the signs of  $D$  and  $A$  are found to be same.

### Discussion and Summary

Even if the  $Mn^{++}$  ions are at the  $Ca(II)$  site, the e.p.r. spectrum could well be like the one observed, if the rhombic component of the crystalline field  $E$  accidentally vanishes. Judging from the crystal structure shown in Fig. 1, this is more than unlikely. Furthermore if the observed spectrum is of such nature, the effect of the fluorine nucleus situating next to the  $Ca(II)$  site should be expected. The sharpness of the observed spectrum seems to defy the presence of such an effect. Therefore, considering such factors as the intensity of the analyzed spectrum, the way these signals grow in the firing process, and the total amount of  $Mn^{++}$  ions initially introduced, we conclude that in a sample of synthetic calcium fluorophosphate most of the  $Mn^{++}$  ions are at the site of  $Ca(I)$ .

No attempt has been made to analyze the weak signals around the center portion of the spectrum. Judging from their positions most of these signals probably are due to the points other than  $\theta = \pi/2$  on curve 3.

The signs of  $D$  and  $A$  generally are not obtainable from the e.p.r. data alone. For  $Mn^{++}$  ion, however, the sign of  $A$  is almost always negative. We believe, therefore, that for the  $Mn^{++}$  ion of our particular case the signs of  $D$  and  $A$  are both negative. Watanabe has made a theoretical calculation on the ground level splitting of  $Mn^{++}$  ion in a

crystalline field.<sup>7</sup> According to his result, an axial field as large as 428 gauss could occur only in the negative region, in accordance with our deduction given above.

**Summary.**—(1) The e.p.r. spectrum of  $Mn^{++}$  ion in a polycrystalline sample of calcium fluorophosphate can be well explained by a spin Hamiltonian of the form

$$\mathcal{H} = g\beta H \cdot S + D \{S_z^2 - 1/3S(S+1)\} + A_{\parallel} S_z I_z + A_{\perp} (S_x I_x + S_y I_y)$$

and the values of the parameters therein are, at 290°K.

$$\begin{aligned} g &= 2.0005 \pm 0.0005 & A_{\parallel} &= 94.4 \pm 0.5 \text{ gauss} \\ D &= 428.0 \pm 2 \text{ gauss} & A_{\perp} &= 92.4 \pm 0.5 \text{ gauss} \end{aligned}$$

(2) The analysis of the e.p.r. spectrum of a polycrystalline sample has been thought to be extremely difficult when the fine structure splitting becomes comparable to, or larger than the hyper-

(7) H. Watanabe, *Progr. Theoret. Phys.* (Kyoto), **18**, 405 (1957).

fine structure splitting.<sup>8,9</sup> We have succeeded in showing that, at least for the case of axially symmetric crystalline field, the analysis is quite possible, leading to a fairly accurate determination of the spin Hamiltonian parameters.

(3) As discussed in the section on the sample preparation, the firing reaction employed for the synthesis of apatite is in near completion after only 10 min. of firing at 1150°. It is interesting to note that the  $Mn^{++}$  ions first diffuse into  $Ca_2P_2O_7$  grains which in turn seem to convert into apatite with further firing. These results suggest the potentiality of the e.p.r. technique for studying the hitherto little known mechanism of a solid—solid reaction typified by our example.

The author wishes to express his sincere appreciation to Dr. M. Emoto and Miss Iijima for preparing the valuable samples, and to Mr. T. Mitsuishi for his helpful discussion.

(8) Van Wieringen, *Discussions Faraday Soc.*, **19**, 118 (1955).

(9) W. D. Hershberger and H. N. Leifer, *Phys. Rev.*, **88**, 714 (1952).

## ON ENZYME CATALYZED EQUILIBRIUM POLYMERIZATIONS.<sup>1</sup>

### I. LINEAR POLYMERS BY DIRECT REACTION AND THROUGH PRIMER INITIATION

BY LEONARD PELLER<sup>2</sup> AND LEWIS BARNETT

*Department of Chemistry, University of Wisconsin, Madison, Wisconsin*

*Received September 5, 1961*

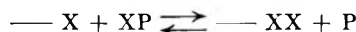
The most probable molecular weight distributions corresponding to two kinds of equilibria are derived and applied to polysaccharide and polyribonucleotide synthesis by phosphorolytic enzymes. It is demonstrated that with current estimates of the equilibrium constants for these synthetic reactions only small extents of polymerization can be expected for an equilibrium involving direct reaction of the monomer sources. An inhibited equilibrium where such direct reactions are excluded and growth occurs on some pre-existing minimal sized primer can lead to high degrees of polymerization. A kinetic picture involving direct reaction of monomers is presented which permits a high degree of polymerization at an intermediate stage in the reaction but which leads ultimately to a small extent of polymerization consistent with the thermodynamics of the systems.

#### Introduction

There are a large number of enzyme systems which reversibly bring about the formation of polymeric species from simple monomeric sources. Examples of such systems are provided by the phosphorylases which reversibly catalyze the formation of glycosidic bonds yielding linear polysaccharide chains.<sup>3</sup> The recently discovered nucleotide phosphorylases which synthesize polyribonucleotides from nucleoside diphosphates as monomer sources<sup>4</sup> also belong to this class of enzymes.

It is the purpose of this communication to develop the equilibrium molecular weight distributions for systems where the reactions involved may

be represented stoichiometrically by steps such as



In the above reaction XP represents the monomeric source—an ester of orthophosphoric or pyrophosphoric acid—and P represents orthophosphate. The chain is lengthened by the addition of successive X units which may themselves be phosphate esters, *e.g.*,  $XP \equiv ADP$  where ADP is adenosine diphosphate.

In many studies of these polymerizing systems there is considerable evidence for the "requirement" of a primer to initiate the reaction (see ref. 3). The primer is frequently a low molecular weight polymer and growth is presumed to occur at one end of the chain of the initiator. We interpret the role of the primer as removing a *kinetic barrier* to growth that exists for the direct reaction of the simple monomeric sources. The equilibrium molecular weight distribution of course is derivable without any assumptions concerning the detailed mechanisms of the polymerization processes (except for the question of primer function).

(1) Presented in part at the 138th National Meeting of the American Chemical Society, New York, N. Y., September 11–16, 1960.

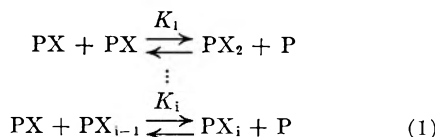
(2) National Institutes of Health, Bethesda 14, Maryland.

(3) (a) H. M. Kalekar, in "The Mechanism of Enzyme Action," ed. by W. D. McElroy and B. Glass, Johns Hopkins Press, Baltimore, 1954, pp. 675–728; (b) E. J. Hehre, in "Advances in Enzymology," ed. by F. F. Nord, Interscience, New York, N. Y., Vol. 11, 1951, pp. 297–337; (c) P. Bernfeld, in "Advances in Enzymology," ed. by F. F. Nord, Interscience, New York, N. Y., Vol. 12, 1951, pp. 379–428.

(4) M. Grunberg-Manago and S. Ochoa, *J. Am. Chem. Soc.*, **77**, 3165 (1955).

### A. Linear Polymerization by Direct Reaction of the Monomeric Sources

We first consider the case where there is no kinetic barrier to the attainment of equilibrium through the direct reaction of the monomeric sources. The various steps in the polymerization may be represented by the reactions



If the system is at equilibrium, then one can write a series of mass action expressions of the form

$$\frac{(m_i)(m_P)}{(m_{i-1})(m_{XP})} = K_i \quad (2)$$

where the activities have been approximated by the molar concentrations ( $m$ ). Invoking the assumption that all bonds formed are thermodynamically equivalent, *i.e.*,  $K_1 = \dots = K_i \equiv K$ , the molar concentration of  $i$ -mer can be written as

$$m_i = (m_{XP})(\lambda K)^{i-1} \quad (3)$$

where  $\lambda = m_{XP}/m_P$ . The mole fraction of  $i$ -mer from eq. 3 is then

$$\frac{m_i}{\sum_{k=1}^{\infty} m_k} = (1-p)p^{i-1} \quad (4)$$

where  $p = \lambda K$ . Equation 4 is of course the customary result corresponding to the most probable distribution<sup>5</sup> where  $p$  is interpreted as the equilibrium probability of bond formation.

There are two conservation conditions to be considered—(a) conservation of the monomeric moiety (X) and (b) the orthophosphate moiety (P). These conditions can be written respectively as

$$\sum_{k=1}^{\infty} k(m_k) = \sum_{k=1}^{\infty} k(m_k)_0 \quad (5a)$$

$$\sum_{k=1}^{\infty} m_k + m_P = \sum_{k=1}^{\infty} (m_k)_0 + (m_P)_0 \quad (5b)$$

where the subscript zero refers to the initial state of the system. Employing eq. 3 for the molar concentration of  $k$ -mer and eliminating  $(m_{XP})$  from eq. 5a and 5b yield the expression for  $p$

$$\frac{(1-p)^2}{p} K \langle k \rangle_0 + (1-p) \langle k \rangle_0 - \frac{(m_P)_0}{\sum_{k=1}^{\infty} (m_k)_0} - 1 = 0 \quad (6)$$

where

$$\langle k \rangle_0 = \frac{\sum_{k=1}^{\infty} k(m_k)_0}{\sum_{k=1}^{\infty} (m_k)_0}$$

is the initial number average degree of polymerization.

With only the monomer source present initially, *i.e.*

(5) P. J. Flory, "Principles of Polymer Chemistry," Cornell University Press, Ithaca, N. Y., 1953, p. 319.

$\langle k \rangle_0 = 1$  and  $(m_P)_0 = 0$ , then

$$p = \frac{1}{1 + 1/K^{1/2}} \quad (7)$$

Under these conditions number and weight average degrees of polymerization independent of the initial concentration of monomer source XP are obtained, thus

$$\nu \equiv \langle k \rangle = \frac{\sum_{k=1}^{\infty} k(m_k)}{\sum_{k=1}^{\infty} (m_k)} = \frac{1}{1-p} = 1 + K^{1/2} \quad (8)$$

$$\omega \equiv \frac{\langle k^2 \rangle}{\langle k \rangle} = \frac{\sum_{k=1}^{\infty} k^2(m_k)}{\sum_{k=1}^{\infty} k(m_k)} = \frac{1+p}{1-p} = 1 + 2K^{1/2} \quad (9)$$

For  $K = 100$  (a much higher value than usually quoted for either polysaccharide synthesis from glucose-1-phosphate or polyribonucleotide synthesis from various nucleoside diphosphates<sup>6</sup>),  $\nu = 11$  and  $\omega = 21$  so that only quite low degrees of polymerization can be anticipated. As will be apparent in the next section, the presence of high molecular weight material *at equilibrium* with  $K$  of the order of 1–10 is a consequence of the "requirement" of a primer.

It should be remarked that the polyribonucleotide phosphorylases appear to catalyze phosphodiester bond formation only at the end of the chain containing a free 3'-hydroxyl group.<sup>7</sup> Hence the equilibrium constant for the first step,  $K_1$ , should be greater by a factor of two than the equilibrium constants for subsequent steps. Making this slight amendment yields the following expression for  $p$  with only XP present initially

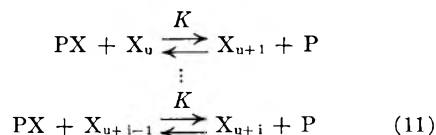
$$\frac{p^2}{(1-p)^2} [1 + (1-p)^2] = K \quad (10)$$

where  $K_1$  has been set equal to  $2K$ . Even for slight degrees of polymerization, *e.g.*,  $p = 0.75$ , the above expression closely approximates eq. 9. In any event a small dependence of  $K_i$  on  $i$  may be anticipated without seriously impairing the validity of the arguments in this paper.

### B. Linear Polymerization with a Linear Primer

We next consider the case of an equilibrium where growth takes place on some pre-existing primer species. An example of such a system might be the synthesis of polyribonucleotides from nucleoside diphosphates initiated by an oligonucleotide as a primer.<sup>8</sup>

The various steps in the polymerization may be represented as



(6) M. Cohn in "The Enzymes," ed. by P. D. Boyer, H. Lardy, and K. Myrback, Academic Press, New York, N. Y., 1961, 2nd. Ed., Vol. 5, p. 192.

(7) M. Grunberg-Manago in ref. 10, p. 260.

(8) Ref. 7, pp. 268–280.

with the explicit assumption that the equilibrium constants are identical for all these steps. For this inhibited equilibrium direct reaction of XP as in eq. 1 is presumed not to occur nor any reaction of XP with oligomers of degree of polymerization less than  $u$ , which represents the chain length of the minimal sized primer. In essence we have assumed that the enzyme is an effective catalyst for formation of chains only beyond some critical length. The implications of this assumption will be discussed further below. It might be remarked at this point that kinetic studies in the phosphorylation of oligonucleotides suggest a value for  $u$  of about two.<sup>9</sup>

For thermodynamic equilibrium in the above case we can write simple mass action expressions of the same form as in eq. 2

$$\frac{(m_{u+i})(m_P)}{(m_{u+i-1})(m_{XP})} = K \quad (12)$$

Recursive solution of these equations leads to a relation like eq. 3

$$m_{u+i} = (m_u)(\lambda K)^i \quad (13)$$

and a most probable distribution of the form

$$\frac{m_{u+i}}{\sum_{k=0}^{\infty} m_{u+k}} = (1-p)p^i \quad (14)$$

with the same definition of  $p$  as in section A.

The equilibrium probability of bond formation,  $p$ , is raised to the power  $i$  in eq. 13 and 14 rather than  $i-1$  in eq. 3 and 4 as we are counting in terms of the number of "reactive" monomeric elements in the polymeric chain.

In contrast to the case discussed previously there are three conservation conditions corresponding to (a) conservation of monomeric moiety, (b) conservation of orthophosphate, and (c) conservation of the number of chains. The last condition is peculiar to polymerizations requiring a primer which initiates synthesis at a chain end. These constraints are embodied, respectively, in the three expressions

$$\sum_{k=0}^{\infty} k(m_{u+k}) + (m_{XP}) = \sum_{k=0}^{\infty} k(m_{u+k})_0 + (m_{XP})_0 \quad (15a)$$

$$(m_{XP}) + (m_P) = (m_{XP})_0 + (m_P)_0 \quad (15b)$$

$$\sum_{k=0}^{\infty} (m_{u+k}) = \sum_{k=0}^{\infty} (m_{u+k})_0 \quad (15c)$$

Utilizing eq. 13 in conjunction with the above conservation equations yields an expression for  $p$  in terms of  $K$  and the initial concentrations, namely

$$(p-1)v_0' \left[ K + p + \left( K - \frac{p}{\lambda_0} \right) \frac{1}{\gamma_0} \right] + p^2 + pK = 0 \quad (16)$$

where

$$\gamma_0 = \frac{\sum_{k=0}^{\infty} (m_{u+k})_0}{(m_{XP})_0} \quad \text{and} \quad v_0' = \frac{\sum_{k=0}^{\infty} k(m_{u+k})_0}{\sum_{k=0}^{\infty} (m_{u+k})_0}$$

The number average degree of extension of the chain,  $\nu'$ , can be written

(9) M. F. Singer, *J. Biol. Chem.*, **232**, 211 (1958).

$$\nu' = \frac{\sum_{k=0}^{\infty} k(m_{u+k})}{\sum_{k=0}^{\infty} (m_{u+k})} = \frac{p}{1-p} = v_0' \left[ 1 + \frac{1}{\gamma_0} \frac{(1-\lambda/\lambda_0)}{(1+\lambda)} \right] \quad (17)$$

The actual number average degree of polymerization of the chains,  $\nu$ , exclusive of the unreacted XP, is

$$\nu = \frac{\sum_{k=0}^{\infty} (u+k)(m_{u+k})}{\sum_{k=0}^{\infty} m_{u+k}} = u + \nu' = u + \frac{p}{1-p} \quad (18)$$

The analogous weight average degree of polymerization,  $\omega$ , is given by

$$\omega = \frac{\sum_{k=0}^{\infty} (u+k)^2(m_{u+k})}{\sum_{k=0}^{\infty} (u+k)(m_{u+k})} = u + \frac{p(1+p) + up(1-p)}{p(1-p) + u(1-p)^2} \quad (19)$$

It is worthwhile examining eq. 16 under certain extreme polymerizing conditions, namely; only the minimal sized primer present initially, *i.e.*,  $(m_{u+k}) = 0$ ,  $k \neq 0$  and no orthophosphate present initially, *i.e.*,  $(m_P)_0 = 0$  or  $1/\lambda_0 = 0$ . Under these conditions  $v_0' = 0$ , as the minimal sized primer contains no reactive X units and  $v_0'/\gamma_0 = (m_{XP})_0/(m_u)_0$ . Solving the awkward quadratic eq. 16 for  $p$ , one obtains

$$p \cong \lambda K = \frac{- \left[ \frac{(m_{XP})_0}{(m_u)_0} + 1 \right] K + \left\{ K^2 \left[ \frac{(m_{XP})_0}{(m_u)_0} + 1 \right]^2 + 4K \frac{(m_{XP})_0}{(m_u)_0} \right\}^{1/2}}{2} \quad (20a)$$

Expanding the square root with retention of the first two terms yields

$$p \cong \frac{1}{1 + (m_u)_0/(m_{XP})_0} \quad (20b)$$

For  $K \sim 10$  and  $(m_{XP})_0/(m_u)_0 \sim 10$  such a truncated expansion is valid and indicates that  $p \rightarrow 1$  as the ratio of monomeric source to primer becomes large. High degrees of polymerization thus are obtainable by increasing the concentration ratio of monomeric source to potential chain ends. This is of course the common method of producing high molecular weight material in certain effectively irreversible polymerizations as evidenced by polypeptide syntheses.<sup>10</sup> In this latter case, however, a narrow Poisson distribution<sup>11,12</sup> can be obtained.

As  $p \rightarrow 1$ , a good approximation to the equilibrium constant  $K$  is provided by  $1/\lambda = (m_P)/(m_{XP})$ . The apparent lack of dependence of the equilibrium ratio  $\lambda$  on primer and initial XP concentration observed when the monomer source is glucose-1-phosphate in the glycogen primed synthesis of polysaccharides<sup>13</sup> doubtless is attributable to a low

(10) E. Katchalski and M. Sela in "Advances in Protein Chemistry," ed. by C. B. Anfinsen, K. Bailey, M. L. Anson, and J. T. Edsall, Academic Press, New York, N. Y., Vol. 13, 1958, pp. 302-307.

(11) P. J. Flory, *J. Am. Chem. Soc.*, **62**, 1561 (1940).

(12) L. Gold, *J. Chem. Phys.*, **28**, 91 (1958).

concentration of chain ends compared to monomeric source.<sup>14</sup> Equating  $K$  to  $1/\lambda$  has been a common practice in the biochemical literature without a clear recognition of the conditions necessary to validate such a procedure. The dependence of  $\lambda$  on the initial concentrations when the above conditions are not met will be discussed further in the following paper for glycogen. The latter functions as a branched chain primer in the phosphorylase catalyzed formation of 1,4-glycosidic bonds.

While the *exact* proximity of  $p$  to unity does not sensibly affect the magnitude of the equilibrium ratio  $\lambda$ , it of course enormously affects the extent of polymerization. However, even as  $p \rightarrow 1$  in the case discussed above of only a limit primer initially present and  $(m_P)_0 = 0$  or  $1/\lambda_0 = 0$ , it can be seen from eq. 17 that the increase in the number average degree of polymerization of the chains is limited for a finite equilibrium constant, that is

$$\Delta\nu = \nu' - \nu_0' = \frac{(m_{XP})_0}{(m_u)_0} \frac{K}{K+1} \quad (21)$$

where  $(m_{XP})_0/(m_u)_0$  is of such magnitude that  $p \rightarrow 1$  and  $\lambda \rightarrow 1/K$ . Only for  $K \gg 1$  does  $\Delta\nu$  approach a value to be expected for complete incorporation of XP into polymer, namely  $(m_{XP})_0/(m_u)_0$ . The condition of a high initial concentration of monomeric source compared to the concentration of viable chain ends ensures that for this equilibrium  $\Delta\nu$  will be quite large even if  $K$  is only of the order of unity. Increasing this concentration ratio drives the reactions in the direction of synthesis.

The equilibrium constant introduced in the preceding analysis has referred to the stoichiometric concentrations of all the species. No account has been taken of the variety of ionic forms present so the  $K$  as defined is  $pH$  dependent. It can be written for the case of XP being glucose-1-phosphate in terms of the equilibrium constant for the reaction of the uncharged species  $K_0$  and the three ionization constants of phosphoric acid ( $K_{1P}$ , etc.) and the two ionization constants of the phosphate ester ( $K_{1GP}$ , etc.) as<sup>14</sup>

$$K = K_0 \left[ \frac{1 + \frac{K_{1P}}{(H^+)} + \frac{K_{1P}K_{2P}}{(H^+)^2} + \frac{K_{1P}K_{2P}K_{3P}}{(H^+)^3}}{1 + \frac{K_{1GP}}{(H^+)} + \frac{K_{1GP}K_{2GP}}{(H^+)^2}} \right] \quad (22)$$

The  $pH$  dependence of  $K$  will be more complex for polyribonucleotide than for polysaccharide synthesis inasmuch as the former is a polyelectrolyte. One may have to take into account changes in the effective ionization constants of groups belonging to the nucleotide bases when they are incorporated into a polyelectrolyte chain. Further, the known interactions of these species with cations such as  $Mg^{++}$ , which appear to be essential for enzymatic activity<sup>7</sup>, also may affect the magnitude of the equilibrium constant introduced above.

### Discussion

Developments of the distribution statistics of reactions leading to polymerization usually are based upon the principle of the lack of dependence of the reactivity of a particular functional group

on molecular size.<sup>15</sup> Such an assumption is inherently reasonable for most polymeric systems. However, when the polymerizations are brought about by a catalyst such as an enzyme, there is substantial evidence that those parameters—Michaelis constants and maximum velocities—which characterize the kinetic behavior of the enzyme system are *not* independent of the chain length of the species. Nonetheless, for the reversible polymerizations of much biochemical interest, the equilibrium constant for formation of a particular bond should be substantially independent of chain length. This of course provides a fixed relationship between the kinetic parameters characterizing the rates in the forward and reverse direction of any *particular* step in the polymerization process. For example, if the formation of low molecular weight species as with the oligonucleotides<sup>9,16</sup> is slow compared to subsequent polymerization steps then the reverse reaction or phosphorolysis must be correspondingly slower than the phosphorolysis of higher molecular weight species. In any event the assumption of the thermodynamic equivalence of the bonds formed seems to be a reasonable hypothesis and therefore comprises a useful though restricted principle of equal reactivity independent of chain length.

A catalyst such as an enzyme functions to remove a kinetic barrier to the attainment of a *particular* equilibrium. In this regard the treatment of the polymerization initiated by a primer (section B) presupposes that the enzyme very rapidly catalyzes the growth of these chains compared to the catalysis of the rate of formation of chains *de novo* from the monomeric sources. One inhibition to equilibrium is readily removed by the enzyme while the other involving direct reaction of monomeric sources may effectively remain.

In the case of polyribonucleotide synthesis apparent plateaus in the consumption of nucleoside diphosphate with time at concentration ratios of XP to P of about 1/2 have been reached.<sup>17</sup> However, under similar conditions weight average degrees of polymerization of the order of several thousand have been observed on material separate from the monomeric sources.<sup>18</sup> The assumption of an equilibrium constant of approximately 2 for the polyribonucleotide synthesis<sup>10</sup> is in fact clearly based on the identification of the equilibrium with the inhibited type described in section B ( $p \rightarrow 1$ ). It is quite plain that a large fraction of unreacted nucleoside diphosphate ( $\sim 1/3$ ) accompanied by very high weight average degrees of polymerization is totally inconsistent with an equilibrium as described in section A. The likely presence of low molecular weight oligonucleotides as a contaminant in the preparations of polyribonucleotide phosphorylase<sup>19</sup> apparently is the origin of the initiating primer. It also would account for the qualitative observation that the weight average degree of polymerization depends directly

(15) Reference 5, pp. 75–78.

(16) R. J. Hilmoe, *Ann. N. Y. Acad. Sci.*, **81**, 660 (1959).

(17) M. Grunberg-Manago, P. J. Ortiz, and S. Ochoa, *Biochim. et Biophys. Acta*, **20**, 269 (1956).

(18) R. F. Steiner, *J. Biol. Chem.*, **235**, 2946 (1960).

(19) M. Grunberg-Manago in ref. 10, p. 270.

(13) G. T. Cori and C. F. Cori, *J. Biol. Chem.*, **135**, 733 (1940).

(14) L. Peller, *Biochim. et Biophys. Acta*, **47**, 61 (1961).

on the ratio of the concentration of monomeric source to that of impure enzyme preparation<sup>20</sup> (see eq. 21).

It is beyond the scope of this communication to attempt to develop a complete kinetic scheme to describe these phosphorylase catalyzed polymerizations. Moreover the previous discussion has made evident that it probably is crucial to treat the kinetics of various of the early steps in the polymerization as being characterized by different parameters than later stages. It is just this latter point upon which we would like to enlarge somewhat.

Recognizing that the kinetic parameters which govern the early steps in the direction of synthesis and hence also of phosphorolysis will lead to smaller rates for these two processes compared to these rates at later stages, then one readily can see how direct reaction of the monomeric sources in the absence of primer can lead to high molecular weight material at an *intermediate stage* in the reaction before the attainment of a thermodynamic equilibrium as discussed in section A. For example if production of dinucleotide is slow compared to all subsequent propagation steps, then these "nuclei" once generated will grow rapidly to form a few long chains. Eventually the growth on new "nuclei" will arise from species obtained by phosphorolysis of these long chains. Thus there may be a *high weight average degree of polymerization* from these few long chains at a relatively early stage in the reaction with an ensuing decline to much lower equilibrium values. While there is a steady depletion of nucleoside diphosphate, a maximum in the weight average degree of polymerization and in the polydispersity will occur before the attainment of equilibrium. Some such process may be at work even in the primed polymerizations where a diminution of the specific viscosity has been observed long after an apparent equilibrium has been reached.<sup>21</sup> In describing the above kinetic picture we have rather loosely used the term rate where some sort of rate constant is im-

plied. A quantitative discussion within the framework of steady-state enzyme kinetics would involve a rather large number of kinetic parameters for each step in the reaction scheme.<sup>22</sup>

With respect to polysaccharide phosphorylase, a synthesis of high molecular weight species has been reported recently involving only direct reaction of the monomeric sources, *i.e.*, glucose-1-phosphate.<sup>23</sup> Furthermore, from the absence of a terminal phosphate it has been concluded that the first step is essentially hydrolytic in character.<sup>24</sup> Owing to the effective irreversibility of the hydrolysis of glucose-1-phosphate,<sup>25</sup> the final equilibrium state of polymerization for such a system will be minute. The preceding argument concerning the high molecular weights obtainable at an intermediate stage in the reaction remains intact, however, as does the development in section B.

From a distinctly teleological point of view, it is of interest that chemical reactions without any large thermodynamic driving force toward polymerization (indeed with equilibrium constants of the order of unity) can be utilized to produce high polymers. The explanation seems to lie in the enzyme's kinetic "preference" for long chains. It is in this context that the treatment of section B must be viewed—as the condition where such a preference is so great that only a limited equilibrium is established during the period of observation.

**Acknowledgment.**—The authors are indebted to the Public Health Service and the National Science Foundation for financial support through grants to Dr. R. A. Alberty for whose interest and encouragement we are grateful. L. P. has profited greatly from several discussions of polymerization statistics with Dr. P. J. Flory.

(22) L. Peller and L. Barnett, unpublished work. See R. Simha and J. M. Zimmerman, *J. Polymer Sci.*, **42**, 309 (1959), for a treatment along conventional polymer kinetic lines for the early phases of such a polymerization with the reverse reaction or phosphorolysis neglected.

(23) B. Illingworth, D. H. Brown, and C. F. Cori, *Proc. Natl. Acad. Sci. U. S.*, **47**, 469 (1961).

(24) D. H. Brown, B. Illingworth, and C. F. Cori, *ibid.*, **47**, 479 (1961).

(25) M. R. Atkinson and R. K. Morton in "Comparative Biochemistry," ed. M. Florkin and H. S. Mason, Academic Press, New York, N. Y., 1960, Vol. 2, p. 11, quote a standard free energy of hydrolysis of about  $-5.0$  kcal./mole.

(20) R. F. Beers, *Ann. N. Y. Acad. Sci.*, **81**, 645 (1959); and J. R. Fresco and P. Doty, *J. Am. Chem. Soc.*, **79**, 3928 (1957).

(21) R. F. Beers, *Biochem. J.*, **66**, 686 (1957).

# ON ENZYME CATALYZED EQUILIBRIUM POLYMERIZATIONS.<sup>1</sup>

## II. GROWTH ON A BRANCHED CHAIN PRIMER AND COPOLYMERIZATION

BY LEONARD PELLER<sup>2</sup>

*Department of Chemistry, University of Wisconsin, Madison, Wisconsin*

*Received September 5, 1961*

The distribution statistics at equilibrium are obtained for growth on a branched chain primer. The treatment is applied to the addition of glucose units to a limit dextrin of glycogen. An analysis of some existing data points to only a fraction of the available glucose residues, which possess an unesterified hydroxyl in the 4-position, as being capable of participating in the equilibrium. A matrix formulation for copolymerization statistics is applied to the equilibrium copolymerization of two nucleoside diphosphates. Inasmuch as copolymerization as well as homopolymerization involves phosphodiester bonds between the 3' and 5'-hydroxyl groups of the ribose rings, the chief effect which might argue against random copolymerization would arise from preferential interactions between the purine and pyrimidine bases. The available experimental evidence for the primer-initiated synthesis of single chain polyribonucleotides seems to support the inference of random copolymerization at equilibrium.

### Introduction

In the preceding communication<sup>3</sup> we presented a discussion of the equilibrium molecular weight distributions which might be anticipated for certain enzyme-catalyzed reversible polymerizations. We wish to extend some of the arguments presented there for linear homopolymerizations to two other polymerization processes.

More specifically we will consider the equilibrium polymerization by phosphorylases where growth occurs on some pre-existing branched chain primer. The best known example of this process is provided by studies with glucose-1-phosphate as a monomer source and glycogen as the branched chain primer—the enzyme being a polysaccharide phosphorylase.<sup>4</sup> The presence of 1,6-linkages, the "branches," in this primer doubtless accounts in part for the inability of the enzyme, which catalyzes only the formation of 1,4-linkages, to degrade the primer beyond a "limit dextrin" under phosphorolytic conditions.

The capacity of polynucleotide phosphorylases to synthesize copolymers from various nucleoside diphosphates<sup>5</sup> encourages an examination of equilibrium binary copolymerization along certain simple statistical lines. A detailed treatment of "most probable" copolymerizations will be presented elsewhere.<sup>6</sup>

### A. Linear Polymerization on a Branched Chain Primer

The primer species in this instance is presumed to possess a number of viable chain ends in a single molecule. These would constitute some fraction (see below) of the total number of chains ending in unesterified hydroxyl groups in the 4-position of the pyranose ring for glycogen as the branched chain primer. We designate the molarity of a given polymeric species as  $m_{uij}$ . The basis for this sort of indexing can be seen by reference to Fig. 1,

which represents a glycogen species. The region within the dashed curve is presumed not to be susceptible to enzymatic attack and contains all the glucose units designated by  $u$ . The region external to this dashed curve consists of glucose units which are reactive and are designated by the symbol  $i$ . It is to be noted that the number of *growing* chains,  $j$ , is less than the total number of branches. This non-equivalence is supported by an analysis of some experimental data which will be presented below.

For a particular branched chain primer characterized by a specified number of unreactive glucose residues and growing chains, polymerization involves only a change in the number of reactive units. Hence, for the system at equilibrium simple mass action considerations suffice to relate  $m_{uij}$  to  $m_{u0j}$ , the molarity of the primer with no reactive units (the limit dextrin). We can express this relation in the following form analogous to eq. 13 of the preceding paper

$$m_{uij} = (m_{u0j})g_{ij}p^i \quad (1)$$

where  $p = \lambda K$ . The appropriate combinatorial factor,  $g_{ij}$ , for this type of polymerization has been given by Schulz<sup>7a</sup> and also by Schaeffgen and Flory,<sup>7b</sup> namely

$$g_{ij} = \frac{(i+j-1)!}{i!(j-1)!} \quad (2)$$

Equation 2 simply counts the number of ways of distributing  $i$  glucose residues among  $j$  chains with no restrictions on the number per chain.

From eq. 1 and 2, we can write a simple expression<sup>7a,7b</sup> for the mole fraction of the species ( $uij$ )

$$\frac{m_{uij}}{\sum_{k=0}^{\infty} m_{ukj}} = \frac{(i+j-1)!}{i!(j-1)!} p^i (1-p)^j \quad (3)$$

The summation is over all species with the same number of unreactive units and the same number of growing chains.

Analogously to the treatment of polymerization with a single chain primer, there are three conservation conditions.

$$\sum_{(u,k,j)} k(m_{ukj}) + (m_{XP}) = \sum_{(u,k,j)} k(m_{ukj})_0 + (m_{XP})_0 \quad (4a)$$

(7) (a) G. V. Schulz, *Z. physik. Chem.*, **B45**, 25 (1939); (b) J. R. Schaeffgen and P. J. Flory, *J. Am. Chem. Soc.*, **70**, 2709 (1948).

(1) Presented in part at the 138th National Meeting of the American Chemical Society, New York, N. Y., September 11-16, 1960.

(2) National Institutes of Health, Bethesda 14, Maryland.

(3) L. Peller and L. Barnett *J. Phys. Chem.*, **66**, 680 (1962).

(4) D. H. Brown and C. F. Cori in "The Enzymes," Ed. by P. D. Boyer, H. Lardy, and K. Myrback, Academic Press, New York, N. Y., 2nd Ed., 1959, Vol. 5, pp. 207-229.

(5) M. Grunberg-Manago, ref. 4, pp. 257-280.

(6) L. Peller, *J. Chem. Phys.*, in press.

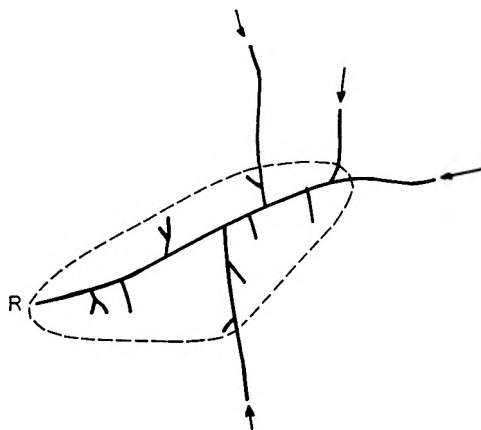


Fig. 1.—Schematic drawing of a glycogen-like branched chain primer with chain ends susceptible to phosphorylase action indicated by arrows. R designates the terminal reducing group.

$$(m_{XP}) + (m_P) = (m_{XP})_0 + (m_P)_0 \quad (4b)$$

$$\sum_{k=0}^{\infty} (m_{ukj}) = \sum_{k=0}^{\infty} (m_{ukj})_0 \quad (4c)$$

It is to be noted that there will be an equation like (4c) applying to each primer species characterized by a given value of  $u$  and  $j$ .

From the above conservation relations and eq. 3 for the distribution of species, we can derive the useful result

$$\frac{p}{1-p} = \frac{\langle k \rangle_0}{\langle j \rangle_0} + \left[ \frac{[1 - \lambda/\lambda_0]}{(1 + \lambda)} \frac{(m_{XP})_0}{\sum_{(u,k,j)} (u+k)(m_{ukj})_0} \right] \frac{\langle u+k \rangle_0}{\langle j \rangle_0} \quad (5)$$

In the absence of any detailed information concerning the initial distribution of species with different values of  $u$  and  $j$ , summations over these indices can only be accomplished formally.  $\langle \rangle$  indicates the number average of a particular quantity. It is to be noted that owing to the nature of the polymerization process  $\langle u \rangle = \langle u \rangle_0$  and  $\langle j \rangle = \langle j \rangle_0$  where the subscript zero refers to initial values of these averages. Reference to eq. 17 of the preceding paper shows that  $p/(1-p) = \nu'$ , the mean extension of a chain, and  $\langle k \rangle_0/\langle j \rangle_0 = \nu'_0$ , the initial number average degree of extension. In terms of these averages and the parameter  $p$  we can calculate the number average degree of polymerization ( $\nu$ ) as

$$\nu = \frac{\sum_{uj} \sum_{k=0}^{\infty} (u+k)(m_{ukj})}{\sum_{uj} \sum_{k=0}^{\infty} (m_{ukj})} \equiv \langle k+u \rangle = \langle u \rangle_0 + \frac{p}{1-p} \langle j \rangle_0 \quad (6)$$

The weight average degree of polymerization ( $\omega$ ) then is given by

$$\omega = \frac{\sum_{uj} \sum_{k=0}^{\infty} (u+k)^2 (m_{ukj})}{\sum_{uj} \sum_{k=0}^{\infty} (u+k)(m_{ukj})} \equiv \frac{\langle (u+k)^2 \rangle}{\langle (u+k) \rangle}$$

$$\frac{\frac{p}{(1-p)^2} \langle j \rangle_0 + \left\langle \left( u + \frac{p}{1-p} \right)^2 \right\rangle}{\langle u \rangle_0 \left[ 1 + \frac{p}{1-p} \frac{\langle j \rangle_0}{\langle u \rangle_0} \right]} \quad (7)$$

It should be noted that eq. 6 and 7 reduce to eq. 18 and 19, respectively, of the preceding article on assuming no polydispersity in  $u$ , i.e.,  $\langle u \rangle_0 = u$  and requiring the functionality of the primer to be unity, i.e.,  $\langle j \rangle_0 = 1$ . The above conditions are appropriate for a single chain primer which adds monomeric units to one end.

The customary index of the polydispersity  $\delta \equiv \omega/\nu$  is given by

$$\delta = \frac{p \langle j \rangle_0 + \langle [u(1-p) + jp]^2 \rangle}{\langle u \rangle_0^2 \left[ (1-p) + p \frac{\langle j \rangle_0}{\langle u \rangle_0} \right]^2} \quad (8)$$

When  $p = 0$ , then  $\delta = \langle u^2 \rangle / \langle u \rangle^2$ , or the polydispersity is characterized by the number of unreactive glucose residues. When  $p \rightarrow 1$ , then  $\delta \rightarrow 1/\langle j \rangle_0 + \langle j^2 \rangle_0 / \langle j \rangle_0^2$ . In this regard it is to be noted that if the average functionality of the glycogen primer,  $\langle j \rangle_0$ , is appreciably greater than unity and there is little polydispersity in this parameter so that  $\langle j^2 \rangle_0 \cong \langle j \rangle_0^2$  then  $\delta \rightarrow 1$  as  $p \rightarrow 1$ . This narrowing of the distribution with increasing functionality was pointed out some time ago for the condensation polymerization of a bifunctional monomer on a multifunctional center all of whose reactive groups are identical.<sup>7a,7b</sup> However, from a variety of studies it appears likely that glycogen is quite polydisperse with respect to the number of chains susceptible to phosphorylase action.<sup>8</sup>

It was pointed out in the previous paper<sup>3</sup> that most studies of phosphorylase catalyzed polymerization on polysaccharide primers were performed under such conditions that  $\lambda$  apparently was independent of the concentration of primer. This can be attributed to a small concentration of available chain ends to initiate growth relative to the glucose-1-phosphate present.<sup>9</sup> In such circumstances  $p$  must be very close to unity and a reliable estimate of  $\nu'$  from a knowledge of  $K$  and a measurement of  $\lambda$  would require an unattainable precision in the determination of these two quantities.

Small extents of polymerization with  $p$  substantially less than one provide some opportunity to estimate  $\nu'$  in the above fashion. In order to obtain a small degree of polymerization for this limited thermodynamic equilibrium, the concentration of primer chain ends must be of comparable magnitude to the initial concentration of monomer source. It also is significant that this condition should have the effect of minimizing the relative importance of any direct reaction of the monomeric sources. This arises from the fact that a chain end of a primer grows by addition of glucose units at a rate orders of magnitude faster than the rate of dimer formation from glucose-1-phosphate at the same concentration.<sup>10</sup>

A few experiments of this sort seem to have been performed some time ago by Hestrin, employing both glycogen and the limit dextrin of glycogen as

(8) S. Erlander and D. French, *J. Polymer Sci.*, **20**, 7 (1956).

(9) L. Peller, *Biochim. et Biophys. Acta*, **47**, 61 (1961).

(10) D. H. Brown, B. Illingworth, and C. F. Cori, *Proc. Natl. Acad. Sci. U. S. A.*, **47**, 479 (1961).

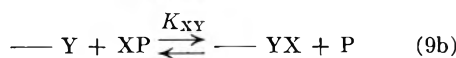
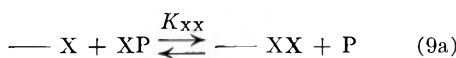


primers.<sup>11</sup> The latter is formed by exhaustive phosphorolysis of glycogen. We have taken his meager data for a given sample of the limit dextrin and calculated the quantity in brackets on the right-hand side of eq. 5.  $\nu' = p/(1 - p)$  has been calculated from his values of  $\lambda$  and  $K = 3.0$  obtained from values of  $1/\lambda$  at the same  $pH = 7.3$  but under conditions where  $p \rightarrow 1$ .<sup>12</sup> A plot of  $\nu'$  against the quantity in brackets on the right-hand side of eq. 5 is shown in Fig. 2. It is seen that the average degrees of extension of the chains indeed are quite small as indicated by the range of ordinates. A reasonably good straight line can be drawn through the three points comprising the available data on the system. The line practically passes through the origin, *i.e.*,  $\langle k \rangle_0 = 0$ , as is to be expected for this initially highly phosphorolyzed sample. The reciprocal of the slope of the line  $\langle \langle j \rangle \rangle_0 / \langle u + k \rangle_0$  which is a measure of the fraction of the total number of glucose units originally present in the primer which can initiate polymerization equals 0.041.

As these data are of course quite fragmentary and of necessity imprecise, it does not seem advisable to attach too great a significance to the above results. However, two conclusions should be emphasized. First, the results can be harmonized readily without invoking an equilibrium constant for bond formation at small degrees of polymerization which differs from that for large degrees of polymerization.<sup>4,13</sup> Secondly, a chemical analysis of the limit dextrin revealed that 0.14 of the glucose units had free hydroxyl groups at the 4-position in the pyranose ring.<sup>11</sup> If all these groups were to initiate chains the slope of the line in Fig. 2 would have to be smaller by more than a factor of three. An imprecision in the data sufficient to account for this seems unlikely. Alternatively, one must concede that only a fraction (less than  $1/3$ ) of those glucose residues possessing unesterified hydroxy groups in the 4-position can participate in this inhibited equilibrium. The remainder of these residues may lie on chains which are so short that kinetic barriers for their reaction still exist. This type of interpretation is intended to be conveyed by Fig. 1, where a number of short chains are located within the dashed curve. Obviously, further careful kinetic and equilibrium studies of a more searching nature are in order for this system.

**B. Copolymerization**

At the outset we will restrict the treatment by assuming that the equilibrium constant for the formation of a bond of a given *type* is independent of the length of the chain. For binary copolymerizations, it is apparent that there will be four equilibrium constants ( $K_{XX}$ , etc.) which must be introduced corresponding to the four reactions



(11) S. Hestrin, *J. Biol. Chem.*, **179**, 943 (1949).  
 (12) W. E. Trevelyan, P. F. Mann, and J. S. Harrison, *Arch. Biochem. Biophys.*, **39**, 419 (1952).  
 (13) M. Cohn, *ref. 4*, p. 192.

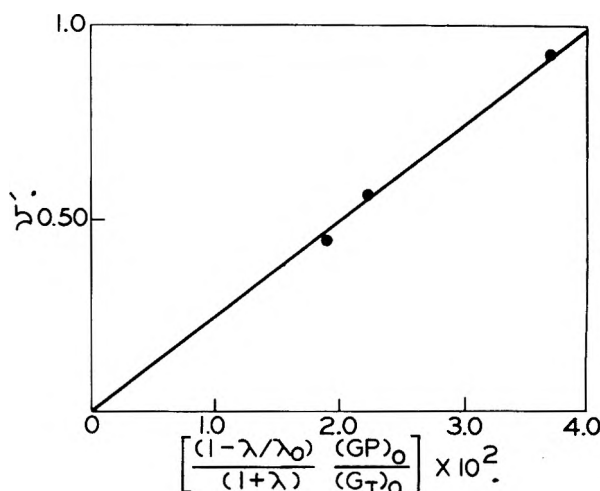
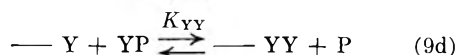
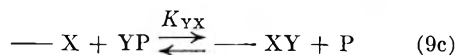


Fig. 2.—A plot of the average chain extension ( $\nu'$ ) against  $\frac{(1 - \lambda/\lambda_0) (GP)_0}{(1 + \lambda) (GT)_0}$  where  $(m_{XP})_0 \equiv (GP)_0$  and  $\sum_{ukj} (u + k) \times (m_{ukj})_0 \equiv (GT)_0$ . Points calculated using data taken from ref. 12.



XP and YP represent two different nucleoside diphosphates.

Proceeding to define a set of sequential probabilities of bond formation for steps of the above type, we have at equilibrium these relations between these probabilities and the above equilibrium constants<sup>6</sup>

$$p_{XX} = \lambda_X K_{XX} \quad (10a)$$

$$p_{XY} = \lambda_X K_{XY} \quad (10b)$$

$$p_{YX} = \lambda_Y K_{YX} \quad (10c)$$

$$p_{YY} = \lambda_Y K_{YY} \quad (10d)$$

$p_{XX}$  is the probability, an X follows an X in the chain, etc., while

$$\lambda_X = \frac{m_{XP}}{m_P} \text{ and } \lambda_Y = \frac{m_{YP}}{m_P}$$

Following an inductive procedure essentially equivalent to that employed in deriving the Ising partition function for a one-dimensional system,<sup>14,15</sup> it is possible to show that the probability of occurrence of an  $r$ -mer ( $P_r$ ), *i.e.*, its mole fraction, is given by the product of three matrices<sup>4</sup>

$$P_r = (1 \ 1) \mathbf{P}^{r-1} (\mathcal{P}_{XP} \ \mathcal{P}_{YP})^T \quad (11)$$

where

$$\mathbf{P} = \begin{pmatrix} p_{XX} & p_{XY} \\ p_{YX} & p_{YY} \end{pmatrix}, \ \mathcal{P}_{XP} = \frac{m_{XP}}{M} \text{ and } \mathcal{P}_{YP} = \frac{m_{YP}}{M}$$

are, respectively, the mole fractions of the nucleoside diphosphates XP and YP, respectively, as  $m_{XP}$  and  $m_{YP}$  are the molar concentrations of these species and  $M$  is the total molar concentration of  $r$ -mers ( $1 \leq r < \infty$ ).  $(\mathcal{P}_{XP} \ \mathcal{P}_{YP})^T$  is the transpose of the indicated row matrix, a column matrix of two elements. The above expression with the  $p$ 's expressed by eq. 10a-10d applies to the equilib-

(14) H. A. Kramers and G. H. Wannier, *Phys. Rev.*, **60**, 252 (1941).  
 (15) (a) E. W. Montroll, *J. Chem. Phys.*, **9**, 706 (1941); (b) E. N. Lassette and J. P. Howe, *ibid.*, **9**, 747 (1941).

rium distribution where direct reaction of the monomeric sources, XP and YP, is presumed to occur. The binary copolymerization thus envisioned is analogous to the homopolymerization described in section A of the previous paper. Furthermore the above relations between the sequential probabilities and the relevant equilibrium constants presuppose a numbering of the chain beginning from the end bearing an unreacted phosphate group.

Some explanation is in order concerning the definition of the  $r$ -mer whose mole fraction is given by eq. 11.  $P_r$  is the total probability of all species containing from 0 to  $r$  X units and  $r$  to 0 Y units, respectively. Therefore we have the relation

$$P_r = \sum_{i=0}^r P_{i, r-i} \quad (12)$$

where  $P_{i, r-i}$  is the probability of occurrence of a species composed of  $i$  X units and  $(r-i)$  Y units. Moreover,  $P_{i, r-i}$  is itself the sum over all possible combinations consistent with the specified number of units of each type. The subsequent discussion in terms of  $r$ -mer rather than in terms of species described in more "detail" as regards their composition and the arrangement of their constituent units obviates the construction of awkward combinatorial factors.

From the definition of  $P_r$  as a probability, it follows that

$$\sum_{r=1}^{\infty} P_r = (1 \ 1) \left[ \sum_{r=1}^{\infty} \mathbf{P}^{r-1} \right] (\phi_{XP} \ \phi_{YP})^T = 1 \quad (13a)$$

Recognizing that the sum in brackets in eq. 13a represents a convergent infinite geometric series in the matrix  $\mathbf{P}$ , one obtains, utilizing the properties of such series,<sup>16</sup> the result

$$\sum_{r=1}^{\infty} \mathbf{P}^{r-1} = (1 - \mathbf{P})^{-1}$$

where  $\mathbf{1}$  is the unit matrix of order 2. On determining the inverse of  $1 - \mathbf{P}$ , premultiplying it by  $(1 \ 1)$ , and postmultiplying it by  $(\phi_{XP} \ \phi_{YP})^T$ , eq. 13a becomes

$$\frac{(1 - p_{YY} + p_{YX})\phi_{XP} + (1 - p_{XX} + p_{XY})\phi_{YP}}{(1 - p_{XX})(1 - p_{YY}) - p_{XY} p_{YX}} = 1 \quad (13b)$$

There are two conservation relationships for the X and Y moieties, respectively, which are given by<sup>6</sup>

$$\frac{M_X}{M} = \frac{1 - p_{YY} - \phi_{YP}}{(1 - p_{XX})(1 - p_{YY}) - p_{XY} p_{YX}} \quad (14a)$$

$$\frac{M_Y}{M} = \frac{1 - p_{XX} - \phi_{XP}}{(1 - p_{XX})(1 - p_{YY}) - p_{XY} p_{YX}} \quad (14b)$$

These expressions are analogous to eq. 2a of the preceding paper with  $M_X$  and  $M_Y$  being the total molar concentrations of X and Y units, respectively. As the polymers synthesized are presumed to possess a terminal unreacted phosphate, the remaining conservation relation governing the orthophosphate moiety will be simply expressed by

$$(M) + (m_P) = (M)_0 + (m_P)_0 \quad (15)$$

This is of course identical to eq. 5b of the preceding paper with the subscript zero denoting initial values of the indicated quantities.

Equations 13–15 serve to define the concentration variables, *viz.*,  $m_{XP}$ ,  $m_{YP}$ ,  $m_P$ , and  $M$  at equilibrium in terms of the four equilibrium constants and the initial conditions. Hence, the number and weight average degrees of polymerization also are defined although convenient expressions for these quantities are better found *via* probabilities of a different type<sup>6</sup> than those given by eq. 10a–10d.

A particularly germane point concerning copolymerization involves the nature of the sequence of X and Y units to be anticipated. Following an inductive procedure of the type utilized in obtaining eq. 11, it can be shown<sup>6</sup> that the average number of times an X unit follows a like unit in the sequence  $\langle (X - X) \rangle$  is given by

$$\langle (X - X) \rangle = p_{XX} \frac{\partial}{\partial p_{XX}} [(1 \ 1) (1 - \mathbf{P})^{-1} (\phi_{XP} \ \phi_{YP})^T] \quad (16)$$

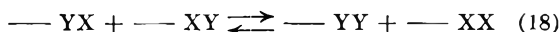
with analogous expressions for  $\langle (Y - Y) \rangle$ , etc. The partial derivative in this equation is understood to be taken holding  $\phi_X$  and  $\phi_Y$  as well as all the sequential probabilities other than  $p_{XX}$  constant. The quantity in brackets is of course equal to the left side of eq. 13b. Calculating the relevant derivatives, one obtains

$$\frac{\langle (X - X) \rangle \langle (Y - Y) \rangle}{\langle (X - X) \rangle \langle (Y - X) \rangle} = \frac{p_{XX} p_{YY}}{p_{XY} p_{YX}} \quad (17a)$$

For a system in thermodynamic equilibrium and described by chemical reactions as in eq. 9a–9d, then

$$\frac{\langle (X - X) \rangle \langle (Y - Y) \rangle}{\langle (X - Y) \rangle \langle (Y - X) \rangle} = \frac{K_{XX} K_{YY}}{K_{XY} K_{YX}} \equiv \mathcal{K} \quad (17b)$$

It immediately is apparent that  $\mathcal{K}$  is simply the equilibrium constant for the reaction



The nature of the copolymerization can be discerned by considering the magnitude of  $\mathcal{K}$ . For  $\mathcal{K} \gg 1$ , there will be a strong preference for bonds between like monomeric units or a tendency for block copolymerization; while for  $\mathcal{K} \ll 1$  there will be a tendency toward an alternating copolymeric structure through a preference for bonds between unlike monomeric elements. When  $\mathcal{K} = 1$ , there is no manifest preference, and a random copolymer will result. The arrangement of the copolymer thus is describable in terms of the position of the equilibrium for the hypothetical reaction in eq. 18. There is a striking parallel between eq. 17b and an expression defining the character of radical copolymerization involving the four rate constants of propagation.<sup>17</sup>

It is of interest that the probability matrix,  $\mathbf{P}$ , plays the same role in copolymerization statistics discussed above as the scalar probability,  $p$ , does in the familiar most probable distribution. To complete this analogy, for a system in equilibrium  $\mathbf{P}$  is factorable into a diagonal matrix,  $\mathbf{A}$ , involving the equilibrium ratios and a matrix,  $\mathbf{K}$ , composed of the elementary equilibrium constants, that is

(16) R. A. Frazer, W. J. Duncan, and A. R. Collar, "Elementary Matrices," Cambridge Univ. Press, Cambridge, 1938, p. 41.

(17) T. Alfrey, Jr., J. J. Bohrer, and H. Mark, "Copolymerization," Interscience Publishers, New York, N. Y., 1952, pp. 136–137.

$$\mathbf{P} = \Lambda \mathbf{K} \quad (19a)$$

$$\Lambda = \begin{pmatrix} \lambda_X & 0 \\ 0 & \lambda_Y \end{pmatrix} \quad (19b)$$

$$\mathbf{K} = \begin{pmatrix} K_{XX} & K_{XY} \\ K_{YX} & K_{YY} \end{pmatrix} \quad (19c)$$

For the particular system under consideration, it should be pointed out that copolymerization as well as homopolymerization involves the formation of bonds between chemically identical groups. Nucleotide phosphorylases catalyze the formation of phosphodiester bonds between the 3'- and 5'-hydroxyl groups of ribose rings. A chemically more satisfactory representation of such copolymers if  $\text{XP} \equiv \text{ADP}$  and  $\text{YP} \equiv \text{UDP}$  where ADP is adenosine diphosphate and UDP is uridine diphosphate would be



with p representing the phosphodiester bridge.

In view of the fact that these bridging groups are identical, one is strongly inclined to believe that the equilibrium constants as introduced at the beginning of this section would be effectively the same. The main possibility for departure from equivalence might lie in preferential interactions between the different nucleotide bases. If  $K_{XX} = K_{XY} = K_{YY} = K_{YX} \equiv K$ , then  $\mathcal{K} = 1$ , and a random copolymer should result. Indeed, this is a particularly stringent condition for random copolymerization. The available experimental data seem to suggest that effectively random copolymers are obtained.<sup>18,19</sup>

If the equilibrium constants for bond formation indeed are independent of the nature of the purine and pyrimidine bases, then it follows regardless of the relative concentrations of the nucleoside diphosphates that

$$p_{XX} = p_{XY} = \lambda_X K \quad (20a)$$

$$p_{YY} = p_{YX} = \lambda_Y K \quad (20b)$$

Let us examine the case where only the two nucleo-

(18) L. A. Heppel, P. J. Ortiz, and S. Ochoa, *J. Biol. Chem.*, **229**, 695 (1957).

(19) R. F. Steiner, *ibid.*, **236**, 842 (1961).

side diphosphates are present initially, *i.e.*,  $(m_P)_0 = 0$ ,  $M_X = (m_{XP})_0$ , and  $M_Y = (m_{YP})_0$ . Solution of eq. 13b, 14a, 14b, and 15 yields for the number average degree of polymerization ( $\nu$ )

$$\nu \equiv \frac{M_X + M_Y}{M} = \frac{1}{1 - (\lambda_X + \lambda_Y)K} = 1 + K^{1/2} \quad (21)$$

where

$$\lambda_X K = \frac{1}{1 + (1/K^{1/2}) \frac{(m_{XP})_0}{(m_{XP})_0 + (m_{YP})_0}} \quad (22a)$$

$$\lambda_Y K = \frac{1}{1 + (1/K^{1/2}) \frac{(m_{YP})_0}{(m_{XP})_0 + (m_{YP})_0}} \quad (22b)$$

Equation 21 is of course identical to eq. 8 of the preceding manuscript inasmuch as the equilibrium constants for copolymerization have been assumed to be identical. Once again only small degrees of copolymerization are contemplated by virtue of the magnitude of  $K$ .

However, the presence of long chains at an apparent equilibrium<sup>19,20</sup> argues for a formulation of the copolymerization which parallels that in section B of paper I. Accomplishing this requires replacement of the two elements in the matrix  $(\mathcal{G}_{XP} \ \mathcal{G}_{YP})^T$  by the probabilities of the occurrence of the minimal sized primer terminated at the growing end by an X and a Y unit, respectively. There then will be two conservation conditions fixing the numbers of chains generated from these two primers. From the manner of derivation, it is evident that eq. 17a and 17b apply to the primer initiated copolymerization as well as to copolymerization by direct reaction of the monomeric sources. Hence, the nature of the high molecular weight polyribonucleotide copolymer synthesized in the presence of the initiator also is presumed to be random at equilibrium.

**Acknowledgment.**—The author wishes to thank Dr. R. A. Alberty for his interest and his encouragement during the course of this research. Several discussions on polymerization statistics with Dr. P. J. Flory were of considerable benefit to the author. This work was supported by grants from the National Science Foundation and the Public Health Service to Dr. R. A. Alberty.

(20) R. F. Steiner, *ibid.*, **235**, 2946 (1960).

# PHOTOLYSIS OF DIETHYL KETONE IN PERFLUORODIMETHYLCYCLOBUTANE<sup>1</sup>

BY R. D. DOEPKER AND GILBERT J. MAINS

Department of Chemistry, Carnegie Institute of Technology, Pittsburgh 13, Penna.

Received September 14, 1961

The photolysis of diethyl ketone in perfluorodimethylcyclobutane solution has been studied in the 2537 Å. region at 26°. The quantum yields for ethylene, carbon monoxide, and butane were found to be of the order of  $10^{-2}$ . Evidence is presented for the disproportionation reaction between ethyl and propionyl radicals as the major route of ethane and ethylene formation at low diethyl ketone concentrations. The ratio of the specific rates of hydrogen abstraction to recombination of ethyl radicals was found to be  $4.2 \pm 0.2 \times 10^{-13}$  cc.<sup>1/2</sup> molecule<sup>-1/2</sup> sec.<sup>-1/2</sup> at 26°. One experiment using a 1:1 mixture of diethyl ketone-diethyl ketone-*d*<sub>10</sub> indicates that the formation of ethane by a "cage" process is negligible. Preliminary results on the photolysis of azoethane in the above solvent also are given.

## Introduction

The vapor phase photolysis of diethyl ketone has been studied extensively.<sup>2</sup> At temperatures above 100°, these investigations have established a well understood mechanism<sup>3-8</sup>; but at temperatures below 100° complicating factors, generally attributed to the increased stability of the propionyl radical, lead to a less certain mode of photochemical decomposition.<sup>4-7</sup> For example, Brinton and Steacie found that the introduction of an inert vapor had a marked effect on the product distribution.

It is not surprising that the liquid phase photolysis of diethyl ketone has received little attention because the nature of the solvent generally would restrict an investigation to temperatures below 100°. Norrish and Bamford<sup>8-10</sup> reported the photolysis of diethyl ketone in a solution of medicinal paraffin. They were unable to observe any decomposition products at 20° but did find some hydrocarbon products at 100°. Ausloos<sup>11</sup> investigated the photolysis of pure liquid diethyl ketone, varying both temperature and intensity, and postulated a mechanism more complex than is generally considered necessary for the vapor phase.

Recent studies<sup>12,13</sup> conducted in this Laboratory using perfluorodimethylcyclobutane as a solvent for the liquid phase photolysis of acetone led to conclusions that were consistent with the normal vapor phase mechanism provided allowance was made for diffusion effects. This solvent has been shown to be chemically inert and unreactive to the radicals formed in the photolysis of acetone.<sup>12</sup>

Photolysis of the solution leads to a system that is homogeneous with respect to reactive species. Because of the advantages of the perfluorinated solvent in acetone photolysis the present investigation was undertaken to examine the possibility of using the normal vapor phase mechanism (allowing for diffusion effects) to explain the photolysis of diethyl ketone in perfluorodimethylcyclobutane solutions.

## Experimental

The solvent employed in this investigation was perfluorodimethylcyclobutane, believed to consist of a mixture of *cis*- and *trans*-1,2-perfluorodimethylcyclobutane. The n.m.r. spectrum of this material indicated the absence of hydrogen and any olefinic impurity. The mass spectra of a liquid sample and of vapor samples collected at different temperatures gave identical patterns. The mass spectra were consistent with ions of the formula C<sub>2</sub>F<sub>8</sub>. The small side peaks which might indicate ions of the formula C<sub>2</sub>F<sub>7</sub>H<sub>2</sub> were accounted for by C<sup>13</sup> isotopes to within 1% of the total side peak. A 75-min. mercury photosensitized oxidation of a vapor phase sample of perfluorodimethylcyclobutane resulted in no change in the mass spectrum of the perfluorocarbon-oxygen mixture. The ultraviolet absorption spectrum showed the solvent to be optically transparent out to 2200 Å.

Fisher diethyl ketone (b.p. 100-102°) was purified by numerous extractions with saturated sodium bisulfite solution<sup>14,15</sup> and then dried and fractionated. The sample used in this investigation was collected at 100.2-100.4°. The diethyl ketone was degassed, distilled under vacuum into ampoules, and stored in the dark until used.

The light source employed in this research was a Hanovia UA-15 lamp coiled into a helix. The quartz reaction vessel previously described<sup>12</sup> was located within the coils of the lamp. The temperature of the reaction cell was controlled to  $\pm 0.5^\circ$  during photolysis by circulating filter solution from a reservoir in a constant temperature bath through the outer jacket of the quartz reaction cell. The filter solution was a 0.02% solution of 2,7-dimethyl-3,6-diazocyclohepta-1,6-diene iodide described by Kasha.<sup>16</sup> This solution restricted the actinic radiation to the mercury lines at 2537 and 2652 Å. Uranyl oxalate was employed as the actinometer. Using the principle of equivalent optical densities,<sup>17,18</sup> a solution of 0.0957 *M* diethyl ketone in perfluorodimethylcyclobutane was found to absorb  $8.8 \times 10^{15}$  quanta cc.<sup>-1</sup> sec.<sup>-1</sup> in the region transmitted by the filter solution.

The procedures of degassing and irradiation of the sample were the same as those employed by Peterson and Mains.<sup>12</sup> After irradiation, the gaseous products were removed by distilling the solution from the reaction vessel into one of two solvent traps. Trap to trap distillation was employed to pump off the gaseous products, which were collected with a Toepler pump. Two line traps between the Toepler

(1) Based upon a thesis submitted by R. D. Doepker in partial fulfillment of the requirements for the degree of Doctor of Philosophy, Carnegie Institute of Technology.

(2) W. A. Noyes, Jr., G. E. Porter, and J. F. Jolley, *Chem. Revs.*, **56**, 49 (1956).

(3) L. M. Dorfman and Z. D. Sheldon, *J. Chem. Phys.*, **17**, 511 (1949).

(4) M. H. J. Wijnen and E. W. R. Steacie, *Can. J. Chem.*, **29**, 1092 (1951).

(5) K. O. Kutschke, M. H. J. Wijnen, and E. W. R. Steacie, *J. Am. Chem. Soc.*, **74**, 714 (1952).

(6) R. K. Brinton and E. W. R. Steacie, *Can. J. Chem.*, **33**, 1840 (1955).

(7) P. Ausloos and E. W. R. Steacie, *ibid.*, **32**, 593 (1954).

(8) R. G. W. Norrish and C. H. Bamford, *Nature*, **138**, 1016 (1936).

(9) R. G. W. Norrish and C. H. Bamford, *ibid.*, **140**, 195 (1937).

(10) C. H. Bamford and R. G. W. Norrish, *J. Chem. Soc.*, 1531 (1938).

(11) P. Ausloos, *Can. J. Chem.*, **36**, 400 (1958).

(12) D. B. Peterson and G. J. Mains, *J. Am. Chem. Soc.*, **81**, 3510 (1959).

(13) R. D. Doepker and G. J. Mains, *ibid.*, **83**, 294 (1961).

(14) H. W. Huyser and A. Schaafsma, *Chem. Abstr.*, **37**, 139 (1943).

(15) A. W. Stewart, *J. Chem. Soc.*, **87**, 185 (1905).

(16) M. Kasha, *J. Opt. Soc. Am.*, **38**, 429 (1948).

(17) D. H. Volman and J. C. Chen, *J. Am. Chem. Soc.*, **81**, 756 (1959).

(18) I. M. Claessen, *Arkiv Kemi*, **10** (1956).

TABLE I  
 PHOTOLYSIS RESULTS AT 26.0° AND 2537 Å.

Diethyl ketone			$R_{CO}$	$R_{C_2H_6}$	$R_{C_2H_4}$	$R_{C_4H_{10}}$	$\frac{R_{C_2H_6}}{R_{C_2H_4}}$	$\frac{R_{C_2H_4}}{R_{C_4H_{10}}}$	$[\frac{1}{2}(C_2H_6 + C_2H_4) + C_4H_{10}]/CO$
Molecules, cc. <sup>-1</sup> × 10 <sup>-19</sup>	Irrad., sec.	Volume gas, cc. at S.T.P.	molecules cc. <sup>-1</sup> sec. <sup>-1</sup> × 10 <sup>-13</sup>						
0.777	660	0.499	23.1	4.82	6.35	1.71	0.76	3.71	0.32
1.61	540	.525	33.0	8.22	8.67	2.57	0.95	3.37	.33
2.63	420	.299	19.5	7.04	5.68	1.15	1.25	4.94	.39
3.52	360	.585	35.7	15.5	11.8	4.86	1.31	2.41	.52
4.70	360	.555	39.6	20.4	13.0	6.38	1.57	2.04	.58
5.76	360	.802	51.4	33.2	16.4	9.80	2.02	1.67	.68

Azoethane			$R_{N_2}$	$R_{C_2H_6}$	$R_{C_2H_4}$	$R_{C_4H_{10}}$	$\frac{R_{C_2H_6}}{R_{C_2H_4}}$	$\frac{R_{C_2H_4}}{R_{C_4H_{10}}}$	$[\frac{1}{2}(C_2H_6 + C_2H_4) + C_4H_{10}]/N_2$
Molecules, cc. <sup>-1</sup> × 10 <sup>-19</sup>	Irrad., sec.	Volume gas, cc. at S.T.P.	molecules cc. <sup>-1</sup> sec. <sup>-1</sup> × 10 <sup>-13</sup>						
2.63	540	0.390	29.1	2.84	3.08	2.37	0.922	1.30	0.18
4.54	360	0.283	29.4	3.30	3.41	2.35	0.968	1.45	0.19

pump and the solvent trap were cooled in a methanol slush bath to condense out any escaping solvent and diethyl ketone. It was found possible to remove essentially all of the carbon monoxide, ethane, and ethylene, and over 95% of the butane by this method. These gaseous products so collected were analyzed with a Consolidated Electro-dynamics Type 21-103C mass spectrometer.

### Results

Six different diethyl ketone ampoules were selected to lead to the widest possible range of sample concentrations. The samples were run in random order to lessen any cumulative effect arising from lamp aging. For each ampoule new solvent was used. These runs are given in Table I.

The quantum yields of the gaseous products observed from the decomposition of a 0.0957 *M* diethyl ketone solution determined in this investigation are given in Table II. Here also are included quantum yields calculated from the data of Kutschke, Wijnen, and Steacie<sup>5</sup> and from data reported by Ausloos.<sup>11</sup> Inasmuch as these data have been taken under somewhat different experimental conditions of light intensity and wave length, the calculated quantum yields must be regarded as qualitative estimates.

TABLE II

QUANTUM YIELDS FOR THE PHOTOLYSIS OF DIETHYL KETONE AT 26° AND 2537 Å.

System	$\Phi_{C_2H_4}$	$\Phi_{CO}$	$\Phi_{C_4H_{10}}$
Diethyl ketone-vapor <sup>a</sup>	8 × 10 <sup>-2</sup>	0.60	0.56
Diethyl ketone-liquid <sup>a</sup>	4.2 × 10 <sup>-2</sup>	5.1 × 10 <sup>-2</sup>	2.7 × 10 <sup>-2</sup>
0.096 <i>M</i> diethyl ketone in per-fluorodimethylcyclobutane	1.9 × 10 <sup>-2</sup>	5.8 × 10 <sup>-2</sup>	1.1 × 10 <sup>-2</sup>

<sup>a</sup> Calculated from data reported in references 5 and 11.

Three major differences between the vapor phase results and the results of this study can be seen in Tables I and II. The ratio of ethylene to butane is greatly increased; at low concentrations the production of ethylene exceeds ethane; and the material balance is much less than one.

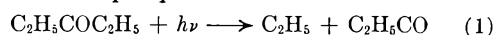
Owing to these observations, results of two experiments using azoethane as the source of ethyl radicals also are given in Table I. A limited supply of fluorocarbon prevented a more extensive study of azoethane photolysis.

One experiment involving a 1:1 mixture of diethyl ketone and diethyl ketone-*d*<sub>10</sub> was undertaken to examine the possibility of a "cage" reaction. The isotopic distribution of ethanes was found to be as follows: C<sub>2</sub>H<sub>6</sub> = 47.7%, C<sub>2</sub>H<sub>5</sub>D =

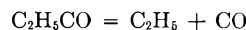
12.1%, C<sub>2</sub>D<sub>5</sub>H = 33.1%, C<sub>2</sub>D<sub>6</sub> = 7.2%. The analysis of the ethylenes gave C<sub>2</sub>H<sub>4</sub> = 68.0% and C<sub>2</sub>D<sub>4</sub> = 32.0%. The mass spectrum of the butane fraction indicated the presence of mixed deuteriobutanes. This fraction was too small for confident analysis.

### Discussion

**Primary Process.**—At temperatures below 60°, the primary process for the photolysis of diethyl ketone in the vapor phase at 2537 Å. is



The propionyl radical eventually may decompose by excess energy carried over from the primary process or by the thermal reaction



Weir<sup>19</sup> concluded that photodissociation of diethyl ketone at 2537 Å. occurs from an excited singlet state. He found no evidence for a triplet state at this wave length. Therefore, it appears that in the liquid phase at 26° the above primary process adequately explains the primary photochemical split of the diethyl ketone molecules. The reduction of the quantum yield from near unity in the vapor phase to 10<sup>-2</sup> in the liquid phase can be explained either by a recombination or a deactivation mechanism. Doepker and Mains<sup>13</sup> observed a decrease in the quantum yield of acetone decomposition to 10<sup>-4</sup> when photolyzed in a perfluorodimethylcyclobutane solution. The observed difference in quantum yield between the liquid phase photolysis of acetone and diethyl ketone may be explained by the absence of a long lived triplet state in diethyl ketone which is present in acetone.<sup>2,19</sup>

It is possible to imagine that geminate recombination may reduce the quantum yield by a factor of 10<sup>-2</sup>, but the results of the photolysis of a mixture of light and heavy diethyl ketone do not indicate the importance of a "cage" reaction as a means of ethane formation. Both C<sub>2</sub>D<sub>5</sub>H and C<sub>2</sub>H<sub>5</sub>D are relatively important products and could not arise from geminate "cage" reactions. If the ratios C<sub>2</sub>H<sub>6</sub>/C<sub>2</sub>D<sub>5</sub>H and C<sub>2</sub>H<sub>5</sub>D/C<sub>2</sub>D<sub>6</sub> are taken as rough measures of the ratio of C<sub>2</sub>H<sub>5</sub> and C<sub>2</sub>D<sub>5</sub> in the bulk solution it is found that there are about 50% more C<sub>2</sub>H<sub>5</sub> radicals than C<sub>2</sub>D<sub>5</sub> radicals. Because the

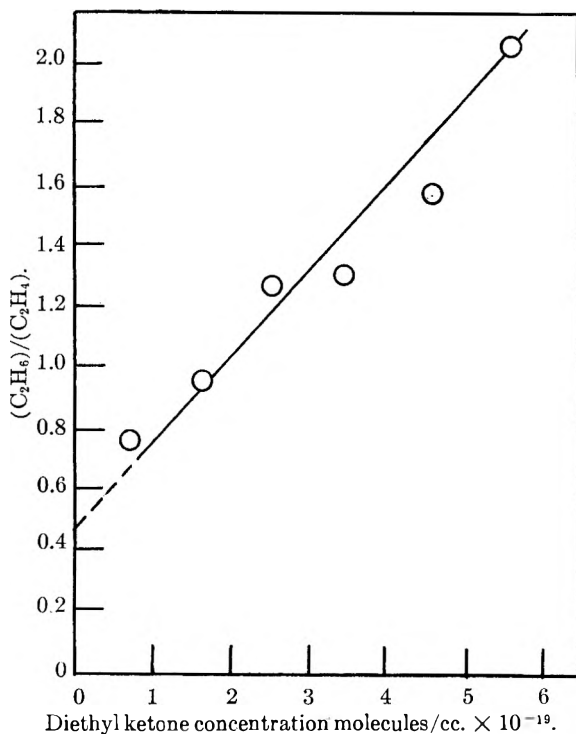


Fig. 1.

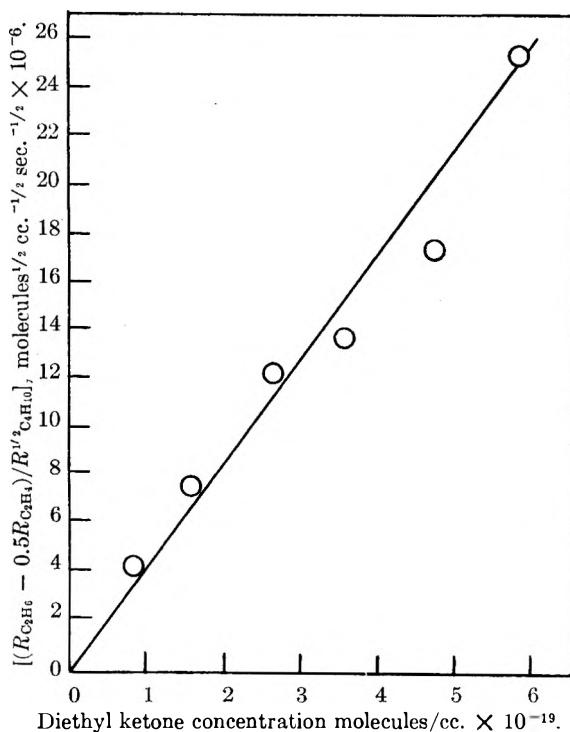
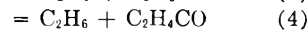
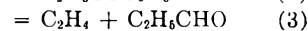
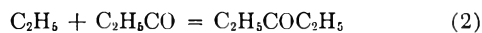


Fig. 2.

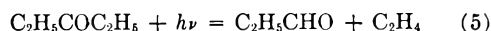
initial ratio of diethyl ketone to diethyl ketone-*d*<sub>6</sub> was analyzed as unity by mass spectroscopy, the decreased yield of C<sub>2</sub>D<sub>6</sub> must be attributed to isotope effects on the primary process in solution. The ratio C<sub>2</sub>H<sub>4</sub>/C<sub>2</sub>D<sub>4</sub> also reflects the abundance of C<sub>2</sub>H<sub>6</sub> radicals in solution and, since these products arise mainly from disproportionation reactions (*v. i.*), an isotope effect on these disproportionations. The following disproportionation and recombina-

tion processes for the ethyl and propionyl radicals within the "solvent cage" and in the bulk liquid must be considered



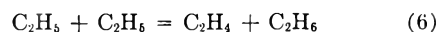
Superficially, it seems unlikely that reaction 2 could be of much importance in the solvent "cage" if (4) is not. Ausloos<sup>11</sup> has estimated that the rate of disproportionation (3) to the rate of the recombination (2) is roughly 0.02 for pure liquid diethyl ketone. This possibly could explain the order of magnitude of the decrease in quantum yield when passing from the vapor into the liquid phase. These experiments cannot distinguish between solvent quenching and primary recombination as the means by which the quantum yield is reduced. However, in the authors' opinion, the sum of evidence seems to favor solvent quenching as the mechanism by which large reductions are accomplished in the quantum yields of ketone photolysis products.

The relatively high ethylene yield could result from a primary process such as



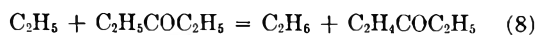
Though the critical experiments using free radical scavengers could not be made owing to the depletion of the supply of perfluorocarbon, Ausloos<sup>11</sup> has placed an upper limit for the quantum yield of this process in pure liquid diethyl ketone at  $5 \times 10^{-3}$ . Since there is no evidence that the nature of the solvent profoundly alters the primary process, it seems reasonable to exclude reaction 5 on the basis of Ausloos' study.

**Secondary Reactions.**—The rate of formation of hydrocarbon products in the vapor phase photolysis of diethyl ketone at 100° has been attributed to the disproportionation to recombination of ethyl radicals



The ratio of disproportionation to recombination of ethyl radical in the vapor phase is generally accepted as 0.12 while here in the liquid phase the ratio of ethylene to butane is considerably higher. The excess ethylene to butane ratio could be explained by assuming some orientation effect due to the solvent, leading preferentially to disproportionation of the ethyl radical. This would be consistent with the results found for azoethane. However, there is no "*a priori*" reason to expect such a highly specific solvation effect in perfluorodimethylcyclobutane. An alternative explanation is that the excess ethylene is formed through the disproportionation of an ethyl radical and a propionyl radical (3). This postulate is consistent with the data reported for azoethane photolysis if it is assumed a reaction similar to (3) will occur with the C<sub>2</sub>H<sub>5</sub>N<sub>2</sub> and C<sub>2</sub>H<sub>5</sub> radicals. Furthermore, if the ratio of disproportionation to recombination of ethyl radicals is the same in the liquid phase as observed in the vapor phase, then reaction 6 is a negligible source of ethane and ethylene. Based upon these arguments the production of

ethane must be accomplished primarily by the abstraction of a hydrogen atom from diethyl ketone by an ethyl radical



and by reaction 4. Assuming reactions 3, 4, and 8 as the only means of producing ethane and ethylene, a plot of the rate of ethane divided by the rate of ethylene *vs.* diethyl ketone concentration should lead to a positive intercept, equal to  $k_4/k_3$ . In Fig. 1,  $k_4/k_3$  is found to be  $0.50 \pm 0.05$ .

Assuming the above value for  $k_4/k_3$ , and that butane is produced solely by reaction 7, then the following equation may be deduced

$$\frac{R_{\text{C}_2\text{H}_6} - 0.50R_{\text{C}_2\text{H}_4}}{R^{1/2}_{\text{C}_4\text{H}_{10}}} = \frac{k_8}{k_7^{1/2}} (\text{DEK})$$

The left-hand side of this equation should be a linear function of diethyl ketone concentration as is observed in Fig. 2, where the data of Table I are plotted.

The slope of the line yields  $k_8/k_7^{1/2}$  directly. The value obtained in this study at  $26^\circ$  is given in

TABLE III

RATIO OF THE SPECIFIC RATE CONSTANTS FOR ABSTRACTION TO RECOMBINATION OF ETHYL RADICALS

Temp., °C.	System	$E_{\text{vis}},^a$ kcal./ mole	$k_8/k_7^{1/2}$		Ref.
			$\text{cc.}^{1/2}$ mole- cules $^{-1/2}$ sec. $^{-1/2}$ $\times 10^{14}$		
25	Diethyl ketone-vapor	0.0	10		11
28	Diethyl ketone-liquid	1.8	26		11
26	Diethyl ketone-perfluoro- dimethylcyclobutane	3.2	$42 \pm 2$		This re- search

<sup>a</sup> Activation energy for viscosity deduced from the temperature dependence of the viscosity of the solvent.

Table III along with the results of other investigations.

It should be noted that the data in Table III are consistent provided the recombination of ethyl radicals is assumed to be diffusion-controlled in the liquid phase. If the activation energy for ethyl radical diffusion is approximately the same as the activation energy for viscosity the increase in  $k_8/k_7^{1/2}$  in passing from the vapor phase to the perfluorodimethylcyclobutane solvent is understood. These trends in the ratio of  $k_8/k_7^{1/2}$  are similar to those observed for methyl radicals.<sup>13</sup> As in the case of acetone the vapor phase photolysis mechanism provides a reasonable explanation of the liquid phase photolysis data. The increased importance of reaction 3 in the liquid phase over the vapor phase can be attributed to solvent stabilization of the energetic propionyl radical. Preliminary studies of the flash photolysis of diethyl ketone<sup>20</sup> find an excess of ethylene as would be expected based upon reaction 3. Therefore it would appear that solvent stabilization of energetic radicals as well as diffusion effects must be considered in the application of vapor phase mechanisms to liquid phase studies.

**Acknowledgment.**—R. D. Doepker wishes to acknowledge financial support provided by a grant from the Petroleum Research Fund of the American Chemical Society. The authors wish to thank Dr. M. H. J. Wijnen for stimulating discussions on the results here reported, and Dr. Amos Newton for valuable criticism of the original manuscript. Grateful acknowledgment is made to Dr. C. A. Sperati and to E. I. du Pont de Nemours & Co. for generously supplying the perfluorinated solvent for these studies.

(20) L. Fischer and G. J. Mzins, unpublished data.

## RARE EARTH DISILICIDES<sup>1</sup>

BY I. P. MAYER, EPHRAIM BANKS, AND BEN POST

*Polytechnic Institute of Brooklyn, Brooklyn, New York*

*Received September 20, 1961*

Disilicides of yttrium and of a number of the heavier rare earth metals have been prepared. X-Ray diffraction analysis indicates that the yttrium compound is dimorphic, crystallizing in the hexagonal system (AlB<sub>2</sub> type) at low temperatures and in the orthorhombic system (distorted form of the tetragonal ThSi<sub>2</sub> structure) at higher temperatures. Tb and Ho disilicides are orthorhombic while the disilicides of Er, Tm, Yb, and Lu are hexagonal. The composition of the YbSi<sub>2</sub> phase was investigated by X-ray diffraction methods; within the limits of experimental error, the unit cell contains two silicon atoms for each ytterbium atom, as indicated by the formula.

The preparation and the crystal structures of many of the rare earth disilicides have been described by Brauer and Haag,<sup>2</sup> and, in greater detail, by Perri, *et al.*<sup>3</sup> The latter reported that the disilicides of the rare earth metals with relatively large atomic radii (Eu, La, Ce, and Pr) were tetragonal and isostructural with ThSi<sub>2</sub>. The corresponding disilicides of the smaller lanthanides (Nd, Sm, Gd, Dy, and Y) were found to crystallize

in a slightly distorted, orthorhombic, version of the ThSi<sub>2</sub> structure.

Zachariasen<sup>4</sup> had found that the disilicides of several actinide metals crystallized in the ThSi<sub>2</sub> structure. He also reported that USi<sub>2</sub> exists in both an "alpha," tetragonal form (ThSi<sub>2</sub> type) and a "beta" hexagonal, form (AlB<sub>2</sub> type). Subsequently, Brown and Norreys<sup>5</sup> found that ThSi<sub>2</sub> itself exists in both these two modifications. The "beta" hexagonal structure also has been reported

(1) Supported by the Office of Scientific Research, U. S. Air Force.  
(2) G. Brauer and H. Haag, *Z. anorg. u. allgem. Chem.*, **267**, 198 (1952).  
(3) J. A. Perri, I. Binder, and B. Post, *J. Phys. Chem.*, **63**, 616 (1959).

(4) W. H. Zachariasen, *Acta Cryst.*, **2**, 94 (1949).  
(5) (a) A. Brown and J. J. Norreys, *Nature*, **183**, 673 (1949); (b) *J. Inst. Metals*, **89**, 238 (1961).

for  $\text{PuSi}_2$ <sup>6</sup> and, more recently, for  $\text{YbSi}_2$ <sup>7</sup> and  $\text{YSi}_2$ .<sup>8</sup>

The present work was undertaken to study further the relations between the crystal structures and the sizes of the metal atoms in rare earth disilicides, with particular emphasis on rare earth metals which had not been investigated previously.

### Experimental

In Table I we list disilicides prepared in the course of the present investigation, the optimum reaction temperatures, and the reaction times. The compounds were prepared either by direct reaction between the metal and silicon, or by silicon reduction of the metal oxides. The silicon monoxide formed in the latter case always was completely removed from the reaction mass in the course of the reaction.

The reactions were carried out in alumina crucibles; the samples were heated by induction in a protective atmosphere of helium; a molybdenum transducer was used. The maximum specimen temperature that was achieved in this way was about 1550°

TABLE I  
PREPARATIVE CONDITIONS: DISILICIDES OF LANTHANIDE METALS

Compound	Temp. of preparation, °C.	Duration of heating, hr.	Starting materials
$\text{TbSi}_2$	1300	1	$\text{Tb}_2\text{O}_3 + \text{Si}$
$\text{HoSi}_2$	1300	1	$\text{Ho} + \text{Si}$
$\alpha\text{YSi}_2$	1500	1	$\text{Y} + \text{Si}$
$\text{ErSi}_2$	1150	4-5	$\text{Er} + \text{Si}$
$\text{TmSi}_2$	1500	4-5	$\text{Tm}_2\text{O}_3 + \text{Si}$
$\text{YbSi}_2$	900-1400	1	$\text{Yb (or Yb}_2\text{O}_3) + \text{Si}$
$\text{LuSi}_2$	1500	4-5	$\text{Lu}_2\text{O}_3 + \text{Si}$
$\beta\text{YSi}_2$	1100	4-5	$\text{Y} + \text{Si}$

In the cases of the Tm and Lu preparations the reactions were not complete even after relatively long heating periods; X-ray diffraction photographs of the reaction products always indicated the presence of some of the starting materials.

X-Ray diffraction methods were used in the analysis of all the reaction products. In most instances a Philips diffractometer was used with filtered  $\text{CuK}$  radiation; where insufficient amounts of material were available, Debye-Scherrer film methods were used.

### Results

Crystal data for the disilicides which we prepared are listed in Table II. It is seen that the orthorhombic modification, reported by Perri, *et al.*,<sup>3</sup> for Nd, Sm, Gd, Dy, and Y disilicides, is also the stable crystalline form of the Tb and Ho disilicides. However, the four heaviest rare earth metals (Er, Tm, Yb, and Lu), all form hexagonal disilicides. In the case of  $\text{YbSi}_2$ , this is somewhat surprising, since, by analogy with  $\text{EuSi}_2$ , a

TABLE II  
CRYSTAL DATA FOR DISILICIDES

Compound	Crystal system	Lattice constants		
		a	b	c
$\text{TbSi}_2$	Orthorhombic	4.045	3.96	13.38
$\text{HoSi}_2$	Orthorhombic	4.03	3.97	13.31
$\alpha\text{YSi}_2$	Orthorhombic	4.05	3.95	13.40
$\beta\text{YSi}_2$	Hexagonal	3.85	..	4.14
$\text{ErSi}_2$	Hexagonal	3.78		4.09
$\text{TmSi}_2$	Hexagonal	3.76		4.07
$\text{YbSi}_2$	Hexagonal	3.77		4.10
$\text{LuSi}_2$	Hexagonal	3.74		4.04

(6) O. J. C. Runnalls and R. R. Boucher, *Acta Cryst.*, **8**, 592 (1955).

(7) I. Binder, *J. Am. Ceram. Soc.*, **43**, 287 (1960).

(8) E. Parthé, private communication.

tetragonal modification might have been expected.<sup>3</sup>  $\text{YSi}_2$  crystallizes in both the orthorhombic and the hexagonal modifications. The hexagonal is the low temperature form.

A number of auxiliary experiments were carried out to check on some of the above findings. Because of the unexpected results encountered with the  $\text{YbSi}_2$  preparation, efforts were made to duplicate the previous preparation of  $\text{EuSi}_2$  from the metal oxide and Si.<sup>3</sup> This again yielded the tetragonal disilicide with the same unit cell dimensions which had been reported by Perri.<sup>3</sup> The preparation of  $\text{YbSi}_2$  from the metal oxide and silicon then was attempted (the original preparation had been made using Yb and Si). This also yielded the hexagonal form of the disilicide with cell dimensions which did not differ significantly from those found previously.

To check the effects of several variables on the formation of the orthorhombic modifications, the following reactions involving Nd and Si were carried out. First, Nd was heated at about 1300° with two parts of Si. This yielded orthorhombic  $\text{NdSi}_2$  just as had the reaction between  $\text{Nd}_2\text{O}_3$  and Si, carried out by Perri.<sup>3</sup> Nd then was heated to 1300° with only one part of Si to one of metal. The X-ray diffraction pattern of the product was complex; presumably a monosilicide had been formed, but there was no indication of the presence of either the orthorhombic or the hexagonal disilicide. Also, no significant reaction occurred when preparations of  $\text{NdSi}_2$  were attempted at temperatures lower than 1100°.

The relative stability of the hexagonal  $\text{YbSi}_2$  phase was investigated by heating Yb and Si in the atomic ratios 1:1, 1:2, and 1:3, in the temperature range from 900 to 1400°. In all cases, hexagonal  $\text{YbSi}_2$  was formed. No other silicide was detected. As expected, peaks due to excess silicon were present on the pattern of the  $\text{YbSi}_3$  preparation; lines due to metallic Yb were present on the  $\text{YbSi}$  pattern. The lattice constants and the relative peak heights of the  $\text{YbSi}_2$  pattern did not vary significantly from pattern to pattern.

When Y was heated with two parts of silicon at 1500°, the orthorhombic disilicide was formed. When prepared at 1100°, the hexagonal form was obtained and this transformed to orthorhombic on further heating to 1500°. Efforts similar to those used with  $\text{YbSi}_2$  were made to prepare  $\text{YSi}$  and  $\text{YSi}_3$  at 1100°. In all cases only the hexagonal disilicide was formed. The reaction was carried out in a helium atmosphere, but in all cases lines due to  $\text{Y}_2\text{O}_3$  and silicon were observed on X-ray patterns.

**Determination of Composition by X-Ray Diffraction Methods:  $\text{YbSi}_2$ .**—It was evident that the composition of the " $\text{YbSi}_2$ " phase was effectively constant in all the preparations. An effort then was made to determine the actual ratio of Si to Yb in the crystal; this was prompted in part by the large deviation from the ideal stoichiometry previously observed in orthorhombic " $\text{GdSi}_2$ ".<sup>3</sup> It was felt that the simplicity of the structure (there are no variable atomic position parameters) greatly favored the possibility of an accurate



determination of the atomic ratio in  $\text{YbSi}_2$  by X-ray methods.

It was assumed that the Yb and Si atoms are located in the positions 1a (0,0,0) and 2d ( $1/3$ ,  $2/3, 1/2$ ) and ( $2/3, 1/2, 1/2$ ), respectively, of  $P6_3/mmm$ ; it was further assumed that, if fewer than one metal atom or two silicon atoms are present in each cell, the atoms actually present would be distributed randomly over the "ideal" positions. The assumption of randomness is strongly supported by the X-ray diffraction data which show no signs of the superlattice formation that would have characterized an ordered defect structure.

The structure factor equation for this structure has the form

$$F_{(hkl)} = f_{\text{Yb}} + n f_{\text{Si}} \left[ \cos 2\pi \left( \frac{h}{3} + \frac{2k}{3} + \frac{l}{2} \right) + \cos 2\pi \left( \frac{2h}{3} + \frac{k}{3} + \frac{l}{2} \right) \right]$$

where  $n$  is the average number of silicon atoms per metal atom in each unit cell. " $\text{YbSi}_2$ " is high melting and therefore must have a small Debye-Waller temperature factor. Since the analysis to be described was confined to reflections occurring at relatively low Bragg angles, the omission of temperature factors from the expressions for " $F$ " could not introduce appreciable errors. The analysis was aimed at determination of " $n$ " in the structure factor expression by comparing observed values of " $F$ " for selected reflections. To avoid difficulties due to preferred orientation of the powdered samples, comparisons were limited to  $F_{(001)}$  vs.  $F_{(002)}$ , and  $F_{(100)}$  vs.  $F_{(110)}$ . Both members of each set should be affected by preferred orientation, if any, in the same way.

Values of the structure factors were computed in the usual way from carefully measured intensities. Measurements were made with a diffractometer using filtered  $\text{CuK}$  radiation in conjunction with pulse height discrimination to reduce background intensity. A scintillation counter was used as radiation detector. Intensity data were recorded on a strip chart while scanning the reflections at  $1/8^\circ$  ( $2\theta$ ) per minute; the areas of the peaks then were measured with a planimeter.

We may illustrate the procedure with a comparison of  $F_{(001)}$  and  $F_{(002)}$ . The former equals  $f_{\text{Yb}} - n f_{\text{Si}}$  and the latter equals  $f_{\text{Yb}} + n f_{\text{Si}}$ . The value of  $n$  for this pair of reflections was calculated from the observed ratio  $F_{001}/F_{002}$  and found to equal 1.92; for the 100/110 pair it was 2.04. Within the limits of experimental error the indicated formula is therefore  $\text{YbSi}_2$ .

### Discussion

Table III shows crystal data for known disilicides of rare earth and actinide metals. The structures encountered are either the tetragonal or orthorhombic  $\text{MeSi}_2$  structures, or the hexagonal  $\text{AlB}_2$  type structure. Although there is a general tendency for these structures to appear in order of decreasing atomic size of the metal atom, it also is necessary to consider the bonding in the silicon network. In both of these structures, each silicon is surrounded by three other silicons in a planar arrangement. In the hexagonal structure, planar

sheets of silicons are present, whereas in the orthorhombic and tetragonal structures, the silicons are connected in a three-dimensional network. These structures may be analyzed conveniently in terms of the shortest Si-Si distances and the volume per  $\text{MSi}_2$  unit.

TABLE III

Compound	Crystal structure	Lattice constants (Å.)			Ref.
		<i>a</i>	<i>b</i>	<i>c</i>	
La	Tetragonal	4.31		13.80	3
Ce	Tetragonal	4.27		13.88	3
Pr	Tetragonal	4.29		13.76	3
Eu	Tetragonal	4.29		13.66	3
$\alpha$ Th	Tetragonal	4.134		14.37	4, 5
$\alpha$ U	Tetragonal	3.97		13.71	4
$\alpha$ Pu	Tetragonal	3.97		13.55	6
$\alpha$ Np	Tetragonal	3.96		13.67	4
Nd	Orthorhombic	4.18	4.15	13.56	3
Sm	Orthorhombic	4.10 <sup>f</sup>	4.035	13.46	3
Dy	Orthorhombic	4.04	3.95	13.34	3
Gd	Orthorhombic	4.09	4.01	13.44	3
$\alpha$ Y	Orthorhombic	4.04	3.95	13.38	3
Tb	Orthorhombic	4.04 <sup>f</sup>	3.96	13.38	This work
Ho	Orthorhombic	4.03	3.97	13.31	This work
$\beta$ Y	Hexagonal	3.85		4.14	This work
$\beta$ Th	Hexagonal	3.99		4.235	5
$\beta$ U	Hexagonal	3.85		4.06	4
$\beta$ Pu	Hexagonal	3.88		4.08	6
Er	Hexagonal	3.78		4.09	This work
Tm	Hexagonal	3.76		4.07	This work
Yb	Hexagonal	3.77		4.10	This work
Lu	Hexagonal	3.74		4.04	This work

Although the positional parameters for silicon in the orthorhombic and tetragonal structures are not accurately known, the shortest Si-Si distances are very close to  $c/6$ ; they are exactly  $a/\sqrt{3}$  in the hexagonal structure.

If we confine ourselves to the lanthanide disilicides, we find that, for the tetragonal disilicides, the shortest distances range from 2.28 to 2.31 Å.; in the orthorhombic modification the distances range from 2.22 to 2.28 Å.; while the distances in the hexagonal modification are limited to the range 2.16 to 2.18 Å. In the latter case, it is clear that the planar silicon layers in the structure are predominant in determining the  $a$  dimension, almost independent of the size of the metal atom, except that only those metals whose sizes fall within a restricted range would be able to form such a structure.

In  $\text{YSi}_2$ , the shortest Si-Si distance is 2.23 Å. in the orthorhombic and 2.225 Å. in the hexagonal modification. The volumes per formula unit are 53.14 and 53.15 Å.<sup>3</sup>, respectively. Since the Si-Si distance is shorter in the hexagonal phase and the volumes are almost identical, the metal-silicon distance in the hexagonal phase is probably the longer of the two. This would be consistent with the hypothesis that the Si-Si bonds in the hexagonal layers are essentially graphitic in nature and that the metal-silicon bonds are of a "pi-complex" type such as that found in the ferrocenes, etc. On the other hand, the shorter metal-silicon bonds in the orthorhombic phase would involve some

direct overlapping with an unhybridized "p" orbital of the silicon. This would account for the greater length of the trigonal bonds between silicon atoms in the orthorhombic structure. The shortening of the silicon-silicon distance in all pairs of polymorphs can be seen from Table IV.

TABLE IV  
Si-Si DISTANCES (Å.) IN DISILICIDES

	Tetragonal (or orth.)	Hexagonal
ThSi <sub>2</sub>	2.39	2.31
USi <sub>2</sub>	2.28	2.225
PuSi <sub>2</sub>	2.26	2.24
YSi <sub>2</sub>	2.23	2.225

That the Si-Si bonding is not the only factor is evident from the fact that the actinide disilicides can crystallize with this structure, even at the cost of stretching the silicon-silicon bonds by as much as 7%, compared to the shortest Si-Si distance.

If we assume that the smallest value found for the Si-Si distance (in LuSi<sub>2</sub>) represents the closest approach to a graphitic structure, with the increase for other compounds attributed to the effect

of larger metal atoms, we can make the following interesting comparison of bond lengths

	Tetrahedral	Planar trigonal
Shortest Si-Si distance (Å.) (in disilicides)	2.351	2.16
C-C distance (Å.) (diamond)	1.542	1.42 (graphite)

The ratio of tetrahedral to trigonal distances is the same for both elements.

The foregoing discussion is necessarily tentative, owing to the lack of precise knowledge of the silicon parameters in the orthorhombic and tetragonal phases, and of the exact stoichiometry of all the phases. The accurate determination of the parameter and the stoichiometry of any one compound would require the use of single crystal data. Fortunately, in those cases where polymorphism exists, the high-temperature phase is the tetragonal (or orthorhombic) modification, so the possibility of growing crystals from the melt exists, although some difficulty may be anticipated in taking these crystals through the transition temperature.

## ON PHYSICAL ADSORPTION. XVIII. LIMITING ISOSTERIC HEATS OF ADSORPTION OF GASES ON GRAPHITIZED CARBON BY THE CHROMATOGRAPHIC METHOD

BY SYDNEY ROSS, JEFFREY K. SAELENS, AND JAMES P. OLIVIER \*

*Department of Chemistry, Rensselaer Polytechnic Institute, Troy, N. Y.*

*Received September 21, 1961*

The heats of adsorption obtained by means of gas-solid chromatography correspond to the limiting values of the isosteric heat of adsorption as the surface concentration tends to zero. The theoretical basis for the comparison of the results obtained by static and dynamic methods is developed. Using as an adsorbent highly graphitized carbon black, for which a quantity of precisely determined adsorption data has been reported, comparisons of the results obtained by the two methods show closer agreement than has yet been reported.

### Introduction

The measurement of the heat of adsorption by means of gas-solid chromatography has been shown<sup>1-3</sup> to yield results that are roughly in agreement with those obtained calorimetrically or from the application of the Clausius-Clapeyron equation to isothermal adsorption data at two or more temperatures. Heats of adsorption obtained by the use of chromatographic techniques usually refer, however, to those at very low surface concentrations; whereas the calorimetric or isosteric heats can be measured with satisfactory accuracy only at appreciable surface concentrations. The heterogeneity of the substrate, if pronounced, can be the cause of large differences between the adsorption heat measured at very low surface concentrations, where those parts of the surface of the greatest adsorptive potentials produce effects that dwarf the remainder, and the heat measured at, say, 20% surface coverage, where the portions of the surface

that have high potentials are no longer significant. Even for substrates of low heterogeneity, the adsorbate-adsorbate interactions, which increase nearly linearly with surface concentration, make comparisons between chromatographic (*i.e.*, dynamic) and static adsorption techniques subject to error. The appropriate comparison for the adsorption heat derived from chromatography is with the limiting isosteric heat as surface concentration tends to zero; unfortunately the usual static adsorption techniques are least accurate precisely for this condition.

The most desirable adsorbent for the purpose of making these comparisons more searching and accurate would be the ideal homotattic<sup>4</sup> surface, which could provide a Henry's law region of the adsorption isotherm within the reach of the static adsorption techniques. Only one adsorbent has, up to the present, made good its claim to be placed even close to this category, namely, graphite in the

(1) S. A. Greene and H. Pust, *J. Phys. Chem.*, **62**, 55 (1958).

(2) J. F. Young in V. J. Coates, H. J. Noebels, and I. S. Fagerson (eds.), "Gas Chromatography," Academic Press, Inc., New York, N. Y., 1958, pp. 15-23.

(3) P. E. Eberly, Jr., *J. Phys. Chem.*, **65**, 68 (1961).

(4) This term was introduced by C. Sanford and S. Ross, *ibid.*, **58**, 288 (1954), who defined a homotattic surface as the surface of a sub-microscopic patch or region, part of a larger surface, which acts as if its structure were uniform and homogeneous. An ideal homotattic surface is one on which every homotattic patch is the same.

form of a heat-treated carbon black. Sams, Constabaris, and Halsey<sup>5,6</sup> have observed and measured the Henry's law region of the adsorption isotherms of neon, argon, krypton, and xenon, as well as hydrogen, deuterium, methane, and deuterio-methane with this adsorbent. From their data, which were measured with great precision, the limiting isosteric heats at zero coverage for these adsorbates can be calculated with a high degree of reliance.

Ross and his collaborators<sup>7,8</sup> have measured the adsorption isotherms up to about 75% monolayer coverage of argon, krypton, and a number of hydrocarbons and halogenated hydrocarbons as adsorbates on the same adsorbent. By means of a newly developed<sup>9,10</sup> method these adsorption isotherms can yield a number of parameters, including the limiting isosteric heats at zero coverage, with a precision not handicapped by the use of graphical extrapolation.

A body of carefully determined data exists, therefore, with which heats of adsorption obtained chromatographically properly can be compared, with the expectation of attaining more critical distinctions and more significant information than has hitherto been forthcoming.

### Experimental

**Apparatus.**—The instrument was a Beckman GC-2A gas chromatograph. The GC-2A is equipped with a filament-type thermal-conductivity detector, which responds to changes in the thermal conductivity of the adsorbate-carrying gas eluted from the column relative to a stream of pure carrier gas (helium). The detector is attached to a Leeds and Northrup Speedomax recording potentiometer (Type G), which has a pen-speed of one second for full-scale deflection.

Gas or vapor was introduced into the apparatus by evacuating the sample valve and then filling it with the gas at any predetermined storage pressure. The pressure head on the column and the flow rate of the gas going through it were measured: the pressure head was measured at a T-joint near the entrance to the column, and the flow rate was measured at the column outlet. The temperature of the column was measured by means of a thermocouple attached to the detector, which is inside the thermal compartment. The packed column, 3 ft. in length, was constructed of standard 1/4 in. stainless steel tubing (i.d. = 0.20 in.). The adsorbent was a sample of highly graphitized carbon black designated Sterling MT (3100°), given to us by courtesy of Dr. W. R. Smith of Godfrey L. Cabot, Incorporated. The powder was sieved, the fraction between 100 and 60 mesh (150 to 250  $\mu$ ) being used to pack the column.

Reproducible pulse volumes of 2 cc. of adsorbate were injected into the helium stream by means of the gas-sampling valve. In all this work the measurements of each adsorbate at each temperature were repeated four times, using different storage pressures, ranging from 0.2 to 1.0 atmosphere. The reproducibility of the measured retention times was always within 1 mm. of chart distance (1.6 sec.), and so testified that the surface concentration of adsorbed gas always was so low that the adsorbate-adsorbate interactions did not contribute significantly to the heat of adsorption. An elution peak, typical of this adsorbent, that of benzene

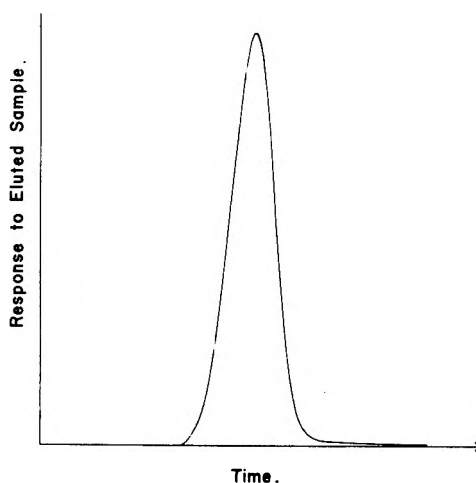


Fig. 1.—Typical elution peak of benzene desorbed from graphitized carbon black at 130°.

at 130°, is shown in Fig. 1. This chromatogram has a symmetry that is not at all customary in gas-solid chromatography, and which is caused by the close approach to uniformity of the adsorbent substrate. The degree of heterogeneity of adsorbents might in fact be estimated from the forward skew of the gas adsorption chromatograms.

The retention time of the adsorbate is suitably measured in the presence of a reference gas that is not adsorbed at the temperature of the column: the retention time of the adsorbate then is obtained as the time interval between the maxima of the two responses. The reference gas used was neon. In the experiments at higher temperatures the peak caused by the neon overlapped that caused by the adsorbate, thus preventing the measurement of the time interval between the two maxima; this effect is due to the small specific surface of the adsorbent ( $\Sigma = 8.4 \text{ m.}^2/\text{g.}$ ) and the use of a short column: the need to economize the adsorbent sample made the short column obligatory. The peak for neon was, therefore, obtained by a separate measurement with neon alone, the adsorbate being injected in its turn without neon. The product ( $t_m F_r$ ) for neon was found to be constant with temperature, and the correction was applied as

$$t_m F_r (\text{adsorbate at } T_1, \text{ obsd.}) - t_m F_r (\text{neon}) = t_m F_r (\text{adsorbate at } T_1, \text{ cor.})$$

where  $t_m$  = retention time and  $F_r$  = flow rate ( $\text{cm.}^3/\text{sec.}$ ), which was measured by a device at room temperature. The correction of  $F_r$  to make it correspond to the actual rate of flow through the column at a temperature  $T_c$  could be made by the multiplying factor  $T_c/T_1$ ; but this is not introduced now or later, for a reason discussed below.

The isosteric heats based on adsorption isotherms are those calculated<sup>10</sup> from published measurements<sup>5,6</sup> or from data soon to be published.<sup>8</sup> The adsorbent used was either the highly graphitized carbon black designated P-33(2700°) or that designated Sterling MT(3100°). They differ in their specific surface areas, but in all the measurements made in this Laboratory using these two adsorbents we have never distinguished any difference in the heats of adsorption when they are interchanged.

### Theory

**1. Isosteric Heats of Adsorption by Gas-Solid Chromatography.**—Let  $n_g$  be the total number of moles of gas in the column, in equilibrium with  $n_a$  moles of gas adsorbed; let  $V_g$  be the interstitial volume of the column and  $V_c$  the volume of the empty column; and let the column be filled with  $w$  grams per  $\text{cm.}^3$  of packed adsorbent, having a specific surface of  $\Sigma \text{ cm.}^2/\text{g.}$ : then

$$f = \text{fractional void space in column} = \frac{V_g}{V_c} \quad (1)$$

$v_a$  = equilibrium surface concn. of adsorbate in moles/

$$\text{cm.}^2 = \frac{n_a}{V_c w \Sigma} \quad (2)$$

(5) J. R. Sams, Jr., G. Constabaris, and G. D. Halsey, Jr., *J. Phys. Chem.*, **64**, 1689 (1960).

(6) G. Constabaris, J. R. Sams, Jr., and G. D. Halsey, Jr., *ibid.*, **65**, 367 (1961).

(7) S. Ross and W. Winkler, *J. Colloid Sci.*, **10**, 319, 330 (1955); S. Ross and W. W. Pultz, *ibid.*, **13**, 397 (1958).

(8) S. Ross and W. D. Machin, in preparation; S. Ross and E. W. Albers, in preparation.

(9) S. Ross and J. P. Olivier, *J. Phys. Chem.*, **65**, 608 (1961).

(10) S. Ross and J. P. Olivier, in preparation.

$s$  = amount of available surface per unit volume of column in  $\text{cm}^2/\text{cm}^3 = \Sigma w$  (3)

$n_e$  = equilibrium gas concentration =  $\frac{n_g}{V_g}$  (4)

The symbols  $f$ ,  $v_e$ ,  $s$ , and  $n_e$  are those defined by Eberly and Spencer<sup>11</sup> in their mathematical description of the process of pulse flow through packed columns. It has been demonstrated<sup>11-13</sup> that the movement of the maximum of a pulse through a packed column is described by the relation

$$\frac{L}{t_m u} = C \quad (5)$$

where

$L$  = length of the packed column in cm.  
 $t_m$  = retention time of the pulse maximum in sec.  
 $u$  = interstitial gas velocity in  $\text{cm}/\text{sec}$ .

The quantity  $C$  is defined<sup>11</sup> as

$$C = \frac{n_e f}{v_e s} \quad (6)$$

which, by means of eq. 1, 2, 3, and 4 can be shown to be equivalent to

$$C = \frac{n_g}{n_a} \quad (7)$$

Let  $\bar{p}$  = the average equilibrium pressure in the gas phase, then

$$\bar{p} V_g = n_g R T_c$$

where  $T_c$  = temperature of the column; therefore

$$n_g = \bar{p} V_g / R T_c \quad (8)$$

Let the average fraction of the adsorbent surface covered at pressure  $\bar{p}$  be  $\bar{\theta}$ , and let us suppose a linear adsorption isotherm (Henry's law region), so that at equilibrium

$$\bar{p} = K \bar{\theta}$$

then

$$n_a = \frac{\bar{\theta} \Sigma w V_c}{\beta N} \quad (9)$$

where  $\beta$  = the two-dimensional van der Waals constant, which is assumed<sup>14</sup> to equal the limiting surface area of an adsorbed molecule at infinite compression. Combining eq. 7, 8, and 9 gives

$$C = \frac{\beta N}{\bar{\theta} \Sigma w V_c} \cdot \frac{\bar{p} V_g}{R T_c} \quad (10)$$

Now let us introduce quantities that have been developed in the treatment of gas-solid adsorption

$$V_\beta (\text{cm}^3 \text{ STP/g.}) = \frac{\Sigma}{\beta N} \times 22,400 \quad (11)$$

and

$$K (\text{mm.}) = \frac{\bar{p}}{\bar{\theta}} \quad (12)$$

(11) P. E. Eberly, Jr., and E. H. Spencer, *Trans. Faraday Soc.*, **57**, 289 (1961). We have tried to retain the symbols originally suggested by these authors as far as possible, but many of them have another significance in the field of physical adsorption, particularly the symbols  $\beta$  and  $\beta'$ , which we have here replaced by  $1/C$  and  $1/C'$ .

(12) A. J. P. Martin and R. L. M. Synge, *Biochem. J.*, **35**, 1358 (1941).

(13) S. A. Greene in R. L. Pecsok (Ed.), "Principles and Practice of Gas Chromatography," John Wiley and Sons, Inc., New York, N. Y., 1959, pp. 29-30.

(14) J. H. de Boer, "The Dynamical Character of Adsorption," Clarendon Press, Oxford, 1953, pp. 172-174.

this makes

$$C = \frac{K}{w V_\beta} \times \frac{V_g}{V_c} \times \frac{22,400}{R T_c} \quad (13)$$

The practical application of eq. 5 requires that it be expressed in terms of quantities actually measured

$F_r$  = flow rate of carrier gas in  $\text{cm}^3/\text{min.}$ , measured by a flow-metering device at room temp.

$p_c$  = column inlet pressure

$p_r$  = column outlet pressure (atmospheric pressure)

The flow rate measured at room temperature ( $F_r$ ) is used to calculate the actual flow rate ( $F_c$ ) inside the column at temperature  $T_c$

$$F_c = F_r T_c / T_r \quad (14)$$

The flow rate sometimes is further corrected to correspond to a zero pressure drop across the column, although for most work, including the present measurements, this correction is too small to be significant. The interstitial gas velocity is related to the volume flow rate by the expression

$$F_c = u a \quad (15)$$

where  $a$  is the interstitial cross-sectional area of the packed column. We then have also, of course, the equation

$$V_g = L a \quad (16)$$

Substituting equations 14, 15, and 16 into equation 5 gives

$$\frac{V_g}{t_m F_r} \times \frac{T_r}{T_c} = C \quad (17)$$

introducing equation 13 and rearranging gives

$$F_r t_m = \frac{w V_c R T_r}{22,400} \times \frac{V_\beta}{K} \quad (18)$$

Note that the factor  $w V_c V_\beta / 22,400$  in equation 18 has the significance of "total number of moles adsorbed by the packed column at infinite compression"; and that the limiting slope of the adsorption isotherm is given by the factor  $K / V_\beta$ .

The parameters  $V_\beta$  and  $K$  in equation 18 are significant for the description of the adsorption characteristics of the solid;  $V_\beta$  is the specific monolayer capacity, hence directly related to the specific surface area of the powder;  $K$  is expressed by the relation

$$K = A^0 e^{-U_0/RT} \quad (19)$$

where  $A^0$  and  $U_0$  have been defined.<sup>9</sup> The limiting isosteric heat of adsorption at infinitely dilute surface concentration can be obtained from the variation of  $K$  with temperature

$$\lim_{\theta \rightarrow 0} q^{st} = R T^2 \frac{d}{dT} (\ln K) \quad (20)$$

or

$$\lim_{\theta \rightarrow 0} q^{st} = -R \frac{d}{d(1/T)} (\ln K) \quad (20A)$$

hence, from equation 18

$$\lim_{\theta \rightarrow 0} q^{st} = R \frac{d}{d(1/T)} [\ln (F_r t_m)] \quad (21)$$

The plot of  $\ln (F_r t_m)$  vs.  $1/T$  provides a curve whose slope at any point equals  $q^{st}/R$  for the temperature in question. The assumption that  $q^{st}$  is invariant with temperature need not be introduced; but,

due to the partial cancellation of various effects, it actually appears to be not far from being so over quite a range of temperature (see Fig. 2).

Previous attempts<sup>2-4</sup> to obtain  $q^{st}$  ( $\theta \rightarrow 0$ ) from chromatograms have not been accurate, as the presence of the factor  $T_c$  in the definition of  $C$  (equation 17) has been overlooked. In this section of the present paper we have presented a thermodynamic analysis of data, leading to the correct way to obtain  $q^{st}$  ( $\theta \rightarrow 0$ ) from gas adsorption chromatograms.

The above development is rather severely limited if it yields only the limiting isosteric heat,  $\theta \rightarrow 0$ . For an adsorbent that is nearly completely homotactic then indeed we do have a measurement characteristic of the material, but such adsorbents are unfortunately exceedingly rare: the large number of adsorbents of current interest show surface heterogeneities that usually are quite pronounced. The limiting isosteric heat,  $\theta \rightarrow 0$ , may, under those conditions, be little more than the reflection of an adventitious surface condition of no particular significance beyond the specimen under observation. If the surface heterogeneity can be represented, however, by a continuous distribution of adsorptive potentials,  $U_0$ , that is symmetrical about a mean value,  $U_0'$ , so that the distribution can be approximated by the Gaussian function

$$\Phi(U_0) = \frac{1}{n} e^{-\gamma(U_0 - U_0')^2} \quad (22)$$

then, it can be shown,<sup>10</sup> the limiting isosteric heat,  $\theta \rightarrow 0$ , is greater by an amount  $1/(2\gamma RT)$  than the limiting isosteric heat of adsorption for a homotactic surface whose adsorptive potential is the same ( $U_0'$ ) as that of the average of the Gaussian distribution.

The chromatographic method promises in this way to offer an important aid to the analysis of adsorption isotherms. In matching experimental isotherms by the Ross-Olivier method<sup>9</sup> there is always a certain latitude in selecting the parameters  $V_\beta$ ,  $\gamma$ ,  $K'$ , and  $2\alpha/\beta$  that best describe the results. As might well be expected with such a number of variables, internal adjustments and compensations make it possible for more than one set of parameters to offer themselves as answers. In equation 18, however, we have, by an independent technique, the means of measuring the limiting slope of the adsorption isotherm, from which we can get another relation between the above parameters. As this is not the main point of the present contribution, we shall leave the matter for development elsewhere.

**2. Variation of the Isosteric Heat with Temperature.**—The isosteric heats of adsorption usually are obtained by a calculation in which the Clausius-Clapeyron equation is applied to adsorption isotherms measured at temperatures within about 20° of each other. The values of  $q^{st}$  thus elicited are plotted as a function of surface concentration; to get the limiting isosteric heat, surface concentration tending to zero, the curve is extrapolated to intercept the axis. For a near-homotactic surface the extrapolation procedure does not introduce an intolerable error, as the heats would rise almost linearly with  $\theta$ ; but for heterogeneous surfaces this

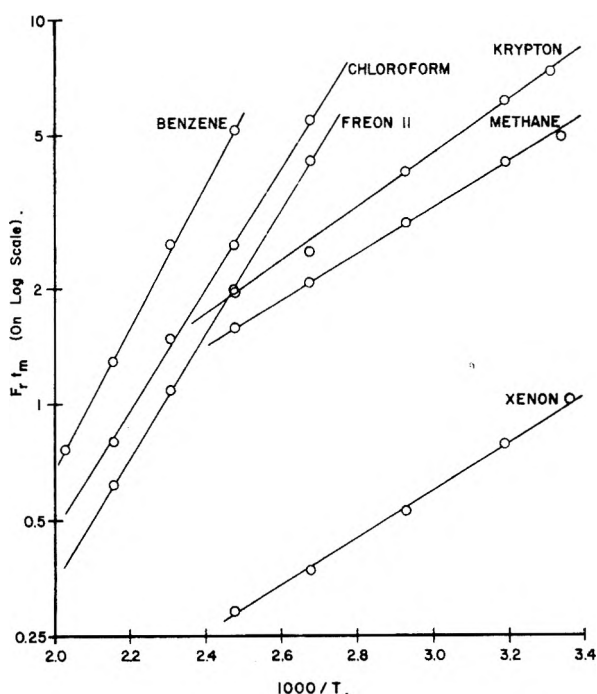


Fig. 2.—The variation of  $\ln F_{T,m}$  vs.  $1/T$  for a number of adsorbates on graphitized carbon black.

saving feature is absent and only crude estimates can be made. An alternative, and slightly more precise, method, for a near-homotactic substrate, is to use eq. 20 or 20A, the parameter  $K$  having been obtained by the method of matching the experimental against computed adsorption isotherms.<sup>9</sup>

The determination of the limiting isosteric heat of adsorption by the chromatograph cannot always be conveniently made at the same temperature, or even within the same temperature range, as the measurements of the adsorption isotherms. A method of estimating the variation with temperature of the limiting heat of adsorption is therefore important. The necessary theory has been developed.<sup>15</sup> For a spherically symmetrical molecule, which is adsorbed from the gas phase without loss of any rotational degrees of freedom, the expression derived is

$$\lim_{\theta \rightarrow 0} q^{st} = U_0' - \frac{Nh\nu}{(e^{h\nu/kT} - 1)} + \frac{3}{2} RT \quad (23)$$

where  $U_0'$  has the significance already described by eq. 22, and  $\nu$  is the vibrational frequency of the adsorbed molecule normal to the surface. These terms are invariant with temperature. Values of  $U_0'$  and  $\nu$  for the inert gases and for methane and hydrogen adsorbed by graphitized carbon have been calculated in this Laboratory from the data of Sams, Constabaris, and Halsey.<sup>5,6</sup> For asymmetric molecules that may be oriented on adsorption, each degree of rotational freedom that is lost is replaced in the adsorbed state by a vibration about the former axis of rotation. Thus, for example, adsorbed chloroform, which is considered<sup>10</sup> to be oriented at a graphite surface with its dipole axis aligned with the surface electric field, thereby has lost two degrees of rotational freedom; these

(15) S. Ross and J. P. Olivier, *Advances in Chem.*, **33**, 301 (1961).

are replaced by two vibrations, which, along with the "adsorption vibration" normal to the surface, make three vibrations of the adsorbed molecule. Assuming that all three vibrational frequencies are equal, the appropriate expression for the variation of  $q^{st}$  with temperature then would be

$$\lim_{\theta \rightarrow 0} q^{st} = U_0' - \frac{3N h \nu}{(e^{h\nu/kT} - 1)} + \frac{5}{2} RT \quad (24)$$

Obviously there is greater possibility of error in the interpretations and assumptions underlying eq. 24 than for the comparatively simple case described by eq. 23.

The heterogeneous substrate described by eq. 22 has an average homotattic patch, whose properties are designated by the prime superscripts as  $U_0'$  and  $K'$ : for the completely homotattic surface, of course, the whole surface consists of this category, and the  $U_0$  of eq. 13 is then equivalent to the  $U_0'$  of eq. 23 and 24.

A theoretical framework for the interpretation of gas adsorption chromatography has been presented by Hanlan and Freeman.<sup>16</sup> The thermodynamic considerations of the present paper would not be affected by any such theoretical framework; but inasmuch as we have referred to a different theoretical model for the adsorption process, a comment on the Hanlan and Freeman treatment is appropriate. These authors have invoked a theory of the gas-solid interaction based on dispersion forces as evaluated by the integration of the Lennard-Jones 12-6 interatomic potential function over a structureless semi-infinite solid. The relative crudeness of this model apart, the theory is not at all applicable to a heterogeneous surface. The chromatograms cited by Hanlan and Freeman are derived from charcoal surfaces of great heterogeneity, for which one doubts if a Henry's law region of the adsorption isotherm could be reached within any practicable range of pressure measurements. Comparisons with results obtained from adsorption isotherms would have revealed the limitations of the treatment, but such comparisons were not made. The portions of the surface that are reflected in the results obtained are, of course, those of the highest adsorptive potentials, which are most active at low pressures.

### Results

For a small number of adsorbates on a graphite substrate the values of  $U_0'$  and  $\nu$  have been obtained, so that the limiting isosteric heat can be

TABLE I  
COMPARISON OF LIMITING ISOSTERIC HEATS (KCAL./MOLE)  
OF ADSORBATES ON GRAPHITE

	Adsorption isotherm				Chromatograph	
	$U_0'$	$\times 10^{-12}$ sec. <sup>-1</sup>	$T$ °K.	$q^{st}$	Temp. range, °K.	$q^{st}$
Krypton	2.754	1.00	352	3.15	302-403	3.20
Xenon	3.654	0.85	350	4.03	297-403	3.94
Methane	2.678	2.48	351	3.13	299.5-403	2.90
Freon-11	8.17	0.76	418	7.9	372-463	7.86
Chloroform	8.05	1.35	418	8.1	372-463	8.00
Benzene	9.41	.64	448	9.1	403-493	9.18

(16) J. F. Hanlan and M. P. Freeman, *Can. J. Chem.*, **37**, 1575 (1959).

calculated either by eq. 23 or 24. In Table I, the values of  $U_0'$  and  $\nu$  are taken from Ross and Olivier.<sup>10,15</sup> The limiting isosteric heat (column 5) is calculated for the temperature designated  $T$ , using eq. 23 for the adsorbates krypton, xenon, and methane; and eq. 24 for the adsorbates Freon-11, chloroform, and benzene. For comparison, the limiting isosteric heats obtained from chromatograms in the temperature range indicated are given (see Fig. 2).

In the next set of comparisons, Table II, the limiting isosteric heats derived from adsorption isotherms, by eq. 20A, are not recalculated to correspond to the temperature range of the chromatograms: either inadequate data or the complexity of the required analysis have hitherto prevented the evaluation of the necessary parameters,  $U_0'$  and  $\nu$ . The temperature corrections obtained in Table I show that less than 100 cal./mole usually is involved.

TABLE II  
COMPARISONS OF LIMITING ISOSTERIC HEATS (KCAL./MOLE) OF ADSORBATES ON GRAPHITE (NOT TEMPERATURE CORRECTED)

	Adsorption isotherm		Chromatograph	
	Temp. range, °K.	$q^{st}$	Temp. range, °K.	$q^{st}$
Ethane	173.1-296.7	4	299.5-372	3.78
Propane	258.2-296.7	6.5	296.5-372	6.26
Butane	258.2-296.7	8	341-433	8.10
Pentane	.....	..	372-463	8.61
Hexane	.....	..	372-463	9.83
Ethylene	229.1-266.2	4.5	313-403	4.40
Butadiene	.....	..	372-463	7.65
Cyclopropane	244.2-296.7	5.5	313-403	5.98
Dimethyl ether	258.2-296.7	6	341-462	5.50
Carbon tetrachloride	231.2-323.2	8.5	372-463	8.35

The agreement between the limiting isosteric heats derived from adsorption isotherms and those derived from chromatograms is, in general and as would be expected, rather better in Table I than in Table II. The chromatograms are likely to give less accurate values for adsorbates with lower heats, such as methane, krypton, and xenon, because of the small extent of the adsorption at the temperatures of the column. But, with one or two exceptions in Table II, the agreements between the two methods are satisfactory. The adsorbent in the chromatograph column cannot, as a preliminary treatment, be out-gassed *in vacuo* or at as high a temperature as the sample in the high-vacuum apparatus; in view of this difference in condition of the adsorbent the agreement between the results of the two methods is even better than might have been expected. The results that appear to be most divergent probably arise from experimental errors in the measurement of the adsorption isotherms rather than from errors in the less exacting technique of gas-solid chromatography.

**Acknowledgments.**—The authors gratefully acknowledge grants in aid of these researches from Esso Research and Engineering Co. and from the donors of The Petroleum Research Fund, administered by the American Chemical Society.

# THE KINETICS OF THE HYDROLYSIS OF CHLORINE. III. THE REACTION IN THE PRESENCE OF VARIOUS BASES, AND A DISCUSSION OF THE MECHANISM

BY ASSA LIFSHITZ AND B. PERLMUTTER-HAYMAN

Department of Physical Chemistry, Hebrew University, Jerusalem, Israel

Received September 27, 1961

The hydrolysis of chlorine in the presence of various anions of weak acids HA has been investigated. The values of  $k_{A^-}$ , the rate constant for the reaction between chlorine and a given anion  $A^-$ , are found to be correlated with the corresponding acid dissociation constants  $K_a$  by the equation:  $k_{A^-} = 1.6 K_a^{-0.54}$ . Since this is the Brønsted catalytic law, the reaction mechanism may be expected to involve rate-determining proton transfer. A different mechanism involving rate-determining rupture of the Cl-Cl bond and formation of ACl is ruled out by further considerations which concern the rate of the back reaction, and the known rate of formation of compounds of the type ACl. The two mechanisms consistent with all the known facts are either a reaction in a single step, or a two-step mechanism in which  $Cl_2OH^-$  is formed in a rate-determining proton transfer between  $A^-$  and the hydrate of chlorine. Theoretical considerations favor the two-step mechanism.

## Introduction

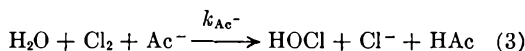
The hydrolysis of chlorine in pure water<sup>1,2</sup> was found to proceed according to



and not



In the presence of acetate,<sup>3</sup> the reaction is much faster and was shown to proceed mainly according to



with some contribution by reaction 1, and a possible contribution by reaction 2.

In the presence of other anions  $A^-$  of weak acids HA we may expect analogous reactions of the type



to take place. A knowledge of the values of  $k_{A^-}$  for different anions might give some insight into the actual mechanism of the reaction.

We therefore investigated the hydrolysis in the presence of the following ions (given in the order of increasing basicity):  $CHCl_2COO^-$ ,  $SO_4^{2-}$ ,  $CH_2ClCOO^-$ ,  $HCOO^-$ , and  $HPO_4^{2-}$ .

## Experimental

The experimental procedure was the same as that described in our previous work.<sup>2,3</sup> The acids and salts employed were either "chemically pure" or "analytical reagent." The temperature was again 9.5°.

## Results

**The Reaction in the Presence of Monochloroacetate.**—Several experiments were carried out in the presence of chloroacetate-chloroacetic acid mixtures. Details of three runs are given in Table I. The initial stoichiometric chlorine concentration is designated by  $a$ ; the amounts hydrolyzed at zero time, and at the end of the reaction by  $x_0$  and  $x_e$ ; the initial concentrations of acid and anion by  $[HA]_0$  and  $[A^-]_0$ . Column 8 shows the value

(1) E. A. Shilov and S. M. Solodushenkov, *Compt. rend. acad. sci. U.R.S.S.*, **1**, 96 (1936); *Acta Physicochim. U.R.S.S.*, **20**, 667 (1945); *J. Phys. Chem. (U.S.S.R.)*, **19**, 404 (1945); **21**, 1159 (1947).

(2) A. Lifshitz and B. Perlmutter-Hayman, *J. Phys. Chem.*, **64**, 1663 (1960).

(3) A. Lifshitz and B. Perlmutter-Hayman, *ibid.*, **65**, 753 (1961).

of  $\Delta H_4$ , the heat of reaction 4, calculated<sup>3</sup> from the total heat effect,  $\Delta T_3 - \Delta T_\infty$  (0.20 to 0.25°); column 9 shows the value calculated from data in the literature. The rate constants  $k_{A^-}$  are defined by the rate equation representing the two parallel reactions 1 and 4, *viz.*

$$dx_i/dt = (a - x_i) [k_{H_2O} + k_{A^-} ([A^-]_0 - x_i)] (1 - \varphi) \quad (I)$$

where  $\varphi$  is the relative contribution of the back reaction.<sup>3,4</sup> The values of  $x_i$  were calculated<sup>3</sup> from the measured values of  $\Delta T_t$ , and those of  $k_{A^-}$  by a trial and error method described before.<sup>3</sup> The application of this method was slightly more tedious than in the case of acetate because the ratio

$$k_{H_2O}/[k_{H_2O} + k_{A^-} ([A^-]_0 - x_i)] \quad (II)$$

is somewhat higher, *i.e.*, the relative contribution of reaction 1 is higher. Furthermore, any uncertainty in  $k_{H_2O}$  introduces a larger uncertainty into  $k_{A^-}$ , the higher the value of the ratio II.

For this reason, and also in order to obtain a sufficient degree of hydrolysis, we employed higher values of  $[A^-]_0$  than in the case of acetate. In spite of this, the reaction is comparatively slow—only about 2 to 3 times faster than in pure water.

Figure 1 shows that  $k_{A^-}$  as defined by equation I is constant during each run,<sup>3</sup> and does not change appreciably from one run to the other, in spite of the variations in  $[A^-]_0$  and  $[HA]_0$ . This fact confirms the rate equation assumed.

The average value of the rate constant is

$$k_{CH_2ClCOO^-} = 57.3 \pm 2.2 \text{ mole}^{-1} \text{ l. sec.}^{-1}$$

## The Reaction in the Presence of Formate.—

The details of 3 runs again are shown in Table I. Figure 2 shows that the appropriate second order plots again yield straight, parallel lines. From the slopes we get

$$k_{HCOO^-} = 193 \pm 3.5 \text{ mole}^{-1} \text{ l. sec.}^{-1}$$

Unfortunately, formate is oxidized by chlorine. Whereas this reaction may be assumed to be too slow to make itself felt during the 0.07 sec. of observation, it somewhat affects the reliability of the analysis of the reaction mixture,<sup>5</sup> and therefore

(4) A. Lifshitz and B. Perlmutter-Hayman, *Bull. Research Council Israel*, **9A**, 200 (1960).

(5) According to J. Thamsen (*Acta Chem., Scand.*, **7**, 682 (1953)) the reaction takes place between formate and chlorine at a specific rate of 8.1 mole<sup>-1</sup> l. sec.<sup>-1</sup> at 25°; the rate constant has not been measured at other temperatures but may be expected to be appreciably lower at

TABLE I  
DETAILS OF EXPERIMENTS CARRIED OUT IN THE PRESENCE OF VARIOUS BASES

Base	$K_a$	$a$	mmole l. <sup>-1</sup>				$\frac{k_A^-}{\text{mole}^{-1} \text{ l. sec.}^{-1}}$	$(-\Delta H_4 \text{ (kcal. mole}^{-1}\text{)})$	
			$x_0$	$x_e$	$[\text{HA}]_0$	$[\text{A}^-]_0$		measured	calcd. a, b
$\text{CH}_2\text{ClCOO}^-$	$^a 1.55 \times 10^{-3}$	49.0	14.15	39.8	50.4	146	57	7.4	7.10
		58.6	15.2	48.8	10.65	148	60.5	7.5	
		53.5	14.6	48.2	30.5	291	55	7.45	
$\text{HCOO}^-$	$^a 1.88 \times 10^{-4}$	51.3	14.35	50.12	23.7	192	189	5.78	5.94
		54.8	14.7	53.7	35.9	252	194	6.25	
		63.0	16.1	61.95	0	250	196	6.18	
$\text{SO}_4^{=}$	$^c 1.70 \times 10^{-2}$	57.6	...	...	0	212	~19	...	...
$\text{CHCl}_2\text{COO}^-$	$^d \sim 5 \times 10^{-2}$	72.0	...	...	0	308	~16	...	...

<sup>a</sup> R. A. Robinson and R. H. Stokes, "Electrolyte Solutions," Butterworths Scientific Publications, London, 1955, p. 496. <sup>b</sup> See reference 22. <sup>c</sup> H. S. Harned and B. B. Owen, "The Physical Chemistry of Electrolytic Solutions," Reinhold Publ. Corp., New York, N. Y., 1950, p. 514. <sup>d</sup> "Handbook of Chemistry and Physics," 40th ed., Chemical Rubber Publishing Co., Cleveland, Ohio, 1958, p. 1744.

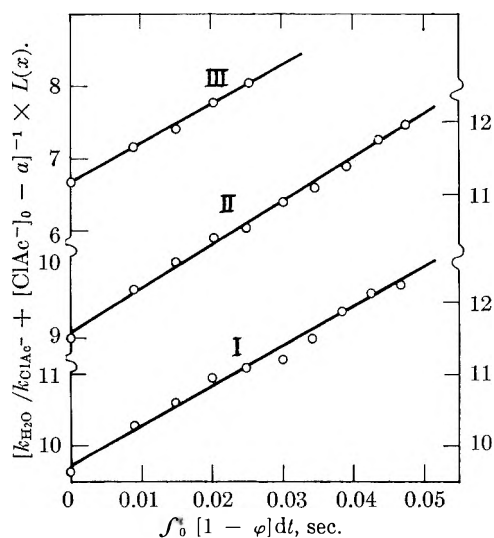


Fig. 1.— $[k_{\text{H}_2\text{O}}/k_{\text{ClAc}^-} + [\text{ClAc}^-]_0 - a]^{-1} \times L(x)$  against "corrected time"<sup>3,4</sup>  $\int_0^x (1 - \phi) dt$ , where  $L$  is defined by  $L \equiv \ln [(k_{\text{H}_2\text{O}}/k_{\text{A}^-} + [\text{A}^-]_0 - x)/(a - x)]$ . Straight parallel lines confirm the assumed rate law. Reactions in the presence of chloroacetate.

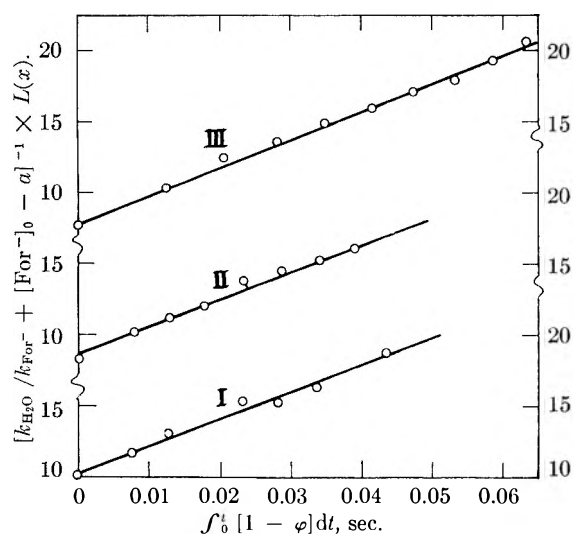


Fig. 2.—As in Fig. 1. Reactions in the presence of formate.

of the dilution ratio, and of the initial concentrations.

9.5°. On the other hand, according to E. A. Shilov and A. I. Slyadnev (*J. Phys. Chem. (U.S.S.R.)*, **22**, 1312 (1948); *Chem. Abstr.*, **43**, 2495 (1949), formic acid also is attacked, though much more slowly.

**The Reaction in the Presence of Phosphate,  $\text{HPO}_4^{=}$ .**—In the presence of  $\text{HPO}_4^{=}$  at initial concentrations between 0.028 and 0.035 M, all the thermistors registered identical temperature effects. This means that already at the first thermistor, or after 8 msec., the amount hydrolyzed was equal to  $x_e$ , and  $\Delta T_\infty$  had been reached—within the limit of experimental error. If we assume that the first measured value is actually equal to at least 0.95  $(\Delta T_\infty - \Delta T_0)$ , we can calculate a lower limit for the rate constant, *viz.*

$$k_{\text{HPO}_4^{=}} \geq 2.5 \times 10^4 \text{ mole}^{-1} \text{ l. sec.}^{-1}$$

(The arbitrariness of this assumption does not materially affect the result.)

In order to slow down the reaction rate as far as possible, we did not employ  $\text{HPO}_4^{=}$  in excess, but rather at concentrations approximately equal to those of chlorine. In some experiments,  $[\text{HPO}_4^{=}]_0$  was even somewhat lower than  $a$ . It is interesting to note that in these cases the initial "instantaneous" temperature drop was followed by an additional small change which was much slower. Clearly, this is due to a further reaction, namely that between chlorine and the  $\text{H}_2\text{PO}_4^-$  formed in the first, rapid part. We did not attempt to calculate  $k_{\text{H}_2\text{PO}_4^-}$  from this qualitative observation.

**The Reaction in the Presence of Dichloroacetate and Sulfate,  $\text{SO}_4^{=}$ .**—The details again are shown in Table I. In the presence of these two comparatively weak bases we employed high values of  $[\text{A}^-]_0$  and chose  $[\text{HA}]_0 = 0$ . In spite of this, the degree of hydrolysis was small, so that  $(\Delta T_\infty - \Delta T_0)$  was low (only about  $-0.1^\circ$ ) and the percentage error in the measured values of  $\Delta T_i$  was larger than usual; furthermore, the contribution of reaction 1 now predominates over that of reaction 4.

For these two reasons, the experimental results cannot be expected to be very accurate. Therefore, certain approximations in the calculation of  $k_{\text{A}^-}$  seem to be justified and we used the rate equation

$$k_{\text{H}_2\text{O}} + k_{\text{A}^-} [\text{A}^-] = 1.07 \frac{K}{K + 3x_e^2} \times \frac{d \ln(x_e - x_t)}{dt} \quad (\text{III})$$

where  $K \equiv K_L [\text{A}^-] / K_a$  ( $K_L$  representing the hydrolysis constant of chlorine),  $[\text{A}^-]$  is the mean



value of  $[A^-]$  during the reaction, and the factor 1.07 is the mean value of the expression  $(K + 3x_0^2)/(K + x_0^2 + x_0x_t + x_t^2)$ —which actually changes gradually from  $\sim 1.14$  for  $x_t = x_0$  to 1.00 for  $x_t = x_e$ . We thus obtain approximate values of  $(k_{H_2O} + k_{A^-}[A^-])$  from simple first order plots of  $\ln(\Delta T_t - \Delta T_\infty)$  vs. time.

The experiments are not sufficiently accurate for a reliable calculation of  $\Delta H_4$ .

### Discussion

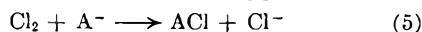
**The Brønsted Catalytic Law.**—Our results show that  $k_{A^-}$  is higher the weaker the acid HA. In Fig. 3 we plotted  $\log k_{A^-}$  vs.  $pK_a$ , including the values obtained previously for water<sup>2</sup> and acetate.<sup>3</sup> (The value of  $k_{H_2O}$  was divided by 55.5 to make it comparable to all the other rate constants which are second order; similarly,<sup>6</sup> we used  $K_{H_3O^+} = 55.5$ .)

We drew a straight line through the two most reliable points, acetate and monochloroacetate; the points for the other 4 bases are seen to deviate only slightly from this line. We thus get

$$k_{A^-} = 1.6K_a^{-0.64} \quad (IV)$$

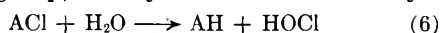
This means that reaction 4 obeys the Brønsted catalytic law.<sup>7</sup>

**Discussion of Reaction Mechanisms.**—The Brønsted law usually applies to general base catalysis, or to other reactions involving rate-determining proton transfer. However, a linear free energy relationship<sup>8a</sup> is conceivable between the acid-base equilibrium and a reaction of the type

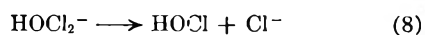
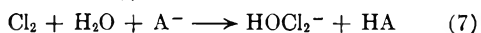


Such a relationship also might lead<sup>9</sup> to eq. IV.

We therefore shall not consider the applicability of the Brønsted Law as a conclusive proof for a mechanism involving proton transfer, and shall include in our discussion a reaction scheme which involves rupture of the Cl-Cl bond in the rate-determining step, namely reaction 5 followed by



(reaction scheme A<sup>10</sup>). Other mechanisms to be discussed are either a one-step mechanism (reaction 4 as it stands), or



The mechanism



(6) See R. P. Bell, "Acid-Base Catalysis," Oxford University Press, London, 1949, p. 45.

(7) J. N. Brønsted and K. J. Pedersen, *Z. physik. Chem.*, **108**, 185 (1924).

(8) See, e.g., A. A. Frost and R. G. Pearson, "Kinetics and Mechanism," John Wiley and Sons, Inc., New York, N. Y., 1953, (a) p. 214 ff., (b) p. 118.

(9) A correlation between "catalytic constant" and basic strength seems to exist in many reactions where we see no room for proton transfer. See, for instance, H. M. Dawson and N. B. Dyson, *J. Chem. Soc.*, 49 (1933), for the hydrolysis of bromoacetic acid; F. J. W. Roughton and V. H. Booth, *Biochem. J.*, **32**, 2049 (1948), for the hydration of CO<sub>2</sub> (the reaction between CO<sub>2</sub> and OH<sup>-</sup> which the authors consider to be uninfluenced by other catalysts may be interpreted as catalysis by OH<sup>-</sup>); A. Lifshitz and B. Perlmutter-Hayman, *J. Phys. Chem.*, **65**, 2098 (1961), for the hydrolysis of Cr<sub>2</sub>O<sub>7</sub><sup>-</sup>.

(10) See A. Lifshitz and B. Perlmutter-Hayman, *Bull. Research Council Israel*, **A8**, 160 (1959), where ABr is suggested as one of two possible intermediates in the hydrolysis of bromine.

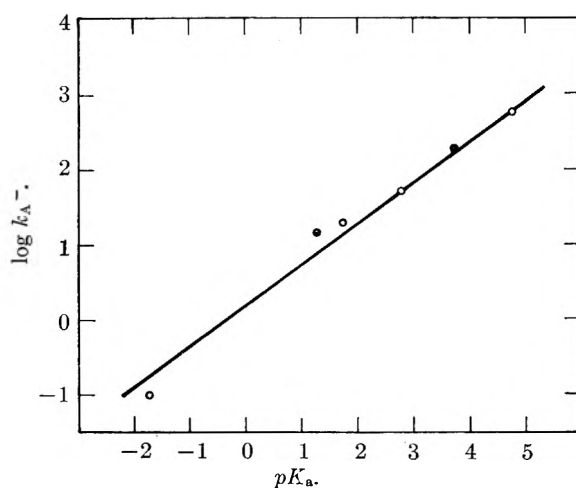


Fig. 3.—The dependence of  $\log k_{A^-}$  on  $pK_a$ .

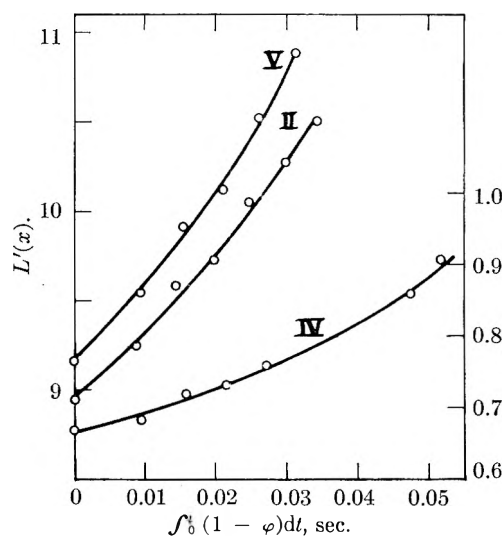


Fig. 4.—Plots of the expression  $([A^-]_0 + k_{H_2O}/k_{A^-}) \log ([A^-]_0 + k_{H_2O}/k_{A^-} - x) - c \log(a - x) \equiv L'(x)$  against  $\int (1 - \varphi) dt$ , for reactions in the presence of acetate. Straight lines would correspond to reactions 7 or 9 constituting a rapid pre-equilibrium.



can be discarded immediately, since it does not account for the accelerating influence of  $A^-$ , unless 9 is a rapid pre-equilibrium. However, the assumption that either reaction 9, or reaction 5 or 7 should constitute a rapid equilibrium in their respective reaction schemes is not compatible with our kinetic results. For 5 or 9 to be a rapid equilibrium, the rate of reaction would have to be inversely proportional to the concentration of the chloride formed during the reaction, and the integrated form of the rate equation would be

$$([A^-]_0 + k_{H_2O}/k_{A^-}) \ln ([A^-]_0 + k_{H_2O}/k_{A^-} - x_t) - a \ln(a - x_t) = \int_0^t (1 - \varphi) dt^{3,4} \equiv 2.3 L'(x) \quad (V)$$

Fig. 4 shows the appropriate plots for 3 typical experiments in the presence of acetate (taken from our previous paper<sup>3</sup>). Curved lines are obtained; this indicates that equation V does not fit our results.

For reaction 7 to be a rapid pre-equilibrium, the reaction rate should be inversely proportional

to  $([HA]_0 + x)$ ; inspection of Table I and of the data reported for acetate-acetic acid<sup>3</sup> shows that this is not the case. Furthermore, when acid and base are involved in a rapid pre-equilibrium, as in 7, we should expect *specific* catalysis.

**Reaction Scheme A.**—Let us now consider scheme *A* with reaction 5 as rate-determining step, and ask whether 6 can be fast enough to constitute a rapid "following reaction." However, nothing is reported in the literature about  $k_6$ . On the other hand,  $k_6'$ , the rate constant for the *back* reaction 6' (*i.e.*, the formation of  $ACl$  from  $HOCl$  and acid) has been estimated in the case of acetic acid on the assumption that reaction 6' is the rate-determining step in the addition of hypochlorous acid to allyl alcohol<sup>11</sup> and allyl acetate,<sup>12</sup> and in the chlorination of *t*-butyl alcohol.<sup>13</sup> All three reactions indeed were found to be zero order with respect to the organic substance, and yielded consistent values for  $k_6'$ , namely,  $(1 \text{ to } 2.4) \times 10^{-1}$  mole<sup>-1</sup> l. sec.<sup>-1</sup>.

We shall now make use of the principle of microscopic reversibility which tells us that a given reaction has to proceed in the forward direction according to the same mechanism (or mechanisms) as in the reverse direction. Therefore, if we can establish the mechanism of the back reaction—formation of chlorine from  $HA$ ,  $HOCl$ , and  $Cl^-$ —then we also know the mechanism of the forward reaction. (As a general principle, this applies of course only to a system in equilibrium. However, in the present case we are trying to decide between three possible mechanisms which all follow the *same* rate law. Therefore, the system will not change from one mechanism to the other as the reaction proceeds, and we can apply the principle during any stage of the reaction.) Furthermore, we know that within a given mechanism the rate-determining step must be the same in both directions. Let us therefore ask whether reaction 6' can be the fast step in the formation of chlorine. This would require

$$k_6' \gg k'_{Ac^-} [Cl^-], \text{ or } [Cl^-] \ll 3 \times 10^{-3} M \quad (VI)$$

Since the actual chloride concentration is always much higher than this—it is at least equal to  $x_0$ , or  $\geq 14 \times 10^{-3} M$ —reaction 6' cannot be the fast step in the back reaction, and reaction 6 cannot be the fast step in the forward reaction; but, as we have seen, neither can reaction 5. Therefore, reaction scheme *A* cannot contribute appreciably to the observed rate in the presence of acetate.

Let us now consider whether the inequality VI might apply for acids other than acetic. When we take a stronger acid,  $k'_{A^-}$  increases. On the basis of theoretical considerations<sup>8a</sup> we may expect  $k_6'$  to increase also. The value<sup>13</sup> of  $k_6' = 18.4$  mole<sup>-1</sup> l. sec.<sup>-1</sup> when the acid is  $H_3O^+$  supports this expectation, but shows that the increase is much less pronounced than that of  $k'_{A^-}$ . It would be only in the presence of very weak acids that the inequality VI might be found to apply. Although this would make it impossible to decide against mechanism *A*, it seems extremely unlikely that

there should be a sudden change in mechanism as we pass from one acid to another.

**Reaction Scheme B.**—We now turn to a discussion of reaction scheme *B*, with reaction 7 as the rate-determining step. The substance  $Cl_2OH^-$  is postulated by Anbar and co-workers<sup>14</sup> as an intermediate in the isotopic exchange of chlorine between  $HOCl$  and  $Cl^-$  in alkaline solution, reaction 8 being assumed to be a fast pre-equilibrium, with  $k_8' \gg 1.3 \times 10^2$  mole<sup>-1</sup> l. sec.<sup>-1</sup>. This assumption is a very reasonable one in view of the fact that the analogous compounds<sup>14,15</sup>  $X_3^-$  are known<sup>15</sup> to be in mobile equilibrium with  $X_2$  and  $X^-$ . Invoking again the principle of microscopic reversibility, we see that reaction 8 *can be* a fast following reaction under our experimental conditions.<sup>16</sup>

Now, on the basis of our results both reaction scheme *B* and a one step reaction represent possible mechanisms. In fact the difference between them might seem trivial. In both schemes there is a rate-determining proton transfer from a water molecule to  $A^-$ , and the concomitant formation of a chemical bond between the  $OH^-$  of this water molecule and one of the chlorine atoms in  $Cl_2$ . The only difference is that in the one-step reaction the  $Cl-Cl$  bond is broken simultaneously with all these rearrangements, whereas in scheme *B* it survives for a short but finite time after the reacting system has passed the main energy barrier. That the differentiation between the two is nevertheless meaningful<sup>17</sup> is perhaps brought out more clearly when we again consider the back reaction. In scheme *B* the rate will be proportional to the—possibly small—concentration of  $Cl_2OH^-$ , and the number of collisions between this substance and  $HA$ . On the other hand, the rate of the one-step reaction is proportional to the number of ternary collisions.

Now, theoretical considerations seem to show that the binary collision frequency in solution is somewhat higher than in the gas phase.<sup>8b,18,19</sup> The same considerations lead to the conclusion that this ratio is still more favorable for ternary collisions; this argues for the plausibility of a one-step reaction. However, the actual factor by which collision numbers in solution should differ from those in the gas phase seems to be rather uncertain. The experimental evidence indicates<sup>18,8b</sup> that for binary collisions this factor is no larger than at most 3 to 4 (in good agreement with the value calculated by Bell<sup>18</sup> from both collision and absolute reaction rate theories). Furthermore, we have found no example in the literature for a reaction in solution which unequivocally

(14) M. Anbar, S. Guttmann, and R. Rein, *J. Am. Chem. Soc.*, **81**, 1816 (1959).

(15) O. E. Myers, *J. Chem. Phys.*, **28**, 1027 (1958).

(16) The compound  $X_2OH^-$  has been suggested by us as one of two possible intermediates in the hydrolysis of bromine (see ref. 10) and has recently been detected (K. Kustin "Abstracts of Papers, 140th National Meeting, Am. Chem. Soc." Washington, D. C., 1961, p. 10-T) as an intermediate in the hydrolysis of iodine.

(17) See S. W. Benson, "The Foundations of Chemical Kinetics," McGraw-Hill Book Co., Inc., New York, N. Y., 1960, p. 306.

(18) R. P. Bell, "Annual Reports," 1939, pp. 88, 89.

(19) S. Glasstone, K. J. Laidler, and H. Eyring, "The Theory of Rate Processes," McGraw-Hill Book Co., New York, N. Y., 1941, p. 409.

(11) G. C. Israel, *J. Chem. Soc.*, 1286 (1950).

(12) A. Chung and G. C. Israel, *ibid.*, 2667 (1955).

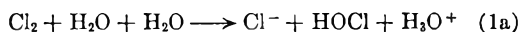
(13) M. Anbar and I. Dostrovsky, *ibid.*, 1094 (1954).

involves ternary collisions. We therefore propose that scheme *B* rather than a one-step reaction constitutes the mechanism of the hydrolysis.

Another question which cannot be answered purely on the basis of the kinetic data is whether the water molecule happens to find itself in a suitable configuration between  $\text{Cl}_2$  and  $\text{A}^-$  at the moment of the reaction, or whether it forms a more or less permanent part of the hydration shell of the chlorine molecule.

Now chlorine is known to form a solid hydrate.<sup>20</sup> Furthermore there is convincing evidence that a chlorine hydrate exists also in solution.<sup>21,22</sup> No matter whether we assign to this hydrate a definite structure<sup>21</sup> or—has been done more recently<sup>22</sup>—consider the interaction between water and chlorine to be of the "iceberg" or "gas hydrate" type, it seems reasonable to suppose that the proton transfer takes place between the  $\text{A}^-$  and one of the water molecules which *already are associated* with chlorine. This should facilitate the simultaneous formation of a covalent bond to form  $\text{HOCl}_2^-$  (or  $\text{HOCl}$ ). We then may say that the water forming part of the chlorine hydrate is more acidic than water in bulk, in analogy<sup>23</sup> with water in a compound of the type  $\text{Fe}(\text{H}_2\text{O})_6^{+++}$ .

**The Reaction between Chlorine and Water.**—We now may return to the consideration<sup>2</sup> of the hydrolysis in pure water. The fact that the data fall so well on the Brønsted plot strongly suggests that the "spontaneous" hydrolysis is not a unimolecular dissociation of a hydrated chlorine molecule but rather that it lies in line with the reaction in the presence of anions. This becomes apparent if we re-write reaction 1 in the form<sup>1</sup>



One water molecule fulfills the same role as in reaction 4, and the same discussion applies to it. The other one serves as base. Mechanism *A* again can be discarded since  $\text{H}_2\text{ClO}^+$  is not formed fast enough<sup>14</sup> from  $\text{H}_3\text{O}^+$  and  $\text{HOCl}$ ; the discussion of a one-step mechanism, and of reaction scheme *B*, applies equally to the present case.

**The Reaction between Chlorine and  $\text{OH}^-$ .**—

(20) See, e.g., L. Mandelcorn, *Chem. Revs.*, **59**, 827 (1959).

(21) H. A. Liebhafsky, *ibid.*, **17**, 89 (1935).

(22) R. E. Connick and Yuan-tsan Chia, *J. Am. Chem. Soc.*, **81**, 1280 (1959).

(23) This analogy was pointed out to us by R. P. Bell in a private communication.

There remains the question of how far reaction 2 is also in line with the mechanism discussed in this paper. Extrapolation of the Brønsted plot to  $pK_{\text{H}_2\text{O}} = 16.28$  yields  $k_{\text{OH}^-} \approx 10^9$ . This value, though very high, is considerably lower than  $k_{\text{OH}^-} \approx 9 \times 10^{10}$  estimated previously<sup>3</sup> on the assumption that reaction 2 contributes somewhat to the observed rate in the presence of acetate. In any case, the extrapolation is so far that it cannot be expected to be accurate. It would seem desirable to confirm the value of  $k_{\text{OH}^-}$  by additional evidence. Unfortunately, we have not been able to do so.

The *direct* reaction between chlorine and  $\text{OH}^-$  is of course much too fast for measurement by the flow method.<sup>1</sup> Reaction 2 can be investigated only in the presence of some other base. It can easily be shown that the value of  $k_{\text{OH}^-}$  obtained in such a system will be more reliable the stronger the base. On the other hand, if the base is too strong (e.g.,  $\text{HPO}_4^{=}$ ) the reaction again becomes too fast for measurement.

All the rate constants obtained in this paper refer to bases weaker than acetate. Even on the assumption of  $k_{\text{OH}^-} = 9 \times 10^{10}$ , reaction 2 makes a negligible contribution in all systems except formate, where it is 11% and cannot serve to calculate a reliable value of  $k_{\text{OH}^-}$ . The most promising system for evaluating  $k_{\text{OH}^-}$  would be a mixture of anion and acid of  $K_a \approx 6$ . However no monobasic inert acid of this  $K_a$  seems to be available.<sup>24</sup>

It might be added that if the correction for reaction 2 were applied to the results of this paper (again using  $k_{\text{OH}^-} = 9 \times 10^{10}$ ), we should get

$$k_{\text{HCOO}^-} = 174 \pm 4 \text{ mole}^{-1} \text{ l. sec.}^{-1}$$

and

$$k_{\text{CH}_2\text{ClCOO}^-} = 55.4 \pm 2.5 \text{ mole}^{-1} \text{ l. sec.}^{-1}$$

The constants for the weaker bases would remain unaffected. The difference between these values of  $k_A$  and those reported above would be noticeable on the Brønsted plot only for formate, which would lie *exactly* on the straight line instead of slightly above. The general conclusions drawn in this paper therefore are unaffected by any assumption we may make about  $k_{\text{OH}^-}$ .

(24) Experiments with mixtures of  $\text{CH}_2(\text{COO})_2^-$  and  $\text{COOHCH}_2\text{COO}^-$  ( $K_a = 2.1 \times 10^{-3}$  at 25°) yielded inconclusive results: high concentrations of acid cannot be applied because (a) the "acid" itself is the anion of a weak acid ( $K_a = 1.6 \times 10^{-3}$  at 25°) and contributes to the observed rate, and (b) the system is oxidized by chlorine.

# A CLOSED FORM ANALYSIS OF THE LCAO-MO $\omega$ -TECHNIQUE. I. IONIZATION POTENTIALS AND ELECTRON AFFINITIES.<sup>1</sup>

BY S. EHRENSON<sup>1</sup>

Laboratory of Molecular Structure and Spectra, Department of Physics, University of Chicago, Chicago 37, Illinois

Received October 2, 1961

Closed form approximations to the results of the  $\omega$ -technique for several special molecular cases have been generated. By means of these solutions the effects of charge redistribution on the energies of neutral conjugated molecules and their ions are analyzed. Generalization of these results indicates the major correction to the Koopmans theorem ionization potentials,  $I$ , provided by this method of charge redistribution is a term dependent upon the number of conjugating  $\pi$ -electrons,  $\eta$ , which reflects stabilization of the cation, *i.e.*,  $I = I - (\eta - 1)\omega\beta^0/\eta$ . The correlation with experiment obtained using the same values of parameters previously used in the cycling procedure is as satisfactory as that obtained through cycling. Predictions of electron affinities by the equation  $\bar{A} = A - (\eta + 1)\omega\beta^0/\eta$  obtained by similar analysis also are discussed.

## Introduction

Streitwieser<sup>2,3</sup> recently has published quite successful correlations of the ionization potentials of a variety of organic molecules with the results of a semi-empirical MO method which he has labeled the " $\omega$ -technique." Less extensive applications of this method also have been made to advantage in other  $\pi$ -electron calculations, especially on ions.<sup>4</sup> However, why this technique superimposed upon the framework of Hückel-type approximations should so markedly improve the simple results is not well understood. By the same token, the reasons for its noted failure for some molecules, *e.g.*, divergence obtained from the iterative self-consistency procedure or convergence to incorrect results, require explanation. The general problem of defining the limits of practical application for such semi-empirical methods also exists; *i.e.*, for which physical phenomena may we expect such a method to work?

In this and an accompanying paper we shall attempt to provide information on these questions by examination of some special molecular cases. The approach is through the generation of closed form approximations to the iterative scheme characterizing the  $\omega$ -technique. Several suggestions as to general computational simplifications are forthcoming from this analysis. The advantages of extending the  $\omega$ -technique as a modification to other simple MO methods, *e.g.*, where overlap is included, also are investigated. Comparisons are made wherever possible with the results of more sophisticated theoretical methods. Special attention is paid to the results of the Pariser-Parr,<sup>5</sup> Pople<sup>6</sup>-type methods.

**1. Theory.**—The basic feature of the  $\omega$ -technique is the assumed linear relationship between Coulomb integral and charge density in the MO framework

$$\alpha_i^{r+1} = \alpha_i^0 + \omega\beta^0(n_i^0 - q_i^r) \quad (1)$$

According to eq. 1, the zeroth order integral,  $\alpha_i^0$ , for atom  $i$  having  $n_i^0$   $\pi$ -electrons available for con-

jugation, will be changed if the charge density,  $q_i$ , obtained from solution of the Hückel determinant is different from  $n_i^0$ . The superscripts indicate the number of iterations;  $q_i^r$ , from the  $r$ th solution of the determinant, yields the new integral value  $\alpha_i^{r+1}$  for the  $(r + 1)$ th determinant. The cycling process is continued until self-consistency in the charge densities is obtained.  $\omega$  is a semi-empirical, dimensionless constant reflecting the sensitivity of the Coulomb integral to charge density changes and  $\beta^0$  is the accompanying energy factor (arbitrarily chosen as the resonance integral for some standard C-C bond, *e.g.*, benzene.)

Equation 1 is a reasonable extension of the theoretically justifiable linear relationship between the Coulomb integral of an atom and its valence state ionization potential.<sup>7</sup> It straightforwardly allows for redistribution of the non-uniform  $\pi$ -charges in the molecule which are imposed through the Hückel-type energy minimization procedures. The latter in effect ignore the differences in Coulomb attraction for an electron of a neutral atom *vs.* the same atom with a charge deficiency or excess. The proper choice of  $\omega$  apparently is able, however, to correct for more than this important neglect. In some way the doubtlessly important  $\pi$ -electronic repulsion changes and  $\sigma$ -electron rearrangements for the physical properties under consideration (especially ionization potentials) are included as an average in  $\omega$ . We shall be more concerned with the specific details of this averaging in the accompanying paper. Here a closed form approximation to the  $\omega$ -technique is generated and its general validity with regards to ionization potentials and electron affinities is investigated.

**2. A Closed Form Approximation to the  $\omega$ -Technique.**—Equation 1 may be rewritten for the molecular cases where all Hückel  $\pi$ -centers ( $N$  in number) are the same as

$$\alpha = \alpha^0 + \omega\beta^0 \left( n^0 - \frac{\eta}{N} \right) \quad (2)$$

where  $\eta$  is the total number of conjugating  $\pi$ -electrons. Similarly, where two different types of  $\pi$ -centers (X and Y) are present

$$\Delta = (\alpha_Y - \alpha_X) = \Delta_0^0 + \omega\beta^0 [(q_X - q_Y) - (n_X^0 - n_Y^0)] \quad (3)$$

Gathering the constant terms, we may more simply write

$$(7) \text{ R. S. Mulliken, } J. \text{ Chem. Phys., } \mathbf{46}, 497 \text{ (1949).}$$

(1) This work assisted by the Office of Naval Research.

(2) A. Streitwieser, Jr., and P. M. Nair, *Tetrahedron*, **5**, 149 (1959).


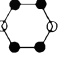
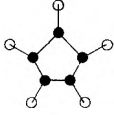
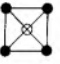
(3) A. Streitwieser, Jr., *J. Am. Chem. Soc.*, **82**, 4123 (1960).

(4) G. W. Wheland and D. E. Mann were the first to use this method, *J. Chem. Phys.*, **17**, 264 (1949); for subsequent applications, *cf.*, N. Muller and R. S. Mulliken, *J. Am. Chem. Soc.*, **80**, 3489 (1958); A. Ron, E. A. Halvevi, and R. Pauncz, *J. Chem. Soc.*, 630 (1960).

(5) R. Pariser and R. G. Parr, *J. Chem. Phys.*, **21**, 466, 767 (1953).

(6) J. A. Pople, *Trans. Faraday Soc.*, **49**, 1375 (1953) and later papers.

TABLE I  
ORBITAL ENERGY LEVEL AND CHARGE DENSITY PARAMETERS FOR X, Y CONTAINING MOLECULES

Molecule type <sup>a, b</sup>	$k/1, 2, 3, 4, 5$	$K^c/1, 2, 3, 4, 5$	$-(q_X - q_Y)$
I. Ring, $X_m Y_m$ , $m > 2$ 	$1, 1, 0, \pm 1, 4\cos^2 \frac{\pi l}{m}$ $l = 1, 2, \dots, m$	$\frac{1}{m}, 4\cos^2 \frac{\pi l}{m}, 1, 4\cos^2 \frac{\pi l}{m}, 1$	$\frac{\Delta}{4m\beta} \sum_j \frac{n_j}{\cos \frac{\pi j}{m}}$
II. Ring, $X_m Y_{2m}$ , $m = 1, 2^c$ 	$1, 1, (-1)^{l+1}, \pm 1, 2$ $2, 1, (-1)^l, 0, -$ $l = 1, \dots, m$	$\frac{1}{2m}, 4, 1, 2, 1$ $-\frac{1}{2m}, 1, 0, 1, 0$	$m = 1^d$ $4 \geq \eta \geq 2$ , for $\Delta = \pm, \mp \left( \frac{\eta-2}{2} \right) + \frac{\Delta}{9\beta} (8-2\eta)$ (4) $m = 2^d$ $6 \geq \eta \geq 4$ , $\mp \left( \frac{6-\eta}{2} \right) + \frac{\Delta}{9\beta} (\eta-2)$ (4) • for $\Delta = \pm,$ $8 \geq \eta \geq 6$ , $\pm \left( \frac{6-\eta}{2} \right) + \frac{\Delta}{9\beta} (10-\eta)$ (4)
III. Per-X Substituted Ring, $X_m Y_m, m > 2$ 	$1, 1, 2\cos \frac{2\pi l}{m}, \pm 1, 1$ $l = 1, 2, \dots, m$	$\frac{1}{m}, 1, 1, 1, 1$	$\frac{1}{m} \sum_j n_j \left[ \frac{\bar{\beta} \cos \frac{2\pi j}{m}}{\left( \beta^2 + \bar{\beta}^2 \cos^2 \frac{2\pi j}{m} \right)^{1/2}} + \frac{\Delta}{2} \cdot \frac{\beta^2}{\left( \beta^2 + \bar{\beta}^2 \cos^2 \frac{2\pi j}{m} \right)^{3/2}} \right]$
IV. Ring with Interl X, $XY_m, m > 2$ 	$1, 1, 2, \pm 1, m$ $2, 1, 2\cos \frac{2\pi l}{m}, 0, -$ $l = 1, 2, \dots, m-1$	$\frac{1}{m}, m^2, 1, m, 1$ $-\frac{1}{m}, 1, 0, 1, 0$	$\frac{1}{m} \left[ \frac{(1+m)\bar{\beta}}{(\bar{\beta}^2 + m\beta^2)^{1/2}} - (1+m-\eta) + \frac{\Delta}{2} \cdot \frac{m(1+m)\beta^2}{(\bar{\beta}^2 + m\beta^2)^{3/2}} \right]$

<sup>a</sup> Examples are given in parentheses; X =  $\circ$ , Y =  $\bullet$ . <sup>b</sup> Important subcases: I:  $m = 1, \omega_3 = K_2 = K_4 = 1$ ; III:  $m = 2, k_3 = \pm 1$ ; IV: Holds if  $\beta = \beta_{YY} = 0$  for all cases where  $m > 1$ . <sup>c</sup> For  $m > 2$  cubic equations in  $\Delta$  are generated. <sup>d</sup> Given here for  $\bar{\beta} = \beta$ ; similar but more cumbersome expressions may be developed without this restraint. <sup>e</sup> These parameters represent average charge density component differences over degenerate levels which will remain degenerate throughout the iterative process.

$$\Delta = \Delta^0 + \omega\beta^0 (q_X - q_Y) \quad (4)$$

Two types of differences are recognized between X and Y in this equation; either they are different atoms, e.g., carbon vs. nitrogen, and/or they occupy different positions in the molecule.<sup>8</sup>

The molecules and ions of the first kind (all  $\pi$ -centers the same) include the simple rings where  $N \geq 2$  and asymptotically such macromolecules as graphite. There is somewhat more variety in the second kind. These include

- (1) heteroatomic rings such as s-triazine, pyrazine, and corresponding larger ring cases
- (2) homoatomic rings with single  $\pi$ -center substituents such as the recently prepared perketocycloalkanes<sup>9</sup>
- (3) cases of the type  $X(Y)_m$  where X is the central atom or  $(Y)_m X - X(Y)_m$  which are really subcases of (2). These include such real molecules as formaldehyde, butadiene, the allyl radical, and glyoxal.
- (4) Any of the above where a multi-atom substituent may be represented by a single group-orbital or as having only an inductive (non-conjugating) effect.

For the molecules with all conjugating sites the same, the iterative procedure requires only a single cycle for convergence. The analytic results for these molecules are easily derivable and will be

(8) It shall become apparent that we may distinguish most of the important features of the method by consideration of these types alone. Extension to cases where three or more types of atoms are present is possible but only at the cost of introducing cubic or higher order equations with more than one difference parameter,  $\Delta$ .

(9) Cf. R. West, H. Niu, D. Powell, and M. Evens, *J. Am. Chem. Soc.*, **82**, 6204 (1960).

presented as they are discussed. The molecules of the second kind are more complicated. It may be shown, however, that the Hückel secular equations for these molecules yield orbital energy levels and charge density difference components of the general form

$$\epsilon_j = \alpha_X + (k_{1j}/2) [(k_{2j}\Delta + k_{3j}\bar{\beta}) + k_{4j} \sqrt{(k_{2j}\Delta + k_{3j}\bar{\beta})^2 + 4k_{5j}\beta^2}] \quad (5)$$

and

$$(c_{jX}^2 - c_{jY}^2) = K_{1j} \frac{K_{2j} - K_{3j}(\epsilon_j - \alpha_X)^2}{K_{4j} + K_{5j}(\epsilon_j - \alpha_X)^2} \quad (6)$$

The  $k$ 's and  $K$ 's are parameters determined solely by the molecular geometry and familiarly the charge density difference,  $q_X - q_Y$ , is obtained by summation of  $(c_{jX}^2 - c_{jY}^2)$  over the filled levels,  $j$ .  $\bar{\beta}$  and  $\beta$  represent the resonance integrals between like and unlike atoms, respectively. Table I, col. 1 and 2, contains the parametric representations of a number of molecules of this type both real and hypothetical. While eq. 4 and 5 in combination with eq. 3 represent analytic forms for the iteration cycle, they are rather cumbersome; considerable simplification is possible, however. It may be easily verified that when

$$K_{2j} = k_{1j}^2 k_{4j}^2 k_{5j} K_{3j} \\ c_{jX}^2 - c_{jY}^2 = \frac{-K_{1j} k_{4j} (k_{2j}\Delta + k_{3j}\bar{\beta})}{\sqrt{(k_{2j}\Delta + k_{3j}\bar{\beta})^2 + 4k_{5j}\beta^2}}$$

$$\frac{-K_{1j}k_{4j}}{\sqrt{4k_{6j}\beta^2 + (k_{3j}\bar{\beta})^2}} \times \left\{ k_{3j}\bar{\beta} + \frac{4k_{2j}k_{6j}\beta^2\Delta}{4k_{6j}\beta^2 + (k_{3j}\bar{\beta})^2} + \dots \right\} \quad (7)$$

The right-hand equality, an expansion in powers of  $\Delta$ , may be satisfactorily truncated after the first term in  $\Delta$  as long as  $\Delta$  is less than  $4k_{6j}\beta$ , as is generally the case for molecules of interest.<sup>10</sup> Cases I and III, Table I, meet the above condition; the electron density difference ( $q_X - q_Y$ ) may be expressed for these cases as a sum of this type of expansion terms and therefore to a very good approximation as a linear function of  $\Delta$ . When  $K_{2j}$  is not equal to  $k_{1j}^2k_{4j}^2k_{6j}k_{3j}$ , as for cases II and IV, the  $c_{jX}^2 - c_{jY}^2$  differences may not be expressed separately by eq. 7 but summation over the occupied levels does allow generation of a factored form of comparable simplicity. Column 3 of Table I contains the ( $q_X - q_Y$ ) quantities for all the cases of interest. Let us designate the approximate linear dependence of the charge density difference upon  $\Delta$  as,

$$(q_X - q_Y) = a + b\Delta \quad (8)$$

Recalling eq. 3 which gives  $\Delta$  a similar dependence upon ( $q_X - q_Y$ ), combination of eq. 3 and 8 yields a closed cycle in the iterative scheme. Therefore

$$\begin{aligned} \Delta^1 &= \Delta^0 + \omega\beta^0(q_X - q_Y)^0 = \Delta^0 + \omega\beta^0(a + b\Delta^0) \\ \Delta^2 &= \Delta^0 + \omega\beta^0(q_X - q_Y)^1 = \Delta^0 + \omega\beta^0\{a + b[\Delta^0 + \omega\beta^0(a + b\Delta^0)]\} \\ &\vdots \\ &\vdots \\ \Delta^n &= \Delta^0 + \omega\beta^0(q_X - q_Y)^{n-1} = \Delta^0 + \omega\beta^0(a + b\Delta^0) \sum_{\mu=0}^{n-1} (\omega\beta^0b)^\mu \end{aligned} \quad (9)$$

When ( $\omega\beta^0b$ ) is less than one, by the familiar summation of geometric series

$$\lim_{n \rightarrow \infty} \Delta^n = \Delta^\infty = (\Delta^0 + \omega\beta^0a)/(1 - \omega\beta^0b) \quad (10)$$

Other necessary relationships are derivable recognizing that  $\eta$  is equal to the sum of  $n_X q_X$  and  $n_Y q_Y$ . These are

$$\alpha_X^\infty = \alpha_X^0 + \omega\beta^0 \left[ 1 - \frac{\eta + n_Y(\Delta^\infty - \Delta^0)/\omega\beta^0}{n_X + n_Y} \right] \quad (11)$$

and

$$(\alpha_Y - \alpha_X)^\infty = (\alpha_Y - \alpha_X)^0 + (\Delta^\infty - \Delta^0) \quad (12)$$

It should be noted that  $\Delta^0$  signifies the heteroatom integral difference. The lack of uniformity in the Hückel charge densities due to the molecular geometry, *i.e.*, in non-alternant hydrocarbons, is reflected in the parameter  $a$ .

### Results and Discussion

Having obtained the general closed form expressions for the self-consistent values of the necessary molecular parameters, we may proceed to compare the results of this method with experimental quantities and with the results of other theoretical methods (see also the paper following). In the interest of clarity, the neutral molecule, positive ion, and negative ion results are presented separately and their salient features are discussed;

(10) *E.g.*, when all  $k$ 's are unity,  $\beta$  equals  $\bar{\beta}$  and  $\Delta$  equals  $(\beta/2)$ , this truncation results in a 4% error.

the appropriate combinations of results for comparisons with the observables then follow.

**1. Neutral Molecules.**—From eq. 4 we obtain the self-consistent neutral molecule delocalization energy,  $\bar{E}$ , as opposed to the zeroth order Hückel energy,  $E$ .

$$\bar{E} = \eta\alpha_X^\infty + \frac{1}{2} \sum_j^0 n_j k_{1j} [(k_{2j}\Delta^\infty + k_{3j}\bar{\beta}) + k_{4j} \sqrt{(k_{2j}\Delta^\infty + k_{3j}\bar{\beta})^2 + 4k_{6j}\beta^2}] \quad (13)$$

Here  $n_j$  is the number of  $\pi$ -electrons in the  $j$ th MO and  $\eta$  is the total number of these electrons.  $\sum^0$  indicates summation to the neutral state of this molecule. Several interesting conclusions may be derived from this expression.

For the neutral molecules having alternant hydrocarbon-like structures, *i.e.*, cases I, II ( $m = 2$ ), III ( $m$  even), and IV ( $\beta_{YX} = 0$ ), the energy is to the first-order independent of whether the calculation is made self-consistent or not. This may be seen by replacing  $\alpha_X^0$  and  $\Delta^\infty$  by their respective equalities in eq. 10 and 11, expanding the quadratic terms in  $\Delta^\infty$  and  $\Delta^0$  (in the  $\bar{E}$  expression) and recognizing that  $n_Y$  is equal to  $\frac{1}{2} \sum_j n_j k_{1j} k_{2j}$ . In general then

$$\begin{aligned} \bar{E} &= E + (\Delta^\infty - \Delta^0) \left( \frac{1}{2} \sum_j^0 n_j k_{1j} k_{2j} k_{4j} \bar{\beta} / \sqrt{k_{3j}\bar{\beta}^2 + 4k_{6j}\beta^2} \right) \\ &= E + (\Delta^\infty - \Delta^0) (\tau^0 - n_Y) \end{aligned} \quad (14)$$

This sum term, hereafter symbolized as ( $\tau^0 - n_Y$ ) and closely related to  $a$  of eq. 8, may be shown to be zero for the alternant but not necessarily zero for the non-alternant type molecules. The latter molecules therefore do have a first-order correction to the energy through cycling, albeit small especially for the larger molecules.<sup>11</sup>

It is worthwhile to note that in general differences between the resonance energies computed by the self-consistent *vs.* the zeroth order methods should vary as  $\bar{E} - E$  since the localized structures are represented by two-center MO's which are alternant in nature.

For all the cases presented there is a first-order correction to the charge densities upon cycling; from eq. 8 and 10 it is apparent that

$$(q_X - q_Y)^\infty = (q_X - q_Y)^0 / (1 - \omega\beta^0b) \quad (15)$$

In agreement with expectation,  $b/\beta$  is generally negative indicating that charge is redistributed from those sites with excesses to those with deficiencies when  $\omega$  is properly chosen as positive. Equation 15 is perfectly general for ions as well as the neutral molecules, with of course different  $b$  values.

While considering the properties of the neutral molecules it is of interest to reflect on the meaning of the parameter  $a$  in eq. 8. As noted above,  $a$  is zero for the alternant type molecules, a condition

(11) For example, for case III the sum term in eq. 14 is

$$\sum_{j=1}^m \left( \bar{\beta} \cos \frac{2\pi j}{m} / \sqrt{\bar{\beta}^2 \cos^2 \frac{2\pi j}{m} + \beta^2} \right)$$

and is equal to zero when  $m$  is even (note,  $k_{1j}$ ,  $k_{2j}$ ,  $k_{4j}$ , and  $k_{6j}$  constant). When  $m$  is odd assuming  $\beta$  equals  $\bar{\beta}$ , this sum decreases in magnitude rapidly from where  $m$  equals 3 ( $-0.187$ ); *e.g.*, where  $m$  is 5, the sum is 0.040.

which is quickly understood when the equality of  $\Delta^\infty$  and  $(\Delta^0 + \omega\beta^0 a)/(1 - \omega\beta^0 b)$  is reviewed; for the alternant hydrocarbons themselves  $\Delta^0$  is zero as must be  $\Delta^\infty$ . For the non-alternants, however,  $a$  is not zero, indicative of the non-uniform charge distributions imposed by the Hückel solutions. The signs for various non-alternant cases are quite illuminating. For example, the members of case III ( $m$  odd), where all atoms are taken to be  $sp^2$  carbon and with equal  $\beta$ 's, are hypothetical molecular relatives of the perketocycloalkanes, some of which have been prepared as dianions.<sup>9</sup> With  $m$  equal to 3 and 7, Table II shows  $a$  to be positive indicating electron redistribution to be favored to the side chains (out of the ring). Of course  $(q_X - q_Y)^\infty$  remains positive, but somewhat smaller than  $(q_X - q_Y)^0$ . The converse is true when  $m$  is 5 where  $a$  is negative. These electron migration tendencies as indicated by the signs of  $a$  interestingly parallel the known behavior of the simple hydrocarbon rings. Cyclopropene<sup>12</sup> and cycloheptatriene both form stable positive ions; cyclopentadiene prefers to form a negative ion. While this seems an interesting correspondence, it certainly would be well to exercise caution in the interpretations of the computed charge distributions such as the immediately preceding consideration. Some further comments on the meaning of these distributions will be made later.

**2. Positive and Negative Ions.**—The correction to the energies of positive and negative ions upon cycling to self-consistency may be expressed in terms similar to eq. 14

$$\bar{E}_\pm = E_\pm \pm \frac{\eta \mp 1}{\eta} \omega\beta^0 + (\Delta_\pm^\infty - \Delta^0) \left( \tau^\pm - n_Y \times \frac{\eta \mp 1}{\eta} \right) \quad (16)$$

where, as before,  $\eta$  is the number of  $\pi$ -electrons in the parent neutral molecule, and

$$\tau^\pm = \frac{1}{2} \sum_j^\pm n_i k_{1j} k_{2j} [1 + (k_{3j} k_{4j} / \sqrt{k_{3j}^2 \beta^2 + 4k_{3j} \beta^2})]$$

When  $n_X$  is equal to  $n_Y$ , it may be seen that  $n_Y(\eta \mp 1)/\eta$  is equal to  $1/2 \sum_j^\pm n_i k_{1j} k_{2j}$ , so for these cases

$$\bar{E}_\pm = E_\pm \pm \frac{\eta \mp 1}{\eta} \omega\beta^0 + (\Delta_\pm^\infty - \Delta^0) \times \left( \frac{1}{2} \sum_j^\pm n_i k_{1j} k_{2j} k_{3j} k_{4j} / \sqrt{k_{3j}^2 \beta^2 + 4k_{3j} \beta^2} \right) \quad (17)$$

This equation is essentially different from eq. 14 by the  $(\eta \mp 1)\omega\beta^0/\eta$  term. Here though the sum term is generally not zero although case I which has  $n_X$  equal to  $n_Y$  is an exception. At the same time, it is important to note that this sum term multiplied by the difference in deltas (infinity value minus zero value) is quite small. For example, for  $\Delta^0$  vanishing and  $\beta$ 's equal,  $|(\Delta_+^\infty - \Delta^0)(\tau^+ - n_Y(\eta - 1)/\eta)|$  is for case I equal to zero, for case II ( $m = 4$ ) less than  $\beta/15$ , and for ( $m = 2$ ) equal to zero. For case III this term is  $\beta/4m$ , and for case IV less than  $\beta/5(1+m)$ . Similarly small values are obtained for the negative ions. As well, to alter these non-zero values appreciably through  $\Delta^0$  contributions,  $b_+ \Delta^0$  must be on the order of  $a_+$  requiring  $\Delta^0$  to be on the order of or greater

than  $\beta^0$ . It should be noted that for all cases where the general expressions are written in terms of the numbers of X and Y sites, this correction term goes to zero as the number of these sites increases!

**3. Ionization Potentials.**—We are now in a position to examine the most important application to which the  $\omega$ -technique has been put. The ionization potential of a molecule is defined as the electronic energy difference between the neutral molecule and its unipositive ion; by this method

$$I = E(\text{cation}) - E(\text{neutral molecule})$$

Now it will be convenient to examine both the Hückel or zeroth order or Koopmans theorem ionization potential,  $I$ , and that of the self-consistent method,  $\bar{I}$ . Clearly, by the Hückel method

$$I = -\alpha^0 - m_N \beta^0$$

where  $\alpha^0$  is the reference Coulomb integral (usually taken as that for  $sp^2$  carbon) and  $m_N \beta^0$  is the energy of the highest filled orbital in the neutral molecule. Since we have derived the self-consistent molecular energies in terms of the zero order approximation values it is easily shown that

$$\begin{aligned} \bar{I} - I &= (\bar{E}_+ - \bar{E}) - (E_+ - E) \\ &= (\bar{E}_+ - E_+) - (\bar{E} - E) \\ &= \frac{\eta - 1}{\eta} \omega\beta^0 + (\Delta_+^\infty - \Delta^0) \left( \tau^+ - n_Y \frac{\eta - 1}{\eta} \right) - \\ &\quad (\Delta^\infty - \Delta^0)(\tau^0 - n_Y) \quad (18) \end{aligned}$$

If the latter two terms may be neglected

$$\bar{I} = -\alpha^0 - \left( m_N - \frac{\eta - 1}{\eta} \omega \right) \beta^0 \quad (19)$$

It appears therefore that we may very easily compute good approximations to the  $\omega$ -technique results if the arguments concerning the small sizes of the latter product terms in eq. 18 hold generally, *i.e.*, to those compounds with more than two types of sites. Table II contains a number of ionization potentials computed employing eq. 19. Also given are the values computed by Streitweiser and the electron impact method experimental values, mainly those quoted by the latter author.<sup>3</sup> These are fairly representative, including besides the aromatic hydrocarbons several methyl-substituted cases which because of the large methyl group Coulomb values used in the cycling procedures should result in the poorest agreement between the two methods of calculation. A few heteroatom cases for which the Hückel orbitals were available also are included to extend the test. The results are in general very satisfactory: the values from eq. 19 agree as well with the results from ref. 3 as the latter do with experiment. It is anticipated that as good agreement will be found with the other molecules already examined by the iterative technique or capable of being so examined.

There are but two cases which exhibit results markedly in disagreement with experiment and/or the iterative technique results. These are graphite and the  $\beta$ -phenylallyl radical. A few words are in order concerning the possible reasons for their failure to fit; both in a sense constitute special cases. For the former, the serious question arises whether the work function value quoted may be equated to a vapor state ionization potential be-

(12) Cf., R. Breslow and P. Gal, *J. Am. Chem. Soc.*, **80**, 5991 (1958).

TABLE II  
 IONIZATION POTENTIALS

Molecule	$\bar{I}$ (in e.v.) <sup>a</sup>			
	Expt.	Eq. 18	Ref. 2 and 3 <sup>b</sup>	Eq. 19
Ethylene	10.62	10.66	10.66	10.66
Benzene	9.52	9.53	9.53	9.53
Allyl radical	8.16	8.13	8.22	7.91
Pentadienyl radical	7.73		7.74	7.52
Butadiene	9.18	9.21	9.22	9.16
		9.03 <sup>c</sup>		8.97 <sup>c</sup>
Styrene	8.86		8.94	8.81
				8.69 <sup>c</sup>
Naphthalene	8.68		8.63	8.52
Phenanthrene	8.62		8.50	8.56
Anthracene	8.20		8.11	8.16
Tetracene	7.71		7.81	7.71
3,4-Benzphenanthrene	8.40		8.36	8.29
Pyrene			8.17	8.05
Graphite	4.39	6.93	6.93	6.93
Cyclopentadiene	8.9		8.91	8.91
Azulene			8.32	8.26
Acenaphthalene			8.73	8.60
Fluoranthene			8.54	8.41
Fulvene			9.07	8.92
Biphenyl			8.79	8.73
Toluene	9.23		9.01	9.24
Xylene, <i>o</i> -	8.97		8.76	9.07
<i>m</i> -	9.02		8.77	9.10
<i>p</i> -	8.88		8.83	9.02
Benzyl radical	7.76		7.76	7.35
Cinnamyl radical			7.57	7.25
Methyl radical	9.95		9.88	9.88
Pyridine	9.70			9.53
$\beta$ -Phenylallyl radical			8.20	7.25
				7.91 <sup>d</sup>
Pyrrrole	8.97		8.61	8.72
Furan	9.03		8.93	8.82

<sup>a</sup> All the computations for this table were made employing  $\alpha$ ,  $\beta^0$ ,  $\omega$  values of  $-9.878$  e.v.,  $-2.110$  e.v., and  $1.4$ , respectively, adopted from ref. 3. <sup>b</sup> Many of these values were obtained from first cycles in the self-consistent scheme; for comparisons with converged results, see section on extrapolation procedures in the accompanying paper. <sup>c</sup> Short (ethylenic) bond not considered. <sup>d</sup> Phenyl group taken as non-conjugating.

cause of crystal polarizability; more will be said on this question in the discussion of electron affinities, where it is of a more crucial nature. The radical presents a different problem. Examination of the Hückel secular equation reveals that there is no conjugation between the phenyl and allyl groups when these are joined at the  $\beta$ - (or 2-) position of the latter. The nine  $\pi$ -electrons therefore are not delocalized over the entire molecular framework: for this type molecule, the potential should be close to that for the fragment with the lowest potential (here the allyl radical), ignoring large inductive effects.

Work is presently underway to refit eq. 19 to the molecular potentials which have been measured by photoionization and spectroscopic techniques. While fewer experimental values have been determined by these methods, they generally are recognized to be more dependable than the impact values. Further, the photoionization process is more closely represented by the ionization model here assumed, *i.e.*, with regards to the verticality of the transition, than is the electron impact process. If the errors may be assumed random in the impact values, it seems rather sure that the photoionization correlation should be even better than the quite satisfactory correlation herein presented.

**5. Electron Affinities.**—The obvious question following a discussion of the merits of the  $\omega$ -technique in the calculation of ionization potentials is whether the same procedure may be used to calculate molecular electron affinities. In principle the answer is yes, since electron affinities of neutral molecules are but the ionization potentials of their corresponding negative ions. In practice, however, the answer is not as readily forthcoming; at present two major difficulties, in a sense inter-related, have prevented any serious attempts in this direction. It may be easily shown employing the same parameters as used for ionization potentials that the electron affinities calculated are always too high by on the order of 4 e.v. or more. At the same time, it should be noted that this conclusion may be drawn only from a very few affinity values and these are of dubious reliability. The latter were not directly obtained by experimental procedures but are from more sophisticated theoretical treatments and/or empirical derivation from reduction potential data.<sup>13</sup> Table III contains the affinities of a number of hydrocarbons computed from the closed form solutions given earlier where

$$\begin{aligned} \bar{A} - A &= (\bar{E} - \bar{E}_-) - (E - E_-) \\ &= \frac{\eta + 1}{\eta} \omega \beta^0 + (\Delta^0 - \Delta^- \infty_-) \left( \tau^- - n_Y \frac{\eta + 1}{\eta} \right) - \\ &\quad (\Delta^0 - \Delta^\infty)(\tau^0 - n_Y) \quad (20) \end{aligned}$$

and

$$A = -\alpha^0 - m_{\bar{N}} \beta^0$$

where  $m_{\bar{N}} \beta^0$  is the Hückel approximation to the energy of the highest filled level in the anion. The first column of Table III gives the complete value according to eq. 20 with  $\omega$  taken equal to 1.4; column two contains the approximation where the last two terms are ignored, *i.e.*

$$\bar{A} = -\alpha^0 - \left( m_{\bar{N}} - \frac{\eta + 1}{\eta} \omega \right) \beta^0 \quad (21)$$

Also included are the values computed by Hush and Pople and whatever experimental (indirect) values are available for these compounds.

As for the ionization potential computations, it appears that the truncated expression is quite a good approximation to the closed form (several hypothetical molecules from Table I show essentially the same behavior as those molecules compared in Table III). However, if we restrict ourselves to the same  $\alpha$  and  $\beta$  values as used in the ionization calculations, problems of divergence in cycling would be encountered. Too large an  $\omega$  is required to provide convergence in cycling and simultaneously to produce affinities anywhere near the empirical values quoted by Hush and Pople, or for that matter their theoretical results. It appears then that the  $\omega$ -technique with cycling is not a possible means of correlation of the affinities under these conditions. The criteria for convergence upon iteration are discussed in detail in the accompanying paper. Using the truncation approximation, one still may use this method. Interest-

(13) N. S. Hush and J. A. Pople, *Trans. Faraday Soc.*, **51**, 600 (1955).



TABLE III  
 ELECTRON AFFINITIES

Molecule	Eq. 20 <sup>a</sup> $\omega = 1.4$	$\bar{A}$ (in e.v.) Calculated			Pople	Semi-empirical Exptl.
		$\omega = 1.4$	Eq. 21 <sup>a</sup> $\omega = 2.0$	$\omega = 3.8^b$		
Ethylene	3.34 (3.10) <sup>c</sup>	3.34 (3.10) <sup>c</sup>	1.44 (1.27) <sup>c</sup>	-4.26	-1.81	
Benzene	4.32	4.32	2.84	-1.62	-1.40	-0.54
Butadiene	4.75	4.88	3.30	-1.45	-0.34	
Allyl radical	5.72	5.94	4.25	-0.14	0.24	2.1
Benzyl radical		6.50	5.05	0.71	0.69	1.8
Styrene		5.16	3.73	-0.54	-0.29	
Methyl radical	3.37	3.37	1.44	-6.16	-1.03	1.1
Triphenylmethyl radical		6.77	5.44	1.44	1.65	2.1
Biphenyl		4.92	3.75	-0.37	-0.37	0.41
Naphthalene		5.32	3.93	-0.25	-0.14	0.65
Phenanthrene		5.44	4.18	0.0	-0.06	0.69
Anthracene		5.84	4.48	0.43	0.64	1.19

<sup>a</sup>  $\alpha = -9.878$  e.v.,  $\beta^0 = -2.110$  e.v. <sup>b</sup> That value of  $\omega$  which makes the predicted graphite electron affinity as much higher than the work function as the predicted ionization potential was lower than the work function for this macromolecule. <sup>c</sup> Short bond taken into account.

ingly, if  $\omega$  is chosen to yield an affinity for graphite as much smaller than the value quoted by Mulliken<sup>14</sup> than the  $\omega$ -technique potential is greater than the work function (for  $\omega$  equal 1.4), the last column in Table III is obtained.<sup>15</sup> Here,  $\omega$  is 3.8 and the correlation with Pople's values and the empirical values he quoted are as good as the latter are with each other with two exceptions. Both of these exceptions are small molecules; ethylene and methyl radical are calculated to be considerably more reluctant to accept an electron than Hush and Pople predict them to be. It does not seem profitable to dwell at any great length upon this attempt at correlation and such discrepancies as these two small molecules present, especially when the almost complete lack of information concerning this molecular property is recalled. Nor do further adjustments of parameters seem justified until at least several quantitative measurements of molecular affinities are available.

### Summary

Examination of closed form approximations for some special molecular cases has revealed the major corrections the  $\omega$ -technique makes to the Hückel molecular orbitals. For the most part, the corrections to neutral molecule properties are minor although some energy corrections are noted for non-alternant hydrocarbon-like molecules. Also,

(14) R. S. Mulliken, *Phys. Rev.*, **74**, 736 (1948) gives the photoelectric work function as 4.39 e.v. (equal to  $I$  and  $A$ ).

(15) The supposition that the vapor station ionization potential and electron affinity of graphite would be, respectively, 2.53 e.v. above and below the work function (for the crystal) was suggested by recent work on the potentials of very large molecules in the solid state, cf. D. R. Kearns and M. Calvin, *J. Chem. Phys.*, **34**, 2026 (1961). In general the solid state potentials were estimated to be on the order of 2 e.v. below the gaseous ionization potentials quoted by R. M. Hedges and F. A. Matsen, *ibid.*, **28**, 950 (1958), which were in turn on an average of 0.56 e.v., below the experimental electron impact values.

$\pi$ -electron charge generally is redistributed proportional to the value of  $\omega$ . Resonance energy is changed identically with the corrections to the delocalization energy of the molecule.

The important effects of the  $\omega$ -technique are found in the ion energies; successful generalizations from the special molecular cases reveal carbonium ions (produced by ionization of a  $\pi$ -electron) to be stabilized to a very good approximation by the quantity  $(\eta - 1)\omega\beta^0/\eta$  more than the predicted Hückel stabilization, where  $\eta$  is the number of conjugating  $\pi$ -electrons in the neutral molecule. Similarly, carbanions are predicted to have extra *destabilization* by the amount  $(\eta + 1)\omega\beta^0/\eta$ .

The former term is able to correct the Koopmans theorem ionization potentials to very good agreement with experiment, in a manner apparently *independent of geometry and dimensions of the molecule*. Whatever spatially dependent effects exist for the neutral molecule and ion seem to be reflected in their Hückel MO's. Recognizing the  $(\eta - 1)/\eta$  factor, the correction term may be sensibly viewed as a decrease in the total electronic repulsion accompanying the removal of one of a "sea" of  $\eta$  electrons in the neutral molecule; the value of  $\omega\beta^0$  then should be dependent upon the nature of the constituent atoms and their bonding characteristics, with special reference to the localized electrons responsible for the  $\sigma$ -framework.

At least one seemingly major deficiency in the  $\omega$ -technique method also has come to light. This lies in the lack of as satisfactory a correlation of electron affinities by complementary arguments and correction expressions, a fault not easily explained. However, experimental verification of the affinity values presently available would seem desirable to determine whether the technique is truly at fault.

## A CLOSED FORM ANALYSIS OF THE LCAO-MO $\omega$ -TECHNIQUE. II. MECHANICS OF THE TECHNIQUE

BY S. EHRENSON<sup>1</sup>

*Laboratory of Molecular Structure and Spectra, Department of Physics, University of Chicago, Chicago 37, Illinois*

*Received October 2, 1961*

Analytic expressions for the ionization potentials of the cyclic polyenes are developed for the Pople method and shown to be fundamentally different from the corresponding  $\omega$ -technique expressions. These differences become pronounced only in the very large molecules, however. The possibility of better agreement upon change of parameters based upon good experimental potentials for large molecules is considered. Some of the possible reasons for divergence encountered in the cycling procedure of this technique also are examined in terms of the closed form solutions obtained. Extrapolation procedures for divergent and slowly convergent cases are presented and discussed. The effects of overlap inclusion in calculations of ionization potentials and electron affinities also are considered and found to be unimportant.

### Introduction

In the preceding paper<sup>2</sup> closed form approximations to the results of the  $\omega$ -technique for  $\pi$ -charge redistribution were developed for some special cases and shown to be generalizable for calculations of delocalization energies of neutral molecules and their singly charged ions. The major corrections to the energies introduced by this technique were shown to lie in the extra stabilization of cations and destabilization of anions (beyond the Hückel effects) by the quantities  $(\eta - 1)\omega\beta^0/\eta$  and  $(\eta + 1)\omega\beta^0/\eta$ , respectively, where  $\eta$  is the number of conjugating  $\pi$ -electrons in the neutral molecule.

The availability of these simple algebraic expressions allow further examination of the reasons whereby this technique is able to improve our picture of the relative ion to neutral molecule energies over that afforded by the Hückel method. The intrinsic workings of the technique are also capable of detailed examination, *e.g.*, under what conditions is divergence to be expected in the cycling procedure and what improvements may be expected from the inclusion of overlap. We shall take advantage of our previous results in an attempt to answer these and similar questions.

### Implicit vs. Explicit Electron Interaction

The ability of the  $\omega$ -technique to improve the correlation of ionization potentials over that afforded by the Hückel method has been attributed mainly to the successful averaging of the electron repulsion terms and  $\sigma$ -framework effects by the empirically chosen value of  $\omega$ . Muller, Pickett, and Mulliken,<sup>3</sup> in comparing the  $\omega$ -value for the ionization potential of isolated  $sp^2$  carbon ( $\sim 4.6$ ) to those acceptable for molecular calculations (1–1.5), concluded the difference was due to polarization of the  $\sigma$ -orbitals by non-uniform  $\pi$ -distributions. Streitwieser<sup>4</sup> has reflected upon the averaging of the  $\pi$ -electron repulsion terms and arrived at the sensible conclusion that the  $\omega$ -technique is substantially different from such treatments as Pople's<sup>5</sup> which explicitly contain these terms.

While little can easily be done directly to evaluate

(1) This work assisted by the Office of Naval Research.

(2) S. Ehrenson, *J. Phys. Chem.*, **66**, 706 (1962).

(3) N. Muller, L. W. Pickett, and R. S. Mulliken, *J. Am. Chem. Soc.*, **76**, 4770 (1954).

(4) A. Streitwieser, Jr., *ibid.*, **82**, 4123 (1960).

(5) J. A. Pople, *Trans. Faraday Soc.*, **49**, 1375 (1953) and later papers.

the  $\sigma$ -electron contributions more quantitatively, Streitwieser's line of inquiry may be extended. Employing the previously presented closed form solutions we may make some specific comparisons with the Pople method which in itself somehow averages the  $\sigma$ -framework effects. Our hope is to shed more light on the means by which the averaging of  $\pi$ -electron repulsions is accomplished. At the same time, the reasons for the failure to predict electron affinities, or at least to provide corresponding results to those given by the Pople method, may be examined.

A particularly tractable family of molecules is available in case I.<sup>2</sup> While this family is for the most part experimentally unknown and perhaps for the higher members is completely hypothetical,<sup>6</sup> it seems a useful subject for two reasons. Closed form and general expressions may be written for its ionization potentials in both the  $\omega$ -technique and Pople approximations. Also, the similarities between the large rings and the fused ring benzenoid hydrocarbons with the same numbers of carbon atoms seem sufficient for conclusions to be drawn cautiously for the latter type of real molecules from the results for the former.

For the hydrocarbon rings,  $C_{2m}H_{2m}$ , which are the special members of case I where all the ring atoms are the same, and restricting ourselves to the more interesting cases where  $m$  is odd ("aromatic sextet" type) and equal to or greater than three, the energies may be written as follows. The bond distances are assumed the same as those in benzene.

$$\bar{E} = 2m\alpha^0 + 4\beta^0 \left[ 1 + \sum_{l=1}^{\frac{m-1}{2}} \cos \frac{\pi l}{m} \right] \quad (1)$$

For the monocations, the  $\omega$ -technique, convergent on a single cycle, yields

$$\bar{E}^+ = (2m - 1)\alpha^\infty + 4\beta^0 \left[ 1 + \sum_{l=1}^{\frac{m-1}{2}} \cos \frac{\pi l}{m} \right] - 2\beta^0 \cos \frac{\pi(m-1)}{2m} \quad (2)$$

From ref. 2, eq. 11, then

$$\bar{E}^+ = (2m - 1)\alpha^0 + \frac{2m - 1}{2m} \omega\beta^0 - 2\beta^0 \sin \frac{\pi}{2m}$$

(6) It seems to be well accepted at present that the large unsaturated rings should have alternation in bond lengths much in the manner of the linear polyenes, *c.f.*, H. C. Longuet-Higgins and L. Salem, *Proc. Roy. Soc. (London)*, **A251**, 172 (1959).

and

$$I = -\alpha^0 + (2m - 1) \omega \beta^0 / 2m - 2\beta^0 \sin \frac{\pi}{2m} \quad (3)$$

in agreement with ref. 2, eq. 19, since  $m_N$  is  $2\beta^0 \sin \pi/2m$ . It is to be noted no  $\tau$  term is applicable because all atoms are the same ( $\Delta$ 's are zero).

At the same time, the Pople method<sup>7</sup> ionization potentials for these molecules are

$$-I = U + \frac{1}{2} \gamma_{11} + 2 \sum_{l>k} c_{Nk} F_{kl} c_{Nl}^* \quad (4)$$

where  $U$  and  $\gamma_{11}$  are, respectively, the one-electron kinetic energy plus core interaction and "self-repulsion" integrals both of which are empirically chosen ( $-9.50$ ,  $10.53$  e.v., respectively, for hydrocarbons). The  $c$ 's are the Hückel AO coefficients (atoms  $k$  and  $l$ ) for the highest filled MO and  $F_{kl}$  is the interaction integral defined as

$$F_{kl} = \beta_{kl} - \frac{1}{2} P_{kl} \gamma_{kl}, \quad k \neq l$$

For the rings where the wave functions,  $\psi_s$ , are written in the imaginary forms, i.e.,  $\frac{1}{\sqrt{2m}} \sum_{r=1}^{2m} \varphi_r \exp\left(\frac{sr\pi i}{m}\right)$ , the bond orders,  $P_{kl}$ , may be shown to be

$$P_{kl} = \sin \frac{\pi}{2} (l - k) / m \sin \frac{\pi}{2m} (l - k) \quad (5)$$

Similarly the sum term may be rewritten

$$\sum_{l>k} c_{Nk} F_{kl} c_{Nl}^* = \left[ \sum_{(l-k)=1}^m F_{kl} \cos \frac{(m-1)\pi(l-k)}{2m} \right] - \frac{1}{2} F_{k,k+m} \cos \frac{(m-1)\pi}{2} \quad (6)$$

Since  $\beta_{kl} = \beta^0 = -2.39$  e.v. only when  $(l - k)$  equals one and is equal to zero otherwise, we have only to concern ourselves with  $\gamma_{kl}$  to analytically express  $F_{kl}$ . In general  $\gamma_{kl}$  is reasonably taken as  $\gamma_{kl}^0 r_{kl}^0 / r_{kl}$ ; for  $(l - k)$  equal 1, 2 and 3, respectively,  $\gamma_{kl}^0$  and  $r_{kl}^0$  have been chosen in ref. 7 as 7.30 e.v. and 1.39 Å., 5.46 e.v. and  $\sqrt{3} \times (1.39 \text{ Å.})$ , and 4.90 e.v. and  $2 \times (1.39 \text{ Å.})$ . For  $(l - k)$  greater than 3, the point charge interaction energy assumption is used and therefore  $\gamma_{kl}^0$  is equal to 14.39 e.v. Å. In the polyene ring with benzene bonds (1.40 Å.) it may be easily shown that  $r_{kl}$  is  $1.40 \text{ Å.} \times (1 - \cos \frac{\pi(l-k)}{m})^{1/2} (1 - \cos \frac{\pi}{m})^{-1/2}$ .

Therefore, combining eq. 4, 5, and 6

$$-I = U + \frac{1}{2} \gamma_{11} + 2 \left[ \beta^0 \sin \frac{\pi}{2m} - \frac{\gamma_{12}}{2m} - \frac{\delta \gamma_{14} \sin \frac{\pi}{2m}}{m \sin \frac{3\pi}{2m}} + \frac{14.39}{5.6m} \left( \sin \frac{\pi}{2m} - 2 \sum_{(l-k)=5}^m \frac{\sin \frac{\pi}{2m}}{\sin \frac{\pi(l-k)}{2m}} \right) \right] \quad (7)$$

where  $\delta$  is  $1/2$  when  $m$  is 3 or otherwise unity.

For  $m$  equal to 3 and 5, the ionization potentials are effectively the same by both methods although

(7) Specifically, N. S. Hush and J. A. Pople, *Trans. Faraday Soc.*, **51**, 800 (1955).

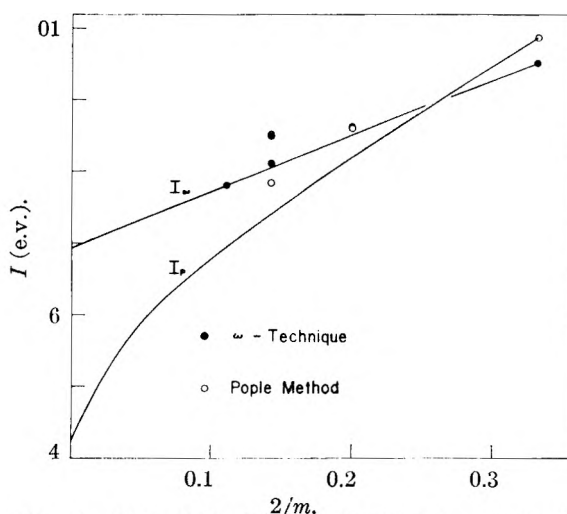


Fig. 1.—Plot of the Pople and  $\omega$ -technique ionization potentials vs. ring size for the cyclic polyenes (curves), for some fused ring aromatics (points).

examination of the terms in the respective equations shows that this is coincidental (the crossing-over in Fig. 1 is indicative of this). When  $m$  is 7 or greater, eq. 7 may be asymptotically expanded<sup>8</sup> with errors less than 0.1% to yield, after replacing  $U$  and  $\gamma_{11}$  by their numerical values

$$-I_P = -4.235 - \frac{2.14}{m} - \left( \frac{10.28 \ln m}{m} \right)$$

Similarly

$$-I_\omega = -6.92 - \frac{8.10}{m}$$

It is now apparent that the two methods are analytically different: examination of Fig. 1 for  $m$  greater than or equal to 7 presents this difference strikingly. Also shown in this figure are the results of the two methods for some of the real benzenoid hydrocarbons. As is to be expected, the  $\omega$ -technique results for the hypothetical rings are better approximations to the real molecule values than are those of Pople; the relatively small  $m_N$  corrections are all that are necessary for the former. In fact, naphthalene, anthracene, and tetracene are almost identical with their hypothetical cyclic polyene counterparts by the  $\omega$ -method. The Pople method, on the other hand, recognizes two major differences. The bond orders,  $P_{kl}$ , are no longer the same for a given value of  $(l - k)$  but depend on the positions of the atoms  $k$  and  $l$ . The  $\gamma_{kl}$  values are, as well, different from those hypothetically chosen since molecular geometry changes the  $r_{kl}$  values.

It is of some interest to note that a correction term may be applied to the hypothetical results quite simply; if one accounts for the existence of the new  $k, k+1$  bonds by multiplying  $\gamma_{12}$  by the appropriate factor to express this increased number of bonds and then scales the values of the other  $\gamma_{kl}$  terms by the changes in  $r_{kl}$ , the true molecular potentials may be well approximated. This doubtlessly is due to the near equality of the average  $P_{kl}$  for a given  $(l - k)$  for the real molecule and the

(8) Asymptotic expansion of the cosecant sum term by the method of G. N. Watson, *Phil. Mag.*, **31**, 111 (1916).

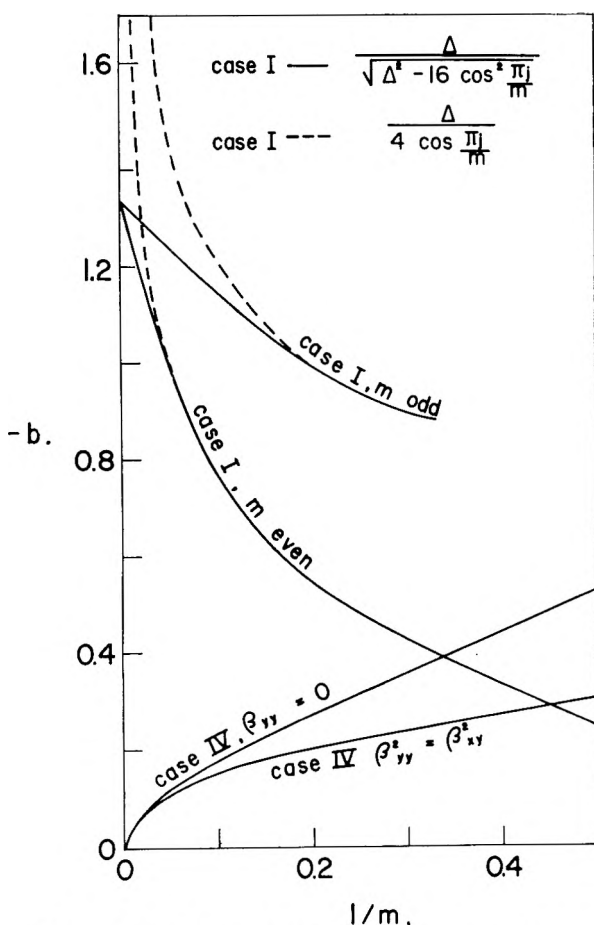


Fig. 2.—Plot of the charge density difference parameter,  $b$ , vs. ring size for closed form cases I and IV (*cf.*, Table I of ref. 2).

corresponding  $P_{kl}$  for the cyclic polyene. Naphthalene, for example, has an average nearest neighbor bond order of 0.622 vs. 0.647 for the cyclic polyene, for bond 1,4,  $-0.218$  vs.  $-0.247$ , and for bond 1,6,  $0.200$  vs.  $0.200$ ; the ionization potential corrected for this molecule in this way is 8.47 e.v.

While we have noted a parallel of results for the two methods for some ionization potentials, no such correspondence exists for electron affinities. It is easily shown that for the  $\omega$ -technique, ref. 2 (eq. 19 and 21), if the same value of  $\omega$  (1.4) is employed, that

$$\bar{I} + \bar{A} = -2\alpha + 2\omega\beta^0 = 13.85 \text{ e.v.}^9$$

In the Pople approximation

$$I + A = -2U - \gamma_{12} = 8.47 \text{ e.v.}$$

We may clearly see here why the affinities computed by the  $\omega$ -technique are found to be generally 5 e.v. higher than those of the Pople method. It is interesting to note as well that the sum of  $\bar{I}$  and  $\bar{A}$  is not a constant in the  $\omega$ -technique when different values of  $\omega$  are employed. A possible and purely empirical way of keeping  $\bar{I}$  plus  $\bar{A}$  constant is to reduce the value of  $\alpha$  for electron affinity calculations to  $-9.878 + (13.85 - 8.47)$  or  $-4.50$  e.v.; this is not generally satisfactory, however, as substitution in eq. 19, ref. 2, indicates.

(9) One may show that this constancy in the sum of  $\bar{I}$  and  $\bar{A}$  is obtainable as well for alternant-hydrocarbon-like molecules from the complete expressions, eq. 18 and 20 of ref. 2.

We may conclude then that not only do distinct differences exist between the Pople and  $\omega$ -technique methods of calculation of ionization potentials, but that quite different results are obtained for some molecules. An important criterion apparently is size; if the Pople method correctly represents the cation-neutral molecule energies for large molecules, then the  $\omega$ -technique does not. Assuming the latter to be true, it is only in a sense fortuitous that the  $\omega$ -technique provides the agreement with experiment that is found. Measurements on larger molecules would have revealed discrepancies: of course, because of their low vapor pressures, measurements in the gas phase on such molecules are precluded. At the same time, the question of whether both theoretical methods are, by virtue of their parameter fitting, correlating with the same ionization potential (vertical or adiabatic, vapor, surface, or solid) must be left open for the present. Similar caution is to be exercised in comparisons of the electron affinities.

It would be well at this time to turn our attention to several other details by which the  $\omega$ -technique is able to profoundly change the Hückel picture of conjugated ions as distinct from neutral molecules.

#### Details on the Mechanics of the $\omega$ -Technique

##### 1. Convergence vs. Divergence in Cycling.—

A general problem encountered in application of the  $\omega$ -method is whether a self-consistent result may be obtained upon iteration for a given molecule and for given parameter choices. Directly from eq. 10 of ref. 2 it is apparent that convergence is obtainable for our closed form cases only when the product of  $\omega$  and  $b$  (the coefficient of  $\Delta$ ) is less than unity, a condition which is sensitive to the molecular geometry.<sup>10</sup> Figure 2 illustrates the dependence of the parameter  $b$ , and thereby also of the maximum  $\omega$  for convergence, upon the variable of ring size for the neutral molecules, cases I and IV. Similar results are obtained for their ions. The two curves for case IV also indicate the strong dependence of  $b$  upon the resonance integrals  $\beta_{YY}$  and  $\beta_{XY}$ . [The allyl radical we may easily ascertain is included in case IV and has a  $b$  value of  $-0.530$  ( $\beta_{YY} = 0$ ,  $\beta_{XY} = 1$ ,  $m = 2$ ).] Note that the convergent value of  $\Delta$  is of course dependent upon  $\omega$ . It may be of interest that for case III there is little variation in  $b$  with ring size; with  $\beta_{XY}$  equal to  $\beta_{YY}$  all converge rapidly under the summation indicated in Table I of ref. 2 to  $b$  approximately equal to 0.60. The even numbered rings converge more quickly than the odd.

While the illustrations involve extension to purely hypothetical cases, there is no reason to believe that similar factors are not involved for all real molecules of interest. Complications are of course to be expected when more than two types of atoms are present. For example, Streitwieser<sup>1</sup> found the related benzyl, cinnamyl, and  $\beta$ -phenyl-

(10) It should be noted that this condition will hold to the first order for any linear relation of Coulomb integral and charge density. Assuming  $\alpha_X = \alpha_X^0 + \omega'\beta(\pi - c\alpha_X)$  with  $c$  a constant smaller than unity will not cause cases which are divergent when  $c$  equals one to converge. Here,  $\Delta = \Delta^0 + c\omega'\beta(\alpha_X - \alpha_Y)$  and obviously  $c\omega'$  fitted to give best correspondence with experiment for all compounds will be  $\omega$  and therefore subject to the same convergence limits as before.

allyl cations all divergent when an  $\omega$  of 1.4 was employed in his calculations but these could be made to converge when  $\omega$  was decreased in size. We may try to understand this behavior in terms of the properties of alternant hydrocarbons in light of the above discussion.

Each of these hydrocarbons has at least one terminal chain site which according to the zeroth order Hückel representation becomes very positive when an electron is removed from its highest occupied orbital (non-bonding). Those sites in the benzyl and cinnamyl cations are, respectively, +0.571 and +0.500, while the corresponding sites (two in number) in the  $\beta$ -phenylallyl cation are +0.383.<sup>11</sup> Little charge is removed from any of the other sites; in other words the non-bonding MO is predominantly composed of the terminal site AO's.

The new  $\alpha$  value generated for the terminal chain sites will be (via eq. 1, ref. 2) numerically very much below those of the other sites as a result and very sensitive to the choice of  $\omega$ . If  $\omega$  is large, this  $\alpha$  will be sufficiently small so as to make the terminal chain sites appear very electron-attracting in the next iteration. The extent of this attraction may be attributed to a complex term involving all the charges to some extent but similar to  $b_+$ . Satisfaction of this demand for electrons must be done at the expense of the other atoms. If a large  $b_+$  type term exists for one of these, its decrease in charge may be large; upon the next iteration then it may over-restore its charge. Such seems to be the case for atoms 1 and 4 in the benzyl cation, both of which have all their charge density contributions in the ions from the most strongly bound MO's.<sup>12</sup>

On the other hand, atoms 2, 3, 5, and 6 which have appreciable charge density contributions from the less strongly bound MO's (specifically the  $1\beta$  zeroth order Hückel level) are not divergent until well after the charges on the other sites have blown up. We may expect therefore that the sites which are nodal in the highest bonding MO's for all these radicals will provide the initial divergences along with and mainly caused by the large charge disparity on the terminal chain sites initially established by the zeroth order Hückel results.

## 2. Further Examination of Charge Densities.—

The question now arises as to why large  $b_+$  type terms exist for atoms 1 and/or 4 in the benzyl, cinnamyl, and  $\beta$ -phenylallyl cations, but not for the allyl cation which also has a non-bonding MO with the described nodal characteristics. It does not seem unreasonable to expect that the tertiary sites (atoms bound to three other conjugating atoms), present in each of the former cases, are of importance in determining the size of these terms. It is of interest in this connection that Hoyland<sup>13</sup> has noted from some improved Pariser-Parr type

calculations that greater  $\pi$ -electron density is predicted for tertiary carbons in alternant hydrocarbonium ions than in their parent neutral molecules when ionization is from an orbital which has a node or near-node at these atoms. Similarly, anomalously low densities are predicted for these atoms in carbanions. These results provide another basis for examination of the mechanism of the  $\omega$ -technique.

It may be easily shown for our alternant hydrocarbon type closed form cases that for  $(q_{X,Y})_+^\infty$  to be greater than one, then  $\pm n_{Y,X}a_+/(1 - \omega\beta^0b_+)$  must be greater than one. Similarly, for the mono-carbanions, for  $(q_{X,Y})_-^\infty$  less than one, then  $\mp n_{Y,X}a_-/(1 - \omega\beta^0b_-)$  must be greater than one. Cases III ( $m$  even) and IV ( $\beta$  equal to zero) from Table I of ref. 2 provide appropriate grounds for comparison with the predictions of the above cited calculations. These molecules, most of which are hypothetical, are all alternant hydrocarbons when X and Y are  $sp^2$  carbon and all have tertiary sites. For case III ( $m$  even),  $a_+$  is quickly shown to be  $-1/\sqrt{2m}$  since  $a_0$  is zero and the electron removed upon ionization comes from the  $k_3$  equals  $-2$ ,  $k_4$  equals 1 level. Since  $\omega\beta^0b_+$  is properly negative, neither  $q_X^\infty$  nor  $q_Y^\infty$  can be greater than unity. We also may note that while somewhat greater electron density is to be found on the ring sites than on the side chain sites the difference is less severe than predicted from the Hückel solutions. In the carbanions,  $a_-$  also equals  $-1/\sqrt{2m}$  (added electron to the  $k_3$  equals 2,  $k_4$  equals  $-1$  level) which does not allow less electron density on the tertiary sites (or side chain sites either for that matter) than in the neutral molecule, independent of the numerical value of  $\omega$  as long as it is positive. For case IV ( $\beta$  equals zero),  $a_\pm$  is  $\pm 1/m$ . Therefore,  $(q_X)_+^\infty$  has a maximum value of unity for  $\omega$  equal to zero; with  $\omega$  positive, no site may have more than one electron in the carbonium ion or less than one electron in the carbanion.

We may conclude then that the  $\omega$ -technique redistributes charge so as to level the differences provided by the Hückel solutions, apparently independent of other criteria such as molecular geometry. The magnitude of the levelling is of course determined by such factors; the reversal of charge redistribution as noted in the studies cited which include electron repulsion does not seem compatible within this method, at least for the special cases examined. It may be tentatively suggested that the problems in divergence encountered for some ions having the structures and orbital arrangements appropriate for the apparently anomalous charge distributions may be due to the restraints imposed by the  $\omega$ -technique preventing such distributions from meeting the criteria for self-consistency. This obviously complicated point is deserving of further investigation.

**3. Extrapolation Procedures.**—The problems of divergence or slow convergence encountered in iterative methods often are overcome by the introduction of extrapolation procedures. Two types are important here. When convergence is slow it is useful to assume a functional form by which the convergence presumably is proceeding and with the

(11) These values may easily be established from the well-known relations for the non-bonding orbital in odd-alternant hydrocarbons given by H. C. Longuet-Higgins, *J. Chem. Phys.*, **18**, 275 (1950).

(12) See Table 5 in A. Streitwieser, Jr., and P. M. Nair, *Tetrahedron*, **5**, 149 (1959), where the atom charges for successive iterations of the benzyl cation are given.

(13) J. R. Hoyland, Ph.D. Thesis, Department of Chemistry, The Pennsylvania State University, June, 1961. See also, A. Brickstock and J. A. Pople, *Trans. Faraday Soc.*, **50**, 901 (1954).

data from several cycles to extrapolate to a "converged" value. If the function assumed is correct, the extrapolated value will be self-consistent; if approximately correct, the extrapolation will approach the correct convergent value from where several more cycles (and perhaps another extrapolation or two) will bring one to the desired self-consistency.

The other extrapolation method attempts to circumvent the frustration of divergency. Here, a parameter expected to be the cause of the divergency is changed until a convergent result is obtained. Further changes in this parameter yield other convergent results from which a functional relationship of the latter to the former may be deduced. Extrapolation to the original value of the varied parameter then may be made. Upon occasion this extrapolation will yield self-consistent results; the reasons for the original divergencies then may be attributed to the starting point properties assumed. (The assumption is made that a continuous passage both conceptually and numerically may be made between the divergent and convergent solutions; however, see section 1 for mention of a possible divergency which would not satisfy this criterion.)

We may examine both of these procedures in the framework of the closed form approximations developed here. For the former case, it often is assumed that the convergence is of the geometric series type.

Then

$$\lim_{n \rightarrow \infty} X_n = X_m + \frac{(X_{m+1} - X_m)^2}{(2X_{m+1} - X_m - X_{m+2})} \quad (8)$$

where  $X_m$  is the value of the particular cycling variable after the  $m$ th iteration. Equations 3 and 8 from ref. 2 for example are the pair of relations which determine the behavior of the special cases chosen upon iteration. If  $X$  is taken to be  $(q_X - q_Y)$  and  $m$  in eq. 8 is assumed zero, then

$$\begin{aligned} \lim_{n \rightarrow \infty} (q_X - q_Y)^n &= (a + b\Delta^0) + \\ &\frac{(a + b\Delta^1 - a - b\Delta^0)^2}{(2a + 2b\Delta^1 - a - b\Delta^0 - a - b\Delta^2)} = (a + b\Delta^0) + \\ &\frac{b(\Delta^1 - \Delta^0)^2}{(2\Delta^1 - \Delta^0 - \Delta^2)} = (a + b\Delta^0) + \\ &\frac{b(\omega\beta^0)^2 (a + b\Delta^0)^2}{\omega\beta^0(a + b\Delta^0 - \omega\beta^0b[a + b\Delta^0])} = (a + b\Delta^0) + \\ &\frac{b(a + b\Delta^0)\omega\beta^0}{(1 - \omega\beta^0b)} = \frac{a + b\Delta^0}{1 - \omega\beta^0b} = (q_X - q_Y)^0 / (1 - \omega\beta^0b) \end{aligned}$$

This is identically eq. 15 of ref. 2, showing that our special cases converge as geometric series; it may be further shown that this result is independent of the choice of iteration,  $m$ . Other more complicated cases (having more than two types of atoms and also with bond order and resonance integral adjustments) also have been examined.<sup>14</sup> These usually required no more than two such extrapolations. The success of the method seems to imply that the  $\omega$ -technique cycling follows a rough geometric series toward convergence.

It is of interest to examine the usefulness of this extrapolation method for the cases which fail to converge. Here it is suggested that "back extrapolation" be employed, or

(14) S. Ehrenson, *J. Am. Chem. Soc.*, **83**, 4493 (1961).

$$\lim_{n \rightarrow \infty} X_n = X_{m+2} + \frac{(X_{m+1} - X_{m+2})^2}{(2X_{m+1} - X_{m+2} - X_m)} \quad (9)$$

The order of points has been reversed, the extrapolation is backward away from divergence or toward convergence. Again substituting with our closed form relations, we find

$$\lim_{n \rightarrow \infty} (q_X - q_Y)^n = (q_X - q_Y)^0 / (1 - \omega\beta^0b)$$

Again, the ref. 2, eq. 15 result is generated: the infinity value for  $(q_X - q_Y)$  is the same as would have been obtained if iterative convergence rather than divergence had occurred with the given value of  $\omega$ .

This result is meaningful in application of the second type of extrapolation. For the cases examined, the functional dependence of  $(q_X - q_Y)$  in iteration upon  $\omega$  was not changed even though divergence occurs beyond a certain threshold value of  $\omega$ . We then might expect an extrapolation of convergent  $(q_X - q_Y)^\infty$  values *vs.*  $\omega$  to values of  $\omega$  which provide cycling divergence, to yield the same result as does this back extrapolation in the cycling procedure. This implies of course that the functional relationship of  $(q_X - q_Y)^\infty$  to  $\omega$  is sufficiently detailed by the convergent points computed to allow a true extension of the curve. The same possibilities of extrapolation extend to other quantities of the system, *e.g.*, energies for which functional relationships with the determined self-consistent quantities are known.

In this light we may examine the specific case of the benzyl cation which Streitwieser<sup>3</sup> studied and found to diverge for the choice of  $\omega$  equal to 1.4. He was able to obtain convergent values for the energy for  $\omega$  equal to 0, 1, and 1.2, however. By a straight line extrapolation he obtained the value of  $(\bar{I} + \alpha)/\beta^0$  to be 1.029 for  $\omega$  equals 1.4, a value which yields good agreement with the experimental ionization potential. Careful examination of the three points fitted by the lower smooth curve in Fig. 3 indicates that these do not lie on a straight line but rather show slight upward curvature (slope for points 1 and 2 is 0.725, for 2 and 3 is 0.825).

Again the similarity with the special cases examined here is noted. According to eq. 16 of ref. 2 and ignoring the final term, a slope of  $(\eta - 1)/\eta$  or 0.857 would be obtained for the benzyl cation but for the more exact relation for  $\bar{I}^+$  and therefore  $\bar{I}$  containing the final term, the slope would be of the form

$$\frac{\eta - 1}{\eta} + \frac{a}{1 - \omega\beta^0b} \times \text{constant}(f[\tau^+, \eta,]) \quad (10)$$

increasing as does the above benzyl cation curve for negative values of  $b$  and  $a \times (\text{constant})$ . Plots for the closed form expression (eq. 10) with arbitrarily chosen  $a \times (\text{constant})$  equal to  $\pm 0.3$  and  $b$  equal to  $-0.75$  are included as the upper curves in Fig. 3 for comparison.

A few words concerning the use of the results of the first iteration seem in order at this point. Streitwieser has remarked on the similarity of the first iteration and converged energy values ( $\chi$ 's) for several of his cases and has employed these results rather widely. It may be shown easily from

TABLE I

Property	PARAMETERS UPON INCLUSION OF OVERLAP				
	Molecule	Ethylene	Benzene	Butadiene <sup>a</sup>	Allyl radical
$(q_X - q_Y)$	Neutral			$8\beta^2\Delta(\bar{\beta}^2 + 4\beta^2)^{-1/2}$	$\left(\frac{3-\eta}{2}\right) + \frac{3\Delta}{4\sqrt{2}\beta}$
	Cation	0	0	$\mp \frac{\bar{\beta}}{2(\bar{\beta}^2 + 4\beta^2)^{1/2}} + \frac{\beta^2\Delta}{2(\bar{\beta}^2 + 4\beta^2)^{3/2}} [12 \pm \bar{S}(3 \pm S^2)]$	
	Anion				
$\Delta^\infty/\beta^0$	Neutral			0	0
	Cation	0	0	$\pm \frac{1/2\omega\beta^0\bar{\beta}(\bar{\beta}^2 + 4\beta^2)}{1 + \frac{\omega\beta^0\beta^2}{2(\bar{\beta}^2 + 4\beta^2)^{3/2}} [12 \pm \bar{S}(3 \pm S^2)]}$	$\frac{1/2\omega\beta^0}{1 + \frac{3}{4\sqrt{2}}\omega S^0}$
	Anion				
$(\bar{I} + \alpha^0 - \frac{\eta-1}{\eta}\omega\beta^0)$		$-\frac{\beta}{1+S}$	$-\frac{\beta}{1+S}$	$\approx \frac{-\sqrt{\bar{\beta}^2 + 4\beta^2} + \bar{\beta} + 2\beta S}{2(1-S-\bar{S}^2)}$	$\approx 0$
$(\bar{A} + \alpha^0 - \frac{\eta+1}{\eta}\omega\beta^0)$		$\frac{\beta}{1-S}$	$\frac{\beta}{1-S}$	$\approx \frac{-\sqrt{\bar{\beta}^2 + 4\beta^2} - \bar{\beta} + 2\beta S}{2(1+S-\bar{S}^2)}$	$\approx 0$

<sup>a</sup> Assuming  $\beta/S$  constant.

eq. 9 and 10 of ref. 2 that for the cases considered here

$$(\Delta^\infty - \Delta^0) = \frac{\Delta^1 - \Delta^0}{1 - \omega\beta^0/b}$$

Since

$$\chi = -m_N\beta^0 + \frac{\eta-1}{\eta}\omega\beta^0 + (\Delta_+^\infty - \Delta_0)$$

$$\left(\tau^+ - n_Y \frac{\eta-1}{\eta}\right) - (\Delta_0^\infty - \Delta_0)(\tau^0 - n_Y)$$

and as we have seen that the last two terms are of small importance, this use of the first iteration values should be quite good. This is especially so for small  $\omega b$ . In fact, the approximation of eq. 19, ref. 2 ignores this fluctuation entirely; its success indicates the  $(\eta - 1)\omega\beta^0/\eta$  is the only correction to the Hückel result of importance.

**4. Extension of the  $\omega$ -Technique to Overlap Included LCAO-MO Theory.**—Charge redistribution by the  $\omega$ -technique has been imposed upon overlap-included as well as Hückel MO calculations.<sup>14,15</sup> The overlap included method has not, however, been used to calculate ionization potentials and electron affinities. A question of some interest is whether this improvement of the MO's would provide more satisfactory correlations of the latter quantities to those calculated by Pople-type methods while maintaining the excellent ionization potential correlations found within the Hückel framework.

The overlap-included results for the four real molecules, ethylene, benzene, butadiene, and the allyl radical, to be found in Table I, suggest the answer to this question is no.

As may be quickly seen, the values of  $\Delta^\infty$  for the allyl radical and ions are independent of whether overlap is included or not. For the butadiene ions, overlap does contribute somewhat to these values but only in a very minor way. The most important contribution of the inclusion of overlap is in the forms of the highest filled levels in the cations and anions; as is well known the former are brought closer and the latter pushed further away from the zero of energy.

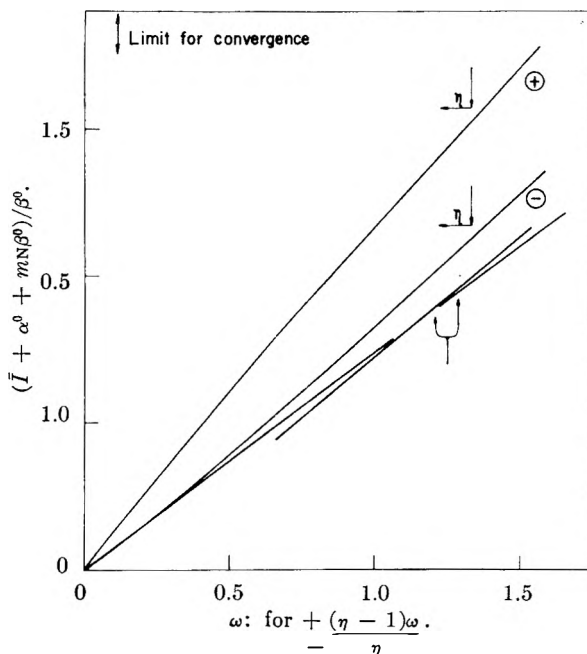


Fig. 3.—Self-consistent energies in the ionization of the benzyl radical vs.  $\omega$ . Upper curves for hypothetical closed form case (see text) with  $\omega$ -limit for convergence decreasing with increasing value of  $\eta$ .

Since the  $\Delta^\infty$  values are of the same order in the Hückel and overlap-included calculations we may employ the same approximation as eq. 19<sup>2</sup>; the self-consistent ionization potential and electron affinity values also are included in Table I. Fitting the observed ionization potentials of these four molecules allows good internal agreement for the  $\alpha$ ,  $\beta^0$ , and  $\omega$  values, respectively, of  $-10.55$  e.v.,  $-2.22$  e.v., and  $1.64$ . The electron affinities of benzene, ethylene, butadiene, and allyl radical are computed to be  $3.33$ ,  $1.82$ ,  $4.05$ , and  $5.67$  e.v., employing these parameters. These results are not significantly better than those reported in Table III of ref. 2, where overlap was neglected. For  $\omega$  taken equal to 3, these values are  $-0.2$ ,  $-2.8$ ,  $0.3$ , and  $1.6$ . Again it is of some interest to take a value of  $\omega$  sufficient to make the affinity of graphite as much greater than the work function of this

(15) Cf., N. Muller and R. S. Mulliken, *J. Am. Chem. Soc.*, **80**, 3049 (1958); A. Ron, E. A. Halevi, and R. Pauncz, *J. Chem. Soc.*, 630 (1960).

species as the  $\omega$ -value of 1.64 makes the ionization potential lower. This value is 3.45 and yields the affinity values (in the same order) of  $-1.4$ ,  $-4.2$ ,  $-1.0$ , and  $+0.4$ . These are quite close to the corresponding values reported previously.

We may only conclude from these results that the inclusion of overlap does not provide significantly better agreement with the electron affinities of Pople than is obtained from the Hückel MO's. The ionization potentials, it would seem from this analysis, also are not significantly different when overlap is included.

### Summary

Detailed comparisons of the  $\omega$ -technique and Pople closed form solutions for the ionization potentials of the cyclic polyenes unambiguously indicate these methods to be fundamentally different. With the parameters presently used for both methods, poor agreement for the potentials of very large molecules is to be expected. Whether either method will yield the correct results for such molecules is a question which must await further experimental work. In the meantime, the correlational usefulness of the  $\omega$ -technique for the smaller organic molecules of common interest so

broadly demonstrated by Streitwieser should not be overlooked.

Extrapolation methods introduced to hasten convergence or circumvent divergence in the cycling procedure are shown to be useful in some calculations. The question of whether a particular case of divergence should be subjected to extrapolation is raised. If the cause is due to the initial choice of parameters or Hückel orbitals and a continuous functional dependence of the property of interest (*e.g.*, energy) upon the latter exists, it would seem that extrapolation is justified. The possibility of intrinsic limitations of the  $\omega$ -technique preventing the correct charge density from being self-consistent must be considered, however. An erroneous result may thereby be obtained upon extrapolation. Until this distinction is more clearly made, justification can only be *a posteriori*; if the result agrees with experiment, extrapolation seems justified.

The extension of the technique to overlap included MO methods also was investigated in terms of some of the closed form cases. For calculations of ionization potentials and electron affinities at least, little if any improvement is to be found over the overlap-included results.

## PROTON MAGNETIC RESONANCE OF SOME NORMAL PARAFFINS AND POLYETHYLENE<sup>1</sup>

BY A. ODAJIMA, J. A. SAUER, AND A. E. WOODWARD

*Department of Physics, Pennsylvania State University, University Park, Pennsylvania*

*Received October 12, 1961*

Proton magnetic resonance spectra have been obtained in the temperature region from 77°K. to the melting point for eleven normal paraffins including  $n$ -C<sub>34</sub>H<sub>70</sub> and for two preparations of polyethylene crystals grown from solution having fold periods of 112 and 120 Å. At, or a few degrees below, the crystal-crystal transition point, the n.m.r. line narrows markedly in a 1–2° range for  $n$ -C<sub>19</sub>H<sub>40</sub>,  $n$ -C<sub>21</sub>H<sub>44</sub>,  $n$ -C<sub>28</sub>H<sub>58</sub>,  $n$ -C<sub>32</sub>H<sub>66</sub>, and  $n$ -C<sub>35</sub>H<sub>72</sub> and at, or just below, the melting point a narrow line characteristic of that found with liquids is obtained. The line-narrowing process for  $n$ -C<sub>35</sub>H<sub>74</sub> takes place in two steps due to the presence of two crystal-crystal transitions. These transitions are believed to be accompanied by the onset of long-axis rotation of the paraffin molecule. The results indicate that considerable methyl group rotation occurs in the  $n$ -paraffins at 77–100°K. The spectra at temperatures 20–30° below the transition points for  $n$ -C<sub>32</sub>H<sub>66</sub>,  $n$ -C<sub>35</sub>H<sub>72</sub>, and  $n$ -C<sub>36</sub>H<sub>74</sub> are found to be markedly dependent on thermal history and purity. For  $n$ -C<sub>44</sub>H<sub>90</sub> and  $n$ -C<sub>94</sub>H<sub>190</sub>, line narrowing, presumably due to torsional oscillation takes place about 25 and 50° below the melting point, respectively. The appearance of a component 0.1 to 2 gauss in width at temperatures of  $\sim$ 200°K. for C<sub>18</sub> to  $\sim$ 300°K. for C<sub>44</sub> was found to be dependent on sample history and purity. One polyethylene crystal preparation (120 Å. fold period) showed a narrow and broad component at 300°K., both of which underwent further narrowing at higher temperatures. Heating the polyethylene crystals at temperatures from 390°K. to the melting point shifted the fine line-narrowing process to lower temperatures and the broad line-narrowing to higher temperatures causing these processes to be coincident with those for melt-formed polymer. The polyethylene crystal sample with 112 Å. fold period and the  $n$ -C<sub>94</sub>H<sub>190</sub> crystals showed no narrow line at 300°K. but one appeared after subsequent heat treatments. This component found for C<sub>34</sub> and polyethylene is attributed to motion of chain segments in crystal defects.

### Introduction

Phase changes and other transformations taking place in normal paraffin compounds in the solid state have been investigated by various physical methods, including: X-ray crystallography,<sup>2,3</sup> proton magnetic resonance<sup>4</sup> (n.m.r.), cooling curves,<sup>3</sup> specific volume,<sup>5</sup> and calorimetry.<sup>6</sup> Using n.m.r.,

Andrew<sup>4</sup> investigated three normal paraffins with an even number of carbon atoms:  $n$ -octadecane (C<sub>18</sub>),  $n$ -octacosane (C<sub>28</sub>), and  $n$ -dotriacontane (C<sub>32</sub>), and reported the presence of considerable motion in all three compounds at temperatures well below their respective melting points. For C<sub>18</sub> at 95°K., the lowest temperature employed, Andrew reported an experimental second moment well below the calculated rigid-lattice value. On

(1) Supported by the U. S. Atomic Energy Commission under Contract AT(30-1) 1858.

(2) A. Müller, *Proc. Roy. Soc. (London)*, **A120**, 437 (1928); **A127**, 417 (1930); **A138**, 514 (1932).

(3) J. D. Hoffman and B. F. Decker, *J. Phys. Chem.*, **57**, 520 (1953).

(4) E. R. Andrew, *J. Chem. Phys.*, **18**, 670 (1950).

(5) P. R. Templin, *Ind. Eng. Chem.*, **48**, 154 (1956).

(6) A. A. Schaerer, C. J. Busso, A. E. Smith, and L. B. Skinner, *J. Am. Chem. Soc.*, **77**, 2017 (1955).



the other hand, C<sub>28</sub> and C<sub>32</sub> were believed to be in a rigid-lattice state at 95°K., but did undergo motional narrowing about 100° below their respective melting points.

In order to obtain further information about motion in the solid state, proton magnetic resonance spectra have been obtained for eleven normal paraffins and one branched paraffin at various temperatures in the range from 77°K. to the respective melting point. The materials studied include a consecutive series of four compounds: C<sub>18</sub>, *n*-nonadecane (C<sub>19</sub>), *n*-eicosane (C<sub>20</sub>), and *n*-heneicosane (C<sub>21</sub>), as well as eight others: hexadecane (C<sub>16</sub>), 2-methylheptadecane (2MHD), C<sub>28</sub>, C<sub>32</sub>, *n*-pentatriacontane (C<sub>35</sub>), *n*-hexatriacontane (C<sub>36</sub>), *n*-tetratetracontane (C<sub>44</sub>), and *n*-tetranonacotane (C<sub>94</sub>). Some effects of thermal history and impurities also have been investigated. The results of these measurements will be presented and discussed herein.

Proton magnetic resonance spectra also have been obtained over a wide temperature range on two samples of polyethylene single crystals grown from solution. It is known<sup>7</sup> that such crystals have a structure at room temperature identical with that for crystals of normal paraffins with the chains being packed normal to layers of thickness 90 Å. or greater. However, for polyethylene this type of packing requires that the chains be folded back on themselves. N.m.r. studies of solution-grown crystals of polyethylene first were given by Herring and Smith<sup>8</sup> and marked differences found between such a sample and melt-formed specimens. Results also have been published by Peterlin, *et al.*,<sup>9</sup> and Slichter.<sup>10</sup> In this paper, the n.m.r. data for the two samples of polyethylene crystals with fold periods of 112 and 120 Å. are compared with those obtained for various normal paraffins.

Thermal treatment of polyethylene crystals is known to affect segmental mobility. For example, Slichter<sup>10</sup> found for single-crystal preparations, which had been heated between 100° and the melting point, that the segmental mobility became irreversibly greater as the annealing temperature was increased. This type of treatment also is found<sup>11,12</sup> to increase irreversibly the long spacing of the crystal lamellae as a consequence of chain refolding. In the present investigation, the effect of thermal treatment and annealing on the occurrence of segmental motion in polyethylene crystals has been studied further by examining two crystal preparations with different fold periods which had received prior heat treatments.

### Experimental

The apparatus and procedures used in this study have been described previously.<sup>13</sup> For samples exhibiting the

narrow n.m.r. lines of width < 0.5 gauss care was taken to avoid modulation broadening by using modulation widths of 0.25–0.04 gauss and a slow scanning rate of 0.2–0.1 gauss/min. To avoid saturation broadening at low temperatures a radio-frequency intensity below that where such effects were noticed was used. The experimental second moments were calculated from the central derivative absorption peak, the limits being where  $d\{f(H)/dH\}$  goes to zero, as determined experimentally.

The samples of C<sub>18</sub>(m.p. 28°), C<sub>28</sub> sample no. 1 (m.p. 56°), and C<sub>32</sub> sample no. 1 (m.p. 68.5°) were purchased from Humphrey-Wilkinson, Inc. A comparison of the melting points given here for C<sub>28</sub> and C<sub>32</sub> with those in the literature<sup>6,6</sup> indicate that these samples contain some impurities, the amounts of which are not known. Upon redistillation and recrystallization a sample of the C<sub>18</sub> was obtained with a 98.5% purity as determined from the boiling point. Other paraffin samples, including C<sub>16</sub>(m.p. 18.0°), 2MHD, C<sub>19</sub>(m.p. 32.0°), C<sub>20</sub>(m.p. 36.6°), C<sub>28</sub> sample no. 2 (m.p. 61.1°), C<sub>32</sub> sample no. 2 (m.p. 69.3°), C<sub>35</sub>(m.p. 73.4–73.8°), C<sub>36</sub>(m.p. 75.9°), C<sub>44</sub>(m.p. 86°), and C<sub>94</sub>(m.p. 114.1–114.5°) were high-purity samples supplied by the American Petroleum Institute Project No. 42 at the Pennsylvania State University. The sample of C<sub>21</sub>(m.p. 39.8°)<sup>14</sup> was furnished by Professor E. R. Fitzgerald of the Pennsylvania State University. Except for the sample of C<sub>94</sub>, most of the n.m.r. measurements were made on solid samples of the above paraffins obtained by cooling from the liquid state; samples with elevated melting points were removed from the oven and allowed to cool in the laboratory atmosphere. As noted on the figures to follow, some samples of the same hydrocarbon were stored at room temperature for 7–21 days prior to measurement and others were measured immediately. N.m.r. measurements also have been made on crystal aggregates of C<sub>21</sub>, C<sub>35</sub>, and C<sub>94</sub>. These crystals were prepared from acetone in the case of C<sub>21</sub> and from *n*-pentane in the case of C<sub>35</sub> and C<sub>94</sub> and were vacuum-dried for 48–72 hr. at 300°K. Following the n.m.r. measurements on this C<sub>94</sub> sample, crystals again were grown using the same material and these were dried at 350°K. under vacuum for 48 hr. In some cases, solid mixtures of paraffins were made up by mixing the components in the liquid state.

One of the polyethylene crystal preparations was supplied by Dr. A. Keller of the University of Bristol, who reported a 120 Å. fold period, as obtained by low angle X-ray diffraction. The second sample, with a reported fold period of 112 Å., was supplied by Dr. F. E. Karasz of the National Physical Laboratory, England; this sample was prepared from a 0.1% xylene solution and was dried under vacuum for 150 hr. at 53° prior to use. Subsequent heat treatments of specimens from both preparations were carried out in a vacuum oven at the temperatures indicated on Fig. 7 and 8.

### Results

N.m.r. spectra have been obtained for melt-formed samples of C<sub>18</sub>, C<sub>19</sub>, C<sub>20</sub>, and C<sub>21</sub> at various temperatures from 77°K. to the respective melting points. The width of the broad component was found to be  $15.5 \pm 0.3$  gauss at 77°K. This width decreased slowly with increasing temperature, reaching values of 14 gauss at 270°K. At the melting point for C<sub>18</sub>, the line narrows from a value of 13 gauss to that observable for liquids (<0.01 gauss). For C<sub>19</sub>, at temperatures prior to melting, the line narrows abruptly from 13 to 5 gauss. This narrowing occurs at 296°K., the temperature of the reported crystal-crystal transition point<sup>6</sup> and the line subsequently narrows to values for liquids at the melting point. A similar behavior is exhibited by C<sub>21</sub> except that the narrowing processes take place a few degrees below the reported transition point<sup>6</sup> and the melting point,

(13) A. Odajima, A. E. Woodward, and J. A. Sauer, *J. Polymer Sci.*, **55**, 181 (1961).

(14) M. H. Broadhurst, Thesis for Ph.D. Degree, The Pennsylvania State University, June, 1960.

(7) A. Keller and A. O'Connor, *Nature*, **180**, 1289 (1957).

(8) M. J. Herring and J. A. S. Smith, *J. Chem. Soc.*, 273 (1960).

(9) (a) A. Peterlin, F. Krašovec, E. Pirkmajer, and I. Levstek, *Macromol. Chem.*, **37**, 231 (1960); (b) A. Peterlin and E. Pirkmajer, *J. Polymer Sci.*, **46**, 185 (1960).

(10) (a) W. P. Slichter, *J. Appl. Phys.*, **31**, 1865 (1960); (b) **32**, 2339 (1961).

(11) A. Keller and A. O'Connor, *Discussions Faraday Soc.*, **25**, 114 (1958).

(12) W. O. Statton and P. H. Geil, *J. Appl. Polymer Sci.*, **3**, 357 (1960).

TABLE I  
 SECOND MOMENTS

n	Calculated values					Experimental values				
	Rigid lattice Struct. 1 <sup>a</sup>	Struct. 2 <sup>b</sup>	CH <sub>2</sub> rot. Struct. 1	Struct. 2	Long axis rot. <sup>c</sup>	77°K.	120-150°K.	300°K.	<Tr.Pt. <sup>e</sup>	>Tr.Pt. <sup>e</sup>
18	30.5	26.8	25.2	22.3	8.8	24.2 ± 0.2	23	19.0 ± 0.5	20(<MP)	..
19	30.4	26.8	25.4	22.5	8.8	25.0 ± 0.1	23	6.5	18	~6.5-7.5
20	30.4	26.7	25.6	22.7	8.8	24.5 ± 0.1	22	19.5	19	~6
21	30.3	26.7	25.8	22.8	8.9	..	23	17	17	~6
28	30.0	26.5	26.6	23.6	9.0	..	..	21.5	19	..
32	29.9	26.5	26.9	23.9	9.0	..	23	21	15	~5
35	29.9	26.4	27.1	24.1	9.1	25	24	21	12	~6
36	29.9	26.4	27.1	24.1	9.1	24.7 ± 0.7	24	21.5	18, 14	~5
44	29.7	26.3	27.5	24.4	9.1	..	25	22.7 ± 0.5	10(<MP)	..
94	29.5	26.2	28.4	25.3	9.3	..	..	22.5	..	..
∞	29.2	26.0	29.2	26.0	9.4	26.2 <sup>d</sup>	25.5 ± 0.5 <sup>d</sup>	21-23 <sup>d</sup>	..	..

<sup>a</sup> Structure given by Teare<sup>22</sup> for  $n$ -C<sub>36</sub>H<sub>74</sub> (1.72 Å. CH<sub>2</sub> proton-proton distance). <sup>b</sup> Increase of CH<sub>2</sub> proton-proton distance to 1.79 Å. <sup>c</sup> From equation of Andrew.<sup>4</sup> <sup>d</sup> Values for linear polyethylene. <sup>e</sup> Tr. Pt. denotes the crystal-crystal transition point temperature.

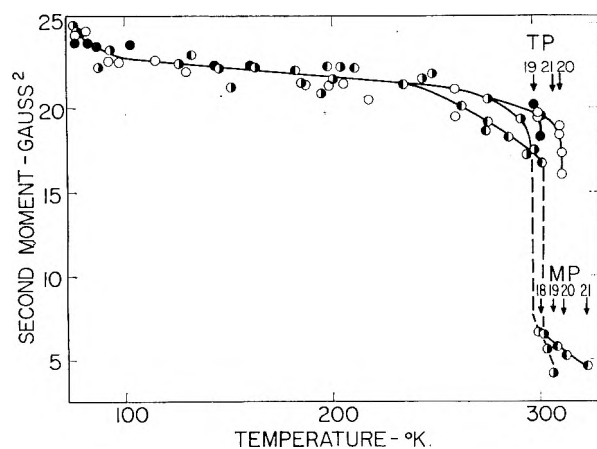


Fig. 1.—Second moment vs. temperature for  $n$ -C<sub>18</sub>H<sub>38</sub> (●),  $n$ -C<sub>19</sub>H<sub>40</sub> (○),  $n$ -C<sub>20</sub>H<sub>42</sub> (○), and  $n$ -C<sub>21</sub>H<sub>44</sub> (○).

respectively. For C<sub>20</sub> the transition point and melting point are very close together and therefore only one narrowing process is observed at 305°K., the line narrowing from a value of 13 gauss.

Experimental second-moment values, obtained from the derivative line shapes for C<sub>18</sub>, C<sub>19</sub>, C<sub>20</sub>, and C<sub>21</sub>, taken in the 77°K. to melting-point range, are plotted in Fig. 1, and some selected values are given in Table I. (In this and subsequent figures T.P. and M.P. indicate reported<sup>5,6</sup> transition points and melting points, respectively.) The second-moment plots are found to be similar in shape to the respective broad line width-temperature curves described above. The results obtained on C<sub>18</sub> are similar to those given earlier by Andrew,<sup>4</sup> except that the presently reported second moment has a greater value just prior to melting.

At temperatures of 190 to 204°K., a narrow line of low intensity appeared for C<sub>18</sub>, C<sub>19</sub>, C<sub>20</sub>, and C<sub>21</sub>, the temperature of its appearance shifting to higher values with increasing chain length as shown in Fig. 2. As is evident from the figure this line undergoes rapid narrowing with increasing temperature. Also shown in Fig. 2 are narrow components for melt-formed samples of C<sub>28</sub>, C<sub>35</sub>, and C<sub>44</sub>. Andrew<sup>4</sup> previously has reported the appearance of a narrow line for C<sub>18</sub> at about 208°K. and for C<sub>28</sub> and C<sub>32</sub> at higher temperatures,

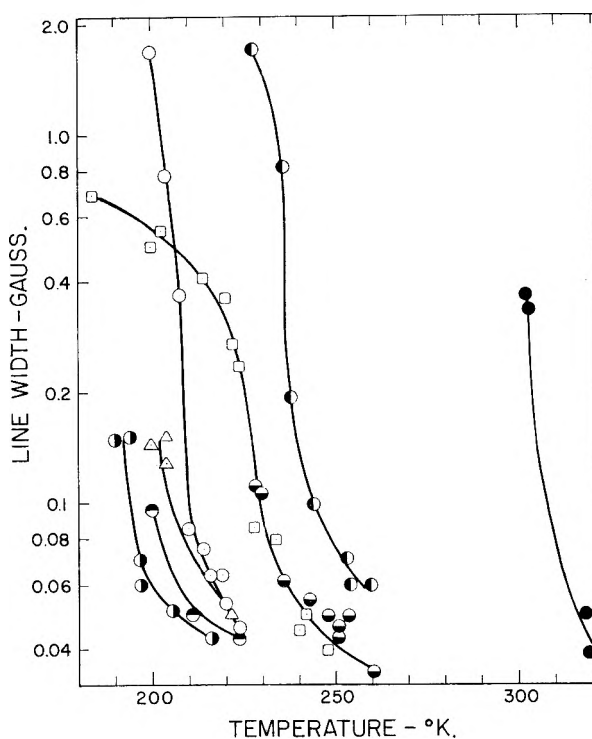


Fig. 2.—Narrow line width vs. temperature for some normal paraffins: C<sub>18</sub> (○), C<sub>19</sub> (●), C<sub>20</sub> (△), C<sub>21</sub> (○), C<sub>28</sub> no. 1 (□), C<sub>28</sub> no. 2 (●), C<sub>35</sub> (○), and C<sub>44</sub> (●).

but the widths observed were of a greater magnitude than those found in the present study, possibly due to modulation broadening in the earlier work.

Crystal aggregates of C<sub>21</sub> prepared from solution were found to have a much reduced narrow component, while for a C<sub>21</sub> sample which had been recrystallized, melted, and then cooled from the melt, no narrow component was evident. Fine lines of very low intensity were observed for the samples of C<sub>32</sub>, C<sub>36</sub>, and solution-grown crystals of C<sub>35</sub>, while a recrystallized, melted, and cooled C<sub>35</sub> sample had none. The sample of C<sub>16</sub> exhibited a narrow line similar to that for C<sub>19</sub> or C<sub>20</sub>, while the sample of 2MHD showed none from 100-280°K., the latter temperature being the melting point as found by n.m.r. Recrystallized C<sub>21</sub>, with 2-3% by weight of C<sub>16</sub> or of 2MHD added,

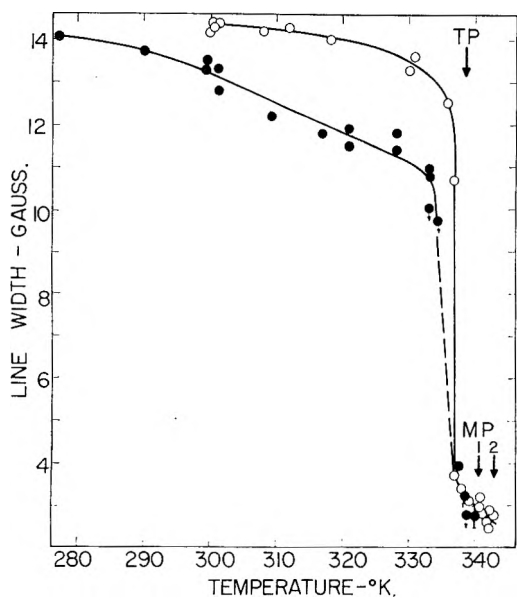


Fig. 3.—Line width vs. temperature for *n*-C<sub>32</sub>H<sub>66</sub> no. 1—m.p., 68.5° (●); no. 2—m.p., 69.3° (○); points with arrows obtained during cooling.

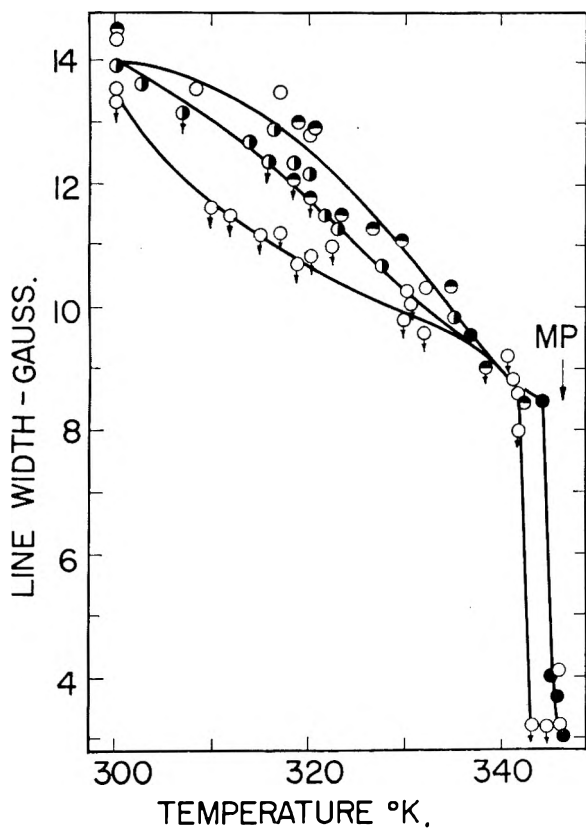


Fig. 4.—Line width vs. temperature for *n*-C<sub>36</sub>H<sub>72</sub>. Cooled from melt and stored (○, ●); cooled from melt (◐); crystals (◑). Points with arrows obtained during cooling.

exhibited narrow components in the 270–300°K. range; while C<sub>36</sub> with 2–3% of C<sub>20</sub> or of C<sub>35</sub> added showed no increase in narrow line intensity at 300°K.

For the various paraffins for which n.m.r. data are given in Fig. 2, the fraction of area under the narrow component, *A<sub>n</sub>*, obtained from the derivative line shape by double integration, changes slowly with

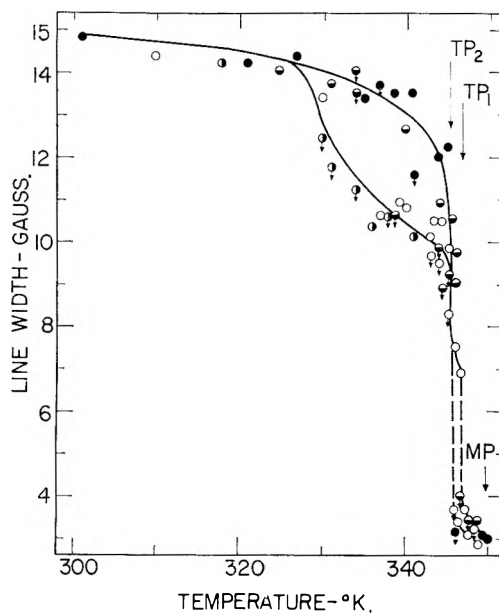


Fig. 5.—Line width vs. temperature for *n*-C<sub>36</sub>H<sub>74</sub>. Cooled from melt and stored (●, ◐); cooled from melt (○, ◑). Points with arrows obtained during cooling.

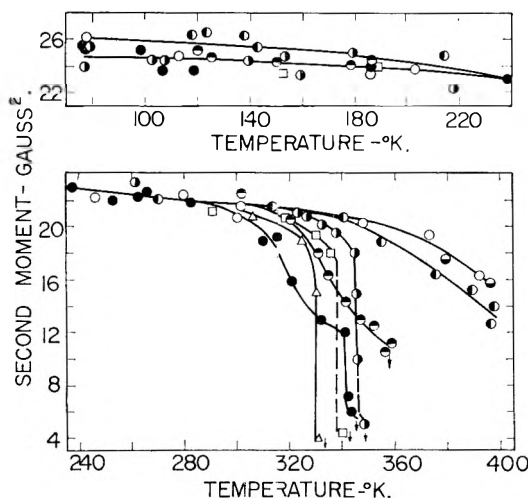


Fig. 6.—Second moment vs. temperature for *n*-C<sub>28</sub>H<sub>58</sub> (Δ), *n*-C<sub>32</sub>H<sub>66</sub> (◻), *n*-C<sub>35</sub>H<sub>72</sub> (●), *n*-C<sub>36</sub>H<sub>74</sub> (◐), *n*-C<sub>44</sub>H<sub>90</sub> (◑), melt formed polyethylene (Marlex 50) (○), polyethylene crystals (◒), and polyethylene crystals heated to 395°K. (◓).

temperature up to a few degrees below the melting point. For C<sub>20</sub>, *A<sub>n</sub>* was ~0.01 at 217°K., 0.055 at 281°K., and 0.07 at 300°K.

N.m.r. line shapes for the broad component were obtained for samples of C<sub>35</sub> and C<sub>36</sub> at various temperatures from 77°K., of C<sub>44</sub> from 120°K., of C<sub>32</sub> from 150°K., and of C<sub>28</sub> from 280°K. to the respective melting points. In the 77 to 280°K. temperature range, the n.m.r. broad-line widths decreased from a value of 16 to 15 gauss for the samples of C<sub>32</sub>, C<sub>35</sub>, C<sub>33</sub>, and C<sub>44</sub>. Below 300°K., only melt-formed samples were investigated while at temperatures above 300°K., samples of different thermal history and purity were studied.

For C<sub>28</sub>, results were obtained for both an impure sample and a pure sample. Little difference was found to occur in line width prior to the melting point of the impure sample. The pure sample

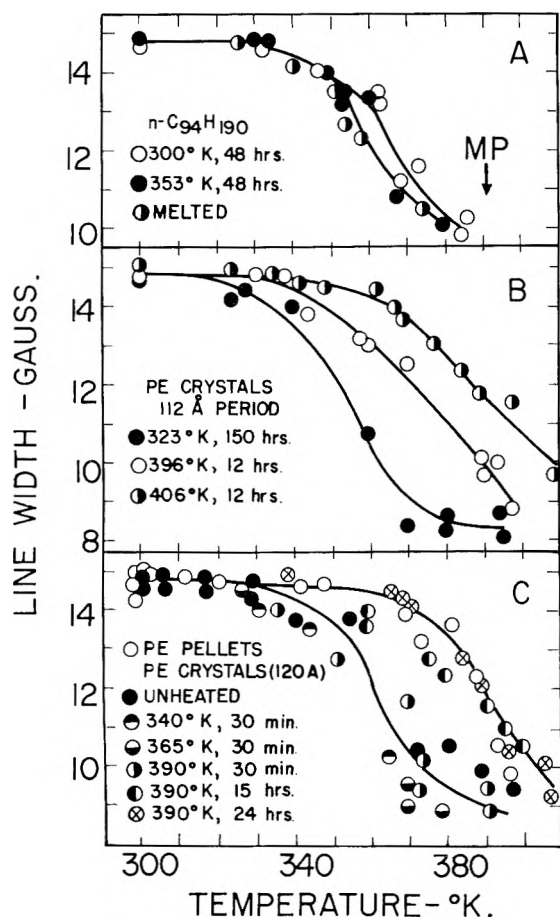


Fig. 7.—Line width (broad component) vs. temperature for  $n\text{-C}_{94}\text{H}_{190}$  (A), polyethylene crystals—112 Å. fold period (B), polyethylene crystals—120 Å. fold period (C), and melt-formed polyethylene (C).

showed a marked line-narrowing process occurring at 331°K., the transition temperature,<sup>5,6</sup> as the samples were warmed and at 328°K. as the samples were cooled. At the melting point, the line narrowed to that characteristic of liquids, a general phenomenon found for all of the paraffins from  $\text{C}_{18}$  to  $\text{C}_{44}$  described herein.

Unlike the situation for  $\text{C}_{28}$ , differences in the line width for pure (no. 2) and impure (no. 1) samples of  $\text{C}_{32}$  are found below the melting point of the impure sample as seen in Fig. 3. The crystal-crystal transition for  $\text{C}_{32}$  (339°K.)<sup>5</sup> is readily apparent although the change takes place 2–3° lower.

N.m.r. line widths are given in Fig. 4 and 5 for samples of  $\text{C}_{35}$  and  $\text{C}_{36}$ , respectively. There is clear evidence for one motional transition process ( $\sim 345^\circ\text{K}$ .) for  $\text{C}_{35}$  and two motional transitions for  $\text{C}_{36}$ , the latter in accord with reported<sup>5,6</sup> transition temperatures of 345 and 347°K. Thermal history effects are clearly evident as well.

For  $\text{C}_{44}$ , considerable line narrowing prior to melting was found for both stored and immediately-tested samples, with the latter showing somewhat lower widths from about 325 to 355°K.

Second-moment values have been obtained from a number of the line shapes for the stored, melt-formed samples of  $\text{C}_{28}$ ,  $\text{C}_{32}$ ,  $\text{C}_{35}$ ,  $\text{C}_{36}$ , and  $\text{C}_{44}$ , and

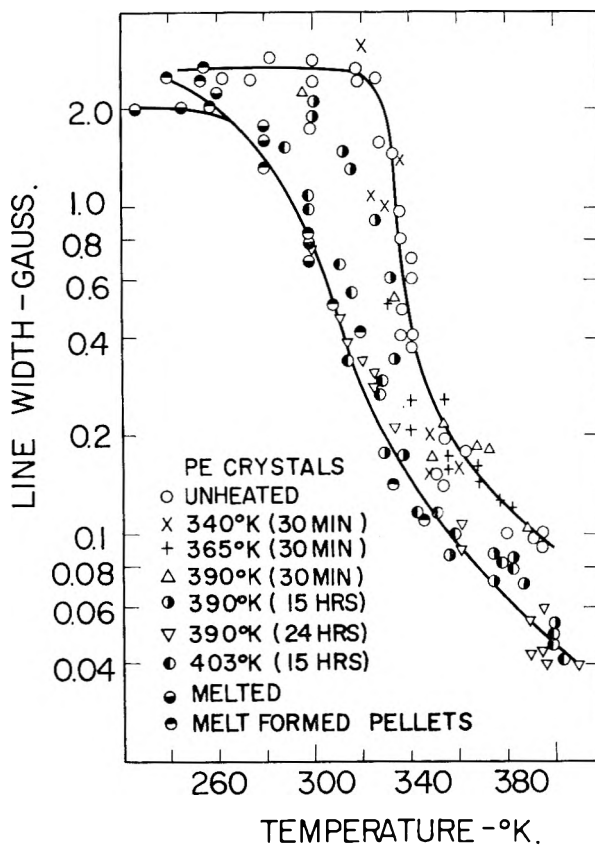


Fig. 8.—Line width (narrow component) vs. temperature for polyethylene crystals and melt-formed polyethylene.

the results are given in Fig. 6. Some selected values also are given in Table I. The values for  $\text{C}_{28}$  are in agreement with those given by Andrew.<sup>4</sup> Second-moment values for impure samples of  $\text{C}_{32}$  and  $\text{C}_{36}$  and for quenched samples of  $\text{C}_{35}$  and  $\text{C}_{36}$  were found to be up to 5 gauss<sup>2</sup> lower above 300°K., but below the transition point, than those given in Fig. 6 for the respective compounds. The second-moment data in the 280–355°K. region for impure  $\text{C}_{32}$  are similar to that given by Andrew.<sup>4</sup>

N.m.r. broad-line widths obtained for the same  $\text{C}_{94}$  sample, treated in three different ways, are given in Fig. 7. Thermal treatment appears to have little effect on the broad-line width. The melt-formed sample showed a small, narrow component of  $\sim 0.1$  gauss width which has  $A_n$  equal to 0.01 at 300°K. The size of this component increases with temperature to a fraction of 0.16 at 350°K. and 0.26 at 367°K., while further narrowing takes place. At room temperature, the fraction of area under this component decreases in going from the melted sample to the 350°K.-dried sample to the 300°K.-dried sample.

The broad-line width as a function of temperature for polyethylene crystals with a 112 Å. fold period is given in Fig. 7B. It is seen that as the annealing temperature is increased the line-width decrease shifts to higher temperatures, becoming similar to that for melt-formed material as given in Fig. 7C. The sample dried at 323°K. did not show a sharp component. However, on heating at 396°K. for 12 hr. a narrow component at 300°K. of  $\sim 1$  gauss width appears; the heating also

causes the broad-line decrease to shift to higher temperatures. A further shift occurs on heating to 406°K. for 12 hr. This type of behavior was noted previously by Slichter.<sup>10b</sup> A sample of these crystals dried at 323°K. was pressed at 8,000–10,000 p.s.i. for 30 min. with no change being found in the n.m.r. spectra at 300°K.; however, after pressing for 10 hr. a sharp component with an  $A_n$  of 0.02–0.03 appears.

More extensive heating studies were carried out on another polyethylene crystal preparation (120 Å. fold period) for which broad-line widths are given in Fig. 7C and narrow-line widths are shown in Fig. 8. Values of  $A_n$  were estimated as follows: 0.02 at 300°K. and 0.11 at 398°K. for the unheated, 120 Å. polyethylene crystals; 0.05 at 300°K. and 0.25 at 390°K. for the 395°K. (15 hr.)-annealed sample; and for the melted crystals, 0.07 at 300°K., and 0.33 at 390°K. The preliminary results presented<sup>15</sup> for samples of this 120 Å. material are considered to be only of qualitative significance due to modulation-broadening effects.

Second moment *vs.* temperature plots for the 120 Å. polyethylene crystal preparation and for a melt-formed sample are included in Fig. 6. At 77°K., the melt-formed sample has a value of 26 gauss<sup>2</sup>, which is 3 gauss<sup>2</sup> lower than that reported for similar samples by workers in these Laboratories.<sup>15,16</sup> In the 200 to 300°K. region, the second moment undergoes a small, almost linear decrease from a value of 24 to 23 gauss<sup>2</sup>, behavior also in disagreement with that previously given.<sup>15,16</sup> In light of these and of similar discrepancies for dry nylon 6-6,<sup>17</sup> it is believed that the previously-reported, low temperature values<sup>15,16</sup> are in error, possibly due to saturation effects.

### Discussion

The appearance of the narrow component in  $C_{18}$ ,  $C_{28}$ , and  $C_{32}$  was attributed previously<sup>4</sup> to the onset of methyl rotation in these compounds. However, the narrowing of the broad line is characteristic of the onset of methyl rotation in polymers like the polymethacrylates<sup>13</sup> and the poly( $\alpha$ -olefins).<sup>20</sup> In addition, the narrowness of the fine line for the  $C_{18}$  to  $C_{44}$  hydrocarbons (see Fig. 2) indicates that motion characteristic of liquids is the cause. The dependence of the intensity of this line on the purity of the sample and on its physical state is an indication that it involves segmental motion in grain boundaries or disordered regions of the material due to the presence of foreign molecules.

(15) A. E. Woodward, R. P. Gupta, A. Odajima, and J. A. Sauer, preprints of papers presented at the 138th National Meeting of the American Chemical Society, High Polymer Division, September, 1960.

(16) R. E. Glick, R. P. Gupta, J. A. Sauer, and A. E. Woodward, *Polymer*, **1**, 340 (1960).

(17) From n.m.r. spectra on nylon 6-6 taken from the same batch as previously run specimens<sup>18</sup> and dried at 120° for 6 days, second-moment values in the 77–300°K. range have been obtained.<sup>19</sup> At 77, 162, 231, and 300°K. values of  $23.4 \pm 1$ ,  $16.5 \pm 0.3$ , and  $14.5 \pm 0.3$  gauss<sup>2</sup> are found. These are 2–4 gauss<sup>2</sup> lower than those given previously.

(18) A. E. Woodward, R. E. Glick, J. A. Sauer, and R. P. Gupta, *J. Polymer Sci.*, **45**, 367 (1960).

(19) J. A. Kail, unpublished results.

(20) A. E. Woodward, J. A. Sauer, and A. Odajima, *J. Phys. Chem.*, **65**, 1384 (1961)

For the polyethylene crystals, the dependence of the intensity of the sharp component and of the temperature of the line-narrowing process on the annealing temperature indicates that crystal defects already present or introduced by the chain unfolding are responsible. Since the narrow component for  $C_{94}$  is similar to that for the polyethylene crystals, in that it is affected by temperature in the same way, similar types of defects may be responsible for it. It is not expected that the  $C_{94}$  chain is long enough to necessitate folding of it in the crystal as is found for polyethylene crystals. Indeed, the independence of the broad-component narrowing process on heat treatment substantiates this. This is evidence that the defects in polyethylene leading to the presence of the narrow component are not in the folds themselves. The shift of the narrowing process for the broad component found for polyethylene crystals to higher temperatures with increasing fold period would appear to be a consequence of the increase in melting point with increase in length of the chain between the folds.

By use of the equation of Van Vleck<sup>21</sup> and the crystal structure for  $n$ - $C_{25}H_{60}$  given by Müller<sup>2</sup> an equation for the rigid-lattice second moment of a normal paraffin in terms of the number of carbon atoms,  $n$ , has been given<sup>4</sup> as:  $26.3 + 19.1/(n + 1)$ . If one adopts the crystal structure given for  $C_{36}$  at 300°K. by Teare<sup>22</sup> and corrects for volume contraction using the data of Cole and Holmes,<sup>23</sup> the rigid-lattice second moment becomes  $29.2 + 24.6/(n + 1)$  at 100°K. By changing the proton-proton distance on the  $CH_2$  group from 1.72 to 1.79 Å., this equation becomes  $26.0 + 15.2/(n + 1)$ , in better agreement with that of Andrew.<sup>4</sup> If rotation of the methyl end groups occurs at frequencies of  $\sim 10^4$  or greater, then the following equations, corresponding to the two above, are found:  $29.2 - 75.9/(n + 1)$  and  $26.0 - 70.1/(n + 1)$ , respectively. The calculated values at 300°K. would be about 2 gauss<sup>2</sup> lower than those obtained using the four above equations due to the effects of thermal expansion.

For rotation of the whole molecule around its long axis, Andrew<sup>4</sup> has given the equation:  $9.4 - 11.6/(n + 1)$ . Using our equations for the rigid lattice and the methyl-rotation cases at 100°K. and Andrew's equation for the long axis rotation case, calculated second-moment values as given in Table I are obtained.

From a comparison of the experimental second-moment values for polyethylene at low temperatures with the calculated ones, it would appear that the equations based on a 1.79 Å. proton-proton distance are the more correct ones. This is also the most reasonable choice in light of the data for the normal paraffins. However, an estimate of the amount of zero-point motion occurring has not been made, and hence this conclusion may have to be modified.

The second-moment values for the lower  $n$ -paraffins indicate that some methyl group rotation

(21) J. H. Van Vleck, *Phys. Rev.*, **74**, 1164 (1948).

(22) P. W. Teare, *Acta Cryst.*, **12**, 294 (1959).

(23) E. A. Cole and D. R. Holmes, *J. Polymer Sci.*, **46**, 245 (1960).

is taking place at 77°K., and the small decrease in the second moment at 77–100°K. for  $C_{18}$ ,  $C_{19}$ , and  $C_{20}$  may be part of a transition involving the onset of such rotation. The decrease in the experimental values with temperature from  $\sim 100^\circ\text{K}$ . up to 200–250°K. for the  $n$ -paraffins is most probably a consequence of volume expansion.

As the temperature approaches the transition points for  $C_{19}$ ,  $C_{20}$ ,  $C_{21}$ ,  $C_{28}$ ,  $C_{32}$ ,  $C_{35}$ , and  $C_{36}$  and the melting point for  $C_{18}$ , some torsional oscillation of increasing amplitude may occur, leading to the second moment reductions observed. The smaller amount of motion in  $C_{28}$  and  $C_{32}$  as compared to  $C_{35}$  below the respective transition points may be a consequence of chain stiffness due to the different crystal packing<sup>24</sup> of the  $\text{CH}_3$  end groups for the odd and even  $n$ -paraffins, an effect to which the alternation of crystal-crystal transition points is attributed (see Fig. 1). However, another cause of the behavior observed herein could be the presence of impurities in the  $C_{35}$  samples not removable by recrystallization. The presence of impurities in

(24) A. E. Smith, *J. Chem. Phys.*, **21**, 2229 (1953).

$C_{32}$  and  $C_{36}$  appears to facilitate either limited, long-axis rotation or a greater amount of torsional oscillation than for the pure compounds prior to the transition point. In fact, it has been found from X-ray analysis that the presence of impurities causes an expansion of the crystal lattice.<sup>21</sup>

Just above the transition points for  $C_{19}$  through  $C_{36}$ , it appears that rotation around the long axis is taking place. Since the experimental values are lower than the calculated rotation values some additional motion is occurring as well.

Unlike  $C_{19}$  through  $C_{36}$ , the second moment values for  $C_{44}$  indicate that, just prior to melting, only rotation about the long axis is taking place. The greater amount of motion found for  $C_{44}$  than  $C_{36}$  in the 300–345°K. range may be due to impurities in the former or possibly is a consequence of an increasing chain flexibility with increasing chain length.

**Acknowledgments.**—We wish to express our thanks to Professor J. A. Dixon of A.P.I. Project No. 42, Professor E. R. Fitzgerald, Dr. A. Keller, and Dr. F. E. Karasz for supplying samples.

## THERMODYNAMIC TREATMENT OF THE ELECTROCAPILLARY CURVE FOR REVERSIBLE ELECTRODES AND PROPERTIES OF THE DOUBLE LAYER

BY DAVID M. MOHILNER<sup>1</sup>

*Coates Chemical Laboratory, Louisiana State University, Baton Rouge, La.*

*Received October 23, 1961*

A thermodynamic derivation is given for the equation of the electrocapillary curve for a reversible electrode. It is concluded from this equation and the theory of the diffuse double layer that, in certain cases, it should be possible to determine the potential difference across the diffuse double layer which prevails at the reversible electrode. Implications in electrode kinetics are indicated.

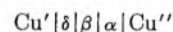
In previous considerations of double layer corrections in electrode kinetics it has been assumed tacitly that for a given electrode potential,  $E$ , the potential drop,  $\phi_2$ , across the diffuse double layer has the same value at the working electrode as at an ideal polarized electrode whose solution has the same composition as in the case of the working electrode except that the reducible or oxidizable substances are excluded. The validity of this assumption has not been tested, apparently because of the prevailing belief that an ideal polarized electrode is the only sort of electrode at which it is possible to determine  $\phi_2$ . Obviously, the requirements for an ideal polarized electrode and for a working electrode are mutually exclusive. It is the purpose of this paper to show how, in certain cases, it is possible to determine  $\phi_2$  for a reversible electrode. This value of  $\phi_2$  then may be used in the double layer correction for the kinetics of the electrode reaction when the reaction is studied near equilibrium as may be done, for example, by relaxation methods.

The approach is based on a consideration of the electrocapillary equation for a reversible electrode and the theory of the diffuse double layer. The

first derivation of such an electrocapillary equation was given by Grahame and Whitney<sup>2</sup> in 1942. The more general derivation which is given below is modeled after the derivation of the electrocapillary equation of an ideal polarized electrode by Parsons and Devanathan.<sup>3</sup>

### Electrocapillary Curve

**The System.**—We shall consider the following cell



$\alpha$  is the metallic phase of the electrode of interest. It is a two component liquid.  $\beta$  is the solution phase and consists of a salt of one of the metals in  $\alpha$ , a second salt and water (the solvent). It is assumed that the two salts in  $\beta$  have a common anion.  $\delta$  is the reference electrode. It consists of a metallic phase and perhaps other solid phases and is reversible with respect to the anion in solution.  $\text{Cu}'$  and  $\text{Cu}''$  represent identical copper terminals to which a potentiometer may be attached.

(2) D. C. Grahame and R. B. Whitney, *J. Am. Chem. Soc.*, **64**, 1548 (1942).

(3) R. Parsons and M. A. V. Devanathan, *Trans. Faraday Soc.*, **49**, 404 (1953).

(1) Postdoctoral Research Associate, 1960–1962.

Let  $\mu_1^\alpha$  be the chemical potential of the metal in  $\alpha$  whose salt is present in  $\beta$  and  $\mu_2^\alpha$  be the chemical potential of the other metal (for example, component 1 might be Zn and component 2, Hg). Then

$$\mu_1^\alpha = \bar{\mu}_1^\alpha + z_1 \bar{\mu}_e^\alpha \quad (1)$$

$$\mu_2^\alpha = \bar{\mu}_2^\alpha + z_2 \bar{\mu}_e^\alpha \quad (2)$$

where  $\bar{\mu}_1^\alpha$  is the electrochemical potential of the ions of metal 1 of valence  $z_1$  in phase  $\alpha$ ,  $\bar{\mu}_2^\alpha$  is the electrochemical potential of the ions of metal 2 of valence  $z_2$  in phase  $\alpha$ , and  $\bar{\mu}_e^\alpha$  is the electrochemical potential of the electrons in phase  $\alpha$ . Since phase  $\alpha$  is in electrochemical equilibrium with the copper terminal  $\text{Cu}''$

$$\bar{\mu}_e^\alpha = \bar{\mu}_e^{\text{Cu}''} \quad (3)$$

where  $\bar{\mu}_e^{\text{Cu}''}$  is the electrochemical potential of the electrons in  $\text{Cu}''$ . Let  $\bar{\mu}_1^\beta$  be the electrochemical potential of the cation of metal 1 in the solution phase and  $\bar{\mu}_2^\beta$  be the electrochemical potential of the other cation in phase  $\beta$ . Let  $\bar{\mu}_3^\beta$  be the electrochemical potential of the common anion. Let  $\mu_{\text{W}}^\beta$  be the chemical potential of the water in the solution. The electrode is assumed to be reversible with respect to cation 1, thus

$$\bar{\mu}_1^\beta = \bar{\mu}_1^\alpha \quad (4)$$

Since the reference electrode is reversible with respect to the anion we have<sup>3</sup> (provided  $\delta$  is of constant composition)

$$|z_3| d\bar{\mu}_e^{\text{Cu}'} = d\bar{\mu}_3^\beta \quad (5)$$

where  $\bar{\mu}_e^{\text{Cu}'}$  is the electrochemical potential of the electrons in  $\text{Cu}'$ .

**The Electrocapillary Equation for the Reversible Electrode.**—The Gibbs adsorption isotherm for the reversible electrode may be written

$$d\gamma = -\Gamma_1^\alpha d\bar{\mu}_1^\alpha - \Gamma_2^\alpha d\bar{\mu}_2^\alpha - \Gamma_e^\alpha d\bar{\mu}_e^\alpha - \Gamma_1^\beta d\bar{\mu}_1^\beta - \Gamma_2^\beta d\bar{\mu}_2^\beta - \Gamma_3^\beta d\bar{\mu}_3^\beta - \Gamma_{\text{W}}^\beta d\mu_{\text{W}}^\beta \quad (6)$$

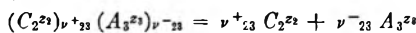
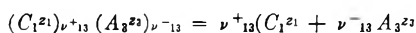
where  $\gamma$  is the interfacial tension at the interface  $\alpha$ - $\beta$  and the  $\Gamma$ 's are the surface excesses at this interface. The first three terms on the right may be written (using eq. 1, 2, and 3)

$$-\Gamma_1^\alpha d\mu_1^\alpha - \Gamma_2^\alpha d\mu_2^\alpha + (\Gamma_1^\alpha z_1 + \Gamma_2^\alpha z_2 - \Gamma_e^\alpha) d\bar{\mu}_e^{\text{Cu}''} \quad (7)$$

We define the total charge  $q^\alpha$  per unit area on  $\alpha$  by the relation

$$q^\alpha/F = \Gamma_1^\alpha z_1 + \Gamma_2^\alpha z_2 - \Gamma_e^\alpha \quad (8)$$

We may consider the electrolyte in  $\beta$  as made up of a mixture of two salts dissociating according to the scheme



where  $C_1^{z_1}$  is the chemical symbol of cation 1 of valence  $z_1$ ,  $C_2^{z_2}$  is cation 2 of valence  $z_2$ , and  $A_3^{z_3}$  is the common anion of valence  $z_3$ . Because of electroneutrality of the salts we have

$$\nu^{+13} z_1 = \nu^{-13} |z_3| \quad (9)$$

$$\nu^{+23} z_2 = \nu^{-23} |z_3| \quad (10)$$

We define the chemical potentials of the salts 13 and 23 by the equations

$$\mu_{13}^\beta = \nu_{13}^{+1} \bar{\mu}_1^\beta + \nu_{13}^{-1} \bar{\mu}_3^\beta \quad (11)$$

$$\mu_{23}^\beta = \nu_{23}^{+2} \bar{\mu}_2^\beta + \nu_{23}^{-2} \bar{\mu}_3^\beta \quad (12)$$

Equations 5, 8, 9–12 give

$$d\gamma = -\Gamma_1^\alpha d\mu_1^\alpha - \Gamma_2^\alpha d\mu_2^\alpha + (q^\alpha/F) d\bar{\mu}_e^{\text{Cu}''} - (\Gamma_1^\beta/\nu^{+13}) d\mu_{13}^\beta - (\Gamma_2^\beta/\nu^{+23}) d\mu_{23}^\beta + (\Gamma_1^\beta z_1 + \Gamma_2^\beta z_2 - \Gamma_3^\beta |z_3|) d\bar{\mu}_e^{\text{Cu}'} - \Gamma_{\text{W}}^\beta d\mu_{\text{W}}^\beta \quad (13)$$

We define the charge per unit area on the solution side of the double layer by

$$q^\beta/F = \Gamma_1^\beta z_1 + \Gamma_2^\beta z_2 - \Gamma_3^\beta |z_3| \quad (14)$$

Furthermore, by the electroneutrality of the interface

$$q^\beta = -q^\alpha \quad (15)$$

Moreover, the electromotive force of the complete cell,  $E$ , is given by

$$FE = \bar{\mu}_e^{\text{Cu}'} - \bar{\mu}_e^{\text{Cu}''}$$

Hence

$$FdE = d\bar{\mu}_e^{\text{Cu}'} - d\bar{\mu}_e^{\text{Cu}''} \quad (16)$$

Equations 5 to 16 give

$$d\gamma = -\Gamma_1^\alpha d\mu_1^\alpha - \Gamma_2^\alpha d\mu_2^\alpha + q^\beta dE - (\Gamma_1^\beta/\nu^{+13}) d\mu_{13}^\beta - (\Gamma_2^\beta/\nu^{+23}) d\mu_{23}^\beta - \Gamma_{\text{W}}^\beta d\mu_{\text{W}}^\beta \quad (17)$$

Now, since the electrode is not ideally polarizable but is reversible with respect to cation 1, we have from eq. 4

$$d\bar{\mu}_1^\beta = d\bar{\mu}_1^\alpha \quad (18)$$

Combining eq. 1, 9, 11, 16, and 18

$$d\mu_{13}^\beta/\nu^{+13} = d\mu_1^\alpha + z_1 F dE \quad (19)$$

Hence

$$d\gamma = -(\Gamma_1^\alpha + \Gamma_1^\beta) d\mu_1^\alpha - \Gamma_2^\alpha d\mu_2^\alpha - (\Gamma_2^\beta/\nu^{+23}) d\mu_{23}^\beta + (q^\beta - \Gamma_1^\beta z_1 F) dE - \Gamma_{\text{W}}^\beta d\mu_{\text{W}}^\beta \quad (20)$$

If  $x_{13}^\beta$ ,  $x_{23}^\beta$ , and  $x_{\text{W}}^\beta$  are the mole fractions of the two salts and of the water in phase  $\beta$ , the Gibbs–Duhem equation for phase  $\beta$  may be written

$$d\mu_{\text{W}}^\beta = -(x_{23}^\beta/x_{\text{W}}^\beta) d\mu_{23}^\beta - (x_{13}^\beta/x_{\text{W}}^\beta) d\mu_{13}^\beta \quad (21)$$

Substituting the value of  $d\mu_{13}^\beta$  given by eq. 19 into eq. 21 one obtains

$$d\mu_{\text{W}}^\beta = -(x_{23}^\beta/x_{\text{W}}^\beta) d\mu_{23}^\beta - (x_{13}^\beta/x_{\text{W}}^\beta) (\nu^{+13} d\mu_1^\alpha + \nu^{+13} z_1 F dE) \quad (22)$$

If  $x_1^\alpha$  and  $x_2^\alpha$  are the mole fractions of the two metals in phase  $\alpha$ , the Gibbs–Duhem equation for this phase is

$$d\mu_2^\alpha = -(x_1^\alpha/x_2^\alpha) d\mu_1^\alpha \quad (23)$$

Combining eq. 20, 22, and 23

$$d\gamma = -\{[\Gamma_1^\alpha - (x_1^\alpha/x_2^\alpha)\Gamma_2^\alpha] + [\Gamma_1^\beta - \nu^{+13}(x_{13}^\beta/x_{\text{W}}^\beta)\Gamma_{\text{W}}^\beta]\} d\mu_1^\alpha - \{[(\Gamma_2^\beta/\nu^{+23}) - (x_{23}^\beta/x_{\text{W}}^\beta)\Gamma_{\text{W}}^\beta] d\mu_{23}^\beta + \{q^\beta - [\Gamma_1^\beta - \nu^{+13}(x_{13}^\beta/x_{\text{W}}^\beta)\Gamma_{\text{W}}^\beta] z_1 F\} dE \quad (24)$$

Following Parsons and Devanathan<sup>3</sup> we define the relative surface excess of metal 1 with respect to metal 2 in phase  $\alpha$  by the equation

$$\Gamma_{1(2)}^\alpha = \Gamma_1^\alpha - (x_1^\alpha/x_2^\alpha)\Gamma_2^\alpha \quad (25)$$

Similarly we define the relative surface excesses of cations 1 and 2 with respect to water in phase  $\beta$  by the equations

$$\Gamma_{1(\text{W})}^\beta = \Gamma_1^\beta - \nu^{+13}(x_{13}^\beta/x_{\text{W}}^\beta)\Gamma_{\text{W}}^\beta \quad (26)$$

$$\Gamma_{2(\text{W})}^\beta = \Gamma_2^\beta - \nu^{+23}(x_{23}^\beta/x_{\text{W}}^\beta)\Gamma_{\text{W}}^\beta \quad (27)$$

Thus eq. 24 becomes

$$d\gamma = -(\Gamma_{1(2)}^\alpha + \Gamma_{1(\text{W})}^\beta) d\mu_1^\alpha - (\Gamma_{2(\text{W})}^\beta/\nu^{+23}) d\mu_{23}^\beta + (q^\beta - \Gamma_{1(\text{W})}^\beta z_1 F) dE \quad (28)$$

Equation 28 is the electrocapillary equation for the interface of the reversible electrode  $\alpha$ - $\beta$ . It is analogous to the electrocapillary equation for an ideal polarized electrode with the same number of components but has one less independent variable. Thus the interfacial tension,  $\gamma$ , is uniquely determined by the composition of phases

$\alpha$  and  $\beta$  since  $E$  is itself a unique function of these compositions.

It follows from eq. 28 that

$$(\partial\gamma/\partial E)_{\mu_1\alpha, \mu_{23}\beta} = q^\beta - \Gamma_{1(w)}\beta z_1 F \quad (29)$$

This equation is the analog for a reversible electrode of the classical Lippmann equation for an ideal polarized electrode. This partial derivative can be experimentally determined by using a Lippmann electrometer containing phase  $\alpha$  of fixed composition and different solutions of the two salts, varying the solution composition in such a manner that  $\mu_{23}\beta$  stays constant while  $\mu_{13}\alpha$ , and therefore  $E$ , changes.

As practical matter it may be noted that, since salt 23 will play the role of an indifferent supporting electrolyte to obviate the consideration of migration in the kinetic studies, its concentration normally will be several orders of magnitude higher than that of salt 13. Hence, changes in the concentration of salt 13 sufficient to produce measurable changes in  $E$  and  $\gamma$  probably will not affect the activity of salt 23 appreciably. Thus in many cases it should be possible to carry out the measurement of  $(\partial\gamma/\partial E)_{\mu_1\alpha, \mu_{23}\beta}$  simply by adding varying, small amounts of salt 13 to a solution of salt 23. On the other hand, it also would be possible, although less convenient, to vary the activity of salt 13 while keeping the activity of salt 23 constant by appropriate selection of the total ionic strength of each solution. This more rigorous method would, of course, depend on the availability of extensive activity coefficient data for the particular mixed electrolyte solutions.

#### Difference of Potential Across the Diffuse Double Layer

$\phi_2$ , the inner potential at the outer Helmholtz plane with respect to the bulk of the solution, may be determined from the differential coefficient in equation 31 provided (a) that the cation of type 1 is not specifically adsorbed and (b) that the mole fraction of salt 13 is small compared to the mole fraction of water. With these restrictions in mind we have, from the theory of the diffuse double layer

$$\Gamma_{1(w)}\beta z_1 F = n_{01} z_1 F \int_0^\infty \{ \exp[-z_1 F \phi(x)/RT] - 1 \} dx \quad (30)$$

where  $n_{01}$  is the number of moles of cation 1 per unit volume in the bulk of the solution and  $\phi(x)$  is the inner potential in the diffuse double layer relative to the inner potential in the bulk of the solution.  $x$  is the distance from the outer Helmholtz plane to the position where  $\phi(x)$  is measured.

For simplification we shall assume that both salts in phase  $\beta$  are of the same  $z$ -valence type. Then

$$z_1 = z_2 = -z_3 = z \quad (31)$$

and

$$n_{01} + n_{02} = n_{03} = n_0 \quad (32)$$

With this simplification, eq. 30 becomes after rearrangement

$$\Gamma_{1(w)}\beta z_1 F = n_{01} z F \int_0^\infty \{ \exp[zF\phi(x)/RT] + \exp[-zF\phi(x)/RT] - 2 \}^{1/2} \exp[-zF\phi(x)/2RT] dx \quad (33)$$

From the theory of the diffuse double layer it is known that

$$dx = (\epsilon/8\pi n_0 RT)^{1/2} \{ \exp[zF\phi(x)/RT] + \exp[-zF\phi(x)/RT] - 2 \}^{-1/2} d\phi(x) \quad (34)$$

where  $\epsilon$  is the dielectric constant in the diffuse double layer. Hence, eq. 33 becomes

$$\Gamma_{1(w)}\beta z_1 F = n_{01} z F (\epsilon/8\pi n_0 RT)^{1/2} \int_{\phi(0)}^{\phi(\infty)} \exp[-zF\phi(x)/2RT] d\phi(x) \quad (35)$$

We know that  $\phi(0) = \phi_2$ , and  $\phi(\infty) = 0$ . Hence, after performing the integration indicated in eq. 35

$$\Gamma_{1(w)}\beta z_1 F = n_{01} (RT\epsilon/2\pi n_0)^{1/2} \{ \exp(-zF\phi_2/2RT) - 1 \} \quad (36)$$

Since

$$q^\beta = -(2RTn_0\epsilon/\pi)^{1/2} \sinh(zF\phi_2/2RT) \quad (37)$$

from the theory of the diffuse double layer it follows that

$$q^\beta - \Gamma_{1(w)}\beta z_1 F = -(2RTn_0\epsilon/\pi)^{1/2} \sinh(zF\phi_2/2RT) - n_{01} (RT\epsilon/2\pi n_0)^{1/2} \{ \exp(-zF\phi_2/2RT) - 1 \} \quad (38)$$

Equation 38 provides a way to calculate  $q^\beta - \Gamma_{1(w)}\beta z_1 F$  as a function of  $\phi_2$  and  $n_0$ . Then the particular value of  $\phi_2$  which gives the same value for  $q^\beta - \Gamma_{1(w)}\beta z_1 F$  as determined experimentally from measurement of  $(\partial\gamma/\partial E)_{\mu_1\alpha, \mu_{23}\beta}$  is the value of  $\phi_2$  for the reversible electrode at the particular value of  $E$  for which the slope  $(\partial\gamma/\partial E)_{\mu_1\alpha, \mu_{23}\beta}$  is determined. The procedure is analogous to that followed for ideal polarized electrodes. Values of  $\phi_2$  may be used for double layer corrections in electrode kinetics particularly when the overvoltage does not exceed a few millivolts, *i.e.*, in relaxation methods.

**Acknowledgment.**—This work was supported by the National Science Foundation. The author is indebted to Professor Paul Delahay for his interest and discussions of this problem.



# THE ROLE OF ADSORPTION IN CONSTANT CURRENT TRANSITION TIME STUDIES—THE HYDROGEN ELECTRODE

BY RONALD A. MUNSON

Research Laboratory, General Electric Company, Schenectady, N. Y.

Received November 2, 1961

A mathematical treatment which takes into account the influence of a pre-electrochemical first-order adsorption step upon galvanostatic transition times is developed. The model fits the experimental results observed with a platinum electrode in hydrogen saturated aqueous solution for three orders of magnitude in the current and a factor of  $10^4$  in the transition time. The adsorption of hydrogen under the experimental conditions is rapid enough to maintain equilibrium between all the adsorbed species and dissolved hydrogen at the electrode surface. The first-order rate of adsorption is estimated to be greater than  $10^{-1}$  cm./sec. Corresponding to this value the rate of desorption is larger than  $30 \text{ sec.}^{-1}$ . Surface concentrations of the adsorbed hydrogen estimated from the results indicate the presence of sites inactive for hydrogen electrooxidation on the electrode surface.

The anodic behavior of hydrogen electrodes is characterized by the appearance of a limiting current density which has been interpreted as evidence for (I) a slow adsorption of hydrogen molecules onto the surface, (II) a rate-limiting surface reaction such as the dissociation of hydrogen molecules to atoms, or (III) current limitation due to slow hydrogen molecule diffusion to the electrode surface. Vetter and Otto<sup>1</sup> have reported agitation independent anodic limiting currents on inactive platinum which they ascribed to a rate-determining adsorption of hydrogen on the platinum surface (step I). The deuterium exchange and separation experiments of Horiuti and co-workers<sup>2</sup> indicate that step II is rate determining on nickel, but that it probably is not mechanistically important on platinum at anodic potentials. Breiter, Knorr, and co-workers<sup>3</sup> have emphasized the importance of step III. These investigators found that the anodic limiting current densities on specially activated platinum, rhodium, and iridium electrodes are strongly dependent upon the flow rate of electrolyte along the electrode, which is indicative of diffusion limitation of the current. Additional evidence for the exclusion of steps I and II as the slow steps on activated platinum is the observed rapid electrochemical oxidation of molecular hydrogen contained in bubbles in contact with a platinum anode surface.<sup>4</sup> The experiments of Frumkin and Aikazian<sup>5</sup> in aqueous solutions of sulfuric and other acids showed the behavior expected for diffusion control at a rotating disk platinum electrode. At high angular velocities, however, limiting currents were found which these authors ascribe to a rate-limiting step subsequent to adsorption of hydrogen on the surface. Schuldiner<sup>6</sup> has interpreted his experiments, in which current limitation due to diffusion was suppressed by vigorous stirring, on rhodium and platinum on

the basis of a rate-limiting dissociation of hydrogen on the electrode surface.

**Mathematical.**—When a constant current is applied to an inert electrode on which an electroactive species is adsorbed which is interconvertible with a non-electroactive species in solution, the depletion of the adsorbed species also causes the depletion of the inert species. The rate at which the inert species is depleted depends upon its diffusion constant, the current density, and the rates with which each of the two species react to form the other. Removal of the electroactive species from the surface leads to a gradual increase in the electrode overpotential until the electroactive species is no longer present on the surface. At this point the overpotential increases rapidly until a second electrode reaction supplies the constant current. This characteristic time representing initial complete depletion of the electroactive species from the surface is called the transition time ( $\tau$ ).<sup>7</sup> Gierst and Juliard<sup>8,9</sup> as well as Delahay and co-workers<sup>10</sup> have emphasized the importance of transition time measurements in elucidating electrode mechanisms and they have developed mathematically and experimentally several important cases. The influence of a preliminary chemical surface reaction upon the transition time has been considered by Gierst,<sup>8,9</sup> and his formulation will be shown to be correct in a limiting case.

If  $[y]$  is the volume concentration of species  $y$  and  $D$  its diffusion coefficient in an electrolyte solution, then its semi-infinite linear diffusion to a flat electrode surface may be represented by

$$\frac{\partial [y]}{\partial t} = D \frac{\partial^2 [y]}{\partial X^2} \quad (1)$$

Under the assumption of a linear adsorption isotherm at the electrode surface,  $y$  adsorbs to form  $y_{ad}$  with a rate constant  $k_1$  (cm./sec.) and  $y_{ad}$  desorbs with a rate constant  $k_2$  (sec.<sup>-1</sup>). If  $n$  represents the number of electrons exchanged with the electrode in the electrochemical reaction of one molecule of  $y_{ad}$  and  $F$  is the Faraday constant the boundary conditions at the electrode surface are

(1) K. J. Vetter and D. Otto, *Z. Elektrochem.*, **60**, 1072 (1956).

(2) (a) J. Horiuti and G. Okamoto, *Bull. Chem. Soc. Japan*, **13**, 216 (1938). (b) J. Horiuti, Chapter 2, "Trans. Symposium on Electrode Processes," E. Yeager, editor, John Wiley and Sons, Inc., New York, N. Y., 1961.

(3) M. Breiter, C. A. Knorr, and R. Meggle, *Z. Elektrochem.*, **59**, 153 (1955); M. Breiter, Chapter 17, ref. 2b.

(4) M. Breiter, C. A. Knorr, and W. Voelkl, *Z. Elektrochem.*, **59**, 681 (1955).

(5) A. N. Frumkin and E. A. Aikazian, *Dokl. Akad. Nauk S.S.S.R.*, **100**, 315 (1955); A. N. Frumkin, *Z. physik. Chem.*, **207**, 321 (1957).

(6) S. Schuldiner, NRL Report 5291, 30 April 1959; NRL Report 5398, 12 November 1959.

(7) J. A. V. Butler and G. Armstrong, *Proc. Roy. Soc. (London)*, **A139**, 406 (1933); *Trans. Faraday Soc.*, **30**, 1173 (1934).

(8) L. E. Gierst and A. Juliard, *J. Phys. Chem.*, **57**, 701 (1953).

(9) L. E. Gierst, *Z. Elektrochem.*, **59**, 784 (1955).

(10) P. Delahay and T. Berzins, *J. Am. Chem. Soc.*, **75**, 2486, 4205 (1953); P. Delahay, C. Mattax, and T. Berzins, *ibid.*, **76**, 5319 (1954); P. Delahay, *Discussions Faraday Soc.*, **24**, 206 (1957).

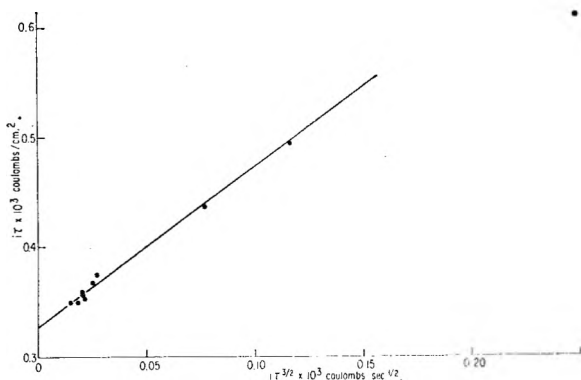


Fig. 1.—Experimental data for short transition times according to equation 9.

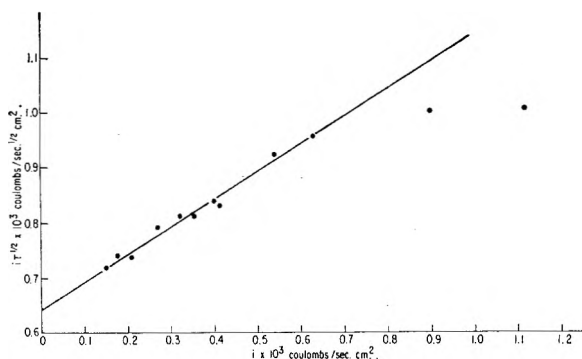


Fig. 2.—Experimental data for long transition times according to equation 10.

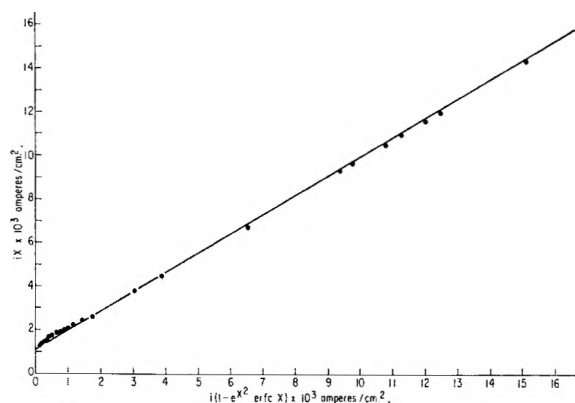


Fig. 3.—Validity of equation 8,  $x = 1.8\tau^{1/2}$ .

$$0 = D \left( \frac{\partial [y]}{\partial X} \right)_{X=0} + k_2 [y_{ad}] - k_1 [y] \quad (2)$$

$$\frac{\partial [y_{ad}]}{\partial t} = k_1 [y] - k_2 [y_{ad}] - \frac{i}{nF}$$

The substitutions

$$\begin{aligned} Z &= [y]_i - [y] \\ Z_{ad} &= [y_{ad}]_i - [y_{ad}] \end{aligned} \quad (3)$$

where  $[y]_i$  and  $[y_{ad}]_i$  are the initial concentrations of  $y$  and  $y_{ad}$ , may be made. Under the assumption that the rate constants are not a function of potential or electrode coverage, eq. 1, 2, and 3 may be solved by performance of Laplace transformations. The solution of the transformed equations has the form

$$\bar{Z} = Me^{-qX} \text{ with } q = \sqrt{\frac{p}{D}} \text{ and } M = \frac{ik_2}{nFD^2q^3(Dq^2 + k_1q + k_2)} \quad (4)$$

Employing the appropriate inverse transformations, we find

$$\begin{aligned} Z_{ad} = \frac{i}{nFD} \left[ 2 \left( \frac{Dt}{\pi} \right)^{1/2} \frac{A+B}{AB} + \frac{B}{A^2(B-A)} (e^{A^2Dt} \operatorname{erfc}(A\sqrt{Dt}) - 1) - \frac{A}{B^2(B-A)} (e^{B^2Dt} \operatorname{erfc}(B\sqrt{Dt}) - 1) \right] \quad (5) \end{aligned}$$

where  $AB = k_2/D$  and  $A+B = k_1/D$ , and  $\operatorname{erfc}$  denotes the error function complement. When  $t = \tau$ ,  $Z_{ad} = [y_{ad}]_i$ . In general, for very short transition times eq. 5 simplifies to

$$[y_{ad}]_i = \frac{i}{nF} \left[ \tau - \frac{k_2}{2} \tau^2 + \frac{8}{15\sqrt{\pi}} \frac{k_1k_2}{\sqrt{D}} \tau^{5/2} - \dots \right] \quad (6)$$

and for very long transition times eq. 5 becomes

$$[y_{ad}]_i = \frac{i}{nFD} \left[ 2 \frac{k_1}{k_2} \left( \frac{D\tau}{\pi} \right)^{1/2} - \frac{k_1^2 - Dk_2}{k_2^2} \right] \quad (7)$$

Equation 7 is essentially that of Gierst, reference 9 eq. (V). Notice, however, that the slope of an  $i\tau^{1/2}$  vs.  $i$  plot may be positive as well as negative depending upon whether the rates of adsorption and desorption are rapid or not. Gierst has discussed the latter case and this paper presents an example of the former.

If the rates of adsorption and desorption are extremely fast so that equilibrium is maintained between solution species at the electrode and the species on the surface, then  $B$  approaches infinity and  $A$  approaches  $k_2/k_1$ . For this special case equation 5 becomes at the transition time

$$\begin{aligned} [y_{ad}]_i = \frac{i}{nFD} \left( \frac{k_1}{k_2} \right)^2 \left[ \frac{2}{\sqrt{\pi}} \frac{k_2}{k_1} (D\tau)^{1/2} + \left( e^{D\tau} \left( \frac{k_2}{k_1} \right)^2 \operatorname{erfc} \left( \frac{k_2}{k_1} \sqrt{D\tau} \right) - 1 \right) \right] \quad (8) \end{aligned}$$

This equation has been derived by W. Lorenz<sup>11</sup> in integral form. If the argument of eq. 8 is small we obtain

$$[y_{ad}]_i = \frac{i}{nFD} \left( D\tau - \frac{4}{3\sqrt{\pi}} \frac{k_2}{k_1} (D\tau)^{3/2} + \frac{D^2\tau^2}{2} \left( \frac{k_2}{k_1} \right)^2 - \dots \right) \quad (9)$$

For large argument eq. 8 reduces to

$$[y_{ad}]_i = \frac{i}{nFD} \frac{k_1}{k_2} \left[ 2 \left( \frac{D\tau}{\pi} \right)^{1/2} - \frac{k_1}{k_2} \right] \quad (10)$$

### Experimental

The constant current was supplied to the cell electrodes by a regulated power supply through series carbon resistors whose resistances were ascertained to within 1% by use of an impedance bridge. The current pulse was turned on and off by a 275 C mercury contact relay activated by appropriate timing circuits. Pulse durations were variable from 10 msec. to 25 sec. and were delayed 4 msec. with respect to the trigger to the oscilloscope. The oscillograms were registered photographically. The cell was constructed of Pyrex glass except for the graded seal to the working electrode which was a horizontal planar disk of platinum with rounded edges of  $5.75 \pm 0.10$  cm.<sup>2</sup> geometric area. It was polished prior to use with 5  $\mu$  diamond dust. The counter electrode, a large coil of platinum wire, was located about 1 in. directly above the working electrode and was separated from it by a fritted disk. A Luggin capillary was used in conjunction with the reference electrode. A Teflon stopcock allowed hydrogen gas to be bubbled through or over the solution. The cell was maintained at 25.0° by a mineral oil-bath.

One molar sodium perchlorate was prepared by the neu-

(11) W. Lorenz, *Z. Elektrochem.*, **59**, 730 (1955).

tralization of analytical reagent 70% perchloric acid with 50% sodium hydroxide (reagent) and dilution with triple-distilled water. The perchloric acid concentration was found to be 0.119 *N*. Ultrapure hydrogen was bubbled through a series of wash bottles containing concentrated sulfuric acid, vanadous chloride (Zn excluded), 50% sodium hydroxide, and triple-distilled water. All connections from the first wash bottle to the gas outlet from the cell were of glass or Teflon tubing.

The working electrode was activated by the use of single anodic pulses until the transition times were reproducible. Prior to each measurement the electrode was pulsed anodically for 250 msec. at an apparent current density of 14 mamp./cm.<sup>2</sup>. Following the reattainment of the hydrogen electrode potential, hydrogen was bubbled vigorously through the solution for 30 sec. The electrode and solution then remained quiescent for 30 sec. prior to the experimental pulse. Deactivation of the electrode was found to be slow. There was no noticeable change of the transition times from 15 sec. to five min. after activation although roughly a 10% decrease in the transition time could be observed after 0.5 hr.

### Results and Discussion

Equation 5 should apply to the hydrogen electrode when  $[y]$  is equated to the dissolved molecular hydrogen concentration and  $[y_{ad}]$  is identified with the total surface hydrogen concentration expressed in terms of molecular hydrogen. The adsorbed species are assumed to be in rapid equilibrium. The results cover geometric current densities from 0.150 to 184 mamp./cm.<sup>2</sup> and transition times in the range of 1.9 msec. to 23 sec. The transition times recorded were corrected for the effect of double layer charging by the assumption of a constant double layer capacity.<sup>4</sup>

Figure 1 illustrates the agreement of the experimental data with eq. 9 at short transition times. The data did not fit eq. 6. For longer transition times the experimental results agreed with the prediction of eq. 10 satisfactorily (Fig. 2). The slopes of Fig. 1 and 2 give values of  $(k_2/k_1)\sqrt{D}$  of 1.9 and 1.7 sec.<sup>-1/2</sup>, respectively. Figure 3 contains the data over the entire range of current densities plotted according to eq. 8 using a value of  $(k_2/k_1)\sqrt{D}$  of 1.8 sec.<sup>-1/2</sup>. The straight line in Fig. 3, which has had its intercept adjusted to best fit the experimental results, has a slope of  $\sqrt{\pi}/2$ . The assumption of rapid reversible adsorption thus is capable of correlating current densities and transition times adequately over a wide range of values. Experimental data obtained in phosphate buffer (pH 3.15) and 0.1 *N* NaOH also could be represented by eq. 8, which suggests that adsorption is rapid in these solutions also.

The diffusion constant of hydrogen in water at 25° is  $4.1 \times 10^{-5}$  cm.<sup>2</sup>/sec.<sup>12</sup>. The solubility of hydrogen gas in water at 25° is  $7.6 \times 10^{-7}$  mole/cm.<sup>3</sup>.<sup>13</sup> The data of Tammann<sup>14</sup> allow an estimate of the solubility of hydrogen in 1 *M* sodium perchlorate of  $6.2 \times 10^{-7}$  mole/cm.<sup>3</sup>. This may be compared to the experimental value for the solubility of hydrogen of  $5.9 \times 10^{-7}$  mole/cm.<sup>3</sup> obtained from the intercept of Fig. 2. The slopes of Fig. 1 and 2 may be used to obtain surface concentrations which are independent of the assumed area of the electrode. Combination of the diffusion constant and the experimentally determined hydrogen solubility with the slopes of Fig. 1 and 2 gives values of  $1.9 \times 10^{-9}$  and  $2.2 \times 10^{-9}$  mole/cm.<sup>2</sup>, respectively. These values may be compared with the current density dependent value  $1.7 \times 10^{-9}$  mole/cm.<sup>2</sup> obtained from the intercept of Fig. 1. Since this value is somewhat smaller than the surface concentrations determined from the slopes of Fig. 1 and 2, it must be concluded that inactive sites on the electrode surface act to offset the influence of surface roughness.

**Kinetic Considerations.**—The use of eq. 5 and 7 makes possible the estimation of the minimum values of the rate constants,  $k_1$  and  $k_2$ . The maximum rates of adsorption and desorption may be estimated crudely from the theory of diffusion under the assumption that each molecule striking the electrode surface adsorbs there. The values are  $10^{-1} < k_1 \lesssim 10^5$  cm./sec. and  $30 < k_2 \lesssim 3 \times 10^7$  sec.<sup>-1</sup>. It must be admitted, however, that the assumptions of first-order adsorption and desorption are not strictly correct, especially at high surface concentrations. Therefore, the constants  $k_1$  and  $k_2$  represent average values over the various surface concentrations. The use of this approximation is justified by its necessity in obtaining a mathematical solution to the problem and the close agreement of the experimental results with the theory.

**Acknowledgment.**—The author expresses his thanks to Dr. M. Breiter for his comments and suggestions concerning this manuscript.

(12) G. Tammann and V. Jessen, *Z. anorg. u. allgem. Chem.*, **179**, 125 (1929).

(13) "Handbook of Chemistry and Physics," 34th ed., Chemical Rubber Publ. Co., Cleveland, Ohio, p. 1532.

(14) G. Tammann, *Z. anorg. u. allgem. Chem.*, **158**, 25 (1926).

# ETHYLENE AS A SCAVENGER IN THE RADIOLYSIS OF LIQUID CYCLOPENTANE<sup>1</sup>

BY RICHARD A. HOLROYD

*Radiation Research Laboratories, Mellon Institute, Pittsburgh, Pa.*

*Received November 2, 1961*

Ethylene, when present as a scavenger during the radiolysis of liquid cyclopentane, leads to two additional products, ethane and ethylcyclopentane. Ethyl radicals are formed by addition of hydrogen atoms to ethylene. Cyclopentyl radicals either add to ethylene or combine with radicals depending on the dose rate. The activation energy for addition of cyclopentyl radicals to ethylene is  $6.7 + \frac{1}{2}E_4$ , where  $E_4$  is the energy of activation for recombination of cyclopentyl radicals in solution. At relatively low dose rates, the rate of formation of ethylcyclopentane is proportional to the ethylene concentration times the square root of the dose rate. It is estimated that the rate of disproportionation of ethyl and cyclopentyl radicals relative to recombination in the liquid phase is 1.7. Radical addition to unsaturates becomes an important secondary reaction at low dose rates in the radiolysis of saturated hydrocarbons if reaction is carried to relatively high conversions.

The purpose of this paper is to report the effect of ethylene on the radiation chemistry of liquid cyclopentane. It has been shown that olefins are scavengers for hydrogen atoms in the liquid phase radiolysis of hydrocarbons.<sup>2</sup> For example, cyclohexene acts as a scavenger in the radiolysis of cyclohexane.<sup>3</sup> Similarly isobutene scavenges hydrogen atoms and radicals in the radiolysis of neopentane.<sup>4</sup> Ethylene as well as propylene is an effective scavenger of H atoms and radicals in the vapor phase radiolysis of simple alkanes.<sup>5,6</sup> The presence of ethylene during irradiation induces the isomerization of *n*-butane to isobutane and isopentane and converts isobutane to isopentane<sup>7</sup>; values for *G*-isomer vary from 200 to 1000 above 300° for pressures from 150 to 600 p.s.i. No thorough investigations of the use of ethylene as a scavenger in the radiolysis of hydrocarbons in the liquid phase have been reported as yet.

Cyclopentane was chosen for the purposes of the present study because its wide liquid range (−94° to +49°) allowed a study of temperature effects and also because a minimum of products are formed in the radiolysis of the pure liquid.<sup>8</sup> Thus there is no difficulty in determining the major products of the scavenging reaction, ethane and ethylcyclopentane. A thorough study of the yields of these products at various temperatures, ethylene concentrations, and dose rates was made in hopes of elucidating the mechanism of ethylene scavenging.

## Experimental

The cyclopentane used in all experiments was Phillips Research Grade (99.98% pure). This was purified further by passage twice through a column packed with carefully dried and degassed activated silica gel. This was necessary to remove the major unsaturated impurity present which was cyclopentene. The ethylcyclopentane was an A. P. I. standard sample.

The ethylene was Phillips Research Grade. This contained a trace of ethane (0.027%). Thus a small correction had to be applied in determining the yield of ethane.

(1) Supported, in part, by the U. S. Atomic Energy Commission. Presented at the 140th National Meeting of the American Chemical Society, Chicago, Illinois, September, 1961.

(2) T. J. Hardwick, *J. Phys. Chem.*, **65**, 161 (1961).

(3) P. J. Dyne and J. W. Fletcher, *Can. J. Chem.*, **38**, 851 (1960).

(4) R. A. Holroyd, *J. Phys. Chem.*, **65**, 1352 (1961).

(5) H. A. Dewhurst, *J. Am. Chem. Soc.*, **83**, 1050 (1961).

(6) R. A. Back, *J. Phys. Chem.*, **64**, 124 (1960).

(7) Esso Research & Engineering Co., British Patent 862,529, March 8, 1961.

(8) G. A. Muccini and R. H. Schuler, *J. Phys. Chem.*, **64**, 1436 (1960).

Ethylene was found to be soluble in cyclopentane in the concentration range used (0.05 to 1.0 mole % ethylene). Samples were prepared by adding a measured amount of ethylene to 2 ml. of cyclopentane in 7-ml. Pyrex cells. The concentration of ethylene in the liquid phase was determined by measuring the fraction,  $\alpha$ , of added ethylene dissolved in the liquid at each temperature. The value of  $\alpha$  varied from 0.71 at 0° to 0.47 at 46°. Over the range studied the concentration of ethylene in solution was proportional to the amount added.

Two identical samples were prepared at each concentration and temperature. After irradiation one sample was transferred to a vacuum line and the fraction volatile at −78° was analyzed for hydrogen and ethane. The other sample was injected into the gas chromatography apparatus for analysis of the C<sub>5</sub> to C<sub>10</sub> products. A 2.5-meter modified silica gel column was used for the separation of ethane from ethylene. This column also was used for the higher molecular weight products. The C<sub>7</sub> fraction was a single peak on the chromatograph and mass spectrometric analysis showed this fraction to be only ethylcyclopentane.

The temperature was varied by circulating a heat exchange fluid through coils surrounding the Co-60  $\gamma$ -ray source. A Co-60 point source of  $\gamma$ -radiation was utilized for the experiments in which the dose rate was varied. Samples placed at distances of 7.5 to 40 cm. from the source were subjected to dose rates in the range 18,700 to 660 rad/hour. Absolute yields were calculated relative to the yield of the Fricke dosimeter ( $G_{Fe^{+++}} = 15.5$ ). For irradiation with a 2.8 m.e.v. electron beam from a Van de Graaff generator smaller samples were used and the beam was focused directly on the liquid. Samples thus were subjected to a dose rate of about  $2 \times 10^{19}$  e.v. ml.<sup>−1</sup> sec.<sup>−1</sup> using a beam current of 1  $\mu$ amp.

## Results and Discussion

The major products of the radiolysis of pure cyclopentane are hydrogen, cyclopentene, and cyclopentylcyclopentane. (Other pentenes may be formed in addition to cyclopentene.)

With ethylene present there are two additional products observed: ethane and ethylcyclopentane. Table I shows the effect of temperature and ethylene concentration on these yields. The radiation yield of ethylcyclopentane increases with temperature and ethylene concentration. The highest yield in these experiments is  $G_{C_7H_{14}} = 4.2$ . From the eighth column in Table I it is obvious that the ethane/ethylcyclopentane ratio is not constant but varies from 0.16 to 2.0. Only at −78° is this ratio constant at  $1.7 \pm 0.2$ . Thus these products cannot be formed only by the disproportionation and recombination of ethyl and cyclopentyl radicals since the ratio then would be a constant independent of temperature and ethylene concentration.

An examination of the ethane yields in Table I shows that the ethane increases with ethylene con-

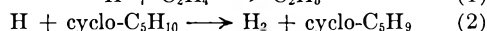
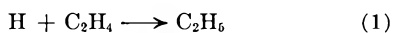
TABLE I

EFFECT OF ETHYLENE CONCENTRATION AND TEMPERATURE ON THE RADIATION YIELDS USING  $\text{Co}^{60}$   $\gamma$ -RAYS<sup>a</sup>

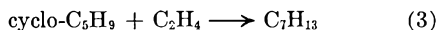
$[\text{C}_2\text{H}_4]$ , mol./ml. $\times 10^{-17}$	Temp., °C.	$\text{H}_2$	$\text{C}_2\text{H}_6$	$G_{\text{H}_2} + G_{\text{C}_2\text{H}_6}$	$G_{\text{C}_7\text{H}_{14}^b}$	$G_{\text{C}_{10}\text{H}_{18}^b}$	$\text{C}_2\text{H}_6/\text{C}_7\text{H}_{14}^b$	$k_3/k_4^{1/2} \times 10^{13}$ , mol. <sup>-1/2</sup> ml. <sup>1/2</sup> sec. <sup>-1/2</sup>
46	46	5.2	0.35	5.6	1.31	0.95	0.27	17.5
108	46	4.8	.51	5.3	3.17	.95	.16	17.9
208	46	..	..	..	4.21	.90	..	15.6
0	28	5.2	..	5.2	0	1.06	..	..
9	28	5.2	.12	5.3	0.20	1.10	.61	13.4
19	28	5.2	.18	5.4	.34	0.97	.54	10.6
38	28	5.0	.25	5.3	.63	1.07	.40	9.7
84	28	5.0	.37	5.4	..	..	..	..
133	28	..	..	..	1.96	0.91	..	9.1
237	28	4.7	.65	5.4	2.88	0.86	.22	7.8
64	15	5.1	.33	5.4	0.58	1.08	.57	5.2
154	15	4.7	.45	5.2	1.14	0.94	.40	4.5
288	15	4.7	.56	5.3	1.81	.75	.31	4.3
0	0	4.9	0	4.9	0	..	..	..
24	0	4.8	0.14	4.9	0.13	.93	1.07	3.3
49	0	4.7	.24	4.9	.26	.94	0.91	3.25
81	0	4.5	.35	4.9	.37	.78	.94	3.1
207	0	4.3	.54	4.8	.75	.75	.72	2.5
305	0	4.2	.61	4.8	1.03	.55	.59	2.7
0	-78	4.3	0	4.3	..	..	..	..
33	-78	4.3	0.30	4.6	0.15	.68	2.0	..
114	-78	4.1	.38	4.5	.26	.62	1.47	..
188	-78	3.9	.45	4.4	.29	.57	1.54	..
422	-78	3.7	.61	4.3	.36	.53	1.68	..

<sup>a</sup> Yields are based on samples given an irradiation dose of about  $3.0 \times 10^{19}$  e.v./ml. D.R.  $\cong 3 \times 10^{15}$  e.v. ml.<sup>-1</sup> sec.<sup>-1</sup>.  
<sup>b</sup>  $G_{\text{C}_7\text{H}_{14}}$  and  $G_{\text{C}_{10}\text{H}_{18}}$  are the yields of ethylcyclopentane and cyclopentylcyclopentane, respectively.

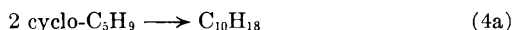
centration and there is a corresponding decrease in the yield of hydrogen. Thus the sum of the yields of hydrogen and ethane is approximately a constant identical with the yield of hydrogen in the absence of scavenger.<sup>9</sup> This relationship suggests that in the presence of ethylene hydrogen atoms add to ethylene forming ethyl radicals, reaction 1, thus lowering the yield of hydrogen formed by abstraction, reaction 2. At low dose rates the ethyl radicals abstract from the solvent to form ethane.



To explain the formation of large yields of ethylcyclopentane it is necessary to postulate an additional reaction. A possibility is the scavenging of cyclopentyl radicals by ethylene (3). Reaction



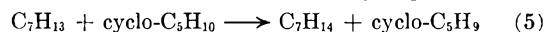
3 competes with the bimolecular disappearance of cyclopentyl radicals (4). The addition of ethylene



thus would remove cyclopentyl radicals, lowering the yields of cyclopentylcyclopentane and cyclopentene. However, these yields are virtually unaffected by the ethylene, at least at the higher temperatures. The average value of  $G_{\text{cyclopentylcyclopentane}}$  with ethylene present is 0.98

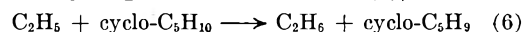
(9) The yields given for  $G_{\text{H}_2}$  in the absence of ethylene are lower than the initial yield of hydrogen as measured by Hardwick (ref. 2,  $G_{\text{H}_2} = 5.78$ ) probably because enough cyclopentene is present during irradiation (total dose  $\sim 3 \times 10^{19}$  e.v./ml.) to scavenge hydrogen atoms.

compared to 1.06 in pure cyclopentane. Similarly  $G_{\text{cyclopentene}}$  is approximately 3.4, independent of the concentration of ethylene. This suggests that cyclopentyl radicals although scavenged in (3) are regenerated by  $\text{C}_7\text{H}_{13}$  radicals abstracting hydrogen from the solvent, cyclopentane (5).

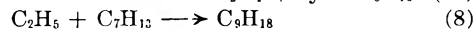
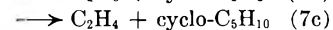
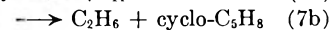
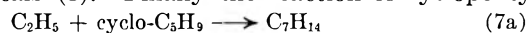


These steps are the elements of a dose rate dependent chain reaction.

The ethyl radical formed in (1) may either abstract a hydrogen to form ethane (6), react with



cyclopentyl radicals to combine or disproportionate (7), or possibly combine with cyclopentylethyl radicals (8). Finally the reaction of cyclopentyl-



ethyl radicals with ethylene (9) may be important



at higher ethylene concentrations. Reactions 8 and 9 lead to a  $\text{C}_9$  product. Since no significant yield of  $\text{C}_9$  hydrocarbon was observed, these last two reactions are neglected.

The mechanism consisting of reactions 1 through 7 satisfies the experimental results quite well. At low dose rates where reaction 7 also may be neglected the yield of dicyclopentyl should remain constant since every hydrogen atom leads to a cyclopentyl radical *via* either (2) or (6) and for each cyclopentyl radical scavenged in (3), a cyclopentyl radical is regenerated in (5).

For the experiments reported in Table I the dose rate is  $3 \times 10^{15}$  e.v./ml./sec. This is low enough so that reaction 7 will be of minor importance compared to ethyl radical abstraction, reaction 6.<sup>10</sup> If reaction 7 is neglected the mechanism requires that

$$R_{\text{ethylcyclopentane}}/(R_{\text{dicyclopentyl}})^{1/2} = k_3(\text{C}_2\text{H}_4)/k_4^{1/2}$$

Values of  $k_3/k_4^{1/2}$  calculated in this way are reported in the last column of Table I. The variation of this ratio with temperature is expressed by the equation

$$\log k_3/k_4^{1/2} = -(1470/T) - 7.16$$

Thus  $E_3$ , the energy of activation for addition of cyclopentyl radicals to ethylene, is  $6.7 + 1/2 E_4 \pm 0.5$  kcal./mole. Some values obtained recently in gas phase studies for the activation energy of addition of radicals to ethylene are: for methyl, 8.7,<sup>11</sup> for ethyl 5.5,<sup>12</sup> and for isopropyl 6.9<sup>13</sup> kcal./mole. The activation energy for methyl radical addition to ethylene in the liquid phase (isoöctane) has been measured by Szwarc<sup>14</sup> to be  $E_a - 1.03$ . Here  $E_a$  refers to the energy of activation for abstraction of a hydrogen atom from isoöctane by a methyl radical. If  $E_a$  is 8 kcal./mole, methyl radical addition will have an activation energy of 7 kcal./mole in solution. No comparable value is available at present for cyclopentyl radicals but the value of  $6.7 + 1/2 E_4$  seems reasonable.

The mechanism also requires that for low dose rates the radiation yield of ethylcyclopentane be inversely proportional to the square root of the dose rate

$$G_{\text{ethylcyclopentane}} = k_3(\text{C}_2\text{H}_4) \left( \frac{50G_R}{k_4 \text{ dose rate}} \right)^{1/2}$$

where  $G_R$  is the yield of cyclopentyl radicals. This relationship was tested over a 400-fold range of dose rates using Co-60  $\gamma$ -radiation. For these experiments the ethylene concentration was constant at  $1.23 \times 10^{19}$  molecules/ml. In Table II the results are given and the product of  $G_{\text{ethylcyclopentane}}$  and the square root of the dose rate is a constant as expected. At  $3.49 \times 10^{15}$  e.v./ml./sec. a higher value is obtained because of a small contribution to  $G_{\text{ethylcyclopentane}}$  by reaction 7.

At  $-78^\circ$  the rates of reactions 3 and 6 will be too slow to contribute to the formation of products because of the high activation energies. The mechanism then requires that  $\text{C}_2\text{H}_6/\text{ethylcyclopentane} = k_{7b}/k_{7a}$ . Although there is some experimental scatter, this ratio is a constant independent of ethylene concentration and has an average value of 1.67 at  $-78^\circ$ . Thus disproportionation is favored over recombination. This value is an upper limit if there are other radicals present which can disproportionate with ethyl radicals (reaction 10). However, cyclopentyl

(10) A similar effect has been reported for neopentane (ref. 4) where methyl radicals are observed predominantly to abstract at dose rates less than  $10^{16}$  e.v./ml./sec. and predominantly to react with radicals at dose rates greater than  $10^{18}$  e.v./ml./sec. at  $28^\circ$ .

(11) R. K. Brinton, *J. Chem. Phys.*, **29**, 781 (1958).

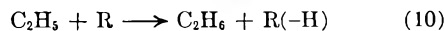
(12) F. W. Lampe and F. H. Field, *Can. J. Chem.*, **37**, 995 (1959).

(13) J. A. Kerr and A. F. Trotman-Dickenson, *Trans. Faraday Soc.*, **55**, 921 (1959).

(14) M. Field and M. Szwarc, *J. Am. Chem. Soc.*, **82**, 3791 (1960).

TABLE II

EFFECT OF DOSE RATE USING Co <sup>60</sup> $\gamma$ -RADIATION ( $\text{C}_2\text{H}_4$ ) = $1.23 \times 10^{19}$ molecules/ml.; temp. = $27^\circ$			
Dose rate, e.v. ml. <sup>-1</sup> sec. <sup>-1</sup> $\times 10^{-15}$	$G_{\text{C}_2\text{H}_6}$	$G_{\text{C}_5\text{H}_{10}}$	$G_{\text{C}_2\text{H}_4} \times (\text{dose rate})^{1/2} \times 10^{-7}$
349.0	1.96	0.9	11.6
24.8	4.95	.9	7.83
13.9	6.40	.9	7.55
6.17	9.32	1.4	7.32
2.22	16.7	1.2	7.86
0.87	25.4	..	7.50



radicals are expected to be the most abundant radical species in irradiated liquid cyclopentane.

An estimate of the disproportionation of ethyl and cyclopentyl radicals to ethylene and cyclopentane (reaction 7c) was obtained by using  $\text{C}_2\text{D}_4$  in place of  $\text{C}_2\text{H}_4$ . Mass spectrometric analysis of the ethylene fraction after irradiation at  $-78^\circ$  showed that  $\text{C}_2\text{D}_3\text{H}$  was formed with a radiation yield of 0.06. Assuming this is all formed by (7c), it is estimated that 13% of the collisions between ethyl and cyclopentyl radicals result in the formation of ethylene and cyclopentane. In a similar experiment at  $28^\circ$  in which  $\text{C}_2\text{D}_4$  was added to cyclopentane, no HD was found in the hydrogen sample. Thus hydrogen atoms normally add to rather than abstract from ethylene in solution.

As a further check on the ratio  $k_{7b}/k_{7a}$  and to see if there was any effect of temperature on this ratio, a few experiments were done at a dose rate of  $2 \times 10^{19}$  e.v./ml./sec. at  $23^\circ$  using an electron beam from a Van de Graaff accelerator. At this high dose rate ethylcyclopentane and ethane are formed mainly by the second-order combination and disproportionation of the cyclopentyl and ethyl radicals (7a) and (7b). The ratio of these products thus is expected to be a constant independent of ethylene concentration. The data of Table III show this to be the case.

TABLE III

Results at a dose rate of $\sim 2 \times 10^{19}$ e.v. ml. <sup>-1</sup> sec. <sup>-1</sup>		
$[\text{C}_2\text{H}_4]$ , mol./ml. $\times 10^{-17}$	Temp., $^\circ\text{C}$ .	$\text{C}_2\text{H}_6/\text{ethylcyclopentane}$
90	23	1.74
140	23	1.64
213	23	1.71

The average of 1.70 is in excellent agreement with the value of  $k_{7b}/k_{7a}$  obtained at  $-78^\circ$  using Co-60  $\gamma$ -rays.

The value of  $k_{7b}/k_{7a} = 1.7$  may be compared with other data for the ratio of disproportionation to combination of radicals. Wagner<sup>15</sup> has predicted on the basis of gas phase results that the disproportionation to recombination ratio should be 1.8 for s-alkyl radicals. Also Freeman<sup>16</sup> suggests that disproportionation of cyclohexyl radicals is 1.86 times the rate of recombination. Gunning,<sup>17</sup> however, has found lower values of this ratio ( $\sim 0.45$  for cyclohexyl radicals and 0.19 for

(15) C. D. Wagner, *J. Phys. Chem.*, **64**, 231 (1960).

(16) G. R. Freeman, *ibid.*, **64**, 1576 (1960).

(17) P. W. Beck, D. V. Kniebes, and H. E. Gunning, *J. Chem. Phys.*, **22**, 672, 678 (1954).

cyclopentyl radicals) from studies of the Hg-sensitized decomposition of these cycloalkanes in the gas phase. If, however, one accepts the value of 1.8 for *s*-alkyl radicals, a value of  $\sim 0.9$  would be expected for  $k_{7b}/k_{7a}$ . On this basis the value of 1.7 found here seems unusually high.

The results of this study illustrate the use of ethylene as a scavenger of both hydrogen atoms and radicals in the radiolysis of hydrocarbon liquids.

The technique provides a means of measuring the activation energy for addition of radicals to ethylene in liquid hydrocarbons. Since ethylene, present in the concentration range 0.05 to 1.0 mole %, is effective in scavenging radicals it is suggested that in general radical addition to unsaturated hydrocarbons can be an important secondary reaction at low dose rates in the radiolysis of hydrocarbons if reaction is carried to 0.1% conversion.

## X-RAY DIFFRACTION STUDY OF ARSENIC TRISULFIDE-IODINE GLASSES

BY T. E. HOPKINS, R. A. PASTERNAK, E. S. GOULD, AND J. R. HERNDON

*Department of Chemistry, Stanford Research Institute, Menlo Park, California*

*Received November 3, 1961*

The structures of arsenic trisulfide glass and of an arsenic trisulfide-iodine glass (46% by weight iodine) have been studied by X-ray scattering techniques. The data for the former indicate a short order arrangement of the atoms similar to that in the (crystalline) orpiment structure. The data for the iodine-containing glass suggest that when iodine is added to arsenic sulfide, the layers are broken up into a structure (probably a twisted chain) having As-I and S-S bonds. The fragmentation of layers also is indicated by the marked decrease in viscosity and softening point.

Arsenic trisulfide glass is of interest at present as a material of high refractive index, transparent in the infrared, which, at the same time, can be processed by techniques suitable for glasses.<sup>1</sup> It recently has been reported<sup>2</sup> that the softening point and the viscosity of arsenic trisulfide glass are greatly lowered by the addition of elemental iodine. Indeed, if sufficient iodine is added, the resulting mixtures, which are also glasses, soften below room temperature. So striking are these effects, particularly in the composition region 42-52 weight % iodine,<sup>3</sup> that we felt a comparative X-ray study of the structure of the iodine-containing glasses and arsenic trisulfide glass itself would be of interest. We are here reporting briefly the results of this investigation. After the conclusion of this work, a structural investigation of glasses in the  $As_2S_3$ -PbS system including pure arsenic trisulfide was reported by Petz and co-workers.<sup>4</sup>

### Experimental

For the X-ray scattering experiments a large flat piece of arsenic sulfide glass as obtained from the American Optical Company was used. The samples of iodine-containing glasses were prepared by fusing appropriate mixtures of powdered arsenic sulfide and elemental iodine; the melts were heated and agitated for 5 min. or more, then poured into a reversed cylindrical sample holder standing on a glass plate and allowed to cool to room temperature. Removal of the plate resulted in a smooth flat surface.

The scattering intensities were measured with a Norelco diffractometer equipped with scintillation counter and pulse

height analyzer. A copper tube operating at 35 kv. and 20 mamp. was used. Since no crystal monochromator was available, matched filters were employed,<sup>5</sup> the pair of filters being  $\frac{1}{3}$  mil nickel, and cobalt oxide-in-plastic.<sup>6</sup>

The intensities were measured with each of the filters at 0.01 intervals in  $s$  ( $=2/\lambda \sin \theta$ ), from  $s = 0.1$  to 1.25, by the constant count technique (12800 cts).

By taking the difference between the intensities measured with the nickel and the cobalt oxide filters, scattering intensities essentially due only to Cu  $K\alpha$  radiation were obtained. They were corrected for polarization and were brought to absolute scale by the method of Norman.<sup>7</sup> The scattering factors for As, S, and I and the method of calculating the incoherent scattering intensities were taken from Compton.<sup>8</sup> Figure 1 shows these corrected intensities, and the calculated total independent scattering curves. These data were converted by the formalism of Warren<sup>9,10</sup> to differential atomic distribution functions and to the atomic distribution functions. In these calculations increments of  $0.01 \text{ \AA}^{-1}$  in  $\sin \theta/\lambda$  were taken, and the distributions evaluated at 0.05  $\text{ \AA}$ . intervals. The radial distribution curves are shown in Fig. 2 and 3. Electronic distribution functions also were calculated but these did not differ in significant details from the atomic functions, except that peaks were broader.<sup>11</sup>

### Discussion

**$As_2S_3$ -glass.**—The differential radial distribution function of  $As_2S_3$  shows only two well-resolved peaks, at 2.3 and 3.5  $\text{ \AA}$ .; a third broad maximum at about 5.5  $\text{ \AA}$ . rises barely above the average density. The two main maxima in the distribution curves obviously represent As-S (2.3  $\text{ \AA}$ .) and combined 1,3 As-As plus 1,3 S-S interactions. From

(5) P. A. Ross, *J. Opt. Soc. Am.*, **16**, 433 (1928).

(6) Obtained by courtesy of Dr. Milburn, General Electric Company, San Francisco.

(7) N. Norman, *Acta Cryst.*, **10**, 370 (1957).

(8) A. H. Compton and S. K. Allison, "X-Rays in Theory and Experiment," D. Van Nostrand Co., New York, N. Y., 1935.

(9) B. E. Warren, H. Krutter, and O. Morningstar, *J. Am. Chem. Soc.*, **19**, 202 (1936).

(10) See also H. P. Klug and L. E. Alexander, "X-Ray Diffraction Procedures," John Wiley and Sons, Inc., New York, N. Y., 1954, p. 605.

(11) The calculations were carried out with a Burroughs 220 computer. Copies of the program, in the Burroughs modification of ALGOL, are available from T. E. H.

(1) The development of arsenic trisulfide glass is described in detail by R. Frerichs, *J. Opt. Soc. Am.*, **43**, 1153 (1953). See also J. Matsuda, *J. Chem. Soc. Japan*, **33**, 208 (1959).

(2) S. S. Flaschen, A. D. Pearson, and W. R. Northover, *J. Appl. Phys.*, **31**, 219 (1960).

(3) Paralleling these effects, the penetrability of arsenic trisulfide-iodine glasses has been found to increase by about five powers of ten if the iodine content is raised from 42 to 52% at 37°. In these tests, the distance penetrated by a needle (tip area about 0.00015 cm.<sup>2</sup>) under loads varying from 50 to 500 g. after a 5-sec. period was measured. (See ASTM Standards, 1958, Part 4, p. 1003.)

(4) J. I. Petz, R. F. Kruh, and G. C. Amstutz, *J. Chem. Phys.*, **34**, 526 (1961).

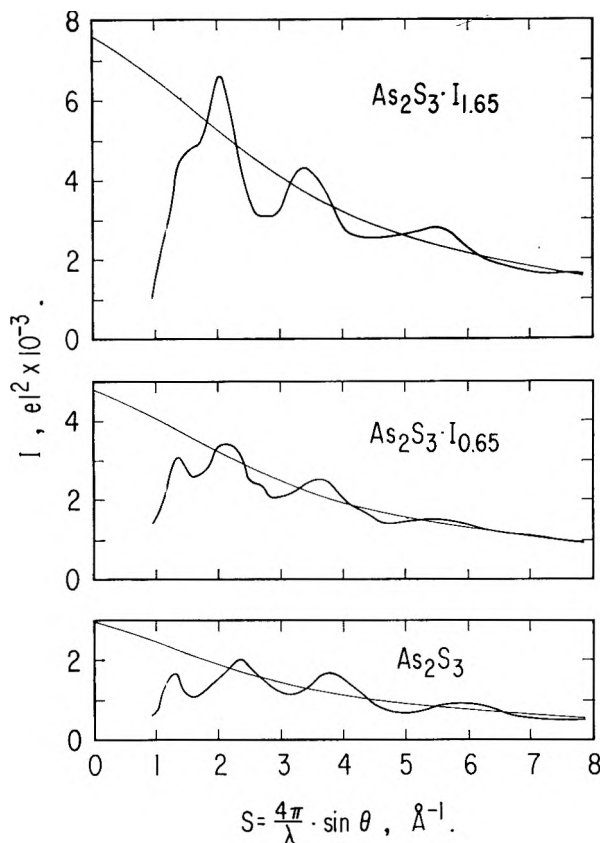


Fig. 1.—Normalized experimental intensities. Monotonically decreasing curves represent total independent atomic scattering.

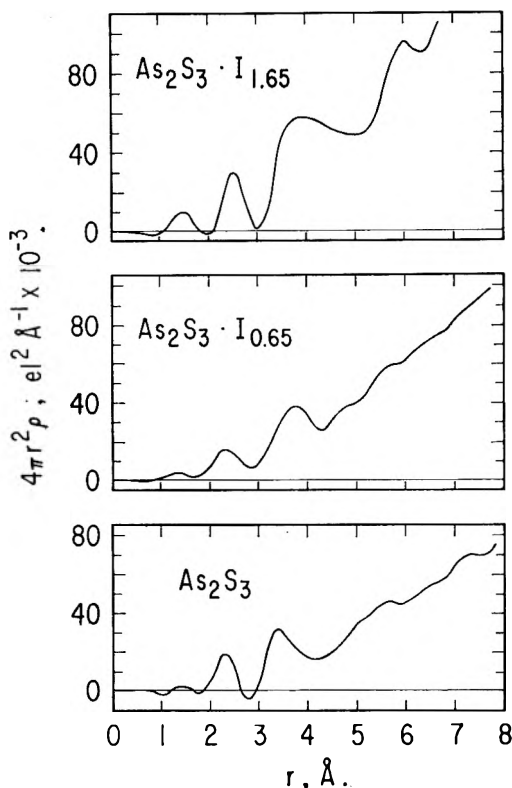


Fig. 2.—Radial distribution curves.

these two distances the average S-As-S and As-S-As bond angle is calculated to be  $99^\circ$ . Further-

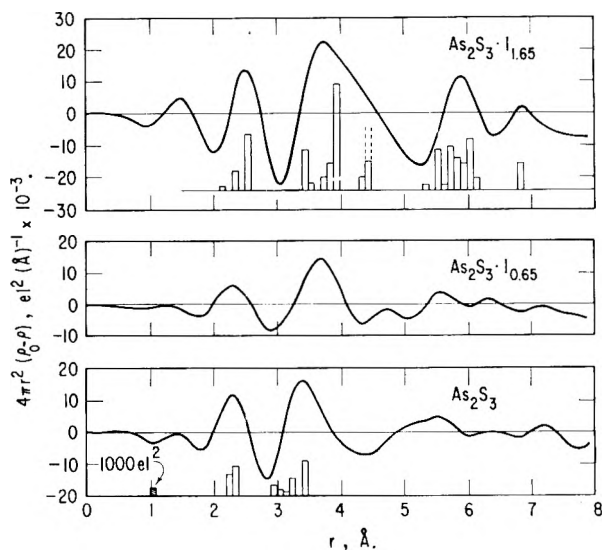


Fig. 3.—Differential radial distribution curves. Bars represent calculated interatomic interaction parameters.

more, from the area of the 2.3 Å peak in the radial distribution curve (Fig. 3), as obtained by integration, the number of As-S interactions was estimated to be 15. Assuming coordination numbers of 3 and 2 for As and S, respectively, twelve interactions would have been expected for the  $\text{As}_2\text{S}_3$  unit. Considering the limited precision of this study and of the technique in general, the agreement is acceptable.

A quantitative interpretation of the area of the second maximum is not justified. On one hand, the definition of the peak is poor; on the other hand, van der Waals interactions between related structural elements almost certainly contribute to this peak also. An appreciable number of As-As, As-S, and S-S packing distances in the 3.5 to 4.0 Å range are found in orpiment (crystalline  $\text{As}_2\text{S}_3$ ),<sup>12</sup> the density of which is only 10% higher than that of the glass.

A short-range structural similarity between the glass and orpiment might be expected. In crystalline  $\text{As}_2\text{S}_3$ , the average bond length is 2.3 Å, the bond angles are approximately  $100^\circ$ , and the coordination numbers of As and S are 3 and 2, respectively. The alternating As and S atoms are arranged in non-planar 12-membered rings, forming two-dimensional sheets. An important feature of the structure is a vector of 4.22 Å between atoms in the ring representing one of the repeat distances of the crystal lattice. The poor resolution of the differential radial distribution shows that order in the glass barely extends beyond the structural unit  $\text{As}_2\text{S}_3$ . Thus, if one assumes that the ring structure of orpiment is present also in the glass,

(12) N. Morimoto, *Mineral. J.* (Sapporo), **1**, 160 (1954), (in English). A number of the observed arsenic-to-arsenic and arsenic-to-sulfur packing distances reported in orpiment are shorter than those corresponding to the sum of the van der Waals radii of sulfur (1.9 Å) and arsenic (about 2.0 Å). However the value for arsenic, which lies close to the radius estimated for the  $\text{As}^{3+}$  ion, is much more appropriate for an arsenic atom bound to hydrogen or carbon than for one bound to oxygen or sulfur. The van der Waals radius for arsenic involved in an As-O or As-S bond (and therefore bearing a partial positive charge) doubtless should be smaller, but it is difficult to say how much smaller.



the rings must adopt a wide range of conformations. Such disorder is in accord with the absence of a maximum of 4.22 Å. in the distribution and with the very small density variation at  $r$  values above 5 Å. A weak maximum at 4.2 Å. is present in the data reported by Petz and co-workers<sup>4</sup>; apparently, their sample retained an additional vestige of orpiment-like order that was not present in our material.

**The Iodine-containing Glass.**—Elemental iodine added to arsenic trisulfide during preparation of the glass is consumed chemically. Very thin layers of the resulting glass do not exhibit the violet color characteristic of molecular iodine, and the radial distribution curve of this glass shows no maximum or shoulder at 2.66 Å., the internuclear distance in molecular iodine. Moreover, as the glass becomes richer in iodine, the 2.3 Å. maximum shifts to 2.45 Å., indicating that some As-S bonds have broken and that As-I bonds have been formed. Our data do not exclude the formation of S-I bonds<sup>13</sup> but because of the low stability of such bonds<sup>13</sup> we assume that they are not present in significant number. If the trivalency of arsenic is maintained, each As-I bond formed releases a sulfur atom having only one bond, almost certainly a thyl radical. Such monovalent sulfur atoms would not be expected to survive as such under conditions of glass preparation, where atomic mobility is high; they instead would undergo coupling to form disulfide linkages. Each two As-I bonds formed thus should result in the formation of one S-S bond, but the S-S interaction, between the two lightest atoms in the ternary systems, would not be expected to appear as a resolved peak in the radial distribution curves.

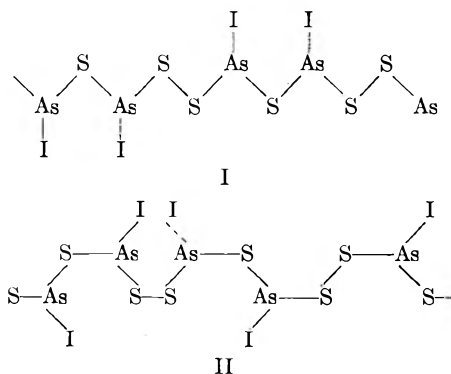
The introduction of monovalent iodine atoms into an array of divalent sulfurs and trivalent arsenics necessarily reduces the average number of bonds per atom in the system and thus lowers the average molecular complexity. The observed decreases in viscosity and softening point reflect this trend; in the glass having 46% iodine by weight (softening point below 60°), very nearly all of the sheets comprising the iodine-free glass have been broken. We have interpreted the radial distribution curves of the iodine-containing glass on the basis of a chain structure, although our data do not preclude the formation of rings containing four or more arsenic atoms. However, such rings would contain ten or more members, and the general difficulty in closing such macro rings in concentrated non-crystalline systems makes the presence of such rings in substantial numbers unlikely.

An iodine content of 46 weight % corresponds to  $\text{As}_2\text{S}_3 \cdot 5/6\text{I}_2$ , or approximately to a 1:1 ratio. Consumption of all added iodine would yield roughly equal numbers of disulfide and monosulfide linkages. Discussion of the structure may be simplified further here by assuming that no arsenic atom is bound to more than one iodine (although a few  $-\text{AsI}_2$  groups may be present, necessarily at

(13) Compounds having the covalent S-I bonds are exceedingly rare. Moreover, sulfur appears to form no binary compounds with iodine under ordinary conditions. (See for example, A. Jakovin and P. A. Archangelski, *Z. anorg. u. allgem. Chem.*, **226**, 350 (1936).)

the ends of chains). Bond lengths chosen are the "standard" values (S-S, 2.08 Å.; As-S, 2.28 Å.; As-I, 2.56 Å.), and the S-As-S and As-S-As bond angles are taken as 100°, in analogy with the angles in orpiment,<sup>11</sup> (some of which lie near 96°, with the others near 103°). Each As-I bond is assumed to make a maximum angle of 120° with the adjoining S-As-S plane, the iodine atom being equidistant from the two sulfurs. This allows a "coordination position" for the one pair of unshared electrons on each arsenic atom.<sup>14</sup>

Neither of the two extreme conformations, shown below, for structures having planar chains is satisfactory. The "all-trans" conformation, I, should result in a pattern having maxima at approxi-



mately 2.3, 3.4, 5.3, and 6.9 Å., corresponding, respectively, to 1,2-, 1,3-, 1,4-, and 1,5-interatomic interactions in the chain. The 2.3 and 6.9 Å. maxima are observed, and the 3.4 Å. maximum conceivably could be included in the large "hill" between 3.3 and 4.8 Å., but there is a minimum observed very near 5.3 Å. In the "cis conformation", II, which is actually an alternation of *cis*- and *trans*-arrangements, the base of each trapezoid in the pattern, corresponding to half of the non-bonded 1,4-interactions in the chain, is only 3.1 Å. This is far less than the sum of the corresponding van der Waals radii; moreover, the radial distribution curve shows a minimum near 3.1 Å. Similar objections apply to other, less regular, planar conformations having both *cis* and *trans* structural units, and also to small ring systems, which consist principally of (slightly distorted) *cis* units.<sup>15</sup>

A twisted chain is much more likely. Because of the very approximate nature of our study, an accurate estimate of the extent of "twist" is not possible, but our data would fit a twist of about 90° at each atom in the chain, *i.e.*, a structure in which the arsenic and sulfur atoms lie on a series of dihedral angles of about 90°, the vertices of which are the bonds constituting the chain. As shown in Fig. 4, this results in a chain in which each bond is nearly parallel to the bond thrice-removed; these

(14) See, for example, R. J. Gillespie and R. S. Nyholm, *Quart. Revs. (London)*, **11**, 368 (1957).

(15) In this discussion, molecular chains are shown with alternating monosulfide and disulfide linkages. This exaggerates the regularity of the structure, since the two types of linkage would be expected to be distributed at random within the chain. In this way, however, all possible intrachain interactions of less than 7.5 Å., except a 1,5-As-As interaction, are considered. This interaction is later incorporated into the semiquantitative treatment with a statistical weight of 1/2.

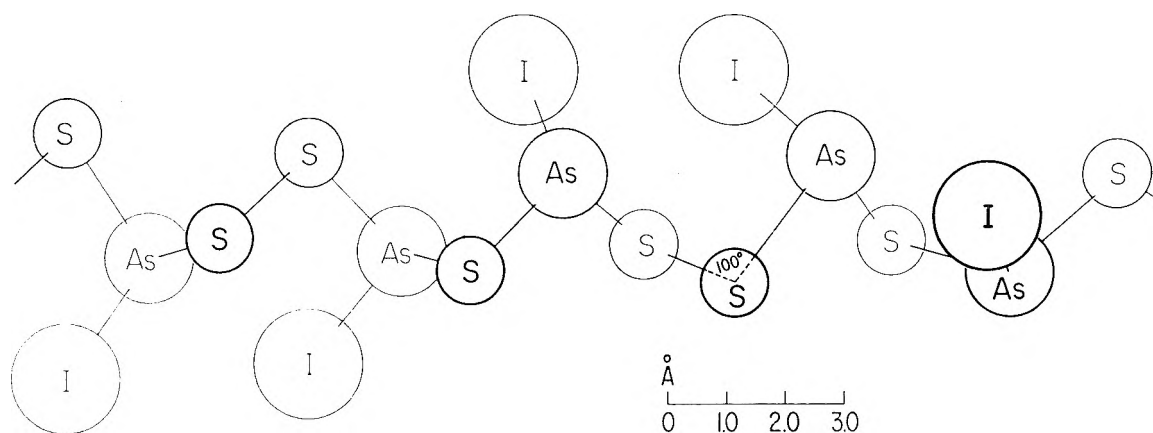


Fig. 4.—Twisted chain structure proposed for arsenic sulfide-iodine glass.

bonds would be truly parallel if the interbond angles, as well as the dihedral angles, were  $90^\circ$ .

In the bottom section of Fig. 3, the differential radial distribution function for the iodine-rich glass is compared with the calculated interatomic interaction parameters (bars). The weight of the interaction between each pair of atoms is assumed to be proportional to the product of the atomic numbers; interatomic distances are estimated by measurement of scale models. (Calculated values only up to 7.0 Å. are included, since limitations in our data and the long range random character of the glass make such comparisons much less meaningful at high interatomic distances.) The first real peak, near 2.45 Å., corresponds to bonded distances, about 2/3 of the weight due to the As-I bonds (2.6 Å.) and about 1/3 to the As-S bonds (2.3 Å.). Many interactions contribute to the second (very broad) peak with a maximum near 3.8 Å. Important contributions arise from the 1,3-iodine-sulfur interactions (3.5 Å.), from arsenic atoms separated by a single sulfur (3.4 Å.), from arsenic atoms separated by a disulfide linkage (4.4 Å.), and from iodine atoms separated by an -As-S-S-As- chain (3.9 Å.).<sup>16</sup> Iodine-iodine van der Waals' contacts between chains (about 4.4 Å.) contribute to this peak also; the latter interaction is indicated with dashed lines, for without knowledge of the mode of packing of chains, the number of such contacts cannot be reasonably predicted. The shape of

(16) This value is significantly less than 4.4 Å., twice the van der Waals radius of iodine. However the iodine-iodine vector in this case makes an angle of only about  $90^\circ$  with the As-I bonds, and non-bonded contact in this direction may be considerably less than the sum of the van der Waals radii. See, for example, L. Pauling, "The Nature of the Chemical Bond," 3rd Edition, Cornell University Press, Ithaca, N. Y., 1960, p. 264.

the curve, however, suggests between one and two (certainly no more than two) interchain iodine-iodine contacts per  $\text{As}_2\text{S}_3\text{I}_2$  unit, corresponding to a very loose packing of chains.

The third peak, having a maximum near 5.0 Å., represents not only the totality of 1,5-interactions in the chain (5.7 Å.), but also the interactions of "trans" iodine atoms (6.1 Å.) separated by -As-S-As- linkages, and a number of additional non-bonded arsenic-iodine interactions (5.5 and 5.9 Å.). The small peak near 6.8 Å., if it is not an artifact, may represent interaction between an arsenic and an iodine separated by a chain of the type -S-As-S-S-As- (6.8 Å.). Thus, within the limits studied, there seems to be no serious inconsistency between our radial distribution curve and the "twisted chain" model proposed for this glass. However, a structure containing large rings, although chemically unlikely, would have much the same short-range order as the chain and should show much the same radial distribution curve.

A detailed analysis of the differential radial distribution function for the low-iodine glass (25% by weight iodine) was not undertaken. The curve is intermediate in character between that of the iodine-free glass and that of the iodine-rich glass, suggesting that the low-iodine glass has structural elements present in both of the other glasses. The relatively low peaks on the low iodine curve indicate that this glass is less ordered than either of the other two glasses, and that a structural analysis would be more formidable.

**Acknowledgment.**—It is a pleasure to acknowledge the assistance of Dr. Maurice Huggins for a number of valuable suggestions during the course of this work.

# THE LIQUID TEMPERATURE RANGE, DENSITY, AND CRITICAL CONSTANTS OF MAGNESIUM<sup>1</sup>

By P. J. MCGONIGAL,<sup>2</sup> A. D. KIRSHENBAUM, AND A. V. GROSSE

Research Institute of Temple University, Philadelphia 44, Pennsylvania

Received November 13, 1961

The density of liquid magnesium was measured over its normal liquid range (923–1390°K.) by the Archimedean method. The dependence of density on temperature is expressed by the linear equation  $D \text{ g./cm.}^3 = 1.834 - 2.647 \times 10^{-4} T \text{ }^\circ\text{K.}$  with a probable error of  $\pm 0.0014 \text{ g./cm.}^3$ . The density of liquid magnesium is  $1.590 \text{ g./cm.}^3$  at its melting point and  $1.466 \text{ g./cm.}^3$  at its boiling point. The volume increase on fusion is 2.96% of the liquid volume. The estimated critical constants of magnesium are:  $T_c = 3850 \pm 400^\circ\text{K.}$ ,  $P_c = 1730 (+800 \text{ or } -700) \text{ atm.}$ ,  $V_c = 59 \pm 8.0 \text{ cm.}^3$ , and  $D_c = 0.41 \pm 0.05 \text{ g./cm.}^3$ . Density values and the temperature coefficient obtained experimentally are in reasonable agreement with those predicted on the basis of an average reduced temperature *vs.* reduced density diagram constructed from data on six metals.

## Introduction

It has been shown<sup>3,4</sup> that the critical temperature of a metal can be estimated from its entropy of vaporization, use of the reduced temperature *vs.* entropy of vaporization curve for mercury (the only metal whose critical temperature has been experimentally determined<sup>5</sup>), and application of the law of rectilinear diameter and the theorem of corresponding states. According to this theorem a metal having a given entropy of vaporization should be at the same reduced temperature as mercury when mercury has that entropy of vaporization. In this work 30,750 cal./g. atom was used as the heat of vaporization at the normal boiling point of 1390°K.<sup>6</sup> The entropy of vaporization then is 22.1 cal./g. atom-deg., which corresponds to a reduced temperature of 0.36 on the entropy of vaporization *vs.* reduced temperature curve of mercury. The critical temperature calculated by this method is  $3850 \pm 400^\circ\text{K.}$  The error is arbitrarily estimated as  $\pm 10\%$ .

Published data on the density of liquid magnesium, as seen in Fig. 1, show considerable disagreement. Reported temperature coefficients vary from  $-0.8 \times 10^{-4}$  to  $-18.1 \times 10^{-4} \text{ g./cm.}^3 \text{ deg.}$  Density data presented in the Liquid Metals Handbook,<sup>7</sup> after critical evaluation of all published data, give  $-10.4 \times 10^{-4}$ , over the range 924 to 1023°K., as the best value. This temperature coefficient differs markedly from the value  $-3.0 \times 10^{-4} \text{ g./cm.}^3 \text{ deg.}$ , which was predicted on a semi-empirical basis utilizing the average reduced temperature *vs.* reduced density curve, constructed from the most reliable density data on mercury,<sup>8,9</sup>

bismuth,<sup>10</sup> lead,<sup>11</sup> silver,<sup>12</sup> gallium,<sup>13</sup> and tin.<sup>14</sup> Except for mercury ideal gas vapor pressures were used in construction of the vapor branch. This curve is shown in Fig. 2. Use of the average of the reported values for the density at the melting point,  $1.587 \text{ g./cm.}^3$ , led to predicted density values of  $1.447 \text{ g./cm.}^3$  at the boiling point and  $0.36 \text{ g./cm.}^3$  at the critical point. Values of 1.466 and  $0.41 \text{ g./cm.}^3$ , respectively, were obtained from the experimental data for magnesium.

## Experimental Procedure

The liquid magnesium was contained under an argon atmosphere in a low-carbon steel tube which was positioned in a bath of liquid lead. The lead was agitated to ensure uniform temperature distribution. Heating was accomplished by means of a furnace with a Nichrome V winding on an aluminum core.

A specially adapted analytical balance was used to determine the apparent decrease in weight of a low-carbon steel float which had a volume of approximately  $13 \text{ cm.}^3$  at room temperature. The exact volume of each float used was determined by calibration in absolute ethanol. The volume of the float was corrected for thermal expansion.<sup>15</sup> Surface tension corrections for the thin iron wire that supported the float were made using the data of Girov.<sup>16</sup> Extrapolation of these data gave values of 571 dynes/cm. at the melting point and 439 dynes/cm. at the normal boiling point. In no case did the surface tension correction amount to more than 0.5% of the total weight loss. Surface tension values of 355 dynes/cm. at the melting point and 300 dynes/cm. at the boiling point were calculated from a general empirical relationship between the surface energy and the critical temperature of a metal, as developed recently.<sup>17</sup> The published experimental values of the surface tension were considered more accurate for use in making the corrections. Since the density determinations were made in a steel apparatus it was necessary to correct for the amount of dissolved iron. The corrections were made on a weight basis using the values of Fahrenhorst and Bulian<sup>18</sup> for the solubility of iron in liquid magnesium. Several samples taken during the experiments and analyzed for iron content were in agreement with the published values. The solubility of iron in liquid magnesium is 0.035–0.040% at 973°K.

(1) This work was supported by the National Science Foundation under Grant 15540.

(2) A report of this work will constitute a portion of a dissertation to be submitted by P. J. McGonigal to the Graduate Council of Temple University in partial fulfillment of the requirements for the degree of Doctor of Philosophy.

(3) A. V. Grosse, "The Liquid Range of Metals and Some of their Physical Properties at High Temperatures," Research Institute of Temple University, September 5, 1960.

(4) A. V. Grosse, *J. Inorg. & Nuclear Chem.*, **22**, 23 (1961).

(5) F. Birch, *Phys. Rev.*, **41**, 641 (1932).

(6) D. R. Stull and G. C. Sinke, "Thermodynamic Properties of the Elements," American Chemical Society, Advances in Chemistry Series, Vol. 18, 1956.

(7) "Liquid Metals Handbook," 2nd Ed., R. N. Lyon, Editor-in-chief, Sponsored by the Committee on Basic Properties of Liquid Metals, Office of Naval Research, Department of the Navy, in Collaboration with the Atomic Energy Commission and the Bureau of Ships, Department of the Navy, Washington, D. C., June, 1952, NAVEXOS P-733 (Rev.).

(8) J. Bender, *Physik. Z.*, **16**, 246 (1915).

(9) J. Bender, *ibid.*, **19**, 410 (1918).

(10) A. D. Kirshenbaum, Final Report on High Temperature Inorganic Chemistry to the National Science Foundation, Research Grant NSF-G 15540, October, 1961.

(11) A. D. Kirshenbaum, J. A. Cahill, and A. V. Grosse, *J. Inorg. & Nuclear Chem.*, **22**, 33 (1961).

(12) A. D. Kirshenbaum, J. A. Cahill, and A. V. Grosse, *ibid.*, in press, 1962.

(13) W. H. Hothar, *Proc. Phys. Soc. (London)*, **48**, 699 (1936).

(14) A. L. Day, R. B. Sosman, and J. C. Hostetter, *Am. J. Sci.*, **37**, 1 (1914).

(15) G. Tammann and G. Bandel, *Archiv Eisenhuettenw.*, **7**, 571 (1934).

(16) V. G. Girov, *Trans. Aluminum-Magnesium Inst. (Russian)*, **14**, 99 (1937).

(17) A. V. Grosse, *J. Inorg. & Nuclear Chem.*, in press, 1962.

(18) E. Fahrenhorst and E. Bulian, *Z. Metallk.*, **33**, 31 (1941).

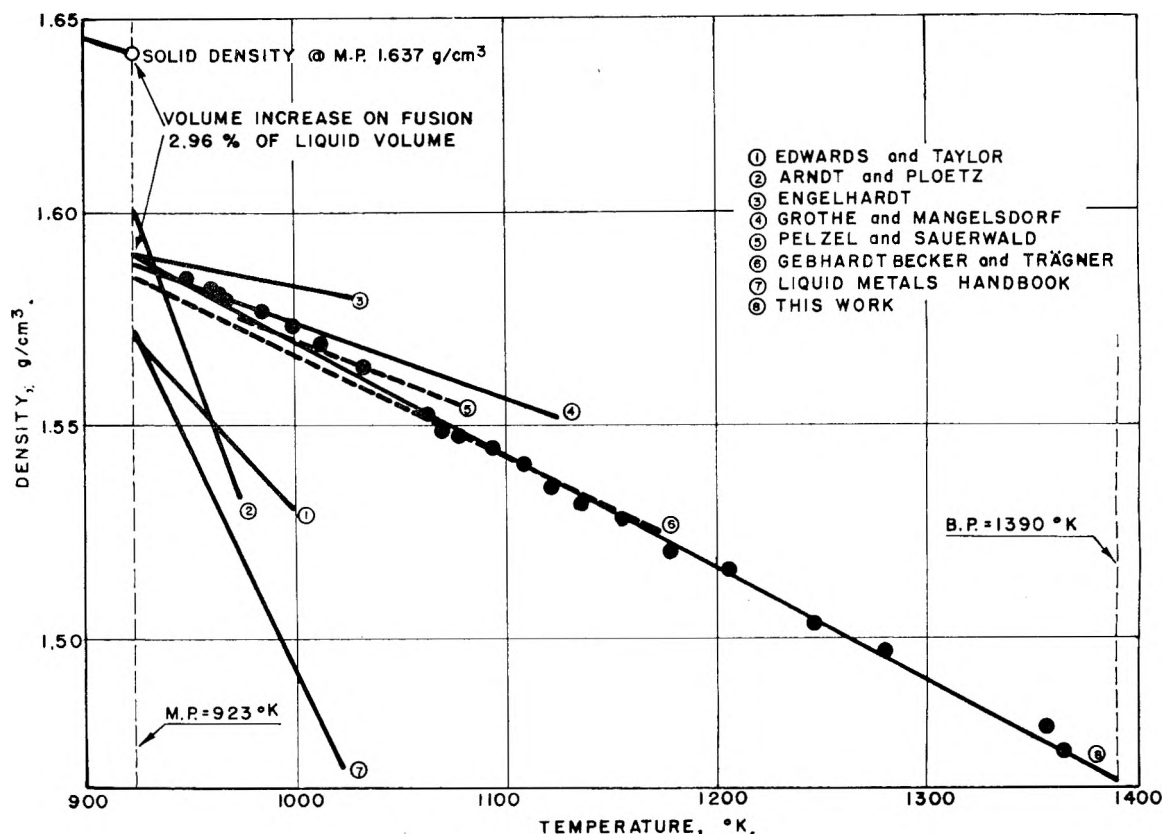


Fig. 1.—Density of liquid magnesium.

and 0.560% at 1373°K. The largest correction was 2.25% (at 1365°K.) of the corrected density. Temperature measurement was accomplished by means of a calibrated Chromel-Alumel thermocouple. The thermocouple was sheathed in a steel tube with a closed end inserted directly into the liquid magnesium.

The magnesium used in this work was supplied by A. D. Mackay, Inc., and had a stated purity of 99.95%. An analysis supplied with the metal listed impurities in p.p.m. as follows: Zn 100; Mn, Fe, Ni, each 50; Al 40; Pb, C, Si, each 30; Au 10.

The oxide coating on the magnesium was carefully removed before use.

### Results

Density determinations were made over essentially the whole normal liquid range of magnesium. Least squares treatment of the experimental data gave the linear relationship

$$D \text{ g./cm.}^3 = 1.834 - 2.647 \times 10^{-4} T \text{ } ^\circ\text{K.}$$

The probable error is  $\pm 0.0014 \text{ g./cm.}^3$ . Figure 1 is a plot of our experimental data corrected for expansion of the float, iron solubility, and surface tension. For purposes of comparison the results of other investigators<sup>19-24</sup> also are shown.

Smoothed densities, atomic volumes, specific volumes, and coefficients of cubical expansion are listed in Table I.

The volume change on fusion is 2.96% of the liquid volume based on this work, the X-ray data

(19) J. D. Edwards and C. S. Taylor, *Trans. Am. Inst. Mining Met. Engrs.*, **69**, 1070 (1923).

(20) K. Arndt and G. Ploetz, *Z. physik. Chem.*, **130**, 184 (1927).

(21) Engelhardt, *Handbuch der techn. Elektrochem.*, **3**, 178 (1934).

(22) H. Grothe and C. Mangelsdorf, *Z. Metallk.*, **29**, 352 (1937).

(23) E. Pelzel and F. Sauerwald, *ibid.*, **33**, 229 (1941).

(24) E. Gebhardt, M. Becker, and E. Trägner, *ibid.*, **46**, 90 (1955).

TABLE I

DENSITY, ATOMIC VOLUME, SPECIFIC VOLUME, AND COEFFICIENT OF CUBICAL EXPANSION OF LIQUID MAGNESIUM

Temp., °K.	Density, g./cm. <sup>3</sup>	Atomic volume, cm. <sup>3</sup> /g. atom	Specific volume, cm. <sup>3</sup> /g.	Coefficient of cubical expansion $\times 10^6$ (°K. <sup>-1</sup> )
923 m.p.	1.590	15.30	0.6289	166.5
950	1.583	15.36	.6317	167.2
1000	1.569	15.50	.6373	168.7
1050	1.556	15.63	.6427	170.1
1100	1.543	15.76	.6481	171.5
1150	1.530	15.90	.6536	173.0
1200	1.516	16.04	.6596	174.6
1250	1.503	16.18	.6653	176.1
1300	1.490	16.32	.6711	177.6
1350	1.477	16.46	.6770	179.2
1390 b.p.	1.466	16.59	.6821	180.6

TABLE II

CALCULATED LIQUID AND VAPOR DENSITIES OF MAGNESIUM ABOVE ITS NORMAL BOILING POINT

T, °K.	Liq. D, g./cm. <sup>3</sup>	Vap. D, g./cm. <sup>3</sup>
1500	1.438	0.0005
2000	1.300	.0052
2500	1.151	.0208
3000	0.989	.0514
3500	0.815	.0932

reported by Foote and Jette,<sup>25</sup> and the solid density data of Pelzel and Sauerwald.<sup>23</sup>

On the basis of our experimental results and the estimated value of  $3850 \pm 400^\circ\text{K.}$  for the critical temperature, the critical density and critical

(25) F. Foote and E. R. Jette, *Phys. Rev.*, **58**, 81 (1940).

TABLE III  
LITERATURE DATA ON THE DENSITY OF LIQUID MAGNESIUM

Lit. ref.	Authors	Year	Temp. range, °K.	Density g./cm. <sup>3</sup> m.p.	$\frac{-dD}{dT} \times 10^4$	Method
19	Edwards and Taylor	1923	923-973	1.572	5.5	Pycnometric
20	Arndt and Ploetz	1927	923-1023	1.601	18.1	Archimedean
21	Not given, reported by Engelhardt	1934	923-1023	1.590	0.8	.....
22	Grothe and Mangelsdorf	1937	953-1123	1.588	1.8	Archimedean
23	Pelzel and Sauerwald	1941	973-1073	1.585	2.00	Archimedean
7	Liquid Metals Handbook	1952	924-1023	1.573	10.4	Summary and crit. eval. of prev. data
24	Gebhardt, Becker, and Trägner	1955	973-1173	1.585	2.40	.....
	This work	1961	923-1390	1.590	2.647	Archimedean

atomic volume were estimated by application of the law of rectilinear diameters, *i.e.*, the critical density lies on the line whose algebraic equation is one-half that of the liquid density *vs.* temperature line.

The critical density and critical atomic volume of magnesium are estimated to be  $0.41 \pm 0.05$  g./cm.<sup>3</sup> and  $59 \pm 8.0$  cm.<sup>3</sup>, respectively, based on our experimental liquid density data. The critical pressure was obtained by extrapolation of ideal gas vapor pressure data<sup>5</sup> and is 1730 (+800 or -700) atm. The errors in the critical density, critical atomic volume, and critical pressure are based on the estimated error in the critical temperature.

Figure 3 shows the complete liquid range diagram of magnesium. The liquid density curve was constructed by subtracting the vapor density at a given temperature from the liquid density given by extrapolation of the experimentally obtained straight line.

Table II shows calculated liquid and vapor densities from 1500 to 3500°K.

**Comparison with Literature Data.**—A comparison of the reported density data in liquid magnesium is shown in Table III and Fig. 1. The disagreement in the *extreme* values of the temperature coefficient is striking. The data of Grothe and Mangelsdorf,<sup>22</sup> Pelzel and Sauerwald,<sup>23</sup> and Gebhardt, Becker, and Trägner<sup>24</sup> are in reasonable agreement with each other and with this work. The data of Edwards and Taylor,<sup>19</sup> Arndt and Ploetz,<sup>20</sup> and those reported by Engelhardt<sup>21</sup> are in definite disagreement.

The low values of Edwards and Taylor as obtained over a short temperature range may possibly be explained on the basis of gas bubbles trapped in their pycnometer. Arndt and Ploetz used a float whose volume was less than one-half cm.<sup>3</sup>; thus, errors in weighing would be relatively large in view of the small apparent decrease in weight. Also, the temperature range over which Arndt and Ploetz made measurements is small. The source of the data reported by Engelhardt is not given. Again, the temperature range is small.

The error in the temperature coefficient depends to a large extent on the temperature range investigated. In this work values were obtained over

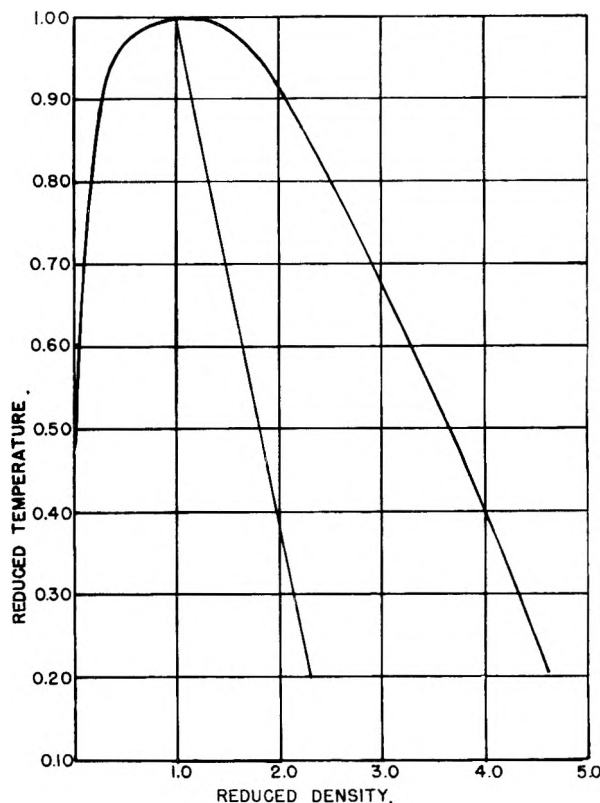


Fig. 2.—Reduced density *vs.* reduced temperature-average curve for Hg, Bi, Ag, Pb, Sn, Ga.

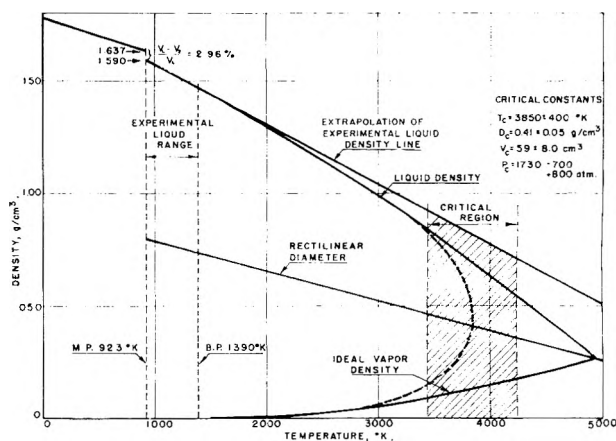


Fig. 3.—The liquid range diagram for magnesium.

essentially the entire normal liquid range (467°) compared with a previous maximum range of 200°.

**Acknowledgment.**—The financial support of

the National Science Foundation is gratefully acknowledged. We thank Mr. J. A. Cahill for his assistance and encouragement and Mrs. Lucia Streng for performing the iron analyses.

## EFFECT OF PROGRESSIVE FLUORINATION OF A FATTY ACID ON THE WETTABILITY OF ITS ADSORBED MONOLAYER

BY E. G. SHAFRIN AND W. A. ZISMAN

*Chemistry Division, U. S. Naval Research Laboratory, Washington 25, D. C.*

*Received November 14, 1961*

A study has been made of the wettability of monomolecular films of a series of heptadecanoic acids with substitutions in the 17-position of perfluoroethyl ( $\phi$ -ethyl),  $\phi$ -propyl,  $\phi$ -pentyl, and  $\phi$ -heptyl groups. Films of these segmented acids were prepared by adsorption from the melt on chromium; films of the  $\phi$ -heptyl compound also were prepared on platinum, nickel, quartz, and soda-lime glass. Films adsorbed on metal substrates exhibited uniformly high contact angles; those on siliceous surfaces were more wettable and more vulnerable to attack by sessile drops of hydrogen-bonding liquids. There was little difference in wettability between the longest terminally fluorinated aliphatic acid and a fully fluorinated acid containing the same perfluoroalkyl moiety ( $\phi$ -octanoic acid, reported previously). Acids with terminal fluorocarbon segments shorter than  $\phi$ -heptyl were more wettable than the analogous fully fluorinated acids. This and the differences in the effects of homology for the two types of acids are discussed in terms of the configuration and orientation of the adsorbed molecules. Models are proposed which take into account the effect of differences in size and van der Waals forces of fluorocarbon and hydrocarbon chains, the steric hindrance to intramolecular bending, and the repulsive effects of uncompensated dipoles at the junction of the  $-\text{CH}_2-$  and  $-\text{CF}_2-$  chains. Future experiments are proposed to confirm the structure of these models.

### Introduction

Previous investigations at this Laboratory have revealed that regular and predictable changes in the contact angles of liquids result from changes in the chemical structure and physical packing of the outermost atoms or atomic groupings in the solid surface being wetted.<sup>1,2</sup> Least wettable of the surfaces studied were those containing the highest concentration and closest packing of perfluoromethyl groups in the exposed surface.<sup>3-6</sup>

Trifluorination of the omega-carbon atom on a long-chain fatty acid or amine was proposed<sup>7</sup> as a way of combining the desirable properties of limited wettability associated with a  $\text{CF}_3$ -rich surface, the closeness of molecular packing resulting from the strong intermolecular cohesive forces between adjacent aliphatic hydrocarbon chains, and the potentially lower cost of compounds having a low degree of fluorination. Although a solid coated with such a film proved less wettable than one covered with a film of stearic acid, it was more wettable than one coated with a film of the perfluorinated fatty acid.<sup>4</sup> The difference in wetting behavior was attributed to the presence of the strong dipole in the  $\text{CF}_3-\text{CH}_2-$  linkage; whereas in the fully fluorinated compounds there is internal compensation between the dipole moment contributions of the  $-\text{CF}_3$  group and its neighboring  $-\text{CF}_2-$  groups in the chain, in the trifluoromethyl-substituted acid the moment of the  $-\text{CF}_3$  dipole is not

compensated by the adjacent  $-\text{CH}_2-$  dipoles of the chain. The resultant uncompensated and strong dipole is located in the outermost portion of the adsorbed monolayer. Since the external electrostatic field of force of the dipole varies as the inverse fourth power of the distance, there results an additional attraction for the molecules of the wetting liquid; hence the surface is made more wettable than one coated by the perfluoro fatty acid. Measurements of the mechanical and electrical properties of such a substance, when spread on water as an insoluble monolayer, were found by Fox<sup>8</sup> to be in accord with the above concept.

Replacing the  $\omega$ -perfluoromethyl group by an  $\omega$ -perfluoroethyl,  $\omega$ -perfluoropropyl, or other  $\omega$ -perfluoroalkyl segment removes the electric center of gravity of the uncompensated dipole further from the exterior surface of the adsorbed monolayer; hence, the longer the perfluoroalkyl group, the smaller should be the effect of the dipole on the wetting behavior of a liquid resting on the outermost surface of the adsorbed monolayer. Providing there are no repulsive forces between neighboring uncompensated dipoles within the monomolecular layer strong enough to seriously interfere with obtaining close packing of the adsorbed molecules, the monolayer then should exhibit the same wetting properties as an equally condensed film of a perfluoroalkanoic acid of the same chain length.

A suitable series of fluorinated heptadecanoic acids has been synthesized recently at the Jackson Laboratory of the E. I. du Pont de Nemours and Company by N. O. Brace and co-workers<sup>9</sup> with the perfluoroheptyl group the longest terminal perfluorocarbon moiety. Pure specimens of these

(1) W. A. Zisman, "Relation of Chemical Constitution to the Wetting and Spreading of Liquids on Solids" in "A Decade of Basic and Applied Science in the Navy," Office of Naval Research, published by the U. S. Government Printing Office, Washington, D. C., 1957.

(2) E. G. Shafrin and W. A. Zisman, *J. Phys. Chem.*, **64**, 519 (1960).

(3) F. Sehulman and W. A. Zisman, *J. Colloid Sci.*, **7**, 465 (1952).

(4) E. F. Hare, E. G. Shafrin, and W. A. Zisman, *J. Phys. Chem.*, **58**, 236 (1954).

(5) M. K. Bennett and W. A. Zisman, *ibid.*, **64**, 1292 (1960).

(6) M. K. Bennett and W. A. Zisman, *ibid.*, **65**, 2266 (1961).

(7) E. G. Shafrin and W. A. Zisman, *ibid.*, **61**, 1046 (1957).

(8) H. W. Fox, *ibid.*, **61**, 1058 (1957).

(9) N. O. Brace, "Long-Chain Alkanoic and Alkenoic Acids with Perfluoroalkyl Terminal Segments," presented at the Symposium on Advances in Fluorine Chemistry, American Chemical Society Meeting, Chicago, Ill., Sept. 3, 1961.

interesting new compounds, which will be designated hereafter as the homologous series of 17-( $\phi$ -alkyl)-heptadecanoic acids, were generously donated by the Organic Chemicals Department, du Pont Company. This report is concerned with the monolayer adsorption on five types of smooth, hard, high-energy solids and the resulting changes in wetting properties of films of the terminally fluorinated, straight-chain alkanolic acids.

**Experimental Materials and Methods.**—All of the compounds studied were highly purified, white, crystalline solids with the reported melting points<sup>9</sup> indicated below; these materials were used as received.

17-(perfluoroethyl)-heptadecanoic acid	m.p. 70–71°
17-(perfluoropropyl)-heptadecanoic acid	73–74.5
17-(perfluoropentyl)-heptadecanoic acid	77–79
17-(perfluoroheptyl)-heptadecanoic acid	91–92

Adsorption experiments were conducted on both metal and non-metal solid substrates. The metals used were: chromium (99% or better purity; major contaminants, manganese and silicon, by spectrographic analysis); nickel (99% or better purity; major contaminant, cobalt, by spectrographic analysis); and high purity platinum. A mirror finish was imparted to the surfaces of these bulk metals by standard metallographic procedures. Prior to each adsorption experiment, the metal specimen was made grease-free by washing with "Tide" solution and polishing metallographically on a grease-free cloth wheel impregnated with 0.3  $\mu$   $\alpha$ -Al<sub>2</sub>O<sub>3</sub> abrasive (Linco Fine Abrasive A-5175) suspended in distilled water. Excess abrasive was removed by touching the metal briefly to a rotating cloth wheel which continuously was being flushed with distilled water. Following flushing of the metal surface with hot distilled water and with triply distilled water, the water-wetted specimen was dried in a grease-free stainless steel oven for 10 min. at 120° and then allowed to cool to the appropriate temperature in an acid-cleaned, covered, glass container. The non-metals used were: soft flint, soda-lime, glass slides ("Gold Seal" brand); and clear, polished, high purity, fused quartz slides (from Amersil Quartz Division of Engelhard Industries, Inc.). The fresh slides were cleaned with a soft camels hair brush in an aqueous solution of the detergent "Tide," then flushed with hot distilled water and triply distilled water. The conditions of oven drying and subsequent cooling used were identical with those used for the metal surfaces; temperatures higher than 120° or more prolonged baking had to be avoided in order to prevent extensive dehydration of the glass surface.<sup>10</sup>

Monomolecular adsorbed films were prepared by the melt method<sup>11</sup> by repeatedly rolling a non-spreading drop of the pure molten compound over the solid surface which was maintained at a temperature just a few degrees above the melting point of the compound. After the liquid had been in contact with the hot adsorbing surface for a given period (10 min., unless otherwise specified), the drop of surplus acid was gently removed from the surface with a flamed platinum wire and the specimen was cooled to 20°. The 17-( $\phi$ -alkyl)-heptadecanoic acids prove particularly amenable to monolayer formation by the melt method because: their melting points are well below their decomposition temperatures; their vapor pressures are low at the melting point; and drops of their non-spreading liquid phase exhibit high contact angles on the adsorbed film. The latter property facilitates removal of molten acid in excess of the monolayer, leaving a surface completely free of visible amounts of the liquid phase.

The wettability of the adsorbed film by each liquid reported was measured at 20° by determining the static contact angle  $\theta$  after advancing the drop slowly over the surface. The source, purity, and surface tension of each of the liquids used have been reported previously<sup>2</sup>; each liquid was used in a freshly purified condition. Each contact angle given represents the average of measurements using many different drops on at least three independently prepared solid surfaces.

**Wettability of Monolayers of 17-(Perfluoroheptyl)-heptadecanoic Acid.**—Condensed monolayers of 17-( $\phi$ -heptyl)-heptadecanoic acid were readily formed since retraction of the molten acid was essentially instantaneous and at a high angle of contact on a variety of adsorbing surfaces (Table I). There were no differences in  $\theta$  between films formed by contacting the molten acid with chromium surfaces for periods of 10 min., 60 min., or 17 hr.; unless otherwise stated a contact period of 10 min. was used. Monolayers formed by the retraction method on chromium at temperatures of from 93 to 103° exhibited identical contact angles. A film formed on the same surface at 125° exhibited a slightly decreased contact angle; hence the data presented in Table I are for films formed at temperatures not in excess of 10° of the melting point of the compound.

Monolayers of this acid adsorbed on chromium exhibited a slightly larger variation in  $\theta$  for a given liquid than the  $\pm 1^\circ$  reported in previous studies of adsorbed monolayers of fatty acids or amines.<sup>4,11,12</sup> Built-up drops of methylene iodide showed average deviations in  $\theta$  of  $\pm 2.5^\circ$  for eleven different locations on a single film of 5 cm.<sup>2</sup> area and for eleven different films adsorbed on a single chromium surface; other liquids exhibited similar variations. Comparable variations in  $\theta$  also were observed for films of this acid adsorbed on nickel surfaces.

Table I lists the average values of  $\theta$  arranged in the order of decreasing surface tension ( $\gamma_{LV}$ ) of the wetting liquid. Measurements of  $\theta$  also were made on some liquids which had been saturated with the 17-( $\phi$ -alkyl)-heptadecanoic acid under study prior to contact with the adsorbed monolayer; the latter data are designated by superscripts. The difference in  $\theta$  for the pure and acid-saturated liquids is small for most liquids, indicating that the adsorbed monolayer is not readily desorbed by the sessile drop of the particular liquid under investigation.

Contact angles observed on films of the acid adsorbed on each type of solid surface are compared in the third through the seventh columns of Table I. Since condensed monolayers adsorbed on the three metals proved indistinguishable within the limits of precision of the measurements of  $\theta$ , the data for films adsorbed on chromium will be considered in the remainder of this report as representative of films on the other metal substrates.

Although the monolayers were just as easy to prepare by the retraction method on metallic as on non-metallic surfaces, the measurements of  $\theta$  revealed that the films adsorbed on quartz and soda-lime glass were more wettable than those adsorbed on the metals. The difference in  $\theta$  using the non-hydrogen-bonding liquids was small but was large for each hydrogen-donating liquid.<sup>13</sup> The data in the last column of Table I for films adsorbed on glass show no large differences in  $\theta$  between the pure liquids and the same liquids containing dissolved acid. Therefore the increase in wettability

(10) E. F. Hare and W. A. Zisman, *J. Phys. Chem.*, **59**, 335 (1955).

(11) R. L. Cottington, E. G. Shafrin, and W. A. Zisman, *ibid.*, **62**, 513 (1958).

(12) O. Levine and W. A. Zisman, *ibid.*, **61**, 1068 (1957).

(13) A. H. Ellison, H. W. Fox, and W. A. Zisman, *ibid.*, **57**, 622 (1953).

TABLE I

CONTACT ANGLES OF LIQUIDS ON MONOLAYERS OF 17-(PERFLUOROHEPTYL)-HEPTADECANOIC ACID ADSORBED ON VARIOUS SOLID SURFACES FROM THE MELT AT 95°

(All contact angles at 20°)

Liquid	Liquid surface tension, $\gamma_{LV}$ , dynes/cm. at 20°	Obsd. contact angles against condensed monolayers on:				
		Metals			Non-metals	
		Chromium	Nickel	Platinum	Fused quartz	Soda-lime glass
Water	72.8	115°	118°	118°	>90° → 70°	25-40°(25°)
Glycerol	63.4	107				
Formamide	58.2	105	107		55	20-40
Methylene iodide	50.8	101	101	98	95	85-95(92°)
Ethylene glycol	47.7	98	102		78	35-55
1,2,3-Tribromopropane	45.4	88				
$\alpha$ -Bromonaphthalene	44.6	87				
Tetrachlorobiphenyl	44.2	93		91		
Pentamethylene glycol	43.3	99				
Tricresyl phosphate	40.9	90	93		82	80
Methylene bromide	39.0	80				
<i>t</i> -Butylnaphthalene	33.7	78			77	74(75°)
Dicyclohexyl	32.8	75	77(78°)	77	70	70(70°)
Bis-(2-ethylhexyl) phthalate	31.3	78	82		72	70
Bis-(2-ethylhexyl) sebacate	31.1	78		75		
Pentaerythritol tetracaproate	30.4	77	82		72	70
Squalane	29.5	77	79	77	70	71
Octanol-1	27.8	68				
Hexadecane	27.6	73	74(73°)	73	68	66(67°)
Octanol-2	26.7	68				
Tetradecane	26.7	70	70	68	64(65°)	63
Tridecane	25.9	68	67			
Dodecane	25.4	66(68°)	67(68°)	(66°)	61(61°)	60(61°)
Undecane	24.7	64				
Decane	23.9	64(63°)	64(63°)	62	(58°)	59(58°)
Octane	21.8	57(59°)	58(57°)	(51°)		50(55°)
Heptane	20.3	52				
Perfluoroalkane (FCD-330)	20.2	41	40		38	38
Trimethyl end-blocked silicones						
Heptadecamer	19.9	61				
Octamer	18.8	58				

° Liquid saturated with 17-(perfluoroheptyl)-heptadecanoic acid.

observed cannot be ascribed to any increased ability of the sessile drop to dissolve the films when adsorbed on silica-rich surfaces.

The former slight decreases in  $\theta$  are presumed evidence for the slightly greater separation of the acids adsorbed on silica and glass than on metals. Similar behavior by adsorbed monolayers of the fatty acids<sup>10</sup> has been reported previously and the explanation advanced was that adsorption occurred through hydrogen bonding with water molecules adsorbed on the silica surface at localized adsorption sites which had a greater average separation than the sites on metal surfaces. The explanation is equally applicable if adsorption occurs at Si-O-H groups in the surface.<sup>14</sup>

The large differences in  $\theta$  observed with such hydrogen-bonding liquids as water, glycerol, etc., are evidence of the preferential wetting of the siliceous surface and desorption of the fluorinated monolayer which can occur when the film is not as closely packed as on a metal substrate. For example, an acid monolayer was adsorbed on both a chromium and a glass surface; half of each film was contacted with a large sessile drop of water for 10

min.; after the water had been removed and the surfaces allowed to equilibrate at 50% relative humidity, pairs of measurements of  $\theta$  for selected liquids were made on both halves of each film. The hexadecane contact angles on a film adsorbed on chromium differed by less than ten degrees; on the same film adsorbed on glass,  $\theta$  decreased from 65° to values of from 30 to 50° between the portions of the monolayers which had not or had been exposed to liquid water. The decrease was even larger for *t*-butylnaphthalene, comparable angles being 73° and from 22 to 42°. For all liquids, the sessile drops were more irregular in periphery on the exposed area of the film on glass. Although less pronounced than in the case of glass, some increase in wettability after contact with water was exhibited by the acid monolayer adsorbed on quartz.

In Fig. 1 the cosine of the contact angle ( $\theta$ ) observed on chromium coated with a condensed monolayer of acid is plotted as a function of the surface tension ( $\gamma_{LV}$ ) of the liquid examined. The graph is similar in every respect with that obtained in previous wetting studies of highly fluorinated, low-energy surfaces.<sup>1-7,13</sup> Graphical points for the *n*-alkanes lie along a straight line, the extrapolation of which to the horizontal line  $\cos \theta = 1$  leads

(14) R. K. Iler, "The Colloid Chemistry of Silica and Silicates," Cornell University Press, Ithaca, N. Y., 1955.



to a critical surface tension of wetting  $\gamma_c$  of 8.0 dynes/cm. The datum point for the highly branched, saturated hydrocarbon squalane also lies on this line, while those for *t*-butylnaphthalene and dicyclohexyl lie slightly above it. All of the data points for liquids with surface tensions below 45 to 50 dynes/cm. fall in a narrow band with the silicones lying below the line characteristic of the *n*-alkanes and the halocarbons lying above it. Considerable deviation from this narrow band exists for the liquids above 50 dynes/cm., the observed enhanced wetting being caused by weak hydrogen-bonding interaction with the surface fluorine atoms.<sup>13</sup>

Values of  $\theta$  for various liquids on condensed monolayers of 17-(perfluoroheptyl)-heptadecanoic acid are nearly identical with those reported previously<sup>4</sup> for the fully fluorinated acid containing the same perfluoroheptyl moiety ( $\phi$ -octanoic acid). Despite the use of different adsorption media in preparing the adsorbed film (melt *vs.* dilute solution in decane) and different adsorbing surfaces (chromium *vs.* platinum), plots of the values of  $\theta$  for the alkanes led to virtually identical values of  $\gamma_c$  (8.0 dynes/cm. for the partially fluorinated acid *vs.* 7.9 dynes/cm. for the perfluoro acid). For six miscellaneous liquids, the differences in  $\theta$  ranged from 1 to 7°, the latter occurring for methylene iodide. Condensed films of the two acids cannot be prepared by the same technique since the melt method is not applicable to  $\phi$ -octanoic acid because of its high vapor pressure at the melting point. Nevertheless, the difference in  $\theta$  for methylene iodide appears real, inasmuch as the 94° angle reported for the perfluoro $\phi$ -octanoic acid film on platinum<sup>4</sup> is close to those reported for films of this acid adsorbed on glass from the vapor phase (97°)<sup>12</sup> and on both glass (96°)<sup>12</sup> and stainless steel (92°)<sup>11</sup> from dilute solution in decane. Since the use of a dilute solution of perfluoro $\phi$ -octanoic acid in methylene iodide does not result in an increase in  $\theta$  over that of the pure liquid for films adsorbed on glass or on platinum foil, it must be assumed that the decrease in  $\theta$  does not result from solution of the monolayer in the sessile drop.

The striking agreement in wetting properties of the condensed monolayers of partially and fully fluorinated acids containing a terminal perfluoroheptyl chain demonstrates that the field of force of the dipole located at the junction of the fluoroalkyl group and the alkyl group has been sufficiently removed from the external surface of the monolayer as to have no influence on the adhesion of the liquid. Moreover, the presence of the 16-carbon hydrocarbon chain in the partially fluorinated acid has no effect on the wetting properties and, therefore, no effect on the closeness of packing of the terminal perfluoroheptyl moieties.

**Effects of Homology on Wettability.**—Measurements of  $\theta$  were made on a condensed monolayer of each of the terminally fluorinated heptadecanoic acid derivatives with each acid adsorbed under standardized conditions using the same methods and procedures described above. As in the case of the  $\phi$ -heptyl derivative, variations in  $\theta$  for a given liquid on a single film of each acid were somewhat

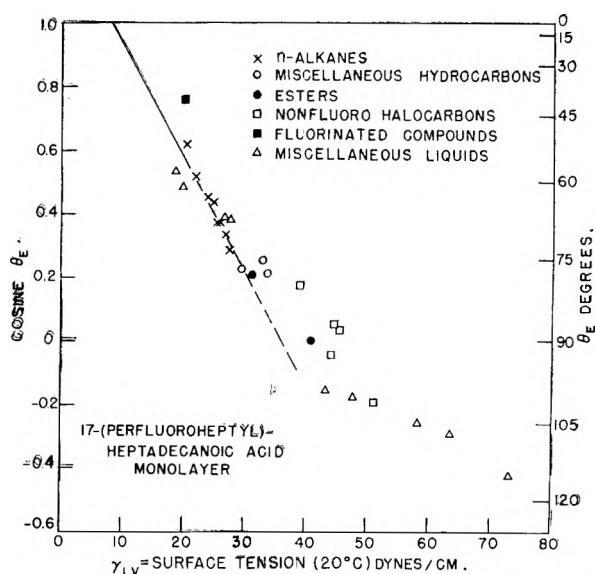


Fig. 1.—The wettability by various liquids of monolayers of 17-(perfluoroheptyl)-heptadecanoic acid adsorbed on chromium by the melt method.

larger than those encountered in previous studies of adsorbed monolayers. The largest variations were observed for films of the  $\phi$ -ethyl derivative. Average deviations of from  $\pm 1$  to  $\pm 2^\circ$  and maximum deviations from  $\pm 3$  to  $\pm 6^\circ$  were common for eleven independent measurements on a single film; an average deviation of  $\pm 3^\circ$  and a maximum deviation of  $\pm 5^\circ$  were obtained for measurements on a single location on the chromium surface coated with eleven independently prepared films of the acid. Unidirectional rubbing of the monolayer neither increased its angle of contact with methylene iodide nor improved its uniformity of wetting, indicating that the variations in wetting were not caused by roughening of the surface as a result of the presence of residual solidified acid in excess of that required for formation of the monolayer. Slight improvement in film uniformity was observed when the period of contact of the molten acid with the metal surface was lengthened to an hour in order to guarantee attainment of adsorption equilibrium, but there was no change in the average value of  $\theta$  observed using methylene iodide or hexadecane. Consequently, as before, contact angles on films formed during a 10-min. adsorption period were considered sufficiently representative of equilibrium films of these compounds.

Results of measurements of  $\theta$  by representative liquids are listed in Table II for chromium coated with a retracted monolayer of each of the partially fluorinated acids. Condensed monolayers of the acid containing the longest fluorinated alkyl group exhibited the largest values of  $\theta$ , and  $\theta$  decreased as the length of the perfluorocarbon moiety decreased; however,  $\theta$  for the  $\phi$ -propyl and  $\phi$ -ethyl-substituted derivatives were nearly indistinguishable.

Wetting by *n*-alkanes and by selected miscellaneous liquids is affected by homology in the adsorbed acid, as shown in Fig. 2A and 2B where  $\cos \theta$  is plotted against the number (*X*) of fluorine-substituted carbon atoms per molecule of adsorbed acid. In a previous study<sup>4</sup> of the effects of homol-

TABLE II

CONTACT ANGLES OF LIQUIDS ON ADSORBED CONDENSED MONOLAYERS OF THE 17-( $\phi$ -ALKYL)-HEPTADECANOIC ACIDS AT 20°<sup>a</sup>

Wetting liquid	Liquid surface tension, $\gamma_{LV}$ , at 20°, dynes/cm.	Contact angles on:			
		$\phi$ -Heptyl-heptadecanoic acid	$\phi$ -Pentyl-heptadecanoic acid	$\phi$ -Propyl-heptadecanoic acid	$\phi$ -Ethyl-heptadecanoic acid
<b><i>n</i>-Alkanes</b>					
Hexadecane	27.6	73°	68°	59°	58°
Tetradecane	26.7	70	65+	55	55
Tridecane	25.9	68	65	51	53
Dodecane	25.4	66(68 <sup>b</sup> )	61+(63 <sup>b</sup> )	52(52 <sup>b</sup> )	52(53 <sup>b</sup> )
Undecane	24.7	64	..	..	49
Decane	23.9	64(63 <sup>b</sup> )	57(58 <sup>b</sup> )	48	46
Octane	21.8	57(59 <sup>b</sup> )	50(50 <sup>b</sup> )	40(37 <sup>b</sup> )	41
Heptane	20.3	52	..	..	35
$\gamma_c$ for <i>n</i> -alkanes, dynes/cm.		8.0	11.4	16.4	16.0
<b>Miscellaneous liquids</b>					
Water	72.8	115°	110°	106°	105°
Formamide	58.2	105	100	97	94
Methylene iodide	50.8	101	94	86	83
Ethylene glycol	47.7	98	92+	84	80
Tricresyl phosphate	40.9	90	81	72	72
<i>t</i> -Butylnaphthalene	33.7	78	73	68	64
Dicyclohexyl	32.8	75	71	62	61
Bis-(2-ethylhexyl) phthalate	31.3	78	75	60	60
Pentaerythritol tetracaproate	30.4	77	72	62	61
Squalane	29.5	77	72	62	61
Perfluoroalkane (FCD-330)	20.2	41	33	23	26

<sup>a</sup> Monolayers adsorbed by retraction on polished chromium during 10-minute contact with molten pure acid. <sup>b</sup> Liquids saturated with appropriate 17-perfluoroalkylheptadecanoic acid.

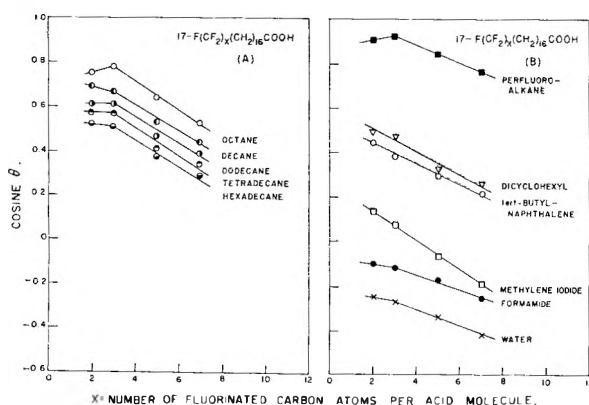


Fig. 2.—The effect on wetting of homology in the segmented acid monolayer adsorbed on chromium from the melt: (A) wetting by *n*-alkanes; (B) wetting by miscellaneous liquids.

ogy in adsorbed molecules of fully fluorinated acids, such plots were linear for each *n*-alkane liquid and were decreasing functions for each of the miscellaneous liquids. As regards the partially fluorinated acids reported here, the smaller number of available homologs and the difficulty of distinguishing differences in  $\theta$  for the two shortest homologs makes such relationships less informative. Nevertheless, it is apparent that the curves of Fig. 2A and 2B for the 17-( $\phi$ -alkyl)-heptadecanoic acids do not resemble those reported for the  $\phi$ -alkanoic acids.

Graphs of  $\cos \theta$  vs.  $X$  for many of the liquids on monolayers of both acid types exhibit linearity over a limited range of  $X$  (from 3 to 7 for the terminally fluorinated acids; from 5 to 11 for the fully fluorinated acids). Although the slopes of the

linear portions of the curves are roughly comparable within a given family of acids, there is a large difference between slopes for the terminally fluorinated and the fully fluorinated acids. The much steeper slope of the rectilinear portion of the graphs for the former deserves explanation.

A second distinctive feature of the curves appears in the region from  $X = 3$  to  $X = 2$ ; the hump in the curves in Fig. 2A indicates that  $\theta$  has become larger for the terminally fluorinated acid than would have been predicted if the effects of homology on wetting were linear over the whole range of values of  $X$ , as was the case with the series of fully fluorinated acids.<sup>4</sup> This cannot be caused by the presence of a large dipole close to the surface, since if any interaction did occur between the electric fields of the dipole and liquid drop it would have made  $\theta$  smaller than predicted, rather than larger, as found experimentally.

The effects of homology in the acid monolayers are better demonstrated by plotting the value of  $\gamma_c$ , obtained from the  $\cos \theta$  vs.  $\gamma_{LV}$  graph of the *n*-alkanes, as a function of  $X$  for the two types of acids (Fig. 3). A straight line represents the data well for the fully fluorinated acids over the range  $3 \leq X \leq 11$ . A rectilinear relation also holds for the terminally fluorinated acids over the range from  $X = 3$  to  $X = 7$ , the latter being the largest value of  $X$  for which compounds currently are available. The point  $X = 7$  appears to correspond to the condition at which the wetting properties of the condensed monolayer become determined solely by the packing of the fluorocarbon segment of the molecule; therefore, for values of  $X \geq 7$  the curve is expected to coincide with that for the fully fluorinated acids. Presumably, the effect on wet-

ting of the uncompensated dipole in the aliphatic chain becomes insignificant when  $X \geq 7$ .

If the rectilinear portion of the curve for terminally fluorinated acids of  $3 \leq X \leq 7$  is extrapolated to the  $X = 0$  axis, the intercept indicates a value of  $\gamma_c$  of 22.4 dynes/cm., in good agreement with published values of 22–24 dynes/cm. for the unfluorinated aliphatic acid, stearic acid<sup>2,7</sup> (Fig. 3). The curve obtained experimentally, however, shows the discontinuity at  $2 < X < 3$ . This makes it of interest to examine the curve at  $X = 1$ .

The datum point corresponding to a  $\gamma_c$  value of 18.4 dynes/cm. for the 17-( $\phi$ -methyl)-heptadecanoic acid reported earlier<sup>7</sup> is included in Fig. 3 at  $X = 1$ ; an open symbol is used to show that, as in the case of the fully fluorinated acids, this value of  $\gamma_c$  was obtained for films adsorbed on platinum during contact with a dilute organic solution rather than the molten pure acid. Directly comparable data for the 17-( $\phi$ -methyl)-heptadecanoic acid adsorbed on chromium from the melt could not be obtained experimentally since poor (*i.e.*, relatively wettable) films are formed under the standardized conditions used here of a 10-min. contact period. The melt method is applicable to this acid, but the films show extreme sensitivity to both the time and temperature of contact with the melt. This may correlate with the tendency, previously mentioned, for greater variation in  $\theta$  on films of the  $\phi$ -ethyl and  $\phi$ -propyl-substituted acids formed during short periods of contact with the molten acid. Such behavior is in contrast with that of stearic acid films which show no sensitivity to the length of contact of the chromium with the molten acid. This difference is indicative of the importance of the short terminal groups in determining equilibrium conditions for the adsorbed monolayer.

**Orientation and Packing in the Monolayers.**—The configuration and packing of the adsorbed molecules comprising the monolayer are determined in large part by the relative sizes of the fluorocarbon and hydrocarbon segments of the molecule and by the balance achieved between the stronger cohesive forces between the adjacent hydrocarbon segments and the weaker forces between the adjacent fluorocarbon segments.

Steric effects resulting from the substitution of fluorine for hydrogen in an aliphatic chain can be determined from measurements on Stuart-Briegleb molecular models.<sup>15</sup> In the solid state, the majority of aliphatic derivatives crystallize with the long hydrocarbon chain in a planar, extended configuration, *i.e.*, with the covalently bonded carbon atoms laid out at the tetrahedral angles along a flat zig-zag; the introduction of fluorine increases the cross-sectional diameter of such an extended hydrocarbon chain by 30% in the plane of the zig-zag, and by 25% in the plane normal to it. In the liquid state, aliphatic compounds are characterized by high internal flexibility, due to the ease of rotation around their C–C bonds; upon fluorination, rotation is severely restricted, due to the larger effective radii of the fluorine than hydrogen atoms. This increase in radius is also a factor in restricting rotation around the  $-\text{CF}_2-$

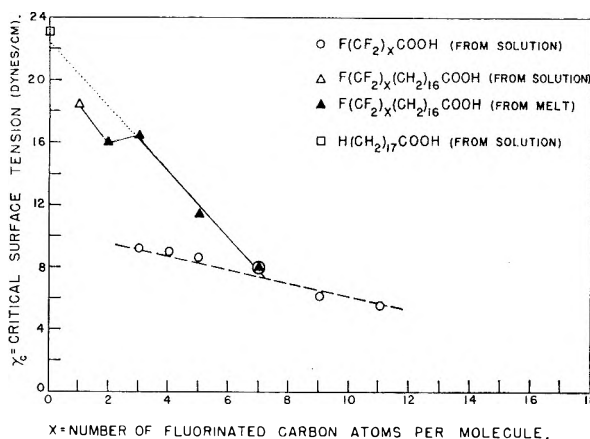


Fig. 3.—The effect of fluorination of the adsorbed acid monolayer on its critical surface tension of wetting by the  $n$ -alkanes.

$\text{CH}_2-$  bond. During rotation of a rigid fluorocarbon chain around this C–C bond, the angle between the long axes of the fluorocarbon and hydrocarbon chains varies from  $0^\circ$  to  $17^\circ$  to  $42^\circ$ , for rotations of  $0^\circ$ ,  $90^\circ$ , and  $180^\circ$ , respectively. After  $180^\circ$  rotation, the hydrocarbon and fluorocarbon chains once again would be coplanar, but the intramolecular bend of  $42^\circ$  which this entails is sterically impossible due to the marked hindrance between the fluorine and hydrogen atoms comprising the  $-\text{CF}_2-\text{CH}_2-$  group.

Consideration of steric factors and intermolecular forces between compounds with appreciable terminal fluorination suggests three interesting models (Fig. 4) consistent with the wetting properties reported here for the more highly fluorinated compounds ( $X \geq 3$ ). Models A and B are based on the postulate that the fluorinated terminal groups are in extended configuration, approaching close packing. In each of these models the larger diameter of the fluorinated terminal groups serves to separate the attached aliphatic chains over at least a portion of their length and thus diminish the cohesive forces between them. This leads to the possibility in Model A that the aliphatic chains can attain only short-range order, a condition normally associated with the liquid state. The existence of such an underlying two-dimensional quasi-liquid phase would not be inconsistent with close packing of terminal fluorocarbon groups because the 25–30% increase in cross-sectional area of a hydrocarbon chain resulting from fluorination is larger than the approximately 15% increase which occurs in the process of melting aliphatic hydrocarbons.<sup>16</sup> A somewhat greater degree of order for the hydrocarbon chains is postulated in Model B so that partial adlineation can occur between those portions of the aliphatic chains furthest removed from the fluorinated end. The neighboring molecules cluster together, the size of the cluster, or two-dimensional micelle, being determined by the relative lengths of the fluorocarbon and hydrocarbon segments of the molecule and by the rela-

(16) S. S. Kurtz, Jr., and A. Sankin, "Density and Refractive Index of Hydrocarbons," in A. Farkas, "Physical Chemistry of the Hydrocarbons, Volume II," Academic Press, Inc., New York, N. Y., 1953, p. 27.

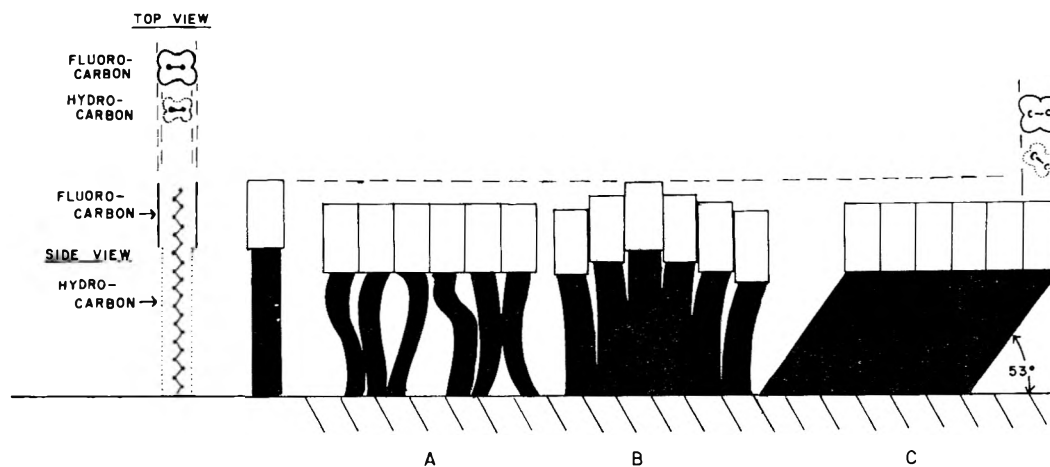


Fig. 4.—Schematic representation of configurations of adsorbed molecules of 17-(perfluoroheptyl)-heptadecanoic acid consistent with close packing of perfluoroheptyl groups. (Variations in thickness and apparent length of hydrocarbon segment symbolize changes in projected dimensions of 16-methylene group chain as it departs from planar, full extension.)

tive displacement of the fluorocarbon chains consistent with the requirements for lateral stability. Epstein<sup>17</sup> had proposed some years ago that fatty acid monolayers adsorbed on glass as 2-dimensional micelles of this same type.

A high degree of order in the hydrocarbon chain is implied in Model C where there is close packing of both the hydrocarbon and fluorocarbon chains when both are in extended configuration. Because of the large differences in the cross-sectional diameters, this requirement can be met for close-packing in only one dimension at a time, and then only by rotating the extended fluorocarbon chain around the  $-\text{CF}_2-\text{CH}_2-$  bond linking it to the extended hydrocarbon chain. This entails the separation of the planes defined by the carbon atoms of the extended chain segments and the introduction of a bend between the long axes of the two chains. Appropriate combinations of angles of rotation and orientation relative to the adsorbing plane can be calculated to satisfy the requirements of Model C for uni-dimensional close-packing (for example, Fig. 4C). Ball models indicate that, for aliphatic chains with terminal fluorocarbon groups containing more than one (or possibly two) carbon atoms, the least steric hindrance is encountered for an orientation of the bent, biplanar molecule in which the fluorocarbon chain has its long axis normal to the plane of the adsorbing surface, necessitating the inclination of the hydrocarbon chain at the angle consistent with the angles of intramolecular rotation and bending. This gives the aliphatic chains an orientation similar to that found in the more common crystalline forms of the solid fatty acids where the long axis of the hydrocarbon chain is inclined at  $63.5^\circ$  to a plane through the carboxyl head groups, an angle attributed<sup>18</sup> to the stable positions of tilt at which the chains interlock after moving relative to each other by one whole zig-zag.

The major objection to Model C is the requirement that the acid molecules adsorb so that there is a parallel alignment of the two sets of planes

defined by the two segments of their carbon skeletons. Even for a completely planar molecule, this is a condition normally met only in crystalline lattices. It is even less likely to be met in a monolayer adsorbed "in situ" unless chemical interaction occurs with the surface. Although chemisorption is a distinct possibility for an acid contacted with a chromium surface, it seems less likely for one adsorbed on platinum, and the contact angles of Table I indicate no differences between the films adsorbed on these two metals. The configurations involving the close-packing of bent molecules, as in Model C, therefore are considered unlikely.

The remaining two configurations (Fig. 4A and 4B) require no more than the usual random azimuthal distribution of the planes defined by the carbon atoms of vertically oriented molecules when incorporated in a monolayer. It is not possible to differentiate between these two configurations on the basis of the data on wetting, since they both result in an exposed surface of the same chemical constitution and nearly the same packing. The nearly identical wetting properties of  $\phi$ -octanoic acid and 17-( $\phi$ -heptyl)-heptadecanoic acid monolayers do show, however, that the introduction of a chain of sixteen methylene groups does not affect the packing of the terminal  $\phi$ -heptyl groups; *i.e.*, that effects due to adlineation of the aliphatic chains are negligible. Such evidence favors Model A for  $X \geq 7$  as depicted in Fig. 4A.

As  $X$  decreases from 7 to 3, the wettability of the surface increases, the effect of homology in the fluorocarbon segment of the molecule being greater for the terminally fluorinated than for the fully fluorinated acids. Apparently the  $\phi$ -alkyl groups do not pack as effectively for the former as for the latter, despite the presence of the methylene chain. Moreover, the packing of the adjacent acid molecules becomes less compact as  $X$  decreases, even though there is no change in the cross-sectional area of the  $\phi$ -alkyl chain. The regularity of the change in wettability as  $X$  decreases to 3 makes it unlikely that the  $\phi$ -alkyl groups undergo any radical reorientation which would alter the packing of the molecules. Therefore the difference in

(17) H. T. Epstein, *J. Phys. Colloid Chem.*, **54**, 1053 (1950).

(18) E. K. Rideal, "An Introduction to Surface Chemistry," 2nd edit., University Press, Cambridge, England, 1930, p. 97.

packing must result from changes in spacing which are not steric in origin.

A regular increase in spacing can arise from the mutual repulsion between the electrostatic dipoles of adjacent, parallel-oriented molecules within the monolayer if there is a progressive decrease in the strength of the forces available to counteract that repulsion, as when the van der Waals cohesive forces between the  $\phi$ -alkyl chains diminish with decreasing  $X$ . Thus, the configurations of Fig. 4A, and, to a lesser extent, Fig. 4B, still are applicable for  $X \geq 3$ , except that the fluorocarbon segments shorter than  $\phi$ -heptyl are less closely packed due to the repulsion between the dipoles at the  $-\text{CF}_2-\text{CH}_2-$  linkage. Since such uncompensated dipoles are not present in the fully fluorinated acids, the intermolecular cohesion and hence the packing in such adsorbed monolayers is less affected by a decrease in  $X$  (Fig. 3).

The marked change in slope in the  $\cos \theta$  vs.  $X$  curve between  $X = 3$  and  $X = 2$  (Fig. 2A) indicates that some additional factor becomes operative for the acids with short terminal groups. If the differences in the effect of varying  $X$  on wettability are due to the presence of a dipole closer to the surface when  $X = 2$  than when  $X = 3$ , the effect should be to lower the contact angles whenever interaction with the wetting liquid can occur. Similarly, if the interaction between adjacent dipoles within the monolayer separates the  $\omega$ -terminal groups of the adsorbed molecules more widely, but does not change their orientation, the effect also should be to lower  $\theta$ . Experiments show, however, that the angles either remain the same or actually increase slightly.

This abrupt reversal of the effects of homology on wettability between  $X = 3$  and  $X = 2$  (Fig. 2A) suggests a radical change in the configuration resulting from the equilibrium between opposing steric and electrical effects when the terminal group is as short as  $\phi$ -ethyl. For example, a considerable change in arrangement could result for Model B if the forces between the terminal groups are not sufficiently strong to align all the terminal groups in the same direction. Adlineation between the segments of the hydrocarbon chain furthest removed from the fluorinated terminal brings the terminal groups together. If there are sufficiently strong, stabilizing, lateral forces, there results a parallel alignment of the large fluorocarbon groups, effectively preventing further adlineation along the hydrocarbon chain. When these forces are absent, crowding of short fluorocarbon groups may be relieved by their rotation around the  $-\text{CF}_2-\text{CH}_2-$  bond. As more molecules group together, progressively larger intramolecular rotation and bending are required to accommodate the end groups. This results in changes in the orientations of the dipoles at the  $-\text{CF}_2-\text{CH}_2-$  linkages of adjacent molecules and an alteration in their mutual interaction. A second result is the exposure of the  $-\text{CF}_2-$  atomic grouping in the wetting surface. Eventually, Model B is changed into a small cluster of molecules (or a surface micelle) comprising perhaps 15 molecules, with extended aliphatic chains in relatively good close packing,

and an outermost surface of randomly oriented  $\phi$ -ethyl groups. Such a surface need not conform to the homology effects consistent with the close packing of unidirectionally oriented perfluoroalkyl groups; it should, however, resemble in its wetting characteristics those surfaces which are rich in both  $-\text{CF}_3$  and  $-\text{CF}_2-$  groups. An example of the latter is the surface of the homopolymer polyhexafluoropropylene.<sup>6</sup> When contact angle data for this surface are compared to the data reported here for adsorbed monolayers of 17-( $\phi$ -ethyl)-heptadecanoic acid, the agreement is excellent for the  $n$ -alkanes and reasonably good for the one cyclic hydrocarbon studied. It is not as good for the remaining miscellaneous liquids; for each of these polarizable liquids,  $\theta$  is lower on the adsorbed monolayer than on the polymer. This is exactly the effect that would be predicted to result for two surfaces of the same chemical constitution if one of them has a large dipole close to the outermost plane of the surface. Therefore, for  $X = 2$ , surface micelles having the modification of Model B in which the fluorocarbon groups have random tilting would be consistent with the data on wettability.

There is no physical crowding of the terminal groups in the monolayer of 17-( $\phi$ -methyl)-heptadecanoic acid. In the planar, extended configuration of the hydrocarbon chain, the C-C bond directions lie at angles of  $35^\circ$  to the long axis of the chain; this so places the terminal carbon atom relative to the molecular axis that a considerable increase in the diameter of a terminal atomic grouping (as in replacing a  $-\text{CH}_3$  group by the larger diameter  $-\text{CF}_3$  group) can be tolerated without serious steric interference to the packing of the hydrocarbon chains. Proof of this lies in: (i) the closeness of the melting points for the 3-dimensional crystalline arrays of stearic and trifluorostearic acid molecules, and (ii) the similar friction behavior of their 2-dimensional arrays where the durability of adsorbed monolayers under repeated friction traverses indicated that both acids form films which are 2-dimensional solids.<sup>19</sup> Both acids therefore are expected to adsorb in the same orientation, *i.e.*, with the hydrocarbon chains extended and their long axes normal to the plane of the adsorbing surface. Differences in packing should be minor and result from the effects of electrostatic repulsion between adjacent dipoles close to the outermost surface of the monolayer. Electron diffraction examination indicated a considerable difference between the packing and orientation of monolayers of stearic acid and 17-( $\phi$ -methyl)-heptadecanoic acid, however, when each was adsorbed on platinum from organic solution.<sup>7</sup> The monolayers of the terminally fluorinated acid were far less densely packed and there was considerable variation of the molecular axis from the essentially  $90^\circ$  orientation found for stearic acid.

From the data presented here for the wettability of an homologous series of terminally fluorinated heptadecanoic acids, it appears that only when  $X \geq 7$  can adsorbed films of such partially fluorinated acids ever result in surface coatings of the same

(19) O. Levine and W. A. Zisman, *J. Phys. Chem.*, **61**, 1188 (1957).

limited wettability as those produced from fully fluorinated acids of the same total fluorocarbon content.

The use of such partially fluorinated acids does, however, provide these advantages: (i) the presence of the long aliphatic chain can be expected to modify the solubility of the acid with respect to some of the more conventional hydrocarbon materials used as solvents in technical applications; (ii) the lowering of the melting point (for the more heavily fluorinated acids) also may facilitate certain types of applications; (iii) the decrease in volatility resulting from the presence of the hydrocarbon chain increases film durability and also lessens the possibility of toxicity hazards; and (iv) finally, and most important of all, the presence of the aliphatic hydrocarbon chain between the carboxyl group and the perfluorocarbon moiety decreases the acid strength of the perfluoroalkanoic acid<sup>20,21</sup>

compound to that of a weak acid like the fatty acids.

The presence of the intermediate aliphatic hydrocarbon chain may alter greatly the lubricating properties of a condensed monolayer adsorbed on a metal. An adsorbed monolayer offers resistance to abrasion and wear to an extent which is sensitive to intermolecular cohesion between molecules of the film.<sup>19</sup> Increasing the total chain length may or may not improve the durability of a lubricating film depending on whether the hydrocarbon portions of the chains adlineate to a certain extent or assume a quasi-liquid configuration.

Film durability measurements and electron diffraction examinations are being made to elucidate further the properties of these unique monolayers.

(20) T. J. Brice, H. G. Bryce, and H. M. Scholberg, *Chem. Eng. News*, **31**, 510 (1953).

(21) W. Sheppard and E. L. Muetterties, *J. Org. Chem.*, **25**, 180 (1960).

## HEAT CAPACITIES AND THERMODYNAMIC PROPERTIES OF GLOBULAR MOLECULES. IV. PENTAERYTHRITYL CHLORIDE, BROMIDE, AND IODIDE FROM 6 TO 300°K.<sup>1</sup>

BY DONALD H. PAYNE AND EDGAR F. WESTRUM, JR.

*Department of Chemistry, University of Michigan, Ann Arbor, Michigan*

*Received November 15, 1961*

The heat capacities of pentaerythrityl chloride, bromide, and iodide were determined by adiabatic calorimetry from 6 to 300°K. and the entropies, enthalpies, and free energy functions evaluated. The entropies at 298.15°K. are 61.54, 69.58, and 75.70 cal. mole<sup>-1</sup> °K.<sup>-1</sup> for the chloride, bromide, and iodide, respectively. Although the general temperature dependences of the heat capacities are of the usual sigmoid character, the chloride and the bromide both show a region of anomalously slow absorption of energy.

### Introduction

Since the original suggestion by Pauling<sup>2</sup> that certain types of solid-solid transitions might be explained by the onset of rotation in the crystalline state, many investigations have been pursued in an attempt to determine the nature of the mechanism of such transformations. Although originally rotational freedom was attributed only to relatively simple molecules, Smyth,<sup>3</sup> through an extensive investigation of the dielectric constants of compounds involving transitions, extended Pauling's view to include many larger and more complex molecules.

Perhaps the most extensive investigations have concerned the transitions in the ammonium halides. Neutron diffraction investigations on the deuterated ammonium halides<sup>4</sup> indicate that these transitions are explained better by an orientational order-disorder type of mechanism than by a rotational one. Moreover, the transition entropy

increments of the ammonium halides also probably are consistent with the order-disorder mechanism.<sup>5</sup> These compounds are examples of relatively simple transitions because of the symmetry features of the ammonium ion. In solid-solid transitions in general, these structures—both molecular and crystallographic—are sufficiently complicated that no adequate general correlation has been demonstrated between the isothermal entropy increments and the mechanism of transition. However, certain stochastic correlations are possible.<sup>6</sup> In transitions involving more complex molecules the factors to be considered apparently are more complicated, but the transitions are actually somewhat more susceptible to study because of the larger number of possible comparison compounds which may be synthesized.

At the initiation of this research a family of compounds of the general type C(CH<sub>2</sub>X)<sub>4</sub> (where X may represent halogen or hydrogen atoms, or hydroxyl groups) was considered to possess inherent interest. A solid-solid transition has been studied in neopentane, C(CH<sub>3</sub>)<sub>4</sub>, by Aston and Messerly<sup>7</sup> and in pentaerythritol, C(CH<sub>2</sub>OH)<sub>4</sub>

(1) Based upon a dissertation submitted to the H. H. R. School of Graduate Studies of the University of Michigan (by D. H. P.) in partial fulfillment of the requirements for the degree of Doctor of Philosophy.

(2) L. Pauling, *Phys. Rev.*, **36**, 430 (1930).

(3) C. P. Smyth, "Dielectric Behavior and Structure," McGraw-Hill Book Co., New York, N. Y., 1955; *J. Phys. and Chem. Solids*, **18**, 40 (1961).

(4) G. H. Goldschmidt and D. G. Hurst, *Phys. Rev.*, **86**, 797 (1952); H. A. Levy and S. W. Peterson, *ibid.*, **86**, 766 (1952).

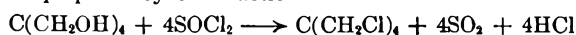
(5) C. C. Stephenson, R. W. Blue, and J. W. Stout, *J. Chem. Phys.*, **20**, 1046 (1952).

(6) G. B. Guthrie and J. P. McCullough, *J. Phys. and Chem. Solids*, **18**, 53 (1961).

by Nitta and his co-workers<sup>8</sup> with the discovery of a remarkably high transition entropy increment in the latter compound. Comparison of the symmetry features of the high temperature cubic modifications of pentaerythritol with the symmetry features of neopentane suggested the halogen homologs of pentaerythritol would be interesting compounds for investigation. Although the literature data on the chloride, bromide, and iodide are not extensive and no transitions were reported, these three compounds nonetheless were studied to provide data for correlation with that of pentaerythritol fluoride and pentaerythritol. This paper therefore reports the results of low temperature investigation of the heat capacities of pentaerythritol chloride, bromide, and iodide.

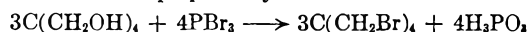
### Experimental

**Preparation of the Pentaerythrityl Halides.**—The pentaerythritol chloride used for the heat capacity measurements was prepared by the reaction



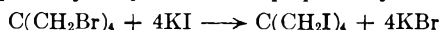
in the manner described by Mooradian and Cloke.<sup>9</sup> Following the addition of water to the pyridine solution to separate the product, the crude product was filtered and washed thoroughly with warm water. It then was recrystallized twice from 95% ethanol, the first time with Norit charcoal suspended in the ethanol. Following the recrystallizations the product was sublimed twice at about 5 mm. at steam-bath temperatures. Gravimetric chloride analysis indicated 67.47% (theoretical: 67.56%); the melting point was 97°.

The pentaerythrityl bromide used for the heat capacity measurements was prepared by the reaction



according to the method outlined in "Organic Syntheses."<sup>10</sup> Purification of the crude product was accomplished by two successive continuous extractions with 95% ethanol, followed by one recrystallization from 95% ethanol using Norit charcoal, and five recrystallizations using 95% ethanol alone. Gravimetric analysis showed 82.65% bromide by weight (theoretical: 82.43%); m.p. 163°.

The pentaerythrityl iodide was prepared by the reaction



according to the method outlined in "Organic Syntheses."<sup>10</sup> For purification the sample was submitted to continuous extraction with 95% ethanol until the melting point reached 233°. The sample then was removed from the thimble of the extractor and recrystallized from benzene. The solvent was removed by high vacuum. Just before use of the sample, it was recrystallized from benzene (to remove decomposition products produced during storage) and then kept in a darkened cold room (-10°) until the sample actually was loaded into the calorimeter. Volhard iodide determination indicated 88.39% iodide (theoretical: 88.17%). The sample melted with some decomposition at 233°.

**The Calorimetric Apparatus.**—The Mark I adiabatic calorimetric cryostat for use over the range 4 to 350°K. was an improved version of one constructed by Westrum, Hatcher, and Osborne,<sup>11</sup> with the essential similarity that helium was used as the lowest temperature refrigerant

(7) J. G. Aston and G. H. Messerly, *J. Am. Chem. Soc.*, **58**, 2354 (1936).

(8) I. Nitta and T. Watanabe, *Bull. Chem. Soc. Japan*, **13**, 28 (1938); I. Nitta, S. Seki, and M. Momotani, *Proc. Japan Acad.*, **26**, 25 (1950); I. Nitta, S. Seki, M. Momotani, K. Suzuki, and S. Nakagawa, *ibid.*, **26**, 11 (1950); I. Nitta, T. Watanabe, S. Seki, and M. Momotani, *ibid.*, **26**, 19 (1950).

(9) A. Mooradian and J. B. Cloke, *J. Am. Chem. Soc.*, **67**, 942 (1945).

(10) H. B. Schurink, "Organic Syntheses, Coll. Vol. II," John Wiley and Sons, New York, N. Y., 1943, p. 476.

(11) E. F. Westrum, Jr., J. B. Hatcher, and D. W. Osborne, *J. Chem. Phys.*, **21**, 419 (1953).

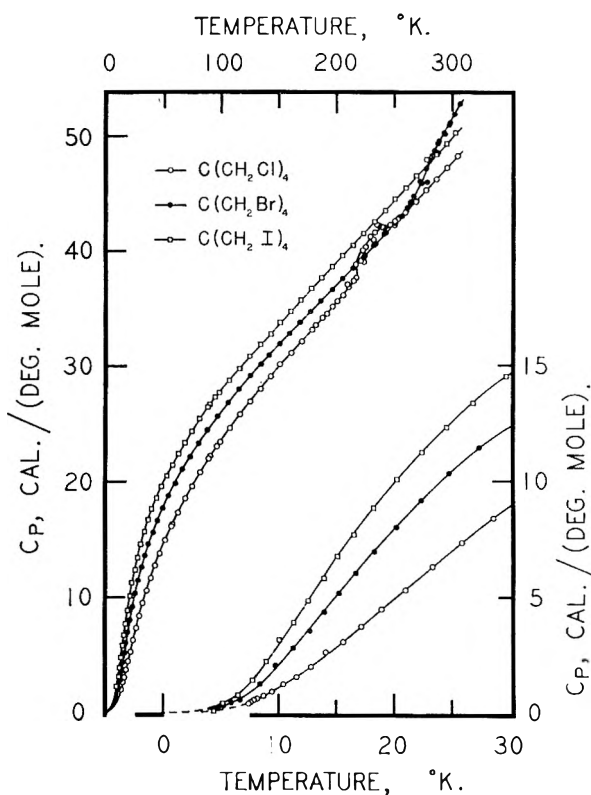


Fig. 1.—Heat capacities of three pentaerythrityl halides.

instead of hydrogen, and that a heat exchanger (called the "economizer") was provided to utilize the enthalpy of the effluent helium gas.

The gold-plated copper calorimeter (laboratory designation W-6) was 3.8 cm. in diameter and 7.7 cm. long. The thickness of the shell was 0.4 mm. Eight vanes of 0.1-mm. copper foil aided in establishing thermal equilibrium. An entrant gold-plated copper heater well contained a platinum capsule-type resistance thermometer (laboratory designation A-3, calibrated by the National Bureau of Standards) within a cylindrical copper heater sleeve carrying 160 ohms of B. and S. No. 40-gage Advance (Constantan) Fiberglass insulated wire, which was wound bifilarly in double threaded grooves and cemented in place with Formvar enamel. Calorimeter W-6 differed from typical calorimeters in that a Monel neck of 15 mm. dia. partially isolated the actual cover from the copper calorimeter, and thus allowed the cover to be soldered in place with Cerroseal solder without appreciably heating the calorimeter or the samples which were placed therein. The heat capacity of the calorimeter-heater-thermometer assembly was determined in a separate set of experiments. Corrections were applied for the small differences in the amount of gaseous helium used in the loaded and empty calorimeter to facilitate thermal contact between sample and calorimeter. After a sample was loaded into the calorimeter, the calorimeter was sealed and the ambient air evacuated by placing the calorimeter within a bulb attached to a high vacuum line. An atmosphere of helium gas at room temperature then was introduced through a small hole which subsequently was soldered shut. The contribution of the calorimeter-heater-thermometer assembly to the heat capacity was less than 10% of the total at 10°K., and increased gradually to 33% at 80°K. and remained approximately constant at higher temperatures; in the case of the bromide and the iodide it was less than 10% at 10°K. and increased to about 55% at 100°K. and higher temperatures. A weighed quantity of Lubriseal stopcock grease was used to obtain thermal contact between the heater, thermometer, and calorimeter; the amount of Cerroseal solder employed to seal the calorimeter was adjusted carefully by weight to equal the quantity used on the empty calorimeter. The masses of the samples (*in*

*vacuo*) used were 84.961, 67.987, and 90.603 g., for the chloride, bromide, and iodide, respectively.

### Results and Discussion

**Heat Capacity Measurements.**—The measured heat capacities of the three pentaerythrityl halides are presented in Table I with the mean temperatures of the determinations indicated. These data are presented in chronological sequence so that the magnitude of the temperature increment employed in the determinations usually may be estimated from the differences in the mean temperatures. Curvature corrections have been applied to correct the experimental values of  $\Delta H/\Delta T$  to the derivatives  $(\partial H/\partial T)_p$ . The data are expressed in terms of the defined thermochemical calorie equal to 4.1840 abs. j. and an ice point of 273.15°K. These data are considered to have a probable error of 0.1% above 25°K., increasing gradually to 1% at 10°K., and may be as large as 5% at lower temperatures. The experimental data are presented graphically in Fig. 1.

TABLE I  
HEAT CAPACITY DETERMINATIONS ON PENTAERYTHRITYL HALIDES [IN CAL. MOLE<sup>-1</sup> °K.<sup>-1</sup>]

Pentaerythrityl chloride; C(CH <sub>2</sub> Cl) <sub>4</sub> , g. mol. wt. = 209.94 g.										
Series I.	T, °K.	C <sub>p</sub>	S°	H° - H <sub>0</sub>	-(F° - H <sub>0</sub> )/T					
24.64	116.20	25.81	125.06	26.94	134.07	28.05	142.99	29.11	151.87	
30.13	160.87	31.14	170.07	32.16	179.22	33.16	188.19	34.20	197.14	
35.14	206.13	36.18	215.09	37.40	223.98	39.03	232.77	40.92	241.51	
41.99	250.43	42.53	259.49	43.31	268.52	44.25	277.56	45.23	286.65	
46.17	295.75	47.18	304.83	48.21	313.22	49.22	322.26	50.21	331.30	
17.31	68.61	18.51	74.74	19.56	81.56	20.78	88.79	21.99	96.04	23.04
Series II.										
57.22	16.27	62.32								
Series III.										
7.40	0.420	7.63	0.510	7.91	0.553	8.19	0.630	8.69	0.769	
9.45	0.936	10.40	1.249	11.57	1.569	12.81	2.016	14.09	2.644	15.59
3.091	17.17	3.737	18.89	4.478	20.97	5.319	23.32	6.322	25.85	7.343
28.59	8.398	31.58	9.480	34.82	10.56	38.33	11.65	42.18	12.72	46.34
13.79	51.01	14.91	56.50	16.10	62.32	17.37	68.76	18.74	75.38	82.22
Series IV.										
210.67	36.87	217.22								
221.46	39.16	225.59	40.35	229.64	41.21	233.64	41.58	237.59		
241.54	42.00	246.46	42.22	253.29	42.74	257.24	43.18	261.19	182.74	
192.06	34.57	201.14	35.65	209.96	37.04	217.14	38.78	222.89		
228.60	41.24	234.29	42.23	240.03	42.01	245.73	42.15	252.32		
42.66										
Pentaerythrityl bromide; C(CH <sub>2</sub> Br) <sub>4</sub> , g. mol. wt. = 387.78 g.										
Series I.	T, °K.	C <sub>p</sub>	S°	H° - H <sub>0</sub>	-(F° - H <sub>0</sub> )/T					
8.40	1.255	9.76	2.064	11.25	2.811	12.69	3.580	13.96	4.388	15.27
16.70	6.032	18.33	6.975	20.21	8.023	22.36	9.153	24.77	10.32	
27.38	11.44	30.20	12.53	33.20	13.58	36.45	14.59	40.10	15.58	44.21
16.60	48.83	17.66	53.92	18.75	59.55	19.85	65.98	21.04	72.70	79.84
22.15	79.84	23.32	87.62	24.48	96.44	25.65	105.83			
115.41	28.02	125.07	29.16	134.33	30.18	141.59	30.95	150.56		
159.37	32.84	168.36	33.79	177.57	34.74	186.78	35.68	195.99		
205.19	37.58	214.38	38.50	223.51	39.47	232.55	40.44	241.64		
250.80	42.41	260.03	43.44	269.34	44.31	278.54	45.93	287.62		
Series III.										
255.18	42.91	264.16	44.18	273.16	45.87	279.90				
284.41	48.69	288.99	49.53	293.63	50.12	298.22	51.12	302.76		
Series IV.										
214.84	38.48	224.47	39.55	233.96						
242.56	41.50	249.99	42.30	255.96	42.96	261.39	43.72	266.84		
272.31	45.97	277.59	47.12	282.66	48.22	287.71	49.32	292.78		
297.80	51.00	302.75	51.86	307.65	52.74					
Pentaerythrityl iodide; C(CH <sub>2</sub> I) <sub>4</sub> , g. mol. wt. = 575.75 g.										
Series I.	T, °K.	C <sub>p</sub>	S°	H° - H <sub>0</sub>	-(F° - H <sub>0</sub> )/T					
90.04	26.63	98.44	27.71	107.11	28.74	115.96	29.80			
125.05	30.85	134.03	31.86	142.81	32.82	151.66	33.80	160.64	34.74	
169.72	35.75	178.79	36.72	187.71	37.65	196.65	38.59	205.68	39.55	
214.76	40.49	223.87	41.49	233.01	42.49	242.06	43.48	251.05	44.44	
260.07	45.43	269.02	46.45	277.81	47.89	286.47	48.32	295.03	49.28	
303.45	50.28	307.75	51.86	307.65	52.74					
Series II.										
4.39	0.090	5.20	0.428	6.48	0.783	7.76				
8.97	2.230	10.09	3.177	11.31	3.891	12.61	4.816	13.93	5.820	
15.16	6.746	16.54	7.687	18.26	8.838	20.29	10.08	22.38	11.23	24.52
26.86	13.37	29.71	14.51	32.91	15.64	36.16	16.64	39.65	17.60	
43.52	18.55	47.75	19.51	52.13	20.44	52.31	20.47	57.18	21.42	62.41
68.15	23.36	74.43	24.32	81.07	25.40	87.97	26.41	95.13	27.30	

Regions in which the heat capacity behaved anomalously and somewhat irreproducibly were

TABLE II  
THERMODYNAMIC PROPERTIES OF PENTAERYTHRITYL HALIDES

T, °K.	C <sub>p</sub>	S°	H° - H <sub>0</sub>	-(F° - H <sub>0</sub> )/T
Pentaerythrityl chloride [C(CH <sub>2</sub> Cl) <sub>4</sub> ]				
10	1.09	0.84	2.72	0.57
15	2.85	1.59	12.32	0.77
20	4.91	2.69	31.70	1.11
25	7.01	4.01	61.54	1.55
30	8.92	5.46	101.4	2.08
35	10.62	6.97	150.4	2.67
40	12.12	8.49	207.3	3.31
45	13.46	9.99	271.3	3.96
50	14.67	11.47	341.6	4.64
60	16.85	14.35	499.5	6.03
70	18.76	17.09	677.6	7.41
80	20.52	19.71	874.1	8.78
90	22.11	22.22	1087.4	10.14
100	23.60	24.63	1316	11.47
110	24.99	26.94	1559	12.77
120	26.29	29.17	1816	14.04
130	27.55	31.33	2085	15.29
140	28.75	33.41	2366	16.51
150	29.92	35.44	2660	17.71
160	31.04	37.40	2965	18.87
170	32.14	39.32	3280	20.02
180	33.24	41.19	3607	21.15
190	34.34	43.01	3945	22.25
200	35.51	44.81	4294	23.34
210	37.05	46.57	4657	24.39
220	38.33	48.35	5038	25.45
230	41.54	50.15	5443	26.48
240	42.01	51.94	5864	27.51
250	42.45	53.66	6285	28.52
260	43.34	55.34	6714	29.52
270	44.35	56.99	7152	30.50
280	45.43	58.63	7601	31.48
290	46.54	60.24	8061	32.44
300	47.64	61.84	8532	33.40
273.15	44.68	57.51	7293	30.81
298.15	47.44	61.54	8444	33.22
Pentaerythrityl bromide [C(CH <sub>2</sub> Br) <sub>4</sub> ]				
10	2.07	0.69	5.18	0.17
15	5.01	2.08	22.81	0.56
20	7.91	3.92	55.23	1.16
25	10.42	5.97	101.2	1.92
30	12.46	8.05	158.6	2.76
35	14.15	10.10	225.2	3.66
40	15.56	12.09	299.6	4.60
45	16.79	13.99	380.5	5.53
50	17.92	15.82	467.3	6.47
60	19.94	19.27	656.8	8.32
70	21.72	22.48	865.3	10.12
80	23.34	25.49	1091	11.86
90	24.81	28.32	1332	13.52
100	26.12	31.01	1586	15.15
110	27.36	33.56	1854	16.71
120	28.56	35.99	2133	18.21
130	29.71	38.32	2425	19.67
140	30.78	40.56	2727	21.08
150	31.84	42.72	3040	22.45
160	32.92	44.81	3364	23.78



170	33.96	46.84	3699	25.08
180	34.99	48.81	4043	26.35
190	36.01	50.73	4398	27.58
200	37.02	52.60	4764	28.78
210	38.04	54.43	5139	29.96
220	39.08	56.22	5524	31.11
230	40.16	57.99	5921	32.25
240	41.24	59.72	6328	33.35
250	42.32	61.42	6745	34.44
260	43.50	63.11	7174	35.52
270	45.39	64.78	7618	36.56
280	47.74	66.47	8084	37.60
290	49.70	68.18	8572	38.62
300	51.40	69.90	9077	39.64
273.15	46.10	65.31	7763	36.89
298.15	51.10	69.58	8983	39.45

Pentaerythrityl iodide  $[\text{C}(\text{CH}_2\text{I})_4]$ 

10	2.91	0.74	7.26	0.01
15	6.61	2.62	31.07	0.55
20	9.90	4.99	72.63	1.36
25	12.52	7.50	128.9	2.34
30	14.61	9.97	197.0	3.41
35	16.29	12.35	274.3	4.51
40	17.69	14.62	359.4	5.63
45	18.89	16.78	450.9	6.76
50	20.00	18.82	548.2	7.86
60	21.96	22.65	758.2	10.01
70	23.67	26.17	986.6	12.08
80	25.20	29.43	1231	14.04
90	26.60	32.48	1490	15.92
100	27.90	35.35	1763	17.72
110	29.12	38.07	2048	19.45
120	30.28	40.65	2345	21.11
130	31.41	43.12	2654	22.71
140	32.51	45.49	2973	24.25
150	33.60	47.77	3304	25.75
160	34.69	49.97	3645	27.19
170	35.77	52.11	3998	28.60
180	36.84	54.18	4361	29.95
190	37.89	56.20	4734	31.28
200	38.94	58.17	5118	32.58
210	39.99	60.10	5513	33.85
220	41.06	61.98	5918	35.08
230	42.16	63.83	6334	36.29
240	43.26	65.65	6762	37.48
250	44.34	67.44	7200	38.64
260	45.42	69.20	7648	39.78
270	46.51	70.93	8108	40.90
280	47.60	72.64	8578	42.00
290	48.71	74.33	9060	43.09
300	49.86	76.00	9553	44.16
273.15	46.85	71.48	8255	41.26
298.15	49.64	75.70	9461	43.97

observed in the chloride sample between 220 and 240°K. and in the bromide sample between ap-

proximately 260 and 290°K. Approximately 2 hr. were required for the bromide to come to thermal equilibrium in the anomalous region, and about 4 hr. for the chloride. The bromide curve appeared to be more reproducible than the chloride one. Large variations in the rate of cooling these samples seemed to produce no effect on the rapidity of reaching equilibrium or upon the heat capacity itself in these regions. It is to be noted that failure to await complete thermal equilibrium may affect the heat capacity curve slightly, but it does not appear to affect total energy under the curve and will have only an extremely small effect on the entropy value. On the last series of measurements on the pentaerythrityl chloride the runs were made in 28 hr. of continuous operation, and the points obtained from these runs were used to determine the heat capacity curve.

The entropy and enthalpy function were obtained by numerical quadrature of large scale plots of  $C_p$  vs.  $\log T$ . These functions, together with the smoothed values of the heat capacity read from these curves, are presented in Table II at selected temperatures. Extrapolations below 6°K. were made by the Debye  $T$ -cubed approximations. The free energy function was obtained by difference. The thermodynamic functions are considered to have a probable error of less than 0.1% above 100°K. Nuclear spin and isotope mixing contributions have not been included in the entropy and the free energy functions; hence, the values given are suitable for chemical thermodynamic purposes. As has been noted previously, the region over which slow equilibrium was obtained does not contribute significant uncertainty to the thermodynamic functions.

Although these three halides have not revealed a "plastically crystalline" phase as originally designated by Timmermans,<sup>12</sup> there is still a possibility that they will undergo transition to this phase before melting. It is proposed to study the higher temperature thermal behavior to ascertain whether or not this is so and to study, where possible, the entropy of fusion to aid in the interpretation of the very interesting closely related molecules, pentaerythrityl fluoride and pentaerythritol.

**Acknowledgment.**—The authors acknowledge with gratitude the partial support of the Division of Research of the U. S. Atomic Energy Commission in this investigation. The cooperation of Dr. D. W. Osborne and the Argonne National Laboratory in making liquid helium available for these studies is appreciated.

(12) J. Timmermans, *Bull. soc. chim. Belg.*, **44**, 17 (1935); *Ind. chim. belge.*, **16**, 178 (1951).

## THE HEATS OF FORMATION OF TRIIODIDE AND IODATE IONS

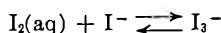
By J. H. STERN AND A. A. PASSCHIER

*Department of Chemistry, Long Beach State College, Long Beach 4, California**Received November 20, 1961*

The heat of reaction of solid iodine with excess aqueous potassium iodide ( $893 \pm 12$  cal./mole) was measured microcalorimetrically at  $25^\circ$ . This value combined with other data yields  $-12.72 \pm 0.15$  kcal./mole for the heat of formation and 56.0 e.u. for the standard entropy of  $I_3^-$  (aq). Measurements of the heats of reduction at  $25^\circ$  of separate solutions of potassium acid iodate and iodic acid with aqueous hydriodic acid to form triiodide ion were combined with the newly determined  $\Delta H_f^\circ$  of  $I_3^-$  and other pertinent heats of formation and dilution to yield  $\Delta H_f^\circ$  of  $IO_3^-$  (aq) =  $-54.8 \pm 0.5$  kcal./mole. It is shown that the values of the heats of formation of triiodide and iodate ions are internally self-consistent within the limits of experimental error.

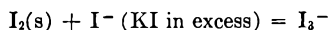
## I. Introduction

Different measurements of the temperature coefficient of the equilibrium constant for



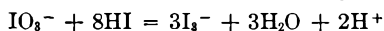
yield values of the heat of complexing of aqueous iodine with iodide ion from  $-3.87$  to  $-5.10$  kcal./mole.<sup>1</sup> These heats combined with the heats of formation of aqueous iodine<sup>1</sup> and iodide ion<sup>2</sup> result in values ranging from  $-11.7$  to  $-12.9$  kcal./mole for the heat of formation of triiodide ion. The National Bureau of Standards<sup>2</sup> lists  $-12.4$  kcal./mole and a standard entropy of 41.5 e.u., which is not compatible with any of the above values when combined with pertinent thermodynamic data. Hence there is a considerable uncertainty associated with the heat of formation of triiodide ion and the heats of formation of other substances which are related to it.

The National Bureau of Standards<sup>2</sup> heat of formation of  $IO_3^-$  (aq) appears to be calculated from data that are between nearly fifty and more than eighty years old. Heats of formation of other halogen compounds and ions based on results taken from the older literature or from indirect measurements sometimes have been found to be in conflict with more recent values.<sup>1</sup> Thus direct and related calorimetric determinations at  $25^\circ$  of the heats of formation of these two important oxidation states of iodine were undertaken. That of triiodide ion was determined from the heat of reaction



The heat of formation depends only on the measured heat and the well established heats of formation and dilution of potassium iodide solutions. The entropy was calculated from the results of these measurements and appropriate thermodynamic data.

The heat of formation of iodate ion was determined from the heat of reduction with excess aqueous hydriodic acid combined with the newly determined



heat of formation of  $I_3^-$  and other data. The stoichiometry of this reaction is well established.<sup>3</sup>

(1) Summarized by H. C. Mel, W. L. Jolly, and W. M. Latimer, *J. Am. Chem. Soc.*, **75**, 3827 (1953).

(2) National Bureau of Standards, Circular 500, "Selected Values of Chemical Thermodynamic Properties," Washington, D. C., 1952, Reprint of July, 1961.

(3) I. M. Kolthoff and E. B. Sandell, "Textbook of Quantitative Inorganic Analysis," 3d Edition, The Macmillan Co., New York, N. Y., p. 594.

Solutions of iodic acid and potassium acid iodate in differing concentrations were used as separate sources of iodate ion in two different sets of measurements. Appropriate heat of dilution corrections also were determined.

## II. Experimental

A. Determination of  $\Delta H_f^\circ$  of  $I_3^-$  (aq).—Materials.—Iodine and potassium iodide were both reagent grade. All solutions of potassium iodide were freshly prepared with triply distilled water.

Microcalorimeter and Experimental Procedure.—The measured heats were less than one calorie per run and were determined with a twin heat-leak microcalorimeter.<sup>4,5</sup> In this apparatus the heat of the reaction taking place within one of the calorimeters is exchanged with the bath. The heat exchange follows Newton's law of conduction and

$$\Delta H = K \int_{t_1}^{t_2} \Delta T dt$$

where  $\Delta H$  is the total heat exchanged between times  $t_1$  and  $t_2$ ,  $K$  is the heat transfer constant, and  $\Delta T$  is the temperature difference between thermostat and reaction calorimeter.  $\Delta T$  is equal to zero before and after the reaction period. The integration is performed graphically by means of a recorder trace of  $\Delta T$  vs.  $t$ , so that

$$\Delta H = K \Delta A$$

where  $\Delta A$  is the area under the traced curve determined by planimeter and  $K$  by electrical calibration. The assumptions have been discussed in detail by Borchardt and Daniels.<sup>4</sup> The microcalorimeter consists of two identical glass vessels with flat bottoms, 35 mm. in diameter with a capacity of 80 ml. One vessel contained both reactants, the other potassium iodide solution only. Both vessels are capped by tight-fitting standard taper 40/50 Teflon covers 3 cm. thick. Passing through each cover is a thin thermistor probe, an off-center propeller-stirrer shaft, and a ramrod for breaking ampoules, all made of glass. The reaction was initiated by crushing a submerged ampoule containing iodine against the bottom of the reaction vessel. No heat effect was observed as a result of breaking an empty ampoule.

A thyatron speed-controlled motor drives separate identical pulleys so that the contents of both calorimeters are stirred at exactly equal rates. Temperature changes as a function of time are plotted on a 10 mv. recorder (Speedo-max G), utilizing the amplified (Leeds & Northrup micro-volt amplifier 9835-A) off-balance potential of a Wheatstone bridge network. The bridge consists of two variable five dial resistance decades set at 2 kilohms, and a matched thermistor (Fenwal G170, 2 kilohms each) in each of the two calorimeter vessels. It is powered by one mercury battery (Mallory RM-42R, 1.34 v.). The circuit is arranged so that the bridge remains balanced when temperature changes occur that are due to causes other than the reaction itself. The recorder trace thus represents the temperature difference between the reactant system in one calorimeter vessel and the inert solution in the other as a function of time.

(4) H. J. Borchardt and F. Daniels, *J. Am. Chem. Soc.*, **79**, 41 (1957).

(5) F. D. Rossini, ed., "Experimental Thermochemistry," Ch. 12, E. Calvet, "Microcalorimetry of Slow Phenomena," Interscience Publishers, Inc., New York, N. Y., 1956.

The calorimeter vessels are immersed to the level of the Teflon caps in a highly insulated enclosed 20-l. water-bath. The temperature is regulated by a proportional controller (Electron-o-therm 148LT) and low-lag knife heater balanced with a submerged refrigeration coil. All runs were made at  $25.000 \pm 0.0015^\circ$  as determined by a platinum resistance thermometer and Mueller bridge.

A heater coil (Manganin, 21.93 ohms) immersed in Octoil and contained in a thin glass tube is used to determine the heat transfer constant  $K$ . The energy for the heater is furnished by two mercury batteries in series. The current is determined by measuring the potential drop across a standard 10-ohm resistance in series with the heater by means of a millivolt potentiometer (Leeds & Northrup 8691). The time of heating is given by an electric stopclock synchronized with the heater switch.

Reactions were carried out in an excess of 2.0 *M* potassium iodide to ensure complete and reasonably rapid conversion to triiodide ion. In a run 50 ml. of potassium iodide was placed in each calorimeter vessel. Thermal equilibrium was attained in less than 5 min. after breaking the submerged ampoule containing a weighed quantity of iodine. The base line was unchanged before and after all runs or calibrations, with  $\Delta T$  estimated to be less than  $0.02^\circ$ .

B. Determination of  $\Delta H_f^\circ$  of  $\text{IO}_3^-$ (aq).—Materials.—Primary standard  $\text{KH}(\text{IO}_3)_2$  (Hach Ver) and reagent grade  $\text{HIO}_3$  (B. and A.) were heated for several hours prior to weighing and were dissolved in distilled water. Aqueous solutions of HI were freshly prepared and analyzed by methods discussed elsewhere.<sup>5</sup>

Calorimeter and Experimental Procedure.—The calorimeter has been described elsewhere.<sup>6</sup> The reductions were carried out in an excess of aqueous hydroiodic acid (200–250 ml.). The iodate solution was weighed into a thin glass ampoule which then was submerged in the reaction solution. After crushing the ampoule, the reaction proceeded very rapidly and thermal equilibrium was attained in less than 60 sec. Heat of dilution corrections were measured similarly. Observed temperature changes were corrected for heat exchange<sup>7</sup> and electrical calibrations were made after each run in the range  $26 \pm 1^\circ$ .

### III. Results

All heats of reaction and dilution are given in the Tables I–IV. Precision indices associated with all average heats are standard deviations.

Heat of Reaction of Solid Iodine with Aqueous Iodide Ion.—The details are given in Table I.

Moles $\text{I}_2 \times 10^3$	$M_{\text{HI}}$	Total energy change, cal.	$\Delta H_1$ , cal./mole $\text{I}_3^-$
0.9949	2.00	0.904	907
1.128	2.00	.996	883
1.047	2.00	.934	888

$$\text{Av. } \Delta H_1 = 893 \pm 12 \text{ cal./mole } \text{I}_3^-$$

Heat of Reduction of Iodate Ion ( $\text{KH}(\text{IO}_3)_2$ ) with Hydroiodic Acid in Aqueous Solution.—The details are given in Table II.

Heat of Reduction of Iodate Ion ( $\text{HIO}_3$ ) with Hydroiodic Acid in Aqueous Solution.—The details are given in Table III.

Heat of Dilution Corrections.—The appropriate heat of dilution corrections of iodic acid were determined in order to correct the calorimetric reaction results of Table III to standard states. The heat of dilution of potassium acid iodate was

(6) J. H. Stern and A. A. Passchier, *J. Chem. Eng. Data*, **7**, 73 (1962).

(7) A. Weissberger, "Physical Methods of Organic Chemistry," Vol. I, Third Edition, Interscience Publishers, Inc., New York, N. Y., 1959, p. 538.

TABLE II  
THE HEAT OF REDUCTION  $\Delta H_2$  OF  $\text{KH}(\text{IO}_3)_2$  WITH HI

Moles $\text{KH}(\text{IO}_3)_2 \times 10^4$	Moles HI	$M_{\text{HI}}$	$\Delta T$ cor. $\pm 0.001^\circ$	Total energy change, cal.	$-\Delta H_1$ , kcal./mole $\text{IO}_3^-$
4.620	0.270	1.35	0.361	77.78	84.20
5.002	.270	1.35	.385	83.60	83.55
4.801	.270	1.35	.375	80.14	83.45

$$\text{Av. } \Delta H_2 = -83.73 = 0.44 \text{ kcal./mole } \text{IO}_3^-$$

TABLE III  
THE HEAT OF REDUCTION  $\Delta H_3$  OF  $\text{HIO}_3$  WITH HI

Moles $\text{HIO}_3 \times 10^3$	Moles HI	$M_{\text{HI}}$	$T$ cor. $\pm 0.001^\circ$	Total energy change, cal.	$-\Delta H_1$ , kcal./mole $\text{IO}_3^-$
2.980	0.252	1.26	1.175	252.7	84.78
2.965	.252	1.26	1.163	250.4	84.44
2.945	.308	1.54	1.167	248.0	84.21
2.975	.308	1.54	1.166	253.5	85.22

$$\text{Av. } \Delta H_3 = -84.66 = 0.45 \text{ kcal./mole } \text{IO}_3^-$$

TABLE IV  
THE HEAT OF DILUTION  $\Delta H_4$  OF  $\text{HIO}_3$

$M_{\text{HIO}_3}$ initial	$M_{\text{HIO}_3}$ final $\times 10^6$	No. of runs	Av. $\Delta H_4$ , kcal./mole $\text{HIO}_3$
0.2536	5.00	2	$-0.45 \pm 0.05$

found to be negligible. Table IV lists summarized values.

### IV. Interpretation of Data

Standard Heat of Formation and Entropy of  $\text{I}_3^-$ (aq).—Unless otherwise specified, all calculations were made using thermodynamic properties from the National Bureau of Standards Tables.<sup>1</sup>

The average  $\Delta H_1$  ( $893 \pm 12$  cal./mole) from Table I combined with appropriate heats of formation and dilution corrections yields  $\Delta H_f^\circ$  of  $\text{I}_3^-$  ( $0.02 M$ ) =  $-12.72$  kcal./mole. Since the concentration of triiodide ion was very low, we assume this result also to be equal to  $\Delta H_f^\circ$  of  $\text{I}_3^-$ (aq) =  $-12.72$  kcal./mole, with an estimated over-all error of  $\pm 0.15$  kcal./mole. Combining this result with pertinent thermodynamic data we calculate  $S^\circ$  of  $\text{I}_3^-$ (aq) = 56.0 e.u.

Standard Heat of Formation of Iodate Ion.—Combining the average  $\Delta H_2$  from Table II ( $\text{KH}(\text{IO}_3)_2$ ) with the newly determined heat of formation of  $\text{I}_3^-$  and other heats, we calculate  $\Delta H_f^\circ$  of  $\text{IO}_3^-$ (aq) =  $-55.07$  kcal./mole. Similarly the average  $\Delta H_3$  from Table III combined with  $\Delta H_4$  from Table IV ( $\text{HIO}_3$ ), yields  $\Delta H_f^\circ$  of  $\text{IO}_3^-$ (aq) =  $-54.59$  kcal./mole. We shall take our final value as the average of the above two,  $\Delta H_f^\circ = -54.8 \pm 0.5$  kcal./mole. This value is in good agreement with those given by the National Bureau of Standards of  $-55.0$  and  $-54.9$  kcal./mole for  $\text{IO}_3^-$ (aq) and  $\text{HIO}_3$ (aq), respectively. This agreement shows that our value of  $\Delta H_f^\circ$  of  $\text{I}_3^-$ (aq) is internally self-consistent with experimental heats reported here and auxiliary heats used in these calculations.

Acknowledgment.—Financial support of this work by the Research Corporation is gratefully acknowledged.

## NOTES

THE VAPOR PRESSURE AND HEAT OF  
SUBLIMATION OF GOLD<sup>1</sup>

By D. L. HILDENBRAND AND W. F. HALL

Research Laboratories, Aeronutronic Division of Ford Motor Co., Newport  
Beach, California

Received May 16, 1961

Although the available literature contains a number of references to experimental determinations of the vapor pressure of gold, the reported values are not in good agreement and the derived heat of sublimation is uncertain by at least several kcal./mole. Some additional vapor pressure data for gold have been obtained recently in this Laboratory in the course of some studies of the reliability of the torsion-effusion method of vapor pressure measurement. It was felt worthwhile to report this information in view of the need for firmly establishing such basic data. When enough information of this type becomes available, it may be possible to establish a reliable set of high temperature vapor pressure standards such as those developed for the standardization of calorimetric measurements. Because of the fundamental importance of vapor pressure measurements in high temperature chemistry studies, the establishment of vapor pressure standards would appear to be desirable.

Data reported here have been obtained by the torsion-effusion method, which has been described previously.<sup>2,3</sup> With this method, one observes the angular deflection induced by effusion of vapor from a multihole effusion cell which is suspended from a filament of small restoring force. The pressure within the effusion cell can be evaluated from the relation

$$P = \frac{2k\theta}{\Sigma afq} \quad (1)$$

where  $k$  is the torsion constant of the filament,  $\theta$  is the measured angular deflection, and  $a$ ,  $f$  and  $q$  are the area, force factor and moment arm of each of the effusion orifices. The force factor corrects for the reduction in effusive force resulting from the finite thickness of the orifice and has been calculated for various tube geometries by Freeman and Searcy.<sup>4</sup> It should be noted that total pressure data so obtained are on an absolute basis and, in addition, are not dependent on the composition of the effusing vapor.

## Experimental

Engelhard Industries mint grade gold of better than 99.99% purity was used for the vapor pressure measurements.

Since the torsion-effusion apparatus will be described in more detail in a forthcoming publication, only a brief description will be given here. All measurements were made

using effusion cells machined from ATJ high density graphite. The cells were of square horizontal cross section and contained four effusion orifices, one each drilled in opposite sides of opposite vertical faces so that the moment arm of each of the orifices with respect to the center of suspension was about 0.55 cm. Orifice depths were of the order 0.04 to 0.05 cm. The effusion cell geometrical factors are given in Table I. Contrary to the experience of Pugh and Barrow<sup>5</sup> and Witt and Barrow,<sup>6</sup> the graphite cells used in this and other research in this Laboratory have proven to be entirely satisfactory as far as reproducibility of results is concerned. In addition, there was no evidence for diffusion of the liquid metal or its vapor through graphite, as reported by Edwards and Downing<sup>7</sup> for mercury, silver and copper. However, it is highly unlikely that diffusion or permeation effects could contribute a net torque and thus, even if present, they should have no effect on the torsion measurements.

TABLE I

THE VAPOR PRESSURE AND HEAT OF SUBLIMATION OF GOLD

$T$ , °K.	$\theta \times 10^3$ , rad.	$P \times 10^5$ , atm.	$\Delta H_{298}$ , kcal./mole
Cell 3			
1669	32.9	1.08	88.1
1691	43.4	1.42	88.3
1741	87.2	2.88	88.3
1722	68.2	2.25	88.3
1705	51.9	1.71	88.3
1655	24.2	0.80	88.3
1705	54.8	1.80	88.1
1744	90.0	2.95	88.3
1762	115.9	3.80	88.2
1733	77.7	2.55	88.3
Cell 4			
1796	60.2	5.88	88.3
1831	96.1	9.18	88.2
1814	73.9	7.14	88.5
1779	46.6	4.60	88.4
1785	48.4	4.78	88.6
1823	80.9	7.78	88.4
1841	107.0	10.22	88.3
1807	60.8	5.92	88.7
1767	36.4	3.66	88.5
Cell 5			
1966	77.7	48.5	88.0
1943	54.4	33.9	88.4
1923	44.3	27.6	88.3
1897	29.8	18.6	88.7
1960	71.6	44.6	87.9
1954	65.2	40.6	88.0
1943	56.7	35.4	88.2
1930	50.6	31.6	88.0
1830	13.8	8.6	88.4

Av. 88.3 ± 0.2

	Cell 3	Cell 4	Cell 5
$a$ , cm. <sup>2</sup>	0.0105	0.0046	0.0010
$\Sigma afq$ , cm. <sup>3</sup>	0.01872	0.00681	0.000977
$k$ , dyne cm./rad.	3.12	3.20	3.09

(1) This work was supported in part by the Advanced Research Projects Agency under Contract NOrd 17980.

(2) A. W. Searcy and R. D. Freeman, *J. Am. Chem. Soc.*, **76**, 5229 (1954).(3) M. D. Scheer, *J. Phys. Chem.*, **61**, 1184 (1957).(4) R. D. Freeman and A. W. Searcy, *J. Chem. Phys.*, **22**, 762 (1954).(5) A. C. P. Pugh and R. F. Barrow, *Trans. Faraday Soc.*, **54**, 671 (1958).(6) W. P. Witt and R. F. Barrow, *ibid.*, **55**, 730 (1959).(7) R. K. Edwards and J. H. Downing, *J. Phys. Chem.*, **59**, 1079 (1955).

A 30-cm. length of tungsten wire, 0.005 cm. in diameter, served as the torsion filament. Oscillations were damped out magnetically. The effusion cell was heated by radiation from a surrounding hollow tantalum cylinder which was in turn heated by high frequency induction. By shielding the cell and heating indirectly, a coupling effect<sup>2</sup> between the cell and the high frequency field was avoided, leading to entirely satisfactory operation. A number of 0.2-cm. diameter holes drilled in the susceptor side and a larger hole in the removable lid allowed for evacuation of the cell region and escape of vapor molecules. Thermal radiation shielding of the susceptor was provided by several layers of tantalum foil joined in such a way as to present a high resistance to eddy currents.

A fused silica tube enclosed the susceptor and cell arrangement and, while measurements were in progress, was evacuated to a pressure of  $5 \times 10^{-5}$  mm., or lower. The bottom of the tube contained a planar optical window protected by a movable shutter. Temperatures were measured with a calibrated disappearing-filament optical pyrometer sighting through the optical window and a hole in the susceptor bottom into a cylindrical black body cavity in the bottom of the effusion cell. The cavity was 1.0 cm. deep and 0.25 cm. in diameter. Temperatures were corrected for reflection losses at window and prism surfaces.

The remainder of the system, the method of determining the torsion constant and the measurement of angular deflection are essentially the same as described by others.<sup>2,3</sup> In this work, the torque angle could be observed directly to within 0.001 radian.

### Results

The experimental vapor pressure data and derived heats of sublimation are given in Table I and are listed in the order of measurement. Data were obtained with three different orifice sizes; the three sets of results are in good agreement, indicating the observed pressures to be equilibrium values. There is no reason to suspect a reaction of the metal with graphite, since it does not form a stable carbide.<sup>8</sup> The extent to which the results may be affected by solution of carbon in gold, with subsequent lowering of the activity, is not known with certainty, but the effect is believed to be inappreciable. The same gold sample was used throughout the measurements, with no observed change in pressure with time such as might be expected for a gradual solution of carbon in the metal in significant amount. Experimental pressures were within the molecular flow range, as required for application of equation 1.

Free energy functions used in the third law treatment of the vapor pressure data were taken from Stull and Sinke.<sup>9</sup> The assumption of monomeric vapor implicit in the calculations appears to be valid since mass spectra of the vapor obtained under both free evaporation<sup>10</sup> and Knudsen<sup>11</sup> conditions indicate less than one mole per cent. polymeric species to be present. The average third law value of the heat of sublimation at 298°K., 88.3 kcal./mole, is assigned an over-all accuracy uncertainty of  $\pm 0.9$  kcal./mole, based on an analysis of experimental errors. An estimate of a possible error of 15° in temperature measurement contributes most of the uncertainty. From the tempera-

ture dependence of pressure, one calculates a second law  $\Delta H_{298}$  of 89.3 kcal./mole, in good agreement with the third law value.

In Table II, the results of this research are compared with third law heats of sublimation derived from the work of other investigators, in all cases using free energy functions from ref. 9. Uncer-

TABLE II  
COMPARISON OF RESULTS FOR Au(s) = Au(g)

Investigator	Ref.	$\Delta H_{298}$ , kcal./mole
P. Harteck	12	90.7
L. D. Hall	13	84.7 $\pm$ 0.7
R. K. Edwards	14	87.0
E. G. Rauh	14	87.2 $\pm$ 0.8
A. N. Nesmeyanov, <i>et al.</i>	15	87.3
R. D. Freeman	16	88.4
P. Grieveson, <i>et al.</i>	17	88.0-89.3
This Research		88.3 $\pm$ 0.9

tainties are included where they have been estimated by the various investigators. All results except those of this research were obtained by the Knudsen effusion technique, although no details concerning the work of Edwards<sup>14</sup> or Rauh<sup>14</sup> are as yet available. Grieveson, *et al.*,<sup>17</sup> used both Knudsen and transpiration techniques; a trend of 1.3 kcal./mole in the derived third law heats over the range of their measurements, however, indicates a temperature dependent error. The ratio of orifice area to surface area employed in the effusion measurements of Harteck<sup>12</sup> appears too large to yield equilibrium pressures and the  $\Delta H_{298}$  value obtained from his data is high by about 0.6 kcal./mole. Except for the unaccountably high pressures obtained by Hall,<sup>13</sup> who used a radioactive tracer technique to monitor the effusion transport, the various sets of data are in reasonable agreement and indicate a best value of  $88.0 \pm 1$  kcal./mole for the heat of sublimation of gold at 298°K.

(12) P. Harteck, *Z. physik. Chem.*, **134**, 1 (1928).

(13) L. D. Hall, *J. Am. Chem. Soc.*, **73**, 757 (1951).

(14) Private communication, quoted by R. Hultgren, *et al.*, "Thermodynamic Properties of Metals and Alloys," Minerals Research Laboratory, University of California, Berkeley, California, 1960.

(15) A. N. Nesmeyanov, L. A. Smakhtin, D. Ya. Choporov and V. I. Lebedev, *Zhur. Fiz. Khim.*, **33**, 342 (1959).

(16) R. D. Freeman, Oklahoma State University, private communication.

(17) P. Grieveson, G. W. Hooper and C. B. Alcock, "Physical Chemistry of Process Metallurgy," Interscience Publishers, Inc., New York, N. Y., 1961, pp. 341-352.

## EFFECT OF INTENSITY ON THE RADIATION INDUCED DECOMPOSITION OF INORGANIC NITRATES<sup>1</sup>

By EVERETT R. JOHNSON

Department of Chemistry, Brookhaven National Laboratory, Upton Long Island, New York

Received August 15, 1961

The radiolysis of the solid inorganic nitrates has been shown to be complex. The yields are dependent upon lattice parameters,<sup>2,3</sup> changes which

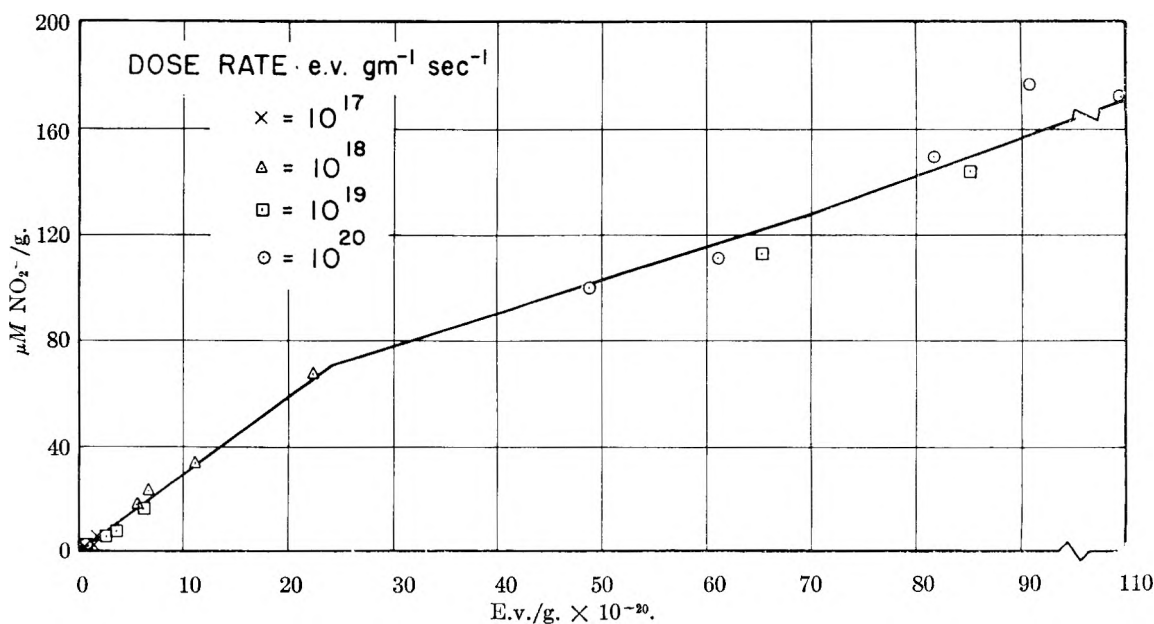
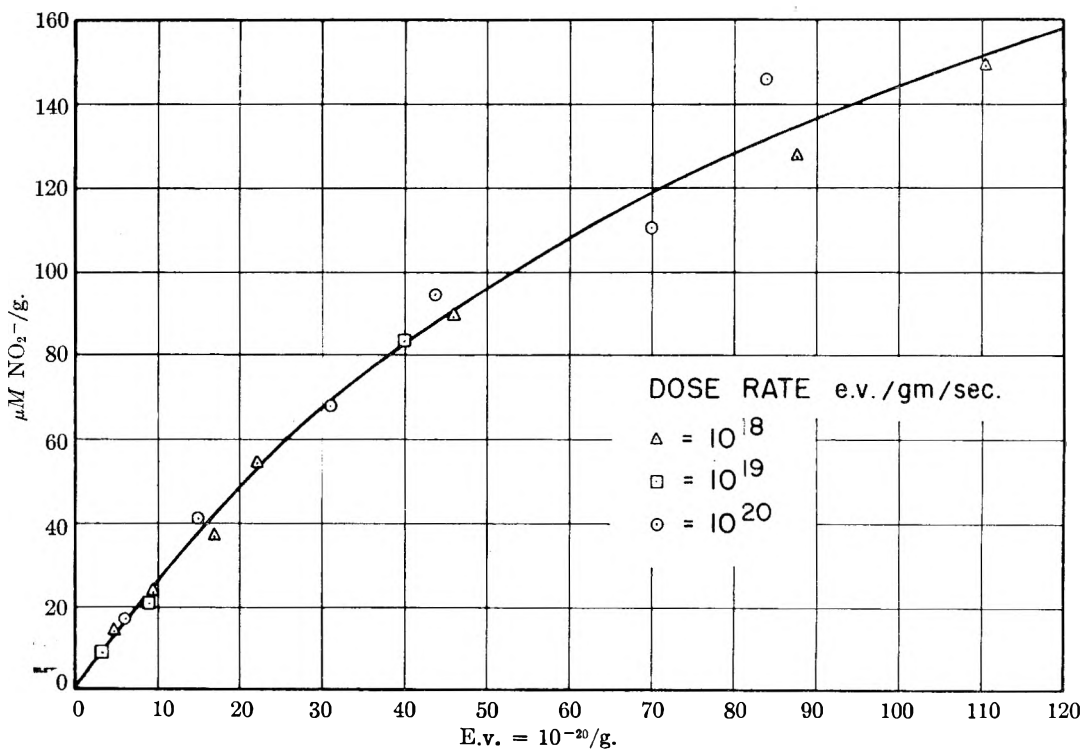
(8) L. Brewer, L. A. Bromley, F. W. Gilles and N. L. Lofgren, Paper 4 in "The Chemistry and Metallurgy of Miscellaneous Materials: Thermodynamics," National Nuclear Energy Series, Vol. 19B, McGraw-Hill Book Co., New York, N. Y., 1950.

(9) D. R. Stull and G. C. Sinke, "Thermodynamic Properties of the Elements," Advances in Chemistry Series, No. 18, American Chemical Society, Washington, D. C., 1956.

(10) J. Drowart and R. E. Honig, *J. Phys. Chem.*, **61**, 980 (1957).

(11) P. O. Schissel, *J. Chem. Phys.*, **26**, 1276 (1957).

(1) Research performed in part under the auspices of the U. S. Atomic Energy Commission, Brookhaven National Laboratory, Upton, L. I., N. Y., and in part under contract No. AT(30-1) 1824.

Fig. 1.—Effect of intensity on decomposition of KNO<sub>3</sub>.Fig. 2.—Effect of intensity on decomposition of CsNO<sub>3</sub>.

occur in the lattice during irradiation,<sup>4,5</sup> and possibly on the stability of the primary products formed, *viz.*, the nitrite ion. One of the factors which has not been clarified in these studies is the effect of intensity on the nitrite yield. It is the intent of this communication to clarify this aspect

(2) (a) J. Cunningham and H. G. Heal, *Trans. Faraday Soc.*, **54**, 1355 (1958); (b) J. Cunningham, *J. Phys. Chem.*, **65**, 628 (1961).

(3) G. Hennig, R. Lees, and M. S. Matheson, *J. Chem. Phys.*, **21**, 664 (1953).

(4) J. Forten and E. R. Johnson, *J. Phys. and Chem. Solids*, **15**, 218 (1960).

(5) E. R. Johnson and J. Forten, *Discussions Faraday Soc.*, **31**, 238 (1961).

of the decomposition of the inorganic nitrates by ionizing radiation.

#### Experimental

One and one-half Mev. electrons from a Van de Graaf accelerator were used as the radiation source. The total current passing through the sample was determined by a current integrator designed by the Electronics Department of the Brookhaven National Laboratory.<sup>6</sup> Nitrite ion was determined by Shinn's method.<sup>7</sup> The molar extraction at 546 mμ was 53,200. To ensure uniform analyses, the entire sample was dissolved and an aliquot taken for nitrite ion analysis.

(6) R. Shuler and A. O. Aller, *J. Chem. Phys.*, **24**, 56 (1956).

(7) M. B. Shinn, *Ind. Eng. Chem., Anal. Ed.*, **13**, 33 (1941).

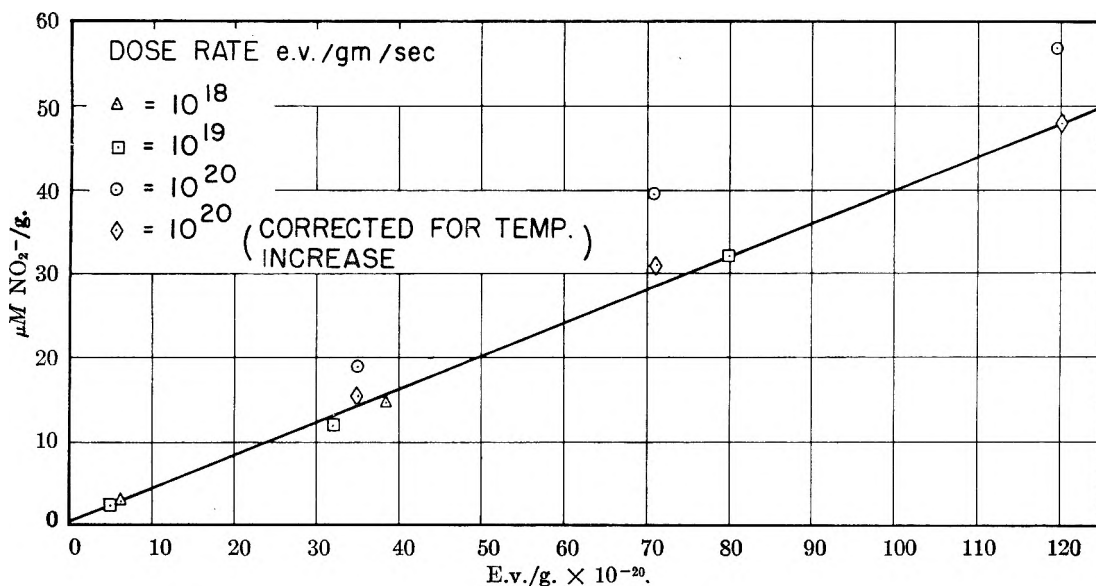


Fig. 3.—Effect of intensity on decomposition of NaNO<sub>3</sub>.

The radiation cells were flat cylinders of Pyrex glass, 14 mm. i.d. and an average of 2.7 mm. inside length in the direction of the beam. This is about half the range of the electrons. The front face of the cell was about 5 to 10 mils thick. There was a single entrance to the cell from the edge, 3 mm. i.d. and about 1 cm. long for sample filling, which was left open during the irradiation.

During the irradiation, the cell was placed behind a grounded 0.25-in. aluminum plate, 3 in. in diameter with a 15-mm. hole directly in front of the cell. Only that portion of the electron beam which penetrated the radiation cell was collected. Behind the cell, a 0.25-in. thick insulated aluminum plate collected the current that passed through the sample. A 2 mil platinum wire attached to the back plate was inserted a few millimeters into the neck of the cell to prevent the accumulation of any static charge in the sample. During irradiation all samples were cooled by compressed air.

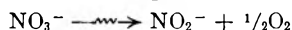
**Results**

The dose rate for the nitrates varied from 10<sup>15</sup> to 10<sup>20</sup> e.v./g./sec. The lower value was obtained from γ-ray results reported in a previous communication.<sup>4</sup> Dosimetry for the electron beam experiments was determined by filling the individual radiation cells with ferrous sulfate dosimetric solution and making a direct determination of the dose. The standard deviation in determining dose was ±5%.

This deviation was due primarily to the fact that exposures for the dosimetry experiments were of the order of 0–2 sec., and the mechanism for cutting off the beam involved an uncertain amount of human error.

The value used for dosimetry calculations was 15.45 molecules of Fe<sup>++</sup> oxidized per 100 e.v.<sup>6</sup> The results are summarized in Fig. 1–4.

**KNO<sub>3</sub>.**—The decomposition of potassium nitrate by ionizing radiation, as with most of the nitrates, yields nitrite ion and oxygen.<sup>2a, 3, 5, 8, 9</sup>



In the case of KNO<sub>3</sub> a distinct break in the nitrite yield vs. dose curve is found.<sup>2b, 4</sup> The G-value before the break (initial slope) was found

(8) C. J. Hochanadel and T. W. Davis, *J. Chem. Phys.*, **27**, 333 (1957).

(9) A. O. Allen and J. A. Ghormley, *ibid.*, **15**, 203 (1947).

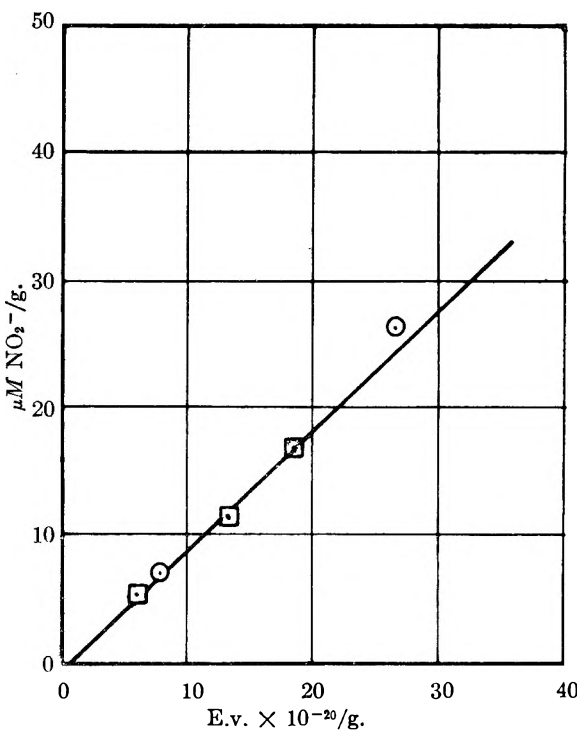


Fig. 4.—Effect of intensity on decomposition of Pb(NO<sub>3</sub>)<sub>2</sub>. Dose rates e.v./g./sec.: □ = 10<sup>19</sup>; ○ = 10<sup>20</sup>.

to be 1.48 ± 0.21 and after the break 0.96 ± 0.06. These may be compared with the values of 1.38<sup>4</sup>, 1.456<sup>2b</sup> ± 0.011, and 1.58<sup>8</sup> found for the initial slope, and 0.93<sup>4</sup> and 0.902 ± 0.029 for that portion of the curve after the break using Co<sup>60</sup> γ-rays.

During the radiolysis of both KNO<sub>3</sub> and NaNO<sub>3</sub> it was found that anomalously high yields of nitrite were obtained during the high intensity experiments (10<sup>20</sup> e.v./g./sec). This could be shown to be due to poor current collection efficiency, which gave a low value of the absorbed dose and consequently a high G-value. The poor collection current was manifested by a slow but steady

decrease in the collected electron beam current during an exposure. It was found that cutting off the beam for a few minutes when the current had decreased 1-2% remedied the situation. Apparently both  $\text{KNO}_3$  and  $\text{NaNO}_3$  stored a large amount of charge; by cutting off the beam for a few minutes, this static charge could bleed off through the platinum wire in contact with the sample. At low intensities the rate at which the static charge bled off was about equal to or less than the rate at which charge could build up. This effect, however, was not observed in either  $\text{CsNO}_3$  or  $\text{Pb}(\text{NO}_3)_2$ .

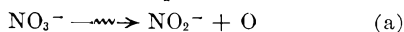
**$\text{CsNO}_3$ .**—The results on intensity effects are shown graphically in Fig. 2. The  $G$ -value for the initial slope was found to be  $1.53 \pm 0.08$  for the intensity range  $10^{18}$ – $10^{20}$  e.v./g./sec. This may be compared with the values of  $1.44$ ,<sup>4</sup>  $1.68 \pm 0.05$ ,<sup>3</sup> and  $1.72 \pm 0.12$ <sup>2b</sup> obtained by  $\gamma$ -radiolysis. In the high dose region there is no basis for comparison with  $\gamma$ -rays from previous work.

**$\text{NaNO}_3$ .**—The results obtained for the decomposition of  $\text{NaNO}_3$  are shown in Fig. 3. The  $G$ -value using only the data obtained at a dose rate of  $10^{18}$  and  $10^{19}$  e.v./g.<sup>-1</sup> sec.<sup>-1</sup> was  $0.22 \pm 0.02$ . This may be compared with the values of  $0.16$ ,<sup>4</sup>  $0.25 \pm 0.02$ ,<sup>8</sup> and  $0.200 \pm 0.004$ <sup>2b</sup> obtained by  $\gamma$ -rays. The results obtained at the highest dose rate ( $10^{23}$  e.v./g.<sup>-1</sup> sec.<sup>-1</sup>) do appear to show an intensity effect. However, although these samples were cooled during irradiation, some unavoidable warming amounting to 8–12° was observed. Cunningham found about a 50% increase in the  $G$ -value of  $\text{NaNO}_3$  when the temperature was increased from 25 to 60°. The results at the high dose rate accordingly were corrected assuming an average temperature rise of 10°.

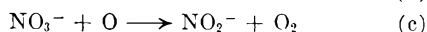
**$\text{Pb}(\text{NO}_3)_2$ .**—The decomposition of lead nitrate (Fig. 4) was studied only in the initial decomposition range. The  $G$ -value found for the initial slope was  $0.53 \pm 0.08$ . This may be compared with the values of  $0.48$ ,<sup>4</sup>  $0.44 \pm 0.04$ <sup>8</sup> and  $0.43$ <sup>2</sup> found by  $\gamma$ -ray radiolysis.

### Discussion

The primary step in the decomposition of the inorganic nitrates has been postulated to be<sup>2b,8-11</sup>



The oxygen fragment produced in (a) reacting as<sup>1a,9,8</sup>



and possibly



It was shown previously<sup>5</sup> that a kinetic scheme using reactions (a), (b), and (c) above gave excellent agreement with experiments for the radiolysis of  $\text{NaNO}_3$ . It is quite possible that a similar reaction scheme will show good agreement for some of the other nitrates, particularly  $\text{CsNO}_3$  and  $\text{AgNO}_3$ .

Considering the range of intensities used in these studies it does not appear, within experi-

mental error, that there is any appreciable intensity effect. Certainly there is no evidence for reaction (d) above. The agreement between  $\gamma$ -ray results and electron beam experiments is as good in most cases as that shown among the different laboratories for the various nitrate decompositions by  $\gamma$ -rays. It was not feasible to extend this work to higher dose rates because of the difficulty of dissipating the large amount of heat generated.

## THE STRUCTURE OF LANTHANUM FAMILY SILICIDES<sup>1</sup>

By A. G. THARP<sup>2</sup>

Department of Mineral Technology, University of California, Berkeley, California

Received August 24, 1961

Perri, Binder, and Post<sup>3,4</sup> have described the structures of several rare earth silicides with  $\text{MSi}_2$  ideal lattice types. Their work agreed with, and expanded upon, that previously reported by Brauer and Haag.<sup>5</sup> The structures of  $\text{LaSi}_2$ ,  $\text{CeSi}_2$ ,  $\text{PrSi}_2$ , and  $\text{EuSi}_2$  were shown to be tetragonal while structures of  $\text{NdSi}_2$ ,  $\text{SmSi}_2$ ,  $\text{GdSi}_2$ ,  $\text{DySi}_2$ , and  $\text{YSi}_2$  are orthorhombic. Perri, *et al.*, postulated that the tetragonal lattice is characteristic of disilicides of those rare earths with relatively large atomic radii.

The orthorhombic structure is a slight distortion of the  $\text{LaSi}_2$  (tetragonal) type structure. At slightly elevated temperatures, where the effective diameters of the atoms are increased by thermal vibration, the orthorhombic phases transform to the tetragonal structure.

Radii of the lanthanum family atoms generally decrease with increased atomic number except that preference for certain electronic configurations causes the radii of some of the atoms to lie off the smooth curve of diameter *vs.* atomic number.

The present work was undertaken to compare the structures of disilicides of the higher atomic number lanthanum family elements, erbium, thulium, ytterbium, and lutetium. If the postulate of Perri, *et al.*, is valid for these elements,  $\text{YbSi}_2$ , if such a phase could be prepared, should crystallize in the tetragonal system as do  $\text{EuSi}_2$  and disilicides of lower atomic number rare earths, while erbium, thulium, and lutetium disilicides should have the orthorhombic or some other structure.

### Experimental

**Preparation of Samples.**—Disilicides of thulium and ytterbium were prepared by direct syntheses from the elements. Disilicides of erbium and lutetium were synthesized by reducing the sesquioxides of the rare earths with an excess of silicon. The rare earth oxides, rare earth metals, and the silicon were 99.9+ % pure.

The reactions between thulium and silicon and between ytterbium and silicon were carried out in tungsten crucibles under a slight positive pressure of helium or argon or *in vacuo*. Vacuum preparation was somewhat undesirable since considerable quantities of thulium or ytterbium would vaporize from the reaction chamber. The argon or helium was dried by passing it through a 30-in. column of phos-

(1) This work was supported by the Office of Naval Research.

(2) Department of Chemistry, Long Beach State College, Long Beach, California.

(3) J. A. Perri, I. Binder, and B. Post, *J. Phys. Chem.*, **63**, 616 (1959).

(4) J. A. Perri, I. Binder, and B. Post, *ibid.*, **63**, 2073 (1959).

(5) G. Brauer and H. Haag, *Z. anorg. allgem. Chem.*, **267**, 198 (1952).

(10) P. Doigan and T. W. Davis, *J. Chem. Phys.*, **27**, 333 (1957).

(11) L. K. Narayanswamy, *Trans Faraday Soc.*, **31**, 1411 (1935).



phoric anhydride and magnesium perchlorate. No evidence of oxidation of either the samples or containers could be observed.

A few preparations were carried out in tantalum, molybdenum, and graphite containers to determine whether or not the phases formed were influenced by reaction with the container. No container reaction could be observed visually or by X-ray analyses.

Er<sub>2</sub>O<sub>3</sub> and Lu<sub>2</sub>O<sub>3</sub> were heated with silicon in tungsten, molybdenum, tantalum, and graphite previously impregnated with silicon. These preparations were usually carried out *in vacuo*.

A reaction temperature of about 1200° was used for synthesis from the elements. Temperatures of 1300 to 1500° were used for synthesis by reduction of an oxide. The samples prepared by reduction of the oxide with silicon were made by raising the temperature very slowly until rapid evolution of gases was obtained as was evident by the quantity of material condensing on the walls of the vacuum system. A temperature of 1350° gave good results. The preparations were heated at maximum temperature for 0.5 to 4 hr.

Thulium disilicide and ytterbium silicide were prepared with a sufficiently large excess of silicon to obtain free silicon

in the preparation. Thulium disilicide also was prepared with enough excess thulium to yield a lower thulium silicide.

### Results

**Crystallographic Data.**—All preparations were examined by powder X-ray diffraction techniques. A 114.59 mm. Debye-Scherrer powder camera was used. Examination of the X-ray diffraction data showed that the four disilicides, ErSi<sub>2</sub>, TmSi<sub>2</sub>, YbSi<sub>2</sub>, and LuSi<sub>2</sub>, crystallize in the hexagonal system. These data were compared with that for other hexagonal disilicides and found to be similar to those for β-USi<sub>2</sub> and β-ThSi<sub>2</sub>. Accordingly, these phases were assigned the space group C6/mmm. The atom positions are one metal atom in (0, 0, 0) and two silicon atoms in ± (1/3, 2/3, 1/2).

Thulium disilicide gave diffraction patterns of especially good quality. Three of these were measured and indexed. Intensities of the diffraction lines were estimated visually. Approximate theoretical intensities were calculated by utilizing the formula

$$I \propto F^2 p \frac{1 + \cos^2 2\theta}{\sin^2 \theta \cos \theta}$$

where  $F$  is the structure factor,  $p$  is the multiplicity factor, and  $1 + \cos^2 2\theta / \sin^2 \theta \cos \theta$  is the trigonometrical polarization correction factor.

The calculated intensities are in good agreement with the observed intensities. These crystallographic data for TmSi<sub>2</sub> are given in Table I.

The diffraction data and intensities for ErSi<sub>2</sub>, YbSi<sub>2</sub>, and LuSi<sub>2</sub> are in excellent agreement with that for TmSi<sub>2</sub>. The YbSi<sub>2</sub> phase gives a diffraction pattern with rather poor back reflections. This indicates poorly formed crystals, but since no splitting of the diffraction lines can be observed, the hexagonal structure is correct. The unit cell dimensions and X-ray densities for ErSi<sub>2</sub>, TmSi<sub>2</sub>, YbSi<sub>2</sub>, and LuSi<sub>2</sub> are given in Table II.

TABLE II  
CELL PARAMETERS AND THEORETICAL DENSITIES

Compound	$a_0$ , Å.	$c_0$ , Å.	Theoretical density, g./cm. <sup>3</sup>
ErSi <sub>2</sub>	3.786	4.089	7.31
TmSi <sub>2</sub>	3.768	4.071	7.48
YbSi <sub>2</sub>	3.77	4.10	7.54
LuSi <sub>2</sub>	3.745	4.046	7.81

### Discussion

Perri and co-workers<sup>3</sup> showed by detailed intensity measurements and calculations that the composition of the gadolinium silicide with the MSi<sub>2</sub> type ideal lattice is about GdSi<sub>1.4</sub>. The hexagonal phases reported in this work appear to have very close to the ideal composition. An excellent X-ray pattern for TmSi<sub>2</sub> was obtained from a sample prepared by combining silicon with thulium in a gram-atom ratio of 3:1. This diffraction pattern showed a very faint silicon pattern, and a very weak diffraction line for the strongest reflection of Tm<sub>2</sub>O<sub>3</sub>.

This sample was studied with the Geiger counter diffractometer. Intensities for these diffraction lines which have an appreciable silicon contribution were measured by determining the area under the diffraction curve. Theoretical intensities were calculated assuming a random absence of silicon atoms

TABLE I

CRYSTALLOGRAPHIC DATA FOR TmSi<sub>2</sub>  
Cu K $\alpha$  Radiation ( $K\alpha = 1.5418$  Å.)

$hk$	$\sin^2 \theta_{\text{obsd}}$	$\sin^2 \theta_{\text{calcd}}$	$I_{\text{obsd}}^a$	$I_{\text{calcd}}$
001	0.0358	0.0359	m <sup>+</sup>	18
100	.0557	.0558	s	50
101	.0915	.0917	vvs	100
002	.1437	.1434	m <sup>b</sup>	11
110	.1675	.1674	s <sup>-</sup>	27
102	.1994	.1992	m <sup>b</sup>	16
111	.2033	.2033	m	10
200	.2229	.2232	m <sup>-</sup>	6
201	.2591	.2591	s	20
112	.3108	.3109	s	19
003	absent	.3227	...	1
202	.3668	.3667	m <sup>-</sup>	6
103	.3778	.3785	m	11
210	.3903	.3907	w <sup>b</sup>	5
211	.4264	.4265	s	18
113	.4904	.4902	w	2
300	.5022	.5023	w	5
212 <sup>+</sup>	.5333	.5332	m <sup>-</sup>	7
301	absent	.5373	...	2
203	.5451	.5451	w	7
004	absent	.5728	...	0
104	.6283	.6306	w <sup>-</sup>	3
302	.6443	.6447	w <sup>b</sup>	8
220	.6693	.6686	w <sup>-</sup>	4
221	.7050	.7044	w	2
213	.7123	.7122	m <sup>-</sup>	13
310	.7250	.7243	w	3
114	.7405	.7399	w	8
311	.7609	.7601	w <sup>b</sup>	14
204	.7960	.7957	w <sup>-</sup>	4
222	.8123	.8118	w	10
303	.8241	.8237	w	3
312	.8679	.8675	m	10
400	.8916	.8915	w <sup>-</sup>	3
005	absent	.8950	...	1
401	.9270	.9273	m <sup>-</sup>	12
105	.9509	.9507	w <sup>b</sup>	15
214	.9628	.9628	m <sup>b</sup>	19
223	.9904	.9908	m	13

<sup>a</sup> vvs = very very strong, s = strong, m = medium, w = weak. <sup>b</sup> This reflection and subsequent ones are for copper K $\alpha_1$  radiation ( $K\alpha_1 = 1.5405$  Å.).

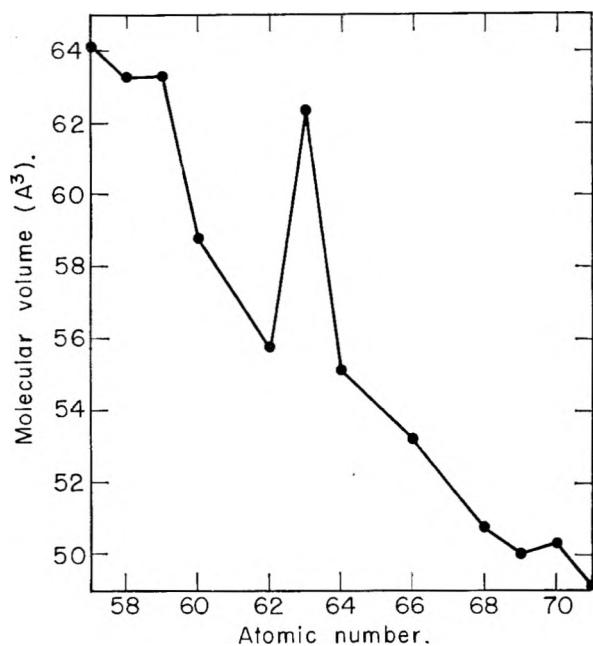


Fig. 1.—Molecular volume of lanthanum metal disilicides vs. atomic number of the metal.

in the lattice and a composition of  $\text{TmSi}_{1.76}$ . These calculated intensities were not in as good agreement with the observed intensities as were the calculated intensities for the composition  $\text{TmSi}_2$ .

Two films of preparations with a silicon to thulium ratio greater than two were measured. Both films show a weak silicon diffraction pattern. The cell parameters for these phases of  $\text{TmSi}_2$  were calculated and the agreement with those for the phase known to be near the composition  $\text{TmSi}_2$  was excellent. No variation in intensities could be observed. It therefore was concluded that the composition of the thulium silicon phase was very close to  $\text{TmSi}_2$ .

X-Ray patterns for samples prepared by varying the silicon to metal ratio showed only the hexagonal  $\text{MSi}_2$  phase and that of a lower silicide for thulium and ytterbium when the gram-atom ratio was about 1.75. Apparently the structures of these phases are not changed by varying the silicon composition as are those of thorium and uranium with the  $\text{MSi}_2$  type ideal lattice. Previous work<sup>6,7</sup> shows that  $\alpha\text{-ThSi}_2$  has about the ideal composition while  $\beta\text{-ThSi}_2$  is silicon deficient. The lower atomic number lanthanum family  $\text{MSi}_2$  phases that are isostructural with  $\alpha\text{-ThSi}_2$  and  $\alpha\text{-USi}_2$ <sup>8</sup> apparently do not show the  $\beta\text{-MSi}_2$  structure modification.

That  $\text{YbSi}_2$  crystallizes in the same crystal system as the other three disilicides reported in this paper is not consistent with the previously reported<sup>3,4</sup> structures for rare earth disilicides if the ytterbium atom is assumed to have the same relatively large size as found in the metal and if the ratio of atom sizes is the important factor in determining the system in which a phase should crystallize. That the cell parameters for  $\text{YbSi}_2$  are

(6) G. Brauer and A. Mitius, *Z. anorg. u. allgem. Chem.*, **249**, 325 (1942).

(7) E. L. Jacobson, R. D. Freeman, A. G. Tharp, and A. W. Searcy, *J. Am. Chem. Soc.*, **78**, 4850 (1956).

(8) W. H. Zachariasen, *Acta Cryst.*, **2**, 94 (1949).

only slightly larger than those of  $\text{TmSi}_2$  and  $\text{LuSi}_2$  suggests that the silicon-silicon contacts determine the crystal volume or that the average number of bonding electrons of ytterbium atoms in  $\text{YbSi}_2$  is more nearly the same as for atoms of adjacent lanthanide elements in their disilicides. The graph of molecular volume of lanthanum family disilicide phases vs. atom number of the metal atoms shown in Fig. 1 demonstrates the variation of cell sizes and consequently of metal atom sizes found in these disilicide phases. The trend in cell dimensions correlates rather closely with the variation in atom sizes for the pure lanthanum family elements. There is, however, somewhat less variation in cell sizes between the hexagonal phases than in the tetragonal and orthorhombic phases.

The hexagonal disilicide phases of erbium, thulium, lutetium, and especially of ytterbium, might be expected to transform at high temperatures to tetragonal or orthorhombic forms isostructural with the disilicides of the lighter lanthanide elements. No evidence of such high temperature transformations could be obtained. Since considerable rearrangement of atoms would be required for the structural transformation to occur, it might be expected that very rapid cooling would quench any high temperature phase. Only the hexagonal phase was observed when samples were cooled at rates of over 500° per min.

## A MODIFIED DIFFUSION TIME-LAG

BY IRVING FATT

Miller Institute for Basic Research in Science and Department of Mineral Technology, University of California Berkeley

Received December 26, 1961

The time-lag measurement described by Barrer,<sup>1</sup> Frisch,<sup>2</sup> and Goodknight and Fatt (GF)<sup>3</sup> often is used to measure diffusion coefficients, or if the coefficient is known, to obtain information on pore structure parameters of porous media. Barrer<sup>1</sup> derives the time-lag equation for a linear porous body in which there are no dead-end pores (cul-de-sacs). Goodknight and Fatt<sup>3</sup> have extended this derivation to include porous media in which there is dead-end pore volume.

The initial and boundary conditions from which Barrer derives his time-lag equation require that the porous plug be initially at a uniform concentration below that which will be imposed at the upstream end at time zero. The outflow end is maintained at the initial concentration and the cumulative amount of material diffusing out of this end is measured as a function of time.

It often is more convenient to have initially in the porous plug a uniform concentration equal to that which will be maintained at the upstream end, and at time zero to lower the concentration at the outflow end. The cumulative amount of material diffusing out of this end is measured as a function of time. This system will be shown below to have a time-lag similar to that of Barrer, differing only by sign and a numerical coefficient. Both time-lags

(1) R. M. Barrer, *J. Phys. Chem.*, **57**, 35 (1953).

(2) H. L. Frisch, *ibid.*, **63**, 1249 (1959).

(3) R. C. Goodknight and I. Fatt, *ibid.*, **65**, 1709 (1961).

can be used to obtain information on the structure of porous media containing dead-end pores.

**Nomenclature**

- A* cross-sectional area of porous body
- A<sub>0</sub>* cross-sectional area of neck between a dead-end pore and flow channel
- c* compressibility
- C* variable concentration
- C<sub>2</sub>* concn. in dead-end pore (variable)
- C<sub>0</sub>* upstream end concn. (*X* = *L*)
- C<sub>b</sub>* downstream end concn. (*X* = 0)
- D* diffusion coefficient
- H* constant coefficient, *H* = *DA<sub>0</sub>*/*l<sub>0</sub>V<sub>0</sub>*
- k* permeability of porous body
- l<sub>0</sub>* length of neck between a dead-end pore and flow channel
- L* length of porous body
- Q<sub>t</sub>* flux parameter, *Q<sub>t</sub>* = *Z<sub>L0</sub>*/*φ<sub>1</sub>A*
- t* time
- T<sub>LF</sub>* time-lag, this paper
- T<sub>LB</sub>* time-lag, Barrer
- V<sub>1</sub>* pore vol. of flow channel (not including dead-end pore vol.)
- V<sub>2</sub>* total vol. of all dead-end pores
- V<sub>0</sub>* volume of a single dead-end pore
- X* distance coordinate
- Z<sub>L0</sub>* cumulative material diffused from outflow end
- Z<sub>La</sub>* cumulative material diffused from outflow end when *Z<sub>L0</sub>* is a linear function of time
- θ* tortuosity (diffusion path length/*L*)
- φ<sub>1</sub>* *V<sub>1</sub>*/*AL*
- μ* viscosity

**Theory**

The time-lag equation will be obtained here for a linear diffusing system with initial and boundary conditions as

$$\begin{aligned}
 C(X, 0) &= C_2(X, 0) = C_0 & (1) \\
 C(L, t) &= C_0 & (2) \\
 C(0, t) &= C_b, t > 0 & (3)
 \end{aligned}$$

For any given set of system parameters, the amount of material diffusing out of the outflow end, *X* = 0, as a function of time can be calculated from eq. 15, 16, and 19 of GF by letting *X* = 0 in their eq. 19. If the porous system is known to be free of dead-end pores than *V<sub>2</sub>* = *H* = 0 in this equation.

For large *t* the GF eq. 15, 16, and 19 with *X* = 0 give the asymptotic straight line

$$Z_{L0} = \frac{D\phi_1 A(C_0 - C_b)}{\theta^2 L} \left[ -t - \frac{\theta^2 L^2}{3D} \left( 1 + \frac{V_2}{V_1} \right) \right] \quad (4)$$

The intercept of this line on the time axis, in a plot of *Z<sub>L0</sub>* vs. *t*, is obtained by setting *Z<sub>La</sub>* = 0 and is the time-lag

$$T_{LF} = - \frac{\theta^2 L^2 (V_1 + V_2)}{3 D V_1} \quad (5)$$

or

$$T_{LF} = - \frac{\theta^2 L(V_1 + V_2)}{3 D \phi_1 A} \quad (6)$$

This is to be compared with the Barrer time-lag

$$T_{LB} = \frac{\theta^2 L^2 (V_1 + V_2)}{6 D V_1} \quad (7)$$

or

$$T_{LB} = \frac{\theta^2 L(V_1 + V_2)}{6 D \phi_1 A} \quad (8)$$

as taken from eq. 23 of GF.

Note that for diffusion the time-lags are dependent upon the ratio of total pore volume to volume of the flow channels. This is in contrast

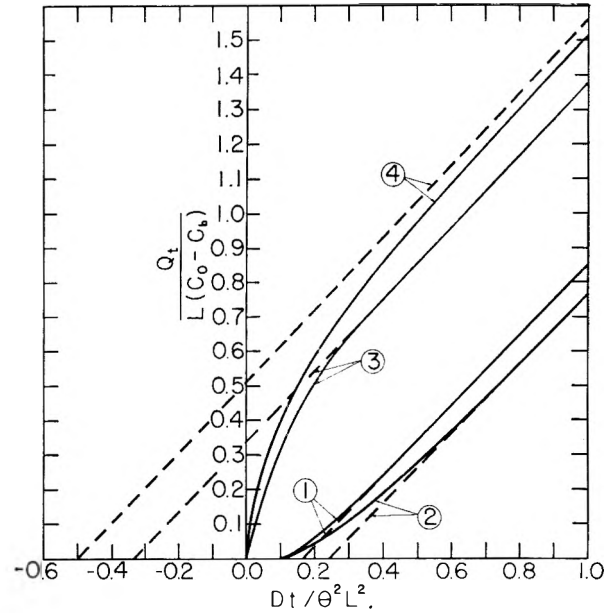


Fig. 1.—Dimensionless cumulative material diffusing out of a linear porous body as a function of the dimensionless time parameter. Curves 1 and 2 are for Barrer's conditions. Curves 3 and 4 are for the conditions given in equations 1, 2 and 3. Curves 1 and 3 are for porous systems with no dead-end pore volume. For curves 2 and 4, (*V<sub>1</sub>* + *V<sub>2</sub>*)/*V<sub>1</sub>* = 1.48, *H* = 0.1347 sec.<sup>-1</sup>. The dashed lines are the linear asymptotes.

to the case for non-steady state flow of a slightly compressible fluid in a porous medium for which the time-lags are given in eq. 9 and 10 and are dependent only on the total pore volume.

$$T_{LF} = - \frac{\mu c L (V_1 + V_2)}{3 k A} \quad (9)$$

and

$$T_{LB} = \frac{\mu c L (V_1 + V_2)}{6 k A} \quad (10)$$

This distinction was not made clear by GF.

This difference in dependence on pore volume distribution results from the difference in definition between the diffusion and permeability coefficients. The permeability is defined for the gross area of a porous material whereas the diffusion coefficient refers to pore area in a unit gross area. As a result the diffusion time-lag equations, 6 and 8, have an area term *Aφ<sub>1</sub>*. In contrast, eq. 9 and 10 for fluid flow have only the *A* term.

**Discussion**

Figure 1 shows a plot of *Q<sub>t</sub>*/*L(C<sub>0</sub> - C<sub>b</sub>)* as a function of the time parameter *Dt*/*θ<sup>2</sup>L<sup>2</sup>* for the Barrer time-lag system and for the system described here, both with and without dead-end pores. These curves were calculated from GF eq. 20 by means of a FORTRAN program on an IBM 704 computer. The curves labeled 1 and 3 are for a porous medium without dead-end pores. The asymptotic straight lines intercept the abscissa at -1/3 and 1/6 as predicted by eq. 5 and 8, respectively. Curves 2 and 4 are examples for a system in which there is dead-end pore volume so that (*V<sub>1</sub>* + *V<sub>2</sub>*)/*V<sub>1</sub>* = 1.48 and *H* = 0.1347 sec.<sup>-1</sup> in GF eq. 12, 13, and 20. Equations 5 and 7 predict that the presence of dead-end pores causes the

time-lag to be multiplied by  $(V_1 + V_2)/V_1$ . This is confirmed by the calculated results shown in Figure 1.

In Fig. 1 the transient part of curve 4 has not yet reached the asymptote at  $Dt/\theta^2 L^2 = 1.0$ . An examination of the calculated data beyond the range of Fig. 1 showed that the linear asymptote was reached at  $Dt/\theta^2 L^2 = 4.0$  and that the intercept of this line on the abscissa is  $-0.494$ , in agreement with eq. 5 and as shown in Fig. 1 for the values of  $V_1$ ,  $V_2$ , and  $H$  chosen above.

**Acknowledgment.**—The author wishes to thank the donors of the Petroleum Research Fund, administered by the American Chemical Society, for their support of the research which led to this paper.

## A CRITICISM OF HEAT OF IMMERSIONAL WETTING PRACTICE

By J. J. CHESSICK

William H. Chandler Chemistry Laboratory, Lehigh University, Bethlehem, Penna.

Received September 21, 1961

The procedural techniques of heat of wetting practice as well as those of data interpretation used by workers in the 1930's generally persist to this day. Some modifications have been introduced, obviously, but these for the most part are either correctional in nature or due to advances in equipment. The question raised here is whether more than modest changes are needed. Evidence is presented to support the view that, indeed, drastic changes are needed to prevent errors of experiment and interpretations of inadequate data in much of the current writing in this field.

The number of articles which in the opinion of the writer could be included here is large. The requirement of brevity alone is sufficient justification for the restriction of discussion to only a limited number of authors. *This, of course, is unfair provided the reader restricts his thinking and judgment to the articles discussed here.* A good portion of the paper treats critically articles co-authored by the writer. The paper suffers as a consequence since in many instances better arguments could have been presented.

### Discussion

**1. The Relationship between Heat of Immersional Wetting and Adsorption Thermodynamics.**—Only a brief discussion of basic relationships, background material for the discussion which follows, will be given. A detailed treatment has been presented.<sup>1</sup>

The integral heat of adsorption of  $N_A$  moles of adsorbate from the vapor state at saturation pressure  $P_0$  and temperature  $T$  is

$$h_{\text{ads.}} = [(h_{I(\text{SL})} - h_{I(\text{SL})})/\Gamma] + \Delta H_L \quad (1)$$

where  $h_{I(\text{SL})}$  and  $h_{I(\text{SL})}$  are, respectively, the heat evolved on immersing an adsorbate-free (evacuated) sample and a sample containing  $N_A$  moles of pre-adsorbed molecules of wetting liquid into this

liquid,  $\Gamma = N_A/\Sigma$ ,  $\Sigma$  is the external area of the solid, and  $\Delta H_L$  the molar heat of liquefaction. The net integral heat of adsorption  $h_{\text{net}} = (h_{I(\text{SL})} - h_{I(\text{SL})})$  is used most frequently and  $h_L$  values are expressed commonly in units of ergs/cm.<sup>2</sup> of surface. The need to define  $h_L$ , the enthalpy change involved in destroying a cm.<sup>2</sup> of liquid surface, will become apparent.

The difference in entropy of the adsorbed film,  $S_A$ , and the entropy of the bulk liquid is given by the expression

$$T(S_A - S_L) = [(h_{I(\text{SL})} - h_{I(\text{SL})})/\Gamma] + \varphi/\Gamma - kT \ln X \quad (2)$$

Here  $X (= P/P_0)$  is the relative equilibrium pressure and  $\varphi (= \gamma_{\text{S}^0} - \gamma_{\text{S}^1})$  the difference in surface free energy of the adsorbate-free solid and one containing adsorbed molecules at a surface concentration  $\Gamma$  (expressed best in moles/cm.<sup>2</sup> to yield conventional entropy units). The equation is valid also if the solid is perturbed on adsorption; the symbol  $S_A'$  is used to denote the entropy of the adsorbate-solid system now.

### 2. The Use of Limited Heat of Wetting Data For the Interpretation of Solid-Liquid Interactions.

—Many workers in the past have reported and used for interpretive purposes only heat values  $h_{I(\text{SL})}$  for the immersion of a given solid into a variety of liquids or different solids into one liquid. Significantly, the writer is co-author of two of these articles. The following references are four of many.<sup>2</sup> Recently, a paper pointing out a few of the dangers inherent in the use of insufficient data was published.<sup>3</sup> Here principal attention was paid to reported  $h_{I(\text{SL})}$  values for the immersion of a rutile ( $\text{TiO}_2$ ) temperature activated at  $500^\circ$ , into a variety of  $n$ -polar paraffin derivatives (three and four carbon compounds such as the acid, amine, alcohol, halides) of references 2a and 2b. There the net heats of adsorption  $(h_{I(\text{SL})} - h_{I(\text{L})})/\Gamma$  at monolayer coverage were compared with calculated interaction energies; the sum of solid-adsorbate energies due to dipole, polarization, dispersion, and adsorbate-adsorbate interaction affects. Further, the slope of the linear curve obtained when the net integral energies of interaction were plotted against the dipole moments of the wetting liquids was used to estimate the average force field emanating from the solid surface.

The calculations of net integral heats of adsorption of  $n$ -butyl derivatives onto rutile<sup>2a,2b</sup> from  $h_{I(\text{SL})}$  values alone required the following assumptions: (1) the formation of a monolayer of wetting liquid molecules oriented perpendicular to the surface, polar groups down, (2) the same number of close-packed adsorbate molecules per unit area of surface for the seven different  $n$ -paraffin derivatives; (3) a value of  $h_{I(\text{SL})}$  at  $\theta = 1$  equal to  $h_L$  for the particular wetting liquid; (4) packing independent of the substrate; (5) physical adsorption alone occurred on high temperature activated

(2) (a) F. H. Healey, J. J. Chessick, G. J. Young, and A. C. Zettlemoyer, *J. Phys. Chem.*, **58**, 887 (1954); (b) J. J. Chessick, A. C. Zettlemoyer, F. H. Healey, and G. J. Young, *Can. J. Chem.*, **33**, 251 (1955); (c) B. V. Il'in and V. F. Kiselev, *Doklady Akad. Nauk, S.S.S.R.*, **82**, 85 (1952); (d) W. D. Harkins, "The Physical Chemistry of Surface Films," Reinhold Publ. Corp., New York, N. Y., 1952.

(3) C. M. Hollabaugh and J. J. Chessick, *J. Phys. Chem.*, **65**, 109 (1961).

(1) J. J. Chessick and A. C. Zettlemoyer, *Advances in Catalysis*, **11**, 263-9 (1959).

rutile and others. The work of Hollabaugh and Chessick<sup>3</sup> demonstrated clearly that some (and undoubtedly all) of these assumptions are incorrect. For example, *n*-butyl halides do not adsorb to form oriented monolayers; rather, flat-wise adsorption as well as multilayer formation was observed. The predicted orientation of alcohol molecules did occur but the packing was not independent of the substrate and chemisorption could not be ruled out. Other workers<sup>2c</sup> made calculations of this type using inadequate data also.

Obviously, the use of plots of  $(h_{I(SL)} - h_{I(SfL)})$  vs. dipole moment to calculate the average field emanating from a solid surface must be viewed with suspicion. Despite the warning given<sup>3</sup> against this practice, such a calculation from too limited experimental data was carried out recently.<sup>4</sup> A serious objection, purely experimental in nature, can be advanced here. The workers of references 2a and 4 used *n*-butyl chloride as an immersion liquid because of its high dipole moment relative to the hydrocarbon, amine, alcohol, etc., completely ignoring the fact that an alcohol and amine possess a peripheral, positive dipole and the chloride a non-peripheral, negative dipole. Their measured  $h_{I(SL)}$  values were large, nevertheless, and in apparent agreement with the predicted increase in heat evolved per unit area of solid with increase in dipole moment of the wetting liquid. These values are experimentally incorrect and result from the presence of unsuspected trace amounts of water in the wetting liquid. Employment of the multi-bulb technique developed by Wightman<sup>5</sup> to remove this trace water reduced the heat of immersion of rutile in *n*-butyl chloride from  $621 \pm 21$  to  $281 \pm 12$  ergs/cm.<sup>2</sup><sup>3</sup>

An understanding of the adsorption process demands isotherm data, preferably measured rather than assumed data, over the range of relative pressure from zero to that of the coverage of interest, as well as heat of immersion values obtained as a function of the amount of wetting liquid pre-adsorbed before immersion. This is a long and tedious process even for one adsorbent-adsorbate systems.

**3. The Use of  $h_L$  Values to Calculate Net Integral Heats of Adsorption; Solid-Organic Liquid Systems.**—Where net integral heats of adsorption  $(h_{I(SL)} - h_{I(SfL)})$ , expressed here in units of ergs/cm.<sup>2</sup> are used for interpretative purposes, most frequently,  $h_L$ , the heat evolved upon destruction of a unit area of (wetting) liquid surface is used in place of  $h_{I(SfL)}$  at  $\theta = 1$  or greater.<sup>6</sup> While this practice may not always lead to serious difficulty, particularly if employed with  $h_{I(SL)}$  values for polar solid-water systems, it can be condemned on grounds that assumed values are unnecessary. The appropriate  $h_{I(SfL)}$  values can be obtained experimentally without difficulty.

(4) L. Romo, *J. Colloid Sci.*, **16**, 139 (1961).

(5) J. P. Wightman, Ph.D. Thesis, Lehigh University, Bethlehem, Pa., 1960.

(6) (a) F. E. Bartell, *J. Phys. Chem.*, **58**, 36 (1954); (b) D. J. Hine and W. C. Wake, *Trans. Faraday Soc.*, **55**, 1017 (1959); (c) R. L. Every, W. H. Wade, and N. Hackerman, *J. Phys. Chem.*, **65**, 25 (1961); (d) See previous references 2a and 2b also. Many others are unlisted.

Further the assumption that  $h_{I(SfL)}$  at  $\theta = 1$  is equal to  $h_L$  for the wetting liquid can be seriously incorrect when organic immersion liquids are employed. The heats of immersion of rutile into *n*-butyl chloride or *n*-propyl alcohol measured as a function of pre-adsorbed wetting liquid revealed that heats evolved per cm.<sup>2</sup> at monolayer coverages are markedly different than the respective  $h_L$  values.<sup>3</sup> Similar findings were reported for graphite samples immersed in toluene, carbon tetrachloride, *n*-heptane, cyclohexane, and *n*-propyl alcohol.<sup>7</sup> The paucity in the literature of heat of immersion curves obtained as a function of  $\theta$  for solid-organic liquid systems, which could justify the use of reasonable, assumed values of  $h_{I(SfL)}$  at  $\theta = 1$  or greater in certain instances, is an additional reason to refrain from the uncertain and carry out the necessary, more tedious chore of obtaining isotherm data and heats of wetting as a function of the amounts preadsorbed. The paucity of such data is convincing evidence that the easy path of limited experiment and unproved assumptions is still with us.

**4. The Use of  $h_L$  Values to Calculate Net Integral Heats of Adsorption: Solid-Water Systems.**—The collection and inspection of the more numerous heat of wetting values obtained as a function of  $\theta$  for the immersion of non-porous polar solids having surface areas ca. 5 to 20 m.<sup>2</sup>/g. in water has shown that rarely does a  $h_{I(SL)}$  value exceed  $h_L$  by more than 20% at  $\theta = 1$ . At higher coverages the use of  $h_L$  rather than the measured value has a good measure of support, provided a duplex film forms. Such an assumption need not be made, however; film type can be determined experimentally.

Heat of immersion values,  $h_{I(SL)}$ , less than  $h_L$  are indicative of systems upon which non-duplex films form. Nevertheless, net integral heats  $(h_{I(SL)} - h_L)$  have been calculated for such systems, e.g., graphite<sup>6c</sup> and silica<sup>6b</sup> in water. The reason for a negative net integral heat of adsorption  $[(h_{I(SL)} - h_L) = (108 - 118) = -10 \text{ ergs/cm.}^2]$  found in this Laboratory for the immersion of the silica Aerosil (now Cab-O-Sil) was revealed by further water and nitrogen isotherm determinations. These showed that the silica surface was 75% hydrophobic (non-duplex film) and 25% hydrophilic (possibly duplex film formation if patches large enough). A similar, fully hydroxylated, 25° outgassed silica had a  $h_{I(SL)}$  value of 435 ergs/cm.<sup>3</sup>

It is true that the quantity  $(h_{I(SL)} - h_L)$  can be used simply as a comparative device. This must be plainly stated, however, when this procedure is employed. Perhaps it would be more convincing to state that the quantity  $(h_{I(SL)} - h_{I(SfL)})$  has thermodynamic significance, irrespective of whether the adsorption is non-duplex or duplex. This is illustrated by the established equation

$$(h_{I(SL)} - h_{I(SfL)}) = (E_A' - E_L) = \int_{\Gamma_2}^{\Gamma_1} q_{st} d\Gamma - \Gamma \Delta H_L \quad (3)$$

Only  $E_A'$ , the molar energy of the adsorbate-solid

(7) J. J. Chessick, A. C. Zettlemoyer, and Yung-Fang Yu, *J. Phys. Chem.*, **64**, 530 (1960).

system, and  $E_L$ , the molar energy of the liquid adsorbate, have not been defined previously. The quantity ( $h_{I(SL)} - h_L$ ) has thermodynamic significance only if  $h_{I(SL)} = h_L$ .

**5. Heats of Immersion of High-Temperature Activated Solids.**—Almost never are solids evacuated at elevated temperatures (300 to 500°) prior to immersion on conventional apparatus protected from the influence of trace amounts of organic contaminants in the system. This statement applies to all references of this paper except 1 (in part), 3, 5, and 7 although it is possible that in some (limited) instances precautions were taken but not reported.

Heat values (ergs/cm.<sup>2</sup>) measured for the immersion of rutile evacuated at 450° to an ultimate vacuum of 10<sup>-6</sup> mm. on a B.E.T.-type adsorption rig were much too erratic to be acceptable.<sup>3</sup> The heat of immersion of rutile outgassed in this manner in water was found to be 708 ± 20 ergs/cm.<sup>2</sup>. Very divergent values were rejected on a statistical basis. If a liquid nitrogen trap separated the sample from the adsorption system during evacuation and further if dry oxygen was introduced in the sample system at the evacuation temperature, the heat of immersion of this rutile sample decreased to 588 ± 9 ergs/cm.<sup>2</sup>. Reduction of the rutile surface is indicated; organics are present on the solid surface and (or) on the rig. Similar divergent heat values were found recently in this Laboratory for the immersion of protected and unprotected samples of alumina activated at 500°. In this instance, the use of the nitrogen trap alone was sufficient to prevent surface contamination; unlike the rutile sample its surface originally was free of organic contaminants.

Footnote 10 of a recent publication which reported the heats of immersion,  $h_{I(SL)}$ , of a variety of rutile and anatase samples in water as a function of temperature of activation<sup>8</sup> reveals a belated recognition of this unsuspected, additional variable. Most articles, reporting immersion values for temperature-activated solids, suffer from this defect.

The assumption made too frequently that polar solids such as anatase,<sup>2d</sup> rutile,<sup>2a,2b</sup> calcium or barium sulfate,<sup>2c</sup> and many others activated at temperatures near 500° only physically adsorb molecules of the wetting liquid can not be accepted without further detailed studies.<sup>3</sup> There is danger also in comparing ( $h_{I(SL)} - h_{I(L)}$ ) values with spreading pressures,  $\phi$ , correctly calculated to  $\theta$ 's at the arbitrarily selected relative equilibrium pressure, both quantities being expressed and compared in units of ergs/cm.<sup>2</sup>.<sup>9</sup>

Free energies, enthalpies, and, particularly, entropies expressed in units of ergs/cm.<sup>2</sup> or ergs/cm.<sup>2</sup>/°C are much more difficult to interpret than those expressed in conventional units. A further need for converting  $\phi$  and  $h_{net}$  values into conventional units is seen from inspection of eq. 2. Spreading pressure values are accurately comparable only to net integral heats when corrected by the  $RT \ln P/P_0$  term; this was not done.<sup>9</sup> In addition, com-

parison of integral heat, free energy, and entropy values at a relative pressure so high that multilayers form suffers because of the insensitivity of such values to surface-adsorbate effects so pronounced in the region zero to monolayer coverage. Capillary effects due to interparticle or particle pores and as a consequence the decrease in area of the solid sample offer further possible complications.

**Acknowledgment.**—The author is grateful to the U. S. Air Force, Wright Air Development Division, Materials Center, Wright-Patterson Air Force Base, Ohio and the National Printing Ink Research Institute, Lehigh University, Bethlehem, Pennsylvania, for support in the development of this paper.

## FLUORINE N.M.R. SPECTROSCOPY. VI. FLUOROCARBON SULFIDES<sup>1</sup>

BY GEORGE VAN DYKE TIERS

Contribution No. 214 from the Central Research Dept., Minnesota Mining & Mfg. Co., St. Paul 19, Minn.

Received October 21, 1961

While nuclear magnetic resonance (n.m.r.) data have been reported for several fluorocarbon derivatives of sulfur hexafluoride,<sup>2,3</sup> and for certain unusual fluorocarbon sulfides,<sup>4,5</sup> such data for simple fluorocarbon mono- or polysulfides have been lacking. The n.m.r. measurements here presented fill this gap; and owing to their high precision several significant generalizations concerning fluorine n.m.r. spectroscopy also emerge from this work.

### Experimental

The syntheses and physical properties of the fluorocarbon sulfides have been reported,<sup>6-8</sup> save for the ultraviolet spectrum and certain constants of 1,4-dithiapentfluorocyclohexane. This compound, b.p. 81.5°, f.p. -6.5°, was studied at a concentration of 1  $\mu$ l./ml. in iso-octane, and had  $\lambda_{max.} = 2232 \text{ \AA.}$  and  $\epsilon_{max.} = 132$ . From its refractive index,  $n_D^{25} 1.3585$ , (lit. 1.3568<sup>8</sup>) and density,  $d^{25} 1.693$ , there is calculated  $M_R = 34.28$ , from which the atomic refractivity 7.40 is obtained for sulfur, in excellent agreement with the value previously given for fluorinated thioethers.<sup>7</sup>

The n.m.r. equipment and techniques have been described.<sup>9</sup>

In Table I are presented numerical shielding values, on the  $\phi$ -scale,<sup>9</sup> for all fluorine positions in each compound studied. Procedures for the approximate conversion of older and less precise numerical data<sup>2-8</sup> into  $\phi$ -values have been given.<sup>9</sup>

### Discussion

Shielding values for the -CF<sub>2</sub>S- group are seen to fall generally in the region 80-95  $\phi$ , about midway between  $\phi$ -values for the isoelectronic P and Cl compounds.<sup>10</sup> Much narrower limits are appropriate when similar structures are compared.

(1) Part III of the latter series; presented at the 138th National A.C.S. Meeting, New York, 1960.

(2) N. Muller, P. C. Lauterbur and G. F. Svatos, *J. Am. Chem. Soc.*, **79**, 1043 (1957).

(3) R. P. Dresdner and J. A. Young, *ibid.*, **81**, 574 (1959).

(4) M. Hauptschein and M. Braid, *ibid.*, **80**, 853 (1958).

(5) C. G. Krespan, *ibid.*, **83**, 3434 (1961).

(6) G. V. D. Tiers, *J. Org. Chem.*, **26**, 3515 (1961).

(7) G. V. D. Tiers, *ibid.*, **26**, 2538 (1961).

(8) C. G. Krespan, U.S. Pat. 2,931,803 (April 5, 1960).

(9) G. Filipovich and G. V. D. Tiers, *J. Phys. Chem.*, **63**, 761 (1959).

(10) E. Piteher, A. D. Buckingham and F. G. A. Stone, *J. Chem. Phys.*, **36**, 124 (1962).

(8) T. H. Wade and N. Hackerman, *J. Phys. Chem.*, **65**, 1861 (1961).

(9) R. L. Every, W. H. Wade, and N. Hackerman, *ibid.*, **65**, 25 (1961).

TABLE I

N.M.R. SHIELDING VALUES FOR FLUOROCARBON SULFIDES

Compound	Conc. <sup>a</sup>	$\phi^*$ Values <sup>b</sup> and multiplicities <sup>c</sup> for				
		$(CF_3-CF_2)$	$(CF_2-CF_2)$	$(CF_2-CF_2)$	$(CF_2-CF_2)$	$(CF_2)_2S_2$
$(n-C_3F_7)_2S$	10.0	80.58 $t^d$	124.22 b; 8.2	...	...	83.81 b; 17
$(n-C_7F_{15})_2S_2$	12.7	80.88 $t^e$	124.21 b; 4.5	...	...	90.80 m(q <sup>2</sup> )
$(n-C_7F_{15})_2S_1$	10.0	80.80 $t^f$	124.22 b; 5.3	...	...	91.82 q <sup>f</sup>
$(n-C_7F_{15})_2S_2$	16.0	81.54 $t^g$	126.5	122.5	119.7	89.79 b; 26
$(CF_3)_4S$	6.0	...	...	...	131.91 $t^h$	87.04 $t^h$
1,4- $(CF_3)_4S_2$	20.0	...	...	...	...	91.08 <sup>i</sup> b <sup>i</sup>

<sup>a</sup> Volume per cent. in  $CCl_3F$  (wt./vol. for perfluoroheptyl disulfide). <sup>b</sup> See ref. 9; standard deviation less than  $\pm 0.01$  for all values given to two decimals, and  $\pm 0.15$  for others. <sup>c</sup> Symbols for multiplicity: s, singlet; t, triplet; q, quadruplet; m, multiplet resolved but not analyzed; b, broad and unresolved peak, width at half-height,  $W_{1/2}$ , being given in c./s. <sup>d</sup>  $J(CF_3-C-CF_2) = 9.5 \pm 0.2$  c./s. <sup>e</sup>  $J(CF_3-C-CF_2) = 9.2 \pm 0.1$  c./s. <sup>f</sup>  $J(CF_3-C-CF_2) = 9.10 \pm 0.05$  c./s. <sup>g</sup>  $J(CF_3-C-CF_2) = 9.40 \pm 0.05$  c./s.; each component is an indistinct triplet having  $J \sim 2.5$  c./s. <sup>h</sup>  $J = 4.4 \pm 0.1$  c./s.; each component appears to be a triplet having  $J = 2.9 \pm 0.5$  c./s. <sup>i</sup> Line width is temp. dependent. At 0% concn.,  $\phi = 91.05$ .

For example, the range 89–91  $\phi$  includes the  $n$ -perfluoroalkyl disulfides having three or more carbons in the chain. The presence of an extra sulfur atom, in the trisulfide, causes only a small increase in shielding; but when both perfluoroalkyl groups are attached to the same sulfur atom the  $-CF_2S-$  peak is displaced downfield by about 7 p.p.m. One might be tempted to attribute this shift to electron withdrawal from sulfur by the perfluoroalkyl group, an effect already apparent in the shift to short wave lengths of the ultraviolet absorption maximum.<sup>6,7</sup> The inadequacy of this explanation is evident, however, in the pronounced *upfield* displacements, about 10 p.p.m., resulting from fluorination of sulfur to the hexavalent state<sup>2,3</sup>; a similar shift is seen in  $n-C_3F_7SO_2F$ , for which the  $\alpha$ - $CF_2$  shielding value is 108.56  $\phi^*$  (10 vol. % concn.). These oxidized sulfur atoms must be considered as much more strongly electron-withdrawing than those of the sulfides.

The very large downfield shifts observed for perfluoroalkyl halides and similar compounds have been attributed to "mixing" of low-lying excited states with the ground state in the magnetic field.<sup>10</sup> While this treatment accounts for the gross position of the  $-CF_2S-$  resonance, it appears to predict the reverse of the observed correlation of ultraviolet maxima with  $\phi$ -values. For the proposed explanation<sup>10</sup> to be correct one must assume that the particular "low-lying excited states" responsible for the observed ultraviolet maxima have the wrong symmetry properties and so fail to affect the n.m.r. spectra.

The effect of a single ring closure upon  $CF_2$  groups is, generally, to shift their n.m.r. peaks as much as 10 p.p.m. to higher values. Such a displacement is seen here in the comparison of the  $\phi$ -values for the  $C-CF_2-C$  groupings of bis-(perfluoropropyl) sulfide, or of bis-(perfluoroheptyl) disulfide, with that of thiaperfluorocyclopentane. The high shieldings for perfluorocyclohexane,

133.25  $\phi^{11}$  and for perfluorocyclobutane, 134.94  $\phi$ , as compared with the typical mid-chain value, 122.5  $\phi$ , found for long  $n$ -perfluoroalkyl groups,<sup>12</sup> illustrate this effect.

The smaller effect of sulfur upon more distant fluorine atoms ( $\beta$  and  $\gamma$ ) can be recognized most readily by comparison of  $\phi$ -values with those for a related fluorocarbon group. Thus, in bis-(perfluoroheptyl) disulfide the  $\phi$ -value  $\beta$  to sulfur is 119.7, or 6.9 p.p.m. lower than the usual value, 126.64  $\phi^*$ , found for  $CF_2$  groups adjacent to  $CF_3$ <sup>12</sup>; the bis-(perfluoropropyl) sulfides show a remarkably constant shift of  $-6.99$  p.p.m. relative to the  $CF_2$  in  $C_3F_8$ , 131.21  $\phi$ . It would appear that only the *nearest* sulfur atom causes the shift. At the  $\gamma$  position the shift is only  $-2.0$  p.p.m. (relative to  $C_3F_8$ ) for the  $CF_3$  group in the perfluoropropyl sulfides, and apparently somewhat less in the long-chain disulfide. From the numerical values cited for the  $\beta$ - and  $\gamma$ -positions in perfluoropropyl chloride, 125.2  $\phi^*$  and 80.7  $\phi^*$ ,<sup>10</sup> it is apparent that very similar  $\beta$  (and  $\gamma$ ) shifts are caused by the isoelectronic chlorine atom; such might be attributed either to the similar size or to the similar polarizability of the S and Cl atoms.

It now is well known that the coupling constant  $J(CF_3-CF_2)$  is very small within perfluoroethyl groups,<sup>13</sup> while in longer chains the coupling of  $CF_3$  to the second  $CF_2$  group, *i.e.*,  $J(CF_3-C-CF_2)$ , is *ca.* 8 to 12 c./s.<sup>10,14,15</sup> In the present work the latter coupling constant is 9.1 to 9.5 c./s., and, in the long-chain disulfide, coupling to the *third*  $CF_2$  group is about 2.5 c./s. It is evident that some further coupling occurs across one and two, but not three, sulfur atoms, for the expected relatively simple  $CF_2S$  quadruplet, slightly broadened due to splitting by the adjacent  $CF_2$  group, is seen only in the latter case. Similar coupling across a nitrogen atom has been reported.<sup>16</sup> In the cyclic sulfide  $(CF_2)_4S$ , couplings between adjacent and between separated  $CF_2$  groups are seen. The coupling constants are about 4.4 and 2.9 c./s., (exact analysis would be exceedingly laborious), but owing to the symmetry of the compound it cannot be determined which is which.

The single broadened line found for 1,4-dithia-perfluorocyclohexane has a temperature-dependent width which undoubtedly results from a slow chair-chair interconversion resembling that of perfluorocyclohexane.<sup>11</sup> Further studies in this area will be reported elsewhere.

**Acknowledgment.**—I thank Donald R. Hotchkiss for careful maintenance and operation of the n.m.r. spectrometer, and Jane E. H. Tiers for measurement of the spectra.

(11) G. V. D. Tiers, *Proc. Chem. Soc.*, 389 (1960).

(12) G. V. D. Tiers, to be submitted for publication.

(13) C. A. Reilly, *J. Chem. Phys.*, 25, 604 (1956).(14) N. Muller, P. C. Lauterbur and G. F. Svatos, *J. Am. Chem. Soc.*, 79, 1807 (1957).

(15) G. V. D. Tiers and J. M. McCrea, paper presented at the N.M.R. Symposium, 132nd National Meeting of the American Chemical Society, New York, 1957.

(16) A. Saika and H. S. Gutowsky, *J. Am. Chem. Soc.*, 78, 4818 (1956).

## FORMATION CONSTANT OF THE 1:1 PYRIDINE-IODINE COMPLEX

BY ARTHUR G. MAKI AND EARLE K. PLYLER

National Bureau of Standards, Washington 25, D. C.

Received October 27, 1951

There has been considerable interest recently in the complexes of halogens with aromatic and amine-like compounds. Plyler and Mulliken<sup>1</sup> have shown that solutions containing the pyridine-iodine complex have an absorption band at 184  $\text{cm}^{-1}$ . This absorption band now has been used to measure the formation constant for the pyridine-iodine complex. Additional measurements also were made on the pyridine absorption band at 601  $\text{cm}^{-1}$ . This band is shifted to 618  $\text{cm}^{-1}$  in the complex and thus may be used to measure the concentration of uncomplexed pyridine.

### Experimental

The far infrared measurements were made using a vacuum spectrometer recently constructed at the Bureau of Standards. In this instrument a 320 lines-per-inch grating was used. Black polyethylene and quartz windows were used as filters and tests showed that the stray radiation was quite negligible. Measurements in the 600  $\text{cm}^{-1}$  region were made with a double-beam infrared spectrometer with a KBr prism.

The sample cells used were constructed of Teflon and had either KBr or quartz windows depending on the wave length studied. Cell lengths of 0.75, 1.0, and 2.0 cm. were used.

All solvents used and the pyridine were spectro grade. The iodine used was reagent grade. The manufacturer states that the pyridine was 99+ % pure and contained less than 0.1% moisture. Subsequent detailed studies of the infrared spectrum of this sample revealed no trace of impurity, thus indicating that the purity is considerably better than 99%.

The spectrophotometric measurements were made on solutions freshly prepared by mixing two previously prepared solutions of pyridine and iodine. All measurements were completed within an hour after the solutions were mixed. In this way any aging process was eliminated. Considerably more time, of the order of 10 hr., was required to give any discernible changes in the solutions although this varied with the solution concentrations.

No special effort was made to obtain accurate temperature regulation. Experimental error was sufficient to mask any small fluctuations in formation constant due to temperature changes. An average sample temperature of 26° is applicable to all measurements.

### Results and Discussion

The experimental determination of the formation constant was made by measurements on the bands at 184 and 601  $\text{cm}^{-1}$ . The measurements on the 601  $\text{cm}^{-1}$  band were used primarily as a check of the results obtained from the 184  $\text{cm}^{-1}$  band. For this check only the peak absorption coefficient was used. Duplicate runs were made on the same solution and five different mixtures were measured. In order to minimize errors due to the non-linearity of a Beer's law plot, the extinction coefficient was measured for pyridine concentrations approximately equal to those measured for the pyridine-iodine solutions.

The concentrations given in Table I and for all other measurements in the 200  $\text{cm}^{-1}$  region were calculated from the known initial concentrations of iodine and pyridine and the value of the con-

centration of the pyridine-iodine complex. To determine the concentration of the complex the absorption was graphically integrated over the entire range for which absorption was evident. This was done by using the integral

$$E_{187}^{197} = \frac{1}{bc} \int_{167}^{197} \log \frac{I_0}{I} d\nu$$

in which  $c$  = concentration in moles per liter of solution,  $b$  = path length in cm., and  $\nu$  is the frequency in  $\text{cm}^{-1}$ . The value of  $E_{187}^{197}$  was determined by using a large excess of pyridine and an amount of iodine sufficient to yield a concentration of complex approximately equal to that found in the unknown solutions. That is to say, the solution used to determine  $E_{187}^{197}$  had an absorption band with about the same area as the absorption band in the unknown solutions. In determining  $E_{187}^{197}$  a correction was made for the non-infinite concentration of pyridine. For this purpose a tentative value of 100 for the formation constant was used. In order to minimize errors due to long term instrumental fluctuations the value of  $E_{187}^{197}$  was re-measured for each determination of the complex concentration.

TABLE I

FORMATION CONSTANT DATA FROM THE 184  $\text{CM}^{-1}$  ABSORPTION BAND WITH CYCLOHEXANE AS SOLVENT

Pyridine	I <sub>2</sub>	Pyridine-I <sub>2</sub> complex	$K_c$ / (l./mole)
0.00592	0.00586	0.00318	92
.00605	.00599	.00305	84
.00605	.00595	.00305	84
.00522	.00578	.00388	128
.00654	.00228	.00256	172
.00715	.00259	.00195	105
.00722	.00265	.00188	98
.00293	.00767	.00183	81
.00268	.00742	.00208	105
.00290	.00764	.00186	84
.00233	.00707	.00243	148

Av. 107 ± 25

$$^a K = [\text{Py} \cdot \text{I}_2] / [\text{Py}] [\text{I}_2]$$

Since a stable ionic complex of pyridine with iodine exists,<sup>2,3</sup> care was exercised throughout this work to ensure that this stable complex, dipyridine-iodine hepta-iodide, was not present in appreciable quantities. The stable complex is ionic and consequently insoluble in most organic solvents. It has infrared absorption bands at 636 and 437  $\text{cm}^{-1}$ , neither of which were observed in the solutions used for this work. Upon standing for several days, however, these solutions were observed to yield a precipitate of this complex.

The formation constants obtained independently from measurements on the two different infrared absorption bands and in the solvents  $\text{CCl}_4$ ,  $n$ -heptane, and cyclohexane all agree within the limits of experimental error. For the formation constant of the 1:1 pyridine-iodine complex ( $\text{Py} \cdot \text{I}_2$ ) the best value obtained by this work is

(1) E. K. Plyler and R. S. Mulliken, *J. Am. Chem. Soc.*, **81**, 823 (1959).

(2) A. B. Prescott and P. F. Trowbridge, *ibid.*, **17**, 859 (1895).

(3) O. Hassel and H. Hoop, *Acta Chem. Scand.*, **15**, 407 (1961).



107  $\pm$  25 l./mole in cyclohexane solution at 26°. This compares quite favorably with the value of 101 found by Popov and Rygg<sup>4</sup> in CCl<sub>4</sub>.

(4) A. I. Popov and R. H. Rygg, *J. Am. Chem. Soc.*, **79**, 4622 (1957).

### THE MECHANISM OF THE "UNIMOLECULAR" YIELD OF HYDROGEN IN THE RADIOLYSIS OF LIQUID CYCLOHEXANE

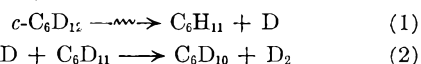
By P. J. DYNE

Research Chemistry Branch, Atomic Energy of Canada Ltd., Chalk River, Ontario

Received November 1, 1961

Some of the hydrogen produced in the radiolysis of cyclohexane is formed by a "unimolecular" or "intramolecular" mechanism where both the hydrogen atoms come from the same hydrocarbon molecule.<sup>1-3</sup> Our experiments<sup>1</sup> have detected this reaction by measuring the yield of D<sub>2</sub> produced in the radiolysis of *c*-C<sub>6</sub>H<sub>12</sub>-*c*-C<sub>6</sub>D<sub>12</sub> mixtures which is first order with respect to the concentration of C<sub>6</sub>D<sub>12</sub>.

Ingalls<sup>4</sup> reports similar studies on the radiolysis of deuterated toluene and suggests that the mechanism of such a "unimolecular" yield may be written (for cyclohexane)



where reaction 2 is a diffusion-controlled reaction between the atom and radical formed in reaction 1. The kinetics of this type of reaction have been studied extensively by Hamill and Williams and their collaborators.<sup>5-7</sup> The yield of deuterium in this reaction sequence would be first order with respect to the C<sub>6</sub>D<sub>12</sub> concentration.

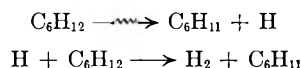
We recently have shown<sup>8</sup> that the "unimolecular" yield of D<sub>2</sub> in these *c*-C<sub>6</sub>H<sub>12</sub>-*c*-C<sub>6</sub>D<sub>12</sub> mixtures is reduced on the addition of benzene and iodine. Since we assumed that the "unimolecular" decomposition did not involve the separation of free deuterium atoms, we argued that the interaction must be by a quenching or energy-transfer type of process. A very reactive hydrogen atom scavenger may, however, compete with reaction 2 and our arguments consequently need re-examination.<sup>9</sup>

Roy, Williams, and Hamill<sup>5</sup> have shown that a scavenger can only compete with a diffusion-controlled radical reaction if the collision efficiency of the reaction between the scavenger and the radical is close to unity. If the collision efficiency is 0.1

or less no effective competition occurs at concentrations of up to 5 mole%.

The collision efficiency of the reaction between H atoms and benzene in the gas phase is 1.3-7.9  $\times 10^{-4}$ .<sup>10</sup> Arguments have been presented to show that gas-phase data for these reactions are relevant to the liquid phase.<sup>11</sup> It consequently is unlikely that benzene could compete with reaction 2.

The inconsistency between known collision efficiencies and those required for competition with a diffusion controlled reaction is seen again in this analogous argument. Our data, when plotted in the manner suggested by Roy, Hamill, and Williams, and interpreted in terms of a diffusion-controlled reaction, show that the collision efficiency for the radical scavenger reaction for both benzene and iodine would have to be close to unity. Since the collision efficiency of the reaction in the gas phase  $\text{H} + \text{C}_6\text{H}_{12} \rightarrow \text{H}_2 + \text{C}_6\text{H}_{11}$  is  $\sim 1 \times 10^{-7}$ ,<sup>11,12</sup> it follows that benzene and iodine should compete with the homogeneous bimolecular reaction sequence



at concentrations  $\sim 10^{-7}$  mole fraction. Experimentally, however, a concentration of benzene  $> 10^{-3}$  mole fraction is required to reduce  $G(\text{H}_2)$  to about one-half its original value.

Similar arguments can be applied to iodine where, as previously has been argued by R. H. Schuler,<sup>13</sup> its effect on  $G(\text{H}_2)$  shows that the collision efficiency of the H atom-iodine reaction is much less than unity.

In studying the photolysis of HI in hydrocarbon solvents, Nash, Williams, and Hamill<sup>14</sup> observed no diffusion-controlled recombination of H and I atoms at room temperature; this they attributed to "the small size of the H atom and the relatively open structure of the solvents." It consequently can be argued that there is a low probability of reaction 2 occurring in a diffusion-controlled reaction.

There seems to be no *a priori* reason why the "unimolecular" decomposition should not go by a true molecular splitting—*i.e.*, a reaction which is mechanistically described by  $\text{C}_6\text{D}_{12} \xrightarrow{\sim} \text{C}_6\text{D}_{10} + \text{D}_2$ , since analogous reactions are well established<sup>15,16</sup> in the vapor-phase radiolysis and photolysis where no diffusion-controlled reactions can occur.

We conclude that (1) we are justified in assuming that benzene and iodine reduce the "unimolecular" yield by a quenching or energy-transfer mechanism, rejecting a scavenging interaction and (2) part, if not all, of the "unimolecular" yield probably occurs by a true molecular splitting.

(1) P. J. Dyne and W. M. Jenkinson, *Can. J. Chem.*, **38**, 539 (1960).

(2) T. D. Nevitt and L. P. Remsberg, *J. Phys. Chem.*, **64**, 969 (1960).

(3) M. Burton and J. Chang, private communication.

(4) R. B. Ingalls, *J. Phys. Chem.*, **65**, 1605 (1961).

(5) J. C. Roy, R. R. Williams, Jr., and W. H. Hamill, *J. Am. Chem. Soc.*, **76**, 3274 (1954).

(6) J. C. Roy, W. H. Hamill, and R. R. Williams, Jr., *ibid.*, **77**, 2953 (1955).

(7) J. C. Roy, J. R. Nash, R. R. Williams, Jr., and W. H. Hamill, *ibid.*, **78**, 519 (1956).

(8) P. J. Dyne and W. M. Jenkinson, *Can. J. Chem.*, **39**, 2163 (1961).

(9) The author is indebted to Dr. H. Schwarz who first drew his attention to this point.

(10) P. E. M. Allen, H. W. Melville, and J. C. Robb, *Proc. Roy. Soc. (London)*, **A218**, 311 (1953).

(11) T. J. Hardwick, *J. Phys. Chem.*, **65**, 101 (1961).

(12) H. E. Schiff and E. W. R. Steacie, *Can. J. Chem.*, **29**, 1 (1951).

(13) R. H. Schuler, *J. Phys. Chem.*, **61**, 1472 (1957).

(14) J. R. Nash, R. R. Williams, Jr., and W. H. Hamill, *J. Am. Chem. Soc.*, **82**, 5974 (1960).

(15) L. M. Dorfman, *J. Phys. Chem.*, **62**, 29 (1958).

(16) Myran C. Sauer, Jr., and L. M. Dorfman, *J. Chem. Phys.*, **35**, 497 (1961).

# COMMUNICATION TO THE EDITOR

## VARIATIONS IN THE COUPLING CONSTANT BETWEEN $^{13}\text{C}$ AND DIRECTLY-BONDED FLUORINE

Sir:

A few measurements of the coupling constant  $J_{^{13}\text{C}-\text{F}}$  in saturated systems have been made,<sup>1,2</sup> but only with carbon, fluorine, and hydrogen atoms directly bonded to the  $^{13}\text{C}$  atom. We have evaluated this coupling constant in the presence of other directly-bonded substituents (Table I). The values exhibit correlations with the position of these substituents in the periodic table. Increase in the atomic number of a substituent atom within a given group of the periodic table is accompanied by an increase in  $J_{^{13}\text{C}-\text{F}}$ . Examples of this regularity are seen in the pairs of molecules  $\text{CF}_4$  and  $\text{CCl}_3\text{F}$ ,  $(\text{CF}_3\text{S})_2$  and  $(\text{CF}_3\text{Se})_2$ ,  $(\text{CF}_3\text{S})_2\text{Hg}$  and  $(\text{CF}_3\text{Se})_2\text{Hg}$ ,  $(\text{CF}_2\text{Cl})_2$  and  $(\text{CF}_2\text{Br})_2$ , and  $(\text{CF}_3)_2\text{NNO}_2$  and  $(\text{CF}_3)_2\text{PCL}$ . The effect of the atoms directly bonded to the  $^{13}\text{C}$  atom appears to be greater than that of remote substituents. This is not always the case for the analogous proton coupling constant,  $J_{^{13}\text{C}-\text{H}}$  (where both the absolute magnitude and the amount of variation are smaller), since its value in methyl groups directly bonded to carbon or nitrogen are similar in magnitude.<sup>3</sup> As the atomic number of a directly-bonded substituent increases within a given row of the periodic table,  $J_{^{13}\text{C}-\text{F}}$  decreases, as can be seen for molecules of the type  $\text{CF}_3\text{X}$ . The lowest value found is that of 259.2 c./s. for  $\text{CF}_4$  itself. The value for  $(\text{CF}_3)_2\text{NNO}_2$  is 273.6 c./s., while for the two  $\text{CF}_3\text{C}$  compounds listed, the coupling constants are 282.5 c./s. and 283.2 c./s.<sup>1</sup> Similarly in the second row of the periodic table the value for  $(\text{CF}_3)_2\text{PCL}$  is greater than any of the three values given for  $\text{CF}_3\text{S}$  compounds. These variations are of lesser magnitude than those within a group of the periodic table, noted above, and are opposite in sign to differences observed for  $J_{^{13}\text{C}-\text{H}}$ .<sup>3</sup> It is of interest to note from Table I that the value of  $J_{^{13}\text{C}-\text{F}}$  for  $\text{CF}_3\text{H}$  is greater than that for  $\text{CF}_4$ ,<sup>2</sup> being roughly the same as that for  $(\text{CF}_3)_2\text{NNO}_2$ .

Malinowski<sup>3</sup> has attempted to show an additivity relation for  $J_{^{13}\text{C}-\text{H}}$  for compounds of the type  $\text{CHXYZ}$  using contributions according to the equation  $J_{^{13}\text{C}-\text{H}} = \zeta_{\text{X}} + \zeta_{\text{Y}} + \zeta_{\text{Z}}$ , and he has obtained good agreement between predicted and observed values. A similar procedure for  $(^{13}\text{C},\text{F})$  coupling constants gives reasonably consistent

(1) G. V. D. Tiers, *J. Phys. Soc. Japan*, **15**, 354 (1960).

(2) S. G. Frankiss, to be published.

(3) E. R. Malinowski, *J. Am. Chem. Soc.*, **83**, 4479 (1961).

TABLE I

VALUES OF THE  $(^{13}\text{C},\text{F})$  COUPLING CONSTANT FOR VARIOUS SUBSTITUENTS, AND THE ASSOCIATED ZETA VALUES

The compounds are arranged in the order of the atomic number of the element for which zeta is quoted.

Molecule	$J_{^{13}\text{C}-\text{F}}$	Atom directly bonded to $^{13}\text{C}$	$\zeta$
(a) Trifluoromethyl compounds			
$\text{CF}_4$	259.2 <sup>2</sup>	F	86.4 <sup>2</sup>
$\text{CF}_3\text{H}$	274.3 <sup>2</sup>	H	101.5
$\text{CF}_3\text{CCl}_3$	282.5 <sup>1</sup>	C	109.7
$\text{CF}_3\text{CO}_2\text{H}$	283.2 <sup>1</sup>	C	110.4
$(\text{CF}_3)_2\text{NNO}_2$	273.6	N	100.8
$(\text{CF}_3)_2\text{PCL}$	320.2	P	147.4
$(\text{CF}_3\text{S})_2$	313.8	S	141.0
$(\text{CF}_3\text{S})_2\text{Hg}$	308.3	S	135.5
$\text{CF}_3\text{SNCO}$	309.4	S	136.
$(\text{CF}_3)_2\text{Se}$	331.3	Se	158.5
$(\text{CF}_3\text{Se})_2$	337.1	Se	164.3
$(\text{CF}_3\text{Se})_2\text{Hg}$	332.5	Se	159.7
(b) Other compounds			
$\text{CF}_2\text{H}_2$	234.8 <sup>2</sup>	H	74.2
$\text{CFH}_3$	157.4 <sup>2</sup>	H	52.5
cyclo- $\text{C}_4\text{F}_8^c$	298.0	C	105.8
$\text{CCl}_3\text{F}$	336.5	Cl	112.2
$(\text{CF}_2\text{Cl})_2$	299.0	Cl	104.4 <sup>b</sup>
$(\text{CF}_2\text{Br})_2$	311.6	Br	115.7 <sup>b</sup>

<sup>a</sup> This value is used in the derivation of all the others.

<sup>b</sup> Assuming  $\zeta_{\text{C}} = 108$ . <sup>c</sup> The  $^{13}\text{C}$  satellite bands of this compound have broadened triplet structure (with 1:1:1 relative intensities), the splitting being 3.0 c./s. Details of the fine structure of the other compounds will be published later.

values for the contributions of directly-bonded substituents (Table I), with the notable exception of hydrogen ( $\zeta_{\text{H}}$  varies markedly in the series  $\text{CF}_3\text{H}$ ,  $\text{CF}_2\text{H}_2$ ,  $\text{CFH}_3$ ).<sup>2</sup> This procedure emphasizes the variation of  $J_{^{13}\text{C}-\text{F}}$  with the atomic numbers of the substituents, since we obtain  $\zeta_{\text{P}} > \zeta_{\text{S}} > \zeta_{\text{Cl}}$ ;  $\zeta_{\text{Se}} > \zeta_{\text{Br}}$ ; and  $\zeta_{\text{Br}} > \zeta_{\text{Cl}} > \zeta_{\text{F}}$ . These empirical correlations may be of use in confirming proposed structures. For example, the value of  $J_{^{13}\text{C}-\text{F}}$  for  $\text{CF}_3\text{-SNCO}$ <sup>4</sup> strongly supports the evidence that the perfluoromethyl group is attached directly to the sulfur atom.

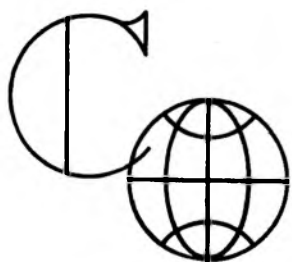
The author is grateful to the Inorganic Chemistry Department, Cambridge University, for the samples of the sulfur- and selenium-containing compounds; and to the Department of Scientific and Industrial Research for a research studentship.

(4) H. J. Emeléus and A. A. Haas, private communication.

THE UNIVERSITY CHEMICAL LABORATORY  
LENSFIELD ROAD  
CAMBRIDGE, ENGLAND

R. K. HARRIS

RECEIVED JANUARY 29, 1962



**NEW**

# International Series in Chemistry

The New INTERNATIONAL SERIES IN CHEMISTRY presents advanced scientific and reference works in chemistry, written by authorities in the field. The books will receive world-wide distribution and will include works by scholars from countries throughout the world. Both English and foreign language editions will be published in conjunction with Prentice-Hall offices abroad.

## First titles in the Series:

### **Regular Solutions**

By *Joel H. HILDEBRAND, Emeritus, University of California, Berkeley, and Robert L. SCOTT, University of California, Los Angeles*

Research in the field of regular solutions has made great advances since 1950. It has progressed to the point at which a remarkably consistent system of quantitative relationships and the factors which determine these relationships now exist. This new book offers a lucid exposition of the current status of the theory of regular solutions.

*April '62*

*192 pages*

*Trade price: \$7.00*

### **The Irreducible Tensor Method for Molecular Symmetry Groups**

by *J. S. GRIFFITH, Fellow of King's College, University of Cambridge*

The irreducible tensor method for molecular symmetry groups is described here for the first time. Employing the theory of the  $V$ ,  $W$ , and  $X$  coefficients as its basic mathematical technique, the material progresses to general formulae for matrix elements in  $n$ -electron systems. The author's work provides a basis for the application of the tensor method to closed-shell systems including aromatic molecules such as benzene or pyridine, or simple inorganic compounds such as silicon tetrachloride.

*June '62*

*160 pages*

*Trade price: \$7.00*

### **Theories of Electrons in Molecules**

by *William T. SIMPSON, University of Washington*

The valence bond and molecular orbital method have for a long time been the backbone of attempts to understand the electronic structure of molecules. This book introduces and explains these methods from a modern viewpoint and with continuity and logical consistency. The independent system approach, which is useful for molecular crystals and certain molecules, is taken up in a similar way, and then related to the other time-honored approaches.

**The books in this series  
are restricted and cannot  
be sampled.**

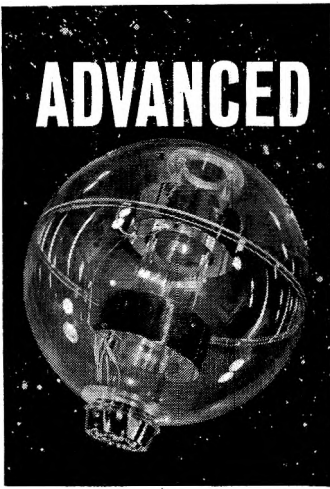
*September '62*

*Trade price: \$8.65*

*For further information, write: Box 903*

**Prentice-Hall, Inc., Englewood Cliffs, New Jersey**

# ADVANCED FLASH TECHNOLOGY



- for
- Flash-induced chemical catalysis.
  - High-speed photography of chemical and process reactions.
  - Motion studies, shock-wave photography.
  - Cloud chamber Physics.
  - Deep-sea photography.
  - U.V. printing and time-marking.
  - Satellite beacon systems.
  - Optical Maser (Laser) light pumps.

EG&G's leadership in flash technology is solidly based on original contributions to the state of the art which have produced more than 40 patents for tubes, circuits and stroboscopic systems.

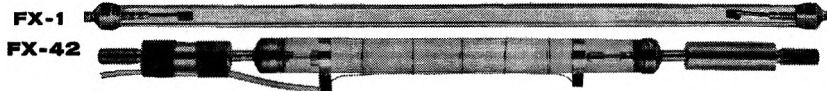
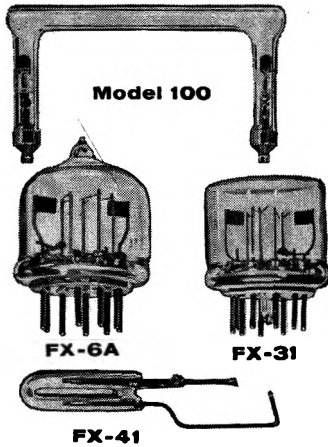
## XENON FLASH TUBES

**Model 100** Designed for Laser and other special applications. Tube configuration ensures maximum light intensity per unit of rod area. Output: 250 HCPS/flash. Input: 100 ws. Price: \$50.

**FX-31** Internally triggered. Non wandering arc. Single flash or strobe. Flat-topped for optimum optical characteristics. Output: 2.5 HCPS/flash. Input: 5 ws. Price: \$30. Standard **FX-6A** type: \$15.

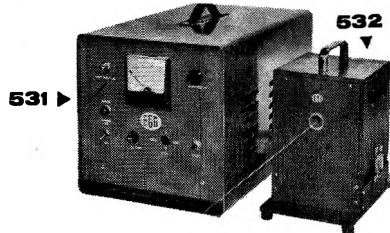
**FX-41** Paper-clip size tube now under development. Inquiries invited.

**FX-38** 3" arc. Output: 400 HCPS/flash. Input: 200 ws. Also available: **FX-1** Output: 2000 HCPS/flash. Input: 400 ws. Price: \$50. **FX-42** Output: 2500 HCPS/flash. Input: 600 ws.



## PULSED POWER SYSTEMS

- FOR LASER STIMULATION FLASH CATALYSIS, ETC.



**Model 531** Output: 400 ws. (1050 mfd at 900 v.) Input: 115 v. 60 cycle a.c. Price: \$795.00. **Model 532** Flash Head with 2 Model 100 tubes: \$395.00. System will drive polished and multicoated ruby rods with low threshold. System Price: \$1190.00.

**Model 522** Two unit 1280 ws. system provides up to 4 kv. into 80 mfd. or 160 mfd. Triggered externally or from front panel. Drives Model 511, 512, 513 Flash Heads with 4 to 10 Model 100 tubes. Accommodates crystals 2" long up to 1/2" dia. Input: 110 v. or 220 v. 60 cycle a.c. Price: \$3345.00 (complete system with 4 tubes).

- FOR MOTION STUDIES, CLOUD CHAMBER PHYSICS, ETC.

**Model 530** Output: 100 ws. (260 mfd. at 900 v.) Input: 115 v. 60 cycle a.c. Price: \$395.00. EG&G TR-36 external trigger transformer: \$13.95. System drives most EG&G flash tubes.

## ELECTRONIC FLASH EQUIPMENT

**Microflash** (.5µsec duration) for ballistic photography... **High-Speed Stroboscope** (6 kc. rate) for photographing shock waves, projectiles, etc. . . . **Flash Illuminator** for macrophotography and photomicrography . . . **Double Flash** for silhouette photography . . . **Multiple Microflash** for superimposition of up to 20 photographs on single negative at up to 100 kc. rate . . . **Mark VI and VII Sensitometers** for rating film sensitivities, etc.



Further information on request on above products and on: Milli-mike® Oscilloscopes and accessories, Hydrogen Thyratrons and Diodes, Triggered Spark Gaps, Transformers, Oceanographic Instruments, Radiation Detection Devices.

TEL. COPLEY 7-9700 • CABLE: EGGINC, BOSTON; TWX: BS 1099

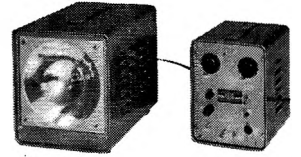
**Edgerton, Germeshausen & Grier, Inc.**

160-D BROOKLINE AVENUE, BOSTON 15, MASSACHUSETTS

WESTERN OPERATIONS: P. O. Box 1912, Las Vegas, Nev.—Santa Barbara Airport, P. O. Box 98, Goleta, Calif.



## ELECTRONIC FLASH EQUIPMENT



**Microflash** Flash Duration: 0.5 microsecond. Peak Light:  $50 \times 10^6$  bea candle power. Energy Input: 8 ws (.C mfd at 18 kv). Recycle Time: 5 second Time Delay: Adjustable from 3 to 10C microseconds. Price: \$975.00. Poi Light Source Attachment: \$35.00.

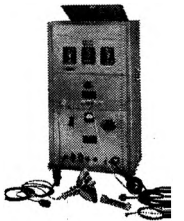
### MARK VI SENSITOMETER

Compact, easy to use, laboratory device. Will accommodate glass plates, 16 mm. or 35 mm films. Exposure Times: 1/100, 1/100-1/10,000 second. Built-in voltage regulator. Color correction filters unnecessary. Price \$600.00. Mark VII Sensitometer, which has the additional range of 1/100,000 and 1/1,000,000, is available at \$1200.00.

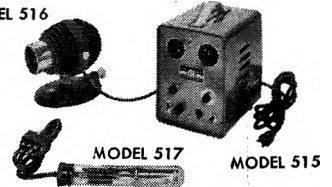


### High-Speed STROBOSCOPE

Light source specially developed for use with high-speed cameras for studies of fast-moving objects such as shock waves and projectiles. Flashing Rate: Up to 6000 flashes per second. Flash Duration: As low as 1.2 microsecond Triggers: From camera, oscillator c contactor. Price: \$3500.00.



MODEL 516



**Microscope Flash Illuminator** Model 516 lamp and 515 power supply provides high intensity flashes (154 microseconds at 100 ws) for extreme close-up photography of delicate subjects without heat damage... e.g human eye, insects, botanical specimens, etc. Model 517, separate lamp assembly permits close-ups of underwater subjects in fish tanks, etc.

## FOR FURTHER INFORMATION, CALL

STATE	CITY	TELEPHONE
Alabama	Huntsville	536-0631
California	San Gabriel	ATlantic 7-9633
	San Carlos	LYtell 3-7693
	San Diego	ACademy 3-713
	Denver	MAin 3-1458
Canada	Willowdale, Ontario	BAldwin 5-7391
Florida	Orlando	CHerry 1-4445
Illinois	Chicago	NAtional 2-8650
Maryland	Towson	VAlley 3-3434
	Wheaton	LOckwood 5-306
Massachusetts	Boston	COpley 7-9700
Michigan	Livonia	453-8414
Minnesota	St. Paul	Midway 8-5531
New Jersey	Ridgewood	GIlbert 4-1400
New Mexico	Albuquerque	AMherst 8-2478
New York	Syracuse	GIbson 6-1771
North Carolina	Winston-Salem	StAte 8-0431
	Dayton	BAldwin 3-9621
Ohio	Cleveland	JAckson 6-3990
Texas	Fort Worth	PERshing 8-2394
Utah	Salt Lake City	EMpire 4-3057
Washington	Seattle	PArkway 3-3320
Wisconsin	Milwaukee	FL 2-2657